

# **Understanding the effect of adding nanoclays into epoxies**

**Tri-Dung Ngo**

**A Thesis**

**in**

**the Department**

**of**

**Mechanical and Industrial Engineering**

**Presented in Partial Fulfillment of the Requirements**

**For the Degree of Doctor of Philosophy at**

**Concordia University**

**Montreal, Quebec, Canada**

**March 2007**

**© Tri-Dung Ngo, 2007**



Library and  
Archives Canada

Bibliothèque et  
Archives Canada

Published Heritage  
Branch

Direction du  
Patrimoine de l'édition

395 Wellington Street  
Ottawa ON K1A 0N4  
Canada

395, rue Wellington  
Ottawa ON K1A 0N4  
Canada

*Your file* *Votre référence*  
*ISBN: 978-0-494-31151-6*  
*Our file* *Notre référence*  
*ISBN: 978-0-494-31151-6*

#### NOTICE:

The author has granted a non-exclusive license allowing Library and Archives Canada to reproduce, publish, archive, preserve, conserve, communicate to the public by telecommunication or on the Internet, loan, distribute and sell theses worldwide, for commercial or non-commercial purposes, in microform, paper, electronic and/or any other formats.

The author retains copyright ownership and moral rights in this thesis. Neither the thesis nor substantial extracts from it may be printed or otherwise reproduced without the author's permission.

#### AVIS:

L'auteur a accordé une licence non exclusive permettant à la Bibliothèque et Archives Canada de reproduire, publier, archiver, sauvegarder, conserver, transmettre au public par télécommunication ou par l'Internet, prêter, distribuer et vendre des thèses partout dans le monde, à des fins commerciales ou autres, sur support microforme, papier, électronique et/ou autres formats.

L'auteur conserve la propriété du droit d'auteur et des droits moraux qui protègent cette thèse. Ni la thèse ni des extraits substantiels de celle-ci ne doivent être imprimés ou autrement reproduits sans son autorisation.

---

In compliance with the Canadian Privacy Act some supporting forms may have been removed from this thesis.

Conformément à la loi canadienne sur la protection de la vie privée, quelques formulaires secondaires ont été enlevés de cette thèse.

While these forms may be included in the document page count, their removal does not represent any loss of content from the thesis.

Bien que ces formulaires aient inclus dans la pagination, il n'y aura aucun contenu manquant.

  
**Canada**

**CONCORDIA UNIVERSITY**

**School of Graduate Studies**

This is to certify that the thesis prepared

By: **Tri-Dung Ngo**

Entitled: **Understanding the effect of adding nanoclays into epoxies**

and submitted in partial fulfillment of the requirements for the degree of

**Doctor of Philosophy (Mechanical and Industrial Engineering)**

complies with the regulations of this University and meets the accepted standards with respect to originality and quality.

Signed by the final examining committee:

_____	Chair
_____	External to the Program
_____	Examiner
Dr. Dorel Feldman	
_____	Examiner
Dr. Paula Wood-Adams	
_____	Examiner
Dr. Martin Pugh	
_____	Thesis Co-Supervisor
Dr. Suong Van Hoa	
_____	Thesis Co-Supervisor
Dr. Minh-Tan Ton-That	

Approved by

\_\_\_\_\_

Chair of Department or Graduate Program Director

\_\_\_\_\_ 2007 \_\_\_\_\_

\_\_\_\_\_

Dean, Faculty of Engineering & Computer Science

# ABSTRACT

## Understanding the effect of adding nanoclays into epoxies

Tri-Dung Ngo, PhD.  
Concordia University, 2007

Different preparation methods and formulations of epoxy nanocomposites have been examined. The effects of each parameter, such as different types of clay, different types of curing agent, and processing conditions (temperature, time, speed), on dispersion of the clay particles were evaluated using different means, such as field emission gun scanning electron microscopy (FEGSEM), X-ray diffraction (XRD), transmission electron microscopy (TEM), and viscometer. Curing behavior was studied by differential scanning calorimetry (DSC) and Fourier transform infrared spectroscopy (FTIR). Thermal properties of epoxy nanocomposites were evaluated by thermogravimetric analysis (TGA), limiting oxygen index (LOI). Dynamic mechanical properties were studied by dynamic mechanical analysis (DMA). Tensile, flexural, compression, impact, surface hardness and fracture toughness were also examined. A new method to disperse organoclay into epoxy without using solvent, and using high speed mixing (TS), is proposed. The results obtained from this study provide a good understanding of the relationship between the formulation, processing conditions and performance. Significant improvement in stiffness and storage modulus was observed in nanocomposites

formulated with better dispersion using TS. However, the extent of the improvement of the nanocomposites' performance depends on the type of the clay and the curing agent. In addition, the processing conditions have great effects on the final properties of epoxy nanocomposites.

## ACKNOWLEDGEMENTS

I thank the Vietnamese Government for a scholarship. I also would like to thank the Natural Sciences and Engineering Research Council of Canada for funding in this project (grant N00784 – Development of Polymer Nanocomposites, and grant N00004 – Analysis and Vibration of Elastic and Viscoelastic Systems).

I would like to express my sincere gratitude to my supervisors **Dr. S. V. Hoa** and **Dr. M. T. Ton-That** for their guidance, instruction, encouragement and support throughout the stages of this study. Not only did these individuals provide invaluable time and assistance regarding polymer science and engineering, but they have been motivational in their love of science and life.

I have been honored to have Dr. D. Feldman, Dr. P. Wood-Adams, Dr. M. Pugh serve on my graduate committee.

I thank Dr. P. Wood-Adams for her help with regard to the study of flow in a concentric cylinder.

I would also like to thank Dr. J. Denault for use of the facilities at the Industrial Materials Institute (IMI)-National Research Council of Canada (NRC).

I am grateful to Dr. Ken C. Cole (from IMI-NRC) for his help and suggestions. I am also thankful to Dr. Ming Xie, Mr. Hang Wang (from the Concordia Center for Composites (CONCOM)), Mrs. Florence Perrin-Sarazin, Ms. Weawkamol Leelapornpisit (from

IMI-NRC) for their assistance with laboratory procedures.

I acknowledge the cooperation and help provided by all technicians who were involved in this study from IMI-NRC and CONCOM.

The friendship and help provided from all of my colleagues at Concordia University are also acknowledged.

I wish to express my appreciation to my family for helping me to know which path to follow. This dissertation is the product of so much more than four years and my family has supported me through it all.

Most of all, and with all of my heart, I would like to thank my wife, Nguyen Thi Buu-Tram, for being the most important part of my life, which is a true proof of love!

There are so many people to whom I have been indebted for support and encouragement.

I thank you all!

Montreal in March 2007

Tri-Dung Ngo

# TABLE OF CONTENT

<b>LIST OF FIGURES .....</b>	<b>xii</b>
<b>LIST OF TABLES .....</b>	<b>xxxiv</b>
<b>LIST OF SYMBOLS, NOMENCLATURES AND ABBREVIATIONS .....</b>	<b>xi</b>
<b>Chapter 1. Introduction .....</b>	<b>1</b>
1.1 Thesis motivation.....	2
1.2 Content of the thesis.....	4
<b>Chapter 2. Background and thesis objectives .....</b>	<b>7</b>
2.1. Development of polymer nanocomposites (PNC) .....	7
2.2. Nano-layered silicates.....	9
2.2.1. Montmorillonite.....	9
2.2.2. Organolay.....	11
2.3. Nanocomposite structures.....	16
2.4. Polymer nanocomposites (PNCs) fabrication.....	21
2.4.1. Thermoset nanocomposites fabrication .....	21
2.4.2. Thermoplastic nanocomposite fabrication.....	24
2.5. Epoxies.....	26
2.5.1. Epoxy resins.....	27
2.5.2. Hardeners (curing agents).....	28
2.6. Epoxy-clay nanocomposites (ECNs) .....	33
2.6.1. Formation of ENC's.....	34
2.6.2. Curing of ENC's.....	38



2.6.3.	Mechanical properties.....	39
2.6.4.	Thermal properties.....	42
2.6.5.	Barrier properties.....	44
2.7.	Summary.....	45
2.8.	Challenges for ECNs.....	48
2.9.	Objectives.....	49
	<b>Chapter 3. Materials and experiments.....</b>	<b>50</b>
3.1.	Selection of materials.....	50
3.1.1.	Epoxy.....	51
3.1.2.	Curing agents (hardeners).....	52
3.1.3.	Clays.....	54
3.2.	Experimental design.....	55
3.2.1.	Study parameters.....	55
3.2.2.	Experimental setup.....	57
3.3.	Stirring methods.....	59
3.3.1.	Room temperature and hand stirring (Rm).....	59
3.3.2.	High temperature and hand stirring (Tm).....	60
3.3.3.	High temperature and medium speed stirring method (TM).....	60
3.3.4.	High speed stirring method.....	61
3.3.5.	High pressure mixing method (HP).....	62
3.4.	Curing of ENC's.....	64
3.5.	ENC's characterization.....	65
3.5.1.	Dispersion behavior.....	65

3.5.2.	Fourier transform infrared spectroscopy (FTIR) analysis .....	74
3.5.3.	Rheological properties .....	75
3.5.4.	Thermal properties .....	77
3.5.5.	Mechanical properties.....	82
<b>Chapter 4. Effects of fabrication process and compositions of constituents on the dispersion and intercalation/exfoliation of clay .....</b>		<b>96</b>
4.1.	Challenges and objectives.....	96
4.2.	Methodology and experiment .....	98
4.2.1.	Effect of the stirring step.....	102
4.2.2.	Effect of the curing step .....	106
4.3.	Effect of the stirring process on the dispersion.....	109
4.3.1.	Micro dispersion .....	109
4.3.2.	The intercalation .....	117
4.3.3.	Rheological properties of epoxy-clay mixtures .....	130
4.4.	Effect of the curing process on the dispersion .....	144
4.4.1.	Effect of curing temperature .....	144
4.4.2.	Effect of chemistry of clay.....	171
4.4.3.	Effect of chemistry of hardener. ....	181
4.5.	Model for the dispersion of clay .....	190
4.5.1.	Van der Waals interaction force acting between two particles or macroscopic bodies.....	192
4.5.2.	Van der Waals interaction forces between two spheres.....	196

4.5.3.	Development of theoretical model of flow of the epoxy-clay mixture in high speed stirring .....	199
4.5.4.	Determination of velocity needed to disperse the clay sheets .....	208
4.5.5.	Application of the above solution to the experimental system .....	216
4.6.	Summary .....	220
	<b>Chapter 5. The curing process of epoxy nanocomposites .....</b>	<b>224</b>
5.1.	Challenges and objectives .....	224
5.2.	Methodology and experimental set up .....	225
5.3.	Modelling .....	228
5.3.1.	Empirical model .....	229
5.3.2.	Activation energy .....	230
5.3.3.	The Avrami model .....	231
5.4.	Effect of clay and level of dispersion on curing process .....	233
5.4.1.	DSC results .....	234
5.4.2.	Activation energy .....	240
5.4.3.	Avrami analysis .....	246
5.5.	Effect of hardener .....	249
5.5.1.	DSC results .....	250
5.5.2.	Activation energy .....	256
5.5.3.	Avrami analysis .....	264
5.6.	Summary .....	268
	<b>Chapter 6. Properties of epoxy nanocomposites .....</b>	<b>272</b>
6.1.	Objectives .....	272

6.2. Methodology and experiment .....	274
6.3. Effect of the stirring process .....	275
6.3.1. Tensile and compressive properties .....	276
6.3.2. Fracture toughness properties .....	286
6.3.3. Dynamic mechanical properties.....	296
6.3.4. Thermal properties .....	301
6.3.5. Barrier properties .....	306
6.4. Effect of the chemistry of clays .....	314
6.4.1. Tensile and flexural properties.....	314
6.4.2. Flammability - limiting oxygen index .....	316
6.5. Effect of the chemistry of hardeners .....	319
6.5.1. Tensile properties.....	319
6.5.2. Flammability - LOI.....	323
6.5.3. Fracture toughness .....	325
6.6. Summary.....	328
<b>Chapter 7. Reinforcing effect of organoclay in epoxy resins with</b>	
<b>characteristics varying over a broad range from rubbery to glassy.....</b>	<b>332</b>
7.1. Challenges and objectives.....	332
7.2. Methodology and experiment .....	333
7.3. Results and discussion .....	336
7.3.1. Dispersion .....	336
7.3.2. Thermal, physical and mechanical properties.....	343
7.4. Modulus prediction .....	365

7.4.1.	Halpin-Tsai and Mori-Tanaka models .....	365
7.4.2.	Representation of intercalated/exfoliated nanoclay .....	370
7.5.	Summary .....	381
	<b>Summary, conclusions, contributions and recommendations for future work.....</b>	<b>384</b>
8.1.	Summary .....	384
8.2.	Conclusions.....	393
8.3.	Contributions.....	395
8.4.	List of publications .....	399
8.5.	Recommendations for future work .....	402
	<b>References .....</b>	<b>404</b>

## LIST OF FIGURES

Figure 2.1. Oxygen transmission rates (OTR) of nylon 6 nanocomposite [27] .....	8
Figure 2.2. Structure of 2:1 phyllosilicates [4, 34].....	10
Figure 2.3. Exchange occurs between the ions of the clay ( $X^+$ ) and those of the electrolyte ( $Y^+$ ) [39].....	12
Figure 2.4. Exchange occurs between $Na^+$ -MMT and organic cation $RH^+$ [41] .....	12
Figure 2.5. Effect of surface treatment [27].....	13
Figure 2.6. The cation-exchange process between alkylammonium ions and cations initially intercalated between the clay layers [41] .....	14
Figure 2.7. (a) The hydrolysis of the silanes and (b) The possible reaction of a silanol group with a hydroxyl group present on the inorganic surface [47].....	15
Figure 2.8. The three idealised structures of polymer-clay composites. ....	17
Figure 2.9. XRD curves of (a) fluorohectorite in HDPE matrix, (b) nanocomposite of fluorohectorite in polystyrene, and (c) nanocomposite of fluorohectorite in silicon rubber [51] .....	18
Figure 2.10. TEM of an amine-cured epoxy clay nanocomposite [45].....	19
Figure 2.11. SEM micrograph of epoxy nanocomposite [18] .....	20
Figure 2.12. AFM phase image of epoxy clay nanocomposite [53].....	20
Figure 2.13. Flowchart presenting the different steps of the “in-situ polymerisation” approach.....	22
Figure 2.14. Schematic illustration of “in-situ polymerisation” approach [4] .....	22

Figure 2.15. Flowchart presenting the different steps of the “solution” approach.....	23
Figure 2.16. Schematic illustration of “solution” approach. The black dots represent the solvent molecules [4].....	23
Figure 2.17. Flowchart presenting the different steps of the “melt intercalation” approach .....	26
Figure 2.18. Schematic illustration of “melt intercalation” process [4] .....	26
Figure 2.19. 2,2- bis [4-(2', 3'- epoxypropoxy) phenyl] propane [73] .....	27
Figure 2.20. Higher molecular weight homologues of epoxy based on diglycidyl ether of bisphenol A (DGEBA) [73-75].....	27
Figure 2.21. Main reactions involved in the cure of epoxy resins with amine curing agents [80].....	30
Figure 2.22. Reactions involved in the cure of epoxy resins with anhydride curing agents [76].....	31
Figure 2.23. Structure of polyamides [76].....	32
Figure 2.24. Reactions involved in the cure of epoxy resins with catalytic curing agents [73, 76].....	33
Figure 2.25. Proposed homopolymerization mechanism of DGEBA catalyzed by alkylammonium ions [81].....	34
Figure 2.26. Comparison of HRR plots for DGEBA/MDA and DGEBA/MDA nanocomposite with 6 wt% of silicate [15].....	44
Figure 3.1. Structure of epoxy EPON828.....	51
Figure 3.2. Structure of (a) DETA, (b) Jeffamine D series, (c) Jeffamine T series, and (d) boron trifluoride monoethylamine [77-79].....	53

Figure 3.3. Experimental procedure.....	58
Figure 3.4. Lightnin mixer (from CONCOM lab) .....	60
Figure 3.5. Photos of (a) EW-04719-00 high-speed homogenizer system; 115 VAC, 50/60 Hz, (b) large-capacity rotor-stator generators, (c) the rotor/stator principle of high speed stirring (from CONCOM lab). .....	62
Figure 3.6. M-110EH microfluidizer processor (from CONCOM lab).....	64
Figure 3.7. Principle of X-ray diffraction [4] .....	66
Figure 3.8. Teflon coated polypropylene mold for XRD samples.....	68
Figure 3.9. A Bruker Discover 8 powder X-ray diffractometer (from IMI lab) .....	69
Figure 3.10. Scheme and structure of SEM (Diagram courtesy of Iowa State University SEM homepage) [110] .....	70
Figure 3.11. The LEICA EMFCS microtome cutter (from IMI lab) .....	71
Figure 3.12. EMITECH K575X high resolution sputter coater (from IMI lab) .....	71
Figure 3.13. The Hitachi-S4700 FEGSEM (from IMI lab).....	72
Figure 3.14. The scattering of electrons from different regions of a TEM specimen [111]......	73
Figure 3.15. A Hitachi H9000 TEM (from McGill University lab).....	74
Figure 3.16. Nicolet Magna 860 FTIR instrument (from IMI lab).....	75
Figure 3.17. Brookfield CAP2000+ viscometer (from CONCOM lab).....	76
Figure 3.18. Brookefield viscometer Model DV-II+ (from CONCOM lab) .....	77
Figure 3.19. Perkin-Elmer instruments -DSC Pyris 1 (from IMI lab) .....	78
Figure 3.20. TA instruments –Q50 (from CONCOM lab).....	79
Figure 3.21. Qualitest LOI chamber (from CONCOM lab).....	81



Figure 3.22. Aluminum mold for casting sample .....	82
Figure 3.23. A schematic of DMA [114].....	84
Figure 3.24. Du Pont 983 DMA (from CONCOM lab).....	84
Figure 3.25. The schematic drawing of tensile test [115] .....	85
Figure 3.26. A Bruker dog-bone cutting machine for tensile specimens (from IMI lab) .....	86
Figure 3.27. The schematic drawing of flexural test [115] .....	87
Figure 3.28. The schematic drawing of compression test [115] .....	88
Figure 3.29. Silicone mold for compression samples.....	88
Figure 3.30. Instron 5500 test machine (from IMI lab) .....	89
Figure 3.31. The schematic drawing of impact test [115].....	90
Figure 3.32. A Tmi notch cutter for impact specimens (from IMI lab) .....	91
Figure 3.33. Impact instrument (from IMI lab) .....	91
Figure 3.34. MTS servo hydraulic testing machine (from CONCOM lab) .....	92
Figure 3.35. Silicone mold for fracture samples.....	93
Figure 3.36. Sample dimensions of three points bend (SENB) .....	93
Figure 3.37 Shore Conveloader instrument (from IMI lab) .....	95
Figure 4.1 Factors affecting dispersion, intercalation/exfoliation of nanoclay in epoxy.....	99
Figure 4.2 Factors affecting dispersion, intercalation/exfoliation of nanoclay in epoxy at stirring step.....	100
Figure 4.3. Factors affecting dispersion, intercalation/exfoliation of nanoclay in epoxy at curing step .....	100

Figure 4.4. Forces imposed on nanoclay (in epoxy) at stirring step, $h$ is the distance between clay platelets, $L$ is the length of clay platelets.....	101
Figure 4.5. Flowchart presenting the experimental steps for studying the mechanical and thermal effects on dispersion, intercalation/exfoliation of nanoclay in epoxy at stirring step: (a) Rm, Tm, TM, RS and TS methods, (b) HP method.....	105
Figure 4.6. Flowchart presenting the experimental steps for studying the effect of curing: (a) temperature and stirring conditions, (b) clay chemistry, and (c) hardener chemistry.....	108
Figure 4.7. (a) SEM micrograph and (b) clay size distribution of epoxy-Cloisite 30B, Rm method.....	109
Figure 4.8. (a) SEM micrograph and (b) clay size distribution of epoxy-Cloisite 30B, Tm method.....	110
Figure 4.9. (a) SEM micrograph and (b) clay size distribution of epoxy-Cloisite 30B, TM method.....	110
Figure 4.10. (a) SEM micrograph and (b) clay size distribution of epoxy-Cloisite 30B, RS method (24000 rpm).....	111
Figure 4.11. (a) SEM micrograph and (b) clay size distribution of epoxy-Cloisite 30B, TS method (120°C and 24000 rpm).....	111
Figure 4.12. Clay size distribution for different stirring methods.....	112
Figure 4.13. The effect of stirring temperature and speed on the size of clay aggregates.....	114

Figure 4.14. The effect of stirring speed and temperature on the size of clay aggregates. ....	116
Figure 4.15. X-ray diffraction curves of C30B and its EPON828-C30B mixtures after being stirred at different temperatures: (a) 0 rpm and (b) 24000 rpm .....	119
Figure 4.16. The effect of stirring temperature and speed on $d_{001}$ of EPON828-C30B mixtures .....	120
Figure 4.17. X-ray diffraction curves of C30B and its EPON828-C30B mixtures after being stirred at different speeds: (a) room temperature and (b) 120°C.....	121
Figure 4.18. The effect of stirring speed on $d_{001}$ of EPON828-C30B mixtures.....	122
Figure 4.19. X-ray diffraction curves of EPON828-C30B mixtures after being stirred using different methods .....	123
Figure 4.20. X-ray diffraction curves of EPON828-C30B mixtures after being stirred at 120°C for different durations with high speed (9500 rpm).....	125
Figure 4.21. X-ray diffraction curves of EPON828-C30B mixtures after being stirred at 120°C for different durations with high speed (17500 rpm).....	125
Figure 4.22. X-ray diffraction curves of EPON828-C30B mixtures after being stirred at 120°C for different durations with high speed (24000 rpm).....	126
Figure 4.23. The effect of stirring duration on $d_{001}$ of EPON828-C30B mixtures.....	127
Figure 4.24. X-ray diffraction curves of EPON828-C30B mixtures after being stirred at room temperature for different durations with high speed (24000 rpm). ....	128

Figure 4.25. X-ray diffraction curves of EPON828-C30B mixtures after being stirred at 180°C for different durations with high speed (24000 rpm).....	128
Figure 4.26. X-ray diffraction curves of EPON828-C30B, EPON828-I30E mixtures after being stirred with Rm and Tm methods .....	130
Figure 4.27. Viscosity-shear rate curves of EPON828-C30B mixtures after being stirred at different temperatures for two speeds: (a) 0 rpm and (b) 24000 rpm.....	131
Figure 4.28. The effect of stirring temperature on viscosity of EPON828-C30B after being stirred at 0 rpm and 24000 rpm for 60 minutes, at shear rate 167 (1/s).....	133
Figure 4.29. Viscosity-shear rate curves of EPON828-C30B mixtures after being stirred at different speeds for two temperatures: (a) RT and (b) 120°C.....	134
Figure 4.30. The effect of speed on viscosity of EPON828-C30B after being stirred at RT and 120°C for 60 minutes, at shear rate 167 (1/s).....	135
Figure 4.31. Viscosity-shear rate curves of EPON828-C30B mixtures after being stirred with different methods.....	136
Figure 4.32. Viscosity of EPON828 and its mixture with C30B after being stirred with different methods for 60 minutes, at shear rate 167 (1/s).....	136
Figure 4.33. Shear stress-shear rate curves of EPON828-C30B mixtures after being stirred with different methods.....	137

Figure 4.34. Viscosity-shear rate curves of EPON 828 and EPON828-C30B mixtures after being stirred by Rm method and RS method for different durations.....	139
Figure 4.35. Viscosity-shear rate curves of EPON 828 and EPON828-C30B mixtures after being stirred by Tm method and TS method for different durations.....	139
Figure 4.36. Viscosity of EPON828-C30B mixtures after being stirred by RS method and TS method for different durations, at shear rate 167 (1/s).....	140
Figure 4.37. Shear stress-shear rate curves of EPON 828 and EPON828-C30B mixtures after being stirred by Rm method and RS method for different durations.....	141
Figure 4.38. Shear stress-shear rate curves of EPON 828 and EPON828-C30B mixtures after being stirred by Tm method and TS method for different durations.....	141
Figure 4.39. Mechanism of dispersion at stirring step.....	143
Figure 4.40. X-ray diffraction curves of nanocomposites at 2 wt% C30B, samples cured at different temperatures.....	146
Figure 4.41. The effect of curing temperature on $d_{001}$ of ENC at 2 wt% C30B.....	146
Figure 4.42. X-ray diffraction curves of EPON828-D230 system, C30B and their nanocomposites at 2 wt% C30B made by different methods and cured at RT.....	148

Figure 4.43. X-ray diffraction curves of EPON828-D230 system, C30B and their nanocomposites at 2 wt% C30B made by different methods and cured at 120°C for 2 h .....	148
Figure 4.44. SEM micrographs of ENC based on EPON828 and D230 with 2 wt% C30B made by different stirring methods: (a) Rm, (b) Tm, (c) TM, (d) RS, (e) TS at 120°C and 24000 rpm, and (f) HP, samples cured at 120°C for 2 h .....	151
Figure 4.45. TEM photos of nanocomposite based on EPON828-D230 with 2 wt% C30B.....	152
Figure 4.46. X-ray diffraction curves of nanocomposites based on EPON828-D230 and 2 wt% C30B made by TS with 9500 rpm for different durations and cured at room temperature.....	153
Figure 4.47. X-ray diffraction curves of nanocomposites based on EPON828-D230 and 2 wt% C30B made by TS with 9500 rpm for different durations and cured at 120°C .....	154
Figure 4.48. The effect of curing temperature on $d_{001}$ of nanocomposites based on EPON828-D230 and 2 wt% C30B made by TS with 9500 rpm for different durations.....	155
Figure 4.49. X-ray diffraction curves of nanocomposites based on EPON828-D230 and 2 wt% C30B made by TS with 17500 rpm for different durations and cured at room temperature.....	155

Figure 4.50. X-ray diffraction curves of nanocomposites based on EPON828-D230 and 2 wt% C30B made by TS with 17500 rpm for different durations and cured at 120°C .....	156
Figure 4.51. The effect of curing temperature on $d_{001}$ of nanocomposites based on EPON828-D230 and 2 wt% C30B made by TS with 17500 rpm for different durations .....	157
Figure 4.52. X-ray diffraction curves of nanocomposites based on EPON828-D230 and 2 wt% C30B made by TS with 24000 rpm for different durations and cured at room temperature.....	158
Figure 4.53. X-ray diffraction curves of nanocomposites based on EPON828-D230 and 2 wt% C30B made by TS with 24000 rpm for different durations and cured at 120°C. ....	159
Figure 4.54. The effect of curing temperature on $d_{001}$ of nanocomposites based on EPON828-D230 and 2 wt% C30B made by TS with 24000 rpm for different durations .....	160
Figure 4.55. SEM photos of nanocomposite based on EPON828-D230 and 2 wt% C30B made by TS with 24000 rpm for (a) 2 minutes, (b) 4 minutes, (c) 10 minutes, (d) 20 minutes, (e) 30 minutes, (f) 45 minutes, and (g) 60 minutes .....	161
Figure 4.56. X-ray diffraction curves of nanocomposites based on EPON828-D230 and 2 wt% C30B made by RS with 24000 rpm for different durations and cured at room temperature.....	163

Figure 4.57. X-ray diffraction curves of nanocomposites based on EPON828-D230 and 2 wt% C30B made by RS with 24000 rpm for different durations and cured at 120°C .....	163
Figure 4.58. The effect of curing temperature on $d_{001}$ of nanocomposites based on EPON828-D230 and 2 wt% C30B made by RS with 24000 rpm for different durations.....	164
Figure 4.59. X-ray diffraction curves of nanocomposites based on EPON828-D230 and 2 wt% C30B made by TS (at 180°C) with 24000 rpm for different durations and cured at room temperature.....	165
Figure 4.60. X-ray diffraction curves of nanocomposites based on EPON828-D230 and 2 wt% C30B made by TS (at 180°C) with 24000 rpm for different durations and cured at 120°C .....	165
Figure 4.61. The effect of curing temperature on $d_{001}$ of nanocomposites based on EPON828-D230 and 2 wt% C30B made by TS (180°C) with 24000 rpm for different durations.....	166
Figure 4.62. Mechanism of dispersion and intercalation/exfoliation of clay particles in epoxy matrix at curing step: (a) big particles, (b) small particles and (c) detail.....	169
Figure 4.63. DSC curves of neat epoxy EPON828, EPON828-C30B and EPON828-I30E in the absence of hardener .....	173
Figure 4.64. FT-IR spectra of (a) uncured EPON828 resin, (b) EPON828-C30B and (c) EPON828-I30E after the first scan in DSC .....	175



Figure 4.65. X-ray diffraction curves of the 8EP and its Cloisite 30B nanocomposites.....	178
Figure 4.66. X-ray diffraction curves of the 8EP and its Nanomer I30E nanocomposites.....	178
Figure 4.67. SEM micrographs of (a) 8EP-2pB-Rm, (b) 8EP-2pB-Tm, (c) 8EP-4pB-Tm, (d) 8EP-2pE-Rm, (e) 8EP-2pE-Tm, (f) 8EP-2pB-Tm at high magnification .....	180
Figure 4.68. TEM micrographs of (a) 8EP-2pE-Rm and (b) 8EP-2pE-Tm.....	181
Figure 4.69. DSC curves of the epoxy with different curing agents at heating rate $2.5^{\circ}\text{C}\cdot\text{min}^{-1}$ .....	183
Figure 4.70. Transformation curves of the epoxy with different curing agents at heating rate $2.5^{\circ}\text{C}\cdot\text{min}^{-1}$ .....	183
Figure 4.71. X-ray curves of the EPON828 and its nanocomposites for samples after being cured at room temperature with (a) DETA, (b) D230, (c) T403, (d) D400 and (e) D2000 .....	188
Figure 4.72. X-ray curves of the EPON828 and its nanocomposites samples after being cured at $120^{\circ}\text{C}$ for 2 h with (a) DETA, (b) D230, (c) T403, (d) D400 and (e) D2000.....	189
Figure 4.73. Shear force imposed on nanoclay (in epoxy) at the stirring step; $h$ is the distance between clay platelets, $L$ is the length of clay platelets. ....	190
Figure 4.74. Schematic for coordinates (a) between a molecule and a block, (b) two blocks.....	193
Figure 4.75. Schematic for coordinates between two spherical particles .....	197

Figure 4.76. The mixer flow geometry.....	200
Figure 4.77. Tangential annular flow between rotating cylinders.....	201
Figure 4.78. Flow of epoxy-clay mixture between rotating cylinders .....	209
Figure 4.79. Flow of epoxy-clay mixture between rotating cylinders (Assumption: clay sheet parallel to rotor and stator).....	213
Figure 4.80. Dimensions of clay particles.....	214
Figure 4.81. Relationship between $\theta$ and time.....	214
Figure 4.82. Velocity $\Omega$ versus interlamellar spacing $h$ .....	218
Figure 4.83. Viscosity of epoxy and its mixtures with C30B at different temperatures.....	220
Figure 5.1. Factors affect curing process of epoxy nanocomposites .....	226
Figure 5.2. Flowchart presenting the experimental steps for studying the curing process of epoxy nanocomposite (a) the effect of clay chemistry and level of dispersion, (b) the effect of hardener chemistry .....	227
Figure 5.3. DSC curves obtained at different heating rates for the epoxy-amine system and its nanocomposites based on Cloisite 30B and Nanomer I30E .....	235
Figure 5.4. Transformation curves corresponding to different heating rates for 8EP and its nanocomposites based on Cloisite 30B and Nanomer I30E .....	237
Figure 5.5. Transformation curves corresponding to epoxy-amine and its nanocomposites at heating rate $2.5^{\circ}\text{C. min}^{-1}$ , (a) with Cloisite 30B, (b) with Nanomer I30E.....	238

Figure 5.6. Kissinger plots for the 8EP system and its nanocomposites .....	241
Figure 5.7. Isoconversional plots corresponding to various degrees of conversion for the 8EP system and its nanocomposites.....	244
Figure 5.8. Activation energies obtained for the isoconversional model .....	245
Figure 5.9. Determination of the Avrami exponent $n$ for the epoxy-amine system and its nanocomposites in the conversion range $\alpha = 0-10\%$ .....	248
Figure 5.10. DSC and transformation curves of the EPON828-DETA system (8DE) and its nanocomposite (8DE-4pB-Tm) at different heating rates, (a) DSC curves; (b) transformation curves .....	251
Figure 5.11. DSC and transformation curves of the EPON828-EPICURE 3046 system (8EP) and its nanocomposite (8EP-4pB-Tm) at different heating rates, (a) DSC curves; (b) transformation curves.....	251
Figure 5.12. DSC and transformation curves of the EPON828-D230 system (8d) and its nanocomposite (8d-4pB-Tm) at different heating rates, (a) DSC curves; (b) transformation curves.....	252
Figure 5.13. DSC and transformation curves of the EPON828-T403 (8T) system and its nanocomposite (8T-4pB-Tm) at different heating rates, (a) DSC curves; (b) transformation curves.....	252
Figure 5.14. DSC and transformation curves of the EPON828-D400 (8 $\delta$ ) system and its nanocomposite (8 $\delta$ -4pB-Tm) at different heating rates, (a) DSC curves; (b) transformation curves.....	253

Figure 5.15. DSC and transformation curves of the EPON828-D2000 (8D) system and its nanocomposite (8D-4pB-Tm) at different heating rates, (a) DSC curves; (b) transformation curves .....	253
Figure 5.16. Kissinger plots for the EPON828 systems and its nanocomposites with different hardeners: (a) DETA, (b) EPICURE 3046 (from section 5.4), (c) D230, (d) T403, (e) D400, and (f) D2000.....	257
Figure 5.17. Isoconversional plots at various conversions for (a) 8DE system and (b) 8DE-4pB-Tm system .....	260
Figure 5.18. Isoconversional plots at various conversions for (a) 8EP system and (b) 8EP-4pB-Tm system (results from section 5.4).....	260
Figure 5.19. Isoconversional plots at various conversions for (a) 8d system and (b) 8d-4pB-Tm system .....	261
Figure 5.20. Isoconversional plots at various conversions for (a) 8T system and (b) 8T-4pB-Tm system.....	261
Figure 5.21. Isoconversional plots at various conversions for (a) 8 $\delta$ system and (b) 8 $\delta$ -4pB-Tm system .....	262
Figure 5.22. Isoconversional plots at various conversions for (a) 8D system and (b) 8D-4pB-Tm system .....	262
Figure 5.23. Activation energies obtained for the isoconversional model for epoxy systems and nanocomposites with different hardeners, (a) DETA, (b) EPICURE 3046 (from section 5.4), (c) D230, (d) T403, (e) D400, and (f) D2000 .....	263

Figure 5.24. Determination of the Avrami exponent $n$ for the 8DE system and its nanocomposites in the conversion range $\alpha = 0-10\%$ .....	265
Figure 5.25. Determination of the Avrami exponent $n$ for the 8EP system and its nanocomposites in the conversion range $\alpha = 0-10\%$ .....	266
Figure 5.26. Determination of the Avrami exponent $n$ for the 8d system and its nanocomposites in the conversion range $\alpha = 0-10\%$ .....	266
Figure 5.27. Determination of the Avrami exponent $n$ for the 8T system and its nanocomposites in the conversion range $\alpha = 0-10\%$ .....	266
Figure 5.28. Determination of the Avrami exponent $n$ for the 8 $\delta$ system and its nanocomposites in the conversion range $\alpha = 0-10\%$ .....	267
Figure 5.29. Determination of the Avrami exponent $n$ for the 8D system and its nanocomposites in the conversion range $\alpha = 0-10\%$ .....	267
Figure 6.1. Factors affecting the performance of epoxy nanocomposites.....	274
Figure 6.2. Tensile properties for EPON828 resin and its nanocomposites made by different stirring methods (a) tensile modulus, (b) tensile strength (the maximum point on the stress-strain curve), (c) tensile strength at break (the last or break point on the stress-strain curve) .....	277
Figure 6.3. Tensile properties for EPON828 resin and its nanocomposites at different clay concentrations made by Tm and TS methods (a) tensile modulus, (b) tensile strength, (c) tensile strength at break .....	281
Figure 6.4. Compressive properties for EPON828-D230 resin and its nanocomposites made by different stirring methods (a) compressive	

modulus, (b) compressive strength at break, (c) compressive strain at break.....	284
Figure 6.5. Compressive properties for EPON828-D230 resin and its nanocomposites at different clay concentrations made by Tm and TS methods (a) compressive modulus, (b) compressive strength at break.....	285
Figure 6.6. (a) $K_{IC}$ and (b) $G_{IC}$ for EPON828-D230 resin and its nanocomposites made by different stirring methods .....	288
Figure 6.7. The effect of size of clay aggregates on (a) $K_{IC}$ and (b) $G_{IC}$ for EPON828-D230 resin and its nanocomposites with 2 wt% C30B.....	289
Figure 6.8. Fracture surface for epoxy; sample cured at 120°C for 2 h: (a) low magnification, (b) high magnification .....	290
Figure 6.9. Fracture surface for sample with room temperature stirring at low speed (2 wt% C30B); samples cured at 120°C for 2 h: (a) low magnification, (b) high magnification .....	292
Figure 6.10. Fracture surface for sample with high temperature stirring (120°C) at low speed (2 wt% C30B); samples cured at 120°C for 2 h: (a) low magnification, (b) high magnification .....	292
Figure 6.11. Fracture surface for sample with high temperature stirring (120°C) at 1000 rpm (2 wt% C30B); samples cured at 120°C for 2 h: (a) low magnification, (b) high magnification .....	293

Figure 6.12. Fracture surface for sample with room temperature stirring at high speed (2 wt% C30B); samples cured at 120°C for 2 h: (a) low magnification, (b) high magnification .....	293
Figure 6.13. Fracture surface for sample with high temperature stirring (120°C) at high speed (2 wt% C30B); samples cured at 120°C for 2 h: (a) low magnification, (b) high magnification .....	294
Figure 6.14. Fracture surface for sample with high pressure (2 wt% C30B); samples cured at 120°C for 2 h: (a) low magnification, (b) high magnification. ....	294
Figure 6.15. (a) $K_{IC}$ and (b) $G_{IC}$ for EPON828-D230 resin and its nanocomposites at different clay concentrations made by Tm, TS and HP methods .....	295
Figure 6.16. Dynamic mechanical analysis measurements: (a) storage modulus vs temperature, (b) loss modulus vs temperature for the EPON828-D230 system and its nanocomposites for different stirring methods.....	298
Figure 6.17. Dynamic mechanical analysis measurements: (a) storage modulus vs temperature, (b) loss modulus vs temperature for the EPON828-D230 system and its nanocomposites at different clay concentrations for methods Tm and TS .....	300
Figure 6.18. TGA results for EPON828 resin and its nanocomposites made by different stirring methods.....	302
Figure 6.19. TGA results for EPON828 resin and its nanocomposites made by Tm and TS stirring methods at different clay loading. ....	303

Figure 6.20. LOI for EPON828-D230 system and its nanocomposites made by different stirring methods.....	305
Figure 6.21. LOI of 8d system and its nanocomposites at different clay loading made by Tm and TS methods .....	306
Figure 6.22. Water absorption profiles for EPON828-D230 system and its nanocomposites made by different stirring methods .....	309
Figure 6.23. Summary of water absorption for EPON828-D230 system and its nanocomposites made by different stirring methods .....	310
Figure 6.24. Nanoclay improves barrier properties [157].....	311
Figure 6.25. Ethanol absorption for the EPON828-D230 system and its nanocomposites made by different stirring methods .....	312
Figure 6.26. Toluene absorption of the EPON828-D230 system and its nanocomposites made by different stirring methods .....	313
Figure 6.27. Tensile properties for 8EP and its nanocomposites: (a) tensile modulus and (b) tensile strength.....	315
Figure 6.28. Flexural properties for 8EP and its nanocomposites: (a) flexural modulus and (b) flexural strength.....	315
Figure 6.29. LOI for 8EP system and its nanocomposites with two different types of clay made by different stirring methods.....	318
Figure 6.30. LOI of 8EP system and its nanocomposites at different clay loading made by Tm and TS methods .....	318



Figure 6.31. Tensile properties for epoxy and its nanocomposites cured with D2000, T403, and DETA: (a) tensile modulus, (b) tensile strength, and (c) strain at break.....	322
Figure 6.32. LOI of epoxy systems and their nanocomposites cured different hardeners.....	324
Figure 6.33. (a) $K_{IC}$ and (b) $G_{IC}$ for EPON828-D2000 resin its nanocomposites made by TS method .....	326
Figure 6.34. (a) $K_{IC}$ and (b) $G_{IC}$ for EPON828-BF <sub>3</sub> resin its nanocomposites made by TS method .....	326
Figure 6.35. (a) $K_{IC}$ and (b) $G_{IC}$ for EPON828-D230 resin its nanocomposites made by TS method (results from Figure 6.15).....	327
Figure 6.36. XRD results for EPON828-D2000, EPON828-D230, EPON828-BF <sub>3</sub> systems and their nanocomposites with 6wt% C30B made by TS method.....	327
Figure 7.1. An example for the structure of rubbery and glassy epoxy systems.....	333
Figure 7.2. Flowchart of sample preparation. ....	336
Figure 7.3. X-ray diffraction curves of epoxy-nanocomposites based on 6 wt% C30B and cured with different ratios of D230/D2000.....	338
Figure 7.4. X-ray diffraction curves of epoxy-nanocomposites based on 6wt% I30E and cured with different ratios of D230/D2000 .....	339
Figure 7.5. FEGSEM micrographs of 6 wt% C30B nanocomposites cured with (a) d0D100 (D2000), (b) d25D75, (c) d35D65, (d) d60D40, and (e) d100D0 (D230).....	340

Figure 7.6. FEGSEM micrographs of 6 wt% I30E nanocomposites cured with (a) d0D100 (D2000), (b) d25D75, (c) d35D65, (d) d60D40, and (e) d100D0 (D230).....	341
Figure 7.7. TEM micrographs of 6 wt% C30B nanocomposites cured with (a, b) D2000 and (c, d) D230.....	343
Figure 7.8. $T_g$ of epoxy systems and their 6 wt% C30B and 6 wt% I30E nanocomposites versus the amount of D230 .....	345
Figure 7.9. $T_g$ for epoxy systems and their nanocomposites cured with D2000 and D230.....	345
Figure 7.10. TGA results of C30B, I30E and their nanocomposites cured with D2000 and D230.....	347
Figure 7.11. Surface hardness of epoxy systems and their 6 wt% C30B, 6 wt% I30E nanocomposites versus percentage of D230. ....	349
Figure 7.12. Typical stress-strain curves for epoxy and its 6 wt% C30B, 6 wt% I30E nanocomposites cured with (a) d0D100 (D2000), (b) d25D75, (c) d35D65, (d) d60D40, and (e) d100D0 (D230).....	350
Figure 7.13. Comparison of typical stress-strain curves for epoxy systems and their 6 wt%C30B, 6 wt% I30E nanocomposites in the same scale. ....	351
Figure 7.14. Tensile modulus of epoxy systems and their nanocomposites versus (a) percentage of D230, and (b) $T_g$ .....	352
Figure 7.15. Tensile modulus of epoxy systems and their nanocomposites cured with different hardeners (a) d0D100 (D2000), (b) d25D75, (c) d35D65, (d) d60D40, and (e) d100D0 (D230) .....	353

Figure 7.16. Tensile strength and tensile strength at break of epoxy systems and their nanocomposites versus percentage of D230 (a) tensile strength (the maximum point on the stress-strain curve), and (b) tensile strength at break (the last or break point on the stress-strain curve) .....	355
Figure 7.17. Tensile strain at break and energy to break (the area under the stress-strain curve) of epoxy systems and their nanocomposites versus percentage of D230 (a) tensile strain at break, and (b) energy to break.....	356
Figure 7.18. Flexural modulus of epoxy systems and their nanocomposites cured with different hardeners (a) modulus versus %D230, and (b) modulus versus $T_g$ .....	357
Figure 7.19. Flexural strength of epoxy systems and their nanocomposites versus $T_g$ .....	357
Figure 7.20. Impact energy of epoxy systems and their nanocomposites versus percentage of D230 .....	358
Figure 7.21. Summary of the reinforcing effect of nanoclay on mechanical properties of epoxy (a) Cloisite 30B, and (b) Nanomer I30E.....	359
Figure 7.22. Fracture surfaces for epoxy cured with different D230-D2000 mixtures, (a) d0D100, (b) d25D75, (c) d35D65, (e) d60D40, and (e) d100D0.....	361
Figure 7.23. Fracture surfaces for 6 wt% C30B epoxy nanocomposites cured with different D230-D2000 mixtures, (a) d0D100, (b) d25D75, (c) d35D65, (e) d60D40, and (e) d100D0 .....	363

Figure 7.24. Fracture surfaces for 6 wt% I30E epoxy nanocomposites cured with different D230-D2000 mixtures, (a) d0D100, (b) d25D75, (c) d35D65, (e) d60D40, and (e) d100D0 .....	364
Figure 7.25. Illustration of the ‘particle’ and ‘matrix’ domains in conventional composite .....	366
Figure 7.26. Results of the Halpin-Tsai model (H-T): dependence of $E/E_m$ on (a), (b) $f_p$ ; (c), (d) $L/t$ and (e), and (f) $E_p/E_m$ .....	368
Figure 7.27. Results of the Mori-Tanaka model (M-T): dependence of $E/E_m$ on (a), (b) $f_p$ ; (c), (d) $L/t$ and (e), and (f) $E_p/E_m$ .....	369
Figure 7.28. Illustration of the ‘effective particle’ and ‘matrix’ domains in nanocomposite .....	370
Figure 7.29. Multi-layer structure of intercalated nanoclay (effective particle) .....	371
Figure 7.30. Relation between volume fraction of clay platelets ( $\chi$ ) and $d_{001}$ at different $N$ .....	372
Figure 7.31. Relation between $f_p/W_s$ and $d_{001}$ at different $N$ with $\rho_m$ of (a) 1.0 g/cm <sup>3</sup> , (b) 1.06 g/cm <sup>3</sup> (D2000), and (c) 1.16 g/cm <sup>3</sup> (D230).....	375
Figure 7.32. Effect of clay structural parameters ( $N$ , $d_{001}$ ), weight fraction of clay and ratio of $E_s/E_m$ on the macroscopic modulus, predicted by the Halpin-Tsai model (a) $d_{001}= 5$ nm, $\rho_m= 1$ g/cm <sup>3</sup> , $E_s/E_m= 100$ , (b) $d_{001}= 5$ nm, $\rho_m= 1$ g/cm <sup>3</sup> , $E_s/E_m= 1000$ , and (c) $N= 5$ nm, $\rho_m= 1$ g/cm <sup>3</sup> , $E_s/E_m= 100$ .....	376
Figure 7.33. Effect of clay structural parameters ( $N$ , $d_{001}$ ), weight fraction of clay and ratio of $E_s/E_m$ on the macroscopic modulus, predicted by the	

Mori-Tanaka model (a)  $d_{001} = 5 \text{ nm}$ ,  $\rho_m = 1 \text{ g/cm}^3$ ,  $E_s/E_m = 100$ , (b)  $d_{001} = 5 \text{ nm}$ ,  $\rho_m = 1 \text{ g/cm}^3$ ,  $E_s/E_m = 1000$ , and (c)  $N = 5 \text{ nm}$ ,  $\rho_m = 1 \text{ g/cm}^3$ ,  $E_s/E_m = 100$ . ..... 377

Figure 7.34. Effect of weight fraction  $W_s$  and  $N$  on the macroscopic modulus of D2000 and D230 nanocomposite systems, predicted by (a, b) the Halpin-Tsai model, (c, d) the Mori-Tanaka model, and (e, f) the rule of mixture ROM. .... 379

Figure 7.35. Effect of  $N$  on the macroscopic modulus of D230 and D2000 nanocomposite systems, predicted by (a, b) the Halpin-Tsai and (c, d) the Mori-Tanaka models compared to experiment results. .... 380

Figure 7.36. Intercalation/exfoliation of clay during the stirring and curing of epoxy nanocomposites ..... 383

## LIST OF TABLES

Table 2.1.	Mechanical properties of nylon 6 nanocomposites [27].....	8
Table 2.2.	Chemical structure of commonly used 2:1 phyllosilicates [36].....	11
Table 2.3.	The structures of some epoxy resins [73-79].....	28
Table 3.1.	Typical properties of EPON828 [77].....	51
Table 3.2.	Characteristic of curing agents [77-79].....	53
Table 3.3.	Technical details of organoclays [27, 49].....	55
Table 3.4.	Study parameters.....	56
Table 3.5.	Mixing methods .....	59
Table 4.1.	Parameters examined for stirring step.....	104
Table 4.2.	Parameters examined for curing step.....	107
Table 4.3.	The average diameter and maximum size of clay particles in epoxy .....	111
Table 4.4.	Summary of XRD results EPON828-C30B mixtures after being stirred using different methods .....	123
Table 4.5.	Summary of XRD results of EPON828-C30B mixtures after being stirred at 120°C for different durations with high speed (9500, 17500 and 24000 rpm).....	126
Table 4.6.	Summary of XRD results of EPON828-C30B mixtures after being stirred at room temperature (RT) and 180°C with high speed (24000 rpm).....	129
Table 4.7.	Variables and experimental conditions for experiment set 4.4.1.....	144

Table 4.8.	Summary of XRD results of C30B and their nanocomposites made by different methods .....	149
Table 4.9.	Summary of XRD results of nanocomposites based on EPON828-D230 and 2 wt% C30B made by TS with 9500 rpm for different durations.....	154
Table 4.10.	Summary of XRD results of nanocomposites based on EPON828-D230 and 2 wt% C30B made by TS with 17500 rpm for different durations.....	156
Table 4.11.	Summary of XRD results of nanocomposites based on EPON828-D230 and 2 wt% C30B made by TS with 24000 rpm for different durations.....	159
Table 4.12.	Summary of XRD results of nanocomposites based on EPON828-D230 and 2 wt% C30B made by RS with 24000 rpm for different durations.....	164
Table 4.13.	X-ray diffraction curves of nanocomposites based on EPON828-D230 and 2 wt% C30B made by TS (at 180°C) with 24000rpm for different durations.....	166
Table 4.14.	Summary of XRD data of samples after being cured at 120°C .....	168
Table 4.15.	Sample specifications for experiment set 4.4.2. ....	171
Table 4.16.	Summary of XRD data.....	177
Table 4.17.	Sample specifications for experiment set 4.4.3. ....	182
Table 4.18.	Summary of XRD data for nanocomposites .....	187
Table 5.1.	Sample specifications for experiment set 5.4 .....	233

Table 5.2.	Curing characteristics for 8EP .....	239
Table 5.3.	Characteristics for 8EP nanocomposites.....	239
Table 5.4.	Activation energies obtained from the Kissinger analysis for E828- EP and its nanocomposites.....	242
Table 5.5.	Average activation energies obtained for the isoconversional model. ....	246
Table 5.6.	Exponents $n$ obtained from Avrami analysis.....	249
Table 5.7.	Sample specifications for experiment set 5.5 .....	249
Table 5.8.	Characteristics for epoxy systems and their nanocomposites with different hardeners .....	255
Table 5.9.	Activation energy for EPON828 and its nanocomposites with different hardeners from Kissinger analysis .....	258
Table 5.10.	Average activation energies obtained for the isoconversional model. ....	264
Table 5.11.	Exponents $n$ obtained from Avrami analysis.....	267
Table 5.12.	The generalization of the effects of chemistry of clay and hardeners and the level of dispersion of clay on curing rate, $E_a$ and exponent $n$ of epoxy nanocomposites compared to epoxy systems .....	271
Table 6.1.	Study parameters for Chapter 6 .....	275
Table 6.2.	Sample specifications for experiment set 6.3 .....	276
Table 6.3.	Dynamic mechanical analysis for pristine EPON828-D230 epoxy and its nanocomposites .....	301
Table 6.4.	Water uptake parameters for EPON828-D230 system and its nanocomposites made by different stirring methods .....	310



Table 6.5.	Solvent resistance for the EPON828-D230 system and its nanocomposites made by different stirring methods after 1970 hrs .....	313
Table 6.6.	Sample specifications for experiment set 6.4 .....	314
Table 6.7.	Sample specifications for experiment set 6.5 .....	319
Table 6.8.	Slope of tensile properties curves versus clay loading .....	322
Table 7.1.	Sample specifications for Chapter 7 .....	335
Table 7.2.	Summary of TGA results for D2000, D230 epoxy systems and their nanocomposites.....	348
Table 7.3.	Components property data used for composite modulus.....	378

## LIST OF SYMBOLS, NOMENCLATURES AND ABBREVIATIONS

3DCM	3, 3'-dimethyl-methylenedi (cyclohexylamine)
AFM	Atomic force microscopy
BAM	Bis-(4-aminocyclohexyl) methane
BF3	Boron Trifluoride monoethylamine
C30B	Cloisite <sup>®</sup> 30B
CEC	Cation exchange capacity
D2000	Jeffamine D2000
D230	Jeffamine D230
D400	Jeffamine D400
DETA	Diethylene Triamine
DGEBA	Diglycidylether of bisphenol A
DMA	Dynamic mechanical analysis
DSC	Different scanning calorimetry
DSC	Differential scanning calorimetry

ECNs	Epoxy-clay nanocomposites
EEW	Epoxy equivalent weight
FEGSEM	Field emission gun scanning electron microscopy
FTIR	Fourier transform infrared spectroscopy
HDPE	High density polyethylene
HP	High-pressure (microfluidizer)
HRR	The total heat release rate
I30E	Nanomer <sup>®</sup> I.30E
LOI	Limiting oxygen index
MMT	Montmorillonite
MT2EtOH	Methyl, tallow, Bis-2-hydroxyethyl, quaternary ammonium
ODA	Octadecyl ammonium
OTR	Oxygen transmission rates
PNC	Polymer nanocomposites
Rm	Room temperature with hand stirring

ROM	Rule of mixture relation
RS	Room temperature and high speed stirring (homogenizer)
RT	Room temperature
SEM	Scanning electron microscopy
T	Tallow
T403	Jeffamine T403
TEM	Transmission electron microscopy
TETA	Triethylene Tetramine
TGA	Thermogravimetric analysis
TGAP	Triglycidyl p-amino phenol
TGDDM	N, N, N', N'-tetraglycidyl-4, 4'-diaminodiphenylmethane
TM	High temperature and medium speed stirring (mechanical stirrer)
Tm	High temperature with hand stirring
TS	High temperature and high speed stirring (homogenizer)
XRD	X-ray diffraction

$\underline{I}$	Identity tensor
$\Delta H\Sigma$	Total heat of the curing reaction
$\Delta Ht$ heating scan	Cumulative exothermic heat evolved at time t during the DSC heating scan
$A$ (Chapter 5)	Pre-exponential factor
$A$	Surface area of clay
$A_p$	Aspect ratio of the particles ( $A_p$ is defined as length divided by thickness of the particles $L/t$ )
$C$	Chemical interactivity between organoclay and epoxy
$d$	Disk-like particle of diameter
$D$	Represents thermodynamic forces
$d_{001}$	Basal spacing
$D_r$	Rotary diffusivity

$d_s$	Silicate sheet thickness
$E$ (Chapter 5)	Activation energy
$E_A$	Attraction energy holding 2 clay sheets together
$E_m$	Young's modulus of matrix
$E_p$	Young's modulus of the particles
$\underline{F}$	Force vector acting on the surface of the clay particle
$f$	Ratio between the attractive area and total area
$F_c$	Force holding clay sheets together
$F_{critical}$	Force that holds the clay together
$F_{DT}$	Total force acting on the clay platelets
$f_p$	Volume fraction of particles in the composite
$G_{IC}$	Critical strain energy release rate
$H_{11}$	Hamaker constant
$h_p$	Planck's constant

$k$ (Chapter 5)	Reaction rate constant
$K_{IC}$	Critical stress intensity factor
$k_B$	Boltzmann's constant
$L$	Length of clay particle
$M$	Molecular weight
$N$	Number of clay layers per stack
$n$ (Chapter 5)	Reaction order
$N_{AV}$	Avogadro number
$P$	Thermodynamic pressure
$p$	Aspect ratio
$Pe$	Rotational Peclet number
$R$ (Chapter 5)	Gas constant
$R_{12}$	Intermolecular distance
$t$ (Chapter 7)	Thickness of the clay particle
$t$	Duration time
$T$	Temperature

$T_g$	Glass transition temperature
$V_p$	Volume assigned to the ‘effective particles’
$V_s$	Volume assigned to the silicate sheets (platelets) in a stack
$W_s$	Weight fraction (ash weight)
$\underline{\underline{\Pi}}$	Total stress tensor
$\underline{\underline{\dot{\gamma}}}$	Rate of strain tensor
$\tau$	Shear stress
$\mu$	Viscosity
$\alpha$ (Chapter 4)	Polarizability
$\alpha$ (Chapter 5)	Degree of cure
$\Omega$	Angular velocity
$\theta$	Bragg diffraction angle (X-ray injection angle)
$\rho$	Density
$\varepsilon$	Relative dielectric permittivity, or the dielectric constant



$\nu$	Stirring speed
$\delta$	Thickness of the clay plate
$\lambda$	Wave length of X-ray
$\theta_0$	Angle at time $t = 0$
$\epsilon_0$	Electric permittivity of vacuum
$\nu_m$	Matrix Poisson ratio
$\zeta$	Positive coefficient depending on the matrix Poisson ratio, $\nu_m$
$\chi$	Volume fraction of clay platelets
$\mu_s$	Viscosity of the suspending fluid

# Chapter 1

## Introduction

Nanotechnology is recognised as one of the most promising avenues of technology development for the 21<sup>st</sup> century. Nowadays, many efforts in material science are focusing to the molecular scale and nanoscale. In the materials area, the development of ceramic and polymer nanocomposites is a rapidly expanding multidisciplinary research activity.

Nanocomposites are a new class of composites. The term “nanocomposite” describes a composite in which the reinforcement has at least one dimension in the range of nanometer ( $10^{-9}$ m) (so called nano-reinforcement or nano-particle). This term is commonly used in two distinct areas of material science: polymers and ceramics. However, this thesis will only consider nanocomposites based on polymers, and in particular thermoset epoxies.

Depending on how many dimensions of the nano-particles are in the nanometer range, three types of nanocomposites can be distinguished. The first type is isodimensional nanoparticles, in which the three dimensions of particles are quite similar and are in the order of nanometers, such as spherical silica nanoparticles [1-4], and semiconductor nanoclusters [5]. When two dimensions are quite similar and in the nanometer scale and the third one is greater, forming an elongated structure, one speaks about nanotubes or

nanofibres, for example, carbon nanotubes or carbon nanofiber [6, 7, 8]. The third type of nano-particles is characterized by only one dimension in the nanometer range. In this case the filler is present in the form of sheets (or lamellar) of one to a few nanometers thick and hundreds to thousands nanometers long such as nano-layered silicates (or nanoclays). This family of nanocomposites can be grouped under the name of polymer-layered silicate nanocomposites, and their study will constitute the main object of this thesis.

## **1.1 Thesis motivation**

Polymer-layered silicate nanocomposites are becoming a very promising new class of materials. The intercalation or exfoliation forms (only event partial exfoliation) of nanolayer silicates in many polymer systems have improved effectively stiffness, strength, fracture toughness, fire resistance, barrier properties, dimensional stability, etc. [9- 14]. The reinforcing ability of nanoclay is due to its high modulus, high strength and high aspect ratio. The greater is the exfoliation of the nanoclays in the polymer matrix, the greater is the reinforcing effect [10]. Good exfoliation of clay in epoxy has also been reported but only by the preparation with solvent.

Mechanical properties of epoxy nanocomposites depend on the quality of clay dispersion and interfacial adhesion between epoxy resin and dispersed clay [15]. Platelet aspect ratios, chemistry and layer charge densities of nanoclay are important parameters that control the dispersion and interfacial adhesion in epoxy nanocomposite [12, 13]. Reinforcing effect of clay in epoxy clay nanocomposites is also dependent on clay loading [10, 12] and clay exfoliation [12].

Processing parameters have an important influence on the dispersion of clay in polymers. Dispersion process parameters mainly include stirring temperature, time, speed, power of ultrason, shearing forces etc. Direct stirring of organoclay and epoxy with mechanical stirring and sonication is widely used to disperse nanoclay in epoxy [9, 11, 16-18]. Although this approach is simple and practical but good dispersion of clay cannot be well achieved in epoxy nanocomposites. Yasmin A. et al. [19] used a three-roll mill to disperse the clay nanoparticles in an epoxy matrix in order to improve the distribution of nanoclay particles in epoxy matrix but not exfoliation. Chen C. and Tolle T. B. [20] achieved a certain exfoliated layer silicate epoxies by high-shear mixing in the presence of a high amount of acetone. Recently, Liu W. P. et al. [21-23] used a “high pressure method” with assistance of acetone solvent to improve the dispersion of clay in epoxy and obtained strong improvement in fracture toughness of epoxy nanocomposites. However, a lot of solvent was used and significant time was required for removing the solvent. There is still work to be done to develop a more economic, practical, and friendly environmental process for fabrication of epoxy nanocomposites with fine dispersions and exfoliated structure. Achieving such exfoliated structure with epoxy-based nanocomposites is a challenge, since high shear is always required to shear the layers apart but common epoxy resins used for most industrial applications has low viscosity, which limit the generation of high shear by conventional devices. Moreover, the mechanism for dispersion of clay in epoxy matrix is still not quite clear. Therefore, the study and exploration of the mechanism of dispersion as well as intercalation and exfoliation of clay in epoxy matrix by using **solvent-free methods** is the motivation of this thesis.

## 1.2 Content of the thesis

In this thesis, different parameters that can affect dispersion and intercalation/exfoliation of organoclay in epoxy matrix were studied. A high-speed with high-temperature-assist method was proposed to disperse organoclay into epoxy matrix in the absence of solvent. The effect of chemistry of clay intercalants, chemistry of hardener and epoxy formulations on processing, curing kinetics, morphology and properties of epoxy nanocomposites were investigated.

**A brief introduction to this Thesis** was presented in Chapter 1. The motivation and the content of the thesis were described.

**A general review of polymer nanocomposites and particularly epoxy nanocomposites** is given in Chapter 2. First of all, materials including natural clay and organoclay were introduced; following by the preparation methods and the properties of nanocomposites. Then the state-of-the art of the development of epoxy nanocomposites was briefly introduced. Finally, the challenges in fabrication of epoxy-clay nanocomposites were pointed out and the objectives of the thesis were also described at the end of this chapter.

**Information on materials used and experimental details** for this thesis were provided in Chapter 3. Materials including epoxy Shell EPON828, several curing agents (DETA, EPICURE 3046, Jeffamine D230, Jeffamine D400, Jeffamine D2000, Jeffamine T403, boron trifluoride monoethylamine -  $\text{BF}_3$ ) and organoclays (Nanomer I30E and Cloisite

30B) were introduced. Different study parameters as well as experiment set ups and equipments to carry out the experiments were also presented in this chapter.

**Results of the dispersion and intercalation/exfoliation of clay in epoxy nanocomposites at different steps during the fabrication process were studied in Chapter 4.** The effects of various parameters of the stirring and curing steps on clay dispersion and intercalation/exfoliation were discussed. For the stirring step, several techniques used to disperse organoclay in epoxy include different devices, speeds, temperatures and durations. For the curing step, effects of curing temperature, chemistry of clay and hardeners were focused. The morphology of epoxy nanocomposites was characterized by scanning electron microscopy (SEM), transmission electron microscopy (TEM) and wide angle X-ray diffraction (WAXRD). The distribution of agglomerates of clay in the nanocomposites was studied using Image Pro Analysis Software. A formation mechanism of dispersion model of the nanocomposites was proposed. An attempt to establish a model for flow in a concentric cylinder high speed stirrer in order to predict the necessary processing conditions for achieving delamination of the clay layers was also described.

**What will happen to the processing of epoxy resins at the curing step in the presence of nanoclay?** The effects of chemistry of clay as well as clay dispersion and chemistry of hardeners on the curing process of epoxy nanocomposites were presented in Chapter 5. Two types of organoclay were used in this study, both based on natural montmorillonite but differing in intercalant chemistry. Different types of hardener were also chosen. The two stirring processes used to prepare the nanocomposites to obtain different levels of

dispersion of clay in epoxy were a room-temperature process and a high-temperature process. The cure kinetics was studied by DSC and was analyzed by means of different models. The activation energy and the Avrami exponent were calculated.

**The effects of clay on mechanical, thermal, and physico-chemical properties of epoxy nanocomposites are discussed in Chapter 6.** In this chapter, the effect of clay dispersion and clay chemistry on the mechanical properties, thermal mechanical properties, thermal and flammability properties, and barrier properties of epoxy nanocomposites were investigated. These effects were also examined for different epoxy systems, which were prepared from different hardeners such as DETA, EPICURE 3046, Jeffamine D230, Jeffamine T403, Jeffamine D2000, and boron trifluoride monoethylamine -  $\text{BF}_3$ .

**Chapter 7 attempts to contribute to some extent to the comprehension of the mechanism that governs the reinforcing effect of organoclay in thermoset epoxy resins,** whose characteristics can vary over a broad range from rubbery to highly glassy. These epoxy matrices were carefully chosen to minimize the difference in chemistry between them. Different mechanism scenarios have been proposed. The prediction of the tensile modulus using Halpin-Tsai and Mori-Tanaka models was also attempted.

**Finally, in Chapter 8, summary and conclusions were drawn based on preparations, characterizations and properties of epoxy nanocomposites.** Contributions and list of publications were also provided. Then recommendations for future research works were proposed. A list of reference was provided at the end.

# Chapter 2

## Background and thesis objectives

The use of organoclays as precursors to nanocomposite formation has been extended into various polymer systems including epoxies, polyurethanes, polyimides, nitrile rubber, polyesters, polypropylene, polystyrene and polysiloxanes, among others. The significant improvement of mechanical properties can be attributed to the special structure and chemistry of the organo-nanoclays. Therefore, in this literature survey, a brief introduction of nanoclays is presented.

Many researchers have applied different methods to obtain nanocomposites including applying various methods to modify the surface of nanoclay, modifying the matrix, using coupling agents to improve the interface, employing different equipment and processing methods to disperse nanoclay into matrix, and so on. A review of these aspects is also included in this chapter.

### 2.1. Development of polymer nanocomposites (PNC)

Polymer-clay interactions have been actively studied during the sixties and the early seventies [24]. Although first reported by Blumstein in 1961 [25], the real exploitation of this technology started in the 1990s. It is only relatively recently that researchers from Toyota [26] discovered the possibility to build a nanostructure from polymer and



organophilic clay. The first company to commercialize these nanocomposites was also Toyota. Researchers from Nanocor reported that the material based on polyamide 6 and organophilic montmorillonite showed dramatic improvements in mechanical properties (Table 2.1), barrier properties (Figure 2.1) and thermal resistance as compared with the pristine matrix and this at low clay content [27].

**Table 2.1. Mechanical properties of nylon 6 nanocomposites [27]**

Nanoclay (Nanomer I24TL) (wt. %)	Flexural modulus (MPa)	Tensile modulus (MPa)	HDT(°C)
0%	2836	2961	56
2%	4326 (+53%)	4403 (+49%)	125 (+123%)
4%	4578 (+61%)	4897 (+65%)	131 (+134%)
6%	5388 (+90%)	5875 (+98%)	136 (+143%)
8%	6127 (+116%)	6370 (+115%)	154 (+175%)

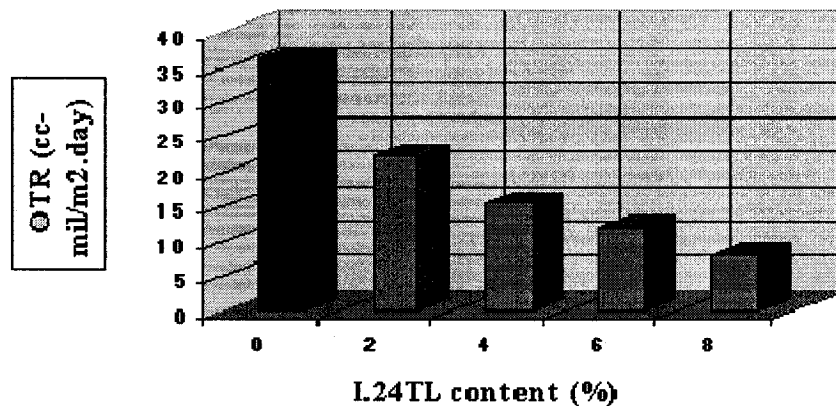


**Figure 2.1. Oxygen transmission rates (OTR) of nylon 6 nanocomposite [27]**

In general, the improvement in properties may be attributed to the following factors: large surface area and aspect ratio, sub-microscopic dispersion of the clay in the polymer

matrix and ionic bonds between the organic polymer and inorganic clay. Following Toyota's lead, a number of other companies also began investigating nanocomposites.

## **2.2. Nano-layered silicates**

Nano-layered silicates, lamellar nano-particles are the most interesting for the production of nanocomposites. The generic term “nano-layered silicates” refers to the natural clays and semi- or fully synthesized clays [28, 29, 30]. Both natural and synthetic clays have been used in the synthesis of polymer nanocomposites.

### **2.2.1. Montmorillonite**

Natural clays have been formed by the weathering of eruptive rock material, usually tuffs and volcanic ash (so called bentonite) [31]. The most popular bentonites are montmorillonite (MMT), hectorite, and saponite. MMT was discovered in 1847 in France by Damour and Salvétat [32], is nowadays the most widely used clay as nanofiller. MMT is known as the most common clay mineral with numerous world-wide localities. In its pristine form, MMT contains in addition varying amounts of crystobalite, zeolites, biotite, quartz, feldspar, zircon and other minerals found in volcanic rocks. MMT, hectorite, and saponite belong to the family of 2:1 phyllosilicates [33-37]. The structure of 2:1 phyllosilicates is given in Figure 2.2. Their chemical formulae are shown in Table 2.2. Their crystal lattice consists of two-dimensional layers where a central octahedral sheet of alumina or magnesia is fused to two external silica tetrahedrons by the tip so that the oxygen ions of the octahedral sheet also belong to the tetrahedral sheets. The layer thickness is around 1 nm and the lateral dimensions of these layers may vary from 300 Å

to several microns and even larger depending on the particular silicate. These layers organize themselves to form stacks with a regular Van der Waals gap in between them called the interlayer or the gallery. Isomorphic substitution within the layers (for example,  $\text{Al}^{3+}$  replaced by  $\text{Mg}^{2+}$  or  $\text{Fe}^{2+}$  as in MMT, or  $\text{Mg}^{2+}$  replaced by  $\text{Li}^{1+}$  as in hectorite) generates negative charges that are counterbalanced by alkali and alkaline earth cations situated on the layer surface. This type of layered silicate is characterized by a moderate surface charge known as the cation exchange capacity (CEC), and generally expressed as milliequivalents per gram (meq/g) or more frequently per 100 g (meq/100 g). This charge is not locally constant, but varies from layer to layer, and must be considered as an average value over the whole crystal. The MMT suitable for preparing nanocomposites should have a CEC of 70 to 150 meq (milliequivalents) /100 g of MMT [38].

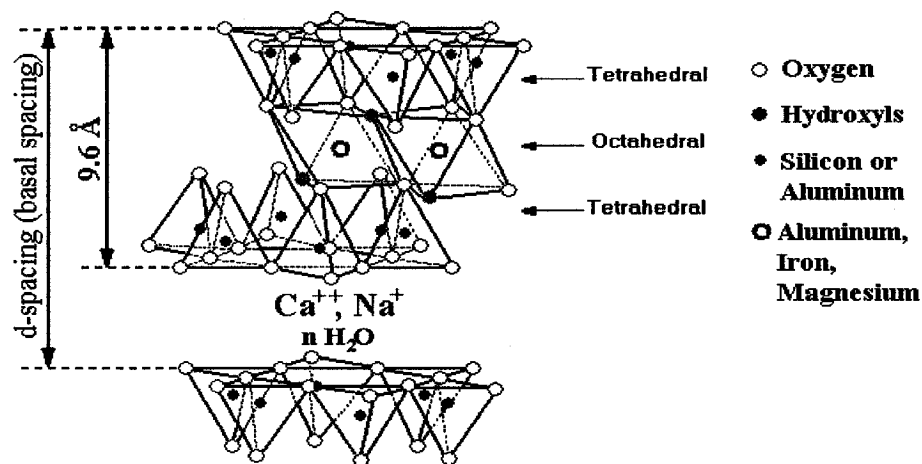


Figure 2.2. Structure of 2:1 phyllosilicates [4, 34]

**Table 2.2. Chemical structure of commonly used 2:1 phyllosilicates [36]**

<b>2:1 Phyllosilicates</b>	<b>Chemical formula*</b>	<b>CEC (meq/100g)</b>
Montmorillonite	$M_x(Al_{4-x}Mg_x)Si_8O_{20}(OH)_4$	110
Hectorite	$M_x(Mg_{6-x}Li_x)Si_8O_{20}(OH)_4$	120
Saponite	$M_xMg_6(Si_{8-x}Al_x)O_{20}(OH)_4$	86.6
<i>*M = monovalent cation; x = degree of isomorphous substitution (between 0.5 and 1.3).</i>		

### 2.2.2. Organoclay

The term organoclay refers to organically modified clay and will be discussed shortly. Although their high aspect ratio is ideal for reinforcement, the nano-layers are not easily dispersed in most polymers due to their preferred face-to-face stacking in agglomerated tactoids (as result of strong interaction by tight electrostatic forces between the layers). Dispersion of the clay tactoids into individual layers (exfoliation) is further hindered by the intrinsic incompatibility between the hydrophilic layered silicates and the more hydrophobic polymers. For these reasons the clay must be treated so it can be incorporated into a polymer. One way of modifying the clay surface to make it more compatible with a polymer is through ion exchanging. Since the cations on the clay surface can be exchanged by other organic cations (so called intercalants), which are tailored to the polymer in which the clay would be become more compatible. This process renders the clay more hydrophobic and helps to open up the clay galleries (as the adding of the intercalant on the clay surface). This facilitates the penetration of polymer in the clay galleries then subsequently exfoliates the clay. As demonstrated by the Toyota group more than twenty years ago, the replacement of inorganic exchange cation in the galleries of the native nanoclays by long chain alkylammonium surfactants can improve

the compatibility between the clay and the hydrophobic polymer matrix. A characteristic feature of smectites such as montmorillonite is their ability to sorb certain cations and to retain them in an exchangeable state. It means that these intercalated cations can be exchanged by treatment of other cations in a water solution. The most common exchangeable cations are  $\text{Na}^+$ ,  $\text{Ca}^{2+}$ ,  $\text{Mg}^{2+}$ ,  $\text{H}^+$ ,  $\text{K}^+$ , and  $\text{NH}_4^+$ . Indeed, if the clay is placed in a solution of a given electrolyte, an exchange occurs between the ions of the clay ( $\text{X}^+$ ) and those of the electrolyte ( $\text{Y}^+$ ) (Figure 2.3) [39].



**Figure 2.3. Exchange occurs between the ions of the clay ( $\text{X}^+$ ) and those of the electrolyte ( $\text{Y}^+$ ) [39]**

The reaction rate depends on the type of clay, medium, type of cation to be exchanged, the reaction conditions, viz. temperature, pH, concentrations and geometry of clay particles, etc. As indicated, this reaction is balanced and the extent to which the reaction proceeds from the left to the right depends on the nature of the cations  $\text{X}^+$  and  $\text{Y}^+$ , on their relative concentrations and often on secondary reactions. The equilibrium of the reaction can be moved to the right by increasing the concentration of the added cation  $\text{Y}^+$  [40]. For example, the cation exchange reaction between sodium MMT ( $\text{Na}^+$ -MMT) and intercalating organic cation  $\text{RH}^+$  is illustrated in Figure 2.4 [41].

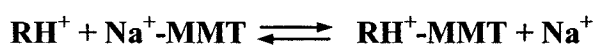


**Figure 2.4. Exchange occurs between  $\text{Na}^+$ -MMT and organic cation  $\text{RH}^+$  [41]**

Surface treatment reduces particle-particle attraction, promoting an expansion of the gallery distance, and improving interactions between clay and matrix (Figure 2.5). Therefore, the particles can be separated further either by diffusion of monomers into the gallery prior to polymerization as in the in-situ polymerization process or by employing shearing force using an extrusion compounder or mixer as in melt compounding of PNC [27].

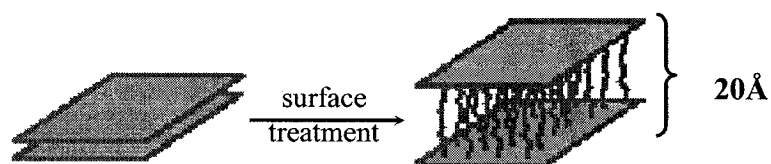


**Figure 2.5. Effect of surface treatment [27]**

Numerous kinds of compatibilizing agent have been used in the synthesis of nanocomposites. The first compatibilizing agents used in the synthesis of nanocomposites based on polyamide 6-clay hybrids by in-situ polymerization were amino acids [26]. Their amine group can be transformed to onium ion to react with clay surface while their acid group can react with the monomers. A wide range of  $\omega$ -amino acids ( $\text{NH}_3^+(\text{CH}_2)_n\text{COOH}$ ) have been intercalated between the layers of MMT [42]. The most popular intercalants are alkylammonium ions because they can be exchanged easily with the ions situated on the clay surface. MMT exchanged with long and linear chain alkylammonium ions can be dispersed in non-polar organic liquids, forming gel structures with high liquid content. This property was first discovered by Jordan [43] and summarised later on by Weiss [44]. Alkylammonium ions offer a good alternative to amino acids for the synthesis of nanocomposites based on other polymer systems than polyamide 6. The most

widely used alkylammonium ions are based on primary alkylamines which can be easily transferred to onium ion in an acidic medium to protonate the amine function. Their basic formula is  $\text{CH}_3\text{-(CH}_2\text{)}_n\text{-NH}_3^+$  where  $n$  is between 1 and 18. Lan et al. [45] showed that alkylammonium ions with chain length greater than eight carbon atoms favoured the synthesis of certain delaminated nanocomposites whereas alkylammonium ions with shorter chains lead to the formation of intercalated nanocomposites. Alkylammonium ions based on secondary, ternary and quaternary amines have also been used [46]. The cation-exchange process of linear alkylammonium ions is described in Figure 2.6.

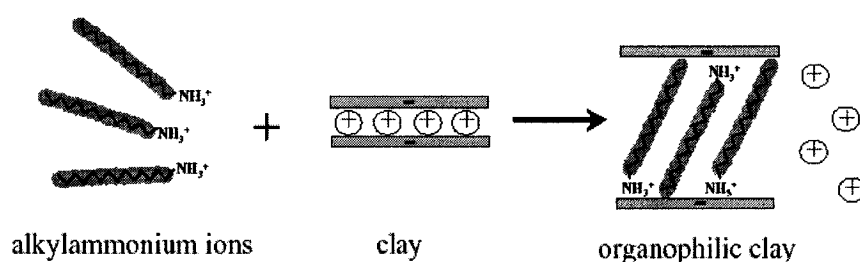


**Figure 2.6. The cation-exchange process between alkylammonium ions and cations initially intercalated between the clay layers [41]**

Silane coupling agents are a family of organosilicon monomers which are characterised by the formula  $\text{R-SiX}_3$ , where R is an organofunctional group attached to silicon in a hydrolytically stable manner and X designates hydrolyzable groups which are converted to silanol groups on hydrolysis. Silanes have been used because of their ability to react with the hydroxyl groups situated possibly at the surface of the reinforcements. In the clay, hydroxyl groups are possibly present on the surface of the layers but also particularly on their edges. It has been proposed that the silane coupling agent is first converted to a reactive silanol form by hydrolysis (Figure 2.7a) which then reacts with





## 2.3. Nanocomposite structures

Depending on the nature of the components used (layered silicate, organic cation and polymer matrix) and the method of preparation, three main types of composites may be obtained when layered clay is associated with polymer [50, 51] (See Figure 2.8).

**Traditional microcomposites:** when the polymer is unable to intercalate between the silicate sheets, a phase separated composite is obtained, whose properties stay in the same range as traditional microcomposites (Figure 2.8a). Beyond this classical family of composites, two types of nanocomposites can be recovered.

**Intercalated structure nanocomposites:** when a single (and sometimes more than one) extended polymer chain is intercalated between the silicate layers resulting in a well ordered multilayer morphology built up with alternating polymeric and inorganic layers (Figure 2.8b).

**Exfoliated or delaminated structure nanocomposites:** when the silicate layers are completely and uniformly dispersed in a continuous polymer matrix, an exfoliated or delaminated structure is obtained (Figure 2.8c).

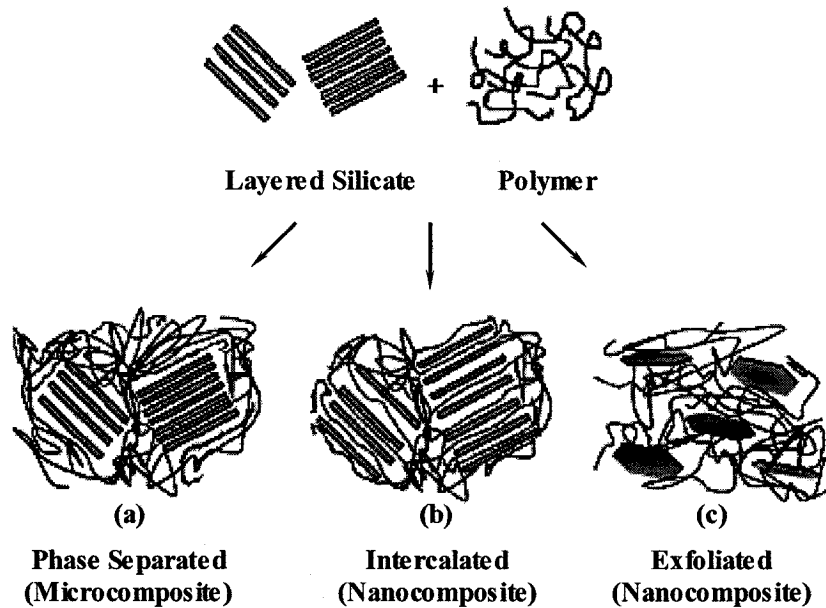


**Figure 2.8. The three idealised structures of polymer-clay composites (a) microcomposite, (b) intercalated nanocomposite, and (c) exfoliated nanocomposite**

Two complementary techniques are used in order to characterize those structures: X-Ray diffraction (XRD) and transmission electron microscopy (TEM). The most straightforward is X-ray diffraction because it is a good way to evaluate the spacing between the clay layers. The sample preparation is relatively easy and the X-ray analysis can be performed within a few hours. XRD uses an incident x-ray beam to interact with the atoms arranged in a periodic manner in 2D to reveal the regular order of crystalline materials. The Bragg equation is used to calculate the basal spacing:  $n\lambda = 2d\sin\theta$ , where  $d$  is basal spacing distance,  $\theta$  is X-ray injection angle,  $\lambda$  is wave length of X-ray, and  $n = 1, 2, 3...$ integers. From there intercalated structures can be identified. Figure 2.9 shows the XRD curves corresponding to different structures [51].

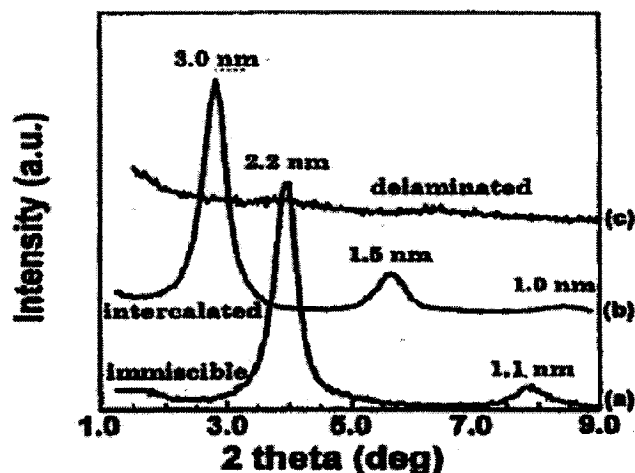
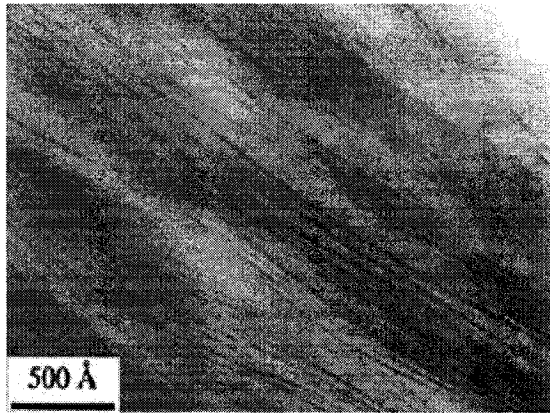


Figure 2.9. XRD curves of (a) fluorohectorite in HDPE matrix (no intercalation, no exfoliation was achieved), (b) nanocomposite of fluorohectorite in polystyrene (intercalation was achieved), and (c) nanocomposite of fluorohectorite in silicon rubber (exfoliation was achieved; diffraction peaks are not visible) [51]

In addition to these two defined structures, both intercalation and partial exfoliation result in a broadening of the diffraction peak. XRD determines the exfoliation structure when the clay gallery distance  $d_{001}$  ( $d$ -spacing) is greater than 8 nm. Due to the limitation of the XRD,  $d_{001}$  is greater than 8 nm can not be detected accurately.

In the case of exfoliated structures, extensive layer separation associated with delamination of the original silicate structure in the polymer matrix leads to the disappearance of any coherent x-ray scattering from the layers. Loss of coherent scattering may be due to either the presence of an extremely large regular ordered spacing between the layers, too large to be detected in the angular range of XRD normally operated (i.e. exceeding 8nm in the case of ordered exfoliated structure), or to the fact that nanocomposite no longer has an ordered layer structure [52]. TEM is therefore used

to determine nanocomposite morphology. Figure 2.10 shows TEM of amine-cured epoxy clay nanocomposite structure [45].



**Figure 2.10. TEM of an amine-cured epoxy clay nanocomposite [45]**

However TEM often focus only in small areas of the samples. The preparation for TEM observation is quite time consuming and expensive. Thus, it is not permitted the observation in different locations in the samples. In addition, clays dispersion often consists of different stages, in which clay particles can be observed at different sizes both micro- and nano-scales.

Scanning electron microscopy (SEM) and atomic force microscopy (AFM) are also used to identify the structure of polymer nanocomposites at the micro-scale that provide us a more general picture of the quality of dispersion. Scanning electron microscopy can be used to investigate clay distribution in the matrix. Figure 2.11 illustrates the morphology of an epoxy clay nanocomposite by using SEM [18].

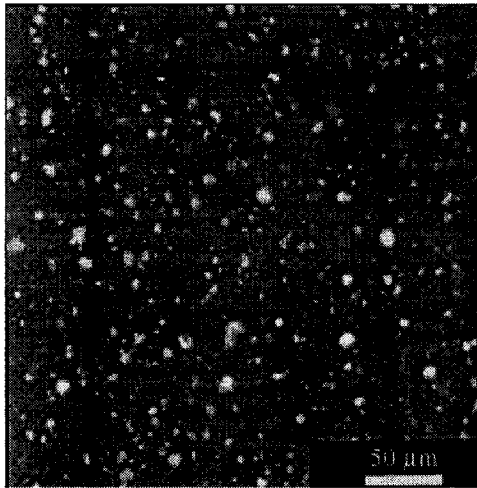


**Figure 2.11. SEM micrograph of epoxy nanocomposite [18]**

AFM can be used to observe the micro-structure but it can also be used in tapping mode for revealing the nanoscale structures of nanocomposites. For example, Chin et al [53] have investigated the clay layer gallery height in epoxy clay nanocomposite (Figure 2.12).

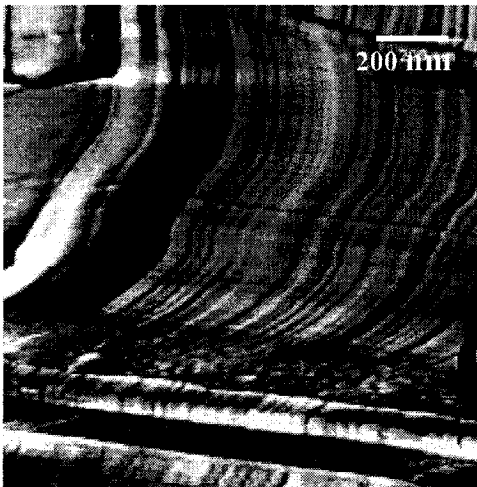


**Figure 2.12. AFM phase image of epoxy clay nanocomposite [53]**

## **2.4. Polymer nanocomposites (PNCs) fabrication**

Fabrication is an important step to obtain nanocomposites and there are many factors that need to be considered in the process. This subsection intends to describe how the nanocomposites are produced.

### **2.4.1. Thermoset nanocomposites fabrication**

In general, researchers developed two processes to fabricate thermosetting nanocomposites: In-situ polymerization process, and solution process.

#### **In-situ polymerisation process**

In-situ polymerization is the conventional process used to synthesise thermoset-clay nanocomposites. Polymer-clay nanocomposites based on unsaturated polyester [54], epoxy [10, 18], polyurethanes [55, 56] have been synthesised by this method. Most researchers used the in-situ polymerization to synthesise thermoset nanocomposite.

The strategy is described schematically in Figure 2.13. First, the organoclay is swollen in the monomer. This step requires a certain amount of time, which depends on the polarity of the monomer molecules, the surface treatment of the organoclay, and the swelling temperature. Then, the reaction is initiated. For thermosets such as epoxies, a curing agent is added to initiate the polymerisation. The schematic illustration of “in-situ polymerisation” approach is shown in Figure 2.14.

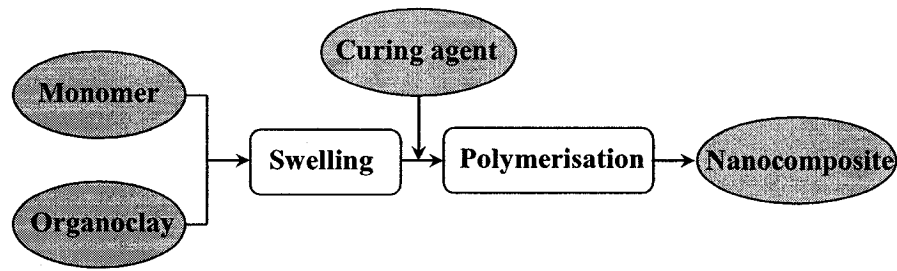


**Figure 2.13. Flowchart presenting the different steps of the “in-situ polymerisation” approach**

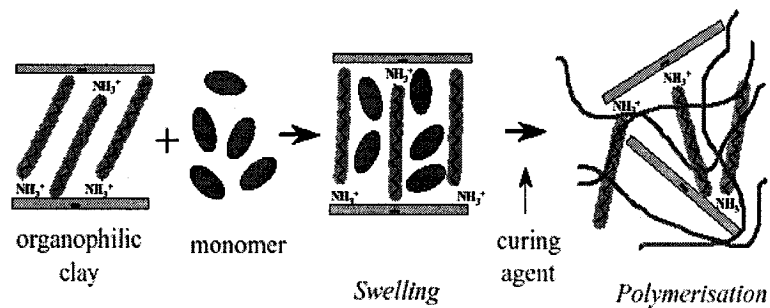


**Figure 2.14. Schematic illustration of “in-situ polymerisation” approach [4]**

It is not always certain that in-situ polymerization can lead to full exfoliation. The key relies on the interaction between the monomer and clay. Several publications have claimed that it is possible to exfoliate the organoclay in epoxy matrix as demonstrated by XRD. However, this claim can not be considered to be valid because no TEM observation can support it.

### **Solution process**

A solution process has also been used to synthesize epoxy-clay nanocomposites [20, 57]. The strategy is similar to the one used in the “in-situ polymerisation” approach. Figure 2.15 describes the different steps of the process. First, the organoclay is dispersed (swollen) in a polar solvent such as toluene, N, N-dimethylformamide, or acetone.

Alkylammonium treated clays swell considerably in polar organic solvents, forming gel structures. Then, the polymer, dissolved in the solvent, is added to the solution and intercalates between the clay layers. As the clays have been pre-intercalated with solvent, the further intercalation of the polymer chain into the clay galleries takes place easier. The last step consists in removing the solvent by evaporation usually under vacuum. Figure 2.16 shows how the polymer is intercalated between the clay layers. A relatively large number of solvent molecules need to be desorbed from the clay to accommodate the incoming polymer chains.

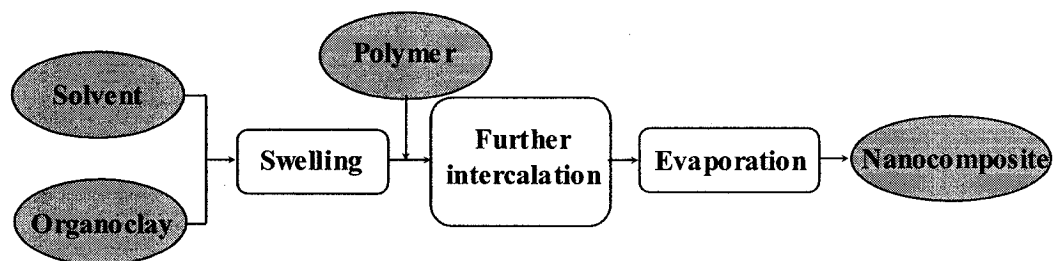


**Figure 2.15. Flowchart presenting the different steps of the “solution” approach**

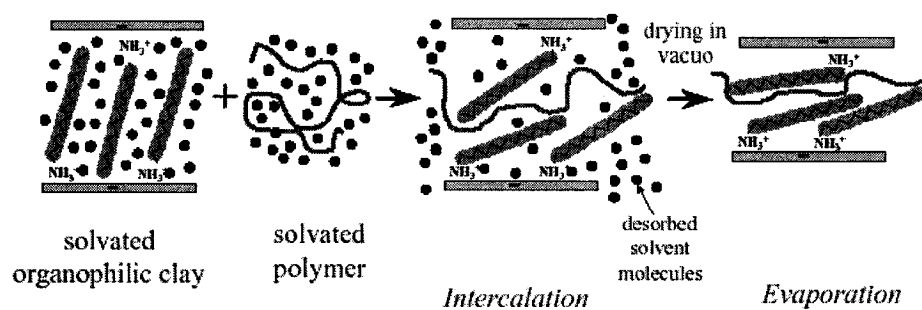


**Figure 2.16. Schematic illustration of “solution” approach. The black dots represent the solvent molecules [4]**

More recently, a new development in which a solution of epoxy, clay and acetone was passed through high pressure chamber at high velocity to break down the agglomerates of



clay has been reported [21]. The method to prepare the organoclay/epoxy nanocomposites in liquid (ethanol and water solution) without any intermediate drying step of clay has been used but full exfoliation still can not be achieved [58]. The major advantage of the solution method is that it offers the possibilities to prepare intercalated nanocomposites from polymers with low or even no polarity. However, the “solution” approach is difficult to apply in industry due to problems associated with the use of large quantities of solvent.

#### **2.4.2. Thermoplastic nanocomposite fabrication**

Three processes to fabricate thermoplastic nanocomposites have been developed by researchers: In-situ polymerization process, solution process, and melt intercalation (or compounding) process.

##### **In-situ polymerisation process**

In-situ polymerisation was the first method used to synthesize polymer-clay nanocomposites based on polyamide 6 [26]. For thermoplastics, the polymerisation can be initiated either by the addition of an initiator or by an increase of temperature [59]. Polyethylene terephthalate [60] has also been synthesised by this method. In a recent work, J. S. Ma et al [61] discussed the synthesis of polypropylene/clay nanocomposites by using in-situ intercalative polymerization. The Na-montmorillonite was modified by hexadecyl-octadecyl trimethylammonium and activated by the Ziegler-Natta catalyst ( $MgCl_2$ ,  $TiCl_4$ ); the activated montmorillonite served as a catalyst for propylene polymerization. During the polymerization, the clay structure would be destroyed and

exfoliated by the growing PP molecules inside the clay galleries. However, due to the incompatibility between the clay and the matrix, the clays collapsed after processing.

### **Solution process**

Nanocomposites based on high-density polyethylene [62], polyimide [63], and nematic liquid crystal polymers [64] have been synthesised by this method. Sometimes, nanocomposites based on untreated clays have also been synthesised using this approach. In this particular case, the polar solvent was deionized water. The polymer must be either able to be dispersed in water like polyoxide(ethylene) [65] or synthesized by emulsion polymerisation as was reported for polymethylmethacrylate [66].

### **Melt intercalation process**

Melt intercalation process was first reported by Vaia et al. [67] in 1993. The melt intercalation process has become increasingly popular because of its great potential for application in industry. Indeed, polymer-clay nanocomposites have been successfully produced by extrusion [68]. A wide range of thermoplastics, from strongly polar polyamide 6 [69] to hydrophobic polystyrene [70] has been intercalated between clay layers using this process. However, polyolefins, which represent the biggest volume of polymers produced, have so far only been intercalated to a very limited extent even the coupling agent was used [71]. The strategy consists in blending a molten thermoplastic with an organoclay under high shear to optimize the polymer-clay interactions (Figure 2.17). Figure 2.18 shows the schematic illustration of “melt intercalation” process. For

semi-crystalline polymers, the mixture can be also annealed at a temperature above the glass transition temperature in order to maximize the performance.

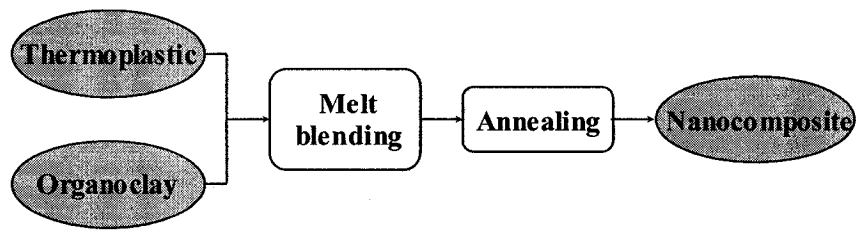


**Figure 2.17. Flowchart presenting the different steps of the “melt intercalation” approach**

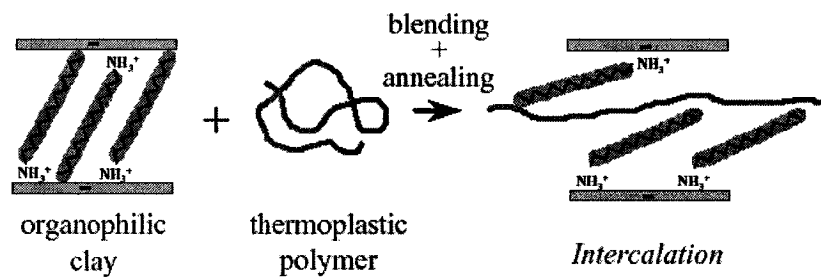


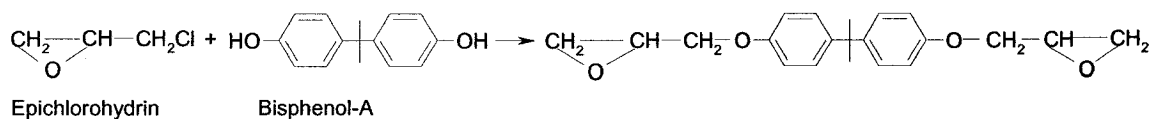
**Figure 2.18. Schematic illustration of “melt intercalation” process [4]**

## 2.5. Epoxies

Epoxies are relatively low molecular weight prepolymers capable of being processed under a variety of conditions. Because of their versatility, epoxies are used in thousands of industrial applications. The cured resins have high chemical and corrosion resistance, good mechanical and thermal properties, outstanding adhesion to a variety of substrates, and good electrical properties [72-75].

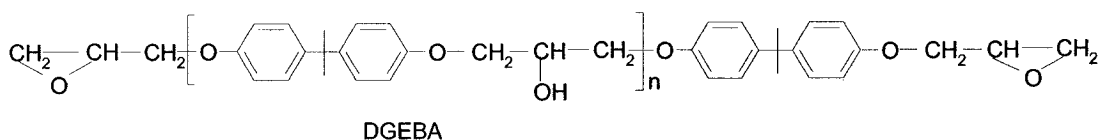
## 2.5.1. Epoxy resins

Epoxy resins are characterized by the presence of a three-membered ring containing two carbons and an oxygen (epoxy group or epoxide or oxirane ring). The liquid diepoxide as the reaction product of bisphenol-A with an excess of epichlorohydrin was reported in 1934 [73]. The structure of the resin is shown in Figure 2.19.



**Figure 2.19. 2,2- bis [4-(2', 3' -epoxypropoxy) phenyl] propane [73]**

The first commercial epoxy resins were obtained by the reaction of bisphenol -A and epichlorohydrin in the presence of strong base, and were first marketed in the 1940s. This resin is commonly called diglycidyl ether of bisphenol A (DGEBA). The higher molecular weight homologues are represented by the following structure (Figure 2.20) [73-75].

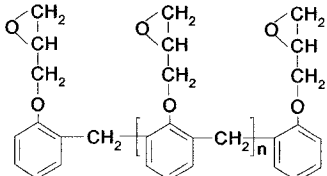
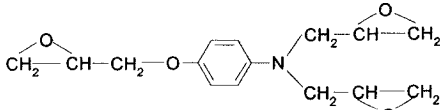
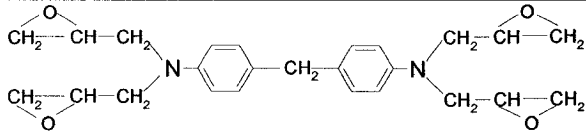
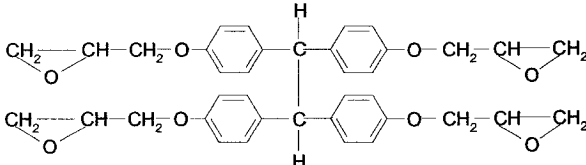


**Figure 2.20. Higher molecular weight homologues of epoxy based on diglycidyl ether of bisphenol A (DGEBA) [73-75]**

The value of  $n$  in liquid resins is less than 2.5 while in high melting point solid resins it can be as high as 18. Liquid DGEBA is used extensively in industry due to its fluidity, processing ease, and good physical properties of the cured resin. As the value of  $n$

increases, the fluidity of resin decreases and, therefore, in the composite industry the general-purpose epoxy resins have a maximum degree of polymerization up to four only [73-75]. The molecular weight of the resin depends on the feed ratio of epichlorohydrin/bisphenol-A and an increase in this ratio results in a decrease in molecular weight. Beside DGEBA, several different types of epoxy resin have been developed and commercialized. The structures of some other epoxy resins are shown in Table 2.3 [73-79].

**Table 2.3. The structures of some epoxy resins [73-79]**

Epoxy	Structure
Epoxy novolac	
Triglycidyl p-amino phenol (TGAP)	
N, N, N', N'-tetraglycidyl-4, 4'-diaminodiphenylmethane (TGDDM)	
Tetraglycidyl ether of tetrakis	

### 2.5.2. Hardeners (curing agents)

The curing of epoxy resins is associated with a change in state from a low molecular weight liquid mixture to a highly cross-linked network. Many commercial hardeners

suitable as curing agents have been used for epoxy resins [73-75]. The most common types of curing agents are (1) primary, secondary polyamines and their adducts, (2) anhydrides, (3) polyamides, and (4) catalytic types.

#### **2.5.2.1. Primary and secondary polyfunctional amines**

Typical of this class of curing agents are aliphatic amine compounds, such as Diethylene Triamine (DETA), Triethylene Tetramine (TETA), and Tetraethylene Pentamine. Room temperature cures are usually employed. Aromatic amines, such as metaphenylene diamine and diamino diphenyl sulfone, are also widely used to achieve higher heat distortion temperatures. Elevated temperature cures are usually employed.

The amines react with the epoxy group through its active amine hydrogen. Each primary amine group is theoretically capable of reacting with two epoxide groups, and each secondary amine group is capable of reacting with one epoxide group. The main reactions that occur are illustrated in Figure 2.21 [80]. Other reaction that can also occur is that between an epoxide ring and a hydroxyl group to form an ether link and a new hydroxyl group, which is then available for further reaction. The epoxide-hydroxyl reaction is generally slower than the epoxide-amine reaction and becomes important only when the cure is performed at high temperatures or when there is an excess of epoxy with respect to amine. The reaction between an epoxide ring and a hydroxyl group is often catalyzed by tertiary amines. The presence of hydroxyls, however, has an important function because they assist in opening the epoxide ring. Alcoholic or phenolic hydroxyls accelerate the primary and secondary amine cures and thus provide for the more rapid gel time of the amine adducts and the higher molecular weight resins. Even if no reactive

amine is present, epoxy resins will polymerize on their own if heated to a sufficiently high temperature. This is attributed to a “homopolymerization” reaction, which may be initiated by impurity groups present in the resin or by (nonreactive) tertiary amine groups. This is generally considered to be difficult to achieve unless specific catalysts such as boron trifluoride complexes are present [77].

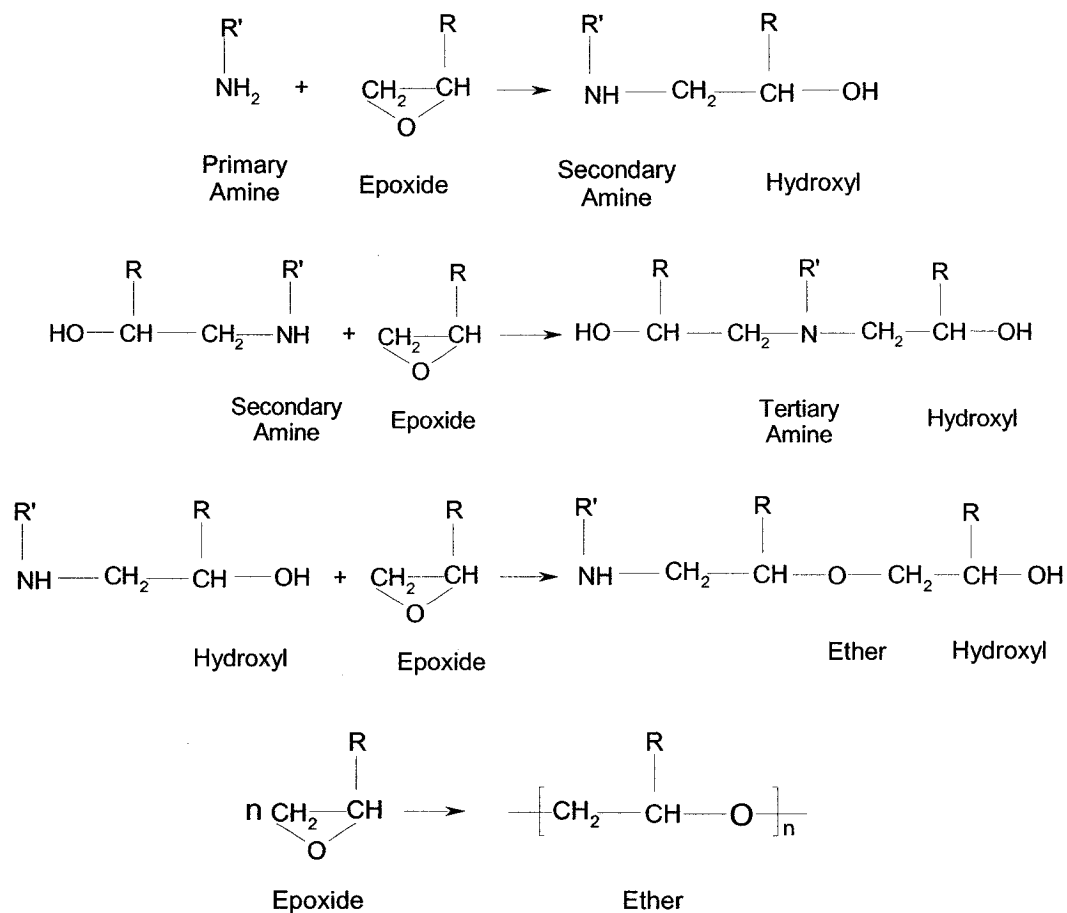


**Figure 2.21. Main reactions involved in the cure of epoxy resins with amine curing agents [80]**

### 2.5.2.2. Anhydrides

Liquid and solid anhydrides are also used to cure epoxy resins but in lesser extent [73, 76]. The reactivity rate of some anhydrides with epoxies is slow. An accelerator, usually a tertiary amine, is often used (0.5% to 3%) to speed up gel time and cure. The reaction of anhydrides with epoxy groups is complex, with several competing reactions capable of taking place. The reactions that occur are illustrated in Figure 2.22.

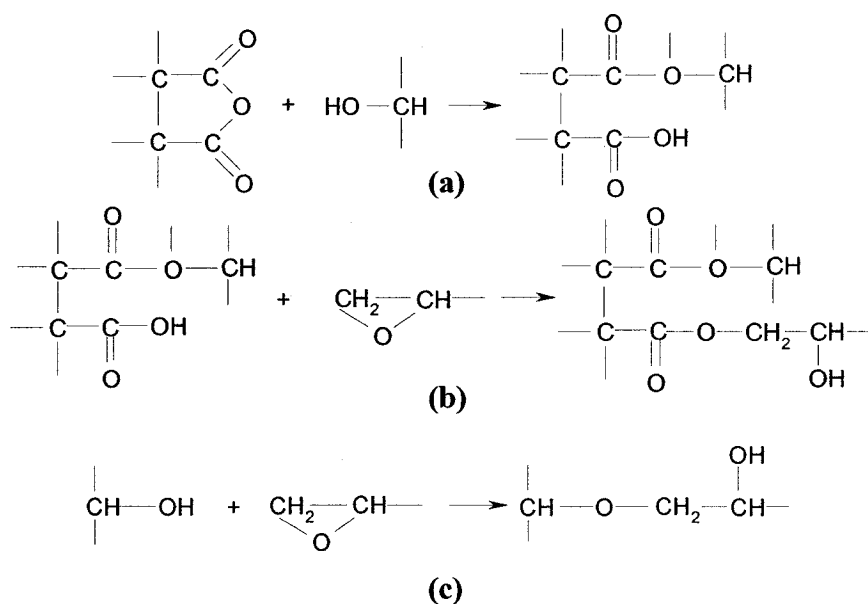


**Figure 2.22. Reactions involved in the cure of epoxy resins with anhydride curing agents: (a) The opening of the anhydride ring with an alcoholic hydroxyl to form the monoester, (b) Subsequent to (a) the nascent carboxylic groups react with the epoxide to give an ester linkage, (c) The epoxide groups react with nascent or existing hydroxyl groups, catalyzed by the acid, producing an ether linkage [76]**

Since reaction can take place independently in the acid medium, the ratio of anhydride to epoxy is less critical than with an amine. It can vary from 0.5 to 0.9 equivalents of



anhydride per equivalent of epoxy and should be determined experimentally to achieve desired properties. Pot life of the mix is usually long; exotherm is low. Elevated temperature cures are necessary and long post cures are required to develop ultimate properties. Electrical and physical strength properties are good over a wide temperature range. Chemical resistance to some reagents is less than with amine-cured systems, but is better against aqueous acids.

### 2.5.2.3. Polyamides

This class of compounds can be considered as modified polyfunctional aliphatic amines, since the polyamides most widely used are the condensation products of dimerized fatty acids and a difunctional amine such as ethylenediamine. Their theorized structure is represented as follows (Figure 2.23)

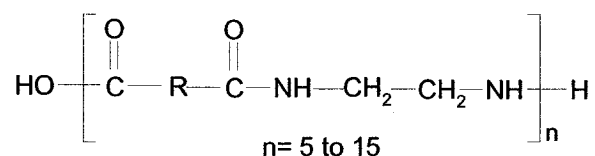


**Figure 2.23. Structure of polyamides [76]**

The reactivity of polyamides with epoxies is similar to that of the aliphatic amines. It is varied quite broadly to obtain properties from hard to semi-flexible. In this sense, the polyamides can be considered resin modifiers as well as curing agents. Polyamide-cured formulations have longer pot life than formulations cured with aliphatic polyamines and their adducts. They cure at room temperature without blushing and show outstanding adhesion. Formulations are high in viscosity and are sometimes incompatible with the resin until reaction has been initiated. They are usually dark in color. Polyamide systems

lose structural strength and insulation value rapidly with increasing temperatures, and are usually restricted to applications under 65°C (149°F) [76].

#### 2.5.2.4. Catalytic curing agents

Catalytic curing agents are those compounds that promote epoxy-to-epoxy or epoxy-to-hydroxyl reactions and do not themselves serve as direct cross-linking agents. Tertiary amines, amine salts, boron trifluoride complexes, and amine borates are in this class [73, 76]. The mechanism of epoxy-to-epoxy polymerization using a tertiary amine catalyst (or other catalytic curing agent) theoretically takes place as in Figure 2.24.

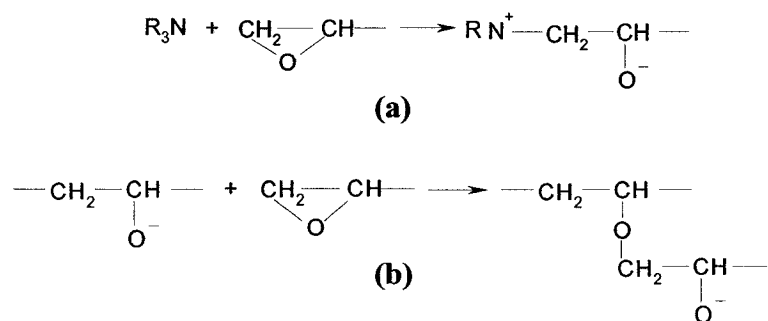


**Figure 2.24. Reactions involved in the cure of epoxy resins with catalytic curing agents: (a) opening of the epoxy group, (b) the ion thus formed is capable of opening another epoxy group [73, 76]**

## 2.6. Epoxy-clay nanocomposites (ECNs)

Epoxy resin reinforced with nanoscopic layered silicates has received increasing attention recently because of the possibility of obtaining improved properties in terms of stiffness, strength, fracture toughness, fire resistance, dimensional stability, etc. [10, 13, 21, 55, 58].

### 2.6.1. Formation of ENCs

The mechanism of formation of exfoliated ENC has been studied. However, much is still unknown. The exfoliation of the clay tactoids into a curing polymer requires the driving force of the polymerization to overcome the attractive electrostatic force between the interlayer cations and the negatively charged silicate layers. If the curing reaction takes place inside the clay galleries slower than outside the galleries (extragallery polymerisation); then delamination of the clay is impeded [45]. Therefore, one needs to find ways to favour the intragallery polymerization as compared with the extragallery polymerization which is not easy to do. This group also proposed that the acidity of the alkylammonium ions may catalyze the homopolymerization of the epoxy molecules inside the clay interlayers but only very high temperature (above 150<sup>0</sup>C) [81]. The proposed mechanism is described in Figure 2.25.

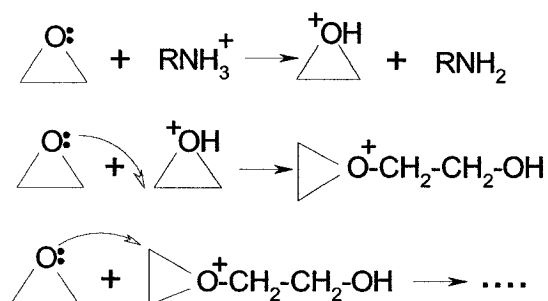


**Figure 2.25. Proposed homopolymerization mechanism of DGEBA catalyzed by alkylammonium ions [81]**

Moreover this research also proposed that long-chain alkylammonium ions allow more epoxy precursors to be accommodated in the gallery, which may be a prerequisite to achieve layer exfoliation upon an intragallery reaction [82]. However, it is not really true

because the long alkyl chain often leads to the higher hydrophobicity which is less compatible with the epoxy matrix.

Ke et al [83] found that the organoclay is easily intercalated by the epoxy precursor during the mixing process, and the clay galleries continue to expand a bit more during the curing process. They also noted that in the cured system, although partial exfoliated clay layers have already formed, an amount of the intercalation structure still remains. On the other hand, the addition of a promoter or coupling agent into the cured system significantly lowers the maximum reaction temperature, and during the curing process the layered organoclay can be gradually broken into nanoscale structures, in which no  $d_{001}$  diffraction peaks are observed. Finally, they claimed that complete exfoliation is achieved at gel time or before but no TEM observation supports for this claim. However, as discussed earlier, absence of XRD peaks do not link directly to the exfoliation. Furthermore, even if exfoliation is achieved, the use of coupling agents is quite expensive and they may also affect the curing process. Lü et al [84] illustrated that the exfoliation takes place under the condition that the exothermal curing heat produced by the intragallery epoxy, before the extragallery epoxy reaches its gel-point, is large enough to overcome the attractive forces between the silicate layers. However this speculation fails due to the fact that hardener is not present in the clay galleries.

Kornmann et al. found that a MMT with a low CEC was already exfoliated during swelling in the epoxy resin prior to curing [10]. A mechanism was proposed in which the homopolymerization of the epoxy resin during the swelling phase causes the diffusion of new epoxy molecules into the clay galleries. Due to its high surface energy, the clay

attracts polar monomer molecules into the interlayers until equilibrium is reached. The polymerization reactions occurring between the layers lower the polarity of the intercalated monomer molecules. This will allow new polar monomer molecules to diffuse between the layers and further exfoliate the clay. The relatively low CEC clay contains a smaller amount of alkylammonium ions. This means that there is more space available for the epoxy molecules at the same  $d$  spacing. The self-polymerization of the epoxy resin within the interlayers can then occur to a larger extent. Unfortunately, this study was conducted on the low aspect ratio clays. It is not really true for the high aspect ratio MMT clays, which have a greater reinforcing effect.

Messersmith and Giannelis [9] have analyzed the effect of different curing agents and curing conditions in the formation of nanocomposites based on the DGEBA and a montmorillonite modified by bis (2-hydroxyethyl) methyl hydrogenated tallow alkyl ammonium cation. They found that the modified clay dispersed readily in DGEBA when sonicated for a short time period as determined by the increase in viscosity at relatively low shear rates and the transition of the suspension from opaque to semitransparent. The increase in viscosity was attributed to the formation of a so-called “house-of-cards” structure in which edge-to-edge and edge-to-face interactions between dispersed layers form percolation structures. XRD patterns of uncured clay/DGEBA also indicate that intercalation occurred during mixing.

Becker et al [85] synthesized epoxy-clay nanocomposites based on organoclay I30E and different epoxy resins: bifunctional DGEBA, trifunctional TGAP, and tetrafunctional TGDDM. I30E was dispersed in these epoxy resins with mechanical stirring. The

hardener was diethyltoluene diamine. The results showed that d-spacing of the DGEBA based nanocomposite system is larger than in the higher functional epoxy systems.

Kornmann et al. have also studied the influence of the nature of the curing agent on nanocomposite structure [10]. Three different curing agents were used: polyoxyalkylene diamine (D230), bis-(4-aminocyclohexyl) methane (BAM) and 3, 3'-dimethyl-methylenedi (cyclohexylamine) (3DCM). The structure of the resulting nanocomposites depended on both the cure kinetics and the rate of the diffusion of the curing agent into the clay gallery. The polarity, molecular flexibility and reactivity of the curing agent greatly affected the kinetics and diffusion rates. Therefore, the resulting structure of the nanocomposite was also influenced. Also, the curing temperature controlled the balance between the extragallery reaction rate of the epoxy system and the diffusion rate of the curing agent into the galleries. Probably at a certain curing temperature, both the rate of diffusion of the epoxy into the clay galleries and the intragallery curing can be favorable than the extragallery curing. However, it is still not clear how chemistry and especially molecular weight of hardener influence the intercalation/exfoliation of clay in epoxy matrix.

Processing parameters have an important influence on the dispersion of clay in polymer. This in turn has an effect on the physical and mechanical properties of nanocomposites. Dispersion process parameters mainly include stirring temperature, time, speed, power of ultrason, and shearing forces etc. Direct mixing of organoclay and epoxy by mechanical stirring and sonication is widely used to disperse nanoclay in epoxy [10, 11, 12, 16, 18]. However it is not enough for good dispersion of clay in epoxy. Many publications

reported on a mixture of intercalation and exfoliation of clay in epoxy nanocomposites but not full exfoliation. Although, the clay galleries were clearly expanded by epoxy matrices and the diffraction peaks were not visible with XRD. However, agglomerates of clay were observed by TEM. The dispersion of nanoclays in epoxy nanocomposites in all cases appears to be very in-homogenous. To our knowledge, besides selecting a right chemistry of the system (clay, epoxy, and hardener) and processing temperature, breaking down the clay agglomerate is also an important key to speed up the intercalation and exfoliation of clay. However, no research on this topic has been fully carried out.

### **2.6.2. Curing of ENCs**

The mechanism and kinetics of epoxy resin curing, which can involve various chemical reactions, have been widely studied [86]. However, the curing reaction of epoxy-clay nanocomposite is complex due to the presence of organoclay. The effect of primary amine-based intercalant on the polymerization of epoxy has been described by Lan et al. [81]. Butzloff et al [87] studied the effects of MMT layered silicates on the curing kinetics of an epoxy resin. Differential scanning calorimetry was used to probe the changes in reactivity due to the presence of MMT and due to the diamine hardener. The enthalpy of polymerization was strongly affected at compositions greater than 5 wt% MMT for epoxy-MMT reactions. However, it is not clear that such effect is caused by the presence of organoclay or the excess of intercalant.

The effect of montmorillonite on the curing kinetics and the structure of epoxy/ organo-montmorillonite ( $\text{CH}_3(\text{CH}_2)_{16}\text{NH}_4\text{-MMT}$ )/methyltetrahydrophthalic anhydride/2-ethyl-4-methyl-imidazole was investigated by the dynamic torsional vibration method (DTVM)

[88]. The addition of Org-MMT reduces the gelation time  $t_g$ , and increases the rate of the curing reaction and the value of the kinetic constant  $k$ . The half-time  $t_{1/2}$  of cure after the gel point decreases with increasing cure temperature, while the values of kinetic constant  $k$  rise as the cure temperature increases. Similar results were also reported [89, 90]. A steric effect of clay on the curing of intercalated epoxy matrix has been discussed by Kornmann et al. [10, 18]. Although the work did not include a kinetics study, they pointed out that there is a competition between diffusion of hardener molecules into the clay galleries and a curing reaction between the hardener and epoxy outside the galleries. Depending on the hardener chemistry and curing temperature, the balance between the two processes may vary.

### **2.6.3. Mechanical properties**

The clay nanolayers are more effective in improving mechanical properties when the polymer is in its rubbery state than in its glassy state. Lan et al [11] mixed the organoclay ( $\text{CH}_3(\text{CH}_2)_{17}\text{NH}_3^+$ -MMT) into to the mixture of epoxy and amine at  $75^\circ\text{C}$  and stirred for 30 minutes. With 7.5 vol% of the organoclay, the strength of elastomeric polymer matrix ( $T_g \sim 40^\circ\text{C}$ ) is improved by more than 10-fold but no significant improvement in glassy epoxy. Although it is not clear that if such effect is solely related to the transition state of the epoxy system or also the difference in chemistry of the matrix and the quality of dispersion of the two systems. The behavior of glassy epoxy-clay nanocomposites in compression was studied by Massam and Pinnavaia [12]. The compressive yield strength and the modulus of the exfoliated nanocomposites were increased by 17 and 27%, respectively, with a clay loading of 10 wt%. However the conventional composites were



completely ineffective in providing reinforcement to the matrix. They also found that interfacial interactions, platelet aspect ratios, and layer charge densities also have a direct impact on the compression behaviour of the nanocomposites. The dimensional stability, thermal stability and solvent resistance of the glassy matrix can also be improved when the clay nanolayers are present. Researchers from Nanocor [27] showed flexural modulus of amine-cured epoxy nanocomposites increased 40% for a high- $T_g$  system (glassy system) at 8 wt% clay but not strength. Zilg et al [91] confirmed that the tensile strength properties of nanocomposites did not improve but decreased depending on types of alkylamine intercalants. Organoclays (alkylamine-treated fluorohectorites) were dispersed in DGEBA (Araldit CY225) at 80°C and 13 mbar pressure. Tensile strength decreased 17% with 10 wt% Butyl-amine treated clay and tensile strength decreased 39.5% with 10 wt% Octadecyl amine treated clay. This can be explained by the poor interface interaction between the epoxy matrix and the organoclay.

Kornmann et al. [18] showed that with octadecyl-amine treated MMT, flexural modulus increases by more than 40% for the EPON 828/Jeffamine D230 system with 10 wt% clay and by 28% for the EPON 828/3DCM system with 8 wt% clay. However, no increase in flexural strength was reported.

Increases in fracture toughness by adding organoclay into epoxy resins systems were reported by many researchers [14, 21, 71, 85, 92-100]. Kornmann et al. [14] showed 112% increase of fracture toughness of TGDDM-DDS matrix reinforced by 4.2 vol% nanoclay. In this study, TGDDM resin and organoclay (hydroxyethyl dihydroimidazolinium-sodium fluorohectorite) was mixed at 100°C under vacuum. There is also

great improvement (nearly 80~90%) of fracture toughness for untreated clay. Kornmann et al. [92] also studied the influence of silicate surface modification on the properties of nanocomposite based on DGEBA. Again, they noted that fracture properties are not substantially affected by the nanoscopic separation of the silicate layers and are also improved for conventionally filled composites. This suggests that mechanisms governing fracture properties of these materials are occurring on the microscale. This seems to be in contrast to the results of filler composites. Moreover the elongation at break of the nanocomposites is lower than that of the pure epoxy. Becker et al [85] found that the improvement in fracture toughness of the epoxy systems with higher functionality is larger than those achieved in the bifunctional DGEBA epoxy system with the presence of clay.

Liu et al [21] prepared intercalated epoxy nanocomposite by high pressure mixing with acetone. The result showed that modification with organoclay (Nanomer I30E) simultaneously improved the fracture toughness and compressive properties of DGEBA/BF<sub>3</sub>.MEA, that is,  $K_{IC}$  and  $G_{IC}$  increased by 1.84 and 2.97 times respectively at 6 phr clay loading. Compressive modulus and fracture strain increased by 25.1% and 9.6% respectively, at 6 phr clay loading. Liu et al [22, 23] also reported that the fracture toughness of the TGDDM-DDS system was greatly improved by adding nanoclay with high pressure mixing method.  $K_{IC}$  and  $G_{IC}$  increased by 2.2 and 5.8 times, respectively, over the pristine epoxy system properties at 4.5 phr (about 3 wt%) clay loading.

The fracture behavior appears to be most dramatically improved in the intercalated system based on EPON825 and Jeffamine D230 [94]. The fracture energy of the

composites was shown to be increased by 100% at clay concentrations of 5 wt %. By investigating the surface roughness and crack propagation under subcritical loading, it has been hypothesized that the creation of additional surface area on crack propagation is the primary means for toughening in intercalated systems. The morphology of this system seems to play an important role in the toughening. The effect of size of nanoclay particles on the fracture toughness of epoxy nanocomposites has also been discussed but the mechanism behind is still unclear.

#### **2.6.4. Thermal properties**

The change in  $T_g$  of epoxy nanocomposites compared to neat epoxy was also reported [9, 13, 101, 102]. Messersmith and Giannelis [9] found that the nanocomposite exhibits a broadened  $T_g$  at slightly higher temperature than the unmodified epoxy. Feng et al [102] reported that  $T_g$  increased with increasing the amount of organoclay. This suggests that the layered silicates hinder the motion of molecules in the epoxy network at least in the vicinity of the silicate surface. Researchers from Nanocor [27] show significantly increased glass transition temperatures (by 10 to 20 °C) for amine-cured epoxy nanocomposites with 7 wt% of Nanomer I30E nanoclay.

However, there is not always an increase in  $T_g$  for epoxy resin with the presence of nanoclays. The reduction in  $T_g$  for DGEBA/BF<sub>3</sub>.MEA was found to be 10°C for the nanocomposites with 6 phr organoclay, and the  $T_g$  of the system decreased further with the increase of clay loading [21]. Becker et al [103] studied the effect of octadecyl amine treated MMT Nanomer I30E on properties of the TGAP and DGEBA system. Nanomer I30E was dispersed in TGDDM resin at 80°C using a stirrer at 500 rpm. They reported

that  $T_g$  decreased 15°C for the TGAP and DGEBA system and 20°C for TGDDM system with the presence of 10 wt% clay. Zilg et al [91] found that the  $T_g$  and properties of nanocomposites changed depending on types of alkylamine intercalants. Organoclay (alkylamine-treated fluorohectorites) was dispersed in DGEBA (Araldit CY225) at 80°C and 13 mbar pressure.  $T_g$  decreased 20°C with 10 wt% butyl-amine treated clay and  $T_g$  decreased 28°C with 10 wt% octadecyl amine treated clay. The reduction in  $T_g$  may be due to the effect of the intercalant (used to treat the clay) on the formation of the crosslink network. Unfortunately, the authors have not paid attention to this issue.

Wang and Pinnavaia [46] compared the thermogravimetric analysis (TGA) curves for an exfoliated nanocomposite prepared from C18A1M-magadiite and an intercalated nanocomposite prepared from C18A3M-magadiite. The lower temperature weight loss (of below 200°C) for the intercalated C18A3M-magadiite nanocomposite is indicative of the decomposition of the quaternary alkylammonium cations (the intercalant) on the magadiite basal planes, because an analogous weight loss is observed for pristine C18A3M-magadiite. Flammability properties of epoxy nanocomposites were studied by Gilman et al [15]. They found that the nanocomposites have reduced flammability. The total heat release rate (HRR) plots of DGEBA/MDA with 6 wt% of clay nanocomposites at 35 kW/m<sup>2</sup> heat flux were reduced by 40% as compared with DGEBA/MDA (Figure 2.26). However, the presence of organoclay reduced the ignition time, which has been speculated due to the low thermal stability of the organic intercalant.

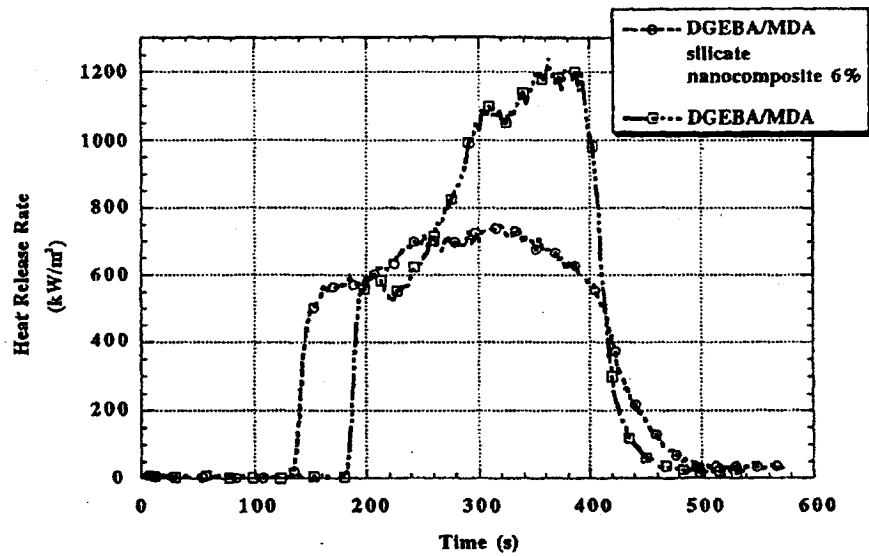


**Figure 2.26. Comparison of HRR plots for DGEBA/MDA and DGEBA/MDA nanocomposite with 6 wt% of silicate [15]**

### 2.6.5. Barrier properties

The barrier properties of nanocomposites depend on the sheet-like structure of the filler: in fact, the nanometre-thin layers act as obstacles to molecules diffusing towards the nanocomposite bulk, extending their path through the polymer and, thus, decreasing its permeability to gases and liquids. Epoxy-organoclay (treated with octadecyl amine) nanocomposites showed excellent reduction water absorption [104]. The difference of water absorption between modified organoclay and unmodified clay can be explained by the fact that the water resistance is strongly dependent on the delamination of clay layers within the epoxy resin and modification of the clay surface. The delamination of clay within the epoxy resin increases the diffusion path of water in the epoxy resin. Thus it takes more time for water to pass through the epoxy resin. The modification of clay by octadecyl amine made the clay surface more hydrophobic and increased the gallery

distance, thus facilitating the delamination. The water uptake behavior, a major concern in glassy high performance epoxy resin systems, was investigated by Becker et al [17]. The results of the water sorption at a temperature of 80°C showed that the equilibrium water uptake of nanocomposites was reduced compared to the neat epoxy system. The concentration of layered silicate did not correlate proportionally with the reduction in equilibrium water uptake. The absolute reduction of water uptake varied between 0.4% and 0.5% for the DGEBA and TGAP and 0.2% for the TGDDM nanocomposites, while the rate of water diffusion remained unaffected.

Chen et al studied the solvent absorption for the aerospace epoxy-organoclay nanocomposite [105]. The solvent absorption of the aerospace epoxy-organoclay nanocomposite in acetone was examined, and the diffusion coefficients of solvent in the nanocomposites were reduced. The solvent uptake for the nanocomposites is significantly low compared with the pristine polymer [12, 106].

## **2.7. Summary**

The polymer layered silicate nanocomposites are becoming a very promising new class of materials. Based on the above survey of the literature, the silicate nanolayers have provided effective reinforcement on the epoxy resins depending very much on the level of their dispersion. The finer the dispersion and exfoliation the better the reinforcing effect. In overall it is still be struggling to produce the epoxy nanocomposites with good exfoliation by industrial processes or processes which can be easily industrialized.

From previous works, the conventional mechanical stirring method to prepare epoxy nanocomposites has been widely used in the research due to its simple, economic and good dispersion. However it is not sufficient to obtain the good dispersion of clay in epoxy because of its low shearing efficiency. The low viscosity of epoxy resin, which is an essential requirement for most processing procedures for the fabrication of epoxy materials, also contribute to the difficulty in generating high shear by conventional devices. In addition, even if delamination of the clay layers can be achieved, the delaminated structure cannot be sure to be maintained during storage if the compatibility between the clay and the epoxy matrix is not good (agglomeration will eventually take place according to the thermodynamic rule). Further, one cannot focus only on the compatibility between the organoclay and the epoxy resin but also between the organoclay and the hardener as well as between organoclay and the intermediate products of the curing (polymerization) process. Thus the delamination of organoclay in the epoxy curing system is quite complex and no study has addressed through all the important elements of this complex process. Beside that other non-practical or unconventional approaches have been explored, like the use of ultrason, high pressurized system, solvent, coupling agent, etc. They show very limited success in delamination in term of quality and uniformity but have very low consistency in the results (work for only few systems) while they appeared to be neither practical nor economical for industrial application. Therefore, it is desirable to have a better understanding about the delamination process in order to propose a practical and economical means to achieve a fine dispersion and improve the intercalation/exfoliation of nanoclay in epoxy nanocomposites for industrial practice.

On the other hand, the curing process of epoxy nanocomposites is also an important issue in the production of epoxy based materials in the industry. In term of chemistry, mineral clays have been known to have no significant effect on the curing process of epoxy just as other mineral filler when they are dispersed in the micro-composites. However, if the clay layers are delaminated, a huge surface area and a great restriction of the molecular mobility can be generated. Such effects on the curing process still remain unknown. In addition the presence of the intercalant on the clay may complicate the curing process. Since commonly used intercalants are based on amine compound, the conversion of amine to ammonium ion for the clay treatment and the cationic exchange reaction of such ion with the cationic ions on the clay surface by industrial process may not be necessary perfect, thus may generate a trace of free amine and free ammonium ion in the organoclay products. In addition, if the ammonium ion is based on primary or secondary amine, even when it is bound on the clay surface by ionic bond, it still contains active hydrogen (in the amine portion). The effect of such elements on the curing process has been discussed rarely in few publications but there is no conclusive understanding. Therefore, it is worth to have a better to understanding of the effect of organoclays which have different levels of intercalant chemistries as well as different stage of dispersion on the curing process in order to provide basic information for the fabrication of epoxy nanocomposite based products by industrial processes.

In principle the reinforcing effect of clay in nanocomposites is just similar to the reinforcing effect of conventional composites, which is strongly dependent on the aspect ratio of the type of clay used and the interface interaction between the clay and the matrix. The quality of clay dispersion and intercalation/exfoliation determines the actual



aspect ratio of the clay aggregates in the system. The finer the dispersion and the greater the intercalation/exfoliation should lead to the higher aspect ratio of the clay aggregates/stacks in the actual system. As mentioned earlier, the quality of dispersion and intercalation/exfoliation is controlled by the mechanical means (to break down the aggregates and to shear the layers apart) as well as the compatibility between the clay and the matrix. The compatibility between the matrix and the clay, beside that, is the main key to control the interface interaction between the two phases. It is evident that the chemistry of the clay intercalant and the chemistry of the resin (both the epoxy and the hardener) play a determined role in this aspect. However, these chemistries not affect only the interface but also the curing process, on one hand it turns to affect the crosslink network structure and on the other hand it has a certain effect on the intercalation and exfoliation as described earlier. Thus the reinforcing effect of clay in epoxy nanocomposites is not straightforward but rather very complicated than expected. A good comprehension of this issue is essential if one desires to fabricate clay epoxy nanocomposites with optimum performance.

## **2.8. Challenges for ENCs**

From the above summary, the scientific challenges in the development of ENCs are very vague. Due to the scope of this thesis, several scientific aspects have been selected to be addressed in this thesis including

- How to fabricate good ENCs by a solvent- free method?
- How to control the dispersion of nanoclays in epoxy resins during the stirring step and curing step?

- What is the effect of the presence of clays on the processing of epoxy based products?
- What is the effect of the chemistry of the epoxy matrix (compositions and molecular weight) and organoclays on the formation of epoxy nanocomposites and thus the nanocomposite properties?

## **2.9. Objectives**

*In order to answer the issues addressed above, this research will focus on several issues as follows:*

- To achieve a better understanding of the formation of epoxy clay nanocomposites.
- To study the effect of different types of clay and hardener on the curing of epoxy clay nanocomposites.
- To study the influence of clay on properties and performance of epoxy clay nanocomposites.
- To analyze the relationships between the formulation, morphology, processing and the properties of epoxy clay nanocomposites.
- To understand the reinforcing effect of the clay on the performance of epoxy systems with characteristics varying over a broad range from rubbery to glassy (at room temperature).
- To further explore non-solvent stirring techniques to improve the intercalation/exfoliation of clay in epoxy matrix and thus improve the performance of epoxy nanocomposites.

# Chapter 3

## Materials and experiments

### 3.1. Selection of materials

Chemistry of clay, matrix formulation and processing parameters are three major factors that may influence the formation of epoxy-clay nanocomposites and need to be studied.

Therefore, this thesis experimental design has mainly considered these three aspects:

✚ Clay: two different types of organoclay which contain different intercalants (organic modifiers)

✚ Matrix: different formulations based on EPON828 and several different curing agents

✚ Processing conditions: different parameters in the processing of epoxy nanocomposites:

- During stirring: different stirring temperatures, residence times of stirring or durations, stirring speeds, and also the use of high pressure device
- During curing: different curing temperature, chemistry of clay, and chemistry of hardener.

### 3.1.1. Epoxy

The resin selected for this study was Shell EPON 828 which is an undiluted clear liquid epoxy resin based on diglycidyl ether of bisphenol-A (DGEBA), a difunctional bisphenol A/epichlorohydrin derived. This is a very common difunctional epoxy resin. The structure and typical properties of epoxy EPON828 are shown in Figure 3.1 and Table 3.1. When cured with appropriate curing agents, very good mechanical, adhesive, dielectric and chemical resistance properties can be obtained.

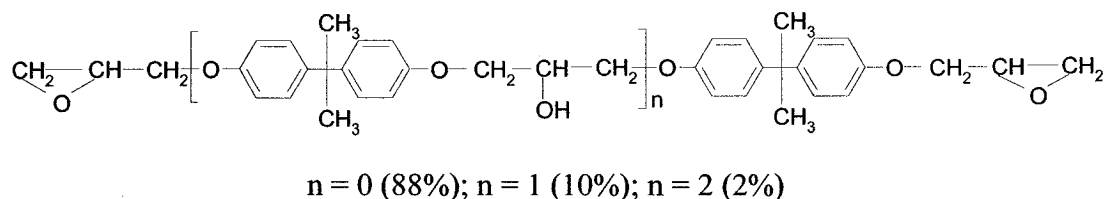


**Figure 3.1. Structure of epoxy EPON828**

**Table 3.1. Typical properties of EPON828 [77]**

Item	Property
<b>Visual appearance</b>	Clear liquid
<b>Epoxy equivalent weight (EEW) (g/eq)</b>	185-192
<b>Viscosity @ 25°C (cPs)</b>	10,000-16,000
<b>Density @ 25°C (g/cm<sup>3</sup>)</b>	1.16
<b>Comments</b>	Liquid DGEBA resin. Common epoxy resin
<b>Supplier</b>	Resolution Performance Products.

### 3.1.2. Curing agents (hardeners)

It is well known that depending on the type of curing agent and curing conditions, the structure of the crosslinked molecular network formed can vary significantly; this greatly influences the properties and the performance of the cured epoxy material. These factors can affect the formation of epoxy nanocomposites as well. Therefore, several kinds of hardeners were selected in this thesis including hardeners which are different in chemistry as well as similar in chemistry but different in molecular weight.

✦ Diethylenetriamine (DETA), which is a low molecular weight triamine and can form a rigid network with epoxy, was obtained from Sigma-Aldrich [79].

✦ Other hardeners were based on diamine-terminated polyoxypropylene diols (Jeffamine D series): Jeffamine D230 (D230), Jeffamine D400 (D400) and Jeffamine D2000 (D2000) having different average molecular weights of approximately 230, 400 and 2000, respectively. To generate epoxy systems with a wide range of  $T_g$  values, mixtures of Jeffamine D230 and Jeffamine D2000 at different ratios were also used. Jeffamine T403 (T403) is a propylene oxide based triamine with medium average molecular weight of 403. All of them were supplied by Huntsman [78].

✦ EPICURE 3046, an aliphatic amidoamine containing triethylene tetramine and tall oil fatty acid polyamide was obtained from Resolution Performance Products.. Tall oil fatty acid is produced by the fractional distillation of tall oil. It is predominately linear chain, 18 carbon mono- and di-unsaturated fatty acids, mainly oleic and linoleic acid [77].

✦ Boron Trifluoride monoethylamine -  $\text{BF}_3\text{NH}_2\text{CH}_2\text{CH}_3$  ( $\text{BF}_3$ ), which is a catalytic curing agent, was obtained from Sigma-Aldrich [79].

Structures and characteristics of curing agents are shown in Figure 3.2 and Table 3.2.

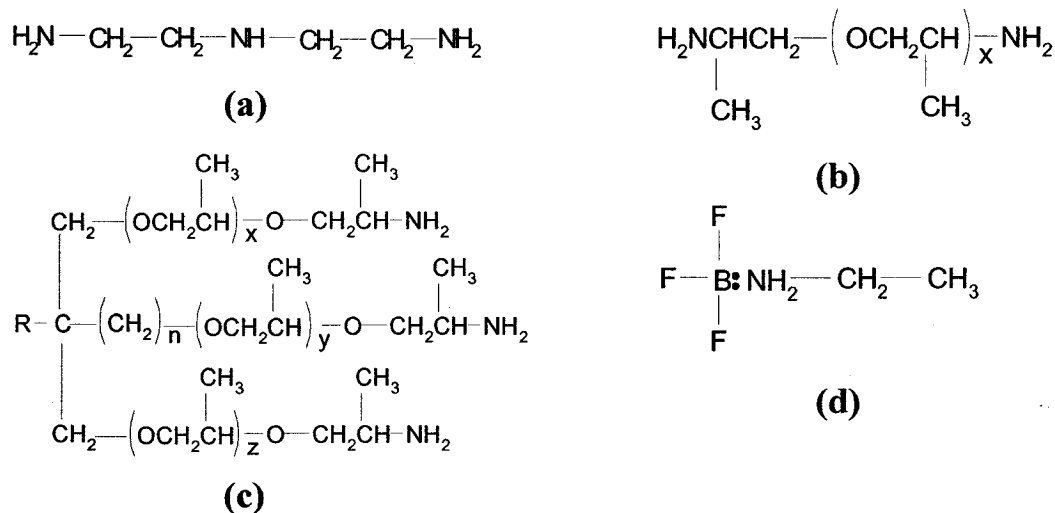


**Figure 3.2. Structure of (a) DETA, (b) Jeffamine D series, (c) Jeffamine T series, and (d) Boron trifluoride monoethylamine [77-79]**

**Table 3.2. Characteristic of curing agents [77-79]**

Curing agents	AHEW* (g/eq)	Viscosity @ 25°C (cps)	phr **	Supplier
Diethylenetriamine (DETA)	20	5.5-8.5	10.9	Sigma-Aldrich Co.
Boron Trifluoride (BF <sub>3</sub> )	28	-	3	
EPICURE 3046	90	120-280	35	Resolution Performance Products.
Jeffamine D series				Huntsman Corp.
Amine-terminated polyoxypropylene diols				
Jeffamine D230 (x = 2.6)	60	9	32	
Jeffamine D400 (x = 6.1)	115	21	55	
Jeffamine D2000 (x = 33.1)	514	247	270	
Jeffamine T series				
Trimethylolpropane; 2,2-bis (hydroxymethyl)-1-butanol based 5-6				
Jeffamine T403 (x + y + z = ~5.3), R = C <sub>2</sub> H <sub>5</sub> , n = 1	81	70	42	
*Amine hydrogen equivalent weight				
** Amount of hardener per 100 g of EPON828				

### 3.1.3. Clays

Currently many types of organoclay are commercially available on the market, mainly from Nanocor Inc [27], and Southern Clay Products Inc [49]. Since these two manufacturers have strong technology and have developed several types of organoclay that are more or less compatible with epoxy resins, the work on new surface treatments was not considered in this project.

The two kinds of organoclay used in this thesis, both based on natural montmorillonites but differing in intercalant chemistry, were Nanomer<sup>®</sup> I.30E (treated with a long-chain primary amine intercalant) and Cloisite<sup>®</sup> 30B (treated with a quaternary ammonium intercalant, less reactive with epoxy than the primary amine). For brevity, these clays are called clay or nanoclay in the following experiments. Henceforth the clays will be designated in shortened form as C30B and I30E, respectively. The technical details of these clays are summarized in Table 3.3.

**Table 3.3. Technical details of organoclays [27, 49]**

Nanoclay Item	C30B	I30E
<b>Organic modifier (intercalant)</b>	<b>MT2EtOH:</b> methyl, tallow, Bis-2-hydroxyethyl, quaternary ammonium $\begin{array}{c} \text{CH}_2\text{CH}_2\text{OH} \\   \\ \text{H}_3\text{C}-\text{N}^+-\text{T} \\   \\ \text{CH}_2\text{CH}_2\text{OH} \end{array}$	<b>ODA:</b> octadecyl ammonium $\begin{array}{c} \text{H} \\   \\ \text{H}-\text{N}^+-\text{H} \\   \\ \text{C}_{18}\text{H}_{37} \end{array}$
<b>Modifier concentration (meq/100 g clay)</b>	90	100
<b>Basal spacing <math>d_{001}</math> (Å)</b>	18.5	23.8
<b>Moisture content (%)</b>	< 2	< 2
<b>Specific gravity (g/cc)</b>	1.98	1.82
<b>Particles sizes in volume (<math>\mu\text{m}</math>)</b>	10% less than 2, 50% less than 6 and 90% less than 13	8 to 10
<b>Supplier</b>	Southern Clay Products Inc.	Nanocor Inc.
<i>T: Tallow (~65% C<sub>18</sub>; ~30% C<sub>16</sub>; ~5% C<sub>14</sub>)</i>		

## 3.2. Experimental design

### 3.2.1. Study parameters

In order to fulfill the objectives described in Chapter 1, the experimental matrix were designed as described in Table 3.4.



**Table 3.4. Study parameters**

Objectives		Variables
Effect of the formation of ENC on the clay dispersion and intercalation/exfoliation	Effect of mixing	<p>Epoxy: EPON 828, clay: C30B, hardener: D230</p> <p>Two main parameters:</p> <p><b>Stirring speed:</b> no speed, low speed (<b>conventional mixer</b>-1000 rpm), high speed (<b>homogenizer at 9500, 17500 and 24000 rpm</b>) and <b>microfluidizer [107]</b> at 15000 psi (103.42 MPa)</p> <p><b>Stirring temperature and time:</b> room temperature, high temperature (120°C), residence time (2, 4, 10, 20, 30, 45 and 60 min)</p>
	Effect of curing	<p>Three main parameters:</p> <p><b>Curing temperature:</b> room temperature, 60, 90 and 120°C</p> <p><b>Chemistry of clays:</b> 2 types of clay: C30B and I30E</p> <p><b>Chemistry of hardeners:</b> types of hardeners: DETA, D230, D400, T403 and D2000.</p>
Effect of clays and hardeners on curing process of ENC	Effect of clay	Epoxy: EPON 828, clay: <b>C30B</b> and <b>I30E</b> , hardener: Epicure 3046
	Effect of hardener	Epoxy: EPON 828, clay: C30B, hardeners: <b>DETA, D230, T403, D400 and D2000</b>
Relationships between formulation, morphology, processing and the properties of ENC	Effect of clay	Epoxy: EPON 828, clay: <b>C30B</b> and <b>I30E</b> , hardener: EPICURE 3046
	Effect of hardener	<p>Epoxy: EPON 828, clay: C30B, hardeners: <b>DETA, T403 and D2000</b></p> <p>Epoxy: EPON 828, clay: C30B, hardeners: <b>D230, D2000</b> and their mixtures</p>

*More details can be found in the next chapters*

### **3.2.2. Experimental setup**

First epoxy and clay were mixed together by using different devices including no mechanical stirring and different speeds of stirring. Then the clay dispersion in the epoxy-clay suspension (in the absence of hardener) was studied by field emission gun scanning electron microscopy (FEGSEM), X-ray diffraction (XRD), rheological properties by viscometer, and curing behavior by differential scanning calorimetry (DSC) and Fourier transform infrared spectroscopy (FTIR). The curing process of epoxy and epoxy nanocomposites was studied by DSC right after mixing the epoxy-clay with hardener. Then, samples for various tests including XRD, FEGSEM, transmission electron microscopy (TEM), DSC, thermogravimetric analysis (TGA), limiting oxygen index (LOI), dynamic mechanical analysis (DMA), tensile, flexural, compression, impact, surface hardness and fracture toughness were molded. Finally, tests on samples were performed to obtain properties. The experimental procedure is as shown in Figure 3.3.

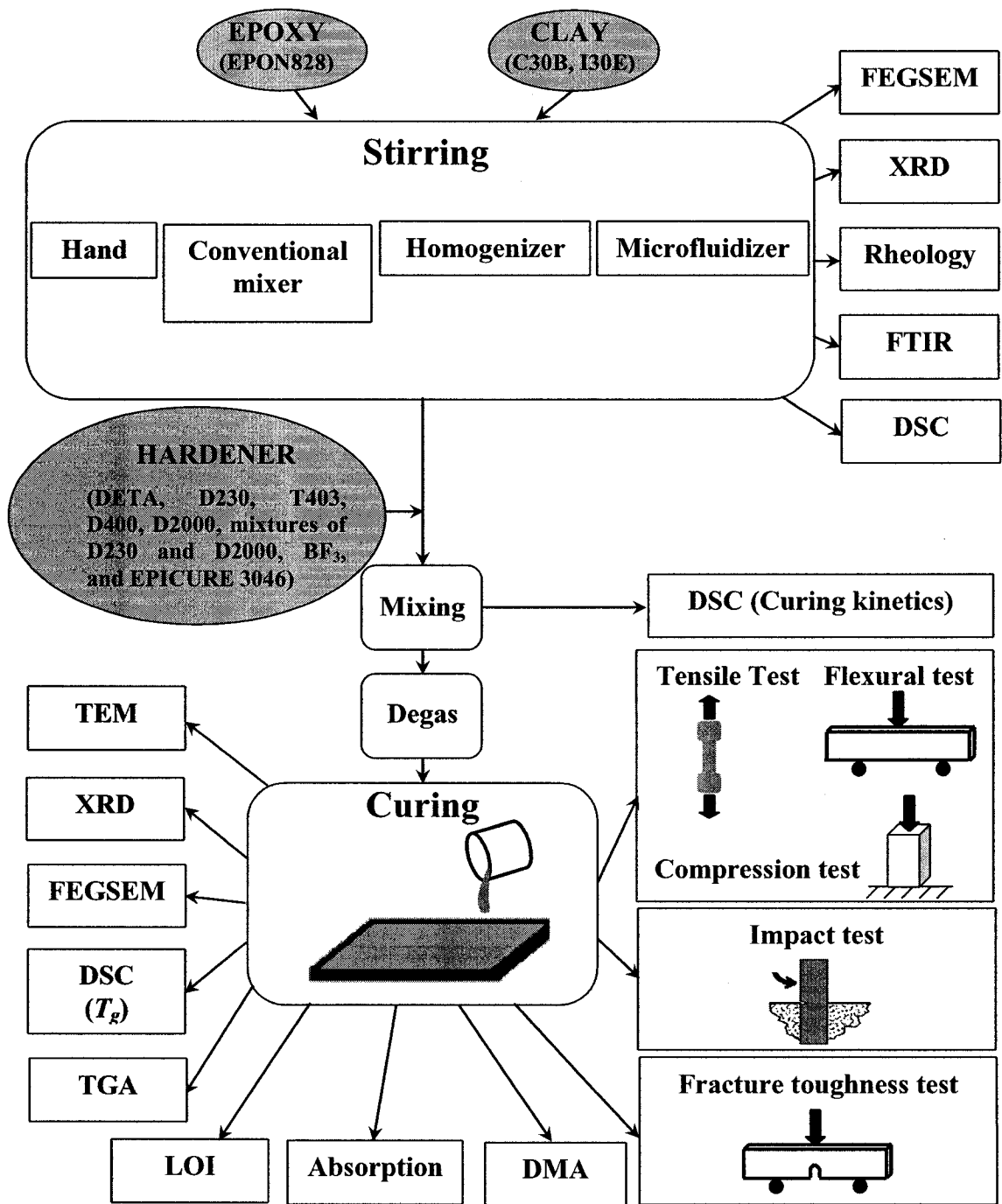


Figure 3.3. Experimental procedure

### 3.3. Stirring methods

Since the stirring temperature and stirring speed may affect the dispersion of organoclay in the epoxy, different methods for stirring the epoxy and clay to generate different shear forces were chosen for this study as shown in Table 3.5.

**Table 3.5. Stirring methods**

<b>Name of stirring method</b>	<b>Equipment</b>
<b>Rm</b>	Room temperature with hand stirring
<b>Tm</b>	High temperature with hand stirring
<b>TM</b>	High temperature and medium speed stirring (mechanical stirrer)
<b>RS</b>	Room temperature and high speed stirring (homogenizer)
<b>TS</b>	High temperature and high speed stirring (homogenizer)
<b>HP</b>	High-pressure (microfluidizer)
<i>The details about stirring conditions such as duration, speed etc. will be described shortly</i>	

#### 3.3.1. Room temperature and hand stirring (Rm)

To separate the effect of temperature and mechanical stirring on the dispersion and intercalation/exfoliation of clay in epoxy resin, a room temperature with hand stirring only was chosen. Organoclay was added into epoxy and stirred by hand at room temperature (RT) for a few minutes to break down the lumps, then kept at RT for 1 hour.

### **3.3.2. High temperature and hand stirring (Tm)**

This method was chosen to understand the effect of temperature on the dispersion of clay in epoxy resin. Organoclay was added into epoxy and stirred as in section 3.3.1 but at 120°C, and then kept in the oven at 120°C for 1 hour.

### **3.3.3. High temperature and medium speed stirring method (TM)**

Organoclay was directly added into epoxy, the mixture was mechanically stirred at about 1000 rpm at 120°C for 1 hour with a mechanical mixer Lightnin (Figure 3.4).

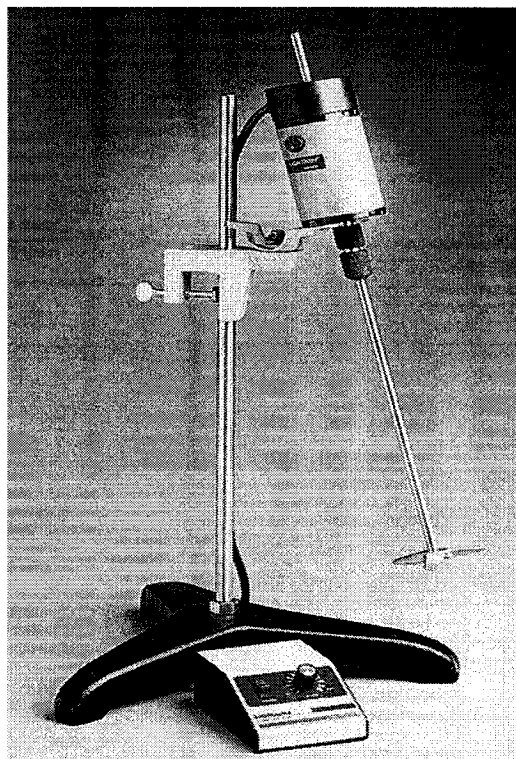


**Figure 3.4. Lightnin mixer (from CONCOM lab)**

### 3.3.4. High speed stirring method

To avoid using solvent, high speed stirring was introduced in this thesis work. Nanoclay was dispersed in epoxy in a high-speed Homogenizer system (Figure 3.5a). The key component is the rotor-stator generator. Shielded in a 316 stainless steel shaft, the rotor acts as a centrifugal pump to re-circulate the liquid and suspended solids through the generator (Figure 3.5b), where shear, impact, collision, and cavitation provide rapid homogenization. It features a powerful force of mixing from a 6500 rpm to 24000 rpm variable-speed motor. Due to the high rotation speed of the rotor, the medium to be processed is automatically drawn axially into the dispersion head and then forced radially through the slots in the rotor/stator arrangement. The high accelerations acting on the material produce extremely strong shear and thrust forces. In addition, high turbulence occurs in the shear gap between rotor and stator, which provides optimum mixing suspension. The dispersion effectiveness is heavily dependent on the product of the shear gradient and the residence time of particles in the shear zone. The rotor/stator principle can be seen in Figure 3.5c.

Two dispersion routes were used: one is that organoclay was dispersed with homogenizer at room temperature (**RS**) for 2, 4, 10, 20, 30, 45 and 60 minutes at 24000 rpm; the other is that organoclay was dispersed with homogenizer at a high temperature of 120°C or 180°C (**TS**). The organoclay was added into epoxy for swelled at 120°C then dispersed at this temperature with a homogenizer at 9500, 17500 and 24000 rpm for 2, 4, 10, 20, 30, 45 and 60 minutes. In another approach, the organoclay was added into epoxy for swelling at 180°C then dispersed with a homogenizer at 24000 rpm for 2, 4, 10, 20, 30,

45 and 60 minutes. All of the samples after preparation were degassed in a vacuum oven at room temperature for 30 minutes to remove the bubbles.

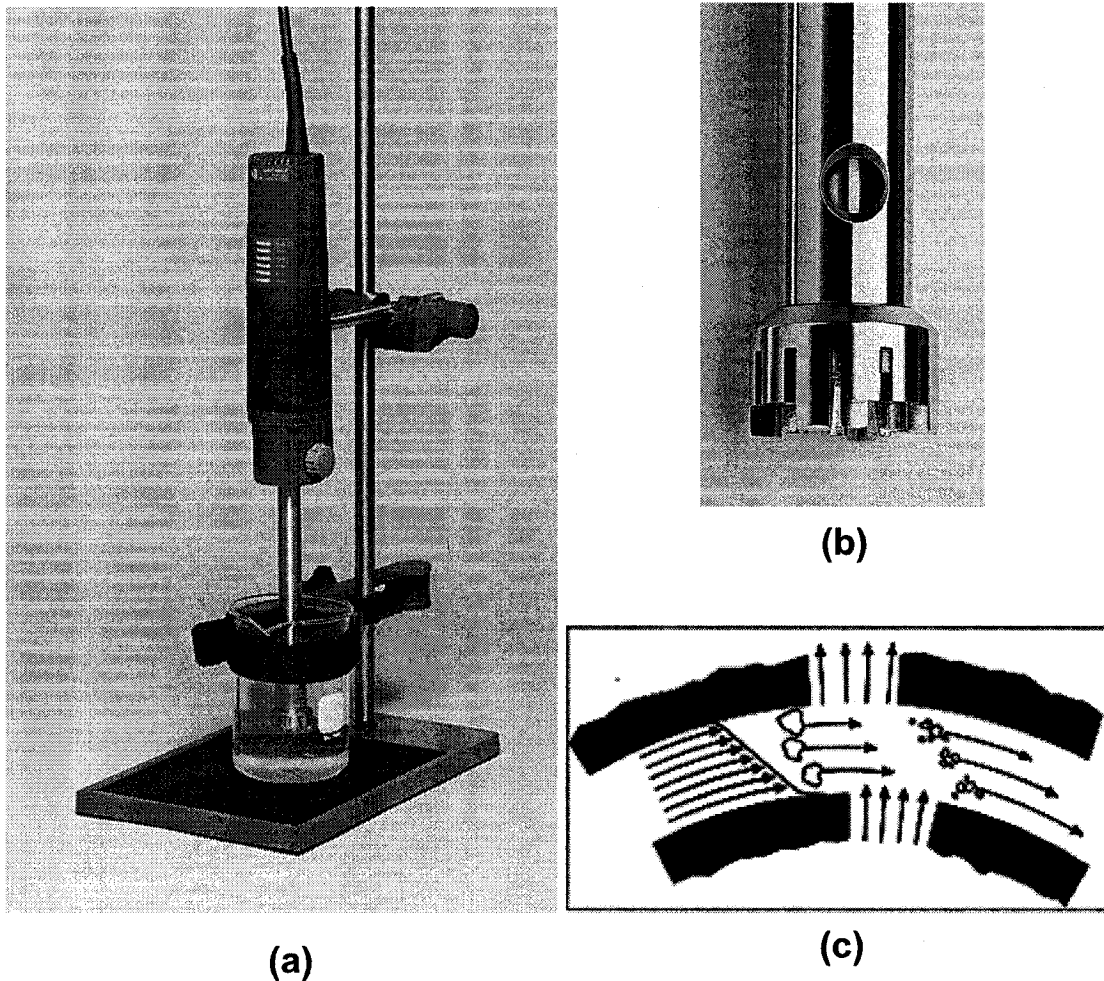


**Figure 3.5. Photos of (a) EW-04719-00 High-Speed Homogenizer System; 115 VAC, 50/60 Hz, (b) large-Capacity Rotor-Stator generators, (c) the rotor/stator principle of high speed stirring (from CONCOM lab)**

### **3.3.5. High pressure mixing method (HP)**

This method was developed by Hoa et al [108]. Nanoclay was dispersed in an organic solvent with the Microfluidizer Processor shown in Figure 3.6. With constant process

pressures ranging from 2500 psi (17.24 MPa) to 25000 psi (172.37 MPa), the microfluidizer maximizes the energy-per-unit fluid volume, resulting in uniform submicron particle and droplet sizes. The basic principle of this machine is based on particle-collision technology: the bombardment of a colloid system or fluid stream against itself inside an interaction chamber of fixed geometry, at high energy. The size of particles is reduced by: crushing forces of the particles against the wall of the chamber; shear forces on the particles within the interaction chamber; crushing forces of the particles hitting themselves; and cavitation forces due to extreme pressure changes in the materials stream.

Due to the high viscosity of epoxy resins at room temperature, it is impossible to directly disperse organoclays in epoxy resins with the Microfluidizer. Organoclays were first dispersed in acetone (about 8% of organoclay in acetone) to form a suspension with the HP method, and then the suspension was added into the epoxy resins.

The exact concentration of clay was measured by drying the solution for 8 hours at 100°C. The desired amount of paste of organoclay and acetone was added to epoxy resins and then the mixture was mixed by hand at room temperature. When the epoxy was visibly dispersed, the mixture was mechanically stirred at 1000 rpm in a fume hood at room temperature for 30 minutes, followed by slow heating to 80°C for 1 hour. Finally, the mixture was degassed under vacuum at 95°C for 30 minutes. There is a large amount of solvent used in this method. Moreover, the size of clay particles before mixing also needs to be considered.



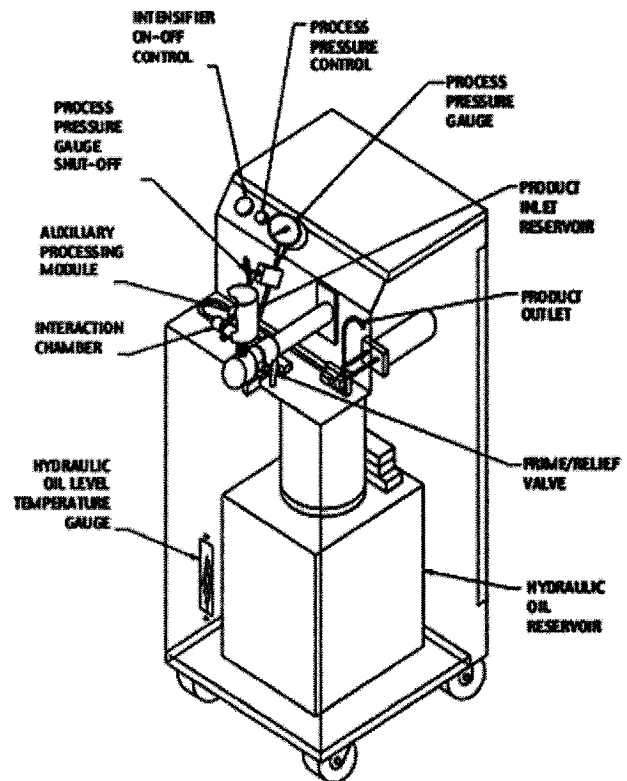
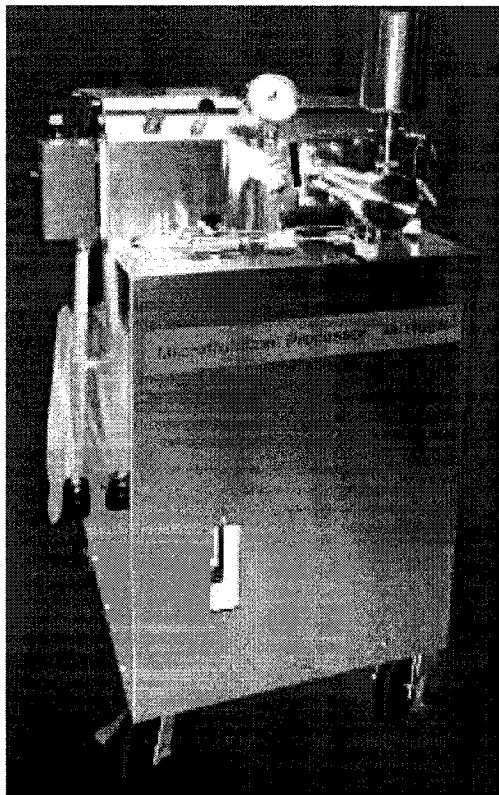


Figure 3.6. M-110EH microfluidizer processor (from CONCOM lab)

### 3.4. Curing of ENCs

The procedure is as follows:

- Add an exact amount of hardener (calculated according to Table 3.2) into epoxy or epoxy-clay mixtures. The amount of materials was estimated based on the required quantity of samples for the tests.
- Mix slowly (to avoid air entrapment in the mixture) the mixture of epoxy or epoxy-clay with hardener at room temperature for 5 minutes using a mechanical stirrer.
- Degas to remove the bubbles in a vacuum oven at 28 mmHg and room temperature for maximum 30 minutes.

➤ Pour the mixture into the either in the non- or pre-heated molds, depending on the requirement. The preheated mold helps to remove the bubbles trapped between the mold and the liquid during casting. Aluminum mold was used for tensile, flexural, impact, DMA, LOI tests. Teflon coated polypropylene molds were used for the XRD test. Silicone molds were used for compression and fracture tests. More details can be found in Section 3.5.

➤ Cure the samples: samples were cured in different ways depending on the tests

For the XRD test: epoxy and ENC were cured at room temperature for 2 days or 60°C, 90°C and 120°C for 2 hours, with subsequent post cure at 140° for 2 hours in all cases.

For the other tests: epoxy and ENC were cured at 120°C for 2 hours, with subsequent post cure at 140° for 2 hours in all cases. Samples in the form of 3 mm thin plaque were prepared for various tests including FEGSEM, DSC, tensile, flexural, impact, fracture toughness, DMA, TGA, LOI, water absorption and solvent resistance.

### **3.5. ENCs characterization**

Various methods have been used to characterize the dispersion, intercalation/exfoliation, physical and mechanical properties of epoxy and its ENCs.

#### **3.5.1. Dispersion behavior**

As described earlier (Chapter 2), the dispersion behavior of nanoclays in the matrix determines the nanocomposite structure, which can be either microcomposites (conventional composites), intercalated or exfoliated nanocomposites. Therefore, it is very important to estimate the level of clay dispersion in epoxy matrix. From literature survey, XRD, AFM, SEM and TEM are the most popular tools for this purpose. In this

project XRD, SEM and TEM were used. XRD can detect the degree of dispersion via the gallery distance; while SEM can illustrate a direct image of dispersion of clay at the micro-level and fracture mechanic; and TEM can provide a direct image of the dispersion of clay at the nano-level.

### 3.5.1.1. X-ray diffraction

XRD is used to identify intercalated structures. In such nanocomposites, the repetitive multilayer structure is well preserved, allowing the interlayer spacing to be determined. The intercalation of the epoxy and hardener molecules usually increases the interlayer spacing, which leads to a shift of the diffraction peak towards lower angle values. Figure 3.7 shows the diffraction from two scattering planes (i.e. two consecutive clay layers or other crystallographic planes of the layers themselves) that are separated by a distance  $d$  (i.e. interlamellar spacing or  $d$ -spacing) and intercept X-rays of wavelength  $\lambda$ , at the incident angle  $\theta$  [109]. The  $2\theta$  value is the angle between the diffracted and incoming X-ray waves. The wave normals connect points of identical phase for incident and diffracted waves.

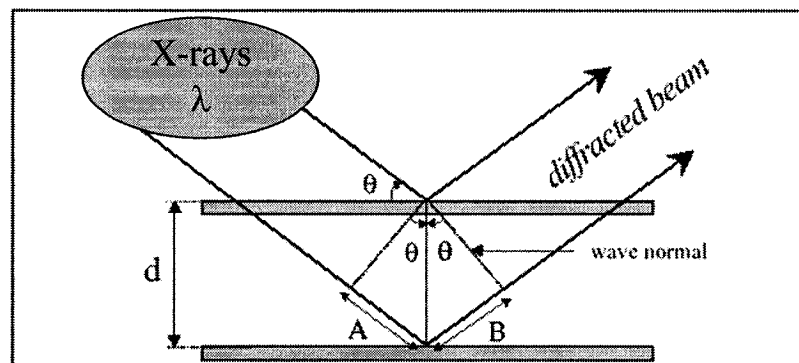


Figure 3.7. Principle of X-ray diffraction [4].

The distance  $(A+B)$  must equal a whole number of wavelengths (i.e.  $n\lambda$ , where  $n$  is an integer) for total constructive reinforcement to occur between the scattering from these planes. Since the direction of  $d$  is normal to the planes, and the wave normal is normal to the wavelets, then the angles opposite A and B are also  $\theta$ . Thus,  $\sin\theta = A/d = B/d$  so that  $(A+B) = 2d\sin\theta$ . Thus, a constructive interference occurs when:

$$n\lambda = 2d_{00n} \sin\theta \quad (3.1)$$

Equation 3.1 is known as the Bragg's Law. The integer  $n$  refers to the degree of the diffraction. Since  $\lambda$  is a constant, after the target tube is selected and  $\theta$  can be controlled and recorded,  $d$  can be calculated from the above equation.

The specimens for X-ray diffraction were prepared by molding in clean Teflon-coated polypropylene molds in order to assure a flat surface and optimize the accuracy for the comparison of the X-ray results. Since the intensity of the XRD peaks is sensitive to the surface, in order to obtain more quantitative results, the specimens should not be deformed or have bubbles and defects. Teflon coated polypropylene molds for XRD samples are shown in Figure 3.8.

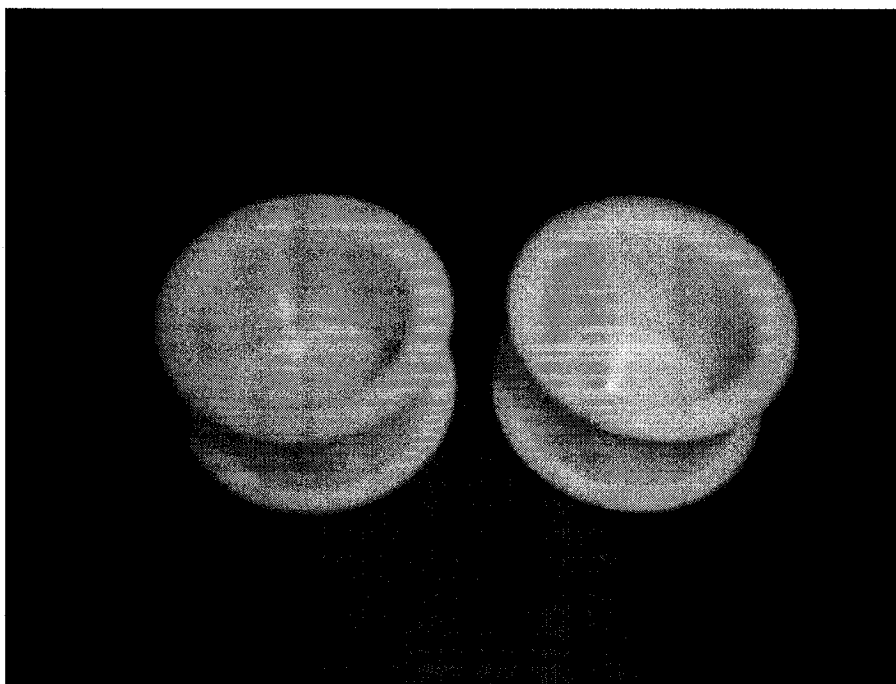


**Figure 3.8. Teflon coated polypropylene mold for XRD samples**

To evaluate the dispersion of the nanoclay in the polymer matrix, X-ray diffraction patterns were obtained from the surface of the samples with a Bruker Discover 8 powder X-ray diffractometer with CuK $\alpha$  radiation (Figure 3.9). The experiments were conducted on the exposed surface of specimens prepared by casting. The scanning uses radiation from a copper target tube (CuK $\alpha$  radiation,  $\lambda= 1.54250 \text{ \AA}$ ) with the  $2\theta$  scan range from  $0.8^\circ$  to  $10^\circ$ . The scanning speed was  $0.67^\circ.\text{min}^{-1}$ . To assure the accuracy, the measurement was performed twice for all samples.

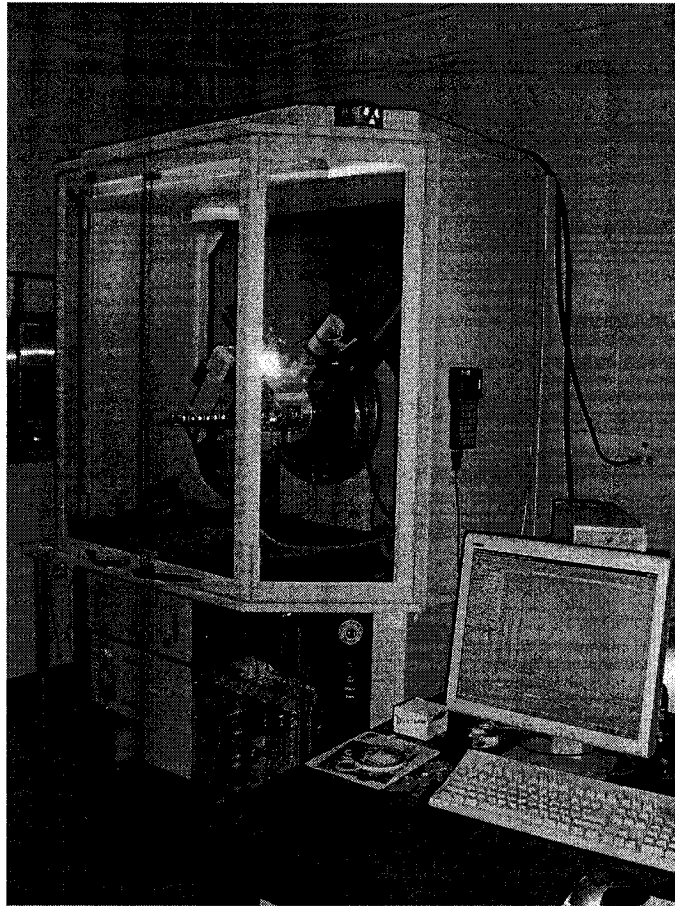


**Figure 3.9. A Bruker Discover 8 powder X-ray diffractometer (from IMI lab)**

### **3.5.1.2. Scanning electron microscopy (SEM)**

The SEM has many advantages over traditional microscopes. It has a large depth of field, which allows more of a specimen to be in focus at one time. The SEM also has much higher resolution compared to traditional microscopes, so closely spaced specimens can be magnified at much higher levels. SEM is very useful in the identification of textures and shapes of mineral grain aggregates. Figure 3.10 shows the schematic drawing of SEM [110]. The definition or resolution of the image is of the order of  $0.01\mu\text{m}$  and is much higher than in traditional microscopes.

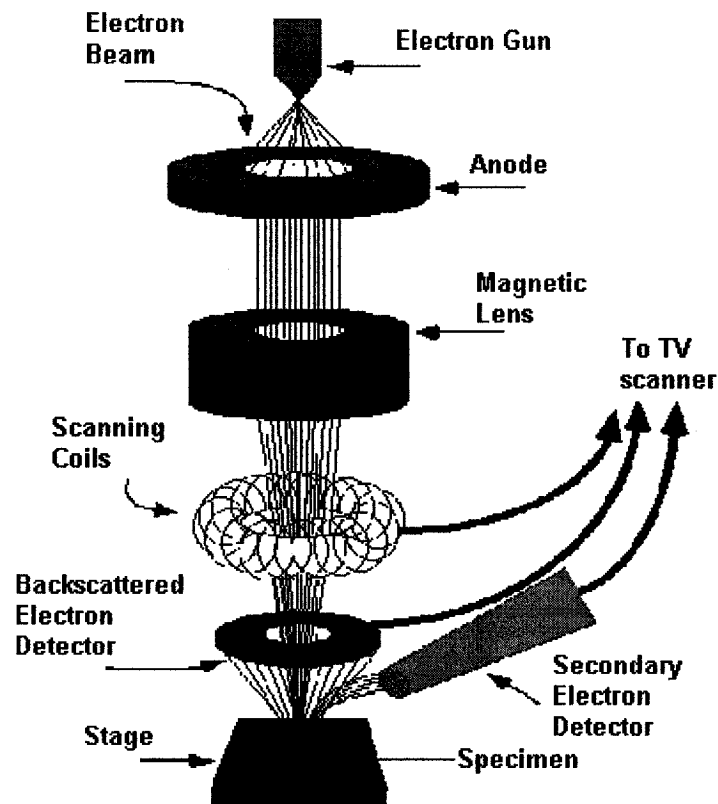


**Figure 3.10. Scheme and structure of SEM (Diagram courtesy of Iowa State University SEM homepage) [110]**

Samples were prepared with a Leica EMFCS cryo-ultramicrotome or came from the fracture surface of tensile test (carefully cut around 8 mm height from the failed surface). Figure 3.11 shows a photo of the microtome machine. Samples also need to be made conductive by covering the sample with a thin layer of conductive material which is usually platinum. This was done by using an EMITECH K575X high resolution sputter coater in which an electric field and argon gas are applied. The sample is placed in a small vacuum chamber. Argon gas and an electric field cause electrons to be removed from the argon, making the atoms positively charged. The argon ions then become attracted to a negatively charged platinum foil. The argon ions knock platinum atoms

from the surface of the platinum foil. Figure 3.12 shows a photo of the EMITECH K575X high resolution sputter coater.

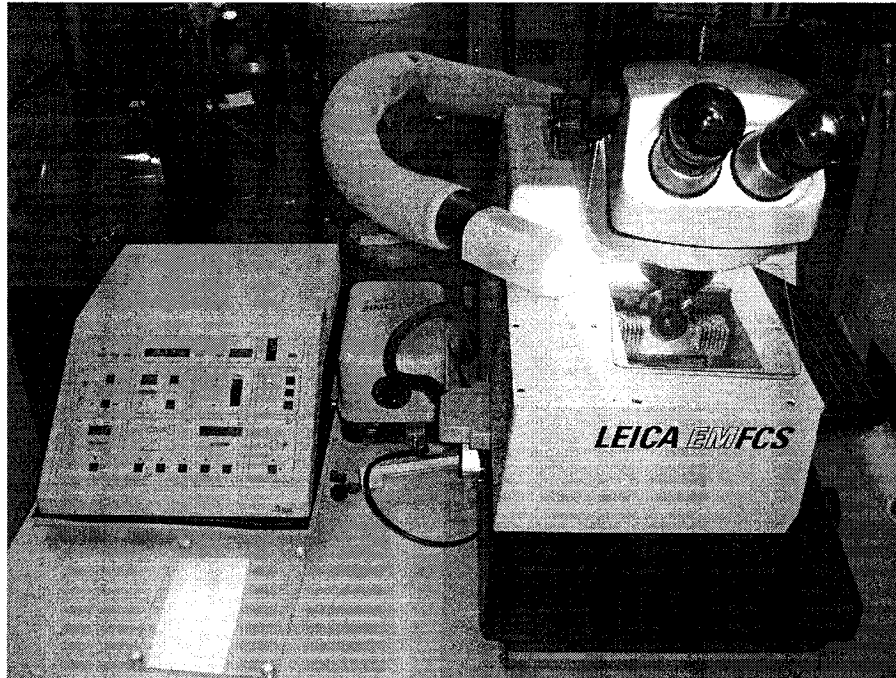


**Figure 3.11. The LEICA EMFCS microtome cutter (from IMI lab)**

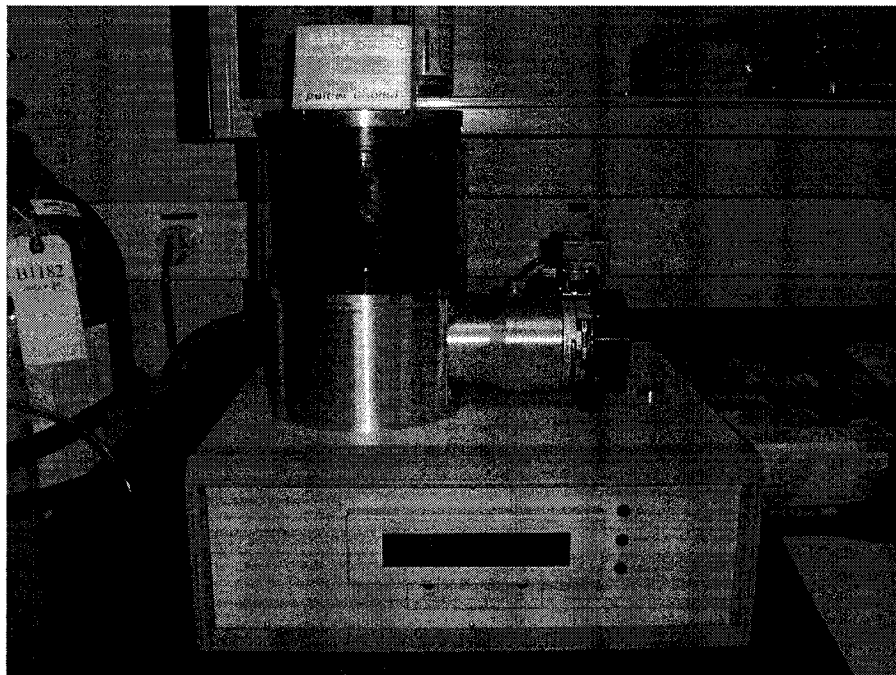


**Figure 3.12. EMITECH K575X high resolution sputter coater (from IMI lab)**



A Hitachi-S4700 field emission gun scanning electron microscope (FEGSEM) was employed to evaluate the traits of dispersion behavior and fracture surface. Figure 3.13 shows a photo of the FEGSEM machine. All water must be removed from the samples because the water would vaporize in vacuum.

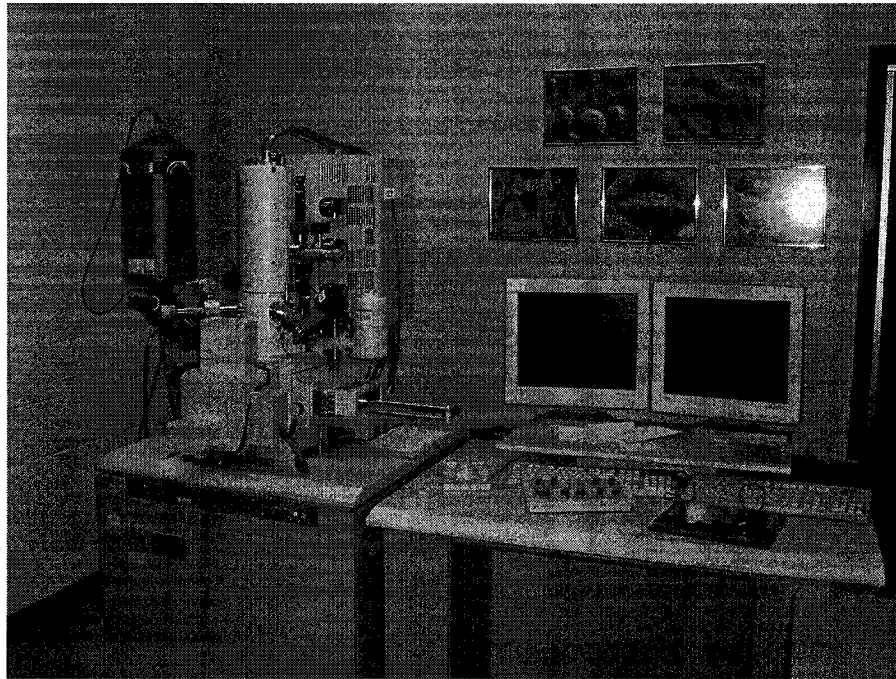


**Figure 3.13. The Hitachi-S4700 FEGSEM (from IMI lab)**

### **3.5.1.3. Transmission electron microscopy (TEM)**

TEM is widely used to characterize polymer-nanocomposites. In transmission electron microscopy, image formation is due to the scattering of electrons as the electron beam passes through the sample. The thickness of TEM specimens should be on the order of 100nm. If the specimen is thin enough to form an image in the TEM, we can assume that the primary electrons that enter the top of the specimen emerge from the bottom. If the objective aperture is centered about the optical axis, then in the absence of a specimen a bright background can be seen. This is known as bright field imaging. Regions of the

specimens which are thicker or higher density will scatter the electron beam more strongly and will appear darker in the image (less and less electrons transmitted). This effect is shown schematically in Figure 3.14. In the thin area (on the left) only a few electrons are scattered and approximately 94% of the incident electrons are un-deviated while in the thicker region of the same material (at the centre) more electrons are scattered and only about 86% remain in the un-deviated beam. For a region of the same thickness but higher density (on the right) even more scattering takes place and only about 74% of the incident electrons pass through the specimen without being scattered [111].

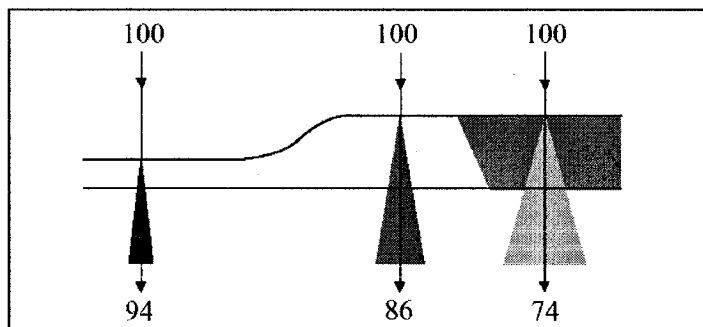


**Figure 3.14. The scattering of electrons from different regions of a TEM specimen**

[111]

A Hitachi H9000 TEM operated at an acceleration voltage of 300 kV was used to observe the dispersion of clay in epoxy matrix at the nano-level. Figure 3.15 shows a photos of the TEM machine. The ultra-thin (50 to 80nm) sections of nanocomposite samples were prepared with a Leica EMFCS cryo-ultramicrotome and supported on a copper 200-mesh grid.

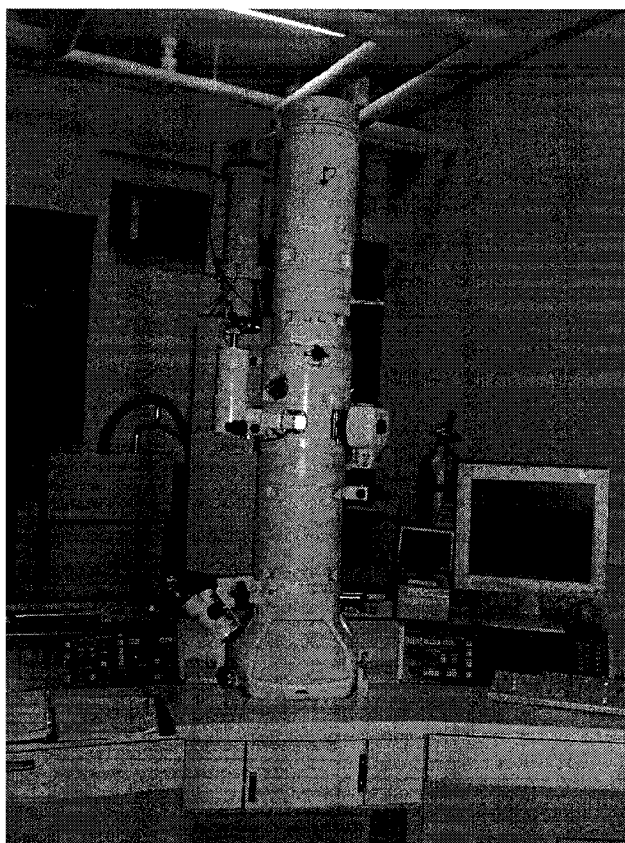


**Figure 3.15. A Hitachi H9000 TEM (from McGill University lab)**

### **3.5.2. Fourier transform infrared spectroscopy (FTIR) analysis**

FTIR analysis was performed at room temperature (approx. 25°C) on a Nicolet Magna 860 Fourier transform instrument at a resolution of 4  $\text{cm}^{-1}$ . Samples for FTIR can be prepared in a number of ways. For liquid samples, the easiest way is to place one drop of sample between two plates of potassium bromide (KBr) or sodium chloride (NaCl). They are transparent to infrared light. The drop forms a thin film between the plates. Solid samples can be milled with potassium bromide to form a very fine powder. This powder is then compressed into a thin pellet which can be analyzed. Alternatively, solid samples can be dissolved in a solvent such as methylene chloride, and the solution placed onto a

single salt plate. The solvent is then evaporated off, leaving a thin film of the original material on the plate. This is called a cast film, and is frequently used for polymer identification. Solutions can also be analyzed in a liquid cell. This is a small container made from KBr or NaCl (or other IR-transparent material) which can be filled with liquid. This creates a longer path length for the sample, which leads to increased sensitivity. Sampling methods include making a mull of a powder with hydrocarbon oil (Nujol) or pyrolyzing insoluble polymers and using the distilled pyrolyzate to cast a film. Films can be placed in an Attenuated Total Reflectance cell and gases in gas cells. The Nicolet Magna 860 Fourier transform instrument is shown in Figure 3.16.

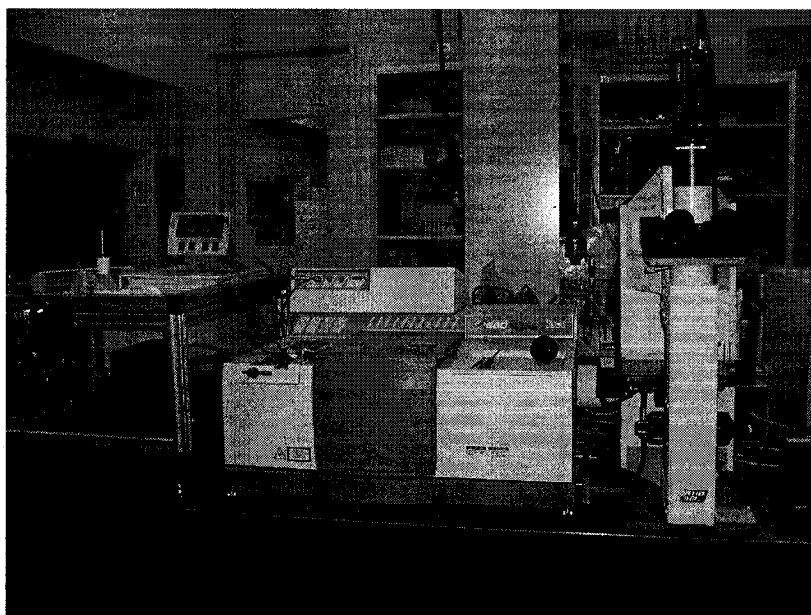


**Figure 3.16. Nicolet Magna 860 FTIR instrument (from IMI lab)**

### **3.5.3. Rheological properties**

Rheological measurements were performed on a Brookfield CAP2000+ viscometer for epoxy and epoxy-organoclay suspensions using cone and plate geometry and a Brookfield viscometer Model DV-II+ with Thermalseal accessory as shown in Figures

3.17 and 3.18. The software used is Capcalc V.20. After the desired temperature was achieved, another 5 minutes was allowed to reach the balance between the sample and spindle.

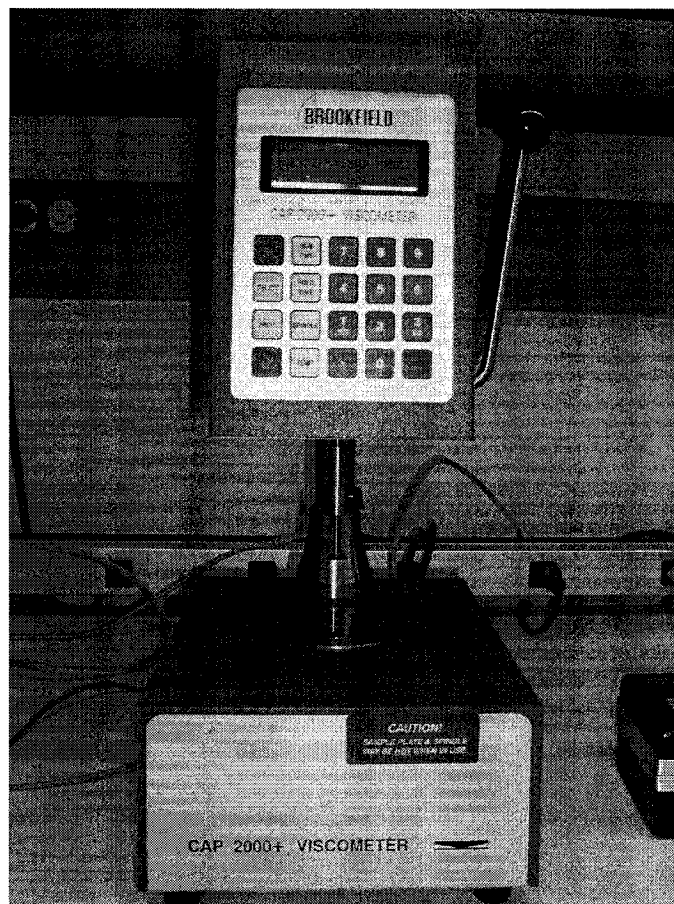


**Figure 3.17. Brookfield CAP2000+ viscometer (from CONCOM lab)**

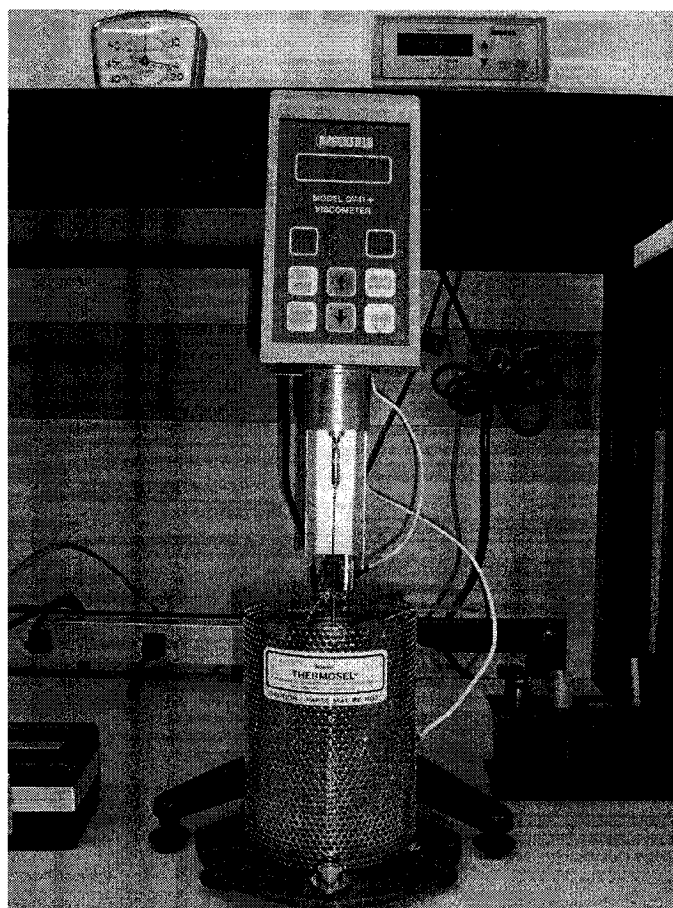


**Figure 3.18. Brookfield viscometer Model DV-II+ (from CONCOM lab)**

### **3.5.4. Thermal properties**

#### **3.5.4.1. Differential scanning calorimetry (DSC)**

DSC is a technique used to determine the temperature and heat flow associated with physical and/or chemical phenomena that can release or absorb heat as a function of time and temperature. It also provides quantitative and qualitative data on endothermic (heat absorption) and exothermic (heat evolution) processes of materials during physical transitions and chemical processes that are caused by phase changes, melting, oxidation, and other heat-related changes. From this information, one can determine the important

transition temperatures, the degree of crystallization, heat capacity, heat of formation and sample purity.

The DSC data were obtained on a Perkin-Elmer Pyris 1 instrument (as shown in Figure 3.19). The samples were heated from 30°C to 250°C (dynamic scan) at five different heating rates (2.5, 5, 10, 15, and 20°C·min<sup>-1</sup>) using nitrogen atmosphere to follow the heat evolution due to the chemical reaction occurring in this temperature range. The cured sample was then cooled to 30°C at 20°C·min<sup>-1</sup> to minimize the enthalpy relaxation in the second heating scan. Finally, the sample was reheated to 250°C at 20°C·min<sup>-1</sup> in order to determine the glass transition temperature ( $T_g$ ) and to confirm the absence of any residual curing. Cryogenic mode with helium atmosphere was used for low  $T_g$  systems.



**Figure 3.19. Perkin-Elmer instruments -DSC Pyris 1 (from IMI lab)**

### 3.5.4.2. Thermogravimetric analysis (TGA)

TGA measures weight changes in a material as a function of temperature (or time) under a controlled atmosphere. Its principal uses include measurement of a material's thermal stability and composition. TGA instruments are routinely used in all phases of research, quality control and production operations.

The TGA data were obtained on a TA-Q50 instrument using nitrogen atmosphere. The samples were heated from 30°C to 1000°C (dynamic scan) at a heating rate of 20°C·min<sup>-1</sup> or at 200°C for 12 hours (isothermal scan) to follow weight changes in a material as a function of temperature (or time) under a controlled nitrogen atmosphere. A photo of the TA-Q50 instrument is shown in Figure 3.20.



**Figure 3.20. TA instruments –Q50 (from CONCOM lab)**



### 3.5.4.3. Limiting oxygen index (LOI)

The advanced limiting oxygen index chamber accurately determines the relative flammability of plastics and other materials, by measuring the minimum oxygen concentration that will support combustion according to ASTM D2863-97 [112] and ISO 4589 specifications. The test specimens are burned in a precisely controlled atmosphere of nitrogen and oxygen. The operator adjusts the supply gases and uses the flow meter readings to calculate the oxygen index.

A photo of the Qualitest LOI analyzer is shown in Figure 3.21. The LOI test apparatus consists of a glass tube 100 mm in diameter and 500 mm in height. A specimen with a height of 80 mm and a width of 10 mm (cut from a plate that was molded in an aluminum mold as shown in Figure 3.22) is supported inside the glass tube. A gas mixture of oxygen and nitrogen is supplied at the bottom of the tube and a small candle-like flame is applied to the top of the specimen in an attempt to ignite it. The objective is to find the minimum oxygen concentration in nitrogen that will result in sustained combustion for at least 3 minutes or excessive flame propagation down the specimen. The oxygen concentration of the mixture used in each successive test is increased or reduced by a small amount until the required concentration is reached. Results are expressed as Equation 3.2

$$LOI = \left[ \frac{O_2}{O_2 + N_2} \right] \times 100 \quad (3.2)$$

where  $O_2$  and  $N_2$  are respectively the minimum oxygen concentration in the inflow gases required to pass the “minimum burning length” criterion and the corresponding nitrogen concentration in the inflow gases.

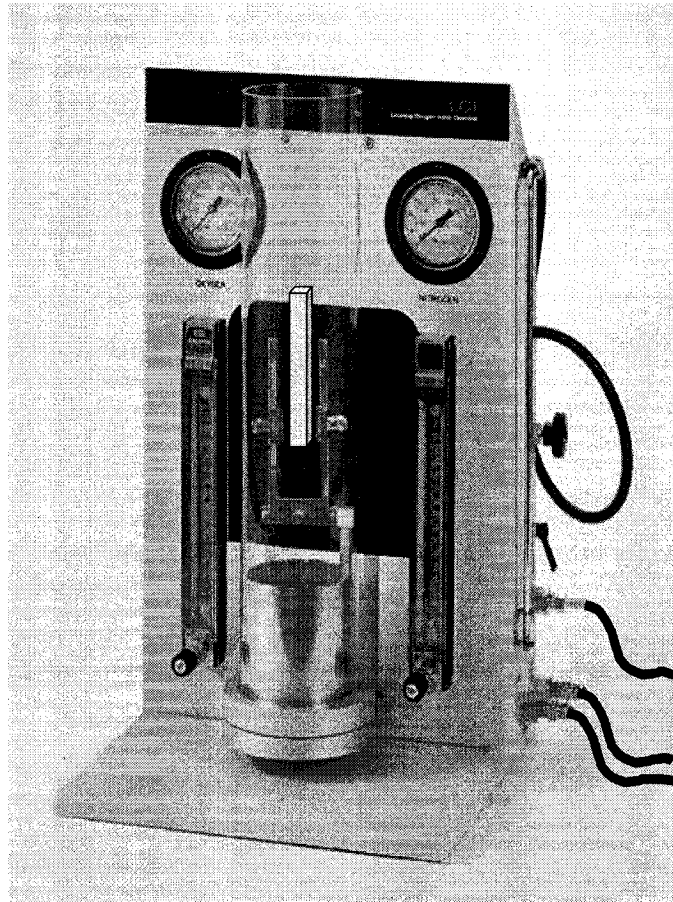


**Figure 3.21. Qualitest LOI chamber (from CONCOM lab)**

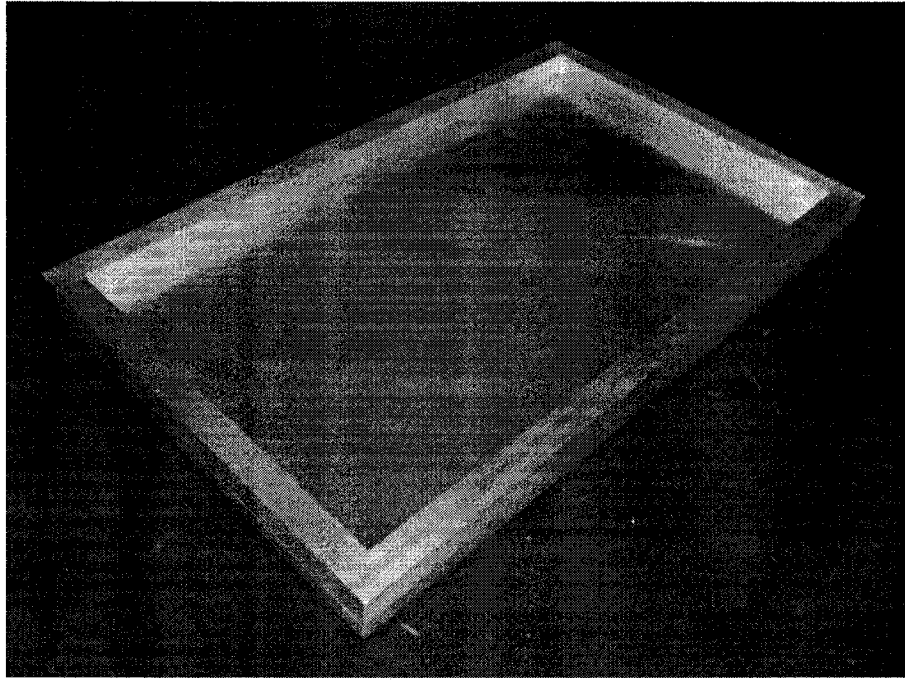


**Figure 3.22. Aluminum mold for casting samples (Note that this aluminum mold was used to prepare plates with sizes of 285x165x3 mm. Samples for tensile, flexural, impact and DMA testing were cut from the plates)**

### **3.5.5. Mechanical properties**

#### **3.5.5.1. Dynamic mechanical analysis (DMA)**

DMA characterizes the viscoelastic properties of materials and simultaneously determines the elastic modulus (stiffness) and energy absorbing (toughness) characteristics of a material as a function of temperature, frequency or time as well. To measure viscoelastic properties, DMA applies a sinusoidal force to a sample then measures the resulting sample deformation or strain. The sample strain response lags behind the input stress wave with respect to time and the lag is known as the phase angle. The ratio of the dynamic stress to the dynamic strain provides the complex modulus that includes both the storage modulus ( $E'$ ) and the loss modulus ( $E''$ ). The  $E'$ , which is the

elastic component, refers to the ability of a material to store energy and represents the change in stiffness of the sample with regards to temperature. The  $E''$ , which is the viscous component, reflects the damping or energy absorbing characteristics which are related to molecular motions [113]. The tangent of phase difference is another common parameter that provides information on the relationship between the elastic and inelastic component. These parameters can be calculated as a function of time, temperature, frequency, or amplitude (stress or strain) depending on the application. DMA can detect coefficient of expansion, glass transition temperature ( $T_g$ ), softening temperatures, phase transitions and sintering. The results of DMA tests include a large amount of information on the sample. The modulus value below the glass transition can indicate levels of molecular orientation and crystallinity. Transitions initialization can be related to the polymer's structure and may be particularly useful where a multiple component composite is under investigation. Dynamic mechanical methods are most sensitive for measuring the glass transition, which is one of the key properties of a polymer from both the structural and processing viewpoint. Figure 3.23 shows a schematic of DMA [114].

A Du Pont 983 DMA (TA instruments) was employed in this experiment. Figure 3.24 shows the exterior of the machine. Samples with dimensions  $L/T > 10$  ( $L$  is the length and  $T$  is the thickness and  $T$  is between 1.5 mm and 3.5 mm) were cut from a plate that was molded in an aluminum mold. The dynamic properties were studied under fixed frequency mode at a frequency of 1Hz, and the amplitude was 0.2mm. The samples were analyzed from 30°C to 160°C at a heating rate of 2°C/min.

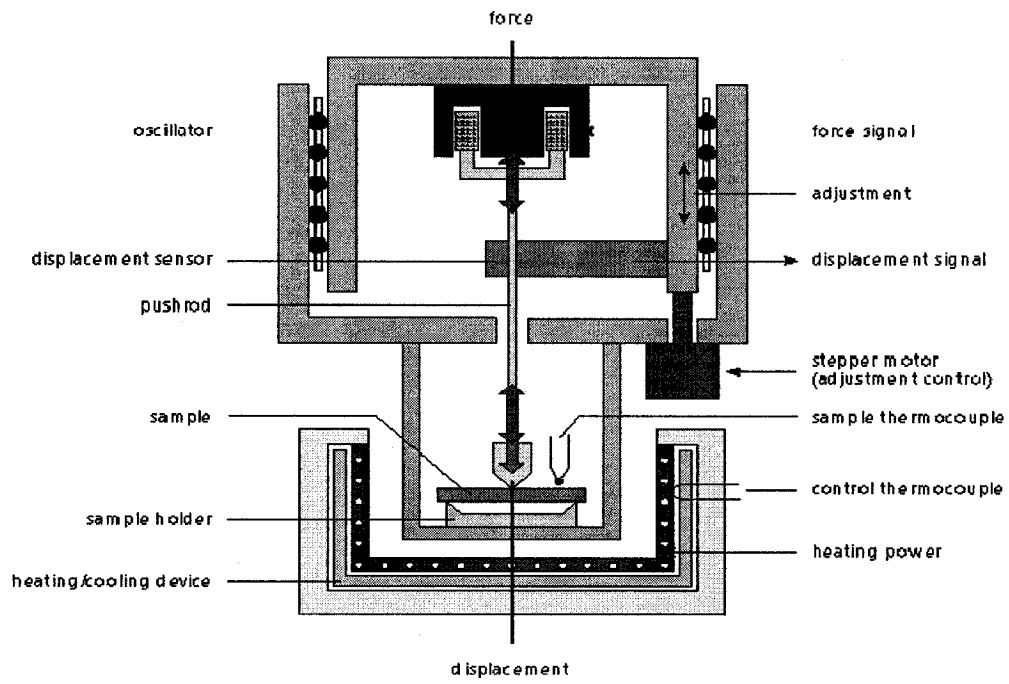


**Figure 3.23. A schematic of DMA [114]**

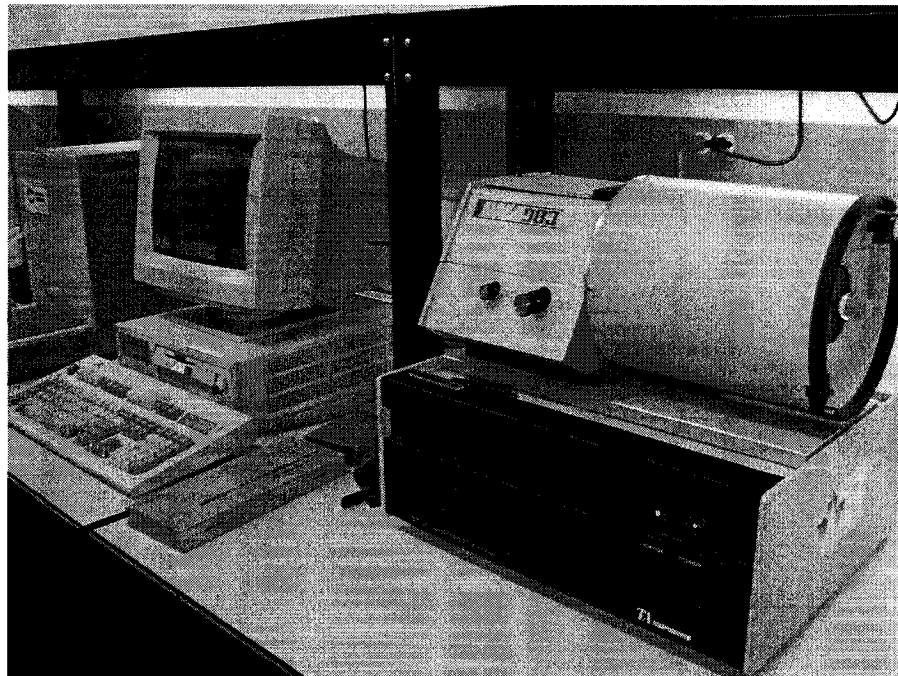


**Figure 3.24. Du Pont 983 DMA (from CONCOM lab)**

### 3.5.5.2. Tensile and flexural tests

Tensile property, the ability of a material to resist breaking under tensile stress, is one of the most important and widely measured properties of plastics used in structural applications. Tensile strength is the force per unit area (MPa) required to break a material in such a manner. The elongation of a plastic is the percentage increase in length that occurs before it breaks under tension. The combination of high ultimate tensile strength and high elongation leads to materials of high toughness. The tensile modulus is the ratio of stress to elastic strain in tension. A high tensile modulus means that the material is rigid - more stress is required to produce a given amount of strain. In polymers, the tensile modulus and compressive modulus can be close or may differ widely. This variation may be 50% or more, depending on resin type, reinforcing agents, and processing methods.

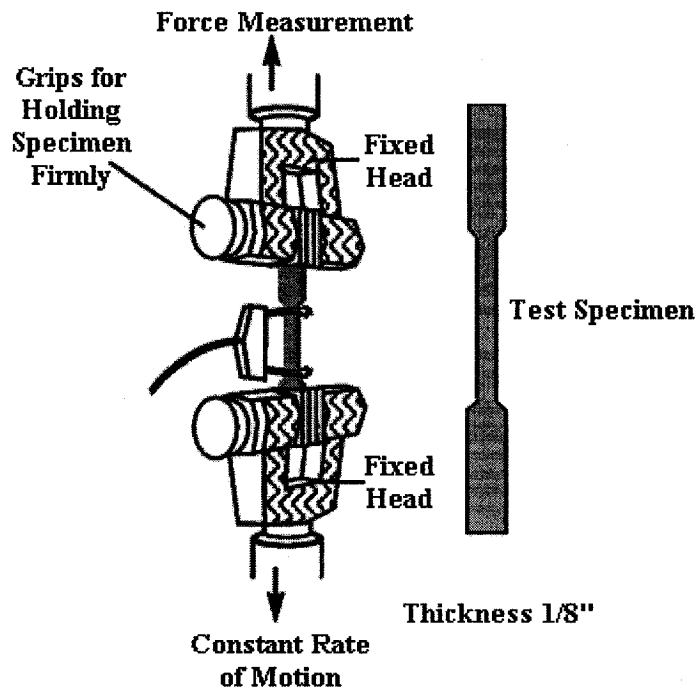
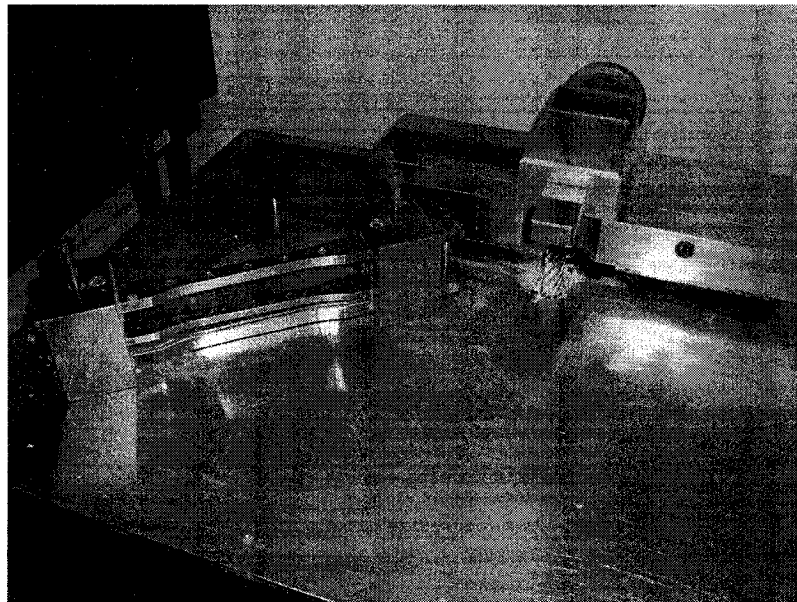


Figure 3.25. Schematic drawing of tensile test [115]

During tensile testing, a machine pulls the sample from both ends and measures the force required to pull the specimen apart and how much the sample stretches before breaking. A schematic drawing of the tensile test is shown in Figure 3.25. According to ASTM D638-02a [116], the crosshead speed at which a sample is pulled apart in the test can range from 1mm to 500mm per minute and will influence the results. In this project, the crosshead speed for the tensile test was 5mm/min and the gauge length was 50mm. The video extension meter (for very soft materials) or micro extension meter was applied during the tensile testing. Samples were prepared as follows: First of all, a large plate of sample cured in an aluminum mold (Figure 3.22) was cut to rectangular shapes. Secondly, these rectangular pieces were machined to form dog bone shape specimens according to the ASTM standard for tensile test. The dog bone cutting machine is shown in Figure 3.26.



**Figure 3.26. A Bruker dog-bone cutting machine for tensile specimens (from IMI lab)**

The flexural strength of a material is its ability to resist flexural deformation under load. Figure 3.27 shows the test geometry. These tests also give the means to measure a material's flexural modulus (the ratio of stress to strain in flexural deformation).

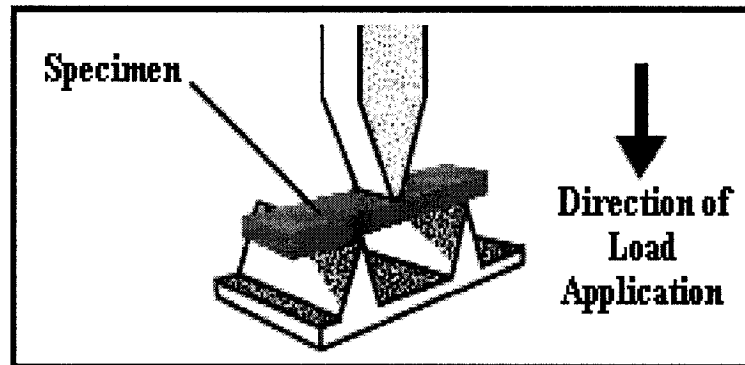


**Figure 3.27. The schematic drawing of flexural test [115]**

According to the ASTM standard D790-03 [117], for all tests, the support span shall be 16 (tolerance  $\pm 1$ ) times the depth (thickness) of the beam. The thickness of the flexural samples in this project was 3 mm, so a 48 mm span was taken for the test. The rate of crosshead motion is calculated by Equation 3.3 [117]:

$$R = ZL^2/6d \quad (3.3)$$

where  $R$ = rate of crosshead motion, mm/min;  $L$ = support span, mm;  $d$ = depth of beam, mm;  $Z$ = rate of straining of the outer fiber, mm/mm/min.

After calculation, the crosshead speed for the flexural test was determined to be 1.3 mm/min.



### 3.5.5.3. Compressive test

ASTM D695-02 [118] is the most commonly used test method. The sample is placed in the compression apparatus and a known load is applied. In this project, the crosshead speed for the compressive test was 1.3 mm/min. Figure 3.28 shows the test geometry.

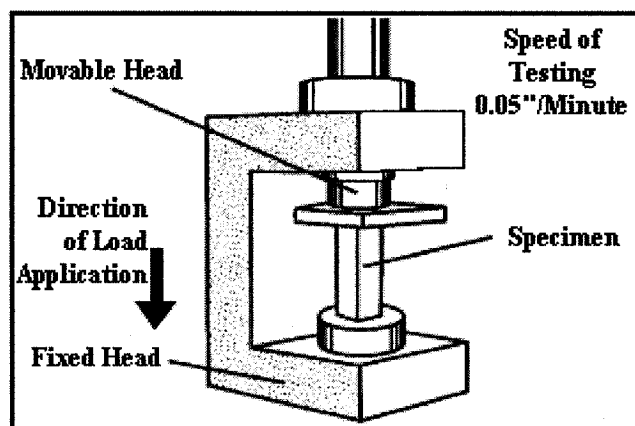


Figure 3.28. Schematic drawing of compression test [115]

Samples of 1/2" x 1/2" x 1" for compression testing were prepared by casting in silicone molds as shown in Figure 3.29. The upper surface of the samples was machined after that.

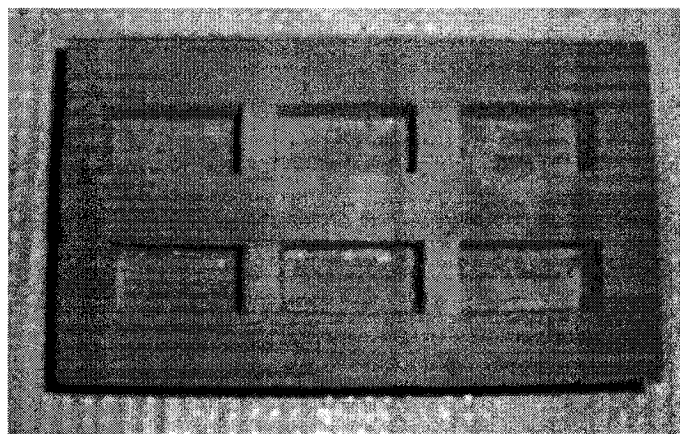
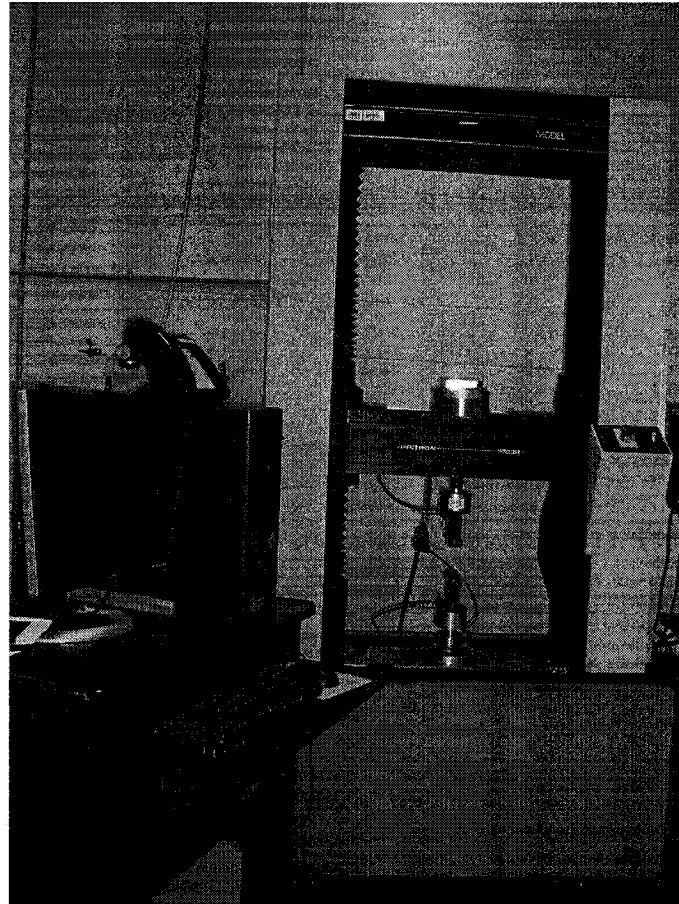


Figure 3.29. Silicone mold for compression samples

In this project, tensile, flexural and compression tests were performed on an Instron 5500R machine. Figure 3.30 shows a photo of this machine. All tests were done at room temperature (23°C), humidity 50%. For each test at least five defect-free specimens were tested.



**Figure 3.30. Instron 5500 test machine (from IMI lab)**

#### **3.5.5.4. Izod impact strength testing of plastics**

Several methods are used to measure the impact resistance of plastics - Izod, Charpy, Gardner, tensile impact, and many others. These impact tests allow designers to compare the relative impact resistance under controlled laboratory conditions and, consequently,

are often used for material selection or quality control. However, these tests generally do not translate into explicit design parameters. The Izod impact test is the most common test in North America. Figure 3.31 depicts the Izod impact strength test apparatus.

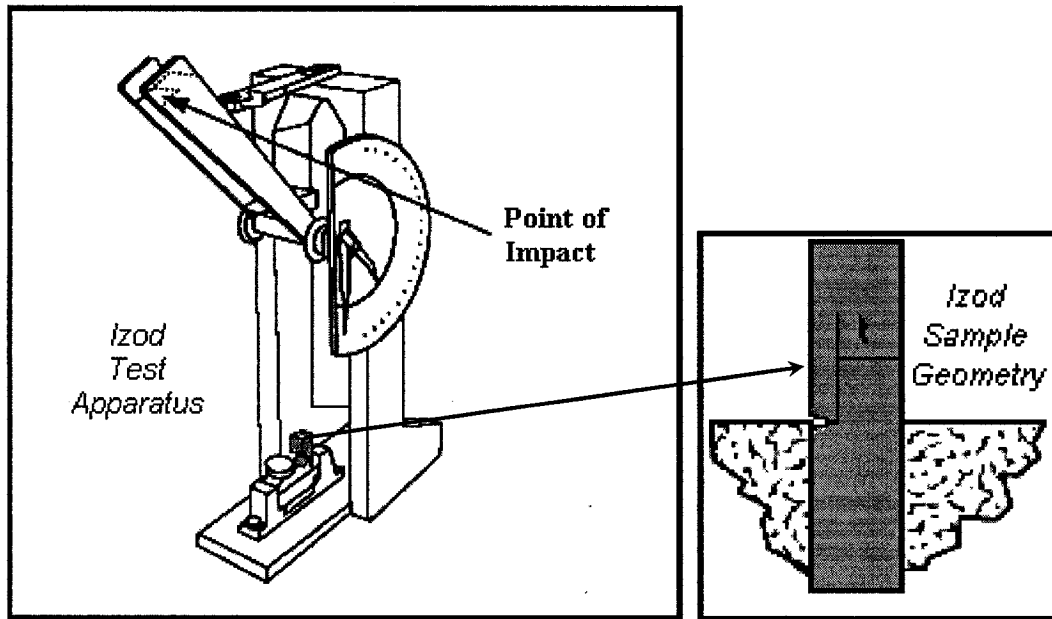


**Figure 3.31. Schematic drawing of impact test [115]**

The test method generally utilized in North America is ASTM D256 [119]. The result of the Izod test is reported in energy lost per unit of specimen thickness (such as ft-lb/in or J/cm) at the notch ('t' in graphic at right). Additionally, the results may be reported as energy lost per unit cross-sectional area at the notch ( $J/m^2$  or ft-lb/in<sup>2</sup>). Samples were cut to rectangular shapes from a large plate that was cured in an aluminum mold (as Figure 3.22). They were then machined on a notch cutter to produce notch. Figure 3.32 shows a photo of the notch cutter. All tests were done at room temperature (23°C), humidity 50% on an Impact tester from Tmi testing machines Inc. For each test at least five defect-free specimens were tested. Figure 3.33 shows a photo of this instrument.

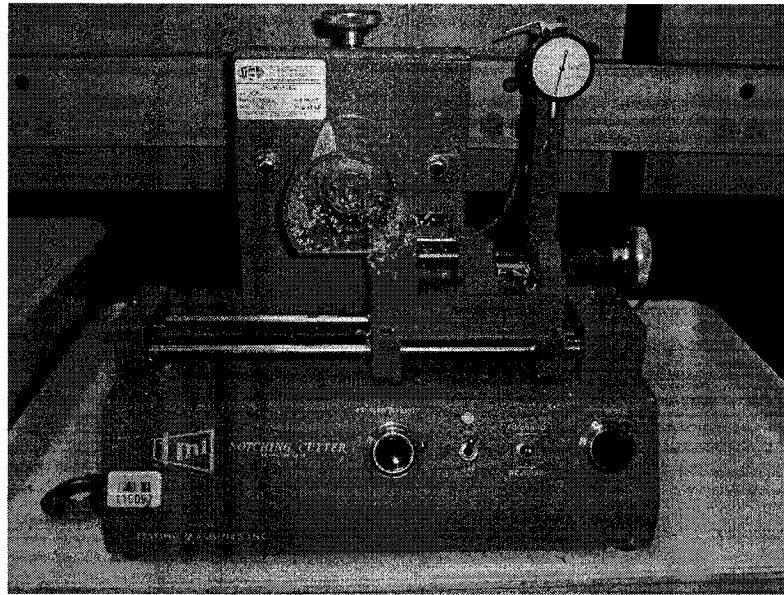


**Figure 3.32. A Tmi notch cutter for impact specimens (from IMI lab)**

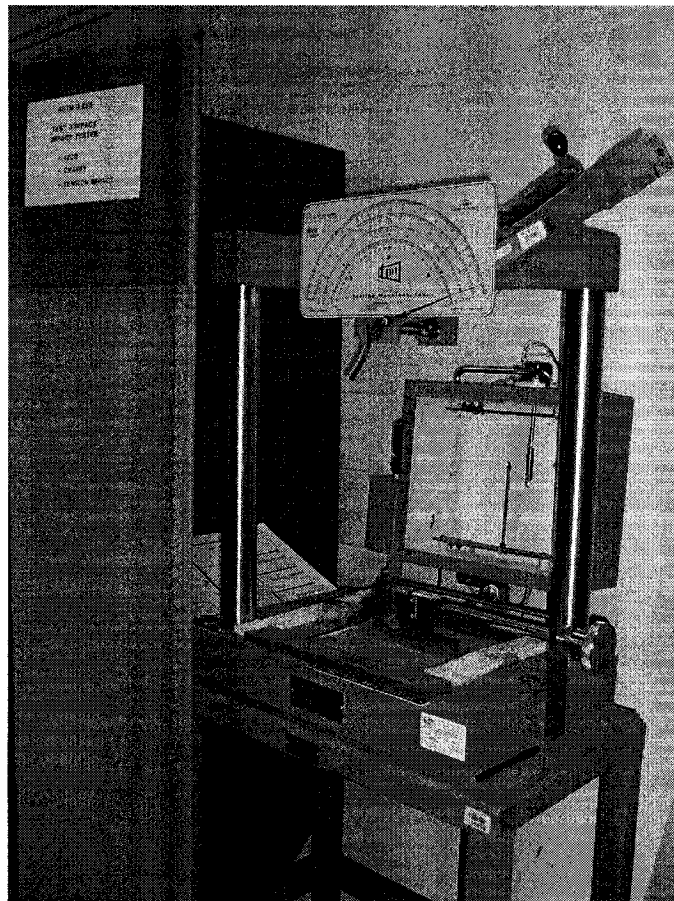


**Figure 3.33. Impact instrument (from IMI lab)**

### 3.5.5.5. Fracture toughness

Fracture tests were performed on an MTS servo hydraulic testing machine at a crosshead speed of 10 mm/min. The support span is 4 times the width of the specimen (according to ASTM D5045-99 [120] at room temperature). Figure 3.34 shows a photo of the machine.

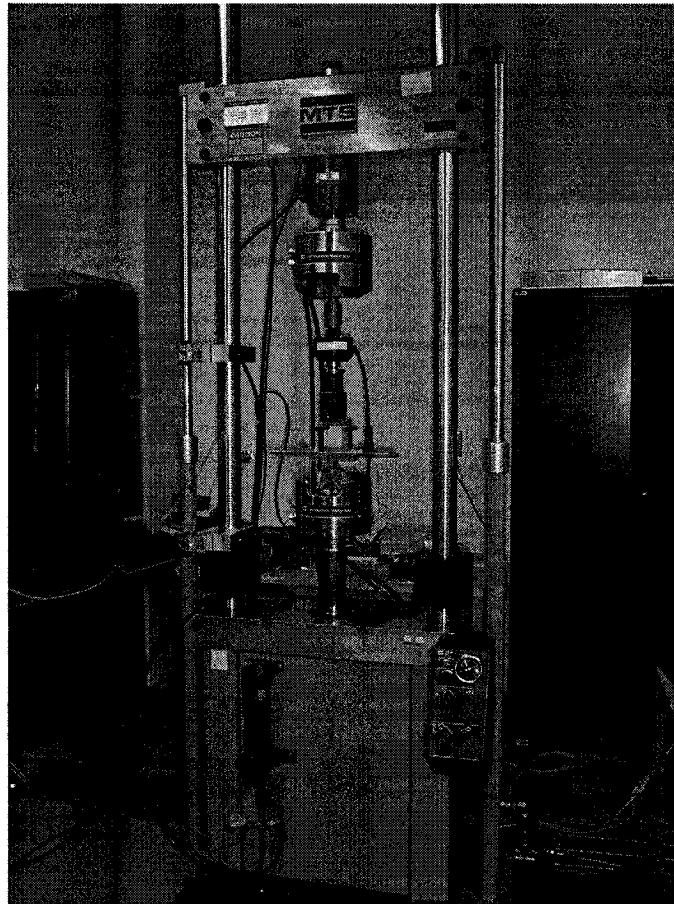


**Figure 3.34. MTS servo hydraulic testing machine (from CONCOM lab)**

Single edge notch bending (SENB) samples, including notch, were cast from a silicone mold as shown in Figure 3.35, their upper surface was machined, and the samples were

pre-cracked by tapping a fresh razor blade into the notch. Samples size and shape are shown in Figure 3.36; at least 5 specimens of each composition were tested.

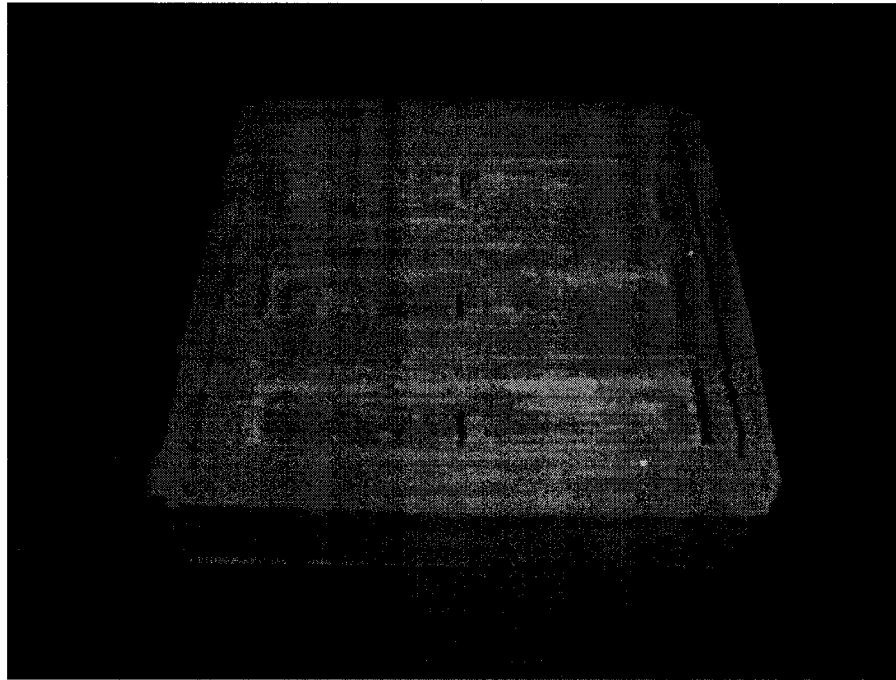


**Figure 3.35. Silicone mold for fracture samples**

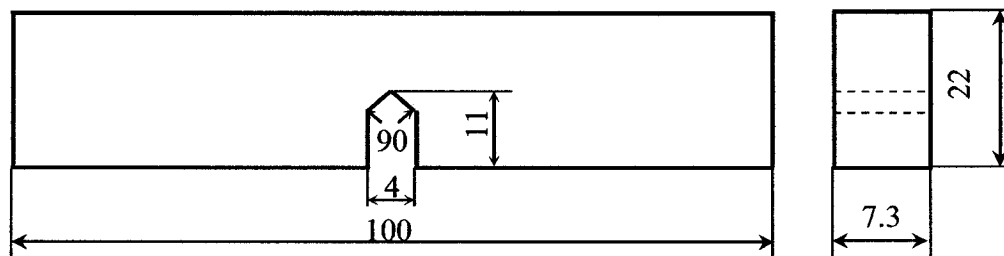


**Figure 3.36. Sample dimensions of three points bend (SENB)**

The critical stress intensity factor ( $K_{IC}$ ) can be calculated from the following formula in units of  $\text{MPa}\cdot\text{m}^{1/2}$  [120]:

$$K_{IC} = \left( \frac{P_{\max}}{BW^{1/2}} \right) f(x) \quad (3.4)$$

where:

$$f(x) = 6x^{1/2} \frac{[1.99 - x(1-x)(2.15 - 3.93x + 2.7x^2)]}{(1+2x)(1-x)^{3/2}} \quad (3.5)$$

$x = a/W$ ,  $P_{max}$  is the max load (kN);  $B$  is the specimen thickness (about 0.7 cm);  $W$  is the specimen width (about 2.2 cm); and  $a$  is the crack length (about 1.1 cm)

The critical strain energy release rate ( $G_{IC}$ ) can be calculated from the following formula, in units of J/m<sup>2</sup> [120]:

$$G_{IC} = U/BW\phi \quad (3.6)$$

where:  $U = (1/2)P_{max}(u_{max} - u_i)$

$$\phi = \frac{A+18.64}{dA/dx} \quad (3.7)$$

$A = [16x^2/(1-x)^2][8.9 - 33.717x + 79.616x^2 - 112.952x^3 + 84.815x^4 - 25.672x^5]$ ; and

$dA/dx = [16x^2/(1-x)^2][-33.717 + 159.232x - 338.856x^2 + 339.26x^3 - 128.36x^4] +$

$16[8.9 - 33.717x + 79.616x^2 - 112.952x^3 + 84.815x^4 - 25.672x^5]$

$\{[2x(1-x) + 2x^2]/(1-x)^3\}$

$u_{max}$  is the maximum displacement; and  $u_i$  is the indentation displacement.

### 3.5.5.6. Surface hardness

The hardness of epoxy and epoxy nanocomposites was determined at room temperature and relative humidity of 50% according to ASTM D2240-00 [121] using a Shore Conveloader instrument (Figure 3.37).

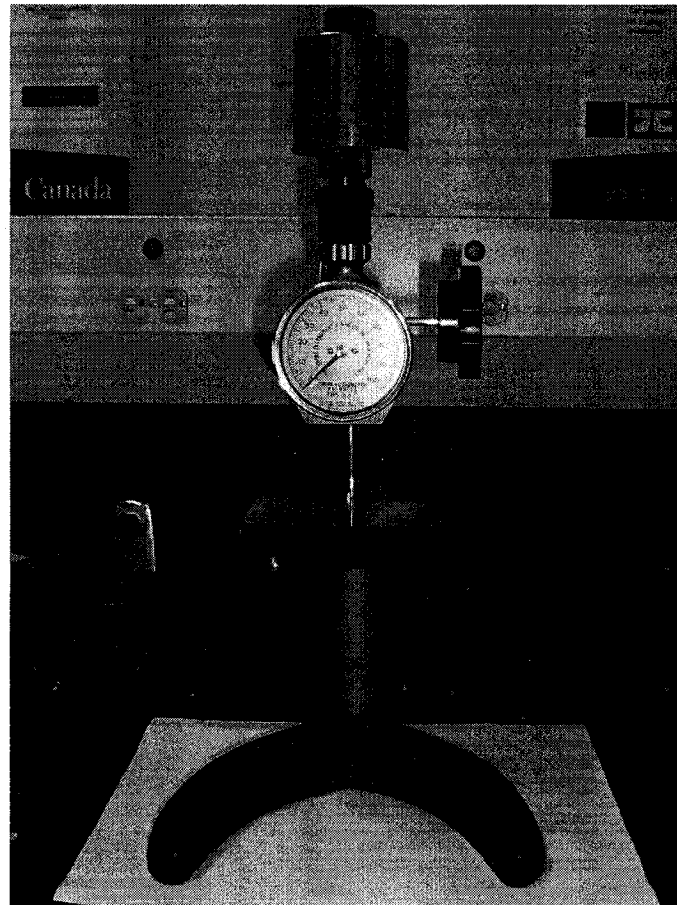


**Figure 3.37. Shore Conveloader instrument (from IMI lab)**



# Chapter 4

## **Effects of fabrication process and compositions of constituents on the dispersion and intercalation/exfoliation of clay**

### **4.1. Challenges and objectives**

Dispersion of organoclays in epoxy is a complex process, which takes place during the stirring step and the curing step. Both pristine and commercially treated clays tend to form stacks rather than individual platelets due to their layer structure and the strong van der Waals force between them. In most cases, the stacks combine and form large aggregates due to such strong secondary interaction. As a result, it is very difficult to break down such interaction in order to disperse the clay layers individually in the epoxy matrix, especially when the two phases are incompatible. In general, there are several different possible levels of dispersion of organoclays in ENCs including 1) exfoliated or delaminated clay layers single platelets; 2) non-intercalated stacks (multiple layers not intercalated by the matrix) or intercalated stacks (multiple layers intercalated either

uniformly or not uniformly by the matrix); 3) multiple-stack aggregates (multiple stacks forming aggregates, on a micrometer-scale) and macro-aggregates (combinations of many multiple-stack aggregates, which are on the macro-scale, in the order of a millimeter). Intercalation is controlled by the diffusion of epoxy resin (both epoxy and hardener) into the clay galleries, which is governed by thermodynamic rules. While breaking down the macro-aggregates into multiple-stack aggregates or further down into single stacks can be effectively done using mechanical forces, such as shear, impact, etc., exfoliation can be achieved either by diffusion of the resin into the galleries or by using mechanical forces. Different stirring procedures have been designed to examine this concept in order to improve the intercalation and exfoliation. In the curing step intercalation and exfoliation will continue but mechanical force cannot be applied by conventional techniques. In addition, the diffusion of monomers and oligomers into the clay galleries in this step may be inhibited by the curing reaction that limits or restricts the molecule mobility. It is important to control the curing temperatures in order to favor the intercalation and exfoliation process.

During the fabrication of epoxy nanocomposites, at first clays are stirred with the liquid epoxy resins. In the absence of the curing agents, the systems can have an extended shelflife at certain elevated temperatures. Therefore, different means such as mechanical shear and thermodynamic force, etc., can be used to facilitate the dispersion. At the end, the system is cured by the use of hardener. At this curing stage, sufficient external shear stress may not be applied, but further dispersion, more specifically intercalation and exfoliation, can continue to take place at the beginning of the curing as the hardener and/or intermediate molecules are still mobile enough to diffuse into the clay galleries;

the motion of these molecules is governed by thermodynamic forces. In general, it is easier to control good clay dispersion in the stirring step than in the curing step.

In this chapter, the effects of mechanical shear and thermodynamic forces on the dispersion of organoclays in epoxy nanocomposites are investigated. The dispersion here means:

- ❖ The size reduction of aggregates of micrometre
- ❖ The diffusion of polymer molecules into the clay galleries (so-called intercalation), and
- ❖ The dispersion into individual clay layers (so-called exfoliation).

## **4.2. Methodology and experiment**

In order to understand the quality of clay dispersion during stirring and curing, it is necessary to understand the factors that may contribute to the dispersion. Several important factors have been identified and are summarized in the flowchart in Figure 4.1.

There are two ways to incorporate the clays into the epoxy systems. In the first case, epoxy and organoclay are mixed together in the stirring step and then hardener is added to the mixture for curing. In the second case clay is stirred with hardener first and then epoxy will be added at the curing step. However, in this study, the first approach was selected because of the toxicity considerations related to the second case (heating toxic amines to high temperature).

In the stirring step, two main factors are considered: mechanical shearing and thermodynamic effect. The effect of mechanical shear on the dispersion and intercalation/exfoliation of clay is a function of  $T$ ,  $\nu$  and  $t$ . The thermodynamic process in this step is the diffusion of epoxy molecules into the clay galleries. It is a function of  $T$ ,  $t$  and chemical interactivity between organoclay and epoxy ( $C$ ). As in all experiments throughout this study, only one type of epoxy resin and two types of clay were used. The factors considered in this study are described in Figure 4.2.

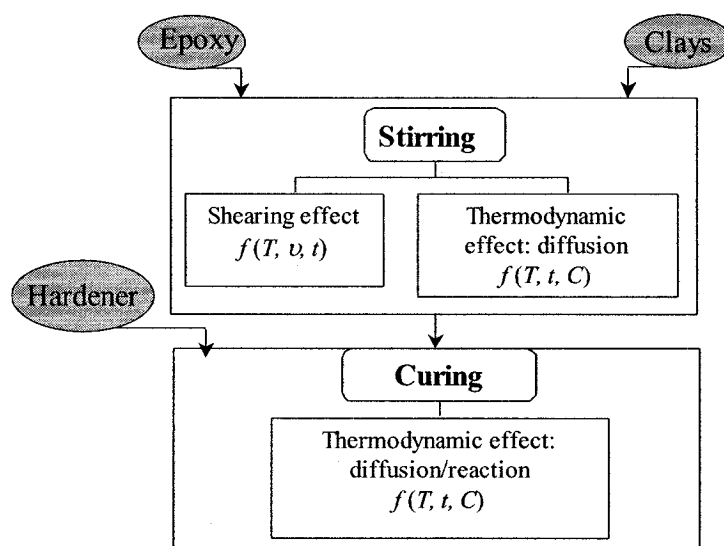


**Figure 4.1. Factors affecting dispersion, intercalation/exfoliation of nanoclay in epoxy at the stirring step,  $T$  = temperature,  $\nu$  = stirring speed,  $t$  = duration, and  $C$  = chemical interactivity between clay - epoxy or clay-hardener**

In the curing step, when the hardener is added to the mixture of epoxy-clay, curing will take place. In this step, external shear cannot be applied, therefore this step is governed only by thermodynamics. The thermodynamics in the curing step can be considered as a function of time ( $t$ ), temperature ( $T$ ), and chemical interactivity between clay-epoxy or clay-hardener ( $C$ ). Chemistry (chemical structure, molecular weight etc) of epoxy,

hardener and clay can all have effects on the dispersion of clay in this step, but in this study only one type of epoxy was used. A summary of thermodynamic effects is shown in Figure 4.3.

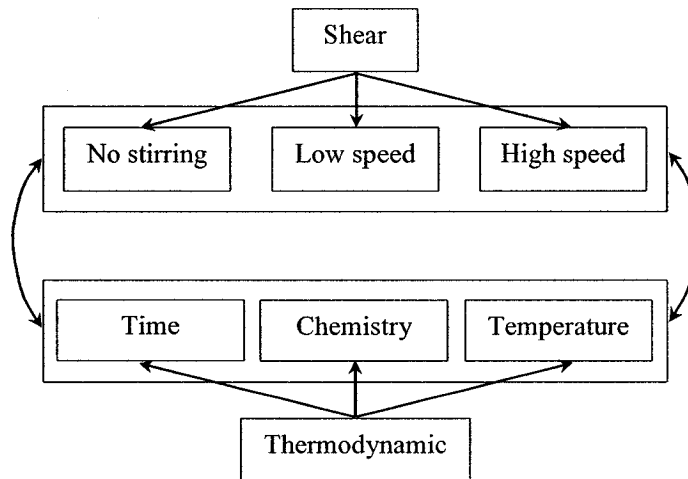


**Figure 4.2. Factors affecting dispersion, intercalation/exfoliation of nanoclay in epoxy at the stirring step**

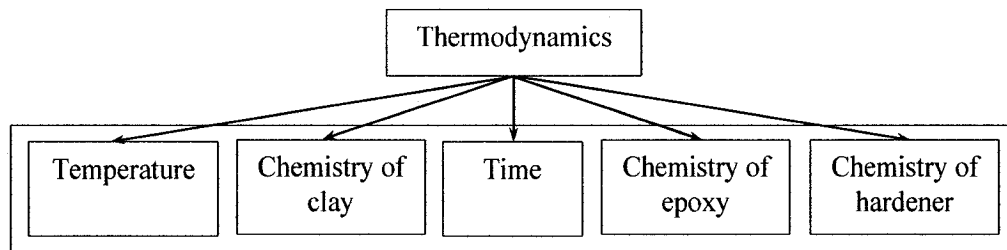


**Figure 4.3. Factors affecting dispersion, intercalation/exfoliation of nanoclay in epoxy at the curing step**

To the knowledge of the author, the effects of mechanical shear and thermodynamic forces on the dispersion of organoclays in epoxy nanocomposites are shown in Figure 4.4, where  $\tau$  represents shear stress and  $D$  represents thermodynamic forces that act on the clay platelets. Thus, the total force acting on the clay platelets can be written as

follows:

$$F_{DT} = D + \tau = D + \eta \frac{dv}{dh} \quad (4.1)$$

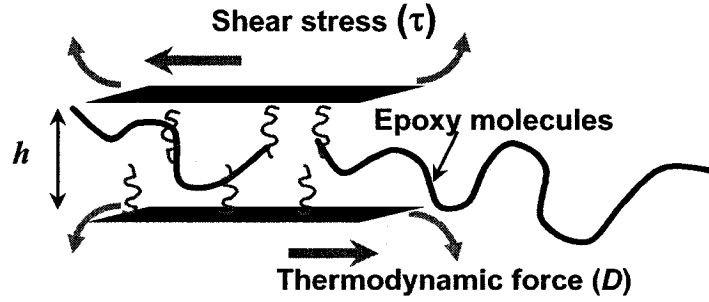


**Figure 4.4. Forces imposed on nanoclay (in epoxy) at the stirring step;  $h$  is the distance between clay platelets,  $L$  is the length of clay platelets**

In Equation 4.1,  $D$  is a function of temperature  $T$ , time  $t$ , and chemical interactivity between clay-epoxy or clay-hardener  $C$  in the mixtures, such that

$$D = D(T, t, C) \quad (4.2)$$

$$\tau = \eta \frac{dv}{dh} \quad (4.3)$$

If  $F_{DT} > F_{critical}$ , where  $F_{critical}$  is the force that holds the clay together, then the clays will be separated into single platelets; otherwise they will remain in the form of stacks. From there, one can see that temperature ( $T$ ), speed ( $v$ ), time ( $t$ ) and chemical interactivity between clay-epoxy or clay-hardener ( $C$ ) are the process parameters that may have an effect on dispersion of clay in epoxy. On the way to disperse the clay, we should consider

two aspects: first the large clay aggregates are broken down into smaller aggregates, and then the smaller aggregates are delaminated. Increasing temperature has an effect on the mobility of the polymer molecules and thus has a positive influence on the diffusion  $D$ . This will contribute to the separation of the clay platelets and it may influence the micro dispersion as well. When the speed increases,  $\tau$  will increase. This will affect the micro-dispersion of the clay aggregates. It may also affect the separation of clay platelets. However it is very difficult to achieve good results if the components in the mixtures are incompatible. Time has an effect on both micro-dispersion and separation of clay platelets. Chemical interactivity between clay-epoxy or clay-hardener in the mixtures ( $C$ ) play an important role in the delamination of the clay layers. Therefore, the experiments in this chapter were designed to investigate the effect of these parameters on the dispersion of clay.

#### **4.2.1. Effect of the stirring step**

The objective of this part is to investigate the effect of stirring parameters on the dispersion and intercalation/exfoliation of clay in epoxy resin. The experiments were organized at 3 different levels of stirring speed: no speed, low speed and high speed. Duration, temperature of stirring and chemistry of clay were also studied.

##### **4.2.1.1. Parameters examined**

In order to fulfill the objective, the experiments were designed as described in Table 4.1. Referring to Chapter 3, three different pieces of equipment were selected in this study:

1. Mechanical stirrer

2. Homogenizer
3. Microfluidizer (reference method)

Different processes were used to stir the epoxy and clay:

- ❖ The first one was a room temperature without mechanical shear process (Rm), in which the clay and epoxy were stirred at room temperature by hand at 100 rpm for a few minutes then kept at room temperature for 1 hour.
- ❖ The second one was a high temperature without shear process (Tm), in which the clay and epoxy were stirred at 120°C by hand at 100 rpm for a few minutes then kept in an oven at 120°C for 1 hour.
- ❖ The third method was a high temperature with low speed process (TM), in which the clay and epoxy were stirred at 120°C for 1 hour by a mechanical stirrer at 1000 rpm.
- ❖ The fourth one was a room temperature and high speed process (RS), in which the clay and epoxy were stirred by a homogenizer at room temperature and high speed for different durations (as in Table 4.1).
- ❖ The fifth method was a high temperature and high speed process (TS), in which the clay and epoxy were stirred by a homogenizer at 120°C and 180°C for different durations and speeds (as in Table 4.1).
- ❖ The sixth one was a high pressure process (HP), in which organoclay was first dispersed in acetone (about 8% of organoclay in acetone) to form a suspension with microfluidizer (15000 psi  $\approx$  103.42 MPa), and then the suspension was added into the epoxy resins. The desired amount of paste of organoclay and acetone was added to epoxy resin and then the mixture was stirred by hand at room temperature. When the epoxy was



visibly dispersed, the mixture was mechanically stirred at 1000 rpm in a fume hood at room temperature for 30 minutes, followed by slow heating to 80°C for 1 hour. Finally, the mixture was degassed under vacuum at 95°C for 30 minutes.

**Table 4.1. Parameters examined for stirring step**

Experiment name		Stirring condition			Equipment
		Temperature (°C)	Duration (min)	Speed (rpm)	
<b>Rm</b>	Room temperature without stirring	Room temperature (RT)	60	100	Hand stirring
<b>Tm</b>	High temperature without stirring	120	60	100	Hand stirring
<b>TM</b>	High temperature with low speed	120	60	1000	Mechanical stirrer
<b>RS</b>	Room temperature with high speed	RT	2, 4, 10, 20, 30, 45, 60	24000	Homogenizer
<b>TS</b>	High temperature with high speed	120	2, 4, 10, 20, 30, 45, 60	9500, 17500, 24000	Homogenizer
		180		24000	Homogenizer
<b>HP</b>	High pressure (103.42 MPa)				Microfluidizer

*100 g of EPON828 was stirred with 2.694 g of C30B (all stirring conditions) or I30E (only Rm and Tm)*

#### 4.2.1.2. Experimental procedure

Figure 4.5 shows the experimental procedure for this study. Epoxy and clay were stirred together using different mixers and the stirring procedure of each mixer is described in section 3.3 and 4.2.1.1. The dispersion of organoclays in epoxy resins after stirring is characterized by field emission gun scanning electron microscopy (FEGSEM), by X-ray diffraction (XRD) and by rheological measurement.

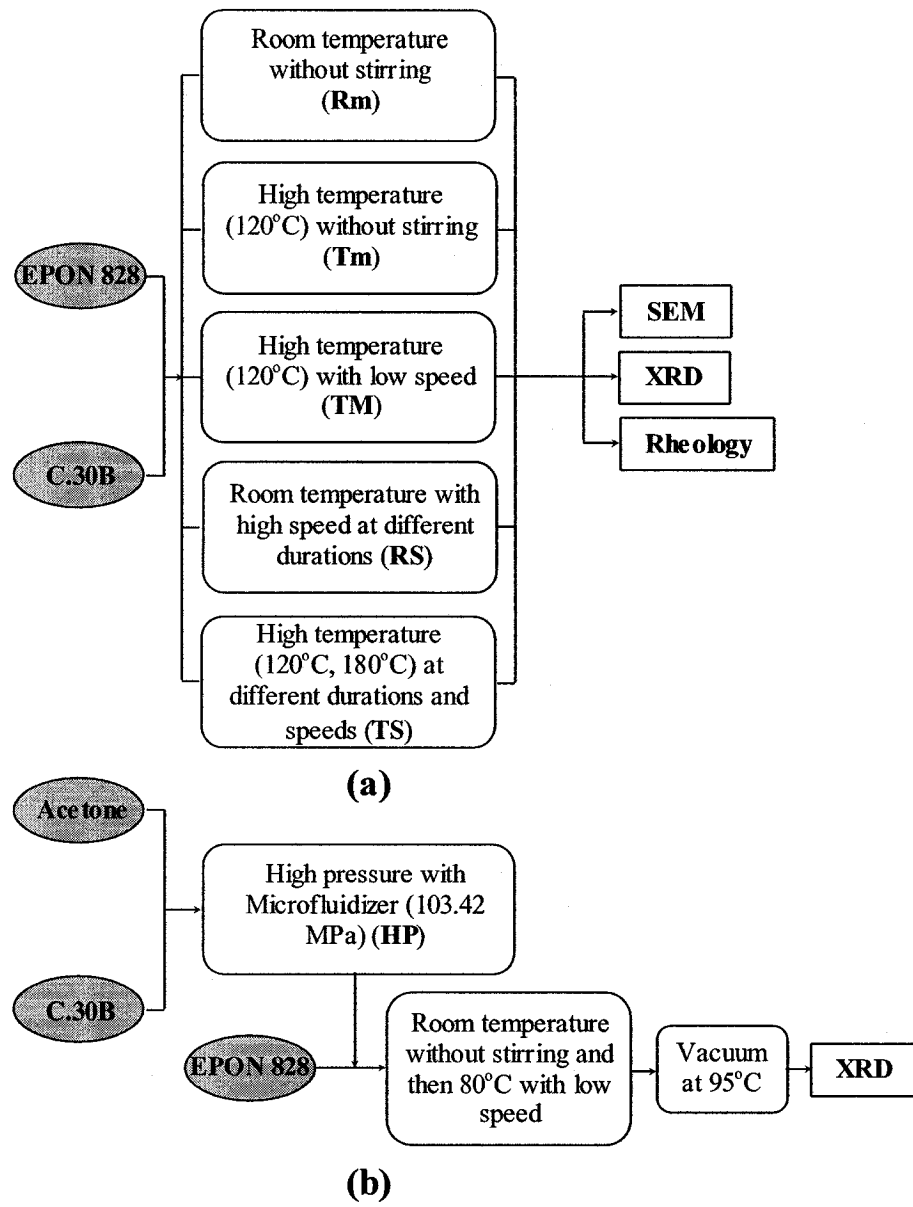


**Figure 4.5. Flowchart presenting the experimental steps for studying the mechanical and thermal effects on dispersion, intercalation/exfoliation of nanoclay in epoxy at the stirring step: (a) Rm, Tm, TM, RS and TS methods, (b) HP method**

## **4.2.2. Effect of the curing step**

The objective of this part is to investigate the effect of the curing step on the dispersion and intercalation/exfoliation of clay in epoxy matrix. Based on the methodology used, temperature, chemistry of clay, and chemistry of hardener are three major factors that influence the dispersion and intercalation/exfoliation of clays in ENC in the curing step. Therefore, the experimental design has considered three aspects:

- Temperature: curing at different temperatures
- Chemistry of clay: using different clays which contain different intercalants
- Chemistry of hardener: using different hardeners (different in molecular weight and structure).

### **4.2.2.1. Parameters examined**

The experiments have been designed as described in Table 4.2.

### **4.2.2.2. Experimental procedure**

Figure 4.6 shows the experimental procedure for the curing. After epoxy and clay were stirred together by different techniques (from the stirring step), epoxy-clay mixtures were then mixed with hardeners according to the stoichiometric ratio. Then they were cured either at room temperature for 2 days or at 60, 90 and 120°C for 2 hours, with subsequent post cure at 140°C for 2 hours in all cases. The quality of dispersion and intercalation/exfoliation after curing were analyzed by XRD, FEGSEM and TEM.

**Table 4.2. Parameters examined for the curing step**

<b>Clay</b>	<b>Stirring method</b>	<b>Hardener</b>	<b>Clay concentration wt%</b>	<b>Curing temperature (°C)</b>
<b>Temperature and stirring conditions</b> (Epoxy-clay mixtures from stirring step)				
<b>C30B</b>	<b>Rm</b>	<b>D230</b>	<b>2</b>	RT, 120
	<b>Tm</b>			RT, 120
	<b>TM</b>			RT, 120
	<b>RS</b>			RT, 120
	<b>TS</b>			<b>RT, 60, 90 and 120</b>
	<b>HP</b>			RT, 120
<b>Chemistry of clay</b>				
<b>C30B, I30E</b>	Rm, Tm	Epicure 3046	(*)	RT, 120
<b>Chemistry of hardener</b>				
<b>C30B</b>	Rm, Tm	<b>DETA</b>	(*)	RT, 120
		<b>D230</b>		
		<b>T403</b>		
		<b>D400</b>		
		<b>D2000</b>		
<p><i>(*) 100 g of EPON 828 was stirred with 2 and 4 g of C30B by Rm and Tm and then the stoichiometric amount of hardener (See Chapter 3) was added in the mixtures for curing.</i></p>				

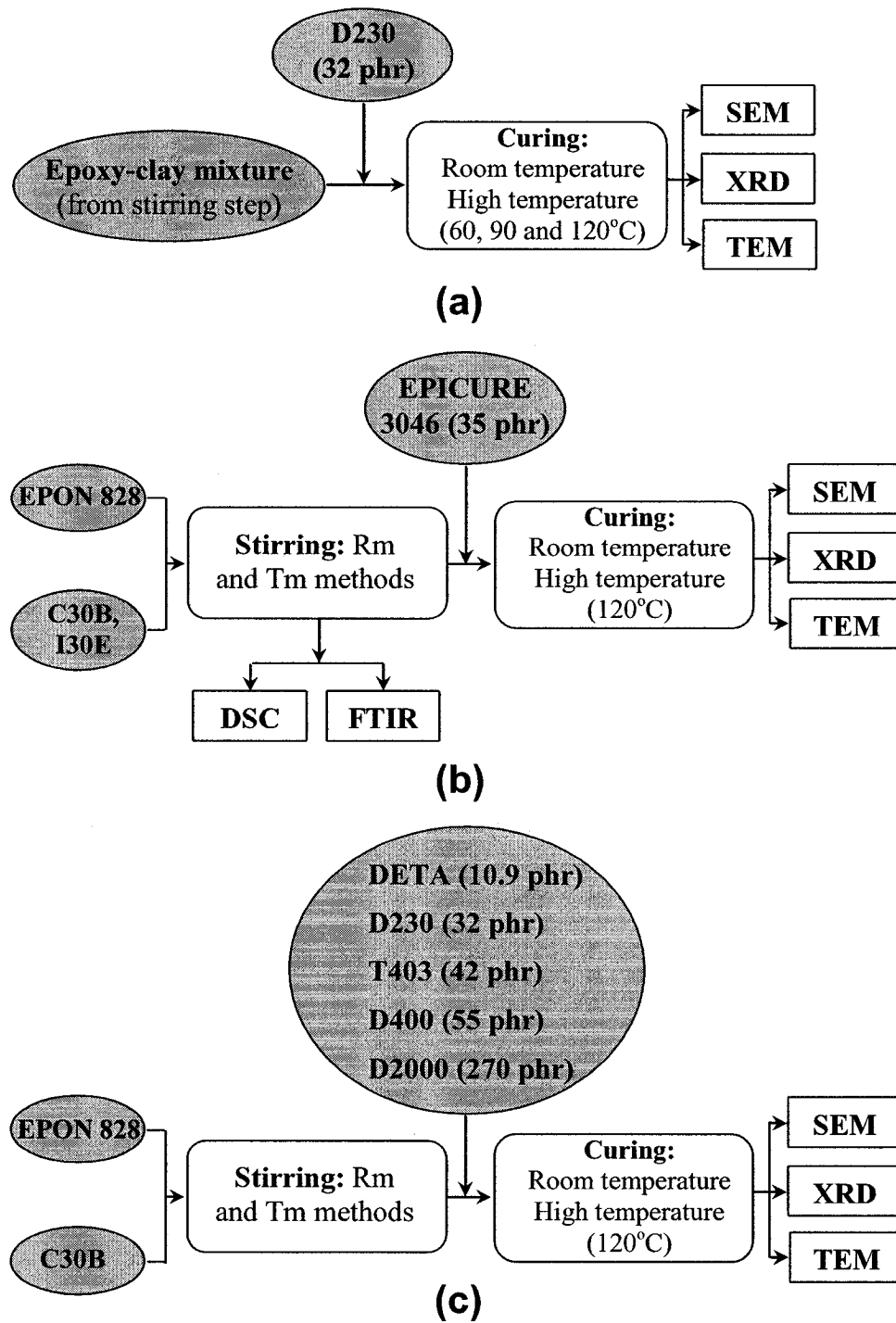


**Figure 4.6. Flowchart presenting the experimental steps for studying the effect of curing: (a) temperature and stirring conditions, (b) clay chemistry, and (c) hardener chemistry**

### 4.3. Effect of the stirring process on the dispersion

#### 4.3.1. Micro dispersion

The microstructures of epoxy-clay mixtures after stirring at different conditions, as observed by SEM, are presented in Figures 4.7a, 4.8a, 4.9a, 4.10a and 4.11a. The bright spots on the backscattered images correspond to clay aggregates at the micro-scale. However, it should be noted here that the nano-scale particles, if they exist, cannot be detected by SEM because of the limitation of the equipment. Apparently, a portion of the clay remains at the micro-scale level with different size populations depending on the stirring conditions. From the SEM images, the distribution of agglomerates of clay in the epoxy is shown in Figure 4.7b, 4.8b, 4.9b, 4.10b and 4.11b (Image Pro Analysis Software was used). A summary of the average diameter, the maximum size and the distribution of clay particles in epoxy made by different methods are given in Table 4.3 and Figure 4.12. The effect of stirring conditions will be discussed shortly.

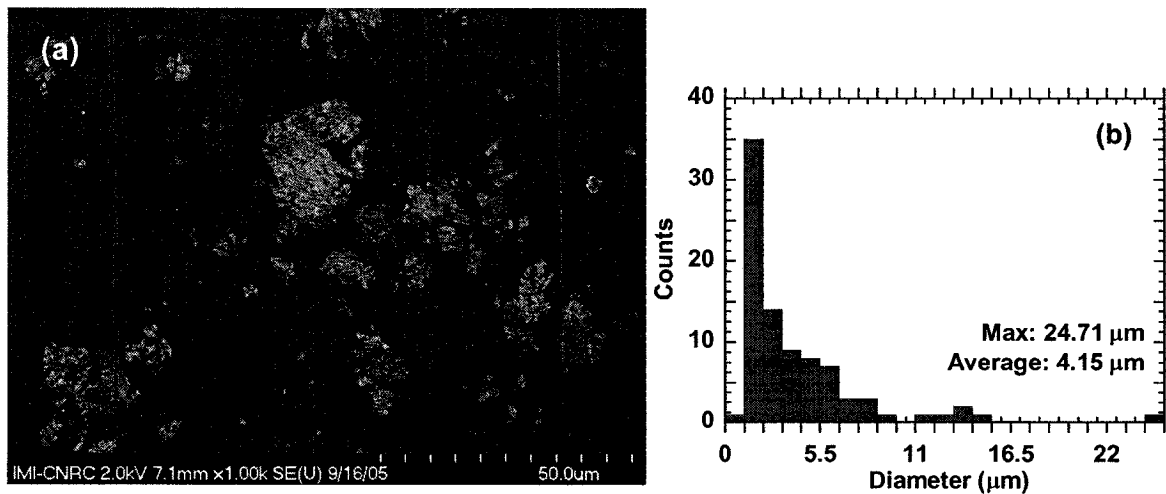


**Figure 4.7. (a) SEM micrograph and (b) clay size distribution of epoxy-Cloisite 30B,**

**Rm method**

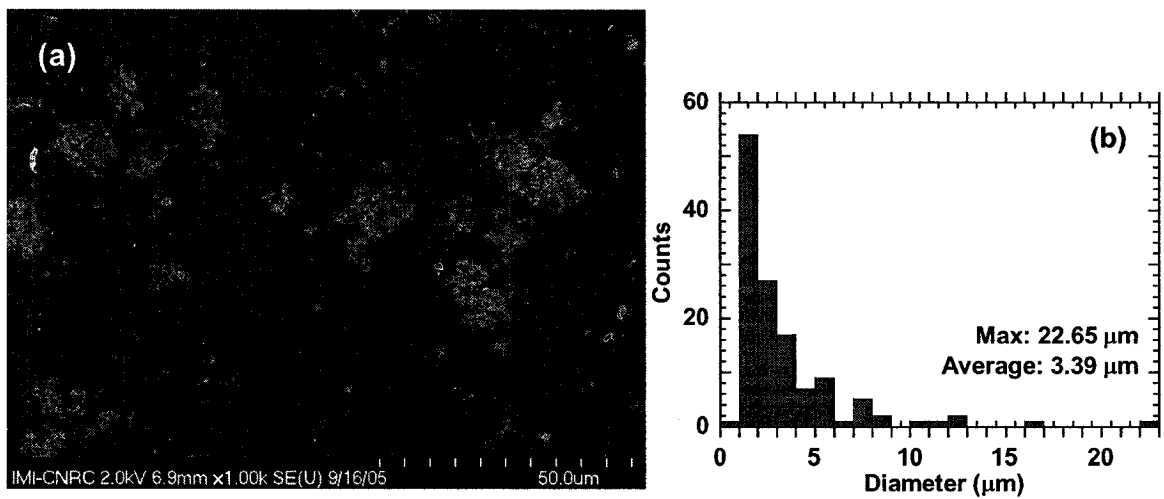


**Figure 4.8. (a) SEM micrograph and (b) clay size distribution of epoxy-Cloisite 30B,**

**Tm method**

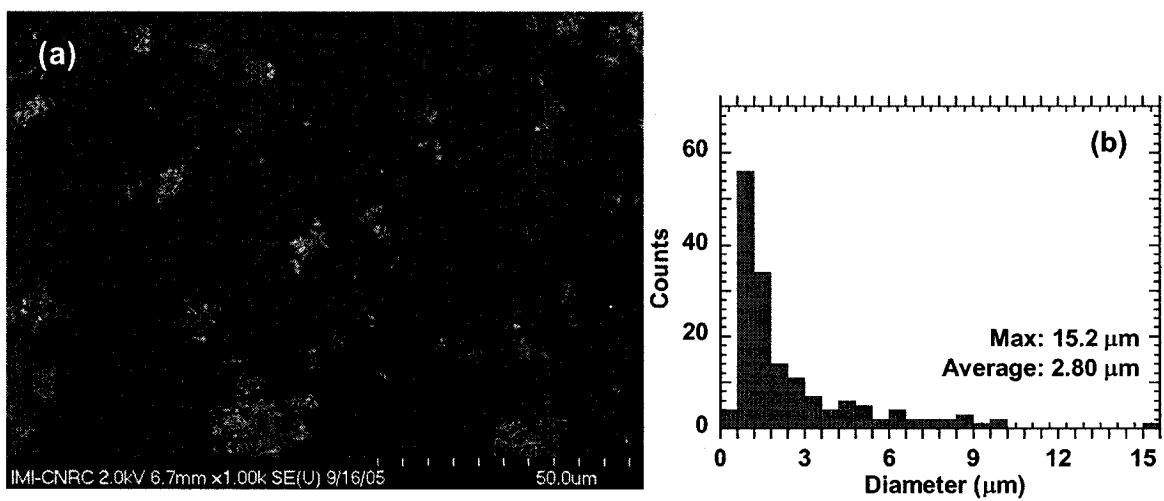


**Figure 4.9. (a) SEM micrograph and (b) clay size distribution of epoxy-Cloisite 30B,**

**TM method**

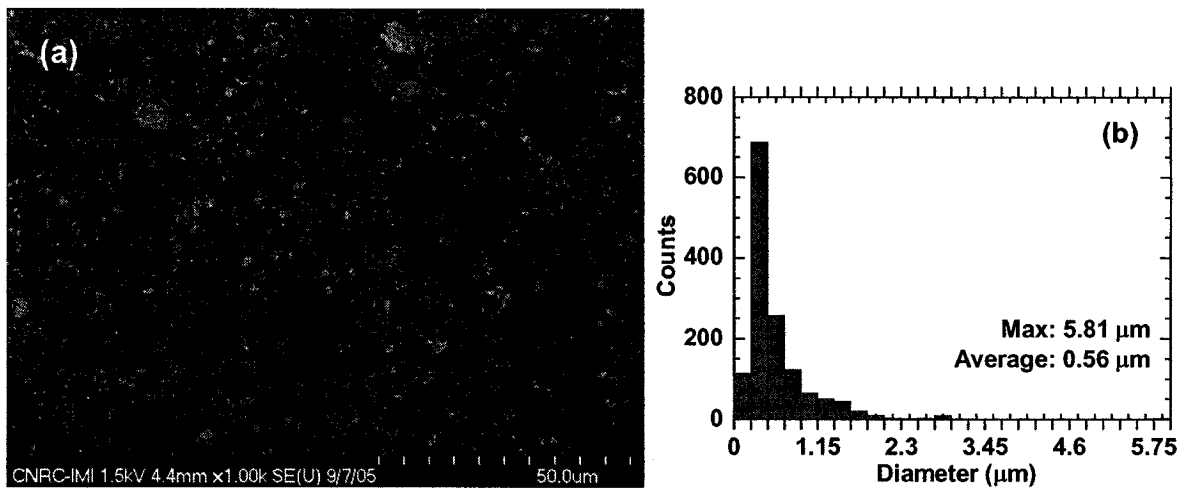


**Figure 4.10. (a) SEM micrograph and (b) clay size distribution of epoxy-Cloisite 30B, RS method (24000 rpm)**

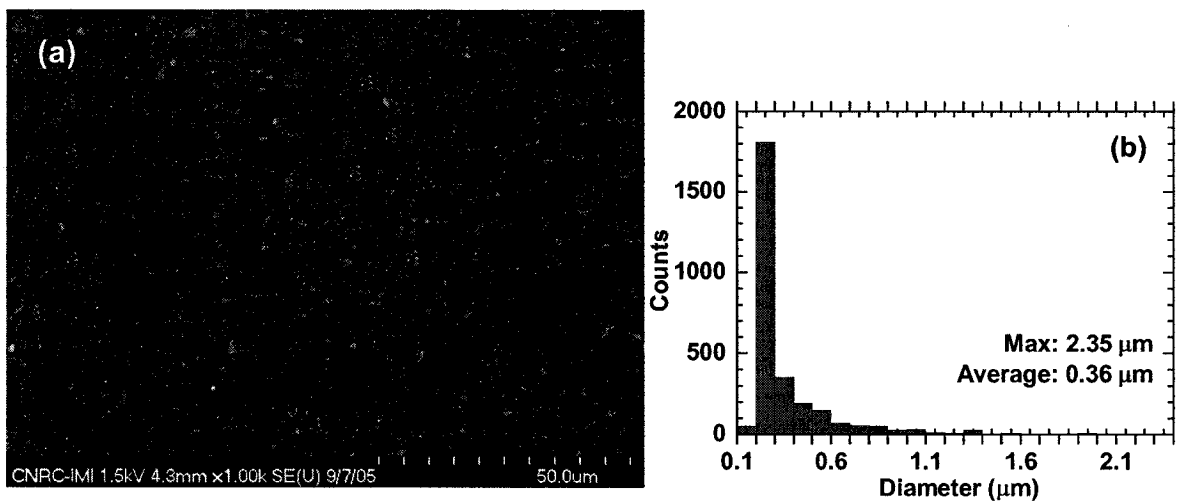


**Figure 4.11. (a) SEM micrograph and (b) clay size distribution of epoxy-Cloisite 30B, TS method (120°C and 24000 rpm)**

**Table 4.3. The average diameter and maximum size of clay particles in epoxy**

Stirring method	Max diameter (μm)	Average diameter (μm)
Rm	24.71	4.15
Tm	22.65	3.39
TM	15.20	2.80
RS	5.81	0.56
TS	2.35	0.36



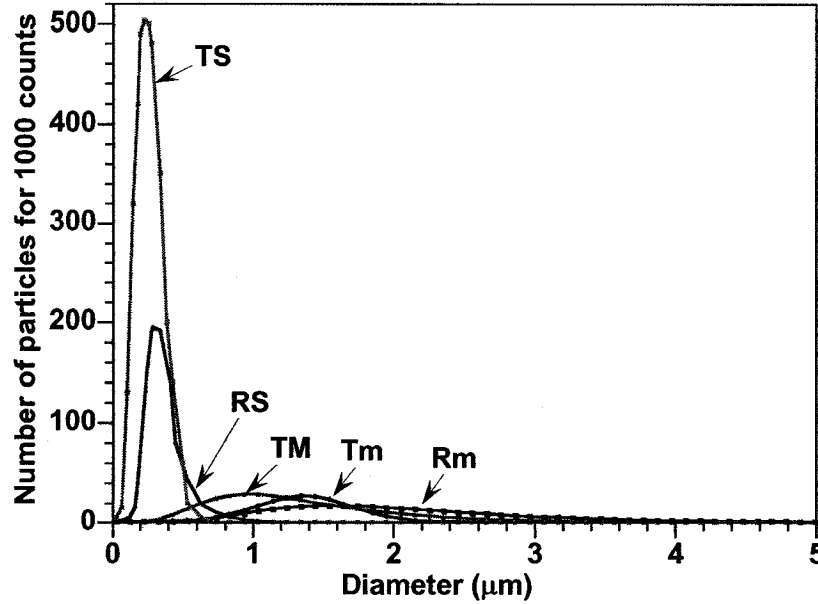
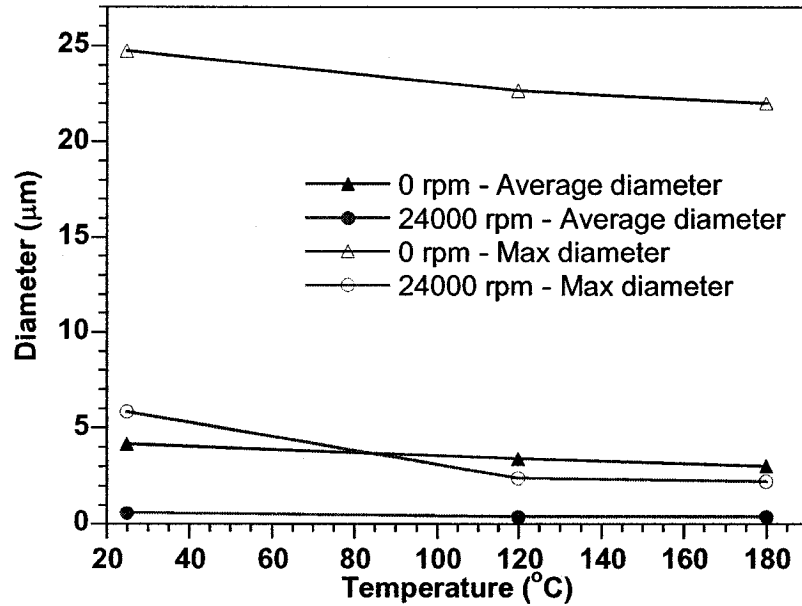


Figure 4.12. Clay size distribution for different stirring methods

#### 4.3.1.1. The effect of stirring temperature

The clay particles are more finely dispersed in epoxy that was prepared at high temperature compared to room temperature. In the absence of high speed stirring, Figure 4.8a (Tm) shows a greater density of small particles and a lower density of large particles than Figure 4.7a (Rm). The average size was reduced from 4.15  $\mu\text{m}$  (Figure 4.7b and Table 4.3 with Rm method) to 3.39  $\mu\text{m}$  (Figure 4.8b and Table 4.3 with Tm method). There is no mechanical stirring effect for these two cases. According to the Equation 4.1 ( $F_{DT} = D + \tau$ ), only  $D$  contributes in these two cases due to the absence of mechanical stirring. In addition the viscosity of the mixture is lower during stirring with Tm (120°C) than stirring with Rm (room temperature), thus  $D_{Tm} > D_{Rm}$ . This may explain why the dispersion of clay in epoxy for the Tm method is better than for the Rm method.

In the presence of high speed stirring, Figure 4.11a (TS-24000 rpm) also shows a greater density of small particles and a lower density of large particles than Figure 4.10a (RS-24000 rpm). The average size was reduced from 0.56  $\mu\text{m}$  (Figure 4.10b and Table 4.3 with RS method) to 0.36  $\mu\text{m}$  (Figure 4.11b and Table 4.3 with TS method). It is expected that at the same stirring speed of 24000 rpm, stirring at room temperature (RS) generates higher shear compared to stirring at 120°C (TS) due to the viscosity reduction at elevated temperature, and high shear can help to separate clay particles better with RS compared to TS; however it is not the case. Although high shear was generated inside the rotor/stator region of the homogenizer, it was difficult to achieve good global stirring at room temperature compared to 120°C. One tried to keep the temperature of the mixture in the RS method as close to room temperature as possible. However, the temperature in between the rotor and stator of the homogenizer is almost around 120°C. Because of this, the shear forces imposed on the clays for these two cases (RS and TS stirring methods) are almost similar ( $\tau_{TS} \approx \tau_{RS}$ ). Moreover,  $D_{TS}$  is higher than  $D_{RS}$  (due to reduction of viscosity for the whole mixture at elevated temperature). Therefore  $F_{DT(TS)} > F_{DT(RS)}$  and this may explain why stirring with TS results in a finer dispersion compared to RS. The effect of temperature on the maximum and average sizes of clay aggregates for the conditions without stirring and stirring at high speed (24000 rpm) is shown in Figure 4.13. The reduction of the size indicates that high-temperature stirring has a positive effect on the general dispersion of the clay in the materials, demonstrating that the thermodynamics of the system plays an important role in the clay dispersion.



**Figure 4.13. The effect of stirring temperature and speed on the size of clay aggregates**

#### 4.3.1.2. The effect of stirring speed

The effect of stirring speed on the dispersion of clay in epoxy was examined. Stirring speed shows a significant effect on the average size of clay particles. The large aggregates disappeared with high speed stirring. The presence of large aggregates mainly indicates poor mixing and poor dispersion. This suggests that high speed helped to reduce the size of particles.

At the same stirring temperature, SEM shows a more homogeneous dispersion with size of particles much smaller for stirring by the homogenizer as compared to stirring by mechanical mixer or by hand (At room temperature: Figure 4.10a (RS) versus Figure 4.7a (Rm), or at 120°C: Figure 4.11a (TS) versus Figure 4.9a (TM) and Figure 4.8a (Tm)).

Speed shows a strong effect on the maximum and on the average sizes of clay particles. The average size was reduced from 4.15  $\mu\text{m}$  (Figure 4.7b and Table 4.3 with 0 rpm - Rm method) to 0.56  $\mu\text{m}$  (Figure 4.10b and Table 4.3 with 24000 rpm - RS method), and from 3.39  $\mu\text{m}$  (Figure 4.10b and Table 4.3 with 0 rpm - Tm method) to 2.80  $\mu\text{m}$  (Figure 4.11b and Table 4.3 with 1000 rpm - TM method) and to 0.36  $\mu\text{m}$  (Figure 4.11b and Table 4.3 with 24000 rpm - TS method). At the same stirring temperature of room temperature, high speed stirring shows a strong effect on dispersion of clay (comparing between RS and Rm). It is clear that  $\tau_{RS} > \tau_{Rm}$  and  $D_{RS} \approx D_{Rm}$  (in general). This results in  $\tau_{tD(RS)} > \tau_{tD(Rm)}$  and the dispersion of clay in epoxy for RS > Rm. At the same stirring temperature of 120°C, mechanical stirring at 1000rpm (TM) does not show a significant change in the morphology of material compared to hand stirring (Tm). The first effect of thermodynamics is similar for TM and Tm methods ( $D_{TM} = D_{Tm}$ ). The second effect of shear  $\tau_{TM}$  may not be strong for TM method while  $\tau_{Tm} \approx 0$ . Because of this, there is no significant difference between  $F_{DT(TM)}$  and  $F_{DT(Tm)}$ . This may explain why the dispersion of clay into epoxy for these two cases is not significantly different. Comparing the TS, TM and Tm methods, it is clear that  $D_{TS} = D_{TM} = D_{Tm}$  (same temperature) and  $\tau_{TS} > \tau_{TM} > \tau_{Tm} = 0$  (speed of stirring in the order of  $\nu_{TS} > \nu_{TM} > \nu_{Tm} = 0$ ). From this  $F_{DT(TS)} \gg F_{DT(TM)} > F_{DT(Tm)}$  and results in the order of dispersion of TS > TM > Tm. The effect of speed on the maximum and average sizes of clay aggregates can be seen in Table 4.3 and Figure 4.14. The reduction of the size in this case indicates that high speed stirring also plays an important role in the clay dispersion.

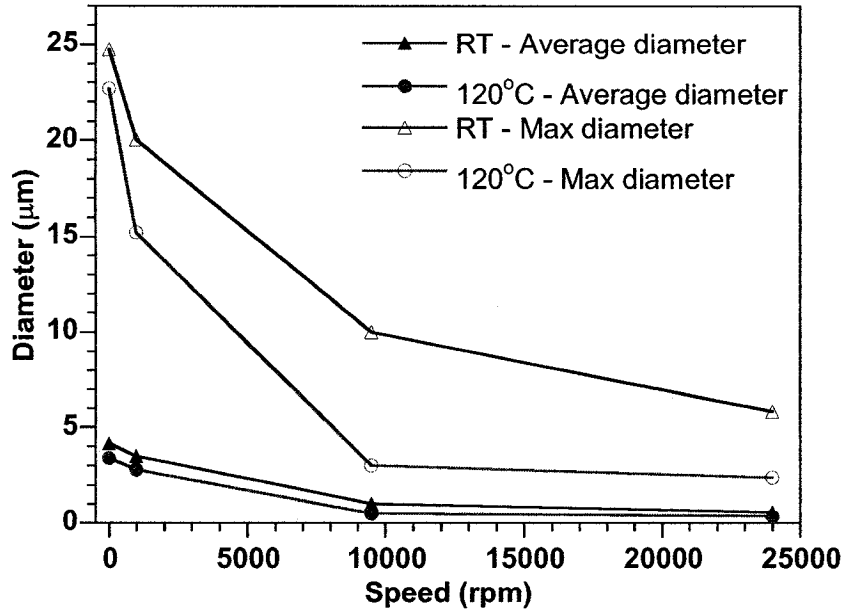


**Figure 4.14. The effect of stirring speed and temperature on the size of clay aggregates**

The results also show that better dispersion of clay in epoxy is obtained from the RS method than from the TM method. One can know that  $\tau_{RS} \gg \tau_{TM}$  and  $D_{RS} < D_{TM}$ . However  $D_{RS}$  is not significantly smaller than  $D_{TM}$ . This results in  $F_{DT(RS)} > F_{DT(TM)}$ . It can be concluded here that high speed plays a very important role in the clay dispersion. In addition, with high speed and temperature (Figure 4.11a), Cloisite 30B is more finely dispersed in the nanocomposite than without mechanical stirring and temperature (Figure 4.7a). Thus both temperature and speed have an effect on the dispersion of clay in epoxy at the stirring step. So far, one can conclude here that the micro dispersion of the clay in epoxy follows the order  $TS > RS > TM > Tm > Rm$ . It can be seen in Figure 4.12, where a shift of the peak to the left indicates that the size of the particles is smaller. Moreover, the peak also becomes narrower in the presence of high speed and high temperature

during stirring. The narrower is the peak on the distribution curve; the better is the mono dispersion of the clay particles in epoxy. Thus large aggregates have been broken down to smaller particles and made more uniform by high speed and high temperature stirring. However, it seems that speed is more powerful compared to temperature.

## **4.3.2. The intercalation**

### **4.3.2.1. The effect of stirring temperature**

XRD is widely used to determine the structure of PNCs due to its simple sample preparation and easy to interpret results. In XRD curves, the peak location (peak at angle  $2\theta$ ), which relates to the gallery distance, can indicate the intercalation degree. The intensity of peaks or area under peaks, which relates to the amount or the size of clay clusters, can indicate the exfoliation degree or the size of clusters. The  $d$ -spacing of organoclay C30B alone and C30B in liquid epoxy resin with different stirring temperatures (in the absence of hardener) were examined by X-ray diffraction and the results are shown in Figure 4.15. C30B has one peak at  $4.8^\circ$  and this is related to the  $d$ -spacing of  $18.5 \text{ \AA}$ . It appears that in epoxy-clay mixtures, there are two distinct peaks at around  $2.3^\circ$  to  $2.4^\circ$  and  $4.7^\circ$  to  $4.8^\circ$ , which may be interpreted in terms of two different extents of clay intercalation. However, according to Bragg's law, the harmonic peak (reflection peak) of the first one (around  $2.3^\circ$  to  $2.4^\circ$ ) should be around the same location at  $4.6^\circ$  to  $4.8^\circ$ . However, by coincidence this second peak is located right at the position of the original C30B peak (Figure 4.15). Therefore it is not clear whether the second peak corresponds to the harmonic peak of the first one, or to the remaining C30B that has not been further intercalated by epoxy resin, or to both of them. Because of this, it is difficult

to say whether there is only one clay intercalation level in the mixtures of epoxy-clay (at the position of the first peak on XRD curves) or whether there are two different clay intercalation levels. It appears from the XRD curves that the first peak shifts to a lower angle for all epoxy-clay mixtures compared to the peak of the starting clay C30B and the intensity also decreases. A shift of the peak to lower angle proves that intercalation has taken place during the stirring step. The clay layer separation (degree of intercalation is around 37.2 Å to 38.1 Å) is considerably higher than in the original C30B (18.5 Å). XRD curves for the epoxy-clay mixtures which were prepared at different temperatures show very similar trends and clays have been well further intercalated by the epoxy resins at the stirring step.

It can also be seen that even with the Tm and Rm methods, the clay has already been intercalated by epoxy resin. This means that liquid epoxy resin can easily diffuse into the clay galleries and further intercalate the clay even without the presence of high speed. It also can be seen here there is a small increase in the *d*-spacing for epoxy-clay mixture which was prepared at high temperature at 180°C and 120°C compared to the mixture which was prepared at room temperature (Figure 4.16). It seems that the diffusion of epoxy molecules into clay galleries almost reached the equilibrium value after 1 hour at room temperature with the Rm method.

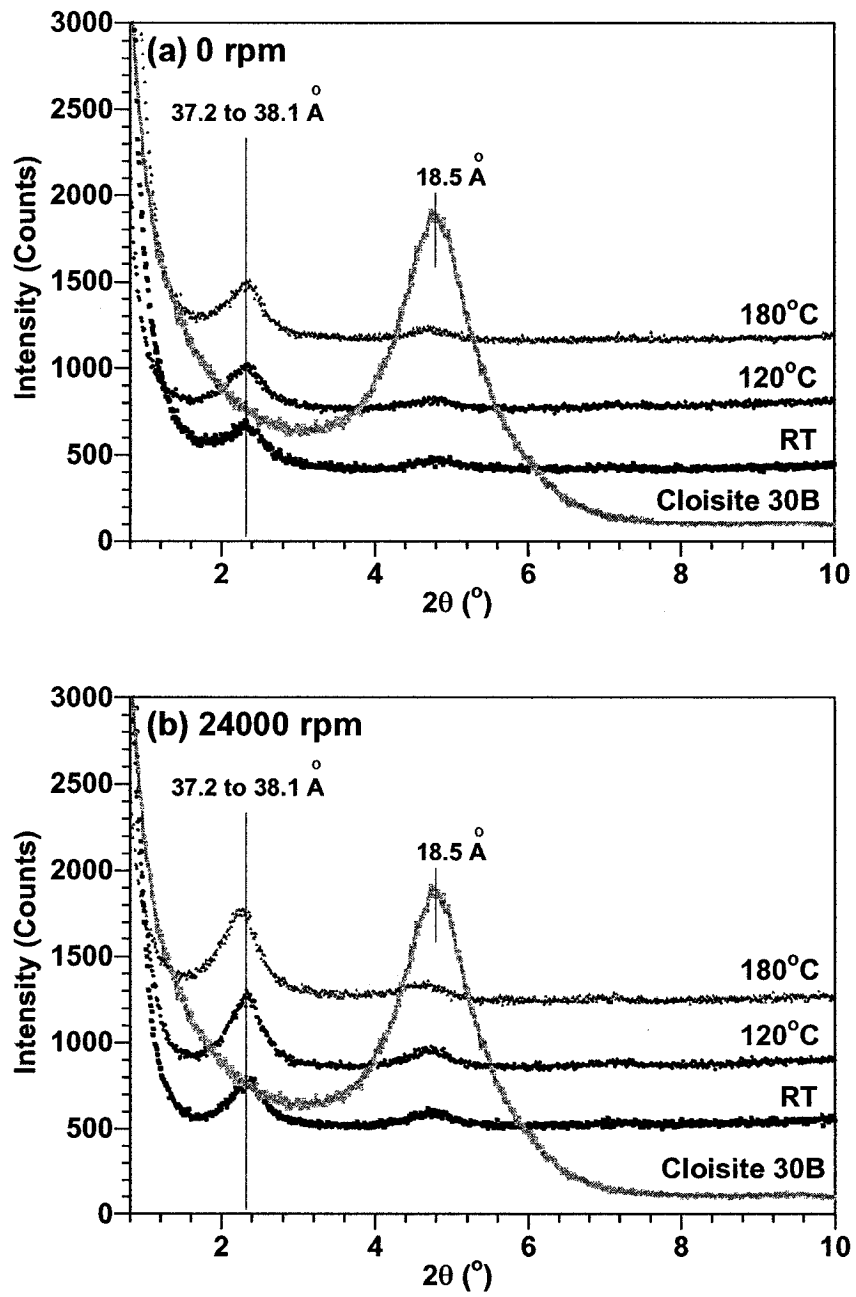
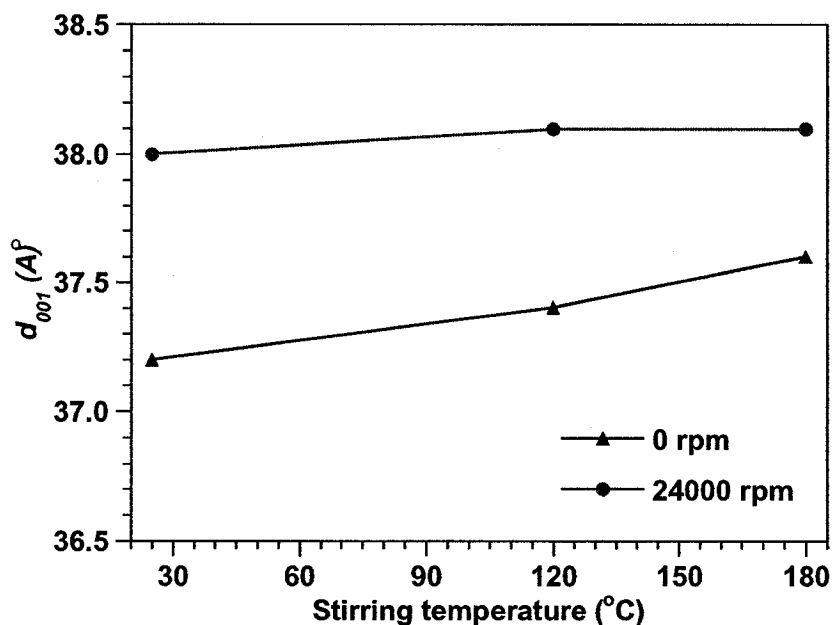


Figure 4.15. X-ray diffraction curves of C30B and its EPON828-C30B mixtures after being stirred at different temperatures: (a) 0 rpm and (b) 24000 rpm





**Figure 4.16. The effect of stirring temperature and speed on  $d_{001}$  of EPON828-C30B mixtures**

#### 4.3.2.2. The effect of stirring speed

The effect of stirring speed on the intercalation/exfoliation of clay in epoxy was examined by XRD. The results are shown in Figure 4.17. There is only a slight increase of the  $d$ -spacing for epoxy-clay mixture which was prepared with high speed at room temperature (RS) compared to the mixture which was prepared without mechanical stirring at room temperature (Rm), and there is a slight increase of the  $d$ -spacing for epoxy-clay mixture which was prepared with high speed and high temperature (TS) compared to the mixture which was prepared without mechanical stirring at high temperature (Tm) (Figure 4.18).

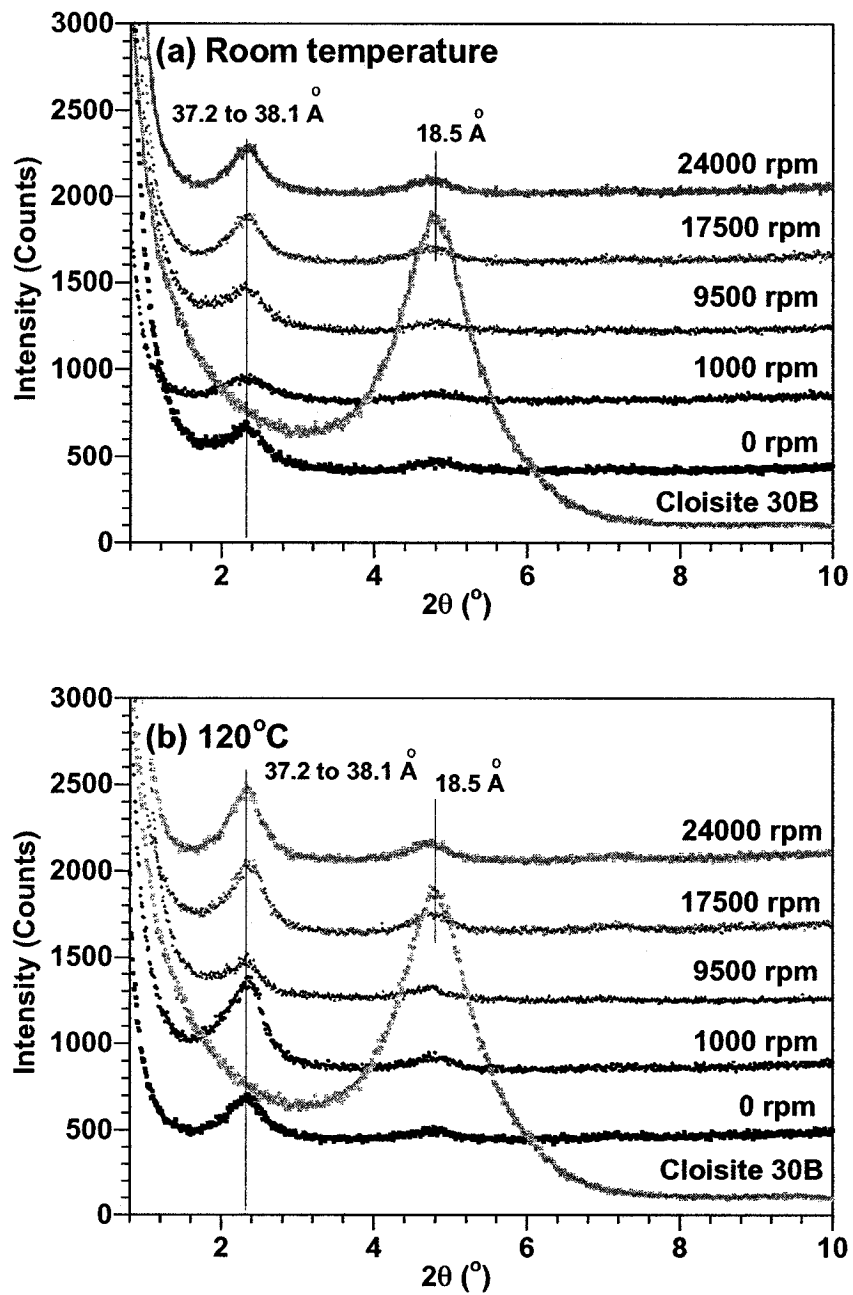
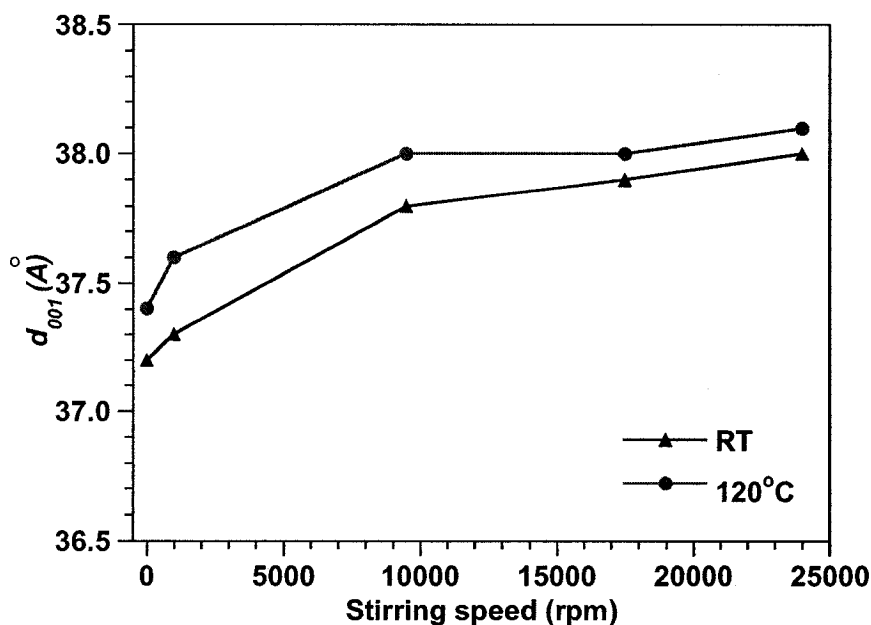


Figure 4.17. X-ray diffraction curves of C30B and its EPON828-C30B mixtures after being stirred at different speeds: (a) room temperature and (b) 120°C



**Figure 4.18.** The effect of stirring speed on  $d_{001}$  of EPON828-C30B mixtures

The X-ray diffraction curves of EPON828-C30B mixtures after being stirred using different methods are shown in Figure 4.19. The summary of the first peak's position ( $d_{001}$ ) on XRD curves of the epoxy-clay mixtures, as well as the difference  $\Delta d$  between the positions of these peaks and that of the peak of C30B, are shown in Table 4.4. Generally speaking,  $d$ -spacing for TS > RS, Tm > Rm, TS > Tm and RS > Rm. However, the increases of the  $d$ -spacing are not significant. The  $d$ -spacing is still around 37.2 Å to 38.1 Å for all cases. Unexpectedly, the basal spacing  $d$  of organoclay in epoxy did not obviously increase even with high temperature and high speed aids. Moreover, the presence of the identical peaks on XRD curves for the epoxy-clay mixtures clearly indicates that the clay was not fully exfoliated at stirring step. From there, it can be concluded that playing with the speed and temperature does not lead to full exfoliation of clay in epoxy resin at the stirring step for this study.

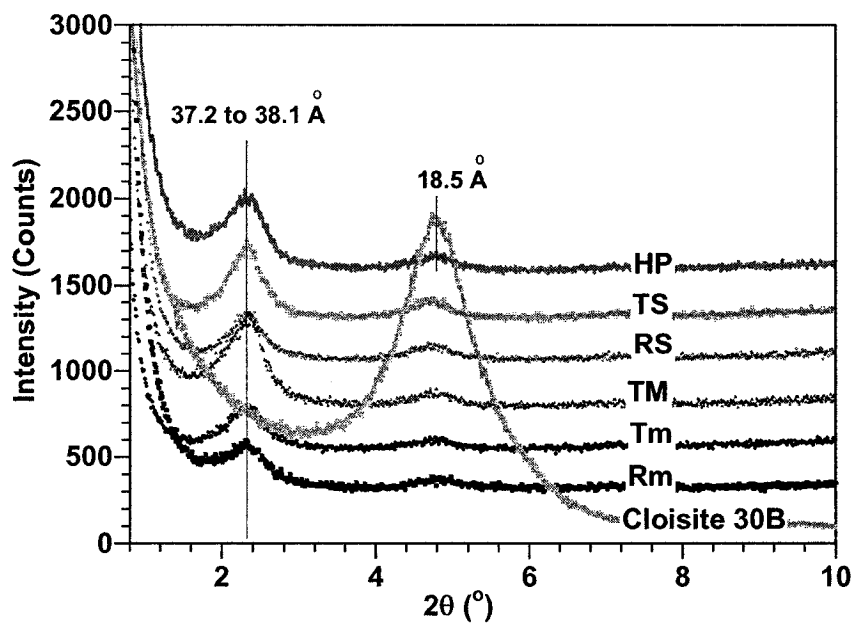


Figure 4.19. X-ray diffraction curves of EPON828-C30B mixtures after being stirred using different methods

Table 4.4. Summary XRD results EPON828-C30B mixtures after being stirred using different methods

Stirring method	Gallery distance (Å)	
	$d_{001}$	$\Delta d$
Cloisite 30B	18.5	
Rm	37.2	18.7
Tm	37.4	18.9
TM	37.6	19.1
RS	38.0	19.5
TS	38.1	19.6
HP	37.3	18.8

#### 4.3.2.3. The effect of stirring duration

The effects of stirring duration on the intercalation/exfoliation of clay in epoxy were also investigated. X-ray diffraction curves of the epoxy and C30B prepared by high speed of stirring at 9500, 17500, and 24000 rpm at 2, 4, 10, 20, 30, 45, and 60 minutes are illustrated in Figures 4.20, 4.21, and 4.22. The summary of the first peak's position ( $d_{001}$ ) on XRD curves of the epoxy-clay mixtures, as well as the difference  $\Delta d$  between the positions of these peaks and that of the peak of C30B, are shown in Table 4.5. Again, it can be seen that the clays have been well intercalated by the epoxy resin. There are two distinct peaks at around  $2.3^\circ$  to  $2.4^\circ$  and  $4.7^\circ$  to  $4.8^\circ$  for all cases. As discussed above, it is also difficult to say if there is only one clay intercalation level in the mixtures of epoxy-clay (at the position of the first peak on the XRD curves) or whether there are two different clay intercalation levels for these cases. There is only a slight difference between the positions of the peak on the XRD curves for all the epoxy-clay mixtures, either at different stirring rates or at different durations. As a consequence, there is only a small increase in the  $d$ -spacing with increase in the durations of stirring (especially if the error of the test is considered), which is not obviously seen (Figure 4.23). It can be noted here that stirring duration does not significantly affect the exfoliation of clay in epoxy resin at this step of fabrication.

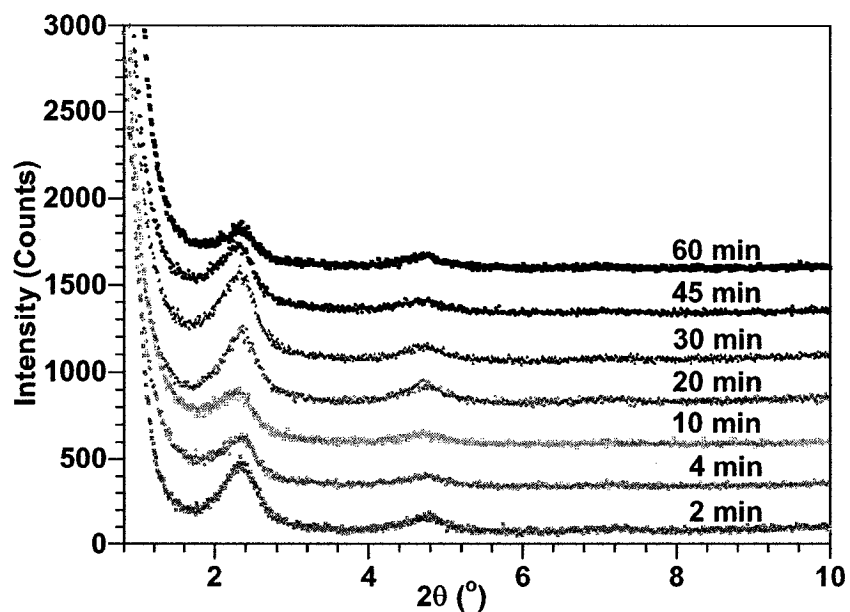


Figure 4.20. X-ray diffraction curves of EPON828-C30B mixtures after being stirred at 120°C for different durations with high speed (9500 rpm)

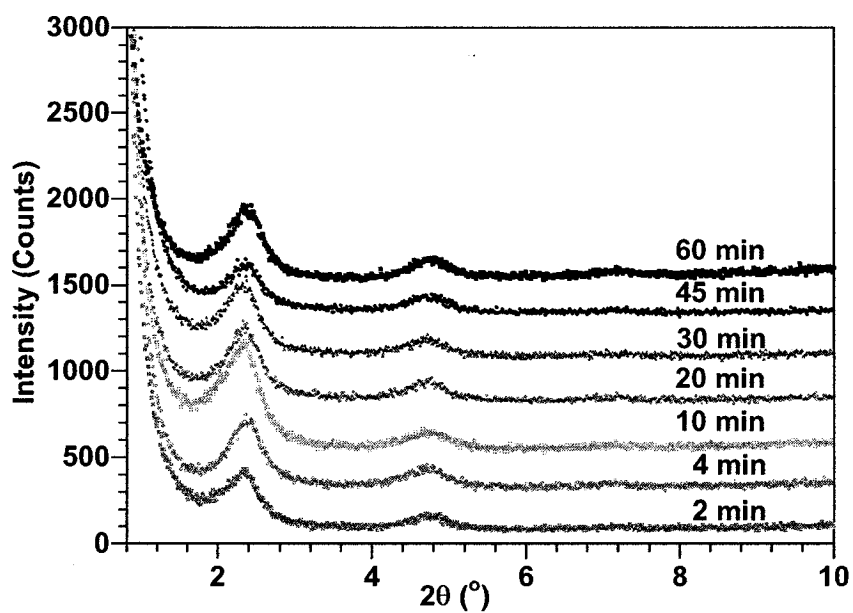


Figure 4.21. X-ray diffraction curves of EPON828-C30B mixtures after being stirred at 120°C for different durations with high speed (17500 rpm)

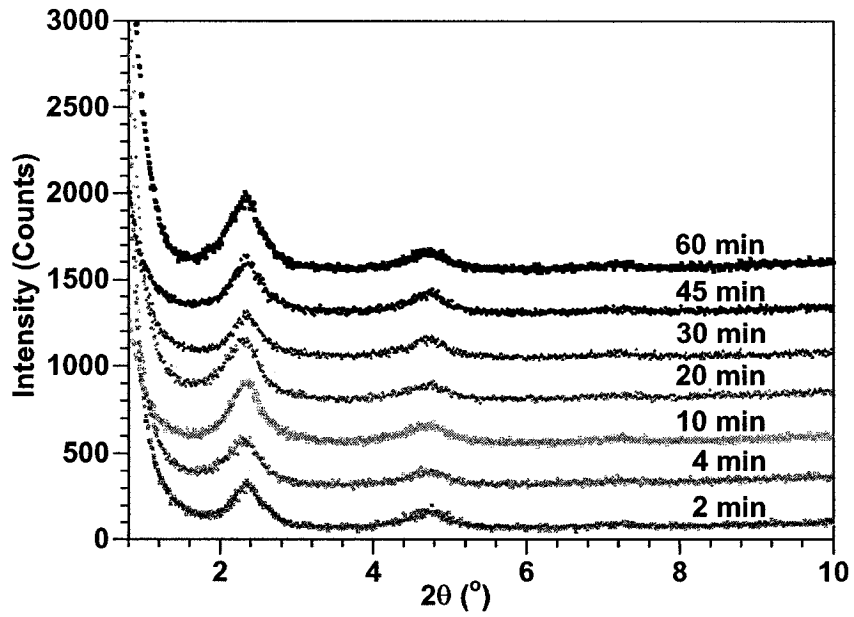
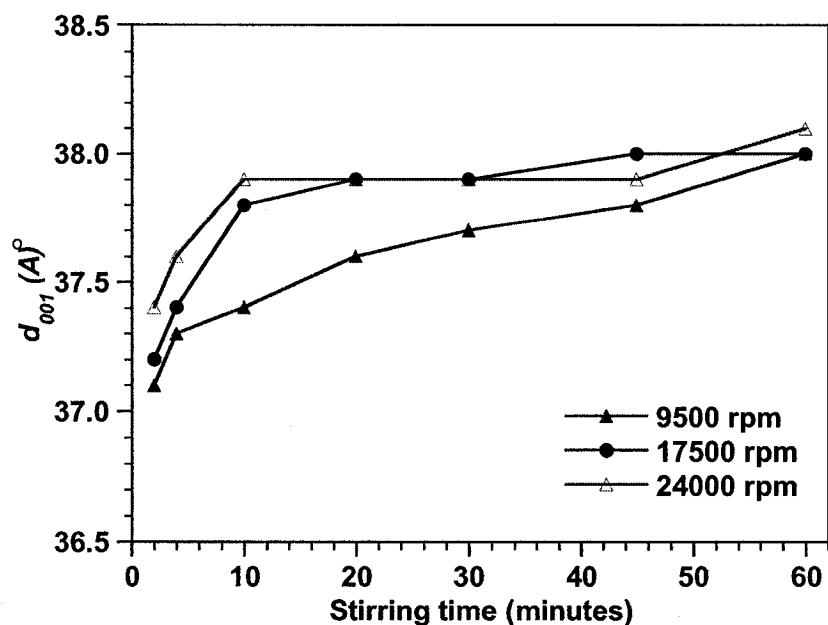


Figure 4.22. X-ray diffraction curves of EPON828-C30B mixtures after being stirred at 120°C for different durations with high speed (24000 rpm)

Table 4.5. Summary XRD results of EPON828-C30B mixtures after being stirred at 120°C for different durations with high speed (9500, 17500 and 24000 rpm)

Duration of stirring (min)	Gallery distance (Å)					
	Stirred at 120°C and 9500 rpm		Stirred at 120°C and 17500 rpm		Stirred at 120°C and 24000 rpm	
	$d_{001}$	$\Delta d$	$d_{001}$	$\Delta d$	$d_{001}$	$\Delta d$
2	37.1	18.6	37.2	18.7	37.4	18.9
4	37.3	18.8	37.4	18.9	37.6	19.1
10	37.4	18.9	37.8	19.3	37.9	19.4
20	37.6	19.1	37.9	19.4	37.9	19.4
30	37.7	19.1	37.9	19.4	37.9	19.4
45	37.8	19.3	38.0	19.5	37.9	19.4
60	38.0	19.5	38.0	19.5	38.1	19.6



**Figure 4.23.** The effect of stirring duration on  $d_{001}$  of EPON828-C30B mixtures

Stirring with high speed (24000 rpm) at room temperature and at 180°C for different durations are also considered. The results are shown in Figures 4.24 and 4.25. The summary of the first peak's position ( $d_{001}$ ) on XRD curves of the epoxy-clay mixtures as well as the difference  $\Delta d$  between the positions of these peaks and that of the peak of C30B, are shown in Table 4.6. Again the results here do not show a significant difference in the peak positions on the XRD curves. All curves show very similar trends. General speaking, organoclay may swell and reach the equilibrium state of the basal spacing. The results also indicated that it is difficult to further expand the clay gallery even with the external action such as stirring. From the XRD results, the stirring step did not lead to full exfoliation of clay. The question here remains whether the clays are partially exfoliated, which the XRD analysis can not reveal.



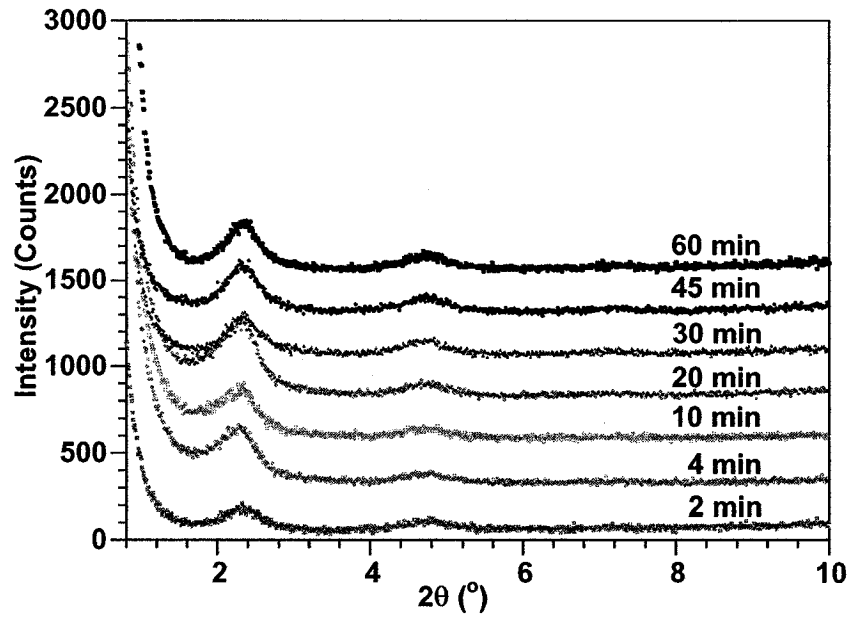


Figure 4.24. X-ray diffraction curves of EPON828-C30B mixtures after being stirred at room temperature for different durations with high speed (24000 rpm)

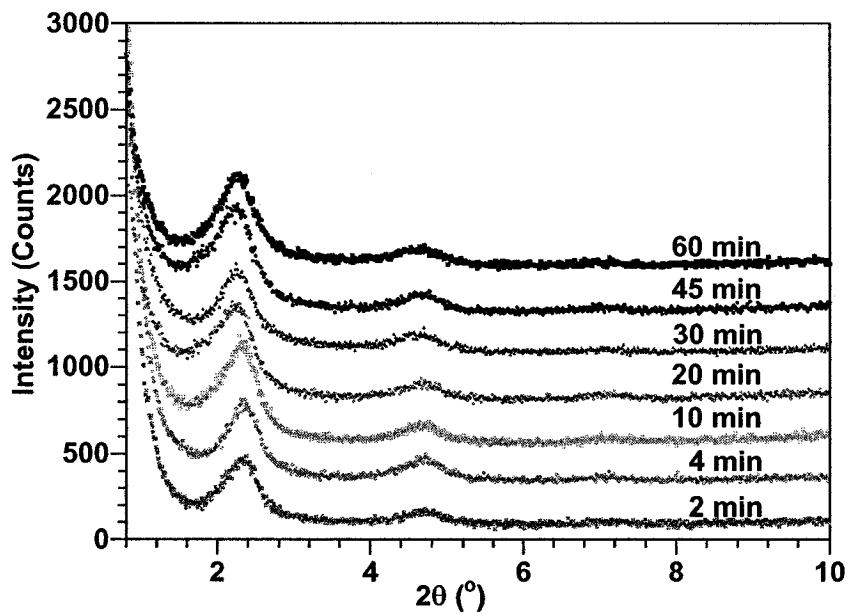


Figure 4.25. X-ray diffraction curves of EPON828-C30B mixtures after being stirred at  $180^\circ\text{C}$  for different durations with high speed (24000 rpm)

**Table 4.6. Summary XRD results of EPON828-C30B mixtures after being stirred at room temperature (RT) and 180°C with high speed (24000 rpm)**

Duration of stirring (min)	Gallery distance (Å)			
	Stirred at RT and 24000 rpm		Stirred at 180°C and 24000 rpm	
	$d_{001}$	$\Delta d$	$d_{001}$	$\Delta d$
2	37.4	18.9	37.6	19.1
4	37.6	19.1	37.7	19.2
10	37.8	19.3	37.7	19.2
20	37.9	19.4	37.8	19.3
30	37.9	19.4	37.9	19.4
45	38.0	19.5	38.0	19.5
60	38.0	19.5	38.0	19.5

#### 4.3.2.4. The effect of clay chemistry

The  $d$ -spacing of C30B and I30E in liquid epoxy resin after being stirred with Rm and Tm (in the absence of hardener) were examined by X-ray diffraction and the results are shown in Figure 4.26. C30B has one peak at 4.8° and this is related to the  $d$ -spacing of 18.5 Å (as discussed above), whereas I30E has two peaks at around 3.7° and 8.0° and they are related to the  $d$ -spacing of 23.8 Å and 11.0 Å, respectively. It appears that in the epoxy-clay mixtures, there are two distinct peaks at around 2.3° to 2.4° and 4.7° to 4.8° for both types of clay. As discussed above, it is difficult to say whether there is only one clay intercalation level or whether there are two different clay intercalation levels in the mixtures of EPON828-C30B due to the fact that the second peak in XRD curve is located right at the peak of the starting clay C30B. On the other hand, the second peak in the XRD curves for the mixtures of EPON828-I30E is located around 4.7° to 4.8°. This second peak may relate to the harmonic peak (reflection peak) of the first one. It appears from the XRD curves that the first peak shifts to a lower angle for EPON828-I30E

mixtures compared to the peak of the starting clay I30E (this is similar to the case for the C30B). A shift of the peak to lower angle proves that intercalation has taken place at the stirring step for both types of clay. The results also indicated that the intercalation is very similar for C30B and I30E after they have been added to epoxy resin. It seems that clay chemistry does not have a strong effect on the intercalation of clay in epoxy (within Rm and Tm methods) at the stirring step.

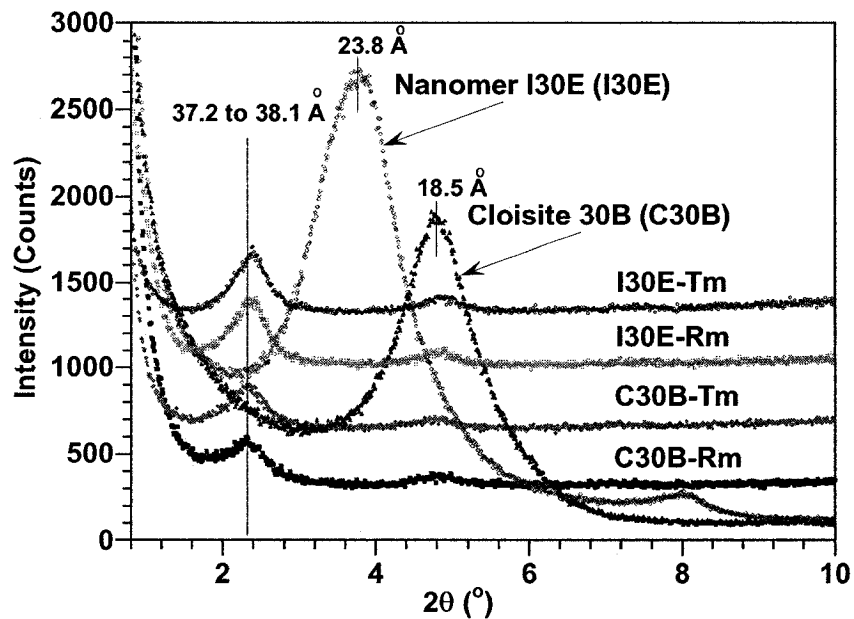


**Figure 4.26. X-ray diffraction curves of EPON828-C30B, EPON828-I30E mixtures after being stirred with Rm and Tm methods**

### 4.3.3. Rheological properties of epoxy-clay mixtures

#### 4.3.3.1. The effect of stirring temperature

The rheological properties of the epoxy-clay suspension were measured with a Brookfield CAP2000+ viscometer, using cone and plate geometry.

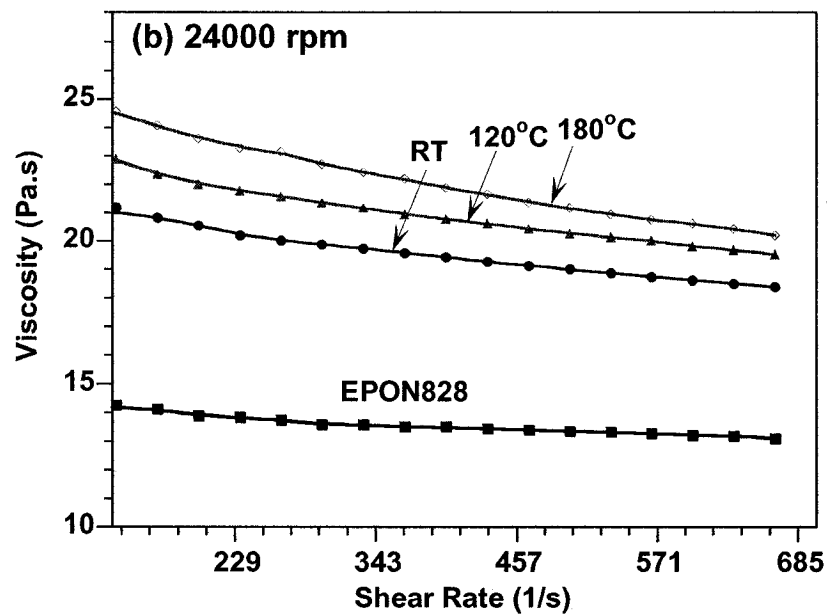
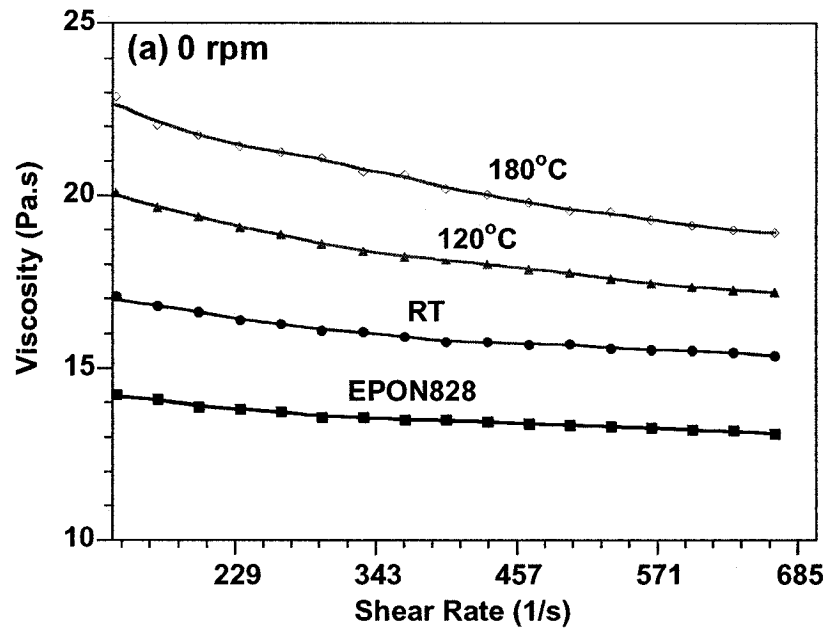


**Figure 4.27. Viscosity-shear rate curves of EPON828-C30B mixtures after being stirred at different temperatures for two speeds: (a) 0 rpm and (b) 24000 rpm**

Figure 4.27 shows the viscosity-shear rate curves at 25°C of epoxy EPON 828 and its mixtures with organoclay C30B after being stirred at different temperatures for two

different speeds of 0 rpm and 24000 rpm. There is only a slight decrease in the viscosity of EPON 828 with the shear rate; thus this epoxy resin can be considered as a Newtonian fluid more or less. With the presence of clay, the viscosity of the epoxy-clay suspension increases compared to epoxy. However, the viscosity of epoxy-clay also decreases with the shear rate.

The effect of stirring temperature on the viscosity of epoxy-clay mixture at a shear rate of  $167.s^{-1}$  is shown in Figure 4.28. Stirring at high temperature for both 0 rpm and 24000 rpm showed higher viscosity compared to room temperature. The higher is the stirring temperature, the higher is the viscosity of the epoxy-clay suspension. In general, the rheological properties of the suspension depend on the following factors: (1) the viscosity of the fluid medium; (2) the content of solid particles; (3) the size and the shape of particles; and (4) the forces of interaction between the particles. As the system is prepared from the same epoxy resin with the same type of clay and the same clay concentration, the increase in the viscosity of the suspension should be related to the size and shape of clay particles in epoxy. Apparently clay particles were broken down into smaller ones during stirring.

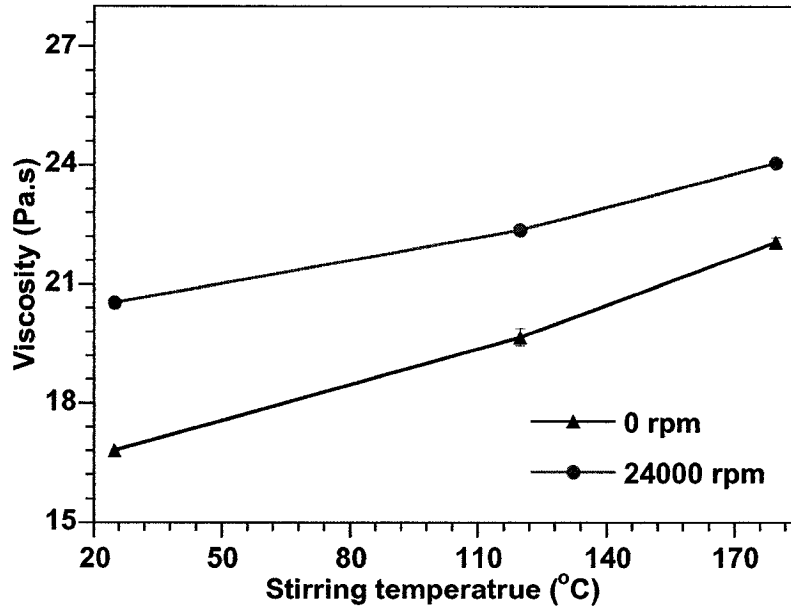


**Figure 4.28. The effect of stirring temperature on viscosity of EPON828-C30B after being stirred at 0 rpm and 24000 rpm for 60 minutes, at shear rate 167 (1/s)**

#### 4.3.3.2. The effect of stirring speed

Figure 4.29 shows the viscosity-shear rate curves at 25°C of epoxy EPON 828 and its mixture with organoclay C30B after being stirred at different speeds of 0 rpm, 1000 rpm, and 24000 rpm for two different temperatures (room temperature and 120°C). In general, stirring at higher speed for both room temperature and 120°C showed higher viscosity compared to low speed. There is not much difference in viscosity between the suspension which was stirred at 1000 rpm and the one without stirring. The effect of stirring speed on the viscosity of epoxy-clay mixture at shear rate of  $167.s^{-1}$  is shown in Figure 4.30. As discussed above, the increase in the viscosity of the suspension may be due to the reduction of size of particles and higher aspect ratio of clay particles after being stirred at high speed compared to without stirring.

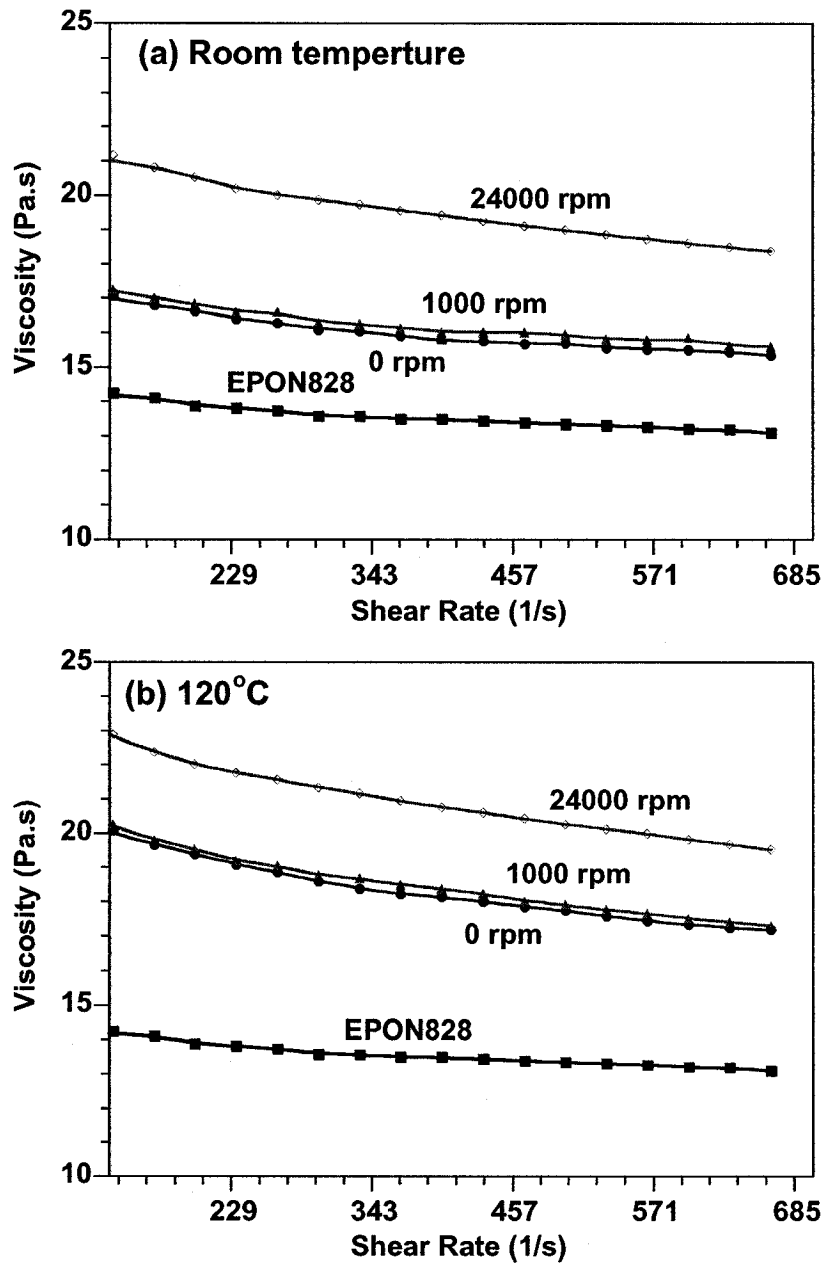
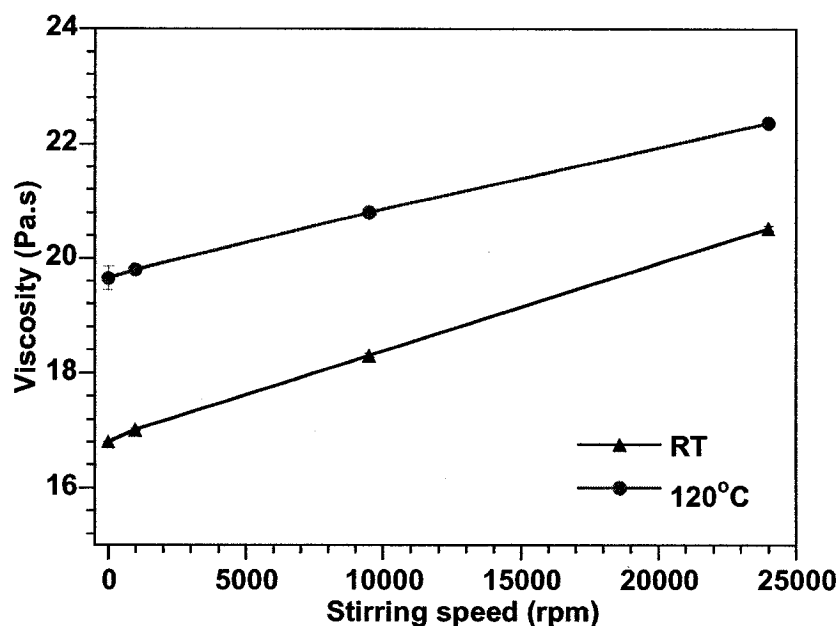


Figure 4.29. Viscosity-shear rate curves of EPON828-C30B mixtures after being stirred at different speeds for two temperatures: (a) RT and (b) 120°C



**Figure 4.30. The effect of speed on viscosity of EPON828-C30B after being stirred at RT and 120°C for 60 minutes, at shear rate 167 (1/s)**

Figure 4.31 shows the viscosity-shear rate curves of epoxy EPON 828 and its mixture with organoclay C30B made by different stirring methods at 25°C. The effect of stirring methods on the viscosity of epoxy-clay mixtures at shear rate of  $167.s^{-1}$  is shown in Figure 4.32. It can be seen here that the viscosity of the suspensions changes according to stirring condition and it is in the following order:  $\eta_{TS} > \eta_{RS} > \eta_{TM} > \eta_{Tm} > \eta_{Rm}$  (Figures 4.31 and 4.32). The temperatures and shear show a positive effect on the viscosity of the suspension. For example:  $\eta_{Tm} > \eta_{Rm}$ ,  $\eta_{TS} > \eta_{RS}$  (temperature effect) and  $\eta_{RS} > \eta_{Rm}$ ,  $\eta_{TS} > \eta_{Tm}$  (speed effect). Again the result here confirms that the clay has a better dispersion in epoxy resin when increased the temperature and high speed are introduced.



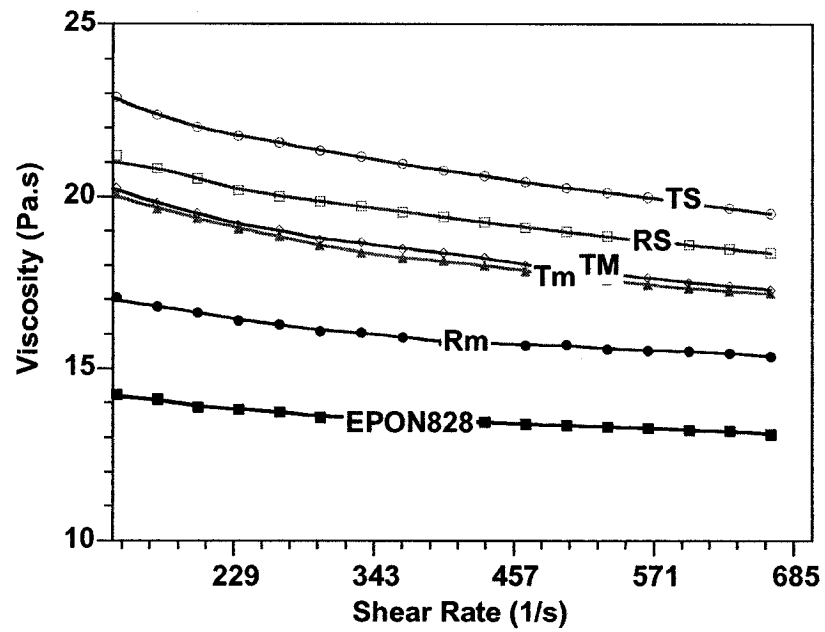


Figure 4.31. Viscosity-shear rate curves of EPON828-C30B mixtures after being stirred with different methods

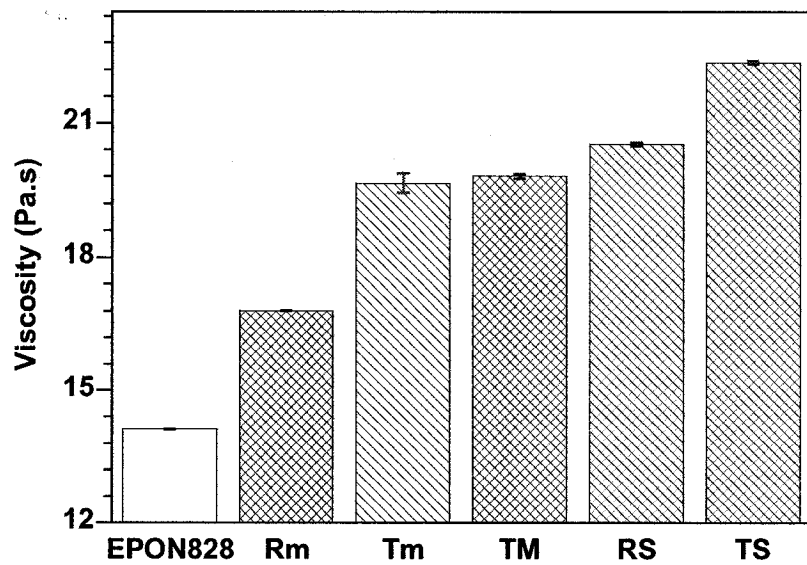


Figure 4.32. Viscosity of EPON828 and its mixture with C30B after being stirred with different methods for 60 minutes, at shear rate 167 (1/s)

The relationship between shear stress and shear rate is shown in Figure 4.33. The shear stress has almost a linear increase with the shear rate for all curves. The apparent viscosity of these suspensions may be obtained by equation as follows

$$\tau = \eta \dot{\gamma} \quad (4.4)$$

where  $\tau$  is the shear stress,  $\dot{\gamma}$  is the shear rate and  $\eta$  is the apparent viscosity.

The results also indicate that the shear stress increases according to the stirring methods and it is in the order  $\tau_{TS} > \tau_{RS} > \tau_{TM} > \tau_{Tm} > \tau_{Rm}$ .

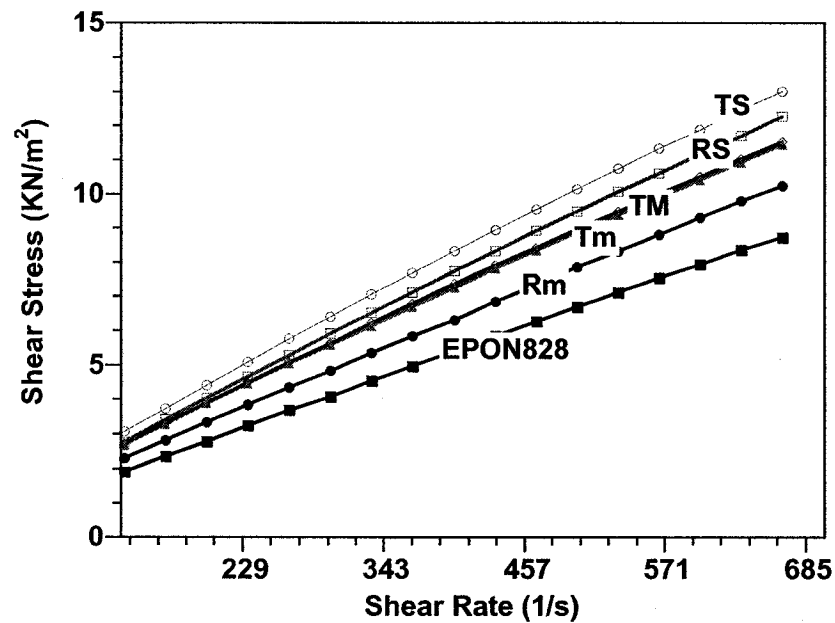


Figure 4.33. Shear stress-shear rate curves of EPON828-C30B mixtures after being stirred with different methods

#### 4.3.3.3. The effect of stirring duration

The rheological properties of the epoxy and its suspension with C30B made by RS and TS for different stirring durations of 2, 4, 10, 20, 30, 45 and 60 minutes were also examined. Figures 4.34 and 4.35 show the viscosity-shear rate curves of epoxy EPON 828 and EPON 828 with organoclay C30B prepared by RS and TS methods at different durations, respectively. The results indicate that with longer stirring duration, the viscosity of the suspension increases. As discussed, the viscosity increase is related to the level of dispersion of clay in epoxy. With increase in duration of stirring, the clay aggregates were broken down to smaller sizes which have higher aspect ratio and result in increase of viscosity. At the same duration of stirring, the viscosity of suspension prepared by TS method is always higher than the viscosity of suspension prepared by RS method. The speed again shows an evident effect on viscosity of the epoxy-clay suspension. At only two minutes stirring with high speed, the viscosity is higher than without mechanical stirring. For instance, the viscosity of epoxy-clay mixture prepared by two minutes with RS is higher than the viscosity of epoxy-clay mixture prepared by one hour with Rm, and the viscosity of epoxy-clay mixture prepared by two minutes with TS is higher than the viscosity of epoxy-clay mixture prepared by one hour with Tm. The order of the effect of stirring time on the viscosity of epoxy-clay mixtures is now  $\eta_{RS60min} > \eta_{RS45min} > \eta_{RS30min} > \eta_{RS20min} > \eta_{RS10min} > \eta_{RS4min} > \eta_{RS2min} > \eta_{Rm}$  (for mixing at room temperature) and  $\eta_{TS60min} > \eta_{TS45min} > \eta_{TS30min} > \eta_{TS20min} > \eta_{TS10min} > \eta_{TS4min} > \eta_{TS2min} > \eta_{Tm}$  (for stirring at 120°C).

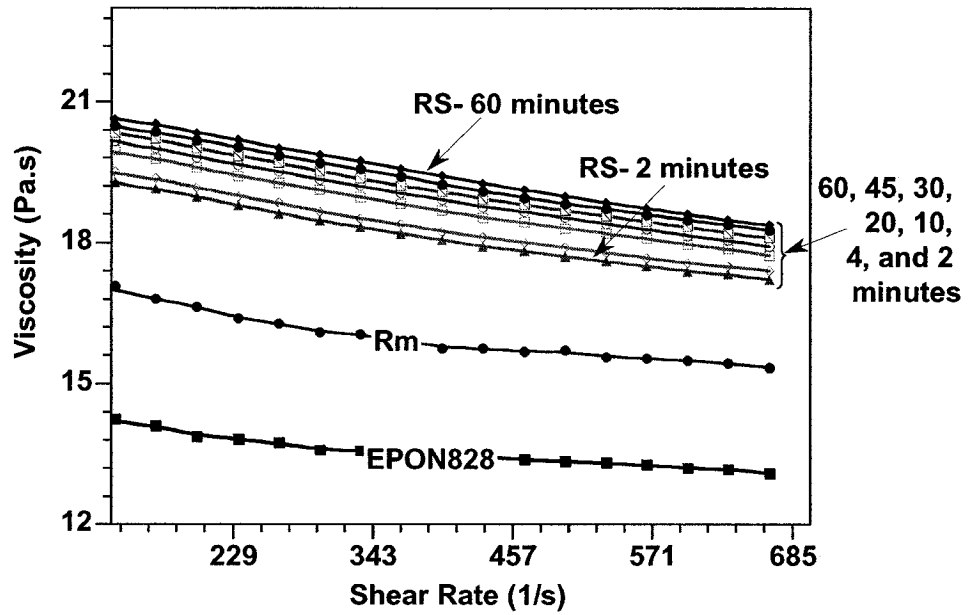


Figure 4.34. Viscosity-shear rate curves of EPON 828 and EPON828-C30B mixtures after being stirred by Rm method and RS method for different durations

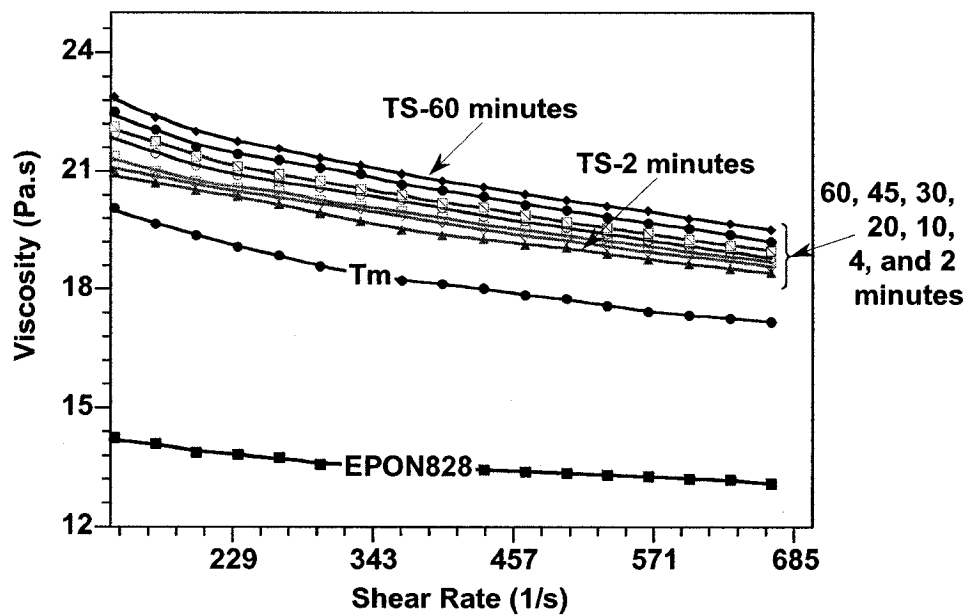
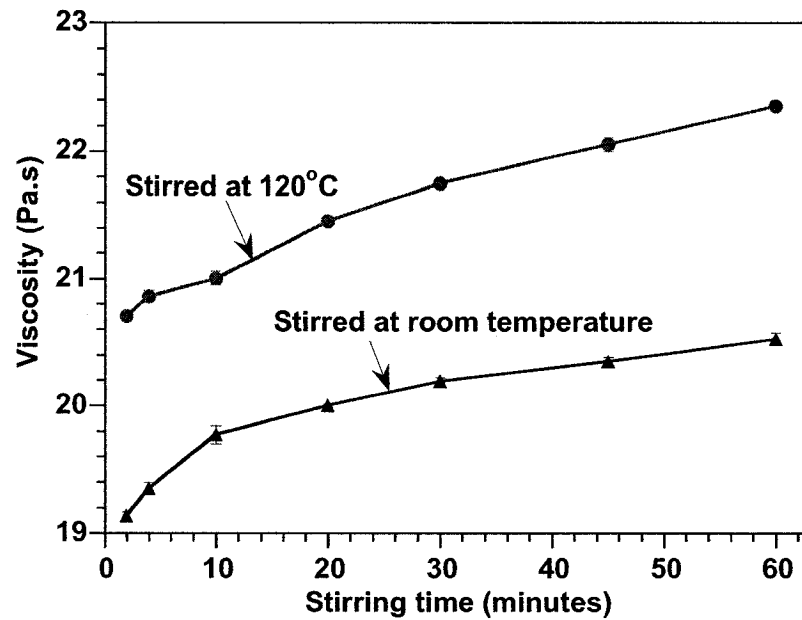


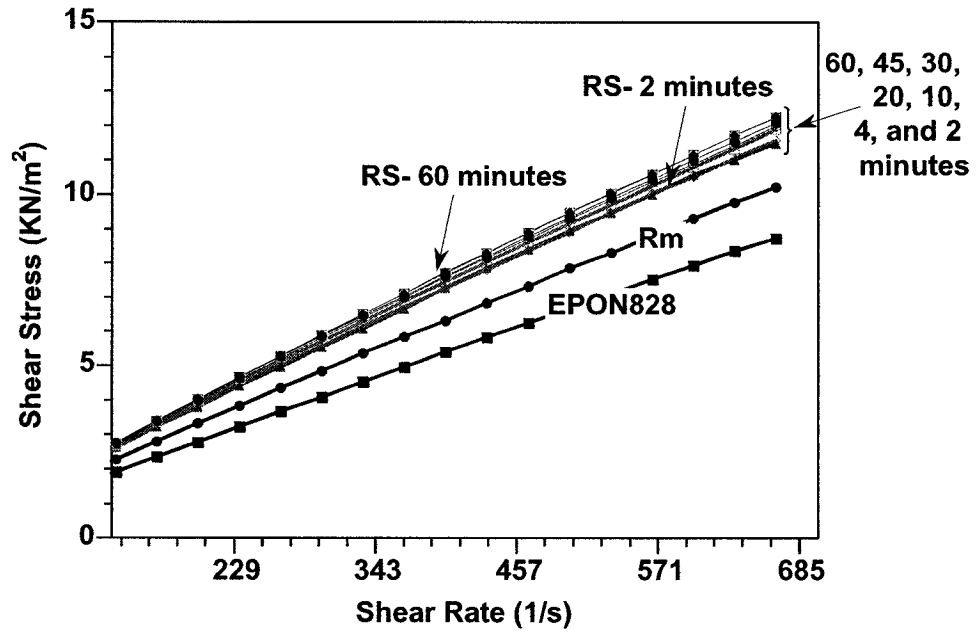
Figure 4.35. Viscosity-shear rate curves of EPON 828 and EPON828-C30B mixtures after being stirred by Tm method and TS method for different durations

Figure 4.36 shows the viscosity of EPON 828 and EPON828-C30B mixtures for different stirring durations after being stirred by RS method and TS method at shear rate 167 (1/s). Apparently, the viscosity of the EPON828-C30B mixtures increases with stirring duration. Thus the longer stirring time results in better dispersion.



**Figure 4.36. Viscosity of EPON828-C30B mixtures after being stirred by RS method and TS method for different durations, at shear rate 167 (1/s)**

Figures 4.37 and 4.38 show the relationship between shear stress and shear rate of epoxy EPON 828 and EPON 828 with organoclay C30B prepared by RS and TS methods for different durations of 2, 4, 10, 20, 30, 45 and 60 minutes, respectively. Shear stress also increases with duration of stirring. The order of the effect of stirring duration on the shear stress of epoxy-clay mixtures is now  $\tau_{RS60min} > \tau_{RS45min} > \tau_{RS30min} > \tau_{RS20min} > \tau_{RS10min} > \tau_{RS4min} > \tau_{RS2min} > \tau_{Rm}$  (for stirring at room temperature) and  $\tau_{TS60min} > \tau_{TS45min} > \tau_{TS30min} > \tau_{TS20min} > \tau_{TS10min} > \tau_{TS4min} > \tau_{TS2min} > \tau_{Tm}$  (for stirring at 120°C).



**Figure 4.37. Shear stress-shear rate curves of EPON 828 and EPON828-C30B mixtures after being stirred by Rm method and RS method for different durations**

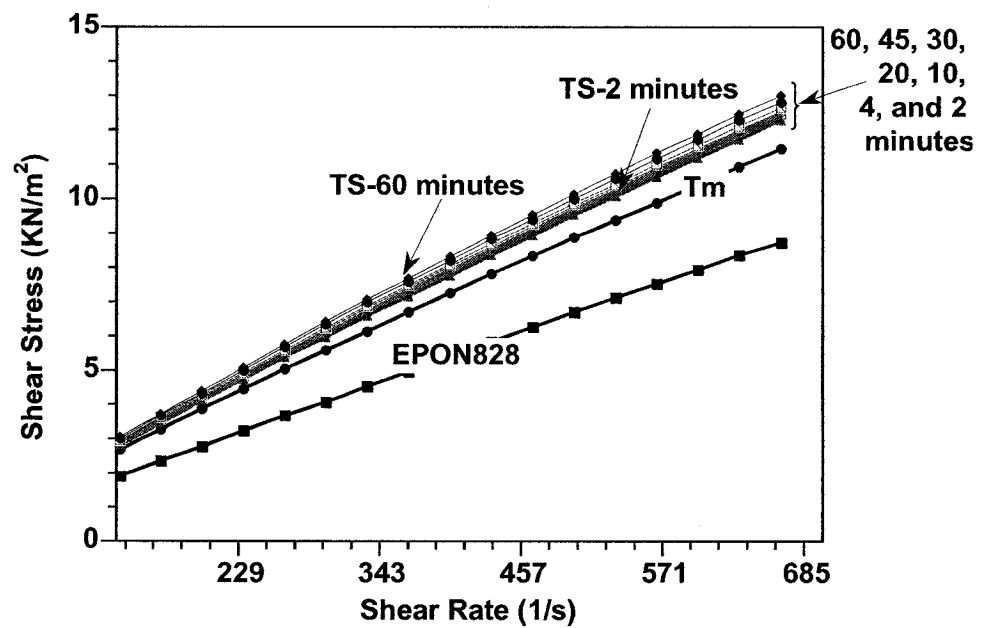


**Figure 4.38. Shear stress-shear rate curves of EPON 828 and EPON828-C30B mixtures after being stirred by Tm method and TS method for different durations**

Generally speaking, with the studied scale, the speed, temperature and duration of stirring do not lead to the exfoliation of clay in epoxy. However, they have influences on the dispersion of organoclay in epoxy resin at the micro level, and thus the mechanism for dispersion of clay in epoxy resin is proposed in Figure 4.39.

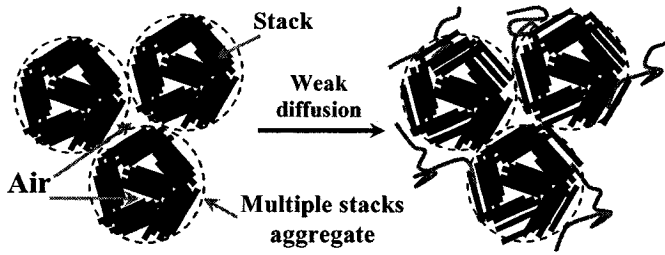
Without mechanical stirring and temperature ( $R_m$ ), a clay is readily intercalated by epoxy matrix (as can be seen in the XRD results, epoxy can easily diffuse into clay galleries even at room temperature). However, such a process can take place easily only on the aggregate surface, but will be very difficult to occur inside the aggregates. In the absence of shear, clays should remain in the form of large aggregates (non uniform intercalation and poor micro dispersion).

With assistance of only high speed ( $R_S$ ), the clay particles (aggregates) can be broken down to smaller sizes (stacks) and lead to fine and uniform dispersion. However, intercalation is likely at the surface of the stacks.

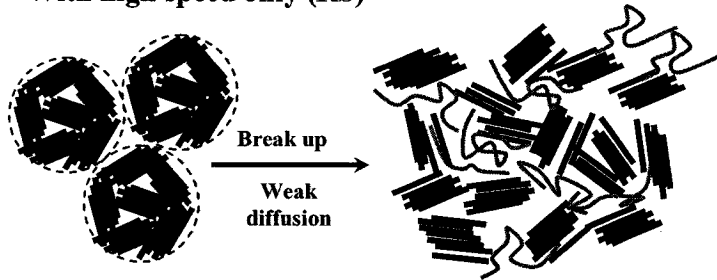
With the assistance of only temperature ( $T_m$ ), the temperature facilitates the diffusion of epoxy into the clay galleries. The intercalation may happen even at the inner stacks. Up to a certain extent, diffusion of epoxy may also help to break down the large aggregates into smaller aggregates but not lead to fine and uniform dispersion.

On the other hand, when high speed and temperature are introduced at the same time ( $T_S$ ), the clay particles (aggregates) can be broken down to smaller sizes (stacks) and lead to very fine and more uniform dispersion. The intercalation takes place even inside all of the stacks.

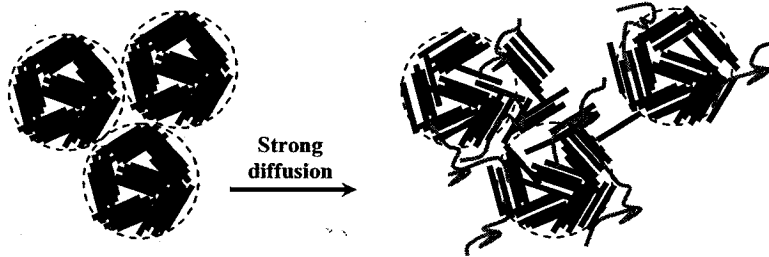
Without mechanical stirring and temperature assist (Rm)



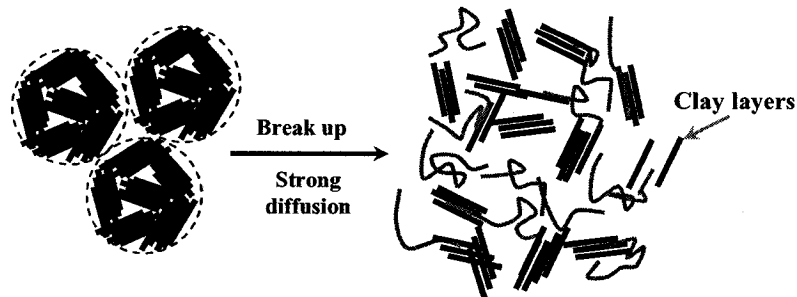
With high speed only (RS)



With high temperature only (Tm)



With high speed and high temperature (TS)



More details about dispersion mechanism with high speed and high temperature

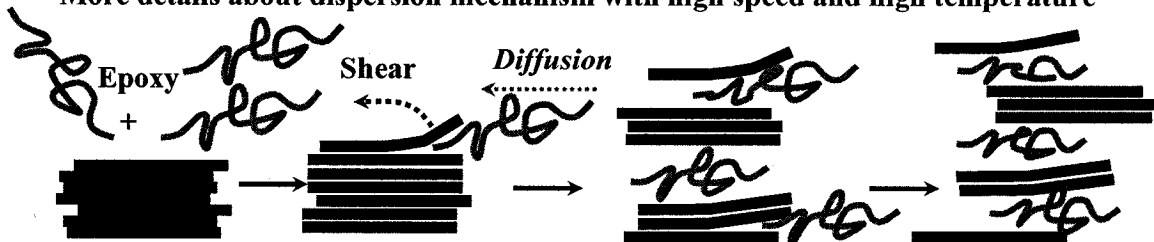


Figure 4.39. Mechanism of dispersion at stirring step



A more detailed description of the effect of mechanical stirring and diffusion on the dispersion of clay in epoxy is also shown in Figure 4.39. During stirring, the bundles of clay can be peeled apart and separated from the big aggregates, while at the same time, polymer molecules can get in to expand the galleries.

## 4.4. Effect of the curing process on the dispersion

### 4.4.1. Effect of curing temperature

Epoxy-clay mixtures from the stirring step were cured with D230 either at room temperature for 2 days or at 60, 90 and 120°C for 2 hours, with subsequent post cure at 140°C for 2 hours in both cases. The variables and experimental conditions of this experiment set are given in Table 4.7.

**Table 4.7. Variables and experimental conditions for experiment set 4.4.1**

Stirring methods	EPON 828	C30B	D230	Curing temperature
Rm	100	2.69	32	RT and 120°C
Tm	100	2.69	32	RT and 120°C
TM	100	2.69	32	RT and 120°C
RS	100	2.69	32	RT and 120°C
TS	100	2.69	32	RT, 60°C, 90°C, and 120°C
HP	100	2.69	32	RT and 120°C

The effect of curing temperature on the dispersion and intercalation/exfoliation of organoclay in epoxy nanocomposites was studied. The XRD results of nanocomposites with 2 wt% of C30B based on EPON828 and D230 which were prepared by TS stirring method at 24000 rpm for 60 minutes and cured at room temperature (RT), 60°C, 90°C and 120°C are shown in Figure 4.40. As mentioned in Section 4.3.2, the position (angle

$2\theta$ ) of the peak in XRD curves is related to the clay gallery spacing and therefore the degree of intercalation, whereas the peak intensity is an indicator of the amount of intercalated clusters or the amount of non-intercalated (i.e. exfoliated) material. On the XRD curves, the intensity of the X-ray diffraction peak decreases with increase in curing temperature. A reduction in the peak intensity indicates that the amount of intercalated clay has decreased, or in other words, the dispersion has been improved by breakdown of clusters or even exfoliation. This figure also shows that there are two peaks in the XRD curve for ENC which was cured at room temperature, around  $2.2^\circ$  and  $4.7^\circ$ , and this corresponds to  $d$ -spacings of 40.1 Å and 18.7 Å. The second peak disappeared for curing at  $60^\circ\text{C}$  and  $90^\circ\text{C}$ . This confirms that with curing at  $60^\circ\text{C}$  and  $90^\circ\text{C}$ , clay has better dispersion and intercalation/exfoliation than at room temperature. It is interesting to observe in Figure 4.40 that when ENC was cured at  $120^\circ\text{C}$ , the peaks shifted to the lower angles at around  $1.3^\circ$  and  $2.2^\circ$ , corresponding to  $d$ -spacing of 66.9 Å and 40.27 Å. This shows that curing at this temperature ( $120^\circ\text{C}$ ) results in a better intercalation/exfoliation than curing at  $90^\circ\text{C}$ ,  $60^\circ\text{C}$  and RT. This can be explained by the fact that when the temperature increases, the mobility of epoxy and hardener molecules increase and because of this, they can diffuse more easily into the clay galleries and further intercalate or exfoliate the clay. Thus, in this particular case a high curing temperature accelerates the diffusion of epoxy and hardener into the clay galleries according to the diffusion rules. All these X-ray results show that curing at higher temperature results in better intercalation than curing at lower temperature, for epoxy nanocomposites. A summary of the effect of curing temperature on  $d_{001}$  of ENC is shown in Figure 4.41. In general, the level of intercalation/exfoliation follows the order  $T_{120} > T_{90} > T_{60} > T_{\text{RT}}$ .

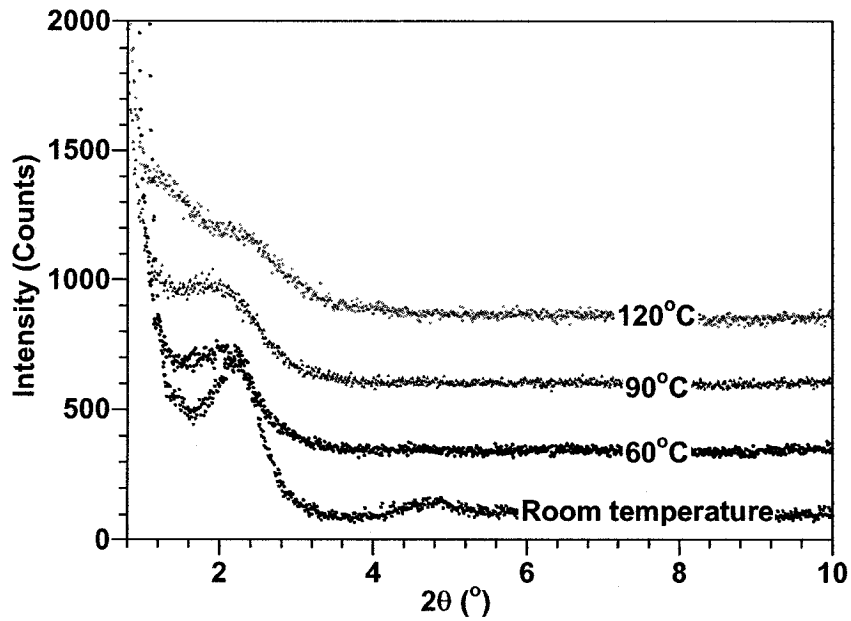


Figure 4.40. X-ray diffraction curves of nanocomposites at 2 wt% C30B, samples cured at different temperatures

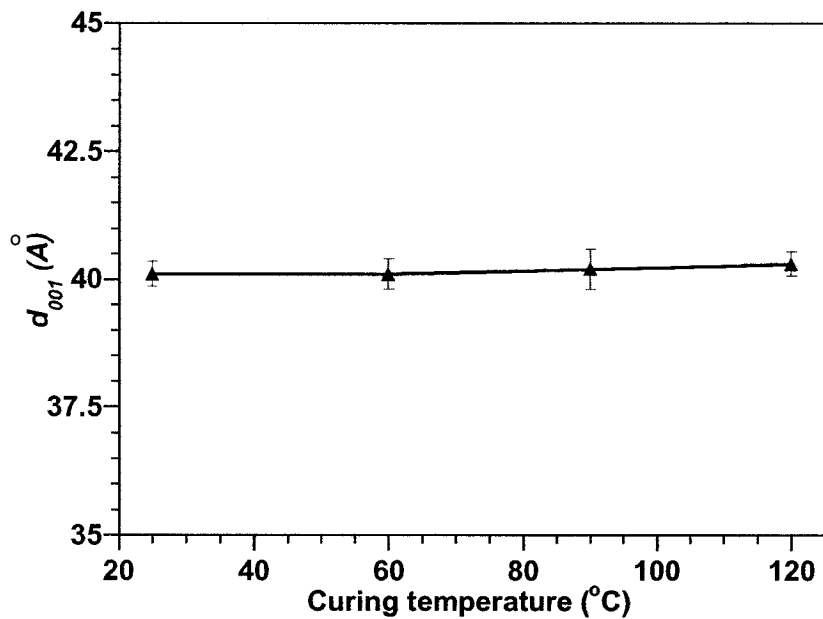


Figure 4.41. The effect of curing temperature on  $d_{001}$  of ENC at 2 wt% C30B

X-ray diffraction curves of the epoxy and its nanocomposites based on C30B and made by different stirring methods are illustrated in Figures 4.42 and 4.43. A summary of the

peak positions of the XRD curves is given in Table 4.8. In all the nanocomposite samples the clay layer separation (degree of intercalation) is considerably higher than in the original C30B. Clays have been well further intercalated by the epoxy matrix for both curing at room and high temperatures.

When samples were cured at room temperature (RT), there is no significant difference between the positions of the peak on the XRD curves. However, the intensity changed depending on stirring methods. At the same loading level of 2 wt% C30B, the ENC made by high temperature method (Tm) shows somewhat better intercalation than the ENC made by room temperature method (Rm). The intensity of the XRD peak for stirring with Tm is lower than for stirring with Rm. This means that stirring at high temperature leads to better delamination of clay than stirring at room temperature. On comparing between high speed at high temperature (TS) and high speed at room temperature (RS), the same phenomenon occurred for two ENCs prepared by these stirring methods. Shear also shows an effect on intercalation/exfoliation of ENC. The intensity of the peak for stirring at room temperature with speed (RS) is lower than stirring at room temperature without speed (Rm), and the intensity of the peak for stirring at high temperature with speed (TS) is lower than for stirring at high temperature with low speed (TM) or without speed (Tm). Stirring with high speed also results in better intercalation/exfoliation of clay in the epoxy matrix at the curing step.

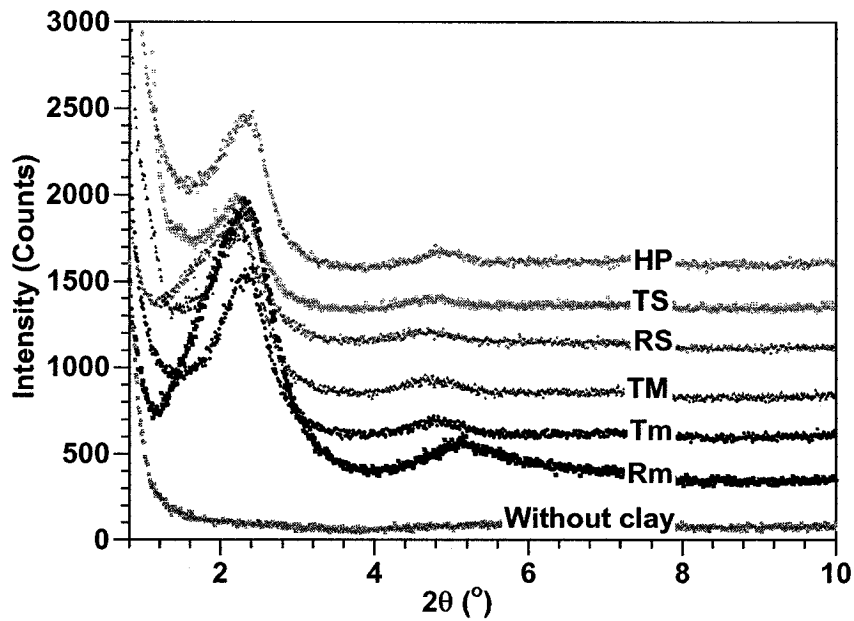


Figure 4.42. X-ray diffraction curves of EPON828-D230 system, C30B and their nanocomposites at 2 wt% C30B made by different methods and cured at RT

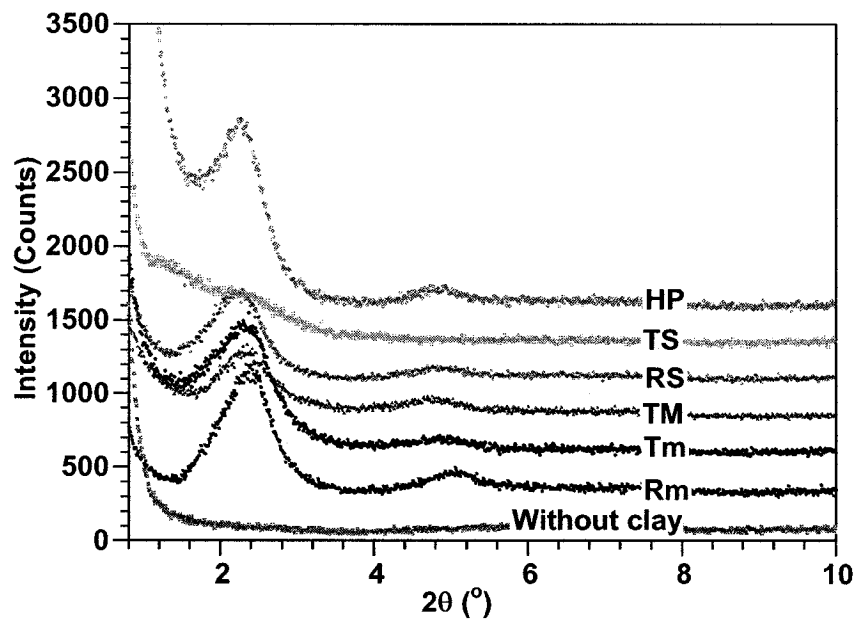


Figure 4.43. X-ray diffraction curves of EPON828-D230 system, C30B and their nanocomposites at 2 wt% C30B made by different methods and cured at 120°C for 2 h

**Table 4.8. Summary of XRD results of C30B and their nanocomposites made by different methods**

Stirring method (Before cure)	Gallery distance (Å)			
	Cured at RT		Cured at 120°C for 2 h	
	$d_{001}$	$\Delta d$	$d_{001}$	$\Delta d$
Cloisite 30B	18.5			
Rm	37.3	18.8	37.6	19.1
Tm	38.3	19.8	38.4	19.9
TM	38.6	20.1	38.6	20.1
RS	39.1	20.6	39.5	21.0
HP	38.3	19.8	39.4	20.9
TS	40.1	21.6	40.3-66.9	21.8-48.4

Again, curing at high temperature provides better intercalation/exfoliation as compared to curing at room temperature. With the same stirring method, the intensity of the XRD peak is lower for curing at 120°C than for curing at room temperature. A similar effect can be seen here (compared to curing at room temperature) on the intercalation/exfoliation of clay in epoxy matrix when temperature and speed were introduced at the stirring step. The intensity of the peak for ENC became smaller when the temperature and speed were introduced in the stirring step. The orders of intercalation/exfoliation are now TS > RS, TM > Tm > Rm, TS > TM > Tm and RS > Rm. Note that there is little difference in intensity of the peak between Tm and TM. It can be seen that there are two peaks in all the XRD curves for ENCs prepared by the Rm, Tm, TM, RS, HP and TS methods. For ENC which was prepared by Rm, Tm, TM and RS, the two peaks were at around 2.3° and 4.8°. The  $d$ -spacings for the ENC can be seen in Table 4.8. However, the peaks shifted to lower angles for the TS method. They are located at 1.3° and 2.2°, corresponding to  $d$ -spacings of 66.9 Å and 40.3 Å, respectively. The TS method shows better intercalation/exfoliation as compared to HP, RS, TM, Tm

and Rm methods. Again, in these cases, the second peak is the reflection of the first one. Because of this, there is only one clay intercalation level in the mixtures of epoxy-clay and this level is located at the position of the first peak in the XRD curves. The intensity of XRD peaks of ENC made by HP method is lower than for the RS method. It is believed that the HP method gives better intercalation/exfoliation than RS although the *d*-spacing is a little lower than RS. In general, it can be noted here that the level of intercalation and exfoliation of clay in epoxy nanocomposites is in the following order: TS > HP > RS > TM > Tm > Rm. The explanation for the better intercalation/exfoliation at this step with ENC prepared with the high speed and temperature stirring methods is that the high speed and temperature helped to break down the clay aggregates to smaller sizes and improve dispersion of clay in the epoxy resin (more homogenous dispersion) during the stirring step. Because of this it can have an indirect effect on the intercalation/exfoliation of clay in epoxy matrix at the curing step. Epoxy and hardener have more chance to diffuse into the clay galleries and further expand the distance between clay platelets especially with high temperature curing when the mobility of the molecules increases.

The microstructures of ENC based on C30B and made by different stirring methods are illustrated by SEM and presented in Figure 4.44. The bright spots on the backscattered images correspond to clay aggregates. Apparently, a portion of the clay remains at the micro-scale level with different size populations depending on the stirring conditions. However, due to the limitation of the SEM, one should not rule out the possibility that some exfoliation does take place. The size of aggregates is reduced significantly with high speed (Figure 4.44d) as compared to without mechanical stirring (Figure 4.44a). The

size of aggregates became much smaller when both high speed and temperature were introduced at the stirring step (Figure 4.44e). Again, it confirms that the micro dispersion of ENC made by different stirring methods follows the order TS > HP > RS > TM > Tm > Rm.

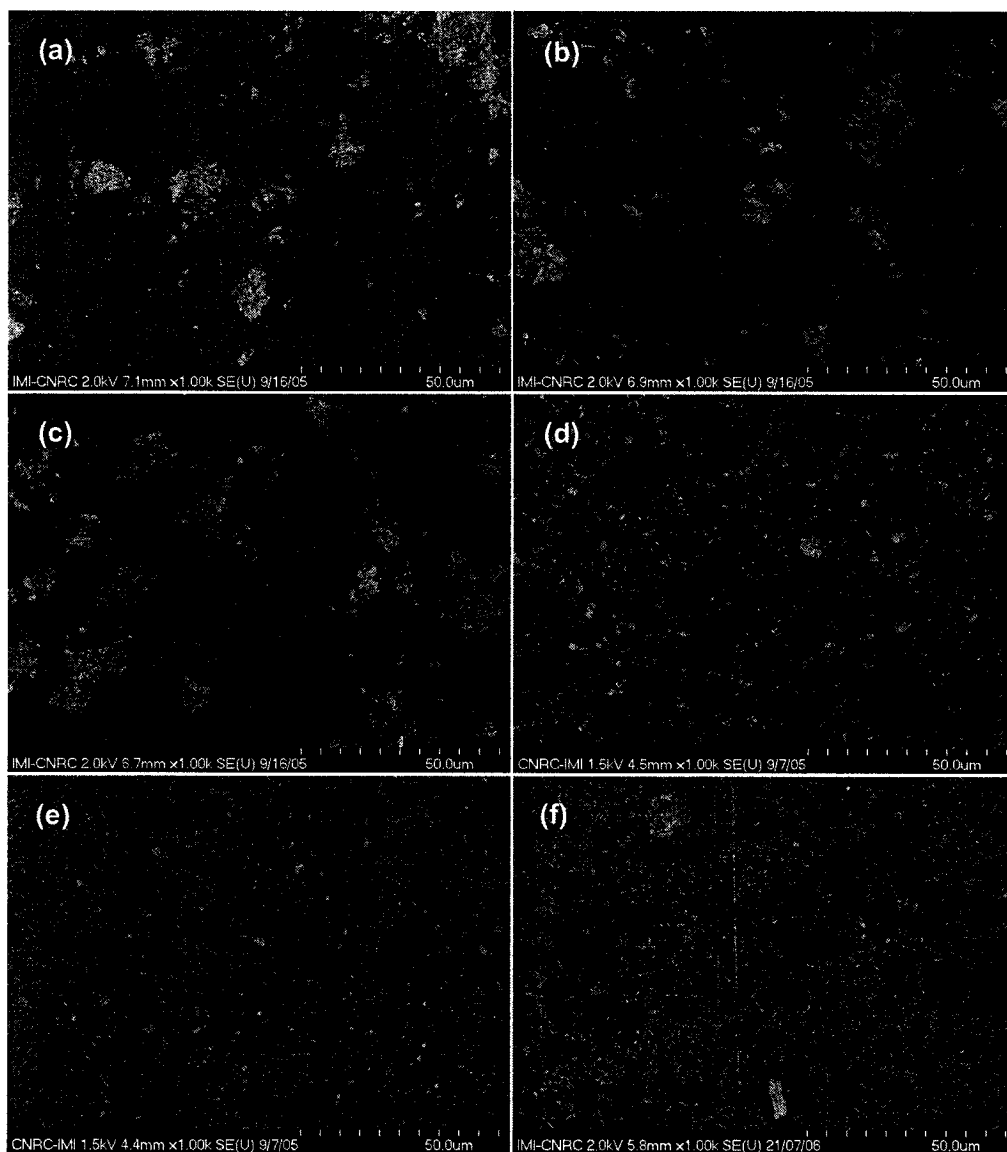


**Figure 4.44. SEM micrographs of ENC based on EPON828 and D230 with 2 wt% C30B made by different stirring methods: (a) Rm, (b) Tm, (c) TM, (d) RS, (e) TS at 120°C and 24000 rpm, and (f) HP, samples cured at 120°C for 2 h**



TEM micrographs for nanocomposites prepared by the TS technique (120°C and 24000 rpm in 1 hour) at different magnifications are shown in Figure 4.45. It can be seen in Figure 4.45a that clays have been well dispersed in the epoxy matrix. The size of small aggregates or clay stacks is less than 0.5 $\mu$ . When the clays are focused at high magnification (Figure 4.45b), the dark lines indicate the silicate nanolayers. Although the clay particles were not completely exfoliated into individual platelets, there are many regions of nanocomposites which contain single, double and triple clay silicate nanolayers. So far, the results from XRD, SEM and TEM combine to indicate that with mechanical stirring and temperature assistance, one can obtain a fine dispersion at the micro scale, good distribution of clay, and good intercalation/exfoliation of clay in the epoxy system.

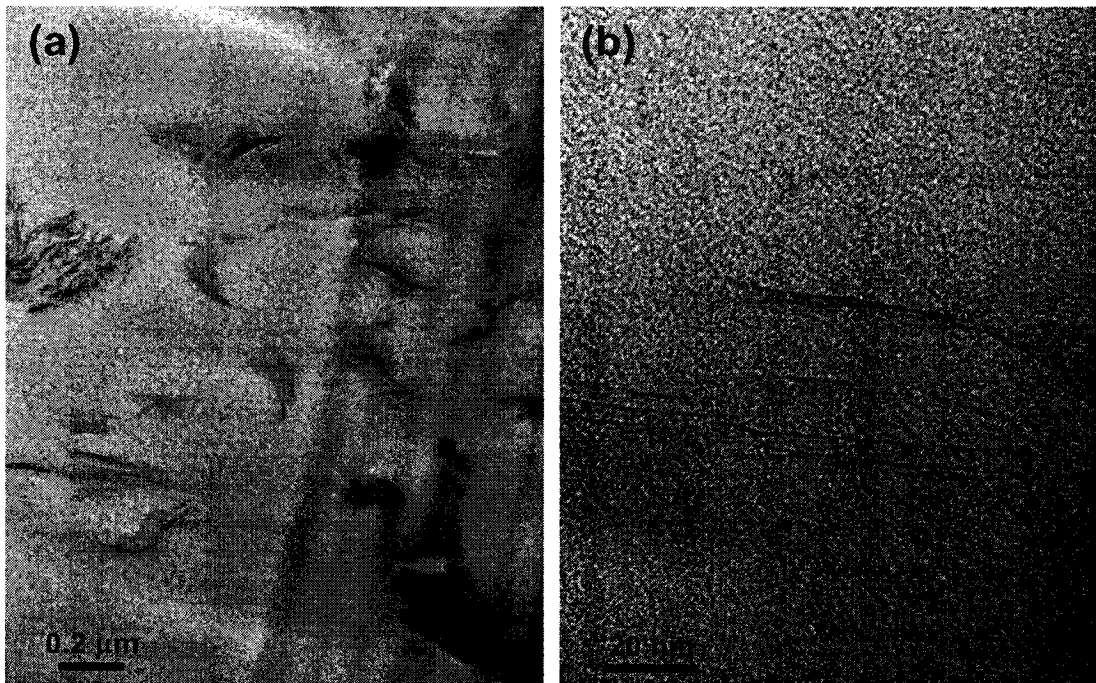


**Figure 4.45. TEM photos of nanocomposite based on EPON828-D230 with 2 wt% C30B**

X-ray diffraction curves of the epoxy and its nanocomposites based on C30B prepared by high speed stirring at 9500, 17500 and 24000 rpm and then cured at room temperature and 120°C are illustrated in Figures 4.46, 4.47, 4.49, 4.50, 4.52 and 4.53. The summary of the first peak's position ( $d_{001}$ ) on XRD curves of the epoxy-clay mixtures as well as the different  $\Delta d$  between the positions of these peaks and that of the peak of C30B are shown in Tables 4.9 to 4.11, and Figures 4.48, 4.51 and 4.54.

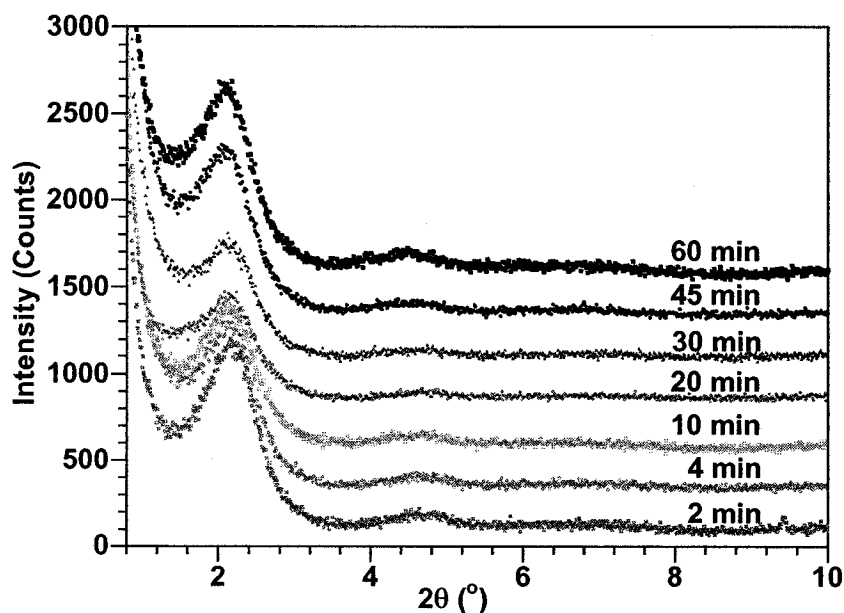


**Figure 4.46. X-ray diffraction curves of nanocomposites based on EPON828-D230 and 2 wt% C30B made by TS with 9500 rpm for different durations and cured at room temperature**

The results show that there are two peaks at around 39.0 Å and 18.5 Å on each XRD curve when ENC is cured at room temperature for all cases in this range of stirring duration and speed. It can be seen at three different speeds of stirring, stirring duration does not significantly improve the intercalation/exfoliation of clay in ENC when they

were cured at room temperature. There is not much difference in the positions and intensity of the peak of the XRD curves for ENC.

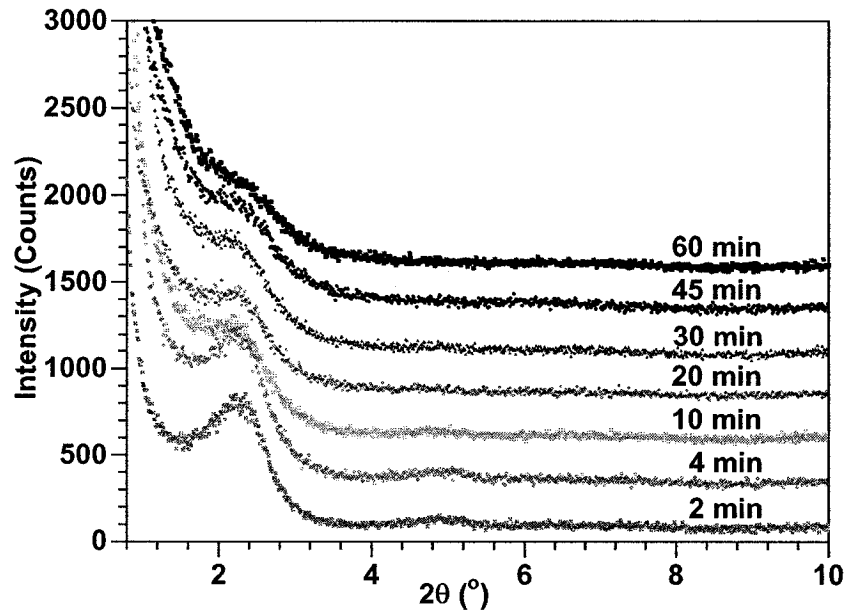


Figure 4.47. X-ray diffraction curves of nanocomposites based on EPON828-D230 and 2 wt% C30B made by TS with 9500 rpm for different durations and cured at 120°C

Table 4.9. Summary of XRD results of nanocomposites based on EPON828-D230 and 2 wt% C30B made by TS with 9500 rpm for different durations

Duration of stirring (min)	Gallery distance (Å)			
	Cured at RT		Cured at 120°C	
	$d_{001}$	$\Delta d$	$d_{001}$	$\Delta d$
2	38.1	19.6	38.0	19.5
4	38.1	19.6	38.1	19.6
10	38.2	19.7	38.4	19.9
20	38.5	20.0	38.6	20.1
30	38.5	20.0	38.7	20.2
45	39.4	20.9	39.4	20.9
60	39.7	21.2	39.5	21.0

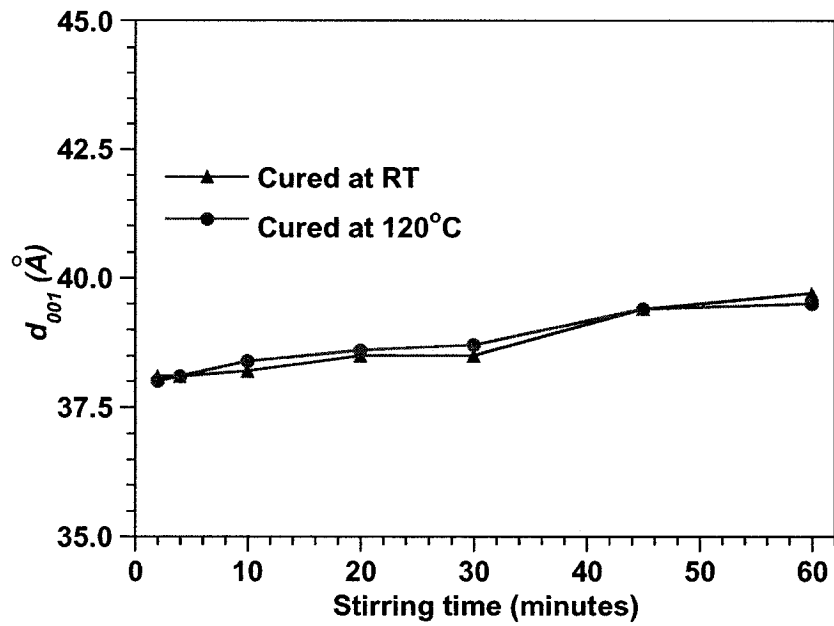


Figure 4.48. The effect of curing temperature on  $d_{001}$  of nanocomposites based on EPON828-D230 and 2 wt% C30B made by TS with 9500 rpm for different durations

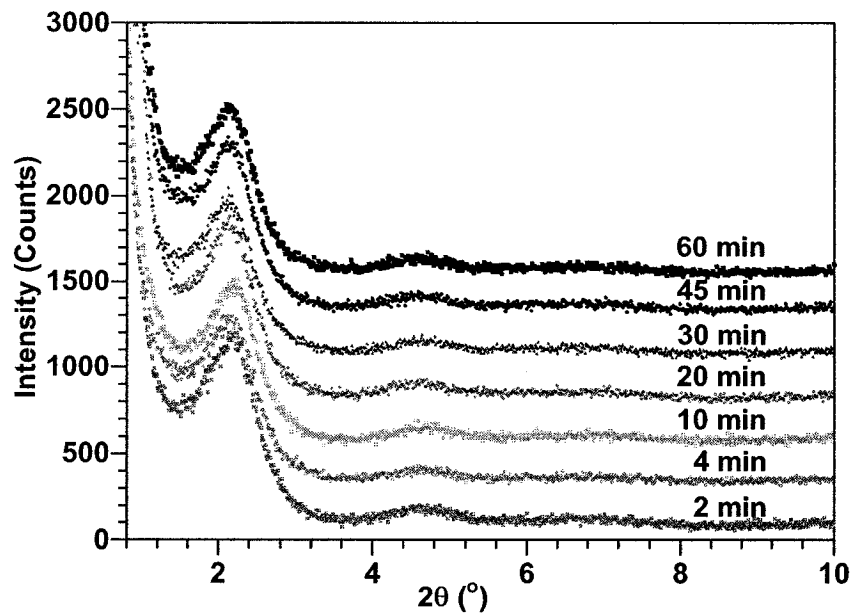


Figure 4.49. X-ray diffraction curves of nanocomposites based on EPON828-D230 and 2 wt% C30B made by TS with 17500 rpm for different durations and cured at room temperature

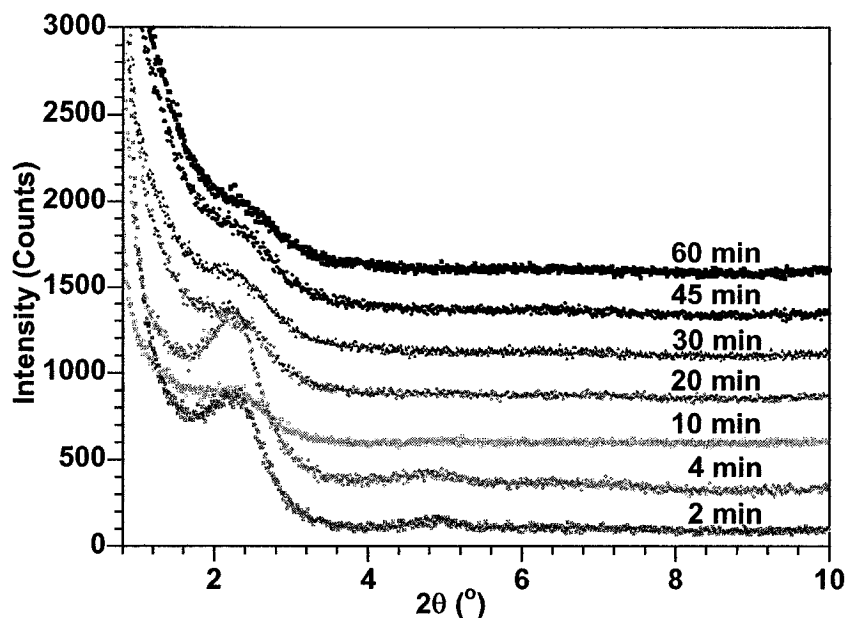
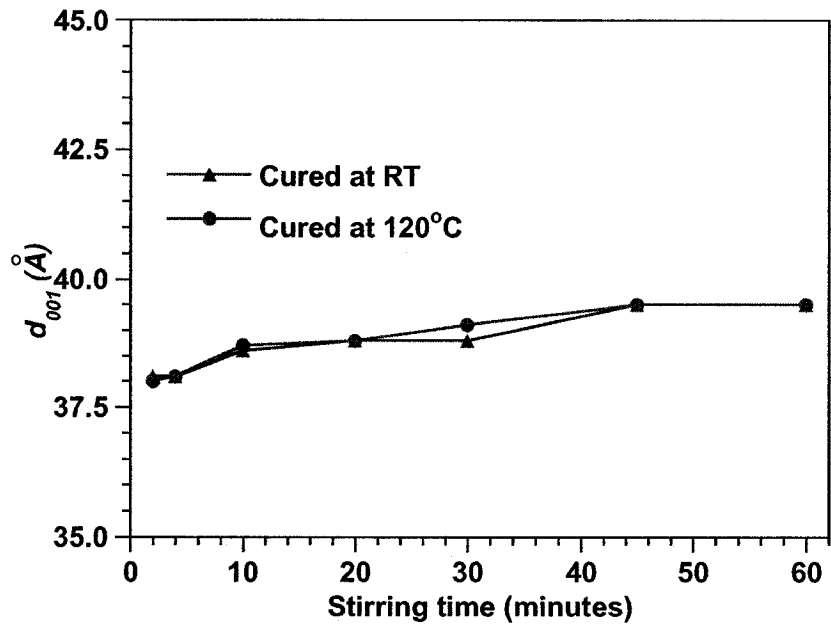


Figure 4.50. X-ray diffraction curves of nanocomposites based on EPON828-D230 and 2 wt% C30B made by TS with 17500 rpm for different durations and cured at 120°C

Table 4.10. Summary of XRD results of nanocomposites based on EPON828-D230 and 2 wt% C30B made by TS with 17500 rpm for different durations

Duration of stirring (min)	Gallery distance (Å)			
	Cured at RT		Cured at 120°C	
	$d_{001}$	$\Delta d$	$d_{001}$	$\Delta d$
2	38.1	19.6	38.0	19.5
4	38.1	19.6	38.1	19.6
10	38.6	20.1	38.7	20.2
20	38.8	20.3	38.8	20.3
30	38.8	20.3	39.1	20.6
45	39.5	21.0	39.5	21.0
60	39.5	21.0	39.5	21.0



**Figure 4.51. The effect of curing temperature on  $d_{001}$  of nanocomposites based on EPON828-D230 and 2 wt% C30B made by TS with 17500 rpm for different durations**

However, when ENC were cured at 120°C, only one peak can be seen clearly for ENCs which were stirred longer than 10 minutes for three different stirring speeds. The second peak at 18.5 Å almost disappeared. A difference in peak intensity is also clearly seen on changing the stirring duration. The longer is the duration of stirring; the lower is the intensity of XRD peaks. A reduction in the peak intensity indicates that the amount of intercalated clay has decreased, or in other words, the dispersion has been improved by breakdown of clusters or even exfoliation. The improvement of dispersion and intercalation/exfoliation by duration of stirring can be understood in term of the better diffusion of epoxy and hardener into the clay galleries. The longer is the duration of

stirring, the smaller is the size of the aggregates (see the next few pages). Because of this, epoxy and hardener have more chance to penetrate at the curing step (as discussed above). In addition, at the same curing temperature and stirring duration up to 30 minutes, the speed of stirring does not show a significant change in the XRD curves. This means that at this temperature and duration of stirring (to 30 minutes), the range of speed from 9500 rpm to 24000 rpm does not show an evident effect on intercalation and exfoliation of clay.

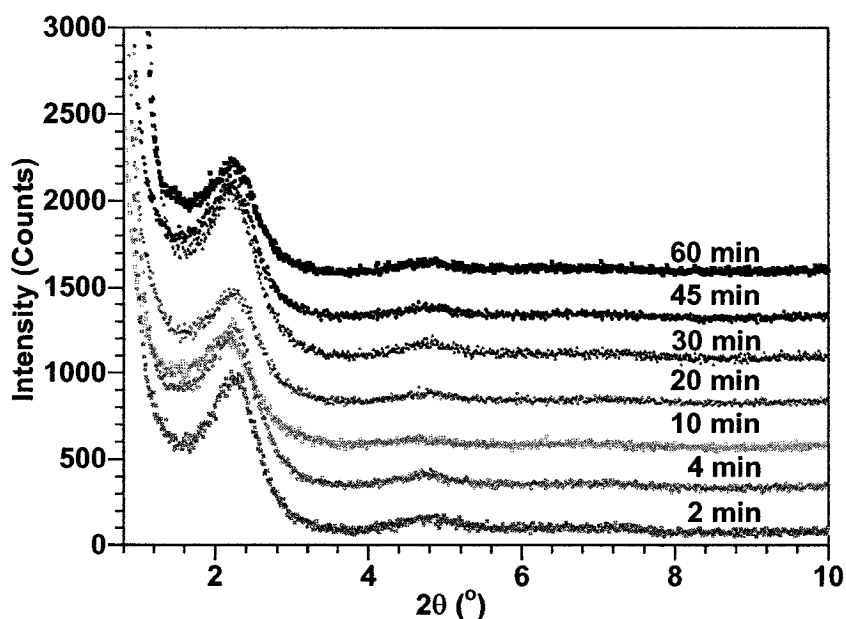


**Figure 4.52. X-ray diffraction curves of nanocomposites based on EPON828-D230 and 2 wt% C30B made by TS with 24000 rpm for different durations and cured at room temperature**

For stirring duration longer than 45 minutes, a difference appears in the XRD curves of ENC made by TS at 24000 rpm compared to 17500 rpm and 9500 rpm. There are two peaks on the XRD curves and they are located at low angles and their *d*-spacings are shown in Table 4.11.

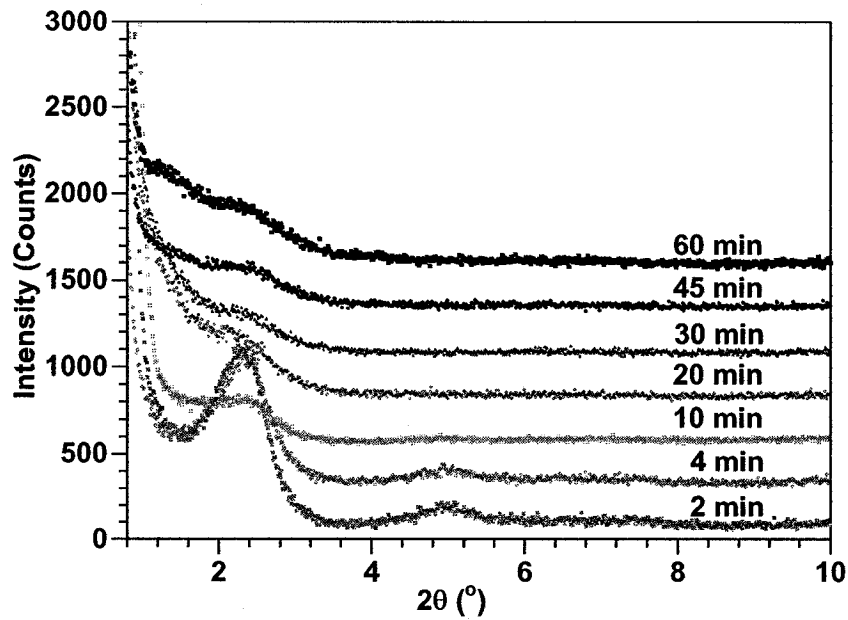
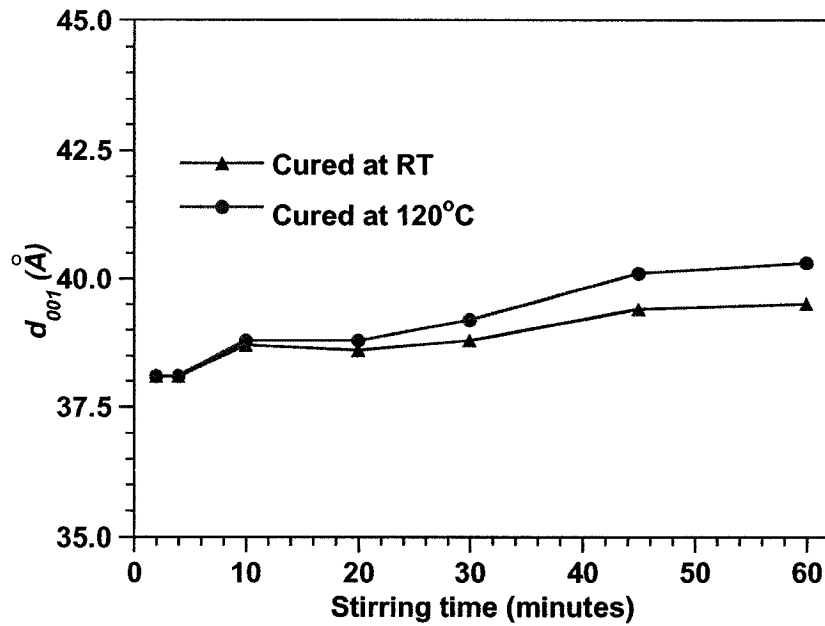


Figure 4.53. X-ray diffraction curves of nanocomposites based on EPON828-D230 and 2 wt% C30B made by TS with 24000 rpm for different durations and cured at 120°C

Table 4.11. Summary of XRD results of nanocomposites based on EPON828-D230 and 2 wt% C30B made by TS with 24000 rpm for different durations

Duration of stirring (min)	Gallery distance (Å)			
	Cured at RT		Cured at 120°C	
	$d_{001}$	$\Delta d$	$d_{001}$	$\Delta d$
2	38.1	19.6	38.1	19.6
4	38.1	19.6	38.1	19.6
10	38.7	20.2	38.8	20.3
20	38.6	20.1	38.8	20.3
30	38.8	20.3	39.2	20.7
45	39.4	21.0	40.2-66.7	21.7-48.2
60	39.5	21.0	40.3-66.9	21.8-48.4





**Figure 4.54. The effect of curing temperature on  $d_{001}$  of nanocomposites based on EPON828-D230 and 2 wt% C30B made by TS with 24000 rpm for different durations**

The effect of stirring duration on the dispersion of C30B in epoxy matrix was also observed by FEGSEM. FEGSEM photos of the ENC based on EPON828-D230 with 2 wt% of C30B made by TS at 24000 rpm for different durations are shown in Figure 4.55. The bright spots on the backscattered images correspond to clay aggregates. Apparently, clay aggregates have been broken down into smaller ones with increase in the stirring duration. It proves that the size of aggregates is smaller with stirring duration and because of this, it can help to improve the level of intercalation and exfoliation of ENC during the curing step.

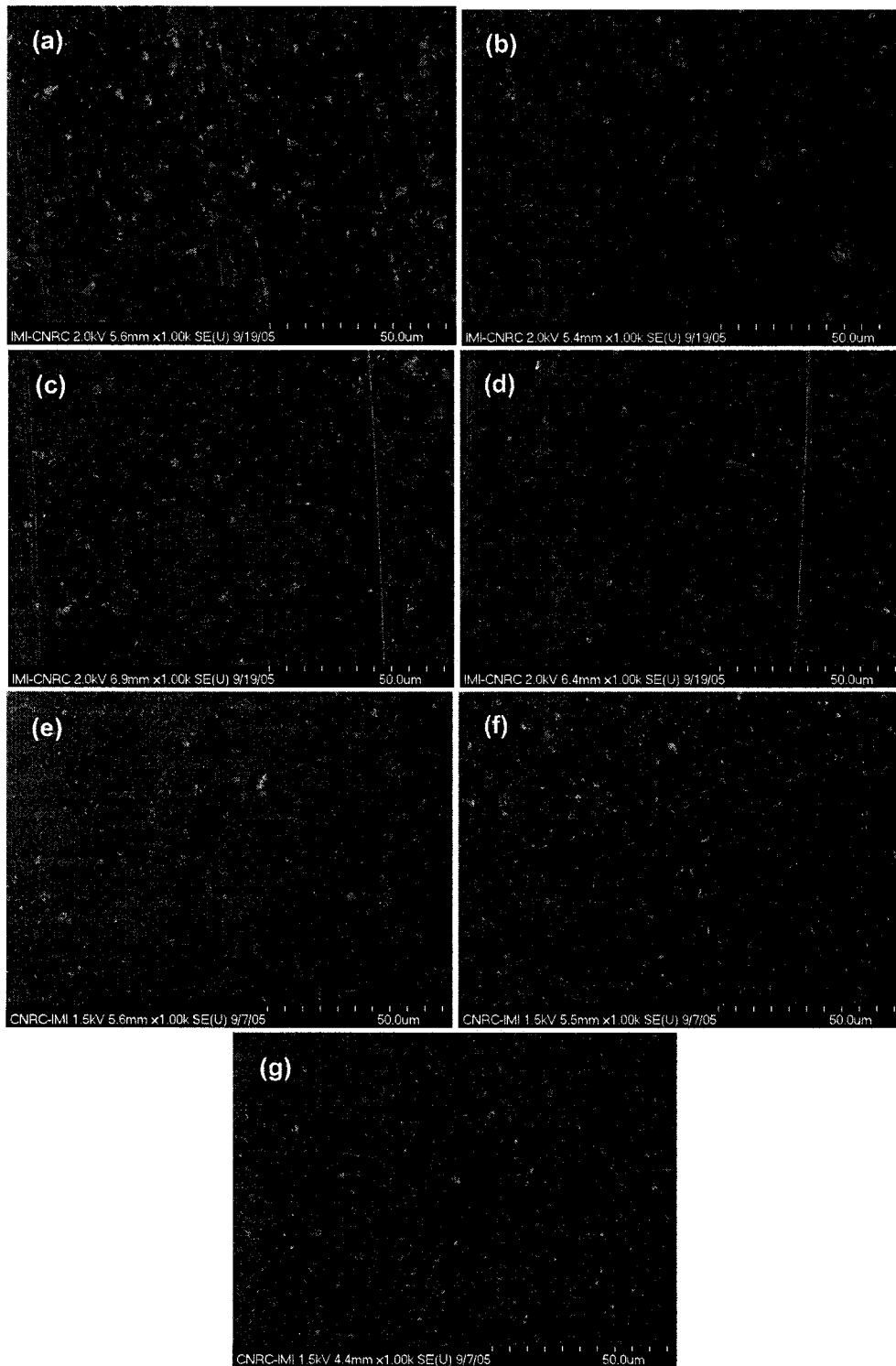


**Figure 4.55. SEM photos of nanocomposite based on EPON828-D230 and 2 wt% C30B made by TS with 24000 rpm for (a) 2 minutes, (b) 4 minutes, (c) 10 minutes, (d) 20 minutes, (e) 30 minutes, (f) 45 minutes, and (g) 60 minutes**

X-ray diffraction curves of EPON828 nanocomposites samples prepared with high speed of 24000 rpm at room temperature and at 180°C and cured at room temperature and 120°C are shown in Figures 4.56, 4.57, 4.59, and 4.60. The summary of the first peak's position ( $d_{001}$ ) of the mixtures as well as the  $\Delta d$  between the positions of these peaks and that of C30B are shown in Tables 4.12, 4.13 and Figures 4.58, 4.60.

For curing at room temperature, the intensity of XRD peaks for mixing at RT, 120°C or 180°C show almost no change. However, the peaks became narrower for 120°C and 180°C compared to RT (Figures 4.52, 4.56 and 4.57), which suggest that better intercalation has taken place for high temperature stirring even when curing was at room temperature. As discussed above, curing at room temperature does not show a significant effect on intercalation of clay when the duration of stirring was changed. Again, it is very clear that at the same stirring temperature, the peak position and intensity of these peaks remains almost the same even if the duration of stirring was changed.

However, duration of stirring has an influence on XRD curves when the samples are cured at 120°C (Figures 4.53, 4.57 and 4.60). The longer is the stirring duration, the better is delamination of clay in epoxy matrix. Stirring temperature also has a significant effect on delamination of clay. There is an evident change in the intensity of the XRD peaks when the temperature of stirring increases from room temperature to 120°C and 180°C. High speed stirring does not show a strong influence on intercalation/exfoliation of cured ENC for the case of stirring at room temperature. The peak remains the same when stirring duration increases. For stirring with high speed at 120°C the peak in the XRD curves becomes smaller when stirring duration increases

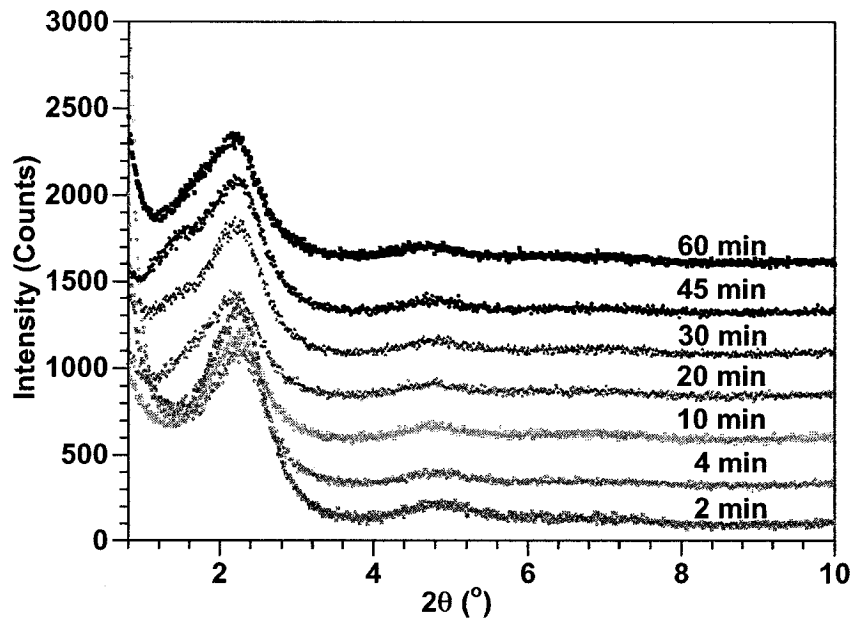


**Figure 4.56. X-ray diffraction curves of nanocomposites based on EPON828-D230 and 2 wt% C30B made by RS with 24000 rpm for different durations and cured at room temperature**

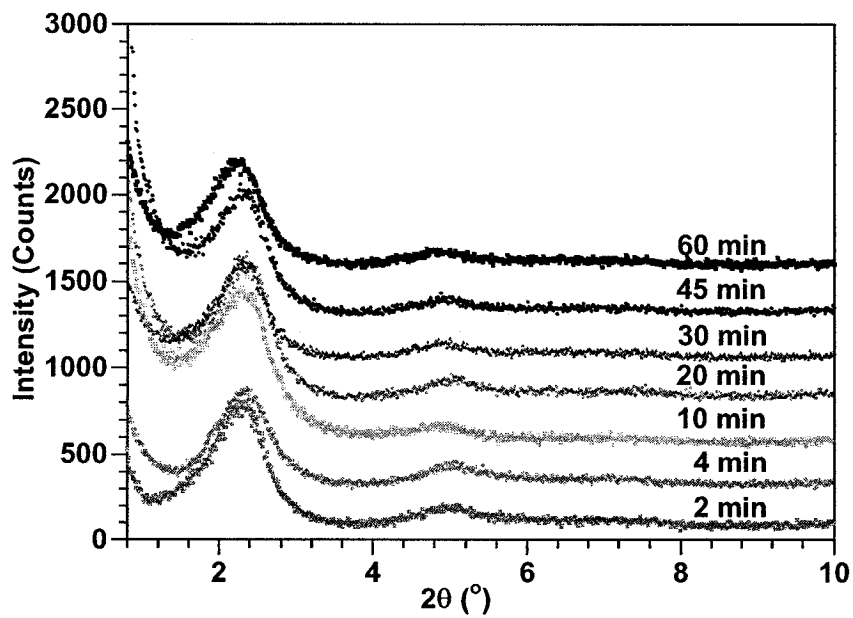


**Figure 4.57. X-ray diffraction curves of nanocomposites based on EPON828-D230 and 2 wt% C30B made by RS with 24000 rpm for different durations and cured at 120°C**

**Table 4.12. Summary of XRD results of nanocomposites based on EPON828-D230 and 2 wt% C30B made by RS with 24000 rpm for different durations**

Duration of stirring (min)	Gallery distance (Å)			
	Cured at RT		Cured at 120°C	
	$d_{001}$	$\Delta d$	$d_{001}$	$\Delta d$
2	37.93	19.43	37.95	19.45
4	38.03	19.53	38.07	19.57
10	38.50	20.00	38.50	20.00
20	38.63	20.13	38.54	20.04
30	38.98	20.48	38.78	20.28
45	39.28	20.78	39.38	20.88
60	39.06	20.56	39.51	21.01

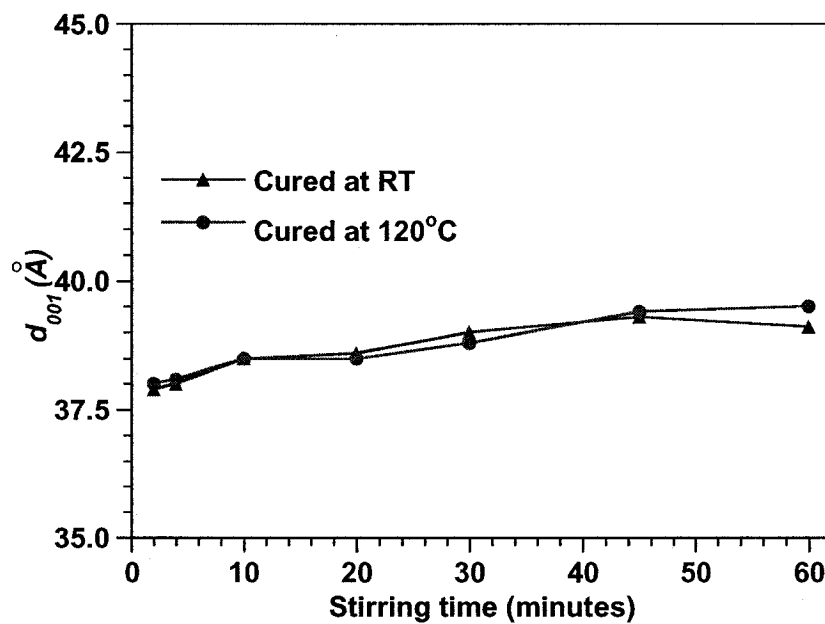


**Figure 4.58. The effect of curing temperature on  $d_{001}$  of nanocomposites based on EPON828-D230 and 2 wt% C30B made by RS with 24000 rpm for different durations**

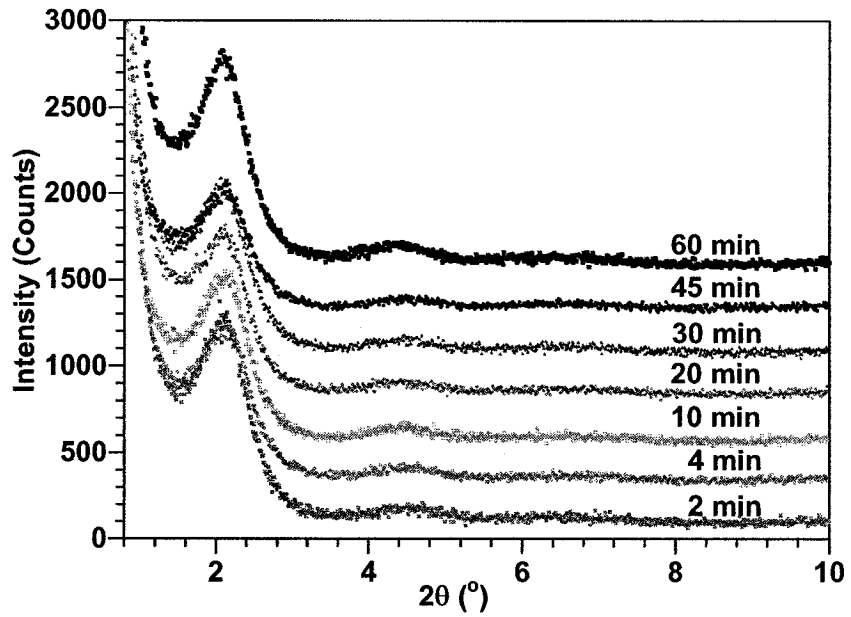


Figure 4.59. X-ray diffraction curves of nanocomposites based on EPON828-D230 and 2 wt% C30B made by TS (at 180°C) with 24000 rpm for different durations and cured at room temperature

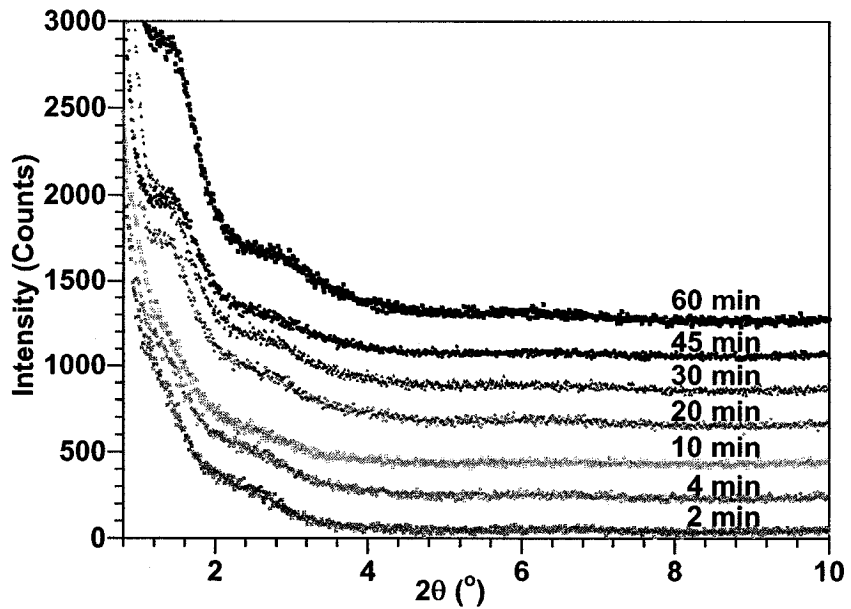
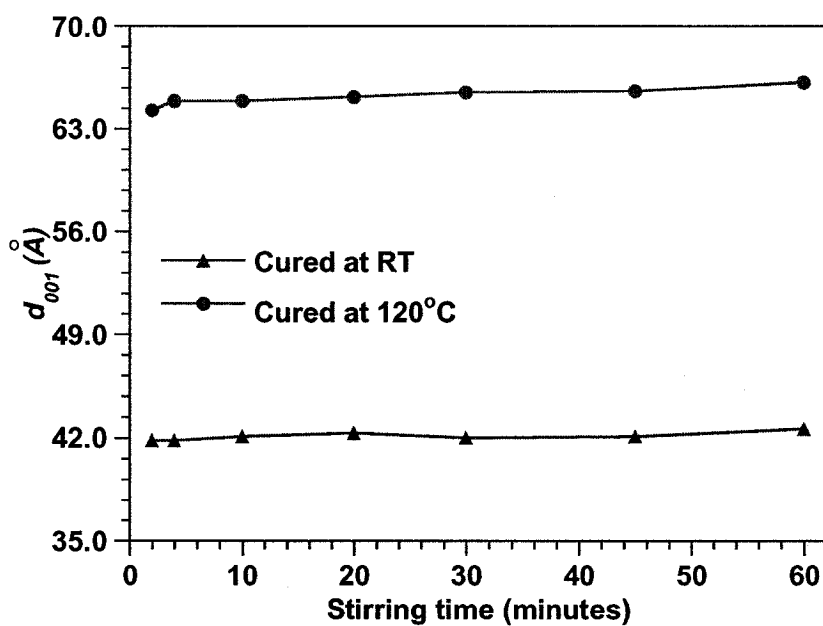


Figure 4.60. X-ray diffraction curves of nanocomposites based on EPON828-D230 and 2 wt% C30B made by TS (at 180°C) with 24000 rpm for different durations and cured at 120°C

**Table 4.13. X-ray diffraction curves of nanocomposites based on EPON828-D230 and 2 wt% C30B made by TS (at 180°C) with 24000rpm for different durations**

Duration of stirring (min)	Gallery distance (Å)			
	Cured at RT		Cured at 120°C	
	$d_{001}$	$\Delta d$	$d_{001}$	$\Delta d$
2	41.8	23.3	64.3	45.8
4	41.8	23.3	64.9	46.4
10	42.1	23.6	64.9	46.4
20	42.3	23.8	65.2	46.7
30	42.0	23.5	65.5	47.0
45	42.1	23.6	65.6	47.1
60	42.6	24.1	66.2	47.7



**Figure 4.61. The effect of curing temperature on  $d_{001}$  of nanocomposites based on EPON828-D230 and 2 wt% C30B made by TS (180°C) with 24000 rpm for different durations**

It has been frequently observed that during exfoliation (especially during the mechanical exfoliation of intercalated clay in a matrix) the position of the XRD peak may remain at the same angular position  $2\theta$ , but it broadens and its intensity decreases. Ishida and co-workers [122] used XRD to calculate the degree of exfoliation  $X_E$  (%):

$$X_E = 100 \left( 1 - \frac{A}{A_0} \right) \quad (4.4)$$

where  $A$  and  $A_0$  are the area under the XRD peak for the polymer nanocomposites and for the mixture with intercalated clay, respectively.

Let us assume there is no exfoliation in the sample which was prepared by hand stirring at room temperature (Rm) and cured at room temperature. In this case,  $A_0$  is the area under the XRD peak for this sample.

The exfoliation level of the ENC made by high speed stirring at room temperature and 120°C (cured at 120°C) was calculated by means of Galactic soft ware (GRAMS AI) and is shown in Table 4.14. The exfoliation levels were calculated based on the reduction in intensity, the percentage of exfoliation of these samples compared to the reference (Rm). The result shows that longer time leads to better exfoliation of the clay in epoxy matrix. In addition stirring at high temperature also shows better delamination compared to stirring at room temperature.



**Table 4.14. Summary of XRD data of samples after being cured at 120°C**

Duration of Stirring (minutes)	Intercalation spacing (Å)		Area A (A <sub>o</sub> )	% Exfoliation
	Main peak	Secondary peak		
<b>RT stirring (Rm)</b>				
60	37.3	17.8	(2370)	0
<b>High speed (24000 rpm) stirring at RT</b>				
2	38.0	17.5	1666	30±2
4	38.1	17.9	879	63±1
10	38.5	18.0	846	64±4
20	38.5	18.0	823	65±3
30	38.8	18.0	771	67±4
45	39.4	18.2	758	68±4
60	39.5	18.6	677	71±1
<b>High speed (24000 rpm) stirring - at 120°C</b>				
2	38.1	17.9	1174	50±2
4	38.1	18.1	695	71±1
10	38.8	18.1	645	73±5
20	38.8	-	541	77±1
30	39.2	-	440	81±2
45	40.2	-	312	87±1
60	40.3	-	249	89±4
<b>High speed (24000 rpm) stirring – at 180°C</b>				
2	64.3	33.8	552	77±2
4	64.9	34.0	441	81±3
10	64.9	34.1	390	84±5
20	65.2	35.6	348	85±1
30	65.5	35.8	332	86±1
45	65.6	35.7	237	90±3
60	66.2	35.6	223	91±2

The mechanism for dispersion and intercalation/exfoliation of nanoclay in epoxy matrix at the curing step is proposed in Figure 4.62. When the clay is stirred with the organic media, the organic media will diffuse into the clay tactoids first in the outer layers and then the inner layers.

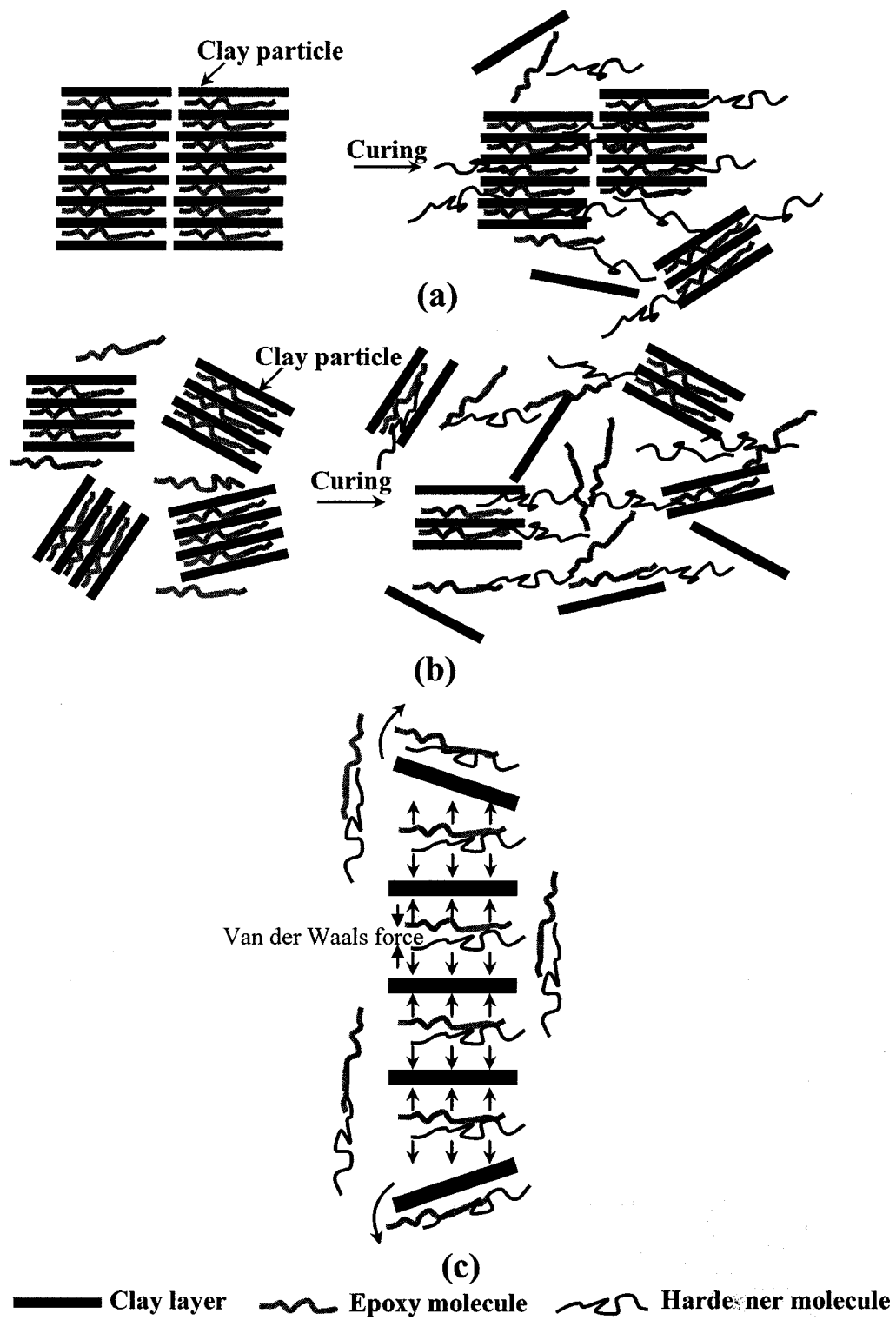


**Figure 4.62. Mechanism of dispersion and intercalation/exfoliation of clay particles in epoxy matrix at curing step: (a) big particles, (b) small particles and (c) detail**

The potential energy of an ion within an ionic solid is not the same as the potential energy of a simple pair of ions as there are many similar and dissimilar neighbors. The inner layers of clay have a higher ionic bonding energy than the surface layers. Because of this, the outer layers of clay have more chance to separate from the big aggregates when the clay swells in the organic media. Moreover, after the epoxy resin and hardener enter the clay galleries, they start to react. They try to push two clay platelets apart. It is also noted that clay platelets are held by (1) electrostatic attractive force coming from intercalant and the negative charge on the clay particles and (2) van der Waals forces. However these forces are balanced with the forces coming from another two adjacent clay layers and make them more difficult to separate from the clay tactoids. Consequently, the surface layers can be separated more easily than the inner layers and the exfoliation process should begin with the separation of surface layers away from the tactoids. Thus, while the outermost gallery expands to an exfoliated gallery height, the adjacent interior galleries remain in their intercalated state, until their turn for exfoliation comes. Full exfoliation results if all layers are separated from all tactoids. However, the separation of clay layers from the tactoids cannot continue when the 3-D epoxy network of epoxy and its hardener is formed at the gel point. At this point the viscosity of the epoxy system rises sharply to very high values. At this stage, relaxation of epoxy molecules is slowed down considerably due to the high viscosity of the surrounding epoxy 3-D network chains and high values of shear stresses acting against the movement of the clay layers. Thus, the gel point provides an upper bound of time available for complete exfoliation of all tactoids. A fully exfoliated system results if all clay layers in all tactoids are exfoliated before the gel point. The gel point, on the other hand, is a

strong function of curing temperature, curing agent, the nature of epoxy molecules, and even the nature of filler particles. It can be delayed or accelerated with proper choice of the ingredients. Because of this, one can believe that the smaller are the tactoids, the better is the separation of clay layers in the epoxy system.

#### 4.4.2. Effect of chemistry of clay

Two processes were used to prepare the epoxy nanocomposites in this study. The first one is the Rm process; the nanoclay content in the epoxy resin in this case was 2 wt%. The second one is the Tm process; the nanoclay content in the epoxy resin in this case was 2 and 4 wt%. For curing, the amine hardener (EPICURE 3046) was added at room temperature at a level of 35 phr. Samples were cured either at room temperature for 2 days or at 120°C for 2 hours, with subsequent post cure at 140°C for 2 hours in both cases. Sample specifications are given in Table 4.15.

**Table 4.15. Sample specifications for experiment set 4.4.2**

<b>Designation *</b>	<b>EPON 828</b>	<b>EPICURE 3046</b>	<b>Nanoclay</b>	<b>Stirring method</b>
8EP	100	35	0	-
<b>Cloisite 30B</b>				
8EP-2pB-M1	100	35	2	Rm
8EP-2pB-M2	100	35	2	Tm
8EP-4pB-M2	100	35	4	Tm
<b>Nanomer I30E</b>				
8EP-2pE-M1	100	35	2	Rm
8EP-2pE-M2	100	35	2	Tm
8EP-4pE-M2	100	35	4	Tm
* 8 = EPON828, EP=EPICURE 3046, 2pB = 2 phr of C30B, 4pB = 4 phr of C30B, Rm = Room temperature stirring method, Tm = high temperature stirring method.				

The difference in chemistry of clay is examined by DSC and FT-IR. The epoxy resin alone and epoxy-clay mixtures without hardener were heated in the DSC at a rate of  $10^{\circ}\text{C}\cdot\text{min}^{-1}$ . Figure 4.63 shows that up to  $250^{\circ}\text{C}$  no exothermic or endothermic peak is observed for the epoxy resin sample and epoxy with C30B, but a strong exothermic peak appeared in the range between  $180$  and  $250^{\circ}\text{C}$  for the mixture of epoxy and I30E. Thus, no chemical reaction occurred either in the epoxy resin or mixture of epoxy and C30B in the temperature range studied, whereas the exothermic peak for the I30E mixture likely indicates that a curing reaction took place during the first heating scan.

To check the effect of the heating process on the physical properties of the sample, a second scan was done. The neat epoxy sample and the C30B mixture showed no change, but the I30E mixture showed a glass transition at  $T_g = 102^{\circ}\text{C}$ . The resin in the mixture had been polymerized to the solid state and the final product was in the form of a brown powder. This transformation can be explained in terms of the polymerization of epoxy groups initiated by the primary amine onium ion of the organo-nanoclay I30E. A similar effect was reported by Lan et al. [81].

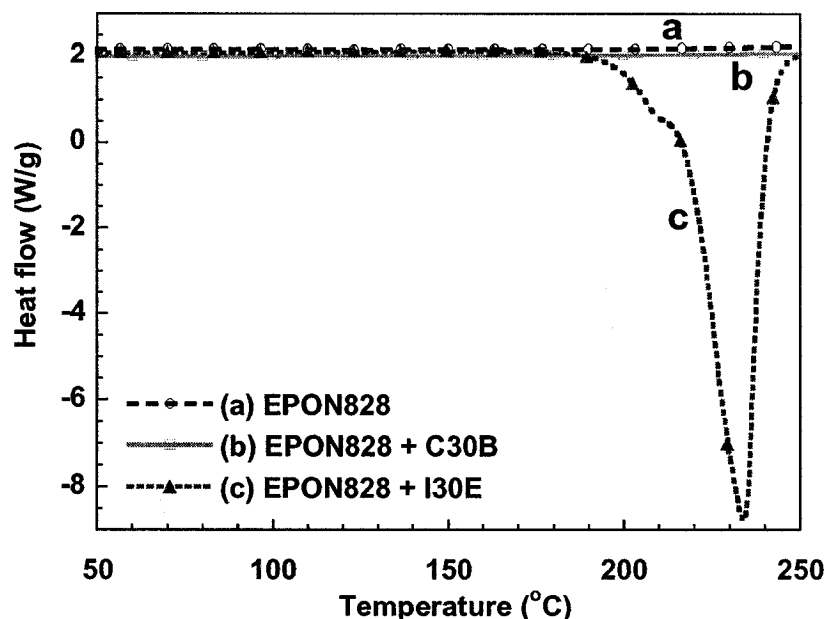


**Figure 4.63. DSC curves of neat epoxy EPON828, EPON828-C30B and EPON828-I30E in the absence of hardener**

Figure 4.64 compares the infrared spectra of uncured EPON828 resin and the epoxy-clay mixture without hardener after heating in the DSC. For EPON828-C30B, the spectra are very similar to that of pure EPON828. There is no evidence of any reaction of the epoxy rings. The only difference (too small to be seen in the Figure 4.64) is a slight variation around  $1100\text{--}1000\text{ cm}^{-1}$  arising from the clay absorption.

For EPON828-I30E, the most significant change is the disappearance of the epoxide ring band at  $915\text{ cm}^{-1}$  upon heating, as have the weaker peaks at  $1430$ ,  $1346$ ,  $971$ , and  $863\text{ cm}^{-1}$ . This is accompanied by the growth of a broad band around  $1170\text{--}1000\text{ cm}^{-1}$  that can be assigned to stretching of the C–O–C ether linkages formed by reaction of the epoxide rings. Thus the IR spectra confirm that the exothermic peak in the DSC curve of the first scan can be assigned to polymerization (etherification) of the epoxy groups

initiated by the onium ion of the organo-nanoclay. In the commercial clay I30E, most of the onium compound is “bound” to the clay surface via ionic bonds, but there is evidence for some unbound material as well. This raises the question of whether the reaction is initiated by the onium ions bound to the nanoclay surface or by the free onium ions. To check this, the free onium salt was removed by washing some I30E clay several times with hot deionized water, followed by drying. The resulting purified clay behaved in the same way as the original clay, indicating that the bound onium ions also play an initiating role for the epoxy polymerization. The primary onium salt  $R-NH_3^+$  probably loses a proton readily and reacts with an epoxide ring to form secondary amine groups and hydroxyl groups. The secondary amine groups can react further to form tertiary amine groups and more hydroxyl groups. Each hydroxyl group can react with an epoxide ring to form an ether linkage and a new hydroxyl group, and this etherification reaction can thus continue until all epoxide rings have been consumed. The etherification reaction is catalyzed by tertiary amine groups, which explains why it is important in the epoxy-clay mixture (even though the number of amine groups may not be high) but is negligible in the neat epoxy resin (even though the latter contains some hydroxyl groups). The epoxy-clay mixture was diluted to 0.2 wt% of clay and the same observation was obtained, indicating that the primary onium salt plays the role of initiator rather than curing agent. It has also been observed that the lower is the heating rate, the lower is the temperature at which the reaction takes place. Under isothermal conditions at 120°C, after 20 min the viscosity of the system increased dramatically while the degree of cure reached approximately 12%.

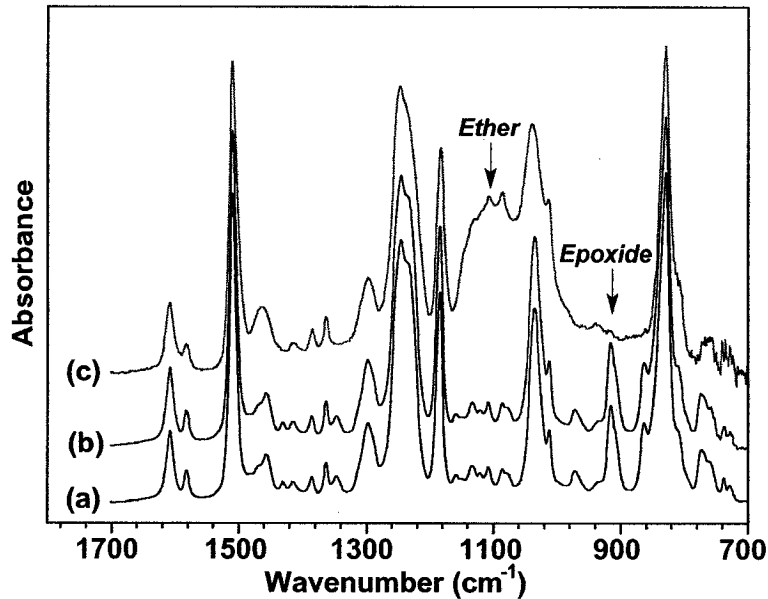


**Figure 4.64. FT-IR spectra of (a) uncured EPON828 resin, (b) EPON828-C30B and (c) EPON828-I30E after the first scan in DSC**

X-ray diffraction curves of the epoxy system and its nanocomposites based on Cloisite 30B and Nanomer I30E are illustrated in Figures 4.65 and 4.66. The *d*-spacing data calculated therefrom are summarized in Table 4.16. In all the nanocomposite samples, the clay layer separation (degree of intercalation) is considerably higher than in the original Cloisite 30B or Nanomer I30E. The gallery distance increases more than double compared to the original clay (Table 4.16). Clays have been further intercalated by the epoxy matrix and the I30E series were better intercalated by the matrix than the 30B ones. In addition, it is also noticed that the high curing temperature leads to a greater clay gallery distance, and it is more pronounced in the Nanomer I30E series. Better intercalation for the I30E series can be explained by the difference in the chemistry of the intercalant of the clays. Nanomer I30E which contains the intercalant based on primary amine can offer a better chemical interaction with the epoxy group of the matrix via the



hydrogen atoms of the amine group and this kind of reaction can take place even at low temperatures. Cloisite 30B consists of quaternary ammonium intercalant containing hydroxyl group, which can also offer a chemical interaction with the epoxy group but it can only take place at elevated temperatures (above 180°C). There is no significant difference between the clay loading levels of 2 phr and 4 phr for Cloisite 30B. However, the difference is more apparent for Nanomer I30E, particularly when the samples were cured at 120°C. Again, it can be speculatively explained by the greater reactivity of the Nanomer I30E at high temperature, resulting in a rapid increase in viscosity as observed during the mixing of clay and epoxy resin. Furthermore it is also observed that at the same loading level of 2 phr, for the 30B series, high stirring temperature shows somewhat better intercalation than the stirring at room temperature, although the effect is more pronounced for room temperature cured samples. For instance, when samples were cured at room temperature, the d-spacing of 8EP-2pB-Tm is 4.23 nm, compared with 3.99 nm for 8EP-2pB-Rm. During stirring of the epoxy and clays, epoxy molecules can diffuse into the clay galleries, and during curing, molecules of amine hardener and/or epoxy can continue to diffuse further into the galleries. Again, a high temperature of stirring speeds up the diffusion of the epoxy into the clay galleries while a high temperature of curing accelerates the diffusion of the epoxy and hardener into the galleries. This indicates that stirring and curing temperature play a very important role in clay intercalation. It should be stressed here that the curing rate of the resin can also have a determining role in the intercalation process. If curing took place very fast, further intercalation by the matrix during curing can be inhibited. As curing rate increases with temperature, high curing temperature should be expected to limit the further intercalation by the matrix. However,

the X-ray results indicate that the curing of the nanocomposites at the higher temperature of 120°C in all cases results in better intercalation than curing at room temperature, for nanocomposites with the same clay loading and stirring method. The X-ray diffraction peak shifts to lower angle, which means the degree of delamination increases in all cases. This can be explained by the fact that the hardener EPICURE 3046, which has a low reaction rate with epoxy even at high temperatures, has minimized this effect. Thus, in this particular case a high curing temperature accelerates further diffusion of the epoxy and hardener into the clay galleries according to the diffusion rules [10].

**Table 4.16. Summary of XRD data**

Sample	Gallery distance (Å)	
	Cured at room temperature	Cured at 120°C for 2 h
8EP	-	
<b>Cloisite 30B</b>	<b>18.5</b>	
8EP-2pB-Rm	39.9	43.8
8EP-2pB-Tm	42.3	44.8
8EP-4pB-Tm	41.7	44.1
<b>Nanomer I30E</b>	<b>23.8</b>	
8EP-2pE-Rm	48.4	56.0
8EP-2pE-Tm	49.4	57.0
8EP-4pE-Tm	47.0	49.9

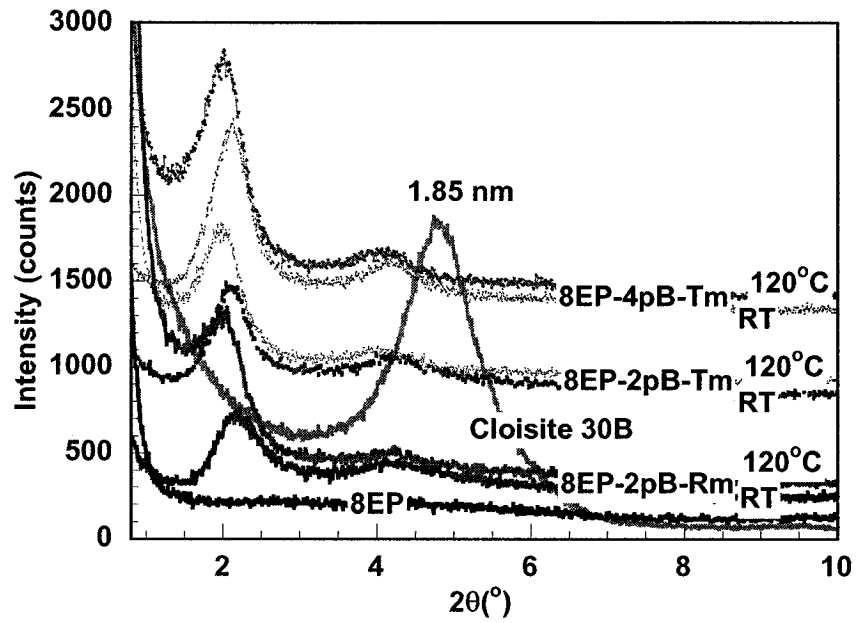


Figure 4.65. X-ray diffraction curves of the 8EP and its Cloisite 30B nanocomposites

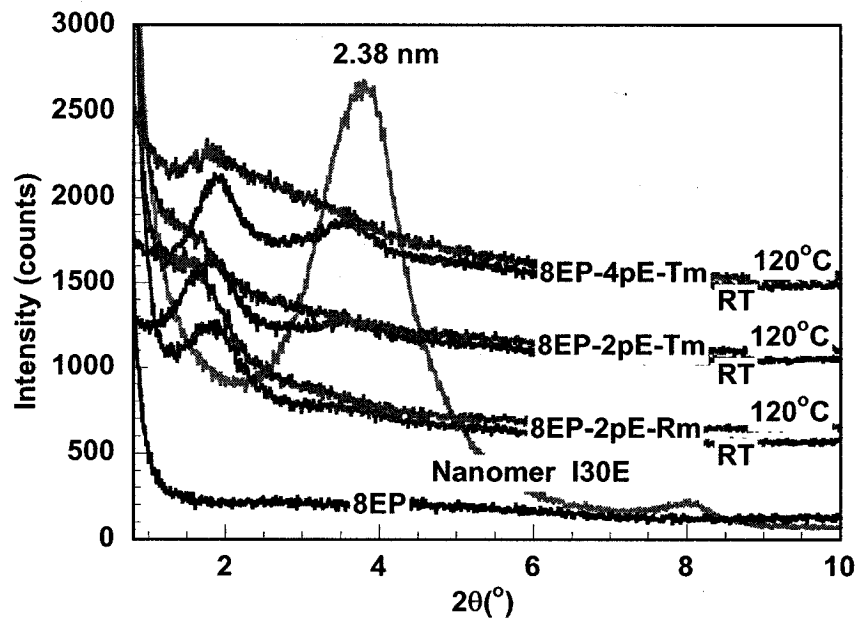
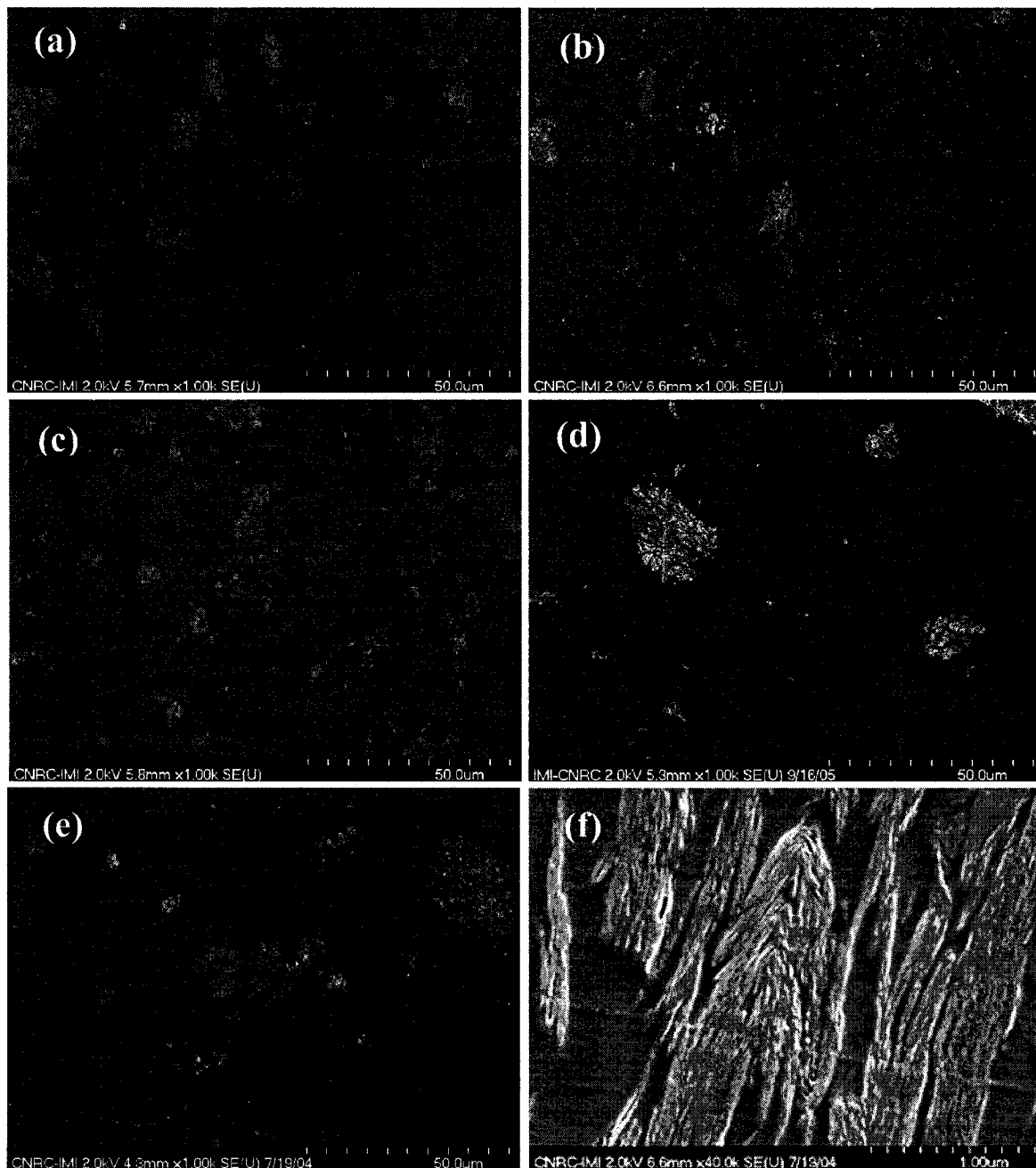


Figure 4.66. X-ray diffraction curves of the 8EP and its Nanomer I30E nanocomposites

Figure 4.67 presents the microstructures of nanocomposite samples observed by SEM. The bright spots on the backscattered images correspond to clay aggregates. Apparently, a portion of the clay remained at the micro-scale level with different size populations depending on the stirring conditions and clay type. However, due to the limitation of the SEM, one should not rule out the possibility of some exfoliation occurring. At the same loading level of 2 phr, the clay particles are more finely dispersed in the nanocomposite that was prepared at high temperature (8EP-2pB-Tm, Figure 4.67b) compared with room temperature (8EP-2pB-Rm, Figure 4.67a). As seen in Figure 4.67b, there is a greater density of small particles (with size below 2 microns) and a lower density of large particles than in Figure 4.67a. This indicates that a high temperature of stirring has a positive effect not only on the intercalation (as identified by XRD) but also on the dispersion of the clay in the materials. Moreover, with the same stirring method at high temperature, when the clay loading increases from 2 phr to 4 phr (Figure 4.67c), the number of aggregates increases but not the particle size. Figure 4.62 also shows that at the same loading level of clay and stirring method, Cloisite 30B is more finely dispersed in the nanocomposite compared to Nanomer I30E.

When the aggregate was examined at high magnification (Figure 4.67f), it was very interesting to observe that the matrix has diffused deeply inside the aggregate to form smaller stacks. Thus the aggregate can be considered as a composite of the small stacks and the epoxy matrix. If sufficient shear was used, it should be believed that these stacks can be further separated to form small particles. It should be stressed here that although clay dispersion remains in a certain proportion at the micro-scale, one should not treat it as a conventional micro-composite because of the presence of the matrix inside the

particles, and each particle can be consider as a nanocomposite.



**Figure 4.67. SEM micrographs of (a) 8EP-2pB-Rm, (b) 8EP-2pB-Tm, (c) 8EP-4pB-Tm, (d) 8EP-2pE-Rm, (e) 8EP-2pE-Tm, (f) 8EP-2pB-Tm at high magnification**

TEM observation for 8EP-2pE-Tm (Figure 4.68) has also confirmed the diffusion of matrix into the clay galleries. Besides large aggregates, a small amount of single-, double- and triple- layer stacks can also be observed in Figure 4.68b. The high stirring temperature provides better dispersion.

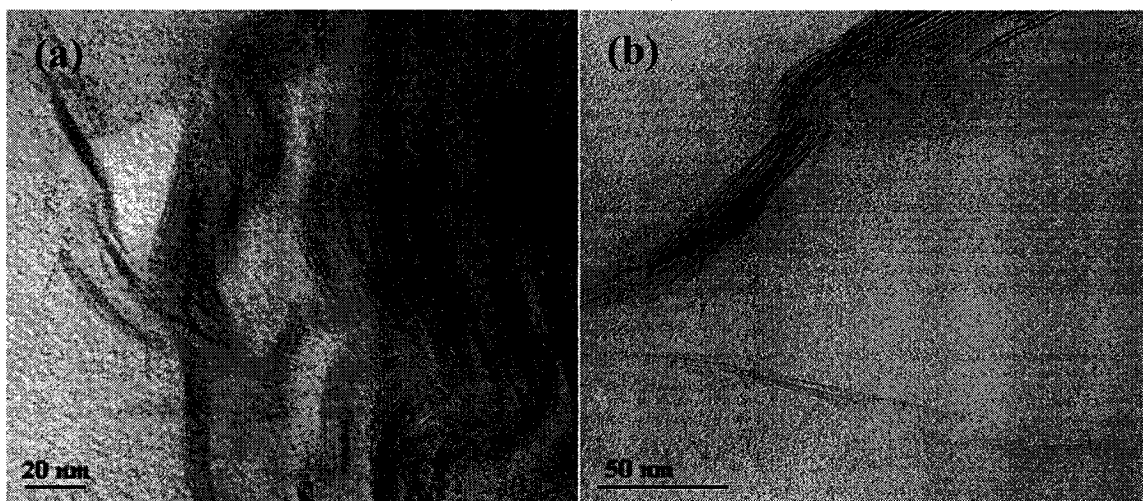


**Figure 4.68. TEM micrographs of (a) 8EP-2pE-Rm and (b) 8EP-2pE-Tm**

#### **4.4.3. Effect of chemistry of hardener**

Five types of curing agent were used in this study. The first one is diethylenetriamine, a low molecular weight triamine that forms a rigid molecular network. The second one is Jeffamine T403, a propylene oxide based triamine with medium molecular weight that forms a less rigid molecular network than diethylenetriamine. The third, fourth and fifth ones are Jeffamine D230, D400 and D2000, which are diamine-terminated polyoxypropylene diols with different molecular weight that can form a rigid to a very flexible network after curing. The nanocomposites were prepared with different concentrations of organoclay, a Southern Clay Products Cloisite C30B. Rm and Tm stirring methods were used. The nanocomposites were cured at room and high

temperature. The intercalation/exfoliation of clay in epoxy systems at different steps of preparing epoxy nanocomposites were analyzed by X-ray diffraction (XRD). Sample specifications are shown in Table 4.17.

**Table 4.17. Sample specifications for experiment set 4.4.3**

Designation*	Epon828	Hardener	C30B	Mixing method
<b>DETA</b>				
8DE	100	10.9	0	-
8DE-2pB-Rm	100	10.9	2	Rm
8DE-2pB-Tm	100	10.9	2	Tm
8DE-4pB-Tm	100	10.9	4	Tm
<b>D230</b>				
8d	100	32	0	-
8d-2pB-Rm	100	32	2	Rm
8d-2pB-Tm	100	32	2	Tm
8d-4pB-Tm	100	32	4	Tm
<b>D400</b>				
8δ	100	55	0	-
8δ-2pB-Rm	100	55	2	Rm
8δ-2pB-Tm	100	55	2	Tm
8δ-4pB-Tm	100	55	4	Tm
<b>T403</b>				
8T	100	42	0	-
8T-2pB-Rm	100	42	2	Rm
8T-2pB-Tm	100	42	2	Tm
8T-4pB-Tm	100	42	4	Tm
<b>D2000</b>				
8D	100	270	0	-
8D-2pB-Rm	100	270	2	Rm
8D-2pB-Tm	100	270	2	Tm
8D-4pB-Tm	100	270	4	Tm
* 8 = EPON828, DE = DETA, d = D230, δ = D400, T = T403, D = D2000, 2pB = 2 phr of C30B, 4pB = 4 phr of C30B, Rm = Room temperature stirring method, Tm = high temperature stirring method.				

#### 4.4.3.1. Curing rate

To clarify the effect of the rate of cure on structure of epoxy nanocomposites, the cure kinetics of these five epoxy systems was then investigated.

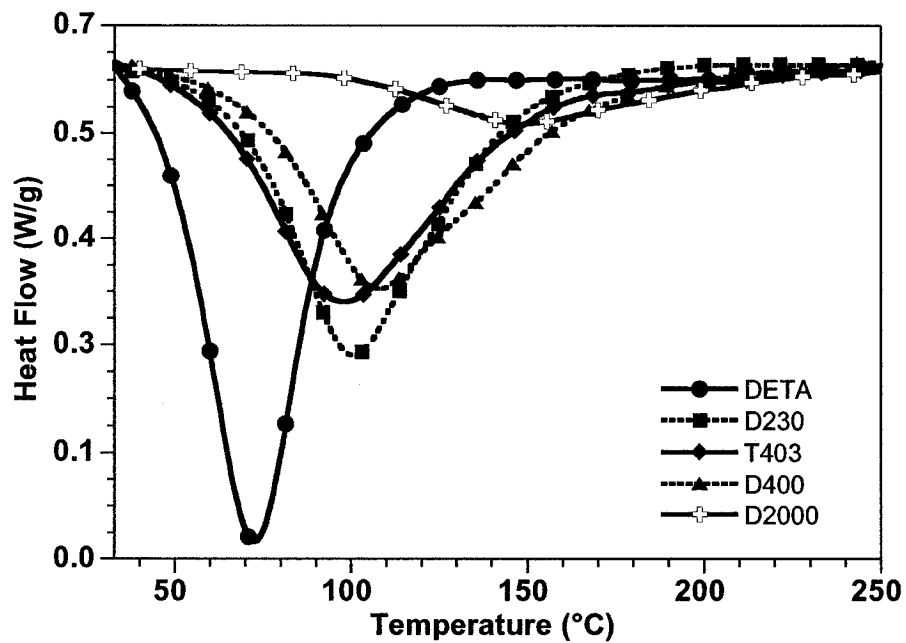


Figure 4.69. DSC curves of the epoxy with different curing agents at heating rate  $2.5^{\circ}\text{C}\cdot\text{min}^{-1}$

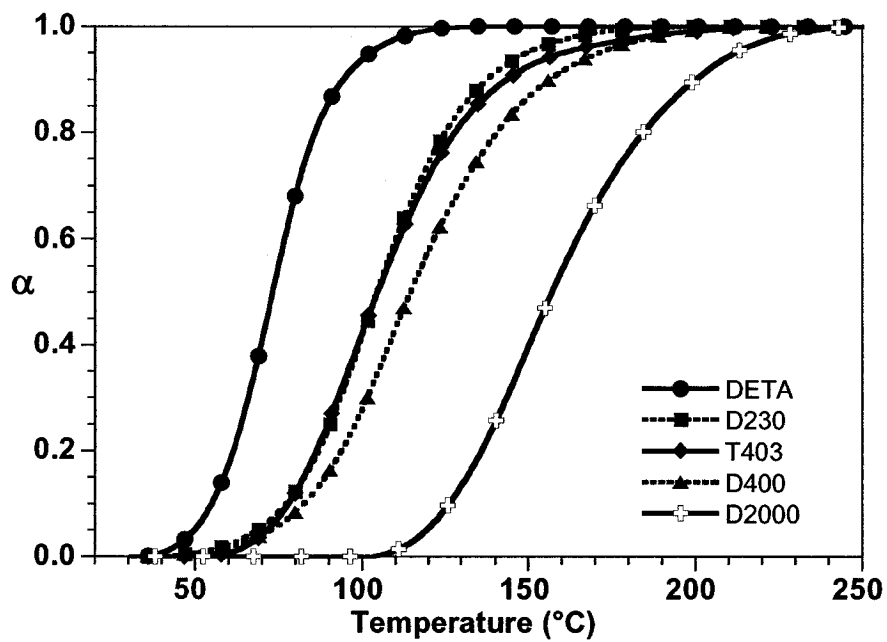


Figure 4.70. Transformation curves of the epoxy with different curing agents at heating rate  $2.5^{\circ}\text{C}\cdot\text{min}^{-1}$



Figure 4.69 shows the DSC curves at heating rate  $2.5^{\circ}\text{C}\cdot\text{min}^{-1}$  of these epoxy systems. The transformation curves derived from the DSC results are shown in Figure 4.70. In these five systems, the epoxy system cured with DETA shows the largest initial slope respectively compared to the others. This means DETA is the most reactive curing agent. Thus the cure rate is significantly higher for the system cured with DETA compared to the systems cured with D230, T403, D400 and D2000. The system based on D2000 shows the lowest reactivity. The rate of cure for these curing agents can be arranged as  $\text{DETA} > \text{D230} \approx \text{T403} > \text{D400} > \text{D2000}$ . Note that the curing rates of D230 and T403 are very close together. These curing rates of five curing agents are very much corresponding to their amine hydrogen equivalent weight (AHEW). The amine hydrogen equivalent weight is 20, 60, 81, 115 and 514 g/eq for DETA, D230, T403, D400 and D2000 respectively. It can be seen clearly that AHEW of DETA is smallest and AHEW of D2000 is highest compared to the AHEW of the other hardeners.

#### **4.4.3.2. Dispersion and morphology**

X-ray diffraction curves of the epoxy systems and their nanocomposites after being cured with different curing agents are illustrated in Figures 4.71 and 4.72. The results show that curing agent has an effect on the delamination (intercalation/ exfoliation) of clay. If one considers 3 hardeners which have similar chemical structure including D230, D400 and D2000, the system cured with D2000 gave a better delamination than D400 and D230. The delamination of these three systems can be arranged as  $\text{D2000} > \text{D400} > \text{D230}$ . However, the length of the molecules of these Jeffamines decreases in the order  $\text{D2000} > \text{D400} > \text{D230}$ , so D230 would be expected to diffuse into the clay galleries

more easily during curing than D400 and D2000. The rate of diffusion of these three hardeners increases in the following order:  $D2000 < D400 < D230$ . However, the curing rate of the EPON828-D2000 system is slower as compared to the EPON828-D400 and the EPON828-D230 systems. As a consequence, it is reasonable to believe that D2000 and possibly EPON828 in EPON828-D2000 system would have more time to diffuse into the clay galleries to exfoliate the clays as compared to the EPON828-D400 and EPON828-D230 systems. On comparing the results presented in Figures 4.69, 4.70, 4.71 and 4.72, there is a correlation between the curing rate of the epoxy system and the level of intercalation/exfoliation of nanoclay in the corresponding nanocomposite. Thus, the lower is the curing reactivity of the epoxy system, the greater is the clay intercalation in the nanocomposites. This observation is in good agreement with the reported literature [18]. Moreover, it is also believed that the size of the D2000 molecules makes a great contribution to the intercalation/exfoliation of clay C30B in epoxy matrix. With larger size compared to the D400 and D230, D2000 can push clay platelets apart and expand the clay galleries more than D400 and D230. The length of D400 molecule is longer than D230. D400 also can push the clay platelets farther apart than D230. Curing temperature also has an effect on intercalation/exfoliation of clay. As curing rate increases with temperature, high curing temperature should be expected to limit further intercalation by the matrix due to faster cure as discussed above. However, the X-ray diffraction peak for curing at high temperature shifts a bit to lower angle and its intensity decreases as compared to room temperature which means the degree of delamination increases. This is very similar to the result from Kornmann et al [18] and Lan et al. [45]. This can be explained by the fact that at higher temperature, the mobility of the epoxy and hardener

molecules increases, thus these molecules can diffuse more easily into the clay galleries and expand them.

As the curing rate of epoxy and DETA is faster than for the Jeffamine curing agents (Figure 4.70) it may be expected that DETA may not have enough time to diffuse into the clay galleries especially when it is cured at high temperature as discussed earlier. However, in reality DETA provides better intercalation and exfoliation than the Jeffamine counter parts (Fig. 4.71b), which means its short molecular chain has given it a better ability to penetrate into the clay galleries.

X-ray results also show that with the same curing rate (D230 and T403), curing with D230 leads to a greater clay gallery spacing than curing with T403 for poorer mixing at room temperature cure. However the delamination for the case of T403 is better than D230 for the high temperature mixing and curing. T403 is a triamine which has three functional groups while D230 is a diamine which has two functional groups. The structure of T403 obstructs the movement of T403 molecule into the clay gallery as compared to D230. Because of this, for room temperature cure and poor dispersion, XRD shows poorer intercalation/exfoliation of clay in the epoxy system cured with T403 than in the one cured with D230. However, at high temperature, the mobility of the epoxy and hardener molecules increases, so T403 can have a better chance to enter the clay galleries. It is worth stressing here that in thermoset systems, the intercalation and exfoliation process that can continue during curing is controlled not only by the rate of diffusion of organic molecules (in this case, the curing agent and the epoxy molecules) into the clay gallery but also by the curing rate of the epoxy system and by the size of the

epoxy and hardener molecules. Because of this, the intercalation/exfoliation of the clay is not only dependent on the reactivity of the epoxy system but also on the rate of diffusion of epoxy and curing agent.

**Table 4.18. Summary of XRD data for nanocomposites**

Sample	Gallery distance (Å)	
	Cured at room temperature	Cured at 120°C for 2 h
<b>C30B</b>	<b>18.5</b>	
<b>DETA (DE)</b>		
8DE-2pB-Rm	37.2	38.2
8DE-2pB-Tm	38.1	38.3
8DE-4pB-Tm	38.1	38.2
<b>D230 (d)</b>		
8d-2pB-Rm	37.4	38.1
8d-2pB-Tm	38.3	38.4
8d-4pB-Tm	37.9	38.3
<b>T403 (T)</b>		
8T-2pB-Rm	36.6	38.1
8T-2pB-Tm	39.3	40.1
8T-4pB-Tm	38.2	39.0
<b>D400 (δ)</b>		
8δ-2pB-Rm	37.4	39.4
8δ-2pB-Tm	39.1	40.3
8δ-4pB-Tm	38.8	40.1
<b>D2000 (D)</b>		
8D-2pB-Rm	-	-
8D-2pB-Tm	-	-
8D-4pB-Tm	-	-

Furthermore it is also observed that at the same loading level of 2 phr, high stirring temperature shows somewhat better intercalation than stirring at room temperature, although the effect is more pronounced for room-temperature-cured samples. High temperature stirring speeds up the diffusion of the epoxy into the clay galleries while high

temperature curing accelerates the diffusion of the epoxy and hardener into the galleries. Epoxy molecules can diffuse into the clay galleries during stirring of the epoxy and clay, and molecules of amine hardener and/or epoxy can continue to diffuse further into the galleries during curing. This indicates that stirring, curing temperature and curing rate play a very important role in clay intercalation.

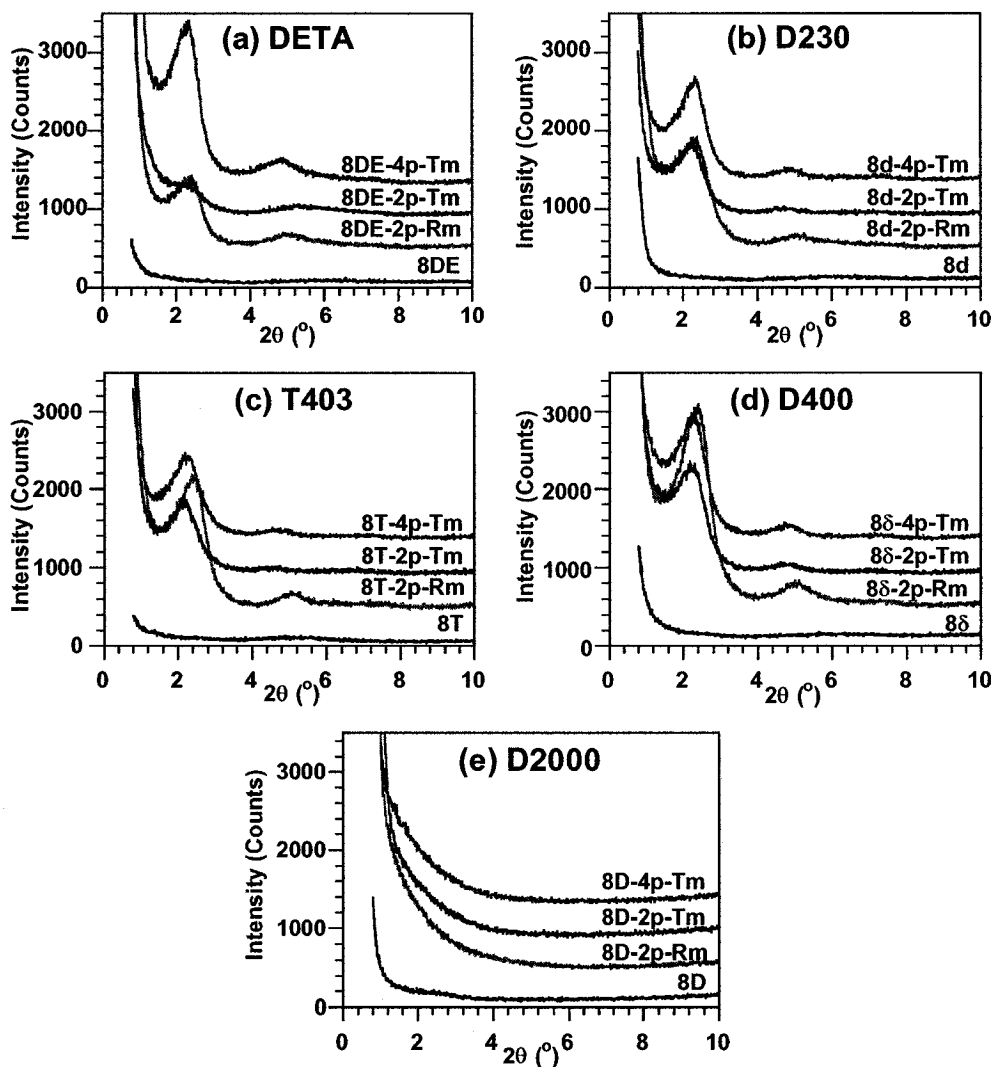


**Figure 4.71. X-ray curves of the EPON828 and its nanocomposites for samples after being cured at room temperature with (a) DETA, (b) D230, (c) T403, (d) D400 and (e) D2000**

Moreover, it is also seen that the intensity of the XRD peak decreases, which means the level of intercalation/exfoliation in all nanocomposite samples after cure increases as compared to their mixture before curing. This indicates that the curing step of preparing nanocomposites also plays an important role in clay intercalation.

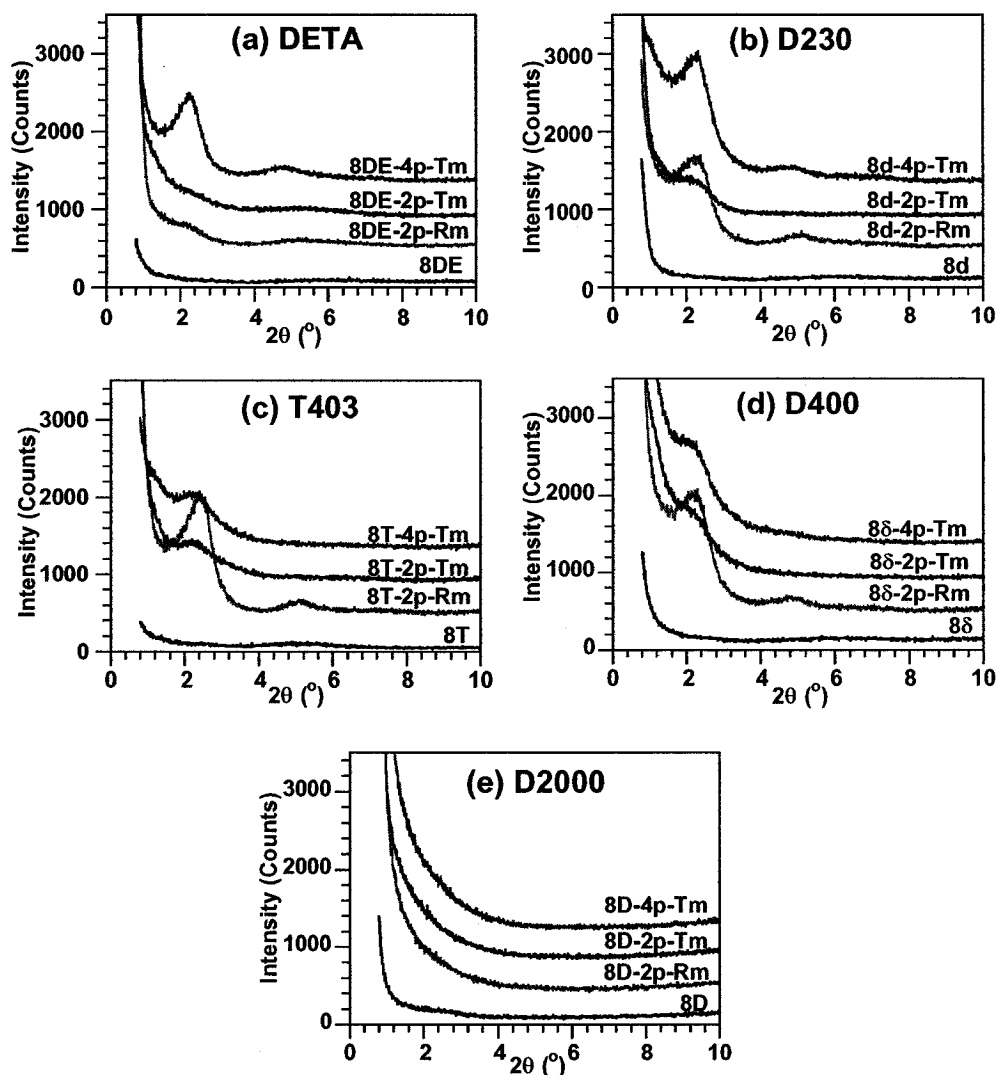


**Figure 4.72.** X-ray curves of the EPO828 and its nanocomposites samples after being cured at 120°C for 2 h with (a) DETA, (b) D230, (c) T403, (d) D400 and (e) D2000

## 4.5. Model for the dispersion of clay

The Equation 4.1 described the effect of both thermodynamic and mechanical terms on the force acting on the clay particles ( $F_{DT} = D + \tau$ ). From the experimental results, the question arises as to why one is not able to achieve the exfoliation of clay at the stirring step. To answer this question, the flow of the epoxy and clay mixture under high speed stirring (homogenizer) was examined from a theoretical point of view. This part of the study was done to investigate further the mechanical effect ( $\tau$ ). Figure 4.73 shows the shear force imposed on the clay layers.

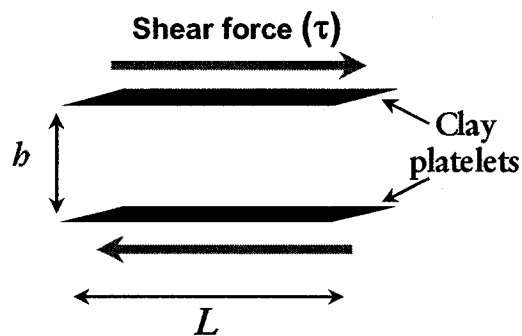


**Figure 4.73. Shear force imposed on nanoclay (in epoxy) at the stirring step;  $h$  is the distance between clay platelets,  $L$  is the length of clay platelets**

The dispersion of clay particles in the polymer matrix can result in the formation of three general types of composites: (a) conventional composites; the clay fraction in conventional clay composites plays little or no functional role and acts mainly as a filling agent for economic considerations, (b) intercalated nanocomposites; these are formed when one or a few molecular layers of polymer are inserted into the clay galleries with a fixed interlayer spacing, (c) exfoliated nanocomposites; the individual 10-Å-thick silicate

layers are dispersed in the polymer matrix and segregated from one another, and the gallery structures are completely destroyed. Both intercalated and exfoliated nanocomposites offer special physical and mechanical properties compared to the conventional composites [50, 123].

The term “dispersion” is used to refer to the complete process of incorporating the powder into the liquid medium such that the final product consists of fine particles distributed throughout the medium. The dispersion of fine particles is normally termed colloidal if at least one dimension of the particles lies between 1 nm and 1  $\mu$ m. Solid particles dispersed in a liquid form a suspension. In many practical uses of powders the primary particle size is sufficiently small that further subdivision is unnecessary. But in the dry state, the powder usually contains aggregates of primary particles and these are attached to other aggregates and/or primary particles forming agglomerates. Aggregates may require considerable energy to break them to the point when the surface of each primary particle is available to the wetting liquid. There are at least three major types of interaction involved in colloidal particles, namely the London – van der Waals forces of attraction, the Coulombic force (repulsive or attractive) associated with charged particles and the repulsive force arising from solvation, or adsorbed layers. The most important forces to consider here are van der Waals forces.

The London-van der Waals attractive forces are based on electronic interaction, due to the interaction of dipoles within the particles. These may be the permanent dipoles of polar particles or the dipoles that may be induced in non-polar particles which are polarisable [124, 125, 126].



### 4.5.1. Van der Waals interaction force acting between two particles or macroscopic bodies

We can understand the origin of dispersion interactions from the following argument. For non-polar atoms, such as the rare gases, the time-average dipole moment is zero. However, at any instant there exists an instantaneous dipole moment determined by the location of the electrons around the nucleus. This dipole generates an electric field, which in turn induces a dipole in nearby neutral atoms. The resulting interaction gives rise to an attraction force between the two atoms whose time average is finite. The same argument applies for the attraction of two non-polar molecules. In 1933 London derived an expression for the attraction between a pair of atoms by solving the Schrödinger equation. He modeled each of the atoms as a charged harmonic oscillator with a characteristic frequency  $\nu$  and obtained attractive interactions between two similar atoms [124].

$$E(R_{12}) = -\frac{3}{4} \frac{\alpha^2 h_p \nu}{(4\pi\epsilon_0\epsilon_r)^2 R_{12}^6} \quad (4.5)$$

and for two dissimilar atoms:

$$E(R_{12}) = -\frac{3}{2} \frac{\alpha_1\alpha_2}{(4\pi\epsilon_0\epsilon_r)^2 R_{12}^6} \left( \frac{h_p\nu_1\nu_2}{\nu_1 + \nu_2} \right) \quad (4.6)$$

In these equations  $h_p$  is Planck's constant and  $h_p\nu$  generally equals the ionization energy of the atoms,  $\alpha$  is the polarizability,  $R_{12}$  is the intermolecular distance,  $\epsilon$  is relative dielectric permittivity, or the dielectric constant,  $\epsilon_0$  is the electric permittivity of vacuum

( $\epsilon_0 = 8.854 \times 10^{-12} \text{ C}^2 \text{J}^{-1} \text{m}^{-1}$ , coulombs<sup>2</sup> per joule per meter). Dispersion forces, like gravitational forces, operate between all atoms or molecules.

Moving on from the analysis of the interaction between two molecules, we consider interaction potentials and forces between two particles that contain many atoms. If we assume pairwise additivity between molecules, we can sum over all possible pairs, one molecule in each body, to obtain the dispersion force between two macroscopic bodies or particles. The discussion that follows represents the two particles as two blocks with planar surfaces of infinite extension separated by a distance  $h$  in vacuum ( $\epsilon_r = 1$ ). In calculating the attractive interaction between pairs of molecules, Equation 4.5 is used. Consider first the interaction between a single molecule (or atom) and a block (block 1) where the normal distance from the molecule to the surface of the block is  $z$ , as shown in Figure 4.74.

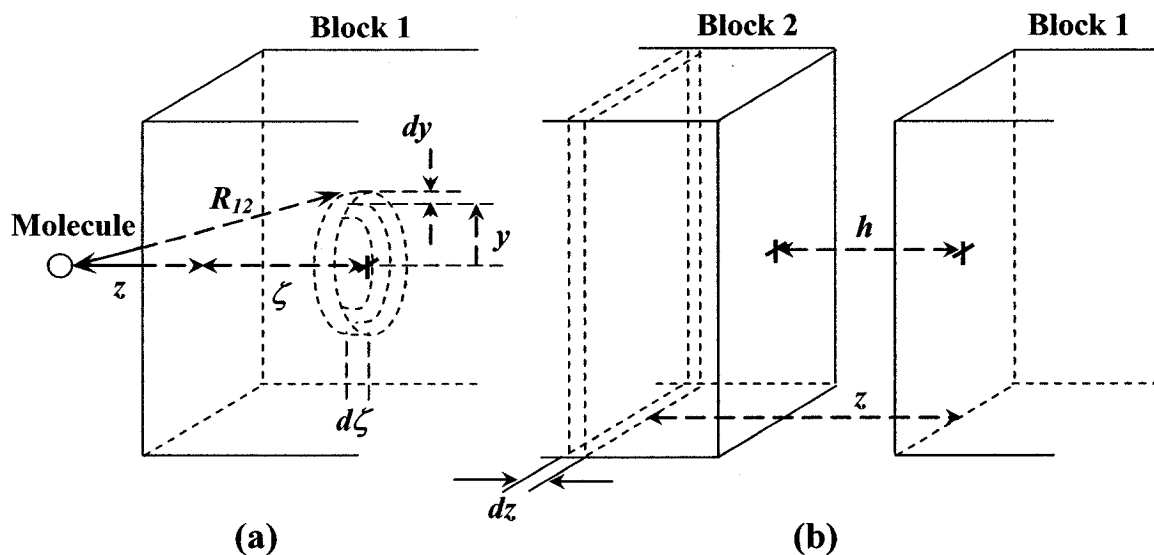


**Figure 4.74. Schematic for coordinates (a) between a molecule and a block, (b) two blocks**

Integration will replace the summation between this molecule and all the molecules in the block. For the ring shape volume element shown in Figure 4.74, the volume is  $2\pi y dy d\zeta$ , and the interaction potential between the single molecule and all the molecules in this small volume is given by [124, 125]

$$dE(R_{12}) = -\frac{C_{disp}}{R_{12}^6} \frac{\rho N_{AV}}{M} 2\pi y dy d\zeta \quad (4.7)$$

Where  $C_{disp}/R_{12}^6$  gives the pairwise interaction potential,  $\rho N_{AV}/M$  ( $\rho$  is density;  $M$  is molecular weight) is the number of molecules per unit volume in the block, and  $2\pi y dy d\zeta$  the differential volume. When the ring is located inside the block.

$$R_{12}^2 = (z + \zeta)^2 + y^2 \text{ and} \quad (4.8)$$

$$dE(z) = -C_{disp} \frac{\rho N_{AV}}{M} \frac{2\pi y dy d\zeta}{\left[ (z + \zeta)^2 + y^2 \right]^3} \quad (4.9)$$

The double intergral of  $dE(z)$  for all values of  $y$  and  $\zeta$  from zero to infinity gives the interaction between the single molecule and the particle at a normal distance  $z$ .

$$E(z) = -\int_0^\infty \int_0^\infty C_{disp} \frac{\rho N_{AV}}{M} \frac{2\pi y}{\left[ (z + \zeta)^2 + y^2 \right]^3} dy d\zeta \quad (4.10)$$

Integration over  $y$  gives:

$$\int_0^{\infty} \frac{ydy}{[(z+\zeta)^2 + y^2]^3} = \frac{1}{2} \int_0^{\infty} \frac{du}{[(z+\zeta)^2 + u]^3} = -\frac{1}{2} \left[ \frac{1}{2[(z+\zeta)^2 + u]^2} \right]_0^{\infty} = \frac{1}{4} \frac{1}{(z+\zeta)^4} \quad (4.11)$$

where  $u = y^2$ ,  $du = 2ydy$

Integration over  $\zeta$  give:

$$\int_0^{\infty} \frac{1}{4} \frac{1}{(z+\zeta)^4} = -\frac{1}{4} \left[ \frac{1}{(z+\zeta)^3} \right]_0^{\infty} = \frac{1}{12z^3} \quad (4.12)$$

Therefore Equation 4.10 becomes

$$E(z) = -\frac{\rho N_{AV}}{M} \frac{C_{disp} \pi}{6z^3} \quad (4.13)$$

Note that the potential energy of interaction between a molecule (atom) and a particle varies with the distance from the surface as  $1/z^3$

One can determine the interaction energy between two blocks by considering the molecule (or atom) to be one of many located inside the second block (block 2). All the atoms in the slice of block 2 located at a distance  $z$  from the first block have an energy given by Equation 4.11.

In a volume element  $dz$  we will have  $(\rho N_{AV}/M)dz$  molecules per unit area, and the interaction potential due to that element per unit area will be

$$dE(z) = -\left( \frac{\rho N_{AV}}{M} \right)^2 \frac{C_{disp} \pi}{6} \frac{dz}{z^3} \quad (4.14)$$

With  $z$  from  $h$  to  $\infty$ , the attraction interaction energy per unit surface area of particles  $E_{att,p}(h)$  is:

$$E_{att,p}(h) = - \left( \frac{\rho N_{AV}}{M} \right)^2 \frac{C_{disp} \pi}{12} \frac{1}{h^2} = - \frac{H_{11}}{12\pi} \frac{1}{h^2} \quad (4.15)$$

In this equation,  $H_{11}$  is called the Hamaker constant, a material constant that measures the attraction between two particles of material in vacuum.

#### 4.5.2. Van der Waals interaction forces between two spheres

The interaction between two infinite blocks separated by a normal distance  $h$  provides the simplest geometry with which to evaluate attraction forces. However one is often interested in the interactions between curved surfaces, particularly spherical particles. When the surfaces of particles are uniformly curved, the interaction can be derived simply by breaking the particles down into a series of planar forms and the interaction energy between two planar surfaces  $E_{att,p}$  can be used for this case. Figure 4.75 shows two spheres of equal radius  $R$  separated by a distance of  $h$ . Approximate the sphere by a series of circular (annular) rings possessing planar faces. The planar faces are separated by a distance  $z$ .

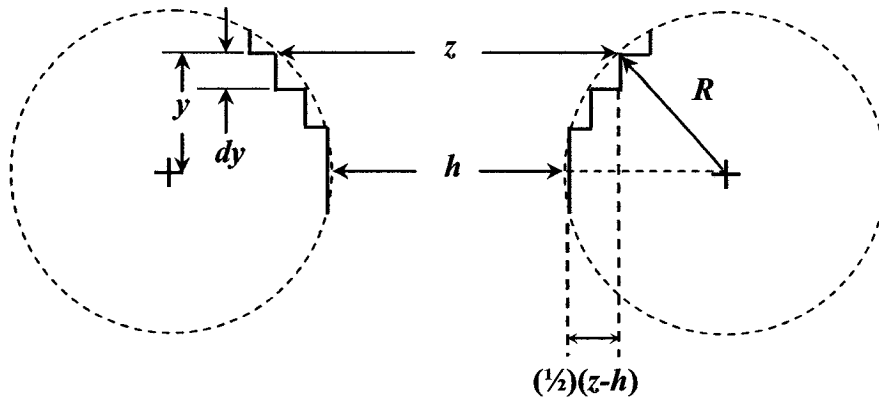


**Figure 4.75. Schematic for coordinates between two spherical particles**

Assume that the main line of interaction occurs along the two centers of two spheres. The interaction energy between the pair of planar rings at a distance  $y$  from the center of the sphere can be calculated as follow:

$$E_{att} dA = E_{att} (2\pi y dy) \quad (4.16)$$

Where  $E_{att}$  is the attractive interaction energy per unit area and  $dA$  is the area of the ring, which can be written as  $2\pi y dy$ .

From the Figure 4.75, we can have:

$$y^2 + \left( R - \frac{(z-h)}{2} \right)^2 = R^2 \quad (4.17)$$

$$y^2 = \left[ R(z-h) - \left( \frac{z-h}{2} \right)^2 \right] \quad (4.18)$$

Differentiating (with  $R = \text{constant}$ ) gives

$$2ydy = \left[ R - \left( \frac{z-h}{2} \right) \right] dz \quad (4.19)$$

From Equation 4.18 we have  $\left[ R - \left( \frac{z-h}{2} \right) \right] = (R^2 - y^2)^{\frac{1}{2}}$  (4.20)

$$2ydy = R \left( 1 - \left( \frac{y}{R} \right)^2 \right)^{\frac{1}{2}} dz \quad (4.21)$$

Substituting into Equation 4.16, we obtain

$$E_{att} dA = \pi R \left( 1 - \left( \frac{y}{R} \right)^2 \right)^{\frac{1}{2}} E_{att} dz \quad (4.22)$$

If the spheres are large compared to their separation distance, then the interaction between them occurs primarily in the regions for which  $y \ll R$ . In this case:  $y^2/R^2 \ll 1$ .

$$E_{att} dA = \pi R E_{att} dz \quad (4.23)$$

Substituting the value of  $E_{att}$  from Equation 4.15 to Equation 4.23 and integrate over all values of  $z$  from  $a$  to infinity (a limit that is justified when the  $R$  of spheres are large compared to their separation), the attraction potential energy of interaction for two identical spheres  $E_{att,s}$  becomes:

$$E_{att,s} = \int_a^{\infty} -\frac{H_{11}R}{12} \frac{dz}{z^2} = -\frac{H_{11}R}{12h} \quad (4.24)$$

Using the same approach to derive the interaction energy between a sphere and a flat surface, Table 4.19 summarizes the values of attractive interaction  $E_A$  for various geometries [124, 125]

**Table 4.19: Potential energy of attraction ( $E_A$ ) between two particles with various geometries [124, 125]**

Particles	$E_A$	Definitions/limitations
Two spheres	$-\frac{H_{11}}{6} \left[ \left( \frac{2R_1R_2}{h^2 + 2R_1h + 2R_2h} \right) + \left( \frac{2R_1R_2}{h^2 + 2R_1h + 2R_2h + 4R_1R_2} \right) + \ln \left( \frac{h^2 + 2R_1h + 2R_2h}{h^2 + 2R_1h + 2R_2h + 4R_1R_2} \right) \right]$	$R_1, R_2 =$ radii, $h =$ separation of surface along line of centers
Two spheres of equal radius	$-\frac{H_{11}}{6} \left[ \left( \frac{2R^2}{h^2 + 4Rh} \right) + \left( \frac{2R^2}{h^2 + 4Rh + 4R^2} \right) + \ln \left( \frac{h^2 + 4Rh}{h^2 + 4Rh + 4R^2} \right) \right]$	$R_1 = R_2 = R$
Two identical spheres of equal radius ( $R \gg h$ )	$-\frac{H_{11}R}{12h}$	$R \gg h$
Two spheres of unequal radius	$-\frac{H_{11}R_1R_2}{6h(R_1 + R_2)}$	$R_1$ and $R_2 \gg h$
Two plates of equal thickness	$-\frac{H_{11}}{12\pi} \left[ \frac{1}{h^2} + \frac{1}{(h + 2\delta)^2} - \frac{2}{(h + \delta)^2} \right]$	$\delta$ is the thickness of the plates.
Two identical blocks	$-\frac{H_{11}}{12\pi h^2}$	$\delta \rightarrow \infty$

### 4.5.3. Development of theoretical model of flow of the epoxy-clay mixture in high speed stirring

The ultimate goal is to determine if it is theoretically possible to separate two layers of clay. The mixer flow geometry (cross-section) is in Figure 4.76. In this schematic, the



dots represent the particles in the fluid. The mixer consists of 2 concentric cylinders, each containing several small notches as shown. The inner cylinder (radius  $R_i$  of 9 mm) spins at a constant angular velocity,  $\Omega$ . The centrifugal force moves the liquid from the middle of the inner cylinder to the gap between the two cylinders where it is sheared before exiting through the notches in the outer cylinder (radius  $R_o$  of 9.5 mm).

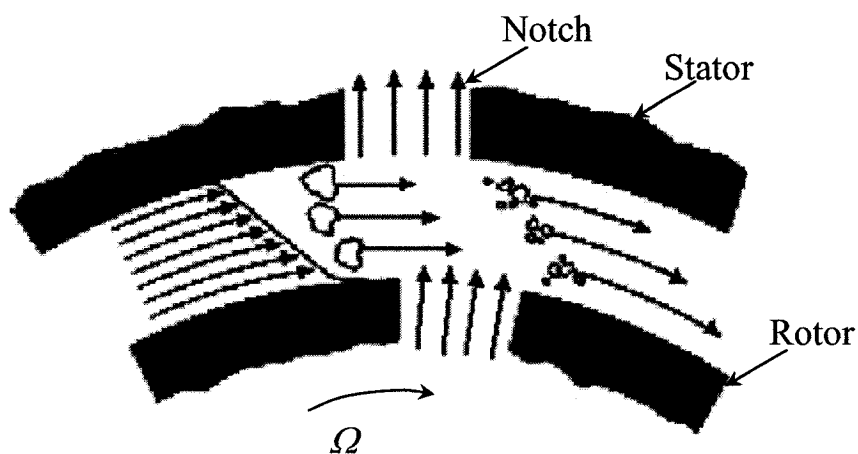


**Figure 4.76. The mixer flow geometry**

To simplify the flow of epoxy and clay mixture in this mixer, the mixer geometry can be considered as in Figure 4.77. That is, a tangential annular flow of a fluid between 2 concentric cylinders when the inner cylinder is turning. The inner cylinder spins at a constant angular velocity,  $\Omega$ .

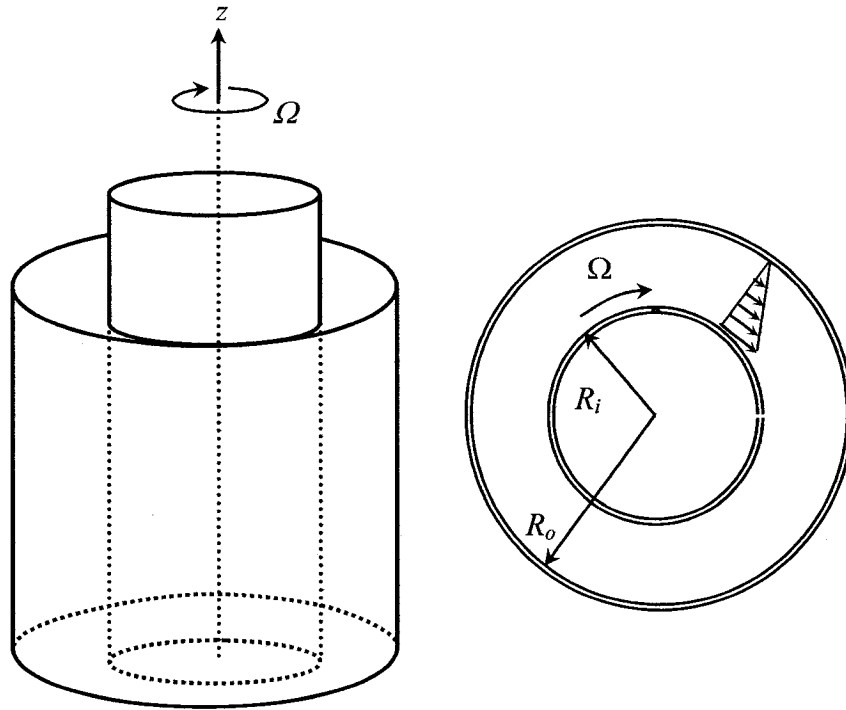


**Figure 4.77. Tangential annular flow between rotating cylinders**

One considers an incompressible, isothermal, Newtonian fluid in steady, laminar flow between the two coaxial cylinders, whose inner and outer wetted surfaces have radii of  $R_i$  and  $R_o$ , respectively. We assume additionally that the effects of the clay particles on the

flow are negligible. Under these conditions  $\frac{\partial}{\partial \theta} = \frac{\partial}{\partial z} = 0$

For an incompressible fluid, the continuity equation is

$$\nabla \cdot \underline{v} = 0 \tag{4.25}$$

where  $\underline{v}$  is the velocity vector

In cylindrical coordinates, Equation 4.25 is written as

$$\frac{1}{r} \frac{\partial(rv_r)}{\partial r} + \frac{1}{r} \frac{\partial v_\theta}{\partial \theta} + \frac{\partial v_z}{\partial z} = 0 \quad (4.26)$$

where  $r$ ,  $\theta$  and  $z$  are the radial, tangential and axial components in cylindrical coordinates.

In steady laminar flow, the fluid is expected to travel in a circular motion. Only the tangential component of velocity exists. The radial and axial components of velocity are zero, so  $v_r = 0$  and  $v_z = 0$ .

$$\underline{v} = \begin{pmatrix} v_r \\ v_\theta \\ v_z \end{pmatrix}_{r\theta z} = \begin{pmatrix} 0 \\ v_\theta \\ 0 \end{pmatrix}_{r\theta z} \quad (4.27)$$

Thus, the continuity equation reduces to:

$$\frac{\partial v_\theta}{\partial \theta} = 0 \quad (4.28)$$

The equation of motion for an incompressible Newtonian fluid [127, 128] is:

$$\rho \left( \frac{\partial \underline{v}}{\partial t} + \underline{v} \cdot \nabla \underline{v} \right) = -\nabla p + \mu \nabla^2 \underline{v} + \rho \underline{g} \quad (4.29)$$

In cylindrical coordinates we have [127, 129]

$$\rho \left( \frac{\partial \underline{v}}{\partial t} \right) = \begin{pmatrix} \rho \frac{\partial v_r}{\partial t} \\ \rho \frac{\partial v_\theta}{\partial t} \\ \rho \frac{\partial v_z}{\partial t} \end{pmatrix}_{r\theta z} \quad (4.30)$$

$$\rho \underline{v} \cdot \nabla \underline{v} = \rho \begin{pmatrix} v_r \left( \frac{\partial v_r}{\partial r} \right) + v_\theta \left( \frac{1}{r} \frac{\partial v_r}{\partial \theta} - \frac{v_\theta}{r} \right) + v_z \left( \frac{\partial v_r}{\partial z} \right) \\ v_r \left( \frac{\partial v_\theta}{\partial r} \right) + v_\theta \left( \frac{1}{r} \frac{\partial v_\theta}{\partial \theta} + \frac{v_r}{r} \right) + v_z \left( \frac{\partial v_\theta}{\partial z} \right) \\ v_r \left( \frac{\partial v_z}{\partial r} \right) + v_\theta \left( \frac{1}{r} \frac{\partial v_z}{\partial \theta} \right) + v_z \left( \frac{\partial v_z}{\partial z} \right) \end{pmatrix}_{r\theta z} \quad (4.31)$$

$$-\nabla p = \begin{pmatrix} -\frac{\partial p}{\partial r} \\ -\frac{1}{r} \frac{\partial p}{\partial \theta} \\ -\frac{\partial p}{\partial z} \end{pmatrix}_{r\theta z} \quad (4.32)$$

$$\mu \nabla^2 \underline{v} = \begin{pmatrix} \mu \frac{\partial}{\partial r} \left[ \frac{1}{r} \frac{\partial}{\partial r} (r v_r) \right] + \mu \frac{1}{r^2} \frac{\partial^2 v_r}{\partial \theta^2} + \mu \frac{\partial^2 v_r}{\partial z^2} - \frac{2\mu}{r^2} \frac{\partial v_\theta}{\partial \theta} \\ \mu \frac{\partial}{\partial r} \left[ \frac{1}{r} \frac{\partial}{\partial r} (r v_\theta) \right] + \mu \frac{1}{r^2} \frac{\partial^2 v_\theta}{\partial \theta^2} + \mu \frac{\partial^2 v_\theta}{\partial z^2} + \frac{2\mu}{r^2} \frac{\partial v_r}{\partial \theta} \\ \mu \frac{1}{r} \frac{\partial}{\partial r} \left( r \frac{\partial v_z}{\partial r} \right) + \mu \frac{1}{r^2} \frac{\partial^2 v_z}{\partial \theta^2} + \mu \frac{\partial^2 v_z}{\partial z^2} \end{pmatrix}_{r\theta z} \quad (4.33)$$

$$\rho \underline{g} = \begin{pmatrix} \rho g_r \\ \rho g_\theta \\ \rho g_z \end{pmatrix}_{r\theta z} \quad (4.34)$$

From the assumptions and analysis of the flow, we obtain

$$\rho \left( \frac{\partial \underline{v}}{\partial t} \right) = \begin{pmatrix} 0 \\ 0 \\ 0 \end{pmatrix}_{r\theta z} \quad (4.35)$$

$$\rho \underline{\underline{v}} \cdot \nabla \underline{\underline{v}} = \rho \begin{pmatrix} -\frac{v_\theta^2}{r} \\ 0 \\ 0 \end{pmatrix}_{r\theta z} \quad (4.36)$$

$$-\nabla p = \begin{pmatrix} 0 \\ 0 \\ 0 \end{pmatrix}_{r\theta z} \quad (4.37)$$

$$\mu \nabla^2 \underline{\underline{v}} = \mu \begin{pmatrix} 0 \\ \frac{\partial}{\partial r} \left( \frac{1}{r} \frac{\partial}{\partial r} (r v_\theta) \right) \\ 0 \end{pmatrix}_{r\theta z} \quad (4.38)$$

$$\rho \underline{\underline{g}} = \begin{pmatrix} 0 \\ 0 \\ 0 \end{pmatrix}_{r\theta z} \quad (4.39)$$

The equation of motion for an incompressible Newtonian fluid in our flow then becomes

$$\rho \begin{pmatrix} 0 \\ 0 \\ 0 \end{pmatrix}_{r\theta z} + \rho \begin{pmatrix} -\frac{v_\theta^2}{r} \\ 0 \\ 0 \end{pmatrix} = \begin{pmatrix} 0 \\ 0 \\ 0 \end{pmatrix}_{r\theta z} + \mu \begin{pmatrix} 0 \\ \frac{\partial}{\partial r} \left( \frac{1}{r} \frac{\partial}{\partial r} (r v_\theta) \right) \\ 0 \end{pmatrix} + \begin{pmatrix} 0 \\ 0 \\ 0 \end{pmatrix}_{r\theta z} \quad (4.40)$$

From which the  $\theta$ - component is:

$$\frac{\partial}{\partial r} \left( \frac{1}{r} \frac{\partial}{\partial r} (r v_\theta) \right) = 0 \quad (4.41)$$

or

$$\left(\frac{1}{r} \frac{\partial}{\partial r}(rv_{\theta})\right) = C_1 \quad (4.42)$$

or

$$\left(\frac{\partial}{\partial r}(rv_{\theta})\right) = C_1 r \quad (4.43)$$

$$rv_{\theta} = C_1 \frac{r^2}{2} + C_2 \quad (4.44)$$

$$\Rightarrow v_{\theta} = C_1 \frac{r}{2} + \frac{C_2}{r} \quad (4.45)$$

By implementing the following boundary conditions:

$$r = R_o, v_{\theta} = 0 \quad (4.46)$$

$$r = R_i, v_{\theta} = R_i \Omega \quad (4.47)$$

The Equation 4.45 becomes

$$0 = C_1 \frac{R_o}{2} + C_2 \frac{1}{R_o} \quad (4.48)$$

$$R_i \Omega = C_1 \frac{R_i}{2} + C_2 \frac{1}{R_i} \quad (4.49)$$

From there the equation 4.48 can be written as

$$C_2 = -C_1 \frac{R_o^2}{2} \quad (4.50)$$

And the Equation 4.49 becomes

$$R_i \Omega = C_1 \frac{R_i}{2} - C_1 \frac{R_o^2}{2} \frac{1}{R_i} \quad (4.51)$$

We obtain

$$C_1 = \frac{2R_i^2 \Omega}{R_i^2 - R_o^2} \quad (4.52)$$

$$C_2 = -C_1 \frac{R_o^2}{2} = \frac{-R_i^2 R_o^2 \Omega}{R_i^2 - R_o^2} \quad (4.53)$$

On substituting for  $C_1$  and  $C_2$ , we can find the velocity profile from Equation 4.45 to be

$$v_\theta = \frac{R_i^2 R_o^2 \Omega}{R_o^2 - R_i^2} \left( \frac{1}{r} - \frac{r}{R_o^2} \right) \quad (4.54)$$

In the above form, the term on the right-hand-side of the equation corresponds to the velocity profile when the outer cylinder is stationary and the inner cylinder is rotating with an angular velocity  $\Omega$ .

The stress tensor for an incompressible Newtonian fluid is

$$\underline{\underline{\tau}} = -\mu \underline{\underline{\dot{\gamma}}} \quad (4.55)$$

where  $\underline{\underline{\tau}}$  is stress tensor,  $\underline{\underline{\dot{\gamma}}}$  is rate of strain tensor and  $\mu$  is viscosity

The rate of strain tensor is

$$\underline{\underline{\dot{\gamma}}} = \nabla \underline{v} + (\nabla \underline{v})^T \quad (4.56)$$

$$\nabla \underline{v} = \begin{bmatrix} \left(\frac{\partial v_r}{\partial r}\right) & \left(\frac{\partial v_\theta}{\partial r}\right) & \left(\frac{\partial v_r}{\partial z}\right) \\ \left(\frac{1}{r} \frac{\partial v_r}{\partial \theta} - \frac{v_\theta}{r}\right) & \frac{1}{r} \left(\frac{\partial v_\theta}{\partial \theta}\right) + \frac{v_r}{r} & \left(\frac{1}{r} \frac{\partial v_z}{\partial \theta}\right) \\ \left(\frac{\partial v_r}{\partial z}\right) & \left(\frac{\partial v_\theta}{\partial z}\right) & \left(\frac{\partial v_z}{\partial z}\right) \end{bmatrix}_{r\theta z} \quad (4.57)$$

Simplifying gives

$$\nabla \underline{v} = \begin{bmatrix} 0 & \left(\frac{\partial v_\theta}{\partial r}\right) & 0 \\ \left(-\frac{v_\theta}{r}\right) & 0 & 0 \\ 0 & 0 & 0 \end{bmatrix}_{r\theta z} \quad (4.58)$$

$$\Rightarrow \underline{\underline{\dot{\gamma}}} = \begin{bmatrix} 0 & \left(\frac{\partial v_\theta}{\partial r} - \frac{v_\theta}{r}\right) & 0 \\ \left(\frac{\partial v_\theta}{\partial r} - \frac{v_\theta}{r}\right) & 0 & 0 \\ 0 & 0 & 0 \end{bmatrix}_{r\theta z} \quad (4.59)$$



$$\underline{\underline{\tau}} = \begin{bmatrix} 0 & \left(2\mu \frac{R_i^2 R_o^2}{R_o^2 - R_i^2} \Omega \frac{1}{r^2}\right) & 0 \\ \left(2\mu \frac{R_i^2 R_o^2}{R_o^2 - R_i^2} \Omega \frac{1}{r^2}\right) & 0 & 0 \\ 0 & 0 & 0 \end{bmatrix}_{r\theta z} \quad (4.60)$$

#### 4.5.4. Determination of velocity needed to disperse the clay sheets

The force on a surface with unit normal  $\hat{n}$  is given by

$$\underline{F} = A \hat{n}^T \cdot \underline{\underline{\Pi}} \quad (4.61)$$

where  $A$  is the surface area of clay,  $\underline{\underline{\Pi}}$  is the total stress tensor, and  $\hat{n} \cdot \underline{\underline{\Pi}}$  is the stress vector acting on an area  $A$  with normal  $\hat{n}$ , and  $\underline{\underline{\Pi}}$  is

$$\underline{\underline{\Pi}} = P \underline{\underline{I}} + \underline{\underline{\tau}} \quad (4.62)$$

where  $\underline{\underline{I}}$  is the identity tensor,  $P$  is thermodynamic pressure. Considering the geometry in Figure 4.78 we develop the following relation for the surface normal unit vector:

$$\text{and } \hat{n} = \begin{pmatrix} \sin \theta \\ \cos \theta \\ 0 \end{pmatrix} \quad (4.63)$$

In our flow the force vector acting on the surface of the clay particle is:

$$\underline{F} = A \hat{n}^T \cdot \underline{\underline{\tau}} \quad (4.64)$$

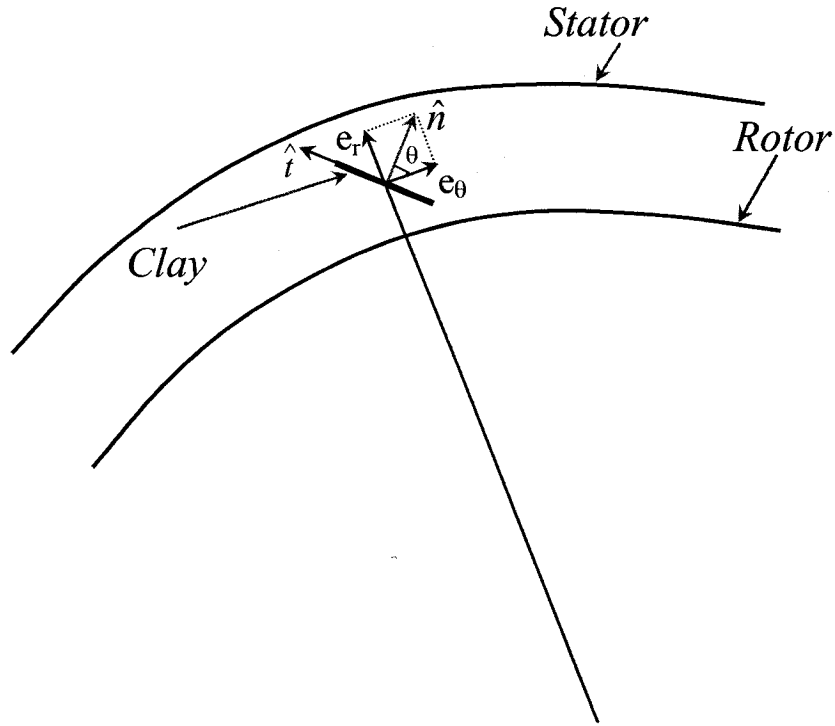


Figure 4.78. Flow of epoxy-clay mixture between rotating cylinders

$$\underline{F} = A \begin{bmatrix} \sin \theta & \cos \theta & 0 \end{bmatrix} \begin{bmatrix} 0 & \left( 2\mu \frac{R_i^2 R_o^2}{R_o^2 - R_i^2} \Omega \frac{1}{r^2} \right) & 0 \\ \left( 2\mu \frac{R_i^2 R_o^2}{R_o^2 - R_i^2} \Omega \frac{1}{r^2} \right) & 0 & 0 \\ 0 & 0 & 0 \end{bmatrix} \quad (4.65)$$

$$\underline{F} = A \left( 2\mu \frac{R_i^2 R_o^2}{R_o^2 - R_i^2} \Omega \frac{1}{r^2} \right) \begin{bmatrix} \cos \theta & \sin \theta & 0 \end{bmatrix} \quad (4.66)$$

We are interested in the force tending to separate the two layers in shear shown in Figure 4.79 which is:

$$F = \underline{F} \cdot \hat{t} = A \left( 2\mu \frac{R_i^2 R_o^2}{R_o^2 - R_i^2} \Omega \frac{1}{r^2} \right) (\cos^2 \theta - \sin^2 \theta) \quad (4.67)$$

and the force tending to separate the two layers in the surface normal direction is:

$$F = \underline{F} \cdot \hat{n} = A \left( 4\mu \frac{R_i^2 R_o^2}{R_o^2 - R_i^2} \Omega \frac{1}{r^2} \right) (\sin \theta \cos \theta) \quad (4.68)$$

From Figure 4.79 it is clear that the particles will be rotating around their center lines because of the unbalanced moment couple due to  $\underline{F}_1 = -\underline{F}_2$ . This is a well known behavior exhibited by particles in dilute suspensions. The rotation of particles in dilute non-Brownian suspensions continues indefinitely under shear flow. It is only under either (1) the conditions of significant particle-particle interactions (i.e. jamming) or (2) conditions of significant Brownian behavior that this rotation stops (or slows). We recall that our model is built on the assumption that the particles have a negligible effect on the flow of the liquid phase. Clearly this assumption is invalid in the case of significant particle-particle interactions. Therefore, our model is only strictly valid when the particles are not jamming and  $\theta$  in the above equation is a function of time. In the case of significant Brownian motion,  $\theta$  will vary only slowly with time and the particles will spend most of the time approximately parallel to the flow direction (this orientation is shown in Figure 4.79). We consider a suspension to be Brownian if the rate at which the particle moves due to Brownian motion is similar to the rate at which it moves due to the flow. We can evaluate this exactly using the rotational Peclet number [130]:

$$Pe = \frac{R_i \Omega}{R_o - R_i} \left( \frac{1}{D_r} \right) \quad (4.69)$$

In the above equation  $D_r$ , the rotary diffusivity, is given by the following equation for a circular disk-like particle of diameter  $d$ :

$$D_r = \frac{3k_B T}{4\mu_S d^3} \quad (4.70)$$

where  $k_B$  is Boltzmann's constant,  $T$  is the absolute temperature, and  $\mu_S$  is the viscosity of the suspending fluid. For our case, at room temperature  $D_r \cong 30$  1/s and the Peclet number is approximately 14000. Since  $Pe \gg 1$  we can consider our particles to be non-Brownian. This means that we expect the angle  $\theta$  to be the following specific function of time:

$$\tan(\theta - 90) = p \tan \left[ \left( \frac{R_i \Omega}{R_0 - R_i} \right) \left( \frac{t}{p + 1/p} \right) \right] + \tan(\theta_0 - 90) \quad (4.71)$$

where  $t$  is time,  $\theta_0$  is the angle at time  $t = 0$ , and the aspect ratio,  $p$ , is:

$$p = \frac{2\delta + h}{L} \quad (4.72)$$

Equation 4.71 results from the integration of the equation of motion for a non-Brownian particle in a flow field [131]. Since the particle consist of two layers, the geometrical parameters for the clay layers are defined in Figure 4.80. In the following analysis we are going to consider the maximum force  $F$  which occurs at  $\theta = 0^\circ$  for shear direction and  $\theta = 45^\circ$  for the surface normal direction, while remembering that each particle will only experience this force during part of its rotation period,  $P$ , which is given by the equation below.

$$P = \frac{\pi(R_0 - R_i)}{R_i \Omega} (p + 1/p) \quad (4.73)$$

Next we note that although our model for the force is only strictly valid for the case of a dilute suspension we can use it to approximate the situation in a semi-dilute suspension by using the suspension viscosity in Equations 4.67 and 4.68 rather than the viscosity of the suspending fluid. The strictly correct approach, valid for dilute suspensions, involves the viscosity of the suspending fluid.

To be able to delaminate the clay we need to have  $F - F_c \geq 0$  or  $F \geq F_c$ , where  $F$  is the force imposed on clay by shearing (see Figure 4.79) and  $F_c$  is the force holding the clay together.

The limiting case of  $F = F_c$  is:

$$A \left( 2\mu \frac{R_i^2 R_o^2}{R_o^2 - R_i^2} \Omega \frac{1}{r^2} \right) (\cos^2 \theta - \sin^2 \theta) = F_c \quad (4.74)$$

for the shear direction

$$\text{or} \quad A \left( 4\mu \frac{R_i^2 R_o^2}{R_o^2 - R_i^2} \Omega \frac{1}{r^2} \right) (\sin \theta \cos \theta) = F_c \quad (4.75)$$

for the surface normal direction

The maximum shearing force experienced by a clay particle will occur at  $r = R_i$  and  $\theta = 0^\circ$  and the maximum stretching force will occur at  $r = R_i$  and  $\theta = 45^\circ$ . The magnitudes of these maximum forces are identical. The relationship between  $\theta$  and time (Equation 4.71) is shown in Figure 4.81. This analysis indicates that most of the time the clay particles are experiencing shearing forces rather than stretching forces.

Therefore by substituting the geometrical conditions for maximum force specified above we find the minimum rotational speed that will allow clay layers to be separated:

$$\Omega_{\min} = \frac{F_c}{A \left( 2\mu \frac{R_o^2}{R_o^2 - R_i^2} \right)} \quad (4.76)$$

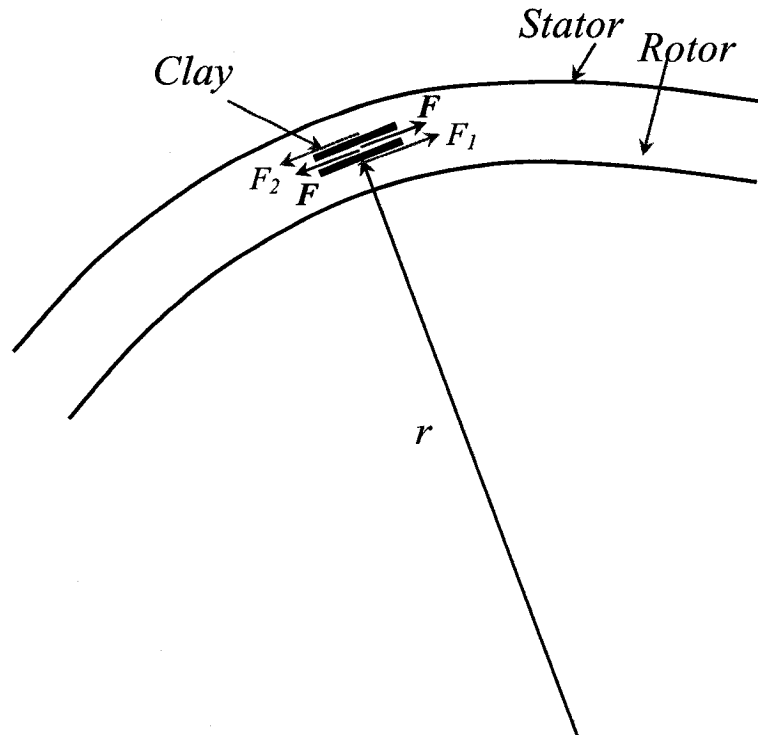


**Figure 4.79. Flow of epoxy-clay mixture between rotating cylinders (Assumption: clay sheet parallel to rotor and stator).  $F_1$  and  $F_2$  are the forces applied on the surfaces of a particle consisting of 2 layers due to the shear flow. They are not exactly equal because of the thickness of the particle. In this analysis we neglect the small difference between  $F_1$  and  $F_2$ , assuming  $F = F_1 = F_2$**

The attraction energy holding 2 clay sheets together is

$$E_A|_h = -\frac{H_{11}}{12\pi} \left[ \frac{1}{h^2} + \frac{1}{(h+2\delta)^2} - \frac{2}{(h+\delta)^2} \right] \quad (4.77)$$

where  $H_{11}$  is the Hamakar constant ( $7.8 \times 10^{-20}$  J) [132, 133, 134],  $h$  is the distance between the surfaces of the plates,  $\delta$  is the thickness of the clay plate, and the dimensions of clay layers are shown in Figure 4.80.

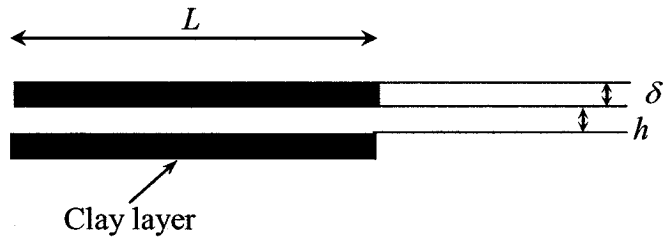


Figure 4.80. Dimensions of clay particles

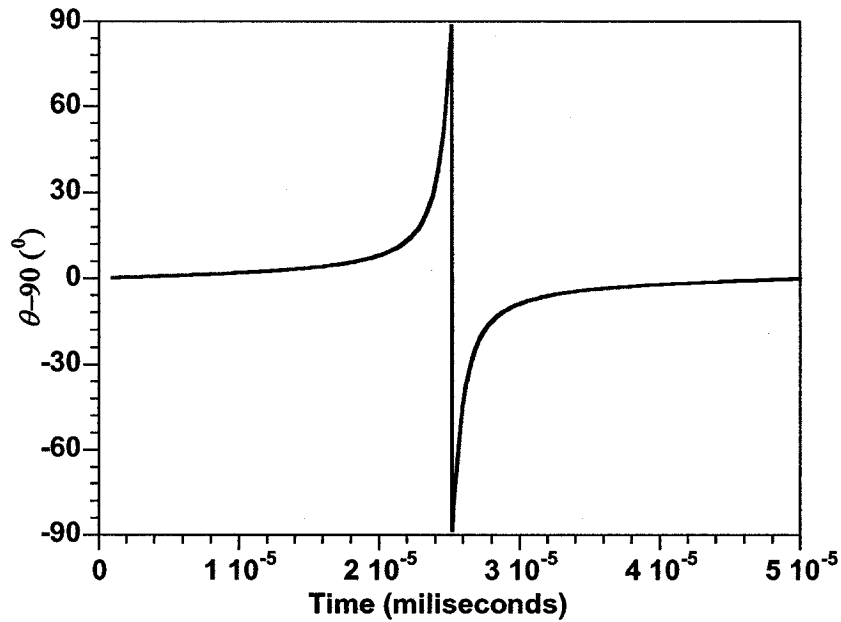


Figure 4.81. Relationship between  $\theta$  and time

$$F_c|_h = \frac{dE_A}{dh}(A) \quad (4.78)$$

$$\frac{dE_A}{dh} = -\frac{H_{11}}{12\pi} \left[ \left( \frac{d\left(\frac{1}{h^2}\right)}{dh} \right) + \left( \frac{d\left(\frac{1}{(h+2\delta)^2}\right)}{dh} \right) - \left( \frac{d\left(\frac{2}{(h+\delta)^2}\right)}{dh} \right) \right] \quad (4.79)$$

$$\frac{dE_A}{dh} = -\frac{H_{11}}{12\pi} \left[ \left( \frac{-2}{h^3} \right) + \left( \frac{-2}{(h+2\delta)^3} \right) - \left( \frac{-4}{(h+\delta)^3} \right) \right] \quad (4.80)$$

$$\frac{dE_A}{dh} = -\frac{H_{11}}{12\pi} \left[ \left( \frac{4}{(h+\delta)^3} \right) - \left( \frac{2}{h^3} \right) - \left( \frac{2}{(h+2\delta)^3} \right) \right] \quad (4.81)$$

Finally we present  $F_c$  and  $E_A$  in terms of the parameters listed above:

$$F_c|_h = \frac{dE_A}{dh}(A) = -\frac{H_{11}}{12\pi} \left[ \left( \frac{4}{(h+\delta)^3} \right) - \left( \frac{2}{h^3} \right) - \left( \frac{2}{(h+2\delta)^3} \right) \right] (A) \quad (4.82)$$

We now assume that the van der Waals forces holding the two platelets together are not directional, giving the following equation for the total attractive force:

$$F_c|_h = \frac{dE_A}{dh}(Af) = -\frac{H_{11}}{12\pi} \left[ \left( \frac{4}{(h+\delta)^3} \right) - \left( \frac{2}{h^3} \right) - \left( \frac{2}{(h+2\delta)^3} \right) \right] (Af) \quad (4.83)$$

where  $f$  is the ratio between the attractive area and total area. Practically speaking this means that we assume that the force to separate the two plates in shear is the same as the force required to separate the plates in the surface normal direction. This assumption is not strictly correct because it applies only for particles having spherical symmetry which



our plates clearly do not have. To further justify this approximation, we recall that the magnitude of the maximum shear force (occurring at  $\theta = 0^\circ$ ) is equal to the magnitude of the maximum normal force (occurring at  $\theta = 45^\circ$ ). Therefore whether we are considering that the delamination occurs in tension or in shear our analysis gives the same results.

Finally we present  $F_c$  and  $E_A$  in terms of the parameters listed above ( $f=1$ ):

$$F_c|_h = \frac{dE_A}{dh}(A) = -\frac{H_{11}}{12\pi} \left[ \left( \frac{4}{(h+\delta)^3} \right) - \left( \frac{2}{h^3} \right) - \left( \frac{2}{(h+2\delta)^3} \right) \right] (A) \quad (4.84)$$

Now we combine this with Equation 4.76 under the conditions for maximum force to find:

$$\Omega_{\min} = \frac{-\frac{H_{11}}{12\pi} \left[ \left( \frac{4}{(h+\delta)^3} \right) - \left( \frac{2}{h^3} \right) - \left( \frac{2}{(h+2\delta)^3} \right) \right]}{\left( 2\mu \frac{R_i^2 R_o^2}{R_o^2 - R_i^2} \right) \frac{1}{r^2}} \quad (4.85)$$

#### 4.5.5. Application of the above solution to the experimental system

The high speed mixer has the following parameters:  $R_i = 9.0$  mm,  $R_o = 9.5$  mm and  $\Omega$  ranges from 6500 rpm to 24000 rpm. We consider that the clay sheet is a plate with a side length of  $L = 100$  nm and a plate thickness  $\delta$  of 0.96 nm. The relationship in Equation 4.85 between minimum rotational speed and viscosity and interlamellar spacing  $h$  is presented in Figure 4.82. It is clear from this figure that, the larger is the interlamellar spacing of clay before mixing; the lower is the speed of stirring necessary to disperse the clay. For example, with the viscosity of the epoxy-clay suspension at 0.1 Pa.s (the third

curve from the top), if the interlamellar spacing  $h$  is 4.0 nm, the minimum velocity necessary to separate the clay platelets is at least 82000 rpm. However if  $h$  is 6.0 nm, the minimum velocity will reduce to 14500 rpm. Also we can observe that the minimum required rotational speed decreases as viscosity increases. With the interlamellar spacing  $h$  of 4.0 nm, if the viscosity is 0.01 Pa.s, the minimum required rotational speed will be 821000 rpm. However if the viscosity increases to 1.0 Pa.s, the minimum required rotational speed will reduce to 8210 rpm. Therefore this model can be used as a guide for the parameters including viscosity, rotational velocity, and the interlamellar spacing that are needed to separate the clay layers.

Taking into account that the  $d$ -spacing of the clay after swelling in epoxy resin is around 38 Å (see Section 4.3.2) and the maximum velocity of the homogenizer of 24000 rpm we can divide the processing space in Figure 4.82 into four areas. The horizontal line in this figure represents the velocity of 24000 rpm (maximum for our mixer) and the vertical line represents the interlamellar spacing  $h$  of 28.5 Å ( $h = d_{001} - \delta = 38.1 \text{ Å} - 9.6 \text{ Å} = 28.5 \text{ Å}$  or 2.85 nm) . These two lines divide the figure into four areas (A, B, C, D). Due to the limitation in speed (24000 rpm) and the interlamellar spacing  $h$  (2.85 nm) of the clay layers after swelling in epoxy, only area A represents processing conditions sufficient to obtain the exfoliated structure of C30B in the EPON828-C30B system at the mixing step with this homogenizer device. Practically speaking, it means the viscosity of the EPON828-C30B system has to be at least 1.5 Pa.s in order for delamination to occur in the present mixer

The results of the XRD studies indicate that good intercalation/exfoliation of clay can be obtained using high speed stirring method at 120°C and 180°C and curing at 120°C (Section 4.3.2). However it is also clear from these results, that it was not possible to separate the clay layers until full exfoliation at the mixing step. We can understand this by considering the model presented above and the viscosity of our suspension.

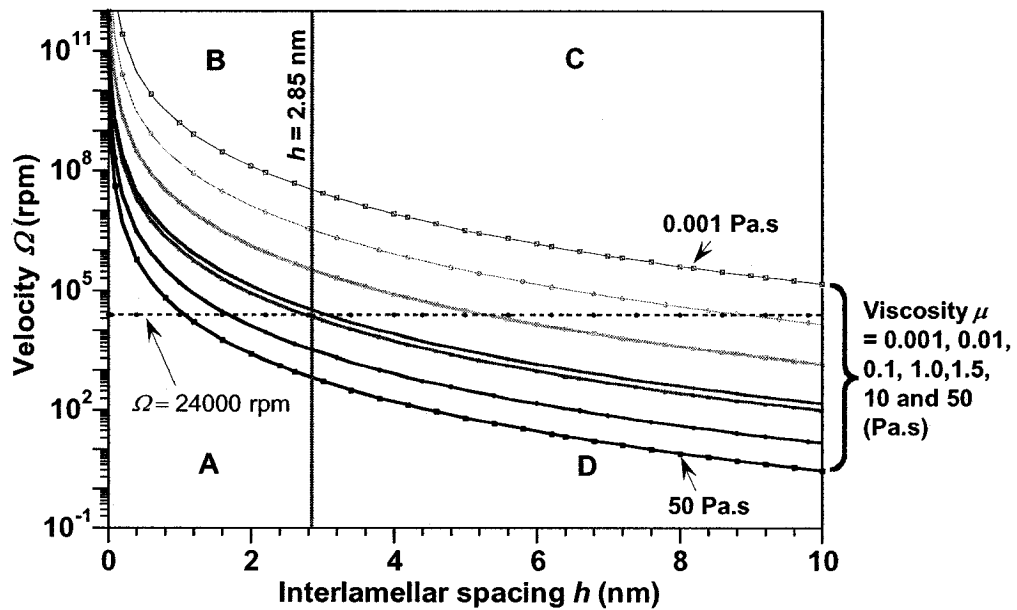


Figure 4.82. Velocity  $\Omega$  versus interlamellar spacing  $h$

On the way to disperse the clay with high speed mixer, we should consider two aspects: first the big clay aggregates are broken down into smaller aggregates, and then the smaller aggregates are delaminated. The delamination can also happen during the breaking down of big aggregates. However, breaking down the big aggregates is easier to achieve than the delamination of clay platelets. There is still work to be done to develop nanocomposites with fine dispersions and exfoliated morphologies. Achieving such morphologies with epoxy-based nanocomposites is a challenge. The model here deals only with the second

aspect. It should be noted that the viscosity of the epoxy-clay mixtures may increase during the stirring due to the dispersion of clay in epoxy due to the breaking of spherical clay particle agglomerates into smaller particles which have higher aspect ratio (see the viscosity results in Chapter 4). It may have a certain effect on the delamination of clay platelets as described in Figure 4.82. By increasing the viscosity of the epoxy-clay suspension, the speed required for delamination of clay can be reduced. In addition, stirring temperature and time also need to be considered, since they have a slight influence on the  $d_{001}$  (Chapter 4), and hence on the interlamellar spacing  $h$ . This also may help to reduce the velocity needed to separate the clay platelets.

To answer the above question, the viscosity of the epoxy EPON828 and its mixtures with C30 at different temperatures was examined with Brookfield Digital Viscosity Model DV-II+. The results are shown in Figure 4.83. As expected, EPON828 has the lowest viscosity at the a give temperature compared to its mixtures with C30B.

From Figure 4.83, at temperatures above 120°C, the viscosity of all EPON828-C30B mixtures and pure EPON828 is lower than 0.1 Pa.s. This value of viscosity is much smaller than 1.5 Pa.s, therefore according to our model we do not expect to be able to achieve the desirable exfoliation of clay at the stirring step. Clearly, if we want to separate the clay by using this equipment for a suspension viscosity around 0.05 Pa.s, we need to have a  $d$ -spacing at the beginning of 60.0 Å (6.0 nm) or more. In other words, we need to increase the clay layer separation by another process prior to stirring with this mixer.

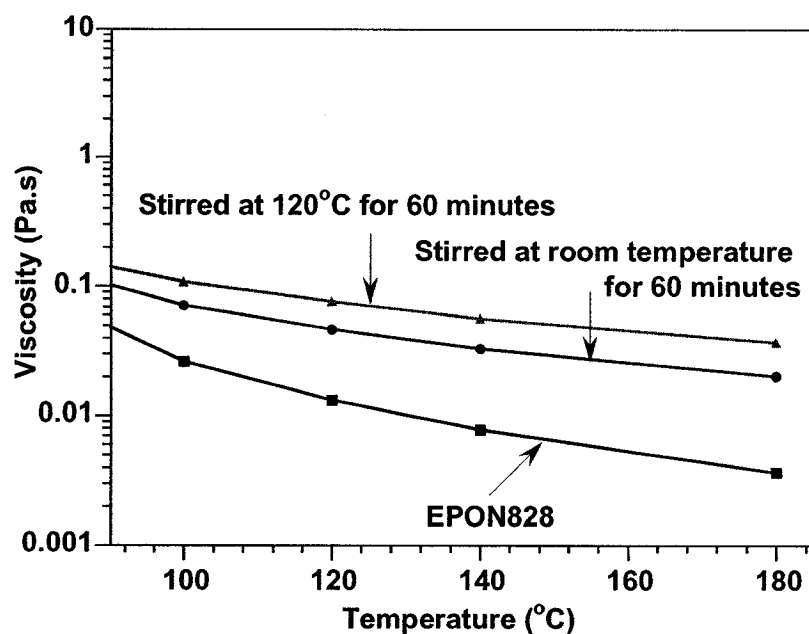


**Figure 4.83. Viscosity of epoxy and its mixtures with C30B at different temperatures**

The present model can also be used to design a new mixer to give the desired shearing force. For example, if we examine Equation 4.85 it is clear that by decreasing the gap between the concentric cylinders in the mixer we can decrease the minimum required rotational speed. If we assume a viscosity of 0.05 Pa.s and an  $R_o$  of 9.5 mm we find that  $R_i = 9.33$  mm (instead of 9.0 mm) is sufficient to reduce the minimum speed for delamination (Equation 4.85) to 24000 rpm.

## 4.6. Summary

Dispersion of organoclays in ENCs is a very complex process. The results have confirmed that there are several different levels of dispersion of organoclays in ENCs depending on the processing conditions. They include: 1) exfoliated or delaminated clay layer (single platelet); 2) non intercalated stacks (multiple layers not intercalated by the

matrix) or intercalated stacks (multiple layers intercalated either uniformly or not uniformly by the matrix); 3) multiple-stack aggregates (multiple stacks forming aggregates, on the micro-scale) and macro-aggregates (combination of many multiple-stack aggregates). The quality of dispersion can be controlled during the stirring (pre-mixing) of the clay with epoxy as well as during curing. Mechanical force and thermodynamic rules govern the dispersion process. Since it is difficult to apply conventional mechanical forces and because of the limited gelation time of the resin in the curing step, it is favorable to emphasize the effort in the stirring step, in which the resin has extended shelf life and it is possible to use different type of forces to facilitate the dispersion process. The results also demonstrated that intercalation is controlled by the diffusion of epoxy resin (both epoxy and hardener) into the clay galleries, which is governed by thermodynamic rules. The chosen organoclays (C30B and I30E) have an acceptable compatibility with the epoxy; therefore, it can diffuse quite easily into the clay galleries even at room temperature. However, high temperature and sufficient time are required to facilitate the diffusion and to obtain uniform intercalation.

On the other hand, breaking the macro-aggregates down into multiple-stack aggregates can be effectively achieved by using mechanical shear forces. However, exfoliation cannot be achieved by using the shear force alone that was generated from the devices used in this study. Exfoliation is more likely controlled by diffusion of the resin into the galleries. It is also evident that although the shear force cannot delaminate the clay stacks into individual platelets, it breaks down the large aggregates into smaller stacks, thus facilitating the diffusion of polymer molecules into the clay galleries. As a consequence, the organoclays have a finer dispersion as well as a more uniform distribution and a more

uniform intercalation in the pre-mixing of clay and epoxy. The dispersion, intercalation and exfoliation are favorable when the stirring intensity and temperature increase.

Intercalation and exfoliation continue to take place during the curing step through the diffusion of the monomers and oligomers into the clay galleries. However, the diffusion of monomers and oligomers into the clay galleries in this step may be inhibited by the curing reaction that limits or restricts the molecule mobility. It is important to control the curing process either by controlling the curing temperature or the chemistry of hardener in order to favor the intercalation and exfoliation process. A good temperature range for favoring the intercalation and exfoliation is dependent on the chemical reactivity and mobility of hardener, and the compatibility between hardener and organoclays.

To facilitate the dispersion, a new processing method using a homogenizer (with high speed and high temperature) have been employed and adopted. This technique is simple, inexpensive and fast. No solvent is needed to achieve a good dispersion and intercalation/exfoliation of clay into epoxy system. High stirring temperature and speed, and longer mixing time improve significantly the dispersion, intercalation and exfoliation of organoclay in the ENCs. Stirring speed (shear force) appears to be a more important parameter because the organoclays and epoxy systems in this study have an acceptable compatibility.

Clay chemistry of the chosen organoclays does not seem to have a strong effect on the intercalation and exfoliation of clay at the stirring step. However, it affects the quality of clay dispersion and clay intercalation in the curing step. The nanocomposites based on I30E were better intercalated than the C30B ones. On the other hand, C30B shows a

better micro dispersion in epoxy than I30E. I30E, which contains the intercalant based on primary amine, can offer a better chemical interaction with the epoxy group of the matrix via the hydrogen atoms of the amine group and this kind of reaction may take place even at low temperatures. C30B consists of quaternary ammonium intercalant containing hydroxyl groups, which can also undergo chemical interaction with the epoxy groups, but only at elevated temperatures.

Chemistry of hardener is also one of the main factors that control the dispersion and intercalation and exfoliation of clay in ENCs. It is important to stress here that in thermoset systems, the intercalation and exfoliation process can continue to occur during the curing step. These processes are controlled not only by the rate of diffusion of organic molecules (in this case, the curing agent and the epoxy molecules) into the clay gallery but also by the curing rate of the epoxy system as well as the size of epoxy and hardener molecules. For medium reactivity hardeners like the Jeffamine series it seems that the larger size and lower curing rate of hardener results in better intercalation/exfoliation of epoxy nanocomposites based on nanoclay C30B. However for high reactivity and short chain hardener like DETA exfoliation can be favored even at high curing temperature.

A model of flow in a concentric cylinder high shear mixer was developed and applied to predict the processing conditions necessary for achieving delamination of the clay layers. The model provides a useful tool for determining the required processing parameters to separate the clay layers in thermosetting polymers. It can also be used to design a new mixer to give the desired shearing force.



# Chapter 5

## The curing process of epoxy nanocomposites

### 5.1. Challenges and objectives

Effects of the fabrication process and compositions on the dispersion and intercalation/exfoliation of clay have been investigated in Chapter 4. What will happen to the processing of epoxy resins at the curing step in the presence of nanoclay? It is well known that, depending on the type of curing agent and curing conditions, the structure of the crosslinked molecular network formed can vary significantly and greatly influence the properties and performance of the cured material. The curing processes of the thermosetting resins involve a multi-step sequence proceeding from a reactive fluid to an elastomer (gelled rubber) to finally a crosslinked solid, and at various stages the reaction mechanism changes from kinetic to diffusion control and the material vitrifies from an elastic gel to gelled glass. Due to the complexities involved that might influence the exfoliation behavior of the clays in the thermosetting matrix, work in this area must be more thoroughly studied. In particular, the question of at which stage complete exfoliation will take place must be clearly understood. In addition, hydrophilic clay is not

highly compatible with the epoxy matrix, resulting in poor dispersion and a weak interface. To improve the interfacial interaction between the nanoclay and the matrix, surface modification of the nanoclay by organic compounds (so-called “intercalants”) is essential as discussed in section 2.2.2. The most popular intercalants are compounds based on onium ions, which contain an amine cation and a long hydrocarbon chain. The presence of intercalant may affect the curing process in terms of chemistry while the presence of clay platelets at an atomic scale may inhibit the curing reaction through a steric effect of the clay. There have been few investigations on the impact of such effects on the mechanism and kinetics of the curing process of epoxy nanocomposites.

The objective of this chapter was to investigate the effect of clays, hardeners and levels of dispersion of clay on the curing process of epoxy nanocomposites. The DSC instrument was used to follow the cure behavior while some empirical approaches were applied to model the kinetics of the cure reaction. The Kissinger and isoconversional models were used to calculate the kinetics parameters while the Avrami model was utilized to compare the cure behavior.

## **5.2. Methodology and experimental set up**

In order to understand the curing of epoxy nanocomposites, it is necessary to understand what factors may contribute to the curing. Several important factors have been identified and are summarized in the flowchart in Figure 5.1.

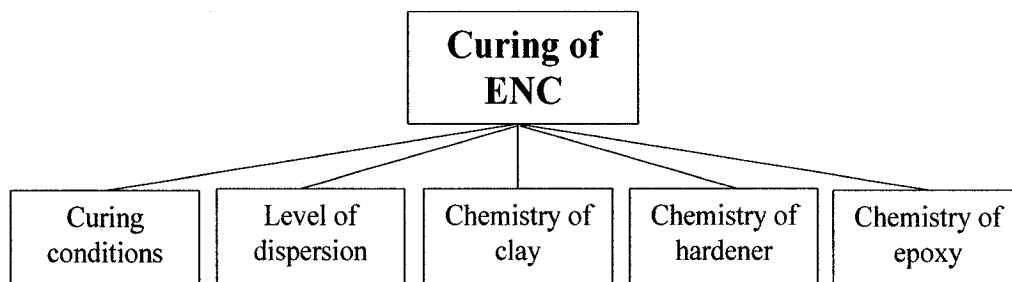
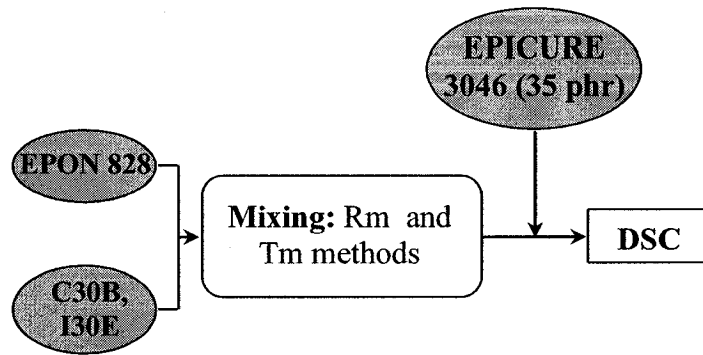


**Figure 5.1. Factors affect curing process of epoxy nanocomposites**

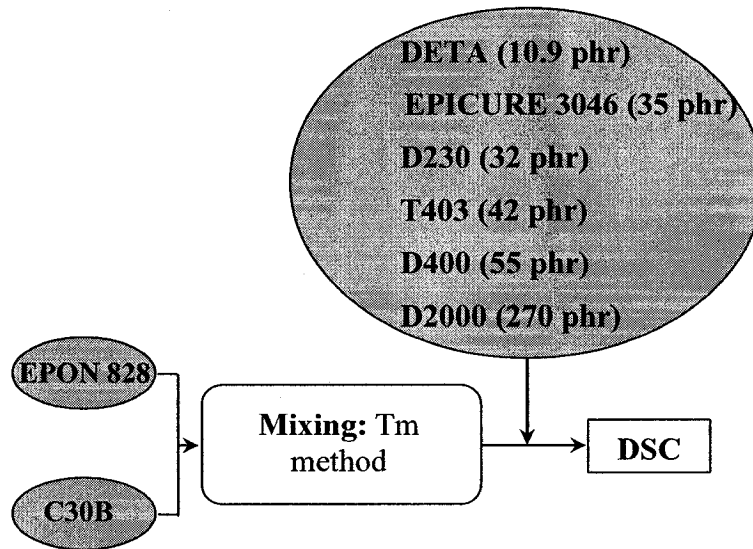
Although curing conditions, level of dispersion of clay, chemistry of epoxy, hardener and clay have effects on the curing of epoxy nanocomposites, only level of clay dispersion, chemistry of clay and hardener are discussed in this chapter as only one type of epoxy was used. The experiments were organized in three series: epoxy with different types of clay, with different levels of dispersion in the presence of the same hardener, epoxy with different hardeners in the presence of one type of clay. Pure epoxies with different hardeners were also used as references.

The DSC data were obtained on a Perkin-Elmer Pyris 1 instrument using nitrogen atmosphere. The epoxy or epoxy-clay mixtures with hardener were heated from 30°C to 250°C (dynamic scan) at five different heating rates (2.5, 5, 10, 15, and 20°C·min<sup>-1</sup>) to follow the heat evolution due to the chemical reaction occurring in this temperature range. The cured sample was then cooled to 30°C at 20°C·min<sup>-1</sup> to minimize the enthalpy relaxation in the second heating scan. Finally, the sample was reheated to 250°C at 20°C·min<sup>-1</sup> in order to determine the glass transition temperature ( $T_g$ ) and confirm the absence of any residual curing.

The experimental procedure for the curing process of epoxy nanocomposites is shown in Figure 5.2.



(a)



(b)

**Figure 5.2. Flowchart presenting the experimental steps for studying the curing process of epoxy nanocomposite (a) the effect of clay chemistry and level of dispersion, (b) the effect of hardener chemistry**

### 5.3. Modelling

To estimate the variation of activation energy of the curing process, the Kissinger [135] and isoconversional models [136, 137] have been widely used. The Kissinger equation calculates an overall activation energy of the curing process while the isoconversional equation provides access to apparent changes in the activation energy throughout the entire conversion.

In another approach that is more physical than chemical, the Avrami model of phase change has also been used to analyze the curing process of thermoset systems in terms of a more macroscopic process involving a heterogeneous structure containing microgel particles [138-141]. The change in the growth of microgels during polymerization should be reflected in the calculated Avrami exponent  $n$  for the different stages of the curing reaction.

In order to determine the evolution of the cure for modeling, DSC data was used. The cumulative exothermic heat ( $\Delta H_t$ ) evolved at time  $t$  during the DSC heating scan is assumed to be proportional to the degree of cure conversion  $\alpha$  in the system. Provided that the cure reaction is the only thermal event and that the specific heat capacity of the resin remains constant, the degree of cure  $\alpha$  at time  $t$  can be obtained from the DSC curve based on the equation:

$$\alpha = \frac{\Delta H_t}{\Delta H_\Sigma} \quad (5.1)$$

where  $\Delta H_\Sigma$  is the total heat of the curing reaction, which is determined by a non-isothermal scan run at a heating rate as low as  $1^\circ\text{C}\cdot\text{min}^{-1}$  from 0 to  $250^\circ\text{C}$  in order to ensure that the curing reaction is fully completed during the scan.

### 5.3.1. Empirical model

The cure kinetics of thermosets are often described in terms of an  $n$ th-order or autocatalyzed mechanism [86, 142, 143]. The  $n$ th-order model is defined by the equation:

$$\frac{d\alpha}{dt} = k(1-\alpha)^n \quad (5.2)$$

where  $n$  is the reaction order and  $k$  is the reaction rate constant, whose temperature dependence is usually expressed by the Arrhenius equation:

$$k = A \exp\left(-\frac{E}{RT}\right) \quad (5.3)$$

where  $E$  is the activation energy,  $R$  is the gas constant,  $A$  is the pre-exponential factor, and  $T$  is the temperature. Autocatalysis can be included by introducing a term in  $\alpha^n$  as follows

$$\frac{d\alpha}{dt} = k\alpha^m(1-\alpha)^n \quad (5.4)$$

A more general autocatalytic expression has also been widely used [144]:

$$\frac{d\alpha}{dt} = (k_1 + k_2\alpha^m)(1-\alpha)^n \quad (5.5)$$

In this case, the influence of the reaction products on the conversion rate is given by the term  $k_2\alpha^m$ . Other non-autocatalytic complex processes can also be represented by the same model.

### 5.3.2. Activation energy

Activation energy is commonly evaluated by one of two methods: the Kissinger equation or the isoconversional equation.

From the Kissinger equation, only an overall activation energy can be calculated [135]. For non-isothermal curing, the relationship between activation energy  $E$ , the heating rate  $q$ , and the temperature  $T_p$  at which the exothermic peak has its maximum can be described as:

$$E = -R \frac{d(\ln(q/T_p^2))}{d(T_p^{-1})} \quad (5.6)$$

where  $R$  is the gas constant, equal to  $8.3144 \text{ J}\cdot\text{K}^{-1}\cdot\text{mol}^{-1}$ . From the dynamic DSC curves measured at different heating rates, the relation between  $\ln(q/T_p^2)$  and  $T_p^{-1}$  can be obtained, and then the activation energy can be calculated from the slope [135].

Unlike the Kissinger approach, the isoconversional approach makes it possible to determine the activation energy corresponding to different stages of cure throughout the entire conversion [135, 136]. The equation used is:

$$E = -R \frac{d(\ln q)}{d(T^{-1})} \quad (5.7)$$

where  $T$  is the temperature corresponding to a selected degree of conversion  $\alpha$  at a given heating rate  $q$ . From the slope of a plot of  $\ln q$  vs.  $T^{-1}$  for a chosen degree of conversion, the activation energy corresponding to that degree of conversion can be obtained.

### 5.3.3. The Avrami model

A number of theories have been proposed to provide insight into underlying molecular processes and the resulting morphology [145]. Among them, the Avrami theory is widely accepted for describing the isothermal crystallization process. The Avrami equation for an isothermal process is:



$$1 - \alpha = \exp(-kt^n) \quad (5.8)$$

where  $k$  and  $n$  are the rate constant and the Avrami exponent, respectively.

The Avrami exponent  $n$  is often used to obtain information about the growth geometry, nucleation behavior, and impingement behavior. After impingement, the spherulitic growth may be restricted in certain directions, and the impingement of the spherulites causes a reduction in the Avrami exponent. Consequently, it is impossible to use a single Avrami equation to describe the whole bulk growth process. Therefore, only data obtained from the early stage of crystallization (less than 10% transformation) are usually used to characterize the crystallization kinetics. In the case of thermoset curing, microgels are formed at an early stage of curing, even at a degree of conversion lower than 5% [141, 143]. Thus intramicrogel polymerization is predominant during the early stage. The number of microgels and their average diameter increase during the cure, so the situation resembles that of polymer crystallization. Hence, the Avrami theory, used for analyzing crystallization kinetics, can be used to describe a polymerization process via growth of microgels [141, 145].

For non-isothermal crystallization, Ozawa [146] has modified the Avrami equation using the assumptions that the cooling crystallization function is constant at a designated temperature  $T$  and the exponent  $n$  is temperature-independent. Apparently, for a large cooling rate range, only a limited number of transformation data,  $\alpha$ , at the same temperature for different cooling rates are available for the foregoing analysis, as the onset of crystallization varies considerably with the cooling rate. In addition, the equation is valid exclusively for primary crystallization before crystal growth

impingement takes place at high transformation. To overcome such problems, Chuah et al. [147] have modified the Ozawa equation so that the cooling function is considered to be temperature-dependent. The Avrami equation for a given heating rate  $q$  has been transformed to:

$$\ln[-\ln(1-\alpha)] = a(T - T_q) \quad (5.9)$$

where  $a$  and  $T_q$  are constants. The data for different heating rates are then related by:

$$T_q = n \frac{\ln q}{a} + T_1 \quad (5.10)$$

where the slope is the Avrami exponent and the intercept  $T_1$  corresponds to the  $T_q$  at  $q = 1$  K·min<sup>-1</sup>.

## 5.4. Effect of clay and level of dispersion on curing process

Sample specifications for experiment set 5.4 are given in Table 5.1.

**Table 5.1. Sample specifications for experiment set 5.4**

Designation	Epon 828	Epicure 3046	Nanoclay	Stirring Method
8EP	100	35	0	-
Cloisite 30B				
8EP-2pB-Rm	100	35	2	Rm
8EP-2pB-Tm	100	35	2	Tm
8EP-4pB-Tm	100	35	4	Tm
Nanomer I30E				
8EP-2pE-Rm	100	35	2	Rm
8EP-2pE-Tm	100	35	2	Tm
8EP-4pE-Tm	100	35	4	Tm

### 5.4.1. DSC results

DSC curves of the epoxy-amine system and its nanocomposites at different heating rates are shown in Figure 5.3. The presence of nanoclay has some effect on the curing process as reflected by the difference in the shape and area of the DSC curves of the epoxy and its nanocomposites. This difference is more apparent at lower heating rates than at higher ones. For the mixture of epoxy and Cloisite 30B, the stirring temperature also affects the curing process. At the same clay loading of 2 phr (based on epoxy resin), the DSC curves of the nanocomposite in which clay and epoxy were stirred at high temperature are different from those of epoxy and the nanocomposite in which clay and epoxy were stirred at room temperature (compare 8EP, 8EP-2pB-Rm and 8EP-2pB-Tm). This may be caused by the presence of clay and the level of dispersion of clay in the epoxy (see Figure 5.3 at heating rates 2.5 and 5°C·min<sup>-1</sup>). On the other hand, with Nanomer I30E, the stirring temperature does not affect the curing process, and the DSC curves of epoxy nanocomposites based on Nanomer I30E are all very similar, although different from the curves of the sample without clay (see Figure 5.3). It is noted here that the reaction between Nanomer I30E and epoxy (the homopolymerization) may take place during the heating in DSC (as indicated in Chapter 4 (section 4.4.2)). However, the reaction between epoxy and amine takes place quite fast even at room temperature, so since in this study the temperature was raised slowly in the DSC device, the epoxy and hardener had enough time to react before the sample reached the critical temperatures. Therefore, the reactions of I30E with epoxy were almost negligible.

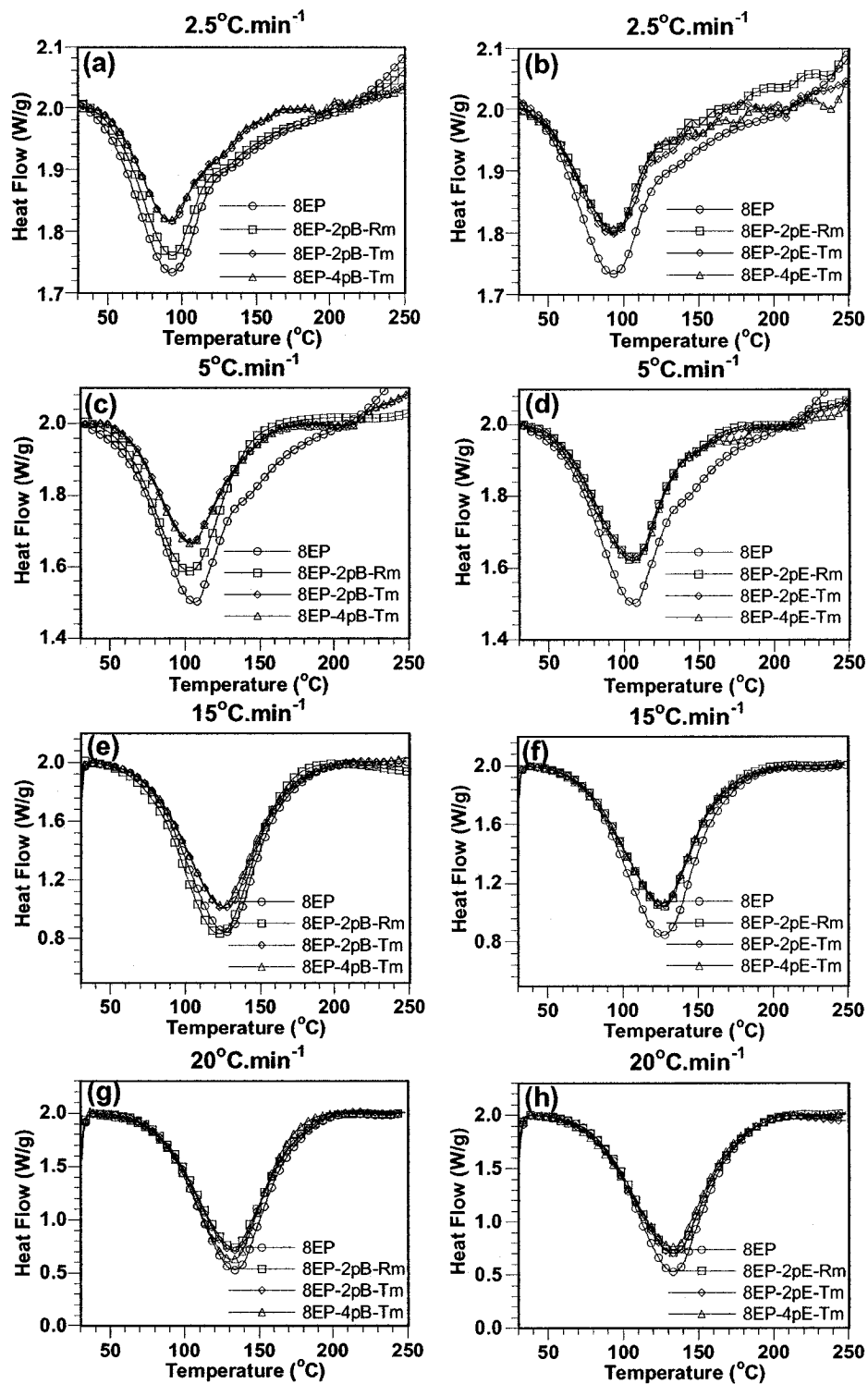


**Figure 5.3. DSC curves obtained at different heating rates for the epoxy-amine system and its nanocomposites based on Cloisite 30B and Nanomer I30E**

The transformation curves derived from the DSC results are shown in Figure 5.4. Generally speaking, the reaction onset and completion occur at lower temperatures at lower heating rates, as can be seen from the  $T_{onset}$  values given in Tables 5.2 and 5.3. There is no large difference between the systems with respect to the  $T_{onset}$ , nor with respect to  $T_p$  (the temperature of the peak maximum in the heat flow curves). However, Figure 5.5 shows that the presence of clay results in a slight difference in curing rate. The curing rate of epoxy nanocomposites is lower in the early stage and faster in the later stage compared to epoxy, especially for the 30B series. This may be because in the early stage of curing (lower temperature), the steric effect of clay reduces the mobility, or because functional groups such as OH groups on the clay surface are attached to epoxy groups via hydrogen bonding and this reduces the possibility of reaction. In the later stage, clay can accelerate the reaction through either epoxy etherification or hydroxyl-hydroxyl reactions. The curing of epoxy with amine involves several different reactions, and the rates of these reactions will vary with temperature in different ways. Thus a change in the heating rate may favour one reaction with respect to another and change the structure of the crosslinked molecular network. This could explain the decrease in the ultimate  $T_g$  observed on increasing the heating rate (Tables 5.2 and 5.3), as well as the variations in  $\Delta H$ . For a given heating rate, the presence of clay does not seem to have a significant effect on  $T_g$ , with the possible exception of sample 8EP-4pE-Tm, where the values are generally a couple of degrees lower. If this effect is real, it could be explained either by a reduction of the crosslink density or by crowding by the intercalant, whose alkyl chain may increase the mobility of the crosslinked network and affect the curing mechanism as well.

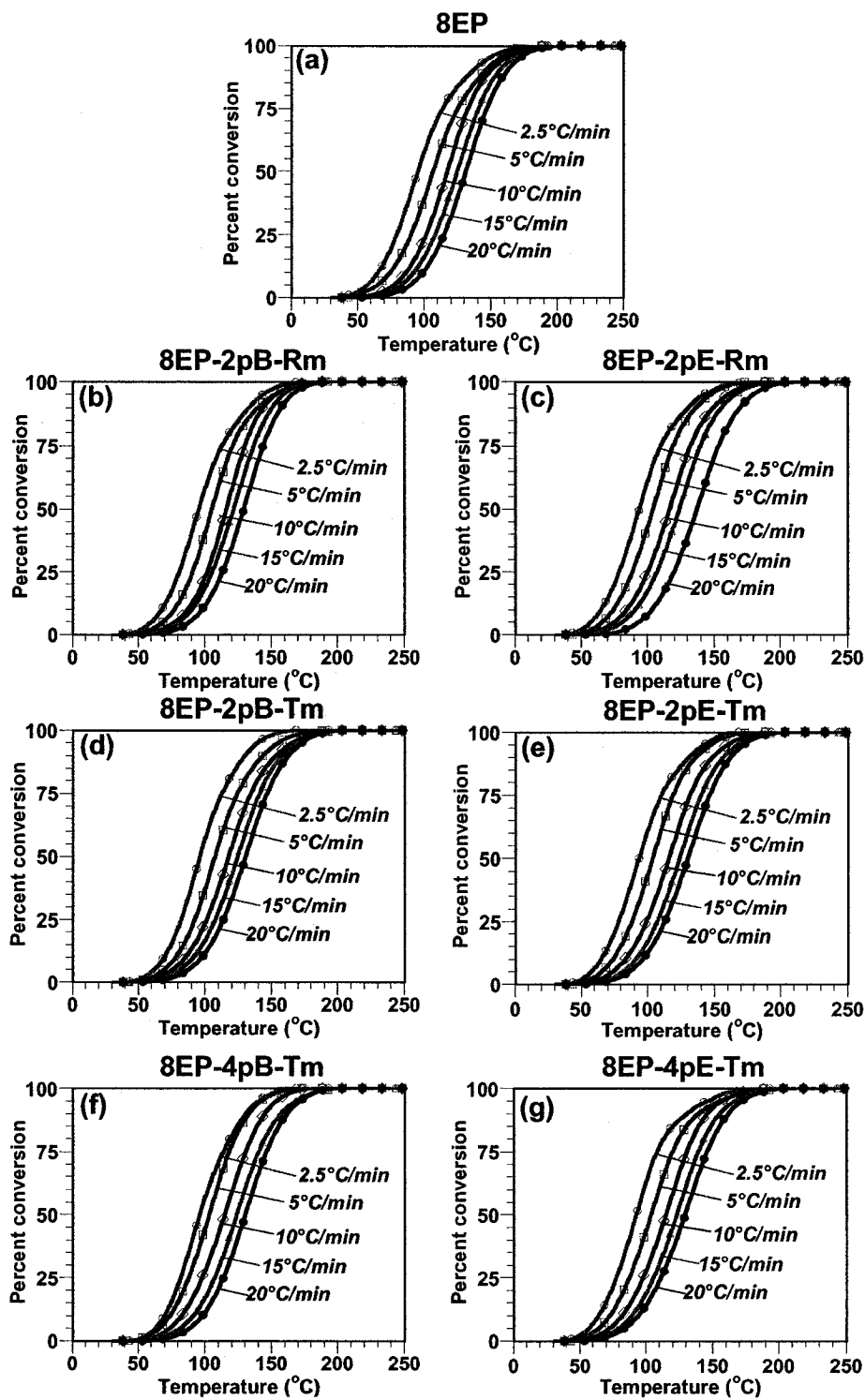


**Figure 5.4. Transformation curves corresponding to different heating rates for 8EP and its nanocomposites based on Cloisite 30B and Nanomer I30E**

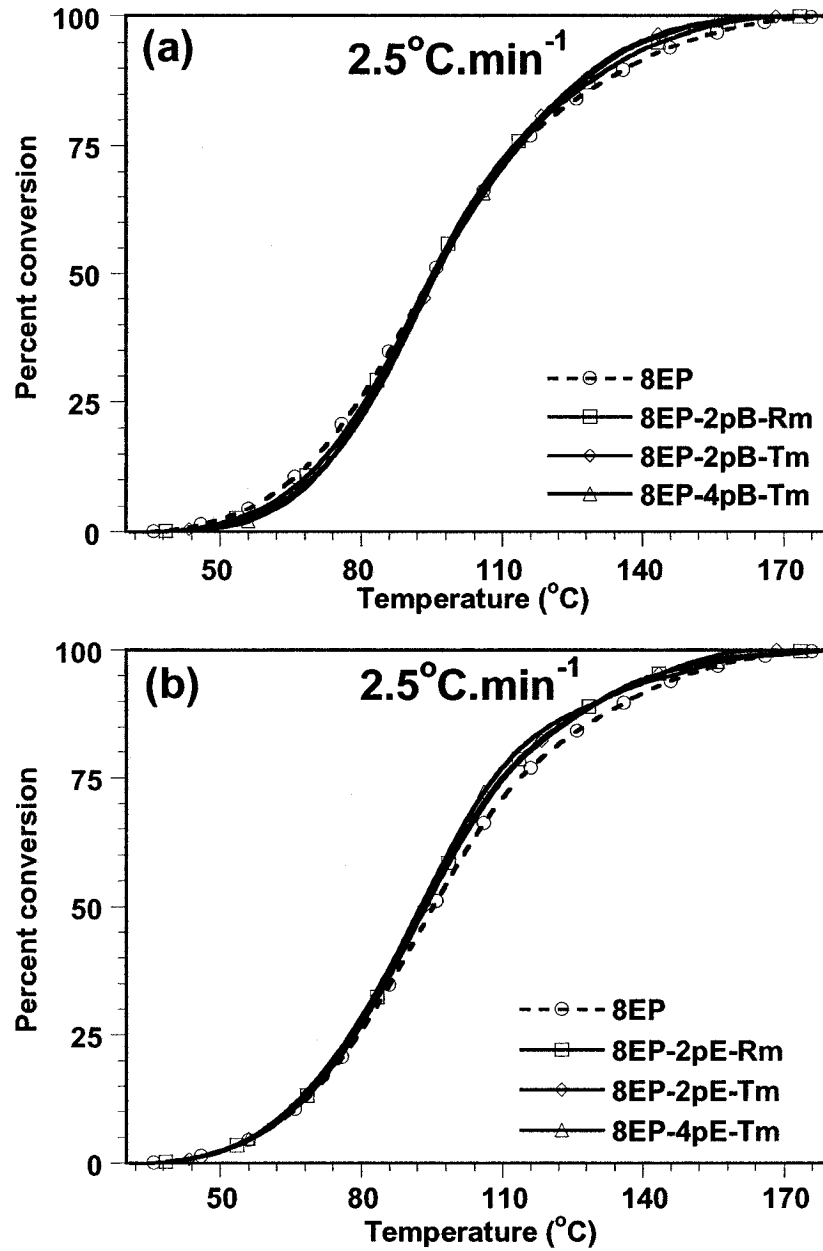


Figure 5.5. Transformation curves corresponding to epoxy-amine and its nanocomposites at heating rate 2.5 °C. min<sup>-1</sup>, (a) with Cloisite 30B, (b) with Nanomer I30E

**Table 5.2. Curing characteristics for 8EP**

q (°C·min <sup>-1</sup> )	T <sub>onset</sub> (°C)	T <sub>p</sub> (°C)	T <sub>g</sub> (°C)
2.5	51.4	92.9	87.7
5	59.2	106.3	86.8
10	69.9	119.0	79.2
15	74.7	126.7	73.9
20	81.6	133.3	72.7

**Table 5.3. characteristics for 8EP nanocomposites**

<b>Cloisite 30B</b>				<b>Nanomer I30E</b>			
q (°C·min <sup>-1</sup> )	T <sub>onset</sub> (°C)	T <sub>p</sub> (°C)	T <sub>g</sub> (°C)	q (°C·min <sup>-1</sup> )	T <sub>onset</sub> (°C)	T <sub>p</sub> (°C)	T <sub>g</sub> (°C)
<b>8EP-2pB-Rm</b>				<b>8EP-2pE-Rm</b>			
2.5	54.8	93.0	87.4	2.5	50.1	93.3	87.5
5	60.2	103.8	83.8	5	59.8	106.4	83.0
10	69.7	116.5	76.6	10	69.7	119.6	76.4
15	75.2	123.2	72.4	15	73.8	127.0	72.8
20	81.8	131.7	71.6	20	80.1	133.8	70.5
<b>8EP-2pB-Tm</b>				<b>8EP-2pE-Tm</b>			
2.5	53.0	93.4	87.5	2.5	48.4	92.2	86.3
5	60.7	104.6	86.3	5	59.8	105.7	82.2
10	69.5	118.5	77.5	10	66.7	119.6	74.0
15	76.1	126.5	71.9	15	73.8	126.8	73.9
20	80.8	132.7	71.0	20	78.2	132.8	69.3
<b>8EP-4pB-Tm</b>				<b>8EP-4pE-Tm</b>			
2.5	54.9	92.0	87.2	2.5	48.3	92.7	83.7
5	62.0	105.2	85.9	5	59.1	105.7	79.1
10	71.6	117.2	77.1	10	64.2	119.6	72.5
15	76.6	125.5	74.7	15	70.8	126.8	72.1
20	83.3	132.1	73.0	20	75.8	132.8	69.4



### 5.4.2. Activation energy

The Kissinger analysis is based on the relationship between the heating rate  $q$  and the temperature  $T_p$  corresponding to the peak in the heat release curve. The Kissinger equation calculates an overall activation energy of the curing process while the isoconversional equation provides access to apparent changes in the activation energy throughout the entire conversion. Figure 5.6 shows the relationship between  $\ln(q \cdot T_p^{-2})$  and  $T_p^{-1}$  for both the epoxy-amine system (8EP) and its nanocomposites. The five points correspond to the five heating rates of 2.5, 5, 10, 15, and 20°C·min<sup>-1</sup>. There is an excellent linear fit in all cases, indicating that the experimental data fit the Kissinger model quite well. From the slopes of these plots the overall activation energy values for epoxy-amine and nanocomposites were calculated and are shown in Table 5.4. The variations observed are believed to be within experimental error and are not considered significant. This is to be expected, given that the  $T_p$  values in Tables 5.2 and 5.3 are effectively the same for a given heating rate. The average activation energy value of 58.4 kJ·mol<sup>-1</sup> is typical for the reaction between epoxy and primary amine.

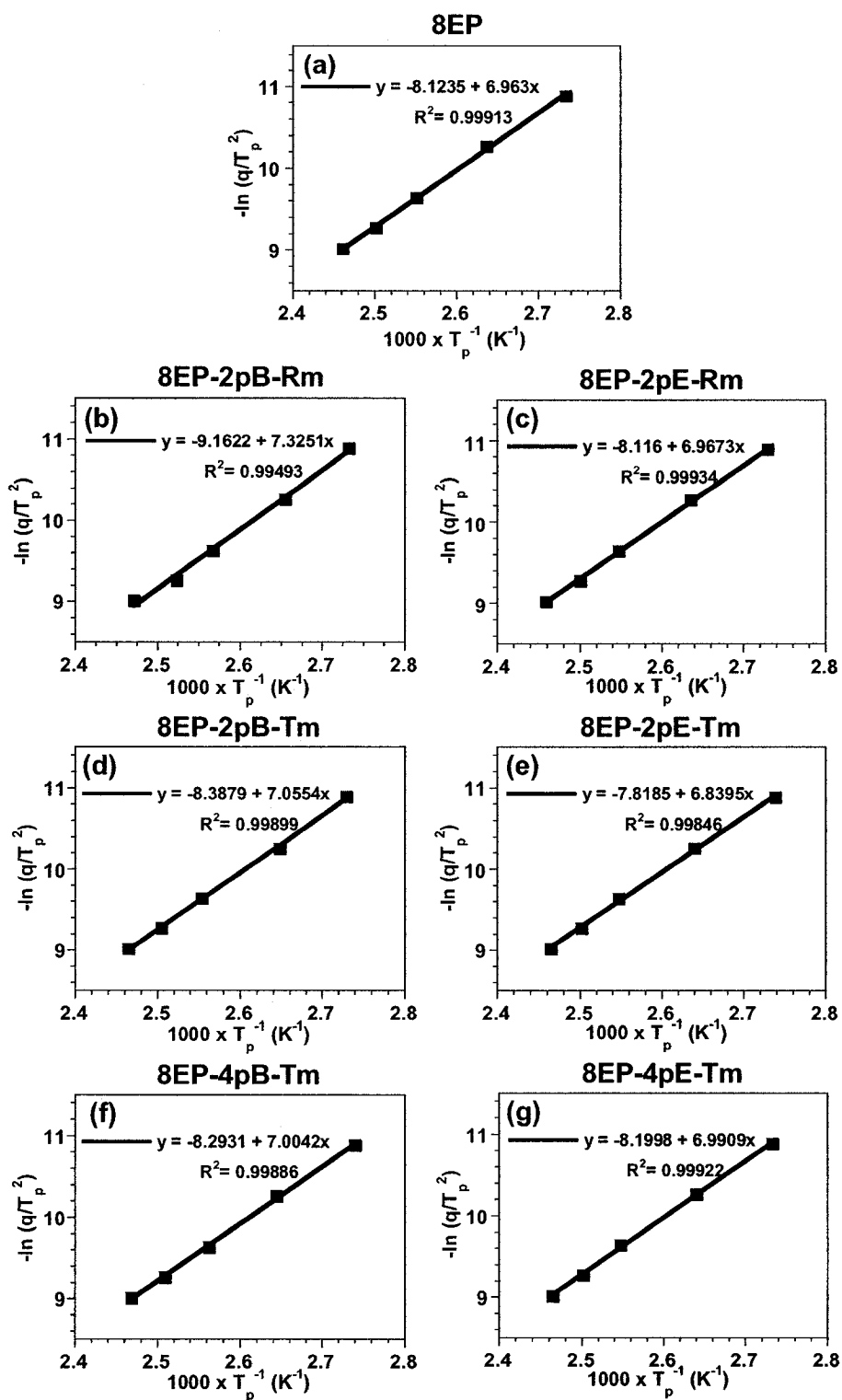


Figure 5.6. Kissinger plots for the 8EP system and its nanocomposites

**Table 5.4. Activation energies obtained from the Kissinger analysis for E828-EP and its nanocomposites**

System	Activation energy (kJ·mol <sup>-1</sup> )
8EP	57.9
8EP-2pB-Rm	60.9
8EP-2pB-Tm	58.7
8EP-4pB-Tm	58.2
8EP-2pE-Rm	57.9
8EP-2pE-Tm	56.9
8EP-4pE-Tm	58.1

The isoconversional analysis is based on the relationship between the heating rate  $q$  and the temperature  $T$  at which a certain degree of conversion is reached. Figure 5.7 shows the relationship between  $\ln q$  and  $T^{-1}$  for nine different degrees of conversion ranging from 0.1 to 0.9. The linear relationship observed in all cases indicates that the approach is applicable for this case. The activation energies  $E_a$  calculated for the four systems are given in Figure 5.8. Some differences are clearly apparent. For the epoxy-amine system without clay, as expected  $E_a$  increases steadily with the degree of cure, particularly in the later stages ( $\alpha > 0.7$ ). For the mixtures of epoxy and Cloisite 30B, when 2 wt% Cloisite 30B is mixed in by Method 1,  $E_a$  behaves in a similar manner except that the values are consistently somewhat higher. Thus, even when not well dispersed, the clay appears to have an effect. However, when the clay is better dispersed using high stirring temperature, whether at 2 or 4 wt % (8EP-2pB-Tm and 8EP-4pB-Tm), the shape of the  $E_a$  vs.  $\alpha$  curve changes considerably. The  $E_a$  decreases slightly as  $\alpha$  increases in the initial stages of cure, then levels off, then rises towards the end, but not as much as when the clay is absent or less well dispersed. It is obvious that the stirring temperature affects the  $E_a$  for epoxy and Cloisite 30B systems. However, for the mixtures of epoxy and

Nanomer I30E, whether stirred at room temperature (8EP-2pE-Rm) or high temperature (8EP-2pE-Tm),  $E_a$  behaves in a manner similar to the epoxy-Cloisite systems stirred at high temperature, except that the values are generally somewhat lower.

Generally speaking, well dispersed clays and clays well intercalated by the matrix lead to a higher  $E_a$  in the early stage of cure. Again this may be because the steric effect of clay reduces the mobility or because functional groups such as OH groups on the clay surface are attached to epoxy groups via hydrogen bonding and reduce the ability of reaction. Moreover, the later stage of cure (at higher temperature) may involve reactions with higher activation energy that could be accelerated by the presence of clay (epoxy etherification, hydroxyl-hydroxyl), as well as the onset of diffusion control. For Cloisite 30B,  $E_a$  is higher for poor dispersion and lower for good dispersion (compared to epoxy without clay). For Nanomer I30E,  $E_a$  is lower in all cases compared to epoxy without clay. This can be explained by the difference in chemistry of the intercalants and the polymerization of epoxy groups initiated by the primary amine onium ion of the organo-nanoclay I30E (See Figure 4.45).

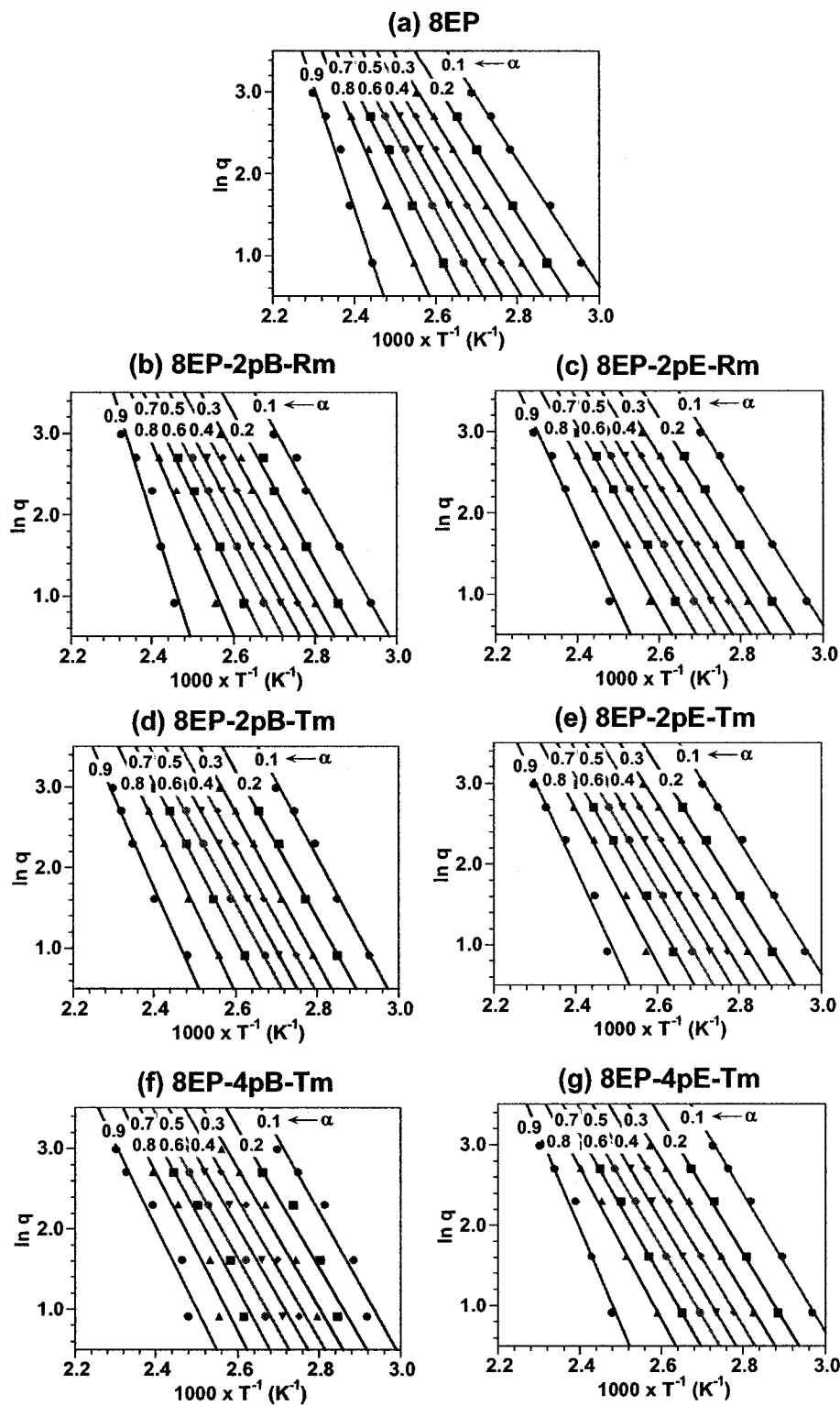


**Figure 5.7.** Isoconversional plots corresponding to various degrees of conversion for the 8EP system and its nanocomposites

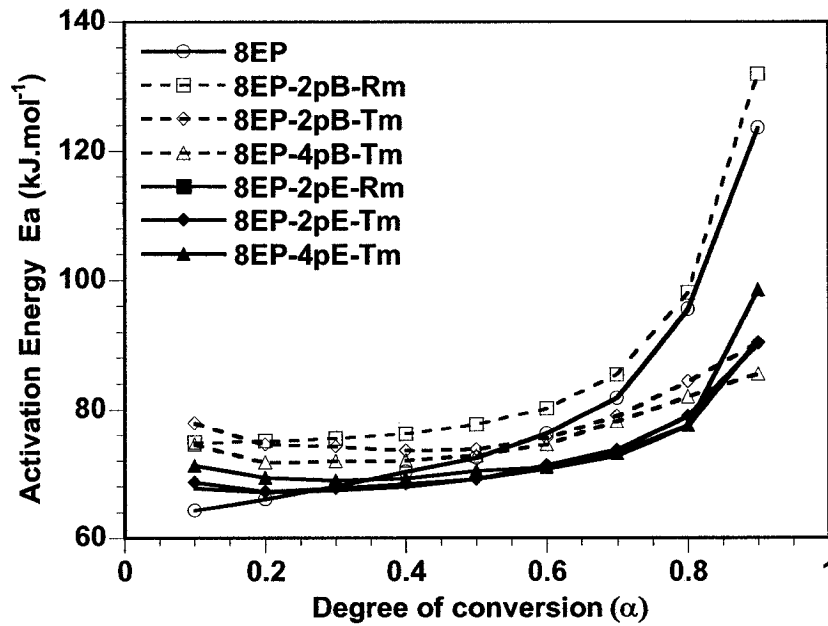


**Figure 5.8. Activation energies obtained for the isoconversional model**

The activation energies obtained by the Kissinger approach (Table 5.4) are lower than the average values obtained by the isoconversional approach (Table 5.5). This can be explained by the differences in assumptions and mathematical approach between the two models. The isoconversional results are more meaningful than the Kissinger ones because the evolution of the chemistry of the system during the cure is partially taken into account. The Kissinger approach is based entirely on the maximum rate of cure, which occurs in this case around the beginning of the curing reaction. Thus it is not surprising that the  $E_a$  values obtained by the Kissinger approach are closer to those obtained at lower degrees of cure by the isoconversional approach rather than to the average isoconversional values.

**Table 5.5. Average activation energies obtained for the isoconversional model**

System	Average activation energy (kJ·mol <sup>-1</sup> )
8EP	79.9
8EP-2pB-Rm	86.1
8EP-2pB-Tm	78.2
8EP-4pB-Tm	76.0
8EP-2pE-Rm	72.4
8EP-2pE-Tm	72.9
8EP-4pE-Tm	74.5

### 5.4.3. Avrami analysis

The change in the growth of microgels during polymerization should be reflected in the calculated Avrami exponent  $n$  for the different stages of the curing reaction. From the DSC results, curves of  $\ln[-\ln(1-\alpha)]$  vs.  $T$  were plotted for two different conversion ranges, namely 0-10% and 10-25%. A linear fit in each range gave the parameters  $a$  and  $T_q$  in Equation 5.9. The results for the five different heating rates  $q$  were then used to make plots of  $T_q$  vs.  $(\ln q)/a$  according to Equation 5.10. The long polymer chains tend to form spherical structures (so-called “microgels”) with high cyclization and crosslinking density after the initial period of polymerization [141, 142]. The number of microgels increases during the early stages. The epoxy and hydroxyl groups of the epoxy resin and the amine groups of the hardener within the microgels continue to react to improve the crosslinking density, while those near the surface react with surrounding monomers and oligomers, leading to increased microgel diameter and microgel interconnection. The Avrami exponent reflects the steric freedom of microgel growth. A higher  $n$  value

indicates greater freedom of growth, and a change of  $n$  value during the cure indicates a marked change in polymerization mechanism.

The results are shown in Figure 5.9. The Avrami exponents  $n$  obtained from the slopes are given in Table 5.6. Similar values were obtained for the more highly exfoliated samples prepared with the use of a solvent [148]. For both epoxy-amine and nanocomposites, the Avrami exponent  $n$  in the early stage of cure is greater than in the second stage. It can be understood that at low conversions, the concentration and the size of the microgels are still small, and their growth is less space-restricted. With the advancement of cure the number of microgels and their size increases, so their growth is restrained and inter-microgelation may occur. When the cure reaches its end, intermicrogelation becomes dominant, a three-dimensional network is formed, and the reaction nearly stops [148].

It can also be seen in Table 5.6 that there is no significant variation in the Avrami exponent  $n$  among the samples. Thus, the presence of clay, regardless of the quality of dispersion, does not seem to have a tremendous effect on the growing of microgels in the systems during curing.



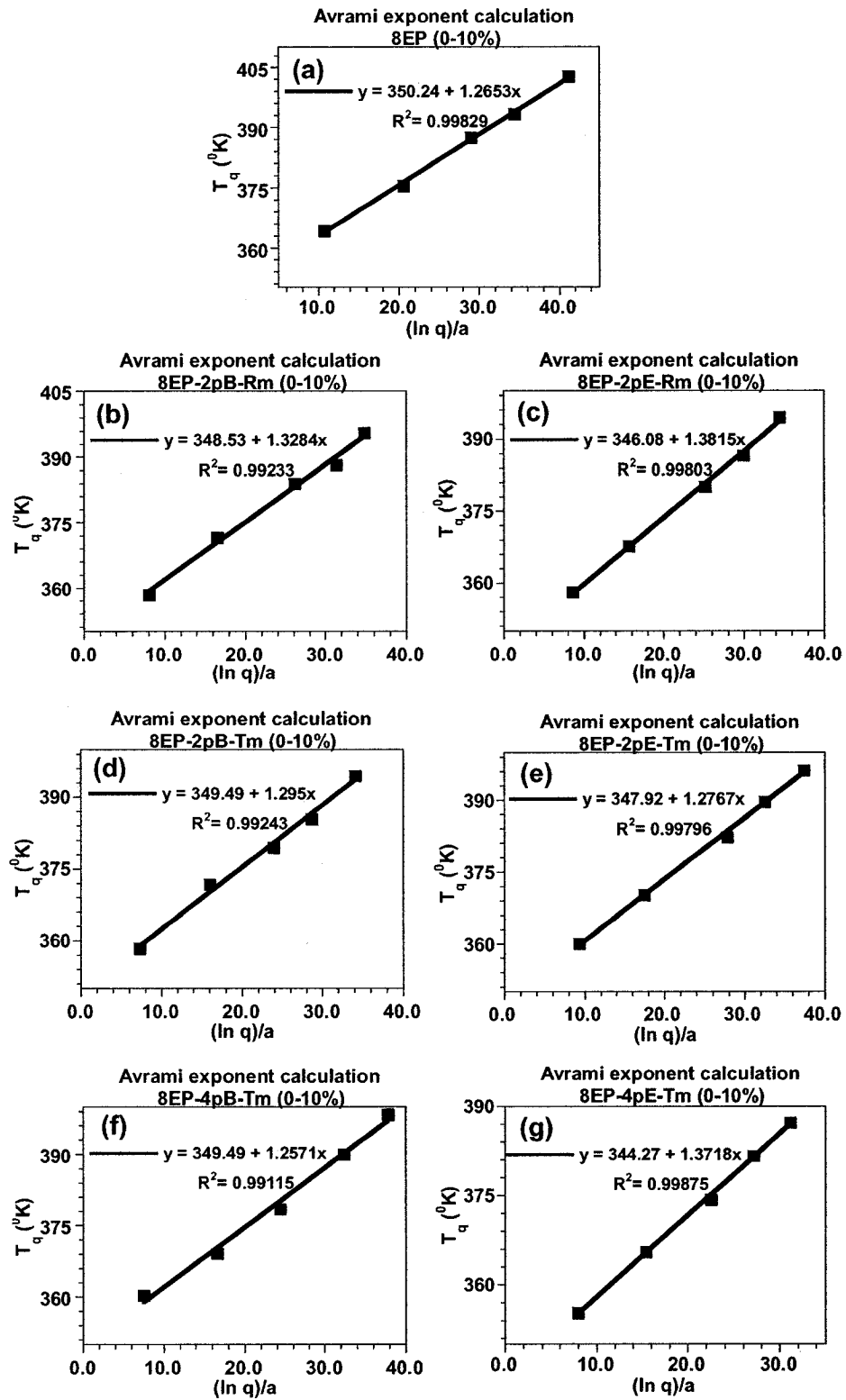


**Figure 5.9. Determination of the Avrami exponent  $n$  for the epoxy-amine system and its nanocomposites in the conversion range  $\alpha = 0-10\%$**

**Table 5.6. Exponents  $n$  obtained from Avrami analysis**

System	$\alpha = 0-10\%$	$\alpha = 10-25\%$
8EP	1.27	1.09
8EP-2pB-Rm	1.33	1.07
8EP-2pB-Tm	1.30	0.97
8EP-4pB-Tm	1.26	1.02
8EP-2pE-Rm	1.38	1.05
8EP-2pE-Tm	1.28	1.01
8EP-4pE-Tm	1.27	1.00

## 5.5. Effect of hardener

Sample specifications for experiment set 5.5 are given in Table 5.7.

**Table 5.7. Sample specifications for experiment set 5.5**

Designation	EPON 828	Hardener	Cloisite 30B	Stirring method
<b>DETA (DE)</b>				
8DE	100	10.9	0	-
8DE-4pB-Tm	100	10.9	4	Tm
<b>EPICURE 3046 (EP) (from section 5.4)</b>				
8EP	100	35	0	-
8EP-4pB-Tm	100	35	4	Tm
<b>Jeffamine D230 (d)</b>				
8d	100	32	0	-
8d-4pB-Tm	100	32	4	Tm
<b>Jeffamine T403 (T)</b>				
8T	100	42	0	-
8T-4pB-Tm	100	42	4	Tm
<b>Jeffamine D400 (<math>\delta</math>)</b>				
8 $\delta$	100	55	0	-
8 $\delta$ -4pB-Tm	100	55	4	Tm
<b>Jeffamine D2000 (D)</b>				
8D	100	270	0	-
8D-4pB-Tm	100	270	4	Tm

### 5.5.1. DSC results

DSC curves of the epoxy-amine systems with different hardeners and their nanocomposites at different heating rates are shown in Figures 5.10a, 5.11a, 5.12a, 5.13a, 5.14a, and 5.15a. As shown by the results in section 4.4 of Chapter 4, the curing rate of the studied systems can be arranged in the order of DETA > EPICURE 3046 > D230  $\approx$  T403 > D400 > D2000.

The presence of nanoclay has some effect on the curing process as reflected by the difference in the DSC curves of the epoxy and its nanocomposite. For curing with DETA, there is a simple cure peak at relatively low temperature cure and the presence of clay results in somewhat faster cure as compared to the one without clay, especially at higher heating rates. The cure is more complex for systems cured with EPICURE 3046, D230, T403 and D400 than for those cured with DETA. An apparent shoulder peak appears at higher temperature for both epoxy and nanocomposite. Again, the clay results in somewhat faster cure than without clay (similar to DETA). The cure is significantly slower for the system cured with D2000 compared to the other two hardeners (DETA and T403), and is barely complete at 250°C. The acceleration effect of clay is not as clearly defined.

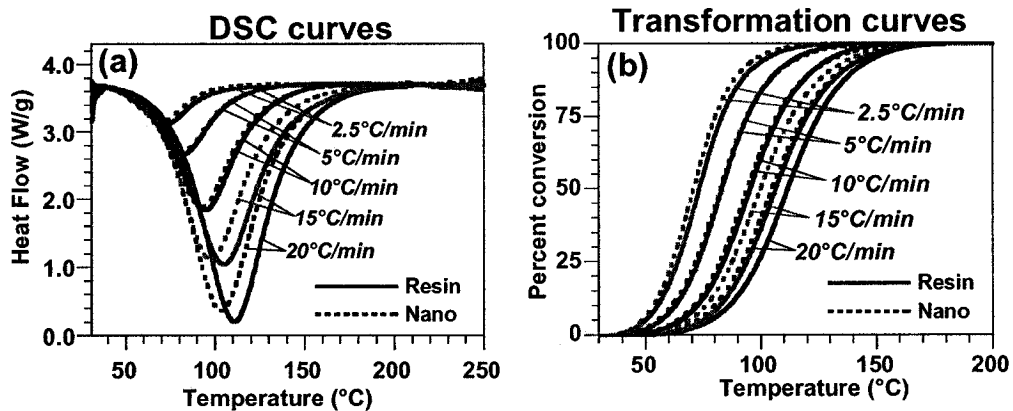


Figure 5.10. DSC and transformation curves of the EPON828-DETA system (8DE) and its nanocomposite (8DE-4pB-Tm) at different heating rates, (a) DSC curves; (b) transformation curves

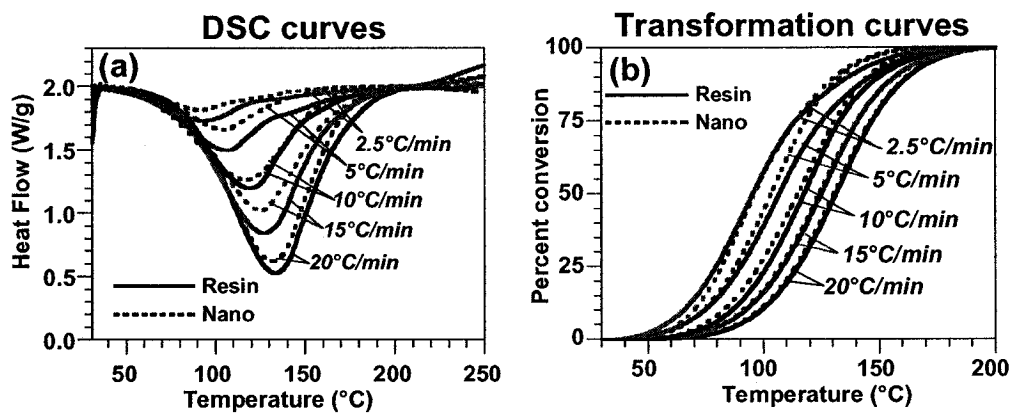


Figure 5.11. DSC and transformation curves of the EPON828-EPICURE 3046 system (8EP) and its nanocomposite (8EP-4pB-Tm) at different heating rates, (a) DSC curves; (b) transformation curves

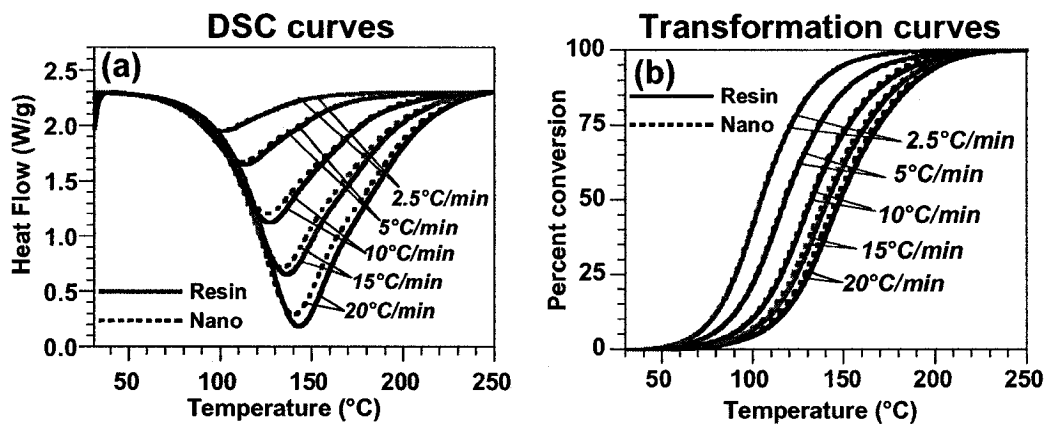


Figure 5.12. DSC and transformation curves of the EPON828-D230 system (8d) and its nanocomposite (8d-4pB-Tm) at different heating rates, (a) DSC curves; (b) transformation curves

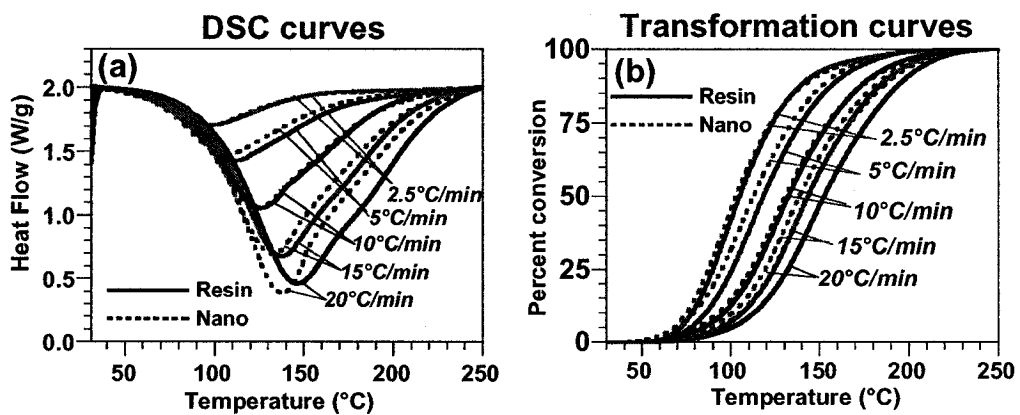


Figure 5.13. DSC and transformation curves of the EPON828-T403 (8T) system and its nanocomposite (8T-4pB-Tm) at different heating rates, (a) DSC curves; (b) transformation curves

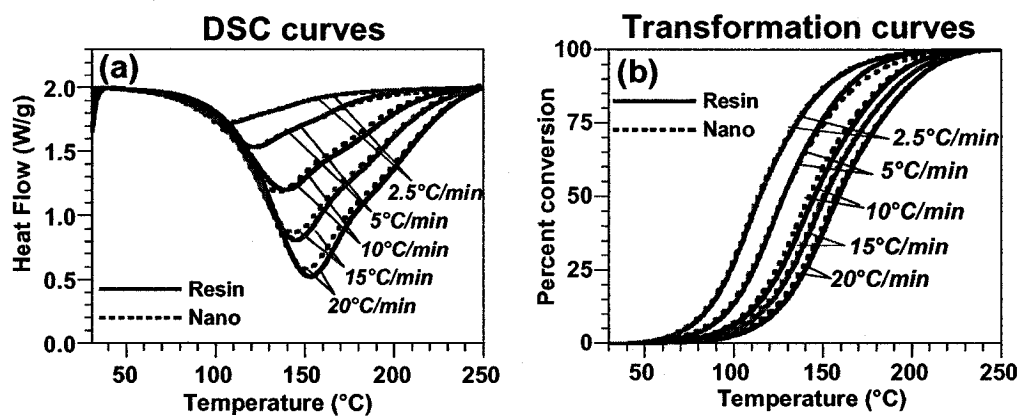


Figure 5.14. DSC and transformation curves of the EPON828-D400 (8 $\delta$ ) system and its nanocomposite (8 $\delta$ -4pB-Tm) at different heating rates, (a) DSC curves; (b) transformation curves

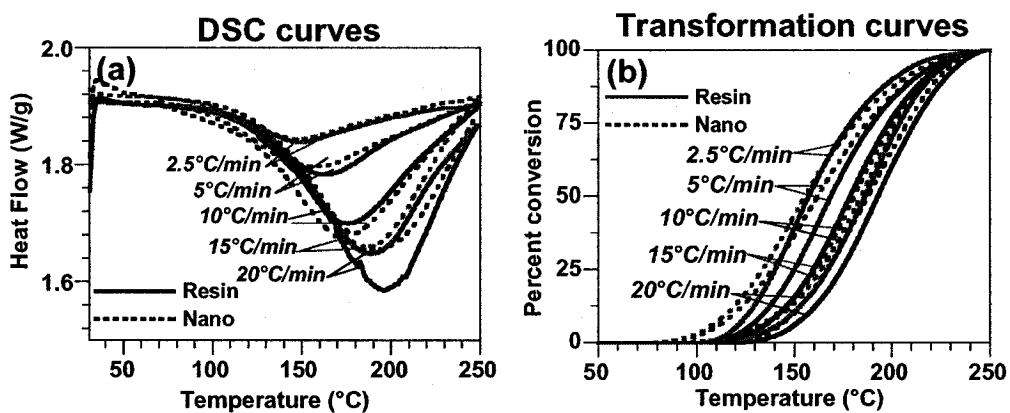


Figure 5.15. DSC and transformation curves of the EPON828-D2000 (8D) system and its nanocomposite (8D-4pB-Tm) at different heating rates, (a) DSC curves; (b) transformation curves

The transformation curves derived from the DSC results are shown in Figures 5.10b, 5.11b, 5.12b, 5.13b, 5.14b, and 5.15b. Generally speaking, the reaction onset and completion occur at lower temperatures at lower heating rates, as can be seen from the  $T_{onset}$  values given in Table 5.8. There is no significant difference between the epoxy and nanocomposite systems with respect to the  $T_{onset}$ , nor with respect to  $T_p$  (the temperature of the peak maximum in the heat flow curves). The curing of epoxy with amine involves several different reactions, and the rates of these reactions will vary with temperature in different ways. Thus a change in the heating rate may favour one reaction with respect to another and change the structure of the crosslinked molecular network. This could explain the decrease in the ultimate  $T_g$  observed for systems on increasing the heating rate, as well as the variations in  $\Delta H$ . However, it appears that the presence of Cloisite 30B has negligible effect on the matrix  $T_g$ .

**Table 5.8. Characteristics for epoxy systems and their nanocomposites with different hardeners**

Epoxy systems				Nanocomposites			
q (°C·min <sup>-1</sup> )	T <sub>onset</sub> (°C)	T <sub>p</sub> (°C)	T <sub>g</sub> (°C)	q (°C·min <sup>-1</sup> )	T <sub>onset</sub> (°C)	T <sub>p</sub> (°C)	T <sub>g</sub> (°C)
8DE				8DE-4pB-Tm			
2.5	46.4	72.6	126.8	2.5	44.2	70.2	126.9
5	53.5	82.2	126.7	5	51.3	81.6	126.3
10	62.6	94.5	126.2	10	60.5	92.7	126.3
15	71.3	104.8	123.3	15	65.2	97.8	126.3
20	76.4	110.9	121.7	20	68.0	103.6	125.8
8EP				8EP-4pB-Tm			
2.5	51.4	92.9	87.7	2.5	54.9	92.0	87.2
5	59.2	106.3	86.8	5	62.0	105.2	85.9
10	69.9	119.0	79.2	10	71.6	117.2	77.1
15	74.7	126.7	73.9	15	76.6	125.5	74.7
20	81.6	133.3	72.7	20	83.3	132.1	73.0
8d				8d-4pE-Tm			
2.5	67.7	101.0	85.7	2.5	66.4	99.9	85.6
5	82.8	113.8	84.8	5	75.8	111.7	84.8
10	87.7	126.8	83.4	10	86.5	125.6	84.6
15	95.2	136.4	82.4	15	92.6	133.6	82.8
20	101.5	142.8	82.3	20	98.9	140.1	82.2
8T				8T-4pB-Tm			
2.5	59.3	97.5	83.4	2.5	57.6	95.3	84.9
5	67.8	111.2	83.2	5	62.3	106.6	84.9
10	79.8	126.5	82.8	10	77.2	124.0	83.5
15	90.2	137.3	82.2	15	85.2	132.5	83.3
20	95.9	145.5	81.1	20	90.7	137.9	83.2
8δ				8δ-4pB-Tm			
2.5	71.7	108.1	47.9	2.5	70.5	106.4	47.3
5	82.5	122.0	47.4	5	79.8	120.2	47.2
10	95.1	139.9	47.4	10	92.1	135.3	47.0
15	100.1	144.9	47.0	15	98.1	143.9	46.3
20	107.0	152.8	47.0	20	103.9	150.5	45.3
8D				8D-4pB-Tm			
2.5	101.9	148.4		2.5	106.8	146.8	
5	111.8	163.6		5	116.4	159.7	
10	125.1	175.3		10	126.9	179.0	
15	127.0	187.7		15	126.6	183.7	
20	135.5	191.3		20	123.0	190.7	



### 5.5.2. Activation energy

Figure 5.16 shows the relationship between  $\ln(q \cdot T_p^{-2})$  and  $T_p^{-1}$  for both the epoxy-amine systems and their nanocomposites. The five points correspond to the five heating rates of 2.5, 5, 10, 15, and 20°C·min<sup>-1</sup>. There is an excellent linear fit in all cases, indicating that the experimental data fit the Kissinger model quite well. From the slopes of these plots the overall activation energy values for epoxy-amine and nanocomposites were calculated and are shown in Table 5.9. The apparent very slight increase in  $E_a$  for the nanocomposites with DETA, EPICURE 3046, D230, T403 and D400 suggesting that the positive effect of the organic intercalant to promote the chemical reaction is weaker than the negative impact of the steric effect of the intercalated/exfoliated clay for these cases. However, with the presence of C30B, the  $E_a$  for the nanocomposite decrease as compared to the neat epoxy when the system cured with D2000.

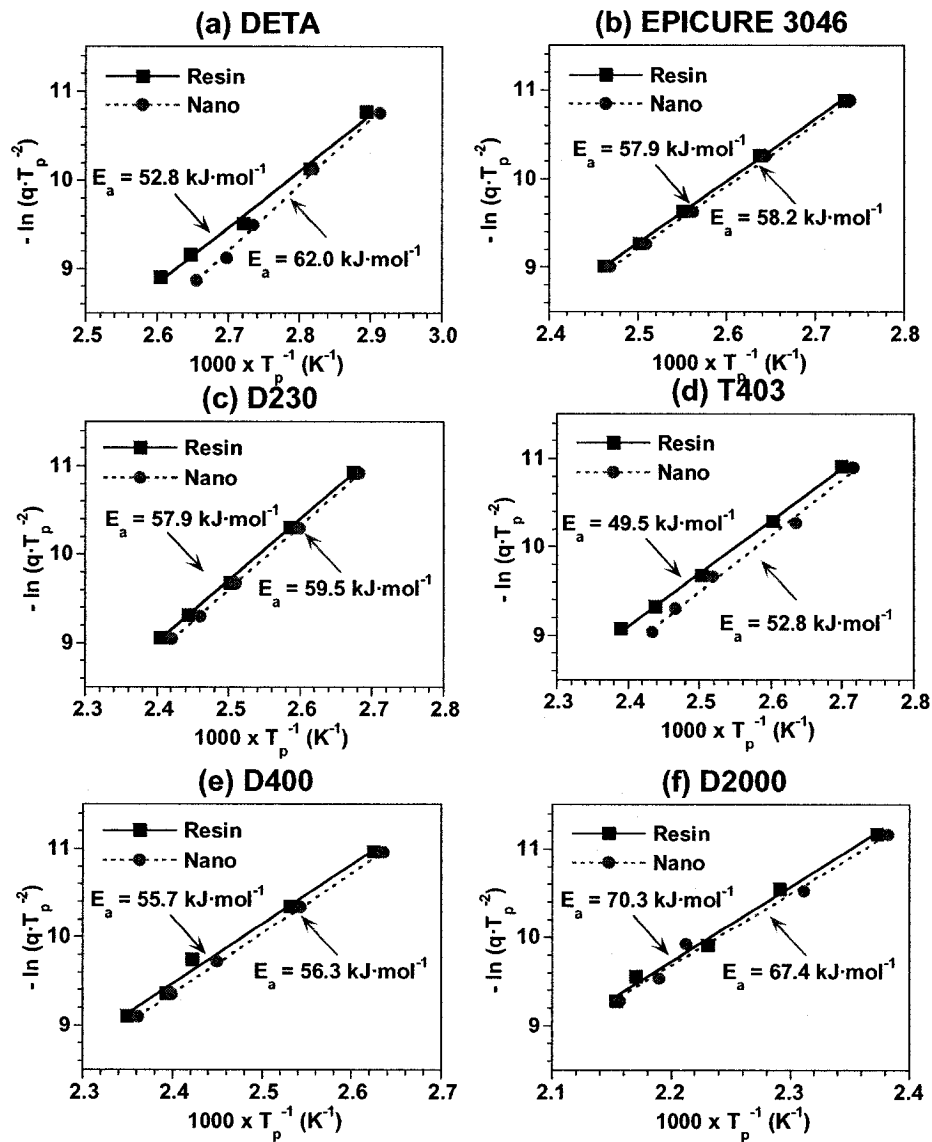


Figure 5.16. Kissinger plots for the EPON828 systems and its nanocomposites with different hardeners: (a) DETA, (b) EPICURE 3046 (from section 5.4), (c) D230, (d) T403, (e) D400, and (f) D2000

**Table 5.9. Activation energy for EPON828 and its nanocomposites with different hardeners from Kissinger analysis**

Hardener	Activation energy (kJ·mol <sup>-1</sup> ) (resin)	Activation energy (kJ·mol <sup>-1</sup> ) (nanocomposite)
DETA	52.8	62.0
EPICURE 3046	57.9	58.2
D230	57.9	59.5
T403	49.5	52.8
D400	55.7	56.3
D2000	70.3	67.4
The results for EPICURE 3046 and its nanocomposite are from section 5.4		

Figures 5.17 to 5.22 show the relationship between  $\ln q$  and  $T^{-1}$  for nine different degrees of conversion ranging from 0.1 to 0.9 for epoxy systems and their nanocomposites with different hardeners. The linear relationship observed in all cases indicates that the approach is applicable for this case. The activation energies  $E_a$  calculated for the four systems are given in Figure 5.23.

For the system cured with DETA, in the epoxy-amine system without clay (Figures 5.17a and 5.23a),  $E_a$  decreases steadily with the degree of cure. With 4 wt% Cloisite 30B (Figures 5.17b and 5.23a),  $E_a$  behaves in a similar manner except that the values are consistently higher; the differences are more clear at the lower degrees of cure. Thus, the clay appears to have an effect.

As discussed above, for systems cured with EPICURE 3046 (Figures 5.18a and 5.23b), in the epoxy-amine system without clay, as expected  $E_a$  increases steadily with the degree of cure, particularly in the later stages ( $\alpha > 0.7$ ). For the mixture of epoxy and Cloisite 30B (8EP-4pB-Tm), the shape of the  $E_a$  vs.  $\alpha$  curve changes considerably. The  $E_a$

decreases slightly as  $\alpha$  increases in the initial stages of cure, then levels off, then rises towards the end, but not as much as when the clay is absent.

For the system cured with D230, in the epoxy-amine system without clay (Figures 5.19a and 5.23c), there is a slight decrease of  $E_a$  with degree of cure. With 4 wt% Cloisite 30B (Figures 5.19b and 5.23c),  $E_a$  behaves in a similar manner except that the values are consistently higher.

For the systems cured with T403 (Figures 5.20 and 5.23d), the  $E_a$  (for both systems with or without clay) changes considerably with the degree of cure. The  $E_a$  decreases slightly as  $\alpha$  increases in the initial stages of cure, then levels off, then rises towards the end, and again at the early stage of cure the presence of clay has more effect on the  $E_a$  than in the later stage of cure. The  $E_a$  of the system with the presence of clay is higher than without clay.

For systems cured with D400 (Figures 5.21 and 5.23e), the  $E_a$  of the epoxy-amine system without clay increases steadily with the degree of cure, particularly in the later stages ( $\alpha > 0.8$ ). For the mixture of epoxy and Cloisite 30B, the  $E_a$  behaves in a similar manner except that the values are consistently higher.

However for the one that was cured with D2000 (Figures 5.22 and 5.23f),  $E_a$  behaves completely contrary to the two other amines; it increases steadily. The curing agent has a different effect on the curing kinetics behavior. The influence of clay also depends on the rate of cure or behavior of hardener.

Generally speaking, hardeners show a different effect on the  $E_a$ . The presence of clay leads to a higher  $E_a$  except for the system cured with very low curing rate D2000 where the intercalant can help to accelerate the curing.

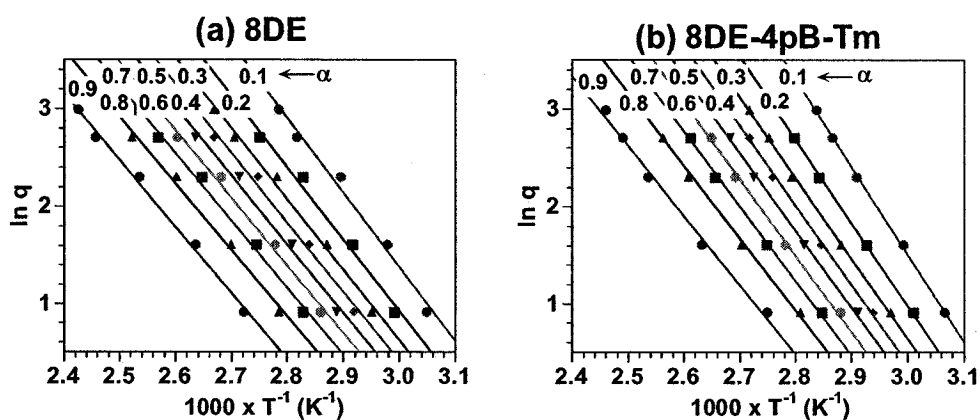


Figure 5.17. Isoconversional plots at various conversions for (a) 8DE system and (b) 8DE-4pB-Tm system

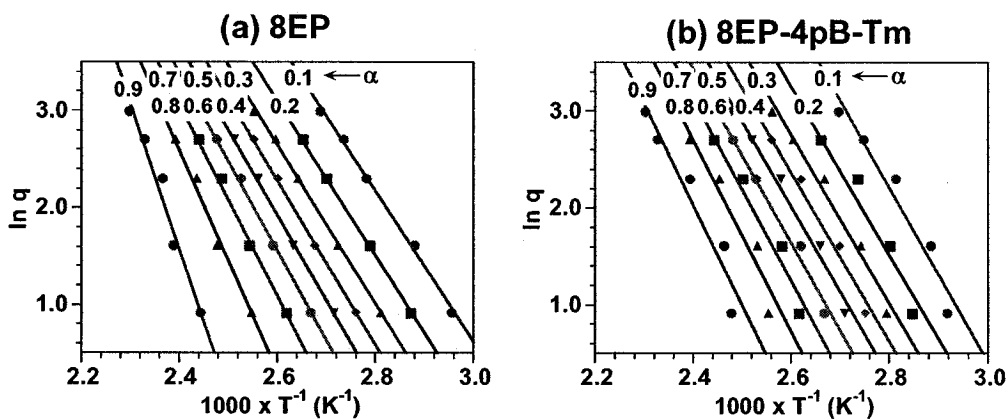


Figure 5.18. Isoconversional plots at various conversions for (a) 8EP system and (b) 8EP-4pB-Tm system (results from section 5.4)

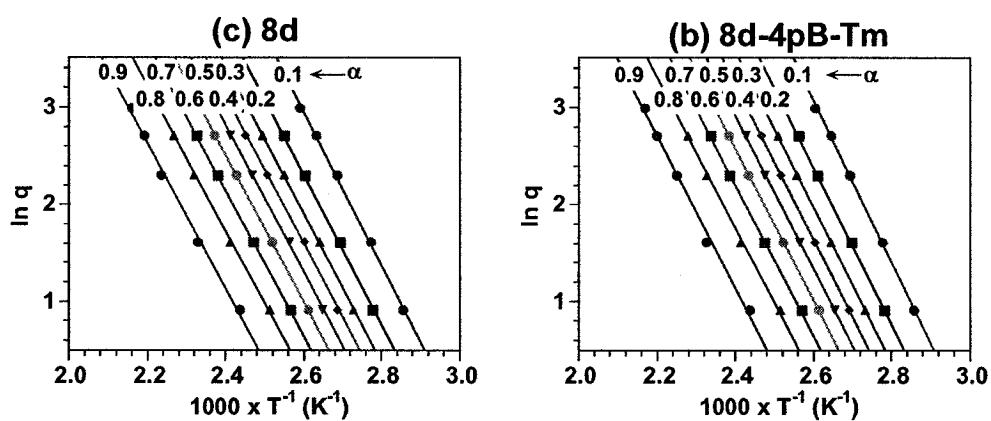


Figure 5.19. Isoconversional plots at various conversions for (a) 8d system and (b) 8d-4pB-Tm system

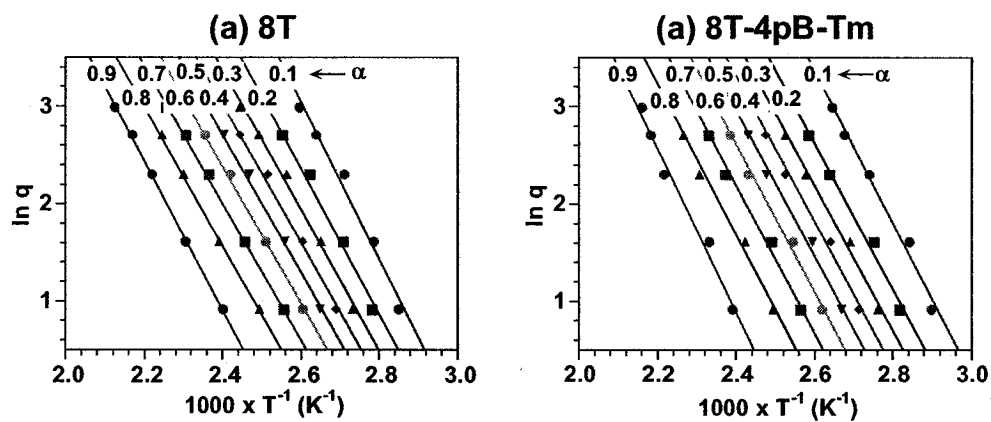


Figure 5.20. Isoconversional plots at various conversions for (a) 8T system and (b) 8T-4pB-Tm system

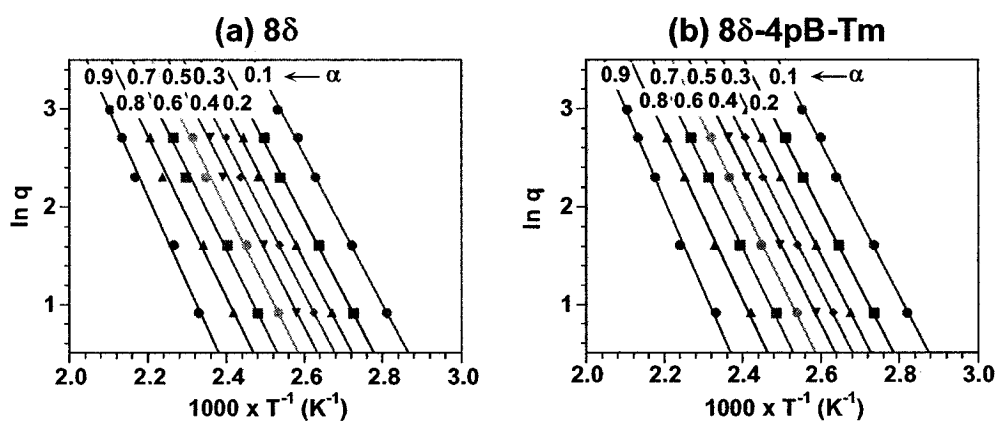


Figure 5.21. Isoconversional plots at various conversions for (a) 8 $\delta$  system and (b) 8 $\delta$ -4pB-Tm system

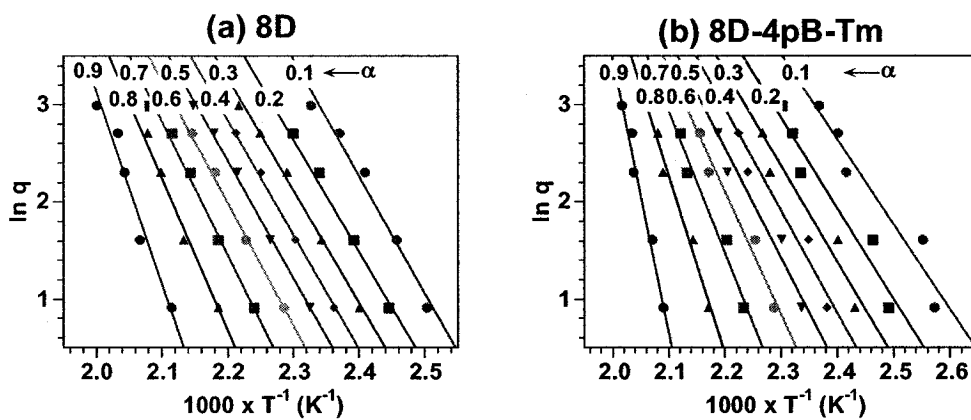


Figure 5.22. Isoconversional plots at various conversions for (a) 8D system and (b) 8D-4pB-Tm system

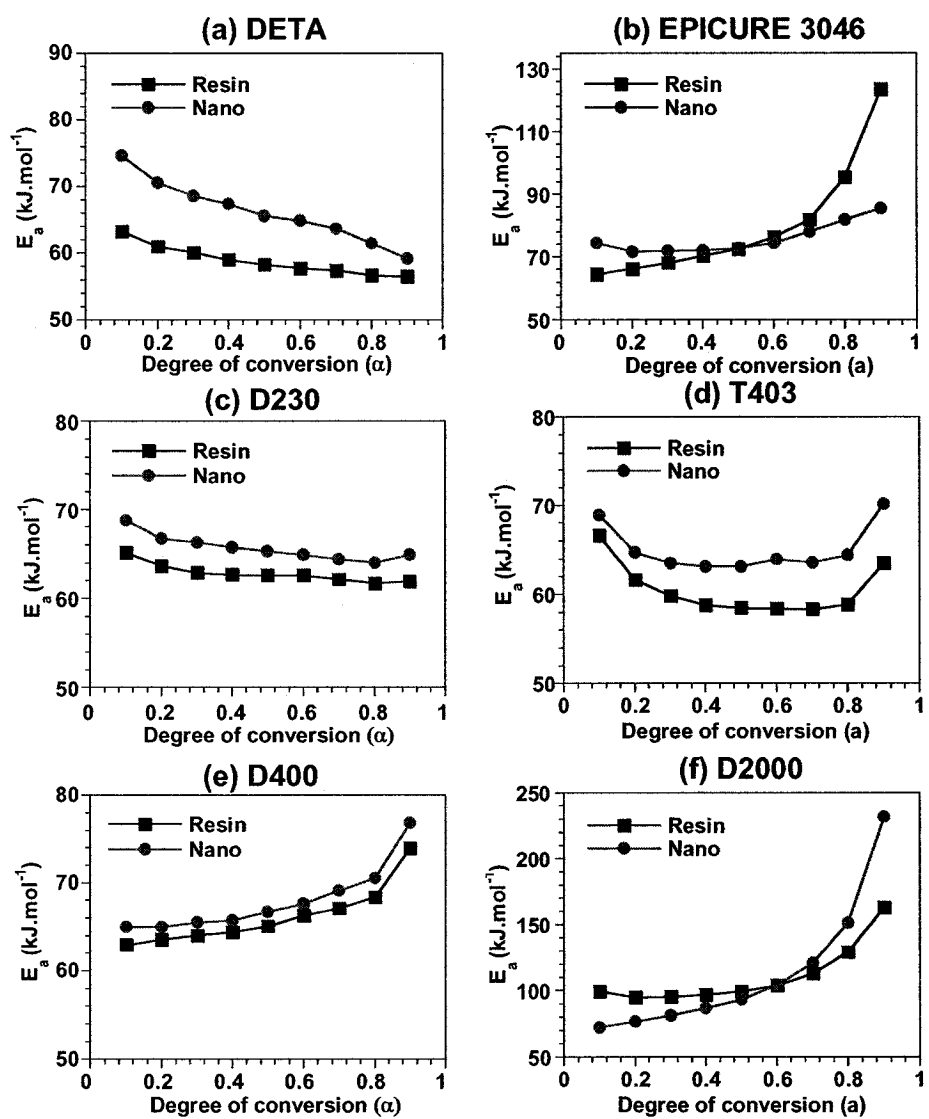


Figure 5.23. Activation energies obtained for the isoconversional model for epoxy systems and nanocomposites with different hardeners, (a) DETA, (b) EPICURE 3046 (from section 5.4), (c) D230, (d) T403, (e) D400, and (f) D2000



**Table 5.10. Average activation energies obtained for the isoconversional model**

<b>Hardener</b>	<b>Average activation energy (kJ·mol<sup>-1</sup>) (resin)</b>	<b>Average activation energy (kJ·mol<sup>-1</sup>) (nanocomposite)</b>
DETA	58.8	66.3
EPICURE 3046	79.9	76.0
D230	62.8	65.7
T403	58.7	63.6
D400	66.2	68.0
D2000	110.8	113.6

Again, the activation energies obtained by the Kissinger approach (Table 5.9) are lower than the average values obtained by the isoconversional approach (Table 5.10). This can be explained by the differences in assumptions and mathematical approach between the two models. The isoconversional results are more meaningful than the Kissinger ones because the evolution of the chemistry of the system during the cure is partially taken into account. The Kissinger approach is based entirely on the maximum rate of cure, which occurs in this case around the beginning of the curing reaction [145]. Thus it is not surprising that the  $E_a$  values obtained by the Kissinger approach are closer to those obtained at lower degrees of cure by the isoconversional approach rather than to the average isoconversional values.

### 5.5.3. Avrami analysis

The curves  $T_g$  vs.  $(\ln q)/a$  according to Equation 5.10 for different hardeners are shown in Figures 5.24, 5.25, 5.26, 5.27, 5.28, and 5.29. The Avrami exponents  $n$  obtained from the slopes of the curves  $T_g$  vs.  $(\ln q)/a$  are given in Table 5.11. For both epoxy-amine and nanocomposites, the Avrami exponent  $n$  in the early stage of cure is greater than in the

second stage. As discussed above, at low conversions, the concentration and the size of the microgels are still small, and their growth is less space-restricted. With the advancement of cure the number of microgels and their size increases so their growth is restrained and inter-microgelation may occur. When the cure reaches its end, intermicrogelation becomes dominant, a three-dimensional network is formed, and the reaction nearly stops. It can also be seen in Table 5.11 that there is no significant variation in the Avrami exponent  $n$  among the system with and without clay except for the system that was cured with DETA, where the  $n$  values are generally lower with the presence of clay. If this effect is real, it could be explained by the steric effect of the clay in these systems. The curing reaction of the system takes place very fast even at low temperature. The growth of microgels is fast in the absence of clay. Because of this, the presence of clay may restrict the growth of the microgels and results in a reduction of  $n$ . Thus, the presence of clay does not seem to have a tremendous effect on the growing of microgels in the epoxy systems during curing, with the possible exception of fast cure epoxy systems such as DETA.

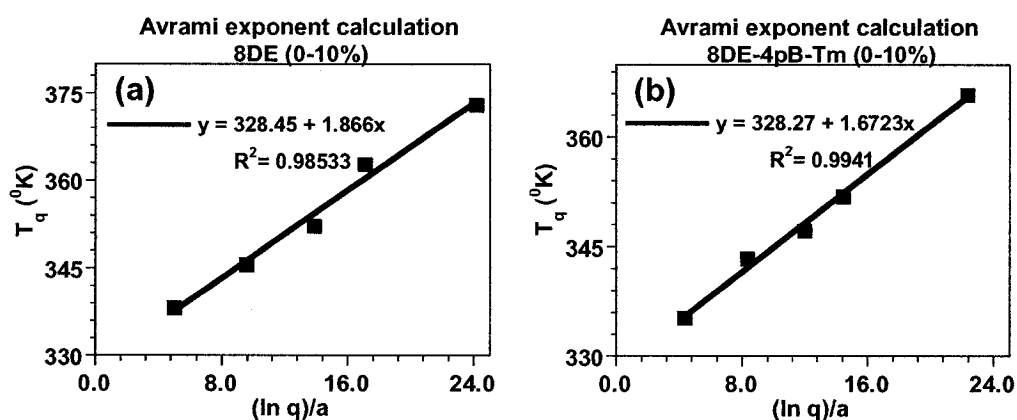


**Figure 5.24. Determination of the Avrami exponent  $n$  for the 8DE system and its nanocomposites in the conversion range  $\alpha = 0-10\%$**

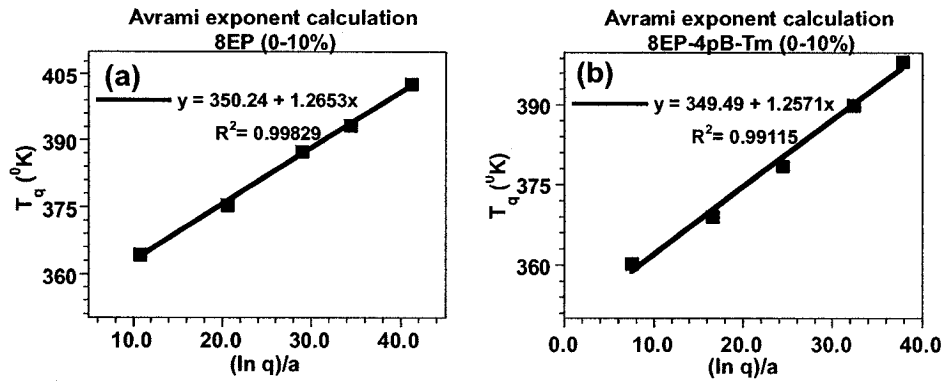


Figure 5.25. Determination of the Avrami exponent  $n$  for the 8EP system and its nanocomposites in the conversion range  $\alpha = 0-10\%$  (results from section 5.4)

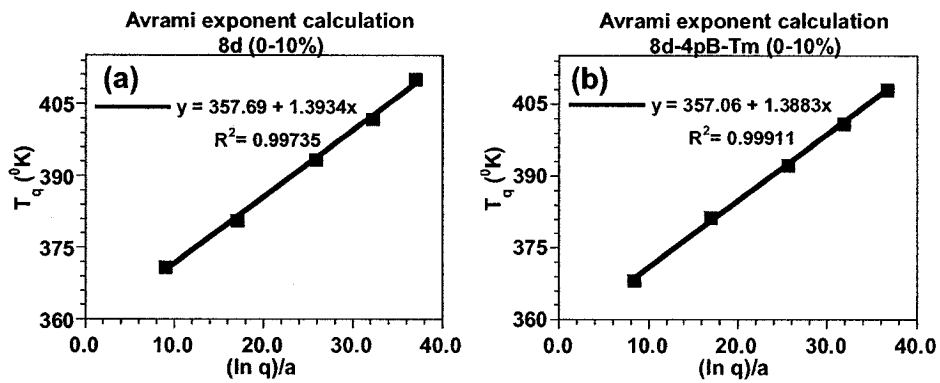


Figure 5.26. Determination of the Avrami exponent  $n$  for the 8d system and its nanocomposites in the conversion range  $\alpha = 0-10\%$

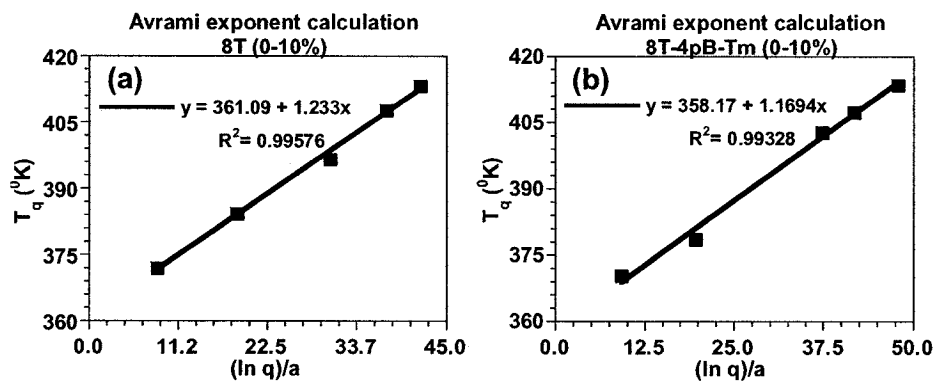
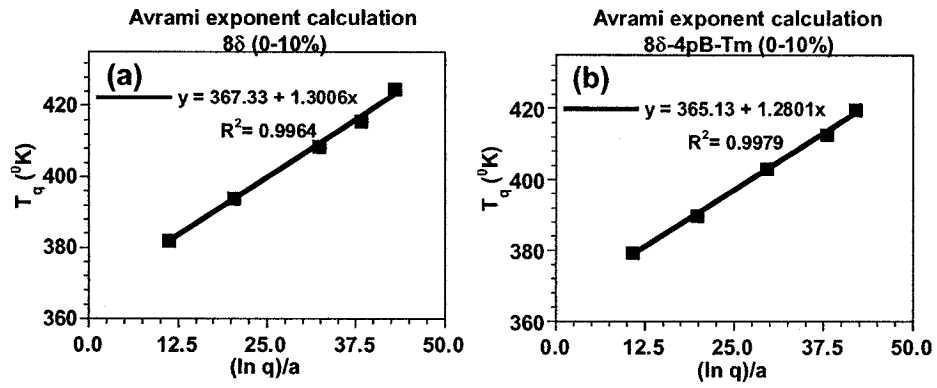
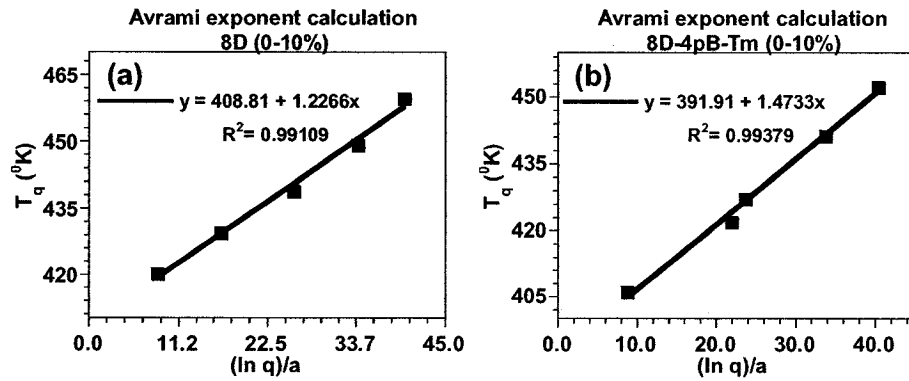


Figure 5.27. Determination of the Avrami exponent  $n$  for the 8T system and its nanocomposites in the conversion range  $\alpha = 0-10\%$



**Figure 5.28. Determination of the Avrami exponent  $n$  for the 8 $\delta$  system and its nanocomposites in the conversion range  $\alpha = 0-10\%$**



**Figure 5.29. Determination of the Avrami exponent  $n$  for the 8D system and its nanocomposites in the conversion range  $\alpha = 0-10\%$**

**Table 5.11. Exponents  $n$  obtained from Avrami analysis**

$\alpha$ Hardener	$\alpha = 0-10\%$		$\alpha = 10-25\%$	
	Resin	Nanocomposite	Resin	Nanocomposite
DETA	1.87	1.67	1.35	1.22
EPICURE 3046	1.27	1.26	1.09	1.02
D230	1.40	1.39	1.13	1.10
T403	1.23	1.17	1.09	1.02
D400	1.30	1.28	1.10	1.05
D2000	1.23	1.47	0.94	0.98

## 5.6. Summary

It is interesting to find out that depending on the intercalant chemistry of the organoclay, the organoclay either can generate or promote certain chemical reactions with the matrix. The C30B, which is based on quaternary ammonium intercalant does not undergo direct chemical reaction with the epoxy matrix. The I30E was treated with an excess amount of primary amine intercalant. Both the primary amine bound to the clay surface and the free amine can react with the epoxy matrix in different ways. The primary amine bound to the clay surface can catalyze the polymerization of the epoxy ring and the hydroxyl group of the DGEBA while the free primary amine can react with the epoxy group (i.e. in the absence of hardener). The first case leads to a dangerous practice since the polymerization liberates a high amount of heat that can generate fire and possible explosion if a large quantity is used. However, the reaction only takes place at high temperatures (above 150°C). The second case is also not favorable because it causes a significant increase in viscosity which is always a challenge in the fabrication of epoxy-based products. However, the reaction is more noticeable at temperatures above 120°C. It is very important to remark here that in the preparation of ENC's with I30E, full attention must be paid to these reactions in order to avoid accident, especially when high temperature is involved. The recommended temperature for the preparation of ENC's with I30E is 120°C and below. If a curing temperature above 120°C is required, it is recommended to raise the temperature slowly or begin the reaction at low temperature for a certain period of time in order to allow the epoxy to react with hardener first.

There is a certain effect of the organoclay type and clay dispersion on the curing kinetics epoxy study by dynamic scan but it is quite minor. The I30E was expected to have a great impact on the results due to its chemical reactivity with the epoxy. However, the reaction between epoxy and amine takes place quite fast even at room temperature and because in this study the temperature was raised slowly in the DSC device, the epoxy and hardener had enough time to react before the sample reached the critical temperatures. Therefore, the reactions of I30E with epoxy were almost negligible.

Generally speaking, the activation energy  $E_a$  increases more or less steadily as a function of the degree of cure. This is probably because at higher degrees of cure (i.e. at higher temperature) the epoxy-hydroxyl reaction, which is known to have higher activation energy, plays a greater role relative to the epoxy-amine reaction. The  $E_a$  of the mixture containing poorly dispersed C30B (stirred at room temperature) is somewhat higher than that of epoxy-amine at all stages of dynamic DSC cure. However, for systems having better dispersion (stirred at high temperature),  $E_a$  is slightly higher in the early stages of cure (i.e. at lower temperature) and lower in the later stages (at higher temperature). The  $E_a$  of the Nanomer I30E mixture is lower than that of the Cloisite 30B mixture (except when the cure approaches 90%) which can be related to the reactivity of I30E with epoxy. On the other hand, the Avrami approach indicates a steric effect of the intercalated/exfoliated clay on the cure of the nanocomposite. The use of these two approaches provides a better understanding of the cure kinetics and mechanism of the nanocomposite formation. Thus the presence of nanoclay and the stirring temperature both affect the cure kinetics.

There is a minor difference in cure kinetics between the epoxy nanocomposites based on Cloisite 30B nanoclay and the corresponding epoxy-amine system without clay. The influence of clay also depends on the rate of cure and behavior of curing agent. The change of activation energy  $E_a$  vs  $\alpha$  cure for epoxy and epoxy nanocomposites depends on hardeners. The presence of clay does not seem to have a tremendous effect on the growing of microgels in the epoxy systems during curing with possible exception of fast cure epoxy system such as DETA.

The results have presented the effects of the chemistry of clay and hardeners and the level of dispersion of clay on the curing kinetics of epoxy nanocomposites. For generalization of the effects, we recall the effect of clay chemistry as the chemical reactivity of clay, the chemistry of hardeners as the chemical reactivity of hardeners. The generalization of the effects of chemistry of clay and hardeners and the level of dispersion of clay on the curing kinetics of epoxy nanocomposites compared to epoxy systems was made and is presented in Table 5.12.

**Table 5.12. The generalization of the effects of chemistry of clay and hardeners and the level of dispersion of clay on curing rate,  $E_a$  and exponent  $n$  of epoxy nanocomposites compared to epoxy systems**

Inputs		Outputs		Curing rate	$E_a$ (Kissinger)	$E_a$ (Isoconversional model)	$n$ (0-10%)
Low chemical reactivity of clay	poor dispersion	slightly higher		slightly higher	slightly higher	slightly higher	
	better dispersion			slightly higher	slightly lower	slightly higher	
High chemical reactivity of clay	poor dispersion			equal	slightly lower	slightly higher	
	better dispersion			slightly lower	slightly lower	slightly higher	
Reactivity of hardeners	high			slightly higher	slightly higher	slightly lower	
	medium			slightly higher	slightly higher (except slightly lower for EPICURE 3046)	slightly lower	
	low		slightly lower	slightly higher	slightly higher		



# Chapter 6

## Properties of epoxy nanocomposites

### 6.1. Objectives

The dispersion and curing process of nanoclays in epoxy have been studied in Chapters 4 and 5. The following stage is the performance properties of epoxy nanocomposites. One knows that the properties of composite materials are strongly influenced by the properties of the components, by the geometry of the filler phase (the size, the shape and the size distribution, thus the aspect ratio), by the morphology of the system, by the nature of the interface between the phases and by the volume fraction of reinforcements etc. For nanocomposites reinforced with nanoclay, their properties also depend on the level of dispersion and intercalation/exfoliation of nanoclay in the matrix. Nanoclay fillers can be present in the form of sheets of one nanometer thick and hundreds to thousands nanometers wide or in the form of stacks or even large aggregates, depending on the quality of dispersion of clays in the matrix. Therefore, they can make a great contribution to the properties of the materials.

From the literature, no improvement in tensile strength but great improvement in compressive strength in glassy ENCs has been reported [11, 12, 18, 27, 41, 45, 91]. The mechanism behind this is still unclear, but it may be speculated that if large clay aggregates or voids (voids are often trapped inside the large aggregates) exist in the

samples they will initiate and propagate the failure across the sample under sufficient tensile stress of the test. Thus there is negligible positive impact of nanoclays on the tensile strength. Tensile strength is sensitive to such defects but not compressive strength. Most of the reports focused on the intercalation and exfoliation aspects but not the micro-dispersion aspect. As pointed out in Chapter 4, the dispersion of organoclay in ENC (also true for PNC) consists of a broad range of structures from macro-aggregates to micro-aggregates, multi-stack aggregates and individual layers, depending strongly on the means of preparation of the ENC. The best intercalation and exfoliation do not automatically provide the best mechanical performance because the mechanical performance is controlled not only by the nano-structure but also by the macro- and micro-structure, that exist in the system. From the fundamental understanding point of view, it is important to clarify the effect of dispersion on the mechanical performance in order to optimize the reinforcing effect of nanoclays. With the improved ENC fabrication processes (mixing process and controlling the curing process) developed in Chapter 4, one can generate different levels of dispersion.

The objective of this chapter was to investigate the performance of the ENC with different levels of dispersion and different chemistries of clays and hardeners. The experiments were organized in three different series: ENC with the same clay and matrix but different dispersion levels of clay (prepared by different mixing methods), ENC with two different types of clays, and ENC with three different hardeners. Neat epoxy was the same in all studies and the neat epoxy systems with corresponding hardeners were also used as references. Different analysis techniques were used to characterize the properties of ENC.

## 6.2. Methodology and experiment

To our knowledge, several factors that may affect the performance of epoxy nanocomposites are: crosslink density of cured epoxy nanocomposites (curing); interface interaction between epoxy matrix (epoxy plus hardener) and clay; the intercalation or exfoliation of clay in epoxy systems; aspect ratio; volume fraction of nanoclay and chemistry of epoxy; curing agent; and clay. These factors are shown in Figure 6.1.

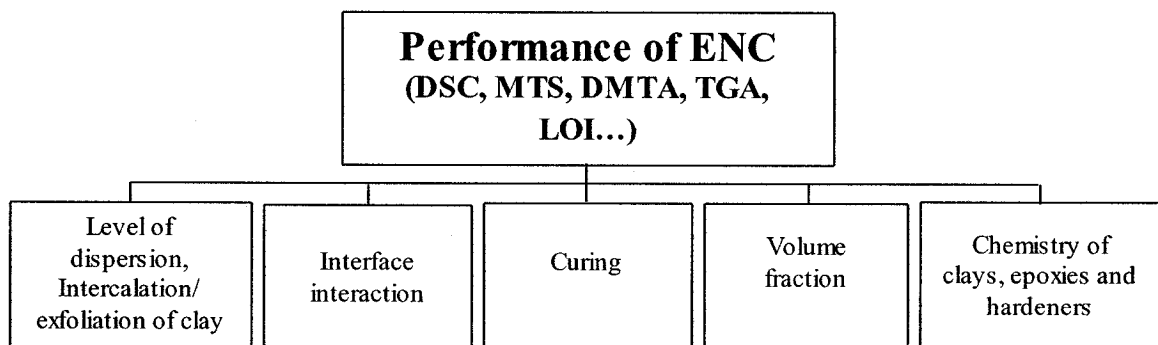


**Figure 6.1. Factors affecting the performance of epoxy nanocomposites**

In order to fulfill the objectives of this chapter, many experiments were designed as described in Table 6.1.

**Table 6.1. Study parameters for Chapter 6**

Clay	Stirring method	Hardener	Clay concentration wt%	Curing (°C)
<b>Temperature and stirring conditions (Epoxy-clay mixtures from stirring step)</b>				
<b>C30B</b>	<b>Rm</b>	<b>D230</b>	2	120°C for 2 hrs and post cure at 140°C for 2 hrs
	<b>Tm</b>		2, 4, 6	
	<b>TM</b>		2	
	<b>RS</b>		2	
	<b>TS</b>		2, 4, 6	
	<b>HP</b>		2	
<b>Chemistry of clay</b>				
<b>C30B, I30E</b>	Rm, Tm	Epicure 3046	(*)	120°C for 2 hrs and post cure at 140°C for 2 hrs
<b>Chemistry of hardener</b>				
<b>C30B</b>	Rm, Tm	<b>DETA</b>	(*)	120°C for 2 hrs and post cure at 140°C for 2 hrs
		<b>T403</b>		
		<b>D2000</b>		
	TS	<b>BF<sub>3</sub></b>	6	115°C for 1 hr + 125°C for 8 hrs and post cure at 175°C for 4 hrs in nitrogen atmosphere
		<b>D230</b>		120°C for 2 hrs and post cure at 140°C for 2 hrs
		<b>D2000</b>		
(*) 100 g of EPON828 was stirred with 2g and 4 g of C30B by Rm and Tm and then the stoichiometric amount of hardener (See Chapter 3) was added in the mixtures for curing.				

### 6.3. Effect of the stirring process

Sample specifications for experiment set 6.3 are given in Table 6.2.

**Table 6.2. Sample specifications for experiment set 6.3**

Designation	EPON828	D230	C30B	Stirring method
8d	100	32	0	-
8d-2B-Rm	100	32	2.69	Rm
8d-2B-Tm	100	32	2.69	Tm
8d-2B-TM	100	32	2.69	TM
8d-2B-RS	100	32	2.69	RS
8d-2B-TS	100	32	2.69	TS
8d-2B-HP	100	32	2.69	HP
8d-4B-Tm	100	32	5.50	Tm
8d-4B-TS	100	32	5.50	TS
8d-4B-HP	100	32	5.50	HP
8d-6B-Tm	100	32	8.43	Tm
8d-6B-TS	100	32	8.43	TS
8d-6B-HP	100	32	8.43	HP

### **6.3.1. Tensile and compressive properties**

#### **6.3.1.1. The effect of stirring temperature and speed on tensile properties**

Tensile and compressive properties of EPON828 resin and its nanocomposites were evaluated. The tensile properties of EPON828-D230 with 2 wt% C30B prepared with different stirring methods are shown in Figure 6.2. The presence of clay results in improvement in modulus for all cases of stirring (Figure 6.2a). A similar effect was reported by other researchers that addition of clay (from 5wt% and above) increases modulus [10, 11]. However, this study demonstrates that even with a small amount of clay of 2wt% the modulus can also significantly be improved. Since clay has a much higher modulus than the epoxy matrix, it is easy to understand, based on the rule of mixtures, why the modulus of the ENCs can be improved by adding nanoclay.

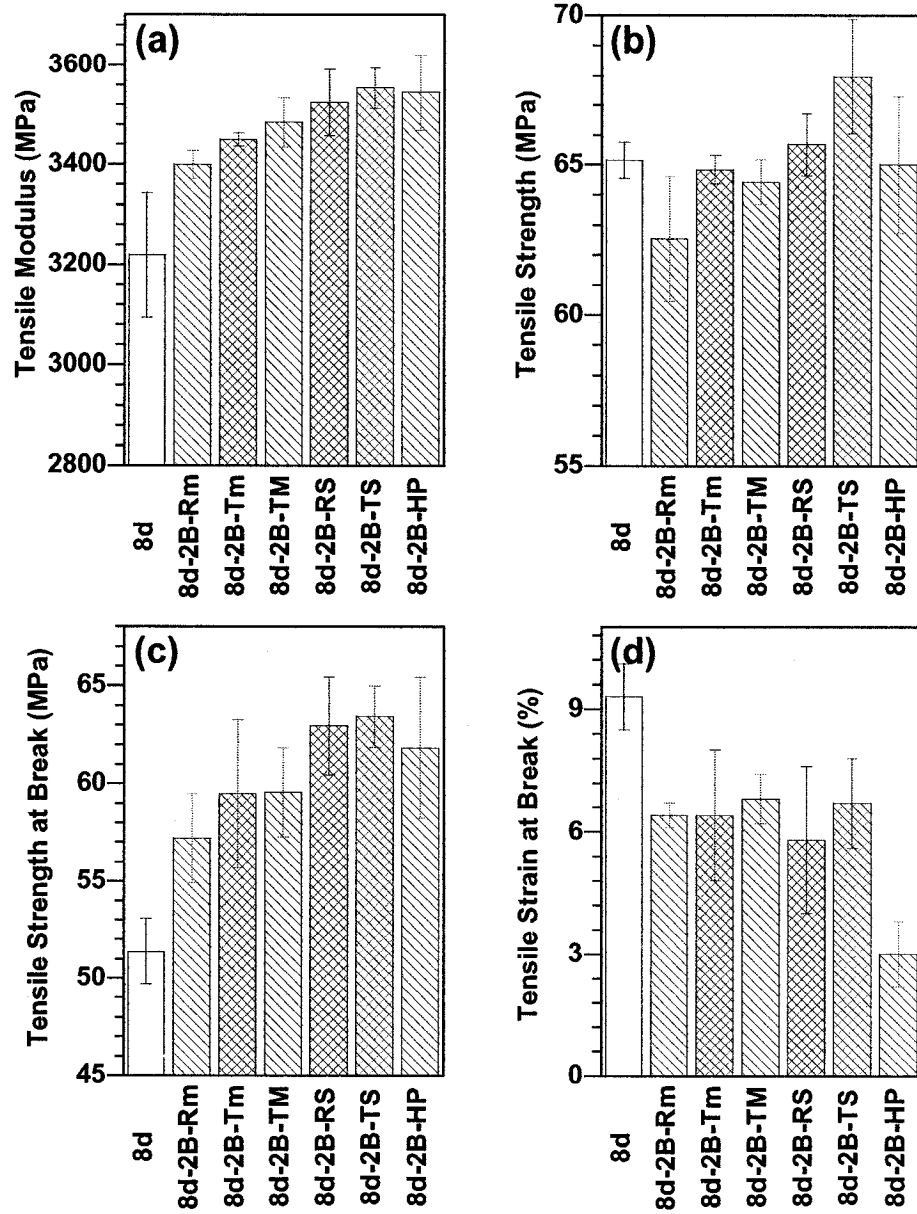


Figure 6.2. Tensile properties for Epon828 resin and its nanocomposites made by different stirring methods (a) tensile modulus, (b) tensile strength (the maximum point on the stress-strain curve), (c) tensile strength at break (the last or break point on the stress-strain curve)

In addition, the modulus of the nanocomposites can follow the order  $E_{TS} > E_{HP} > E_{RS} > E_{TM} > E_{Tm} > E_{Rm} > E_{Epoxy}$ . The level of increase in the modulus of ENCs prepared with TS,

HP, RS, TM, Tm, and Rm stirring methods compared to epoxy is 10.4%, 10.2%, 9.5%, 8.3%, 7.2%, and 5.6% respectively. From the results in Chapter 4, the dependence of dispersion of clay in ENCs on stirring conditions also follows the order of TS > HP > RS > TM > Tm > Rm. Relating to the clay dispersion and the modulus of ENCs, it seems that the better is the dispersion of the nanoclay in ENCs, the higher is the modulus of ENCs.

It can be seen clearly that the modulus of ENCs prepared with Tm stirring method is higher than Rm stirring method ( $E_{Tm} > E_{Rm}$ ) and the modulus of ENC prepared with TS stirring method is higher than RS stirring method ( $E_{TS} > E_{RS}$ ). From there, one can see that the stirring temperature has a positive effect not only on the dispersion, intercalation/exfoliation of clay in ENCs but also on the mechanical performance of ENC.

Stirring speed also shows its effect on the modulus of ENC. At the same stirring temperature of 120°C, the modulus of ENC prepared with high speed stirring method (TS) is higher than that of ENC prepared with low speed stirring method (TM) and without stirring (Tm) ( $E_{TS} > E_{TM} > E_{Tm}$ ). This is similar for stirring at room temperature; the modulus of ENC prepared with RS stirring method is higher than that of ENC prepared with Rm stirring method ( $E_{RS} > E_{Rm}$ ). Both stirring temperature and speed show a positive effect on modulus of ENCs, however, stirring speed appears to have a greater effect.

Unlike the modulus, the strength and strain at break of the materials depend not only on the dispersion of the clay in the matrix but also on the presence of material defects (voids, holes, etc.), the quality of the interface between clay and matrix, and the structure of the

materials. Thus the strength and strain at break do not follow the same trends as the modulus. The tensile strengths of the ENCs are almost the same as that of the epoxy matrix if standard deviation is considered (Figure 6.2b). It is well documented in the literature that improvement in tensile strength was reported only for rubbery epoxy systems while for glassy epoxy systems great reduction in tensile strength was often obtained [11, 12, 18, 27, 41, 45, 91]. For example, a record loss of 39.5% in tensile strength for glassy ENC was provided by Zilg et al [91]. The reason why nanoclays can only improve the strength of rubbery systems but not glassy systems is still unclear up to now. In the following Chapter this matter will be better addressed with different explanations. Therefore, no loss in tensile strength as found in this study should be considered as a positive message, although it would be more gratifying to obtain a gain. If the standard deviation bars are not considered, the general trend of the tensile strength of the ENCs alone in Figure 6.2b is somewhat similar to the trend of the tensile modulus (except for the sample prepared by HP) in Figure 6.2a, which means that the strength has a tendency of increasing with the improvement in dispersion. It can be interpreted that finer and more uniform dispersion can increase the clay surface area for interacting with the matrix and reduce the possibility of stress concentration in the large aggregates that will initiate the failure under stress. Thus the tensile strength is improved. Among them, the sample prepared with TS provides the greatest strength while the poor stirring approach Rm contributes the poorest strength. The exception for HP may be related to the fact that the solvent used in this process was not removed completely from the system.

The tensile strengths at break of the ENCs are greater than that of the matrix and this can be explained by the fact that the strength at break is strongly sensitive to the defects in the



test samples (cracks, microcracks, flaws, voids, holes, etc) and how these defects initiate and propagate the fracture. Epoxy resin is well known for its high residual stress during curing, which can generate defects in the sample. The presence of nanoparticles or even microparticles should improve the situation. Thus it improves the strength at break.

The strains of the ENC's are almost the same for all cases and are significantly lower than that of the matrix (Figure 6.2d). The loss in strain by the presence of nanoclays can be explained by the superior modulus of nanoclay which likely makes the materials more brittle [45, 96], especially in glassy epoxy systems. This issue will be again studied more in depth in the next chapter.

#### **6.3.1.2. The effect of stirring speed and clay loading on tensile properties**

Tensile properties of epoxy nanocomposites according to the various clay concentrations prepared with high speed at high temperature (TS) and at high temperature without mechanical stirring (Tm) are shown in Figure 6.3. The modulus increases almost linearly with the clay loading. The modulus shows a similar trend for both stirring with and without high speed at high temperature (Figure 6.3a). Again, the result shows the better advantage of high speed mixing on the formation of nanocomposites and this advantage becomes greater as the clay loading increases. At the same clay loading, the modulus of the epoxy nanocomposite prepared by high speed is higher than that of the one made without mechanical stirring. For example at a clay loading level of 6wt%, the modulus of the epoxy nanocomposite prepared by the TS method increases 29.3 % with respect to epoxy, compared to 21.3 % for the one without mechanical stirring.

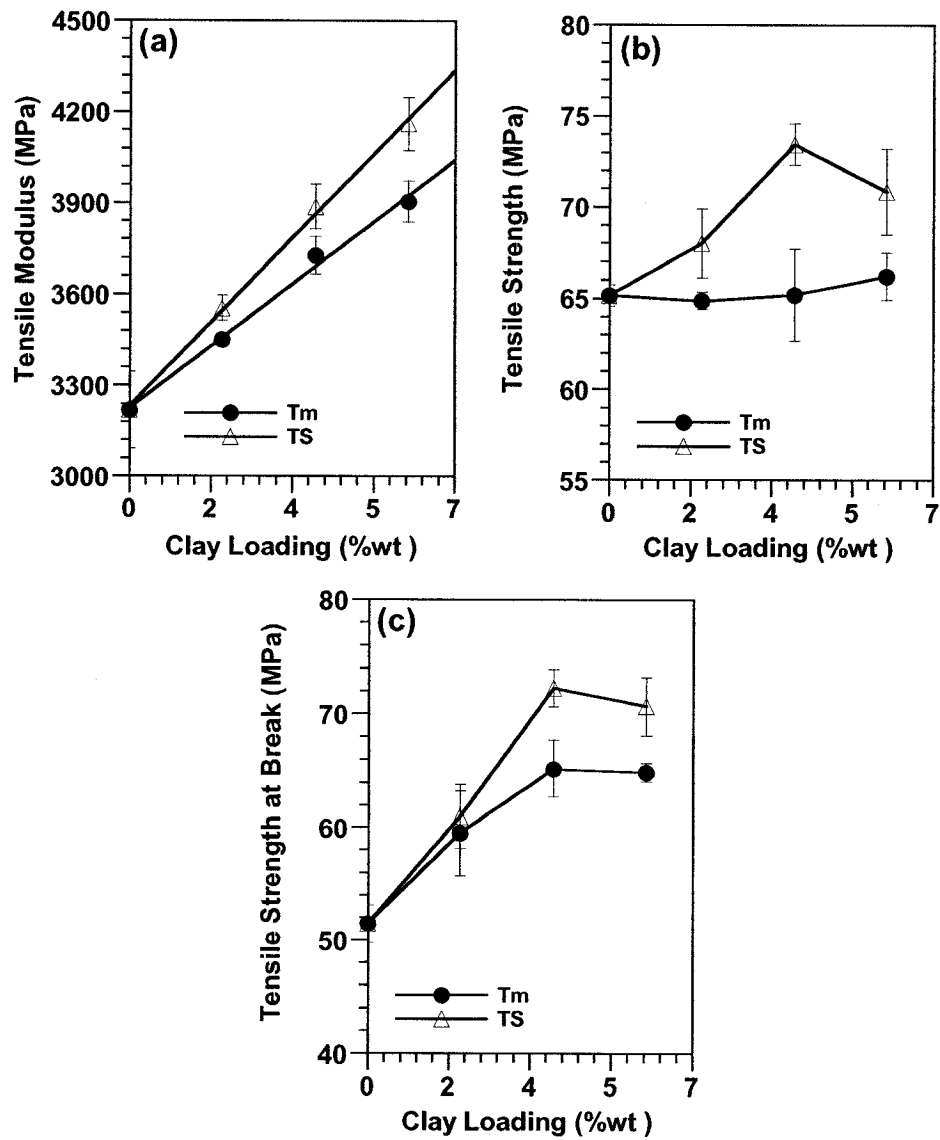


**Figure 6.3. Tensile properties for EPON828 resin and its nanocomposites at different clay concentrations made by Tm and TS methods (a) tensile modulus, (b) tensile strength, (c) tensile strength at break**

The strength of epoxy nanocomposite is also affected by high speed stirring. The strength of samples with high speed stirring appears higher than the strength of samples without mechanical stirring especially at high clay concentrations (Figure 6.3b). Again it

confirms that better dispersion gave better strength. This also occurs for tensile strength at break.

Figure 6.3 also demonstrates that the increase of clay loading increases the modulus as well as the strength. The modulus is quite linearly related to the clay loading in the studied loading range, which likely indicates that this relationship obeys the rule of mixture. Further studies on the rule of mixture and other mechanical theory will be addressed in the following chapter. At higher clay loadings, the reinforcing effect of nanoclays on the tensile strength of the ENC becomes more evident. As discussed earlier, the findings in this study are quite superior to data reported in the literature for glassy ENCs, which show only a loss in tensile strength [11, 12, 18, 27, 41, 45, 91]. The increase in tensile strength seems to reach a plateau at 4 wt% clay loading.

#### **6.3.1.3. The effect of stirring temperature and speed on compressive properties**

In the literature, no improvement in tensile strength but great improvement in compressive strength in glassy ENCs has been reported. Contradictory to the literature, this study found significant improvement in tensile strength by improving the formation of ENCs (mixing process and controlling the curing process). It should be interesting to discover further the advantage of the improved process on the compressive properties of ENCs. Figure 6.4 shows the compressive properties for epoxy and its nanocomposites which were prepared by different stirring methods. Stirring method again shows an effect on compressive properties of nanocomposites (Figure 6.4). The presence of clay results in improvement in modulus for all cases of stirring (Figure 6.4a). In general, the compressive modulus of the nanocomposites also follows the order  $E_{TS} > E_{HP} > E_{RS} > E_{TM}$

$> E_{Tm} > E_{Rm} > E_{Epoxy}$ . The level of increase in the compressive modulus of ENCs prepared with TS, HP, RS, TM, Tm, and Rm stirring methods compared to epoxy is 10.1%, 8.8%, 5.7%, 3.4%, 2.8%, and 2.4% respectively, which is similar to the increase in tensile modulus. Again, it confirms that the better the dispersion of the nanoclays in ENCs, the higher is the modulus of the nanocomposites. Again, it confirmed a slightly better advantage of the Tm over Rm stirring method (if standard deviation was not considered), the TS over the TM and RS stirring methods, and the best advantage of the TS stirring method among all of them.

Compressive strength at break is reduced for ENC prepared with the Rm stirring method compared to neat epoxy (Figure 6.4b) as the result of its poor dispersion with large clay aggregates. Compressive strength at break increases for ENCs prepared with Tm, TM, RS, TS and HP stirring methods compared to neat epoxy and it follows the order of TS > HP > RS > TM > Tm > Epoxy. The explanation for that should be similar to that for tensile strength as discussed earlier. The improvement in compressive strength is more significant than in tensile strength because compressive strength is less sensitive to the defects of the testing sample. Compressive strain at break remains almost unchanged with the presence of the clay, except for the ENC prepared with Rm (Figure 6.4c) where the strain at break lightly decreases with the presence of clay.

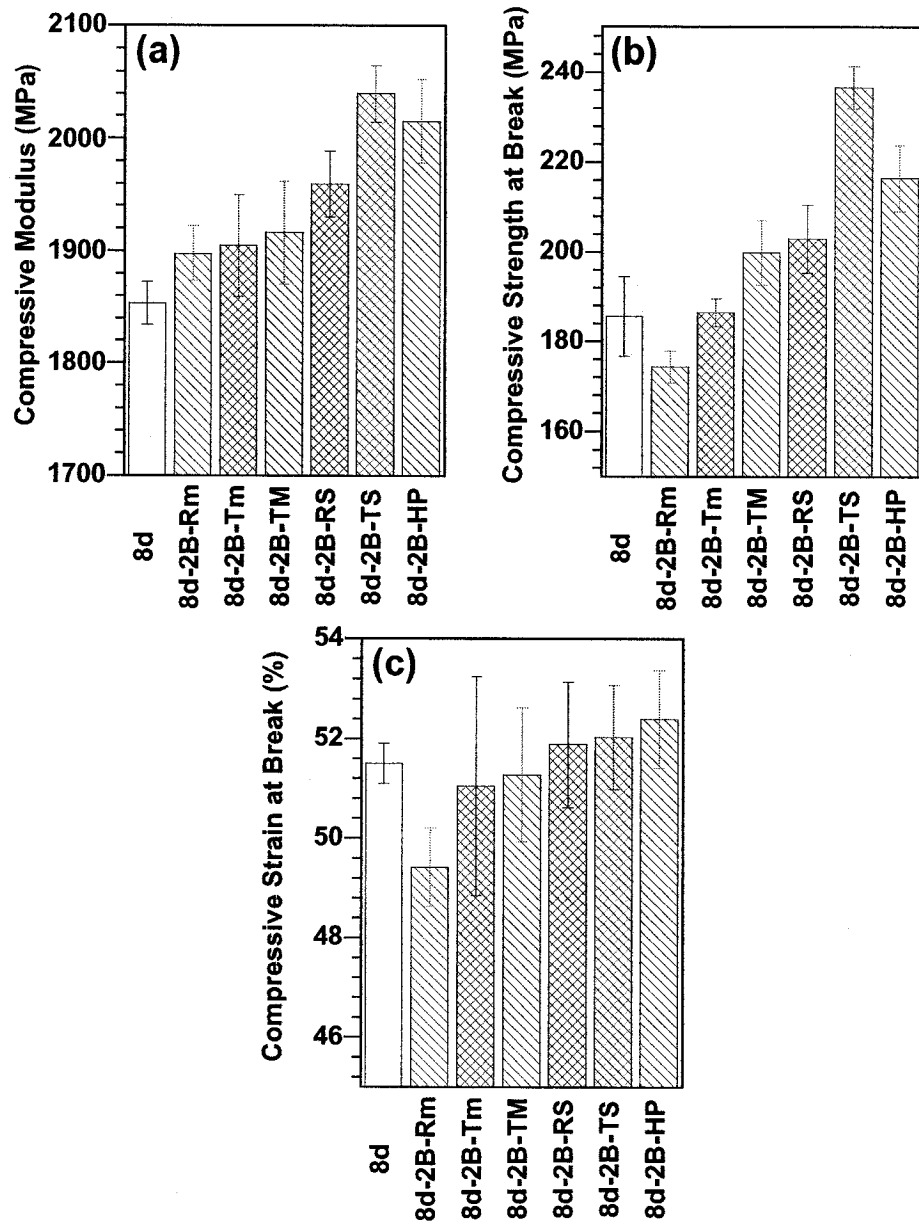
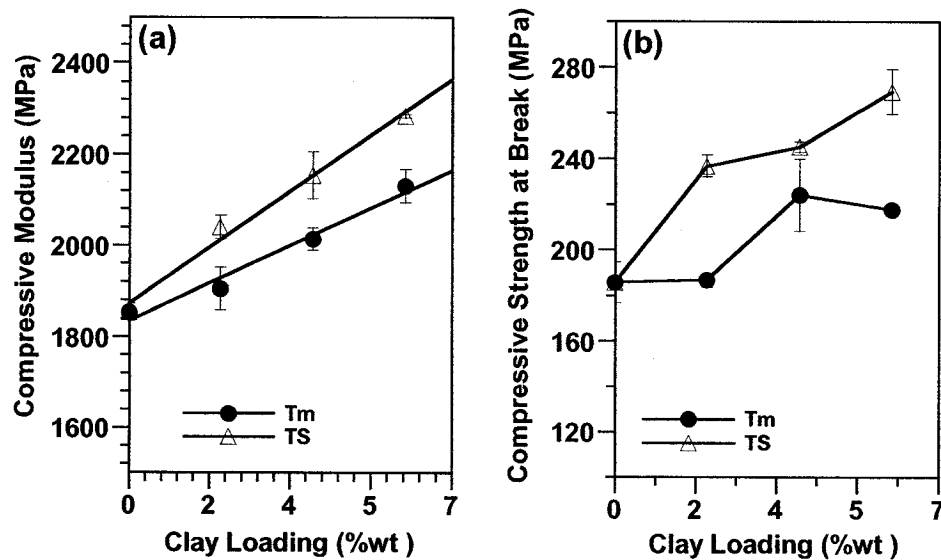


Figure 6.4. Compressive properties for EPON828-D230 resin and its nanocomposites made by different stirring methods (a) compressive modulus, (b) compressive strength at break, (c) compressive strain at break.

#### 6.3.1.4. The effect of stirring speed and clay loading on compressive properties

Comparing the compressive properties of nanocomposites at different clay loadings for stirring with high speed at high temperature (TS) and without mechanical stirring at high temperature (Tm), the modulus shows a similar trend for both cases. The compressive modulus and strength show an improvement with clay loading (Figure 6.5).



**Figure 6.5. Compressive properties for EPON828-D230 resin and its nanocomposites at different clay concentrations made by Tm and TS methods: (a) compressive modulus, (b) compressive strength at break**

However it shows a better improvement when high speed is introduced (Figure 6.5a). The compressive modulus of epoxy nanocomposites at 6 wt% of clay prepared by the TS method increases 23.2 % with respect to epoxy, compared to 15 % for the one without mechanical stirring (Tm). The compressive strength at break of ENC prepared with high speed stirring appears higher than the compressive strength at break of ENC without mechanical stirring at the same clay concentrations (Figure 6.5b). At 6 wt% of clay, the

compressive strength at break increases 45.2% for TS and 32.1% for Tm compared to neat epoxy. It confirms that better dispersion gave a better strength at break.

## **6.3.2. Fracture toughness properties**

### **6.3.2.1. The effect of stirring temperature and speed on fracture toughness properties**

Epoxies are thermoset polymers having versatility in their chemical forms. The characteristics of epoxy resins constitute an excellent combination of chemical and corrosion resistance, and good mechanical and electrical properties. These characteristics, along with a long service life, make epoxies a necessity in the future growth of new technologies. Most of the epoxies are widely used as protective coatings and adhesives, whereas others are used in structural applications such as laminates and composites, tooling, molding, casting, electronics, and construction. Presently, there is high potential for more sophisticated application of high-performance epoxies in both automotive and aerospace industries. However, epoxies have brittle characteristics that may hinder their potential applications in aerospace and automotive applications. For structural applications, for example, epoxy resins tend to be either brittle or notch sensitive. Therefore, tremendous efforts have been focused on improving the toughness of epoxy systems, which has stimulated an overwhelming interest in filling epoxy with inorganic fillers (such as particulates, fibers, and layered fillers) in the pursuit of toughening epoxy resin.

Fracture toughness was measured using three point single-edge notched bending (SENB) (see section 3.5.5.5 in Chapter 3). The critical stress intensity factor ( $K_{IC}$ ) and the critical

strain energy release rate ( $G_{IC}$ ) for the EPON828-D230 system and its nanocomposites at 2 wt% C30B made by different stirring methods are shown in Figure 6.6. Both  $K_{IC}$  and  $G_{IC}$  increase with the presence of clay C30B. The results also show that the stirring methods have an influence on the critical stress intensity factor and the critical strain energy release rate of nanocomposites. The  $K_{IC}$  is increased 35%, 41%, 44%, 50%, 82% and 49% respectively for the Rm, Tm, TM, RS, TS and HP stirring methods. The  $G_{IC}$  is increased 17%, 27%, 40%, 43%, 93% and 48% respectively for the Rm, Tm, TM, RS, TS and HP stirring methods. It is clear that the effect of stirring methods on the improvement for both  $K_{IC}$  and  $G_{IC}$  is in the order of TS > HP > RS > TM > Tm > Rm. This means that the better level of dispersion, intercalation/exfoliation of clay in nanocomposites results in a higher improvement in the  $K_{IC}$  and  $G_{IC}$ . The results are similar to those reported by Liu [22] that the presence of organoclay results in improvement in fracture toughness of epoxy. From there, one can see that the stirring temperature has a positive effect not only on the dispersion, intercalation/exfoliation of clay in ENCs but also on the mechanical performance of ENCs. It can be seen clearly that  $K_{IC}$  and  $G_{IC}$  of ENC prepared with the Tm stirring method are higher than  $K_{IC}$  and  $G_{IC}$  of ENC prepared with the Rm stirring method, respectively and  $K_{IC}$  and  $G_{IC}$  of ENC prepared with the TS stirring method are higher than  $K_{IC}$  and  $G_{IC}$  of ENC prepared with the RS stirring method, respectively.

Stirring speed also shows its effect on  $K_{IC}$  and  $G_{IC}$  of ENC. At the same stirring temperature of room temperature,  $K_{IC}$  and  $G_{IC}$  of ENC prepared with the RS stirring method are higher than  $K_{IC}$  and  $G_{IC}$  of ENC prepared with the Rm stirring method. This is similar for stirring at 120°C;  $K_{IC}$  and  $G_{IC}$  of ENC prepared with high speed stirring method (TS) are higher than  $K_{IC}$  and  $G_{IC}$  of ENC prepared with low speed stirring



method (TM) and without stirring (Tm), respectively. Both stirring temperature and speed show a positive effect on  $K_{IC}$  and  $G_{IC}$  of ENC. However, it seems that stirring speed is more dominant.

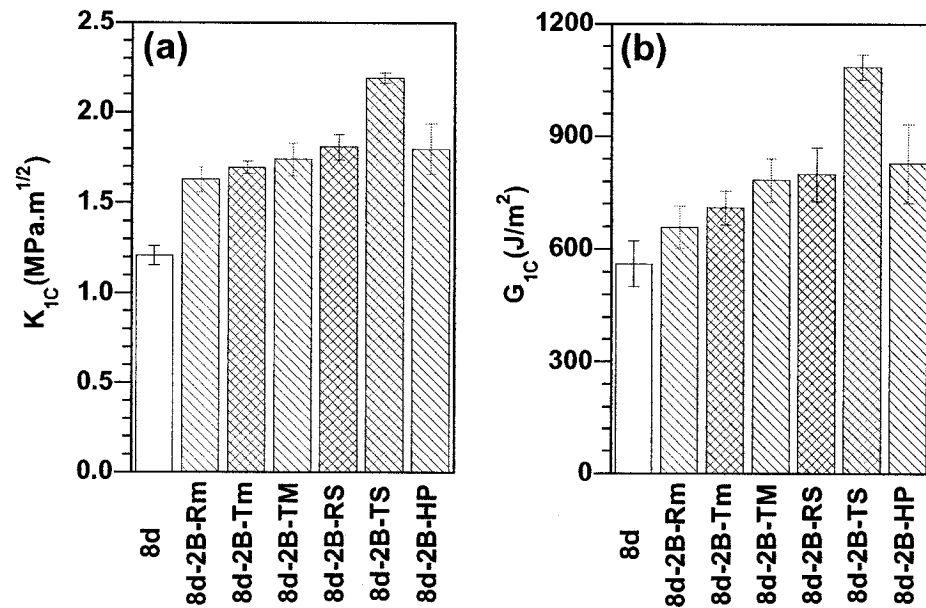


**Figure 6.6. (a)  $K_{IC}$  and (b)  $G_{IC}$  for EPON828-D230 resin and its nanocomposites made by different stirring methods**

The effect of the size of particles on the  $K_{IC}$  and  $G_{IC}$  is shown in Figure 6.7. The results indicated that the size of clay aggregates has a great effect on  $K_{IC}$  and  $G_{IC}$ .  $K_{IC}$  and  $G_{IC}$  increase with decrease of the average size of clay aggregates. There is a jump in the curves at the average below 1  $\mu\text{m}$ . This may be related to the distribution of the clay particles in epoxy (as discussed in Section 4.3.1- Chapter 4) and the level of nano-dispersion at this point. Since particles dispersed in epoxy resin have different moduli and Poisson's ratios from the resin, they usually result in stress concentration. As particles are further partitioned, the stress concentration can be reduced until particle size reaches a certain value [149].

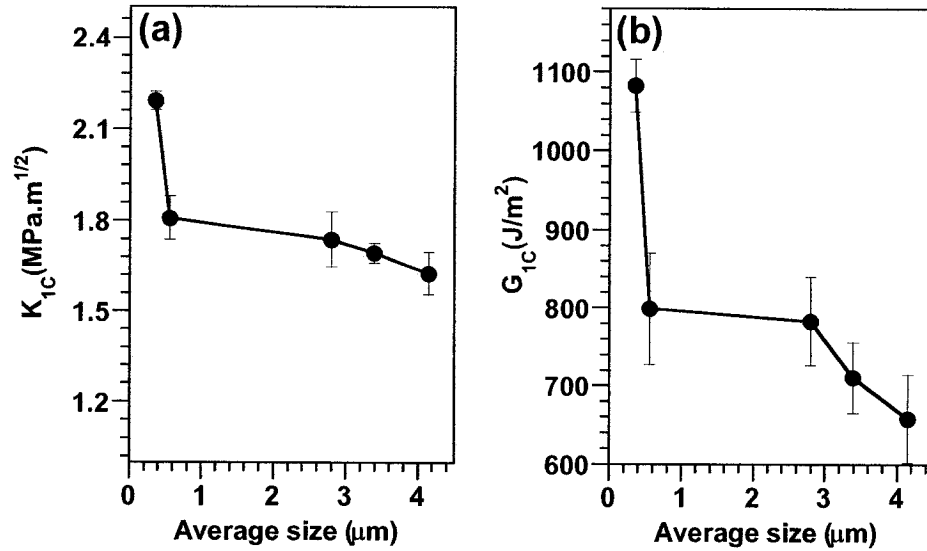


**Figure 6.7. The effect of size of clay aggregates on (a)  $K_{1C}$  and (b)  $G_{1C}$  for EPON828-D230 resin and its nanocomposites with 2 wt% C30B**

The fracture surfaces of specimens made with different stirring methods were observed by FEGSEM and are shown in Figures 6.8 to 6.14. It can be seen that neat epoxy resin exhibits a relatively smooth fracture surface. There are cracks in different planes but almost parallel to the crack-propagation direction, indicated by a white arrow (Figure 6.8). This is a typical fractography feature of brittle fracture behavior, thus accounting for the low fracture toughness of the unfilled epoxy. Compared to the case of neat epoxy, the fracture surfaces of the nanocomposites show considerably different fractographic features. As a representative example, the failure surfaces of the nanocomposites containing 2 wt% of nanoclay made with different stirring methods are shown in Figures 6.9 to 6.14. Generally, a much rougher fracture surface is seen upon adding clay into the epoxy matrix. The increased surface roughness implies that the path of the crack tip is distorted because of the clay platelets, making crack propagation more difficult. More

precisely, the clay is readily able to interact with the growing crack front. Figures 6.9 to 6.11 show that many clay aggregates are observed on the fracture surface, and several distinct agglomerations are indicated by white circles. With high speed or high pressure stirring (Figures 6.11 to 6.13) the clay is already well dispersed in epoxy, so at low magnification FEGSEM, it is difficult to observe clay aggregates in epoxy nanocomposites. Again this confirms that clays have been dispersed better in epoxy with the assistance of high speed stirring. In general, a better dispersion of clay in epoxy results in a rougher fracture surface of epoxy nanocomposites.

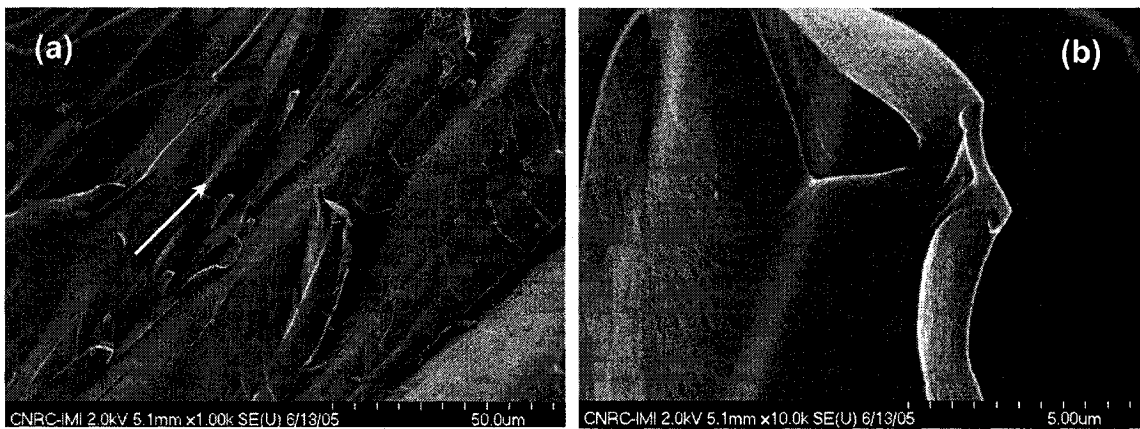


**Figure 6.8. Fracture surface for epoxy; sample cured at 120°C for 2 h: (a) low magnification, (b) high magnification**

It also can be seen that introduction of high speed in the stirring step (Figures 6.12 and 6.13) or high pressure (Figure 6.14) increases the toughness of epoxy nanocomposites compared to without mechanical stirring (Figures 6.9 and 6.10) or with mechanical stirring at low speed (Figure 6.11).

The presence of clay particles or aggregates may cause perturbations along the crack front, thus altering the path of the propagating crack from the straight unperturbed growth seen in the neat resin (Figure 6.9). Consequently, the cracks are deflected by the clay particles into regions surrounding them. Clearly, the crack deflection observed is expected for the increase of strength and toughness obtained by incorporating clay into the epoxy matrix. However, some microvoids can also be seen on the fracture surfaces, as indicated by thick white arrows (Figure 6.9a). At higher magnification (Figure 6.9b), a representative fractographic feature, microvoids, can be clearly observed, as indicated by thick white arrows. Upon fracture the clay particles are very likely to be the stress concentration sites, thus usually resulting in (1) debonding of clay-matrix and (2) cleavage of clay tactoids, consequently producing some micro- or nanovoids and finally reducing the performance. Therefore, it can be believed that the effect of the cleavage of clay tactoids plays a more important role in the fracture toughness of this system. Moreover, high speed and high pressure stirring contributed to reducing the micro-or nanovoids in the epoxy nanocomposite system. Therefore good dispersion, intercalation/exfoliation can help to reduce the negative effect of the cleavage of clay tactoids and bring back the strength of material by incorporating clay into the epoxy matrix.

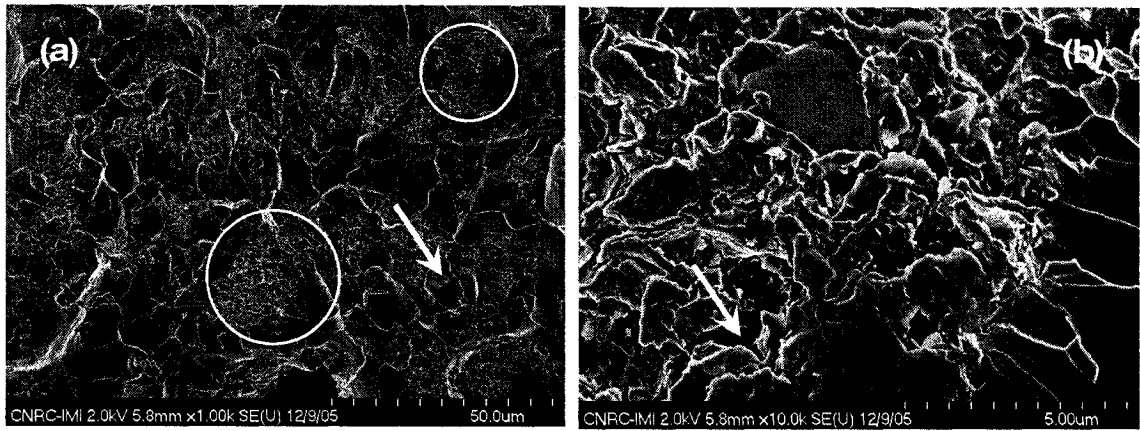


**Figure 6.9. Fracture surface for sample with room temperature stirring at low speed (2 wt% C30B); samples cured at 120°C for 2 h: (a) low magnification, (b) high magnification**

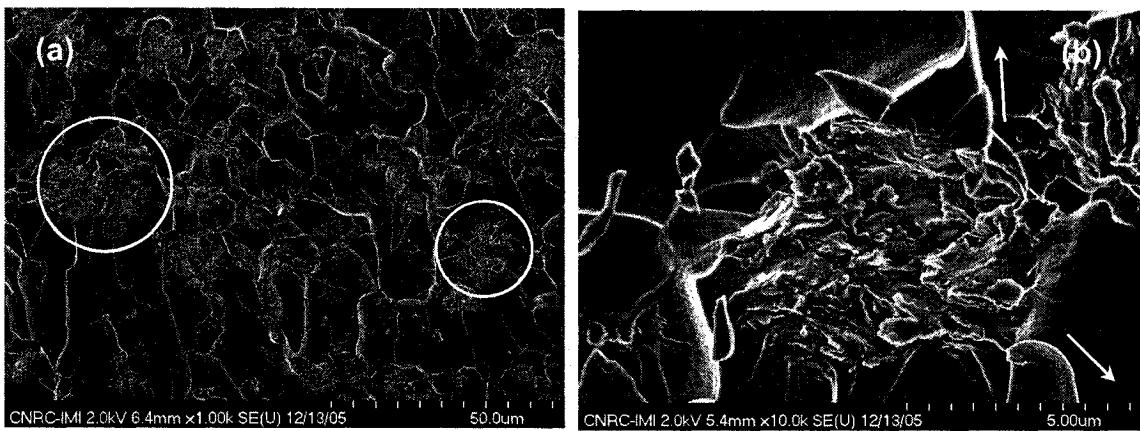


**Figure 6.10. Fracture surface for sample with high temperature stirring (120°C) at low speed (2 wt% C30B); samples cured at 120°C for 2 h: (a) low magnification, (b) high magnification**

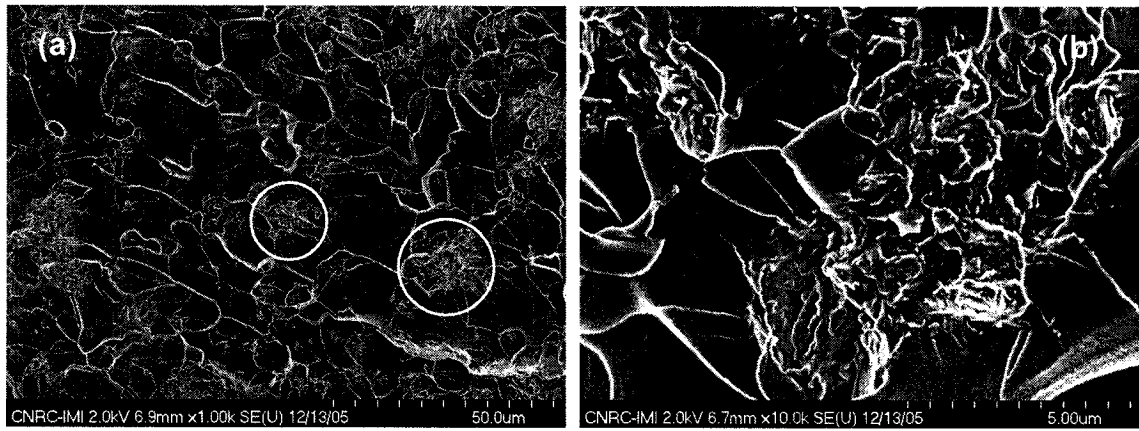


**Figure 6.11. Fracture surface for sample with high temperature stirring (120°C) at 1000 rpm (2 wt% C30B); samples cured at 120°C for 2 h: (a) low magnification, (b) high magnification**

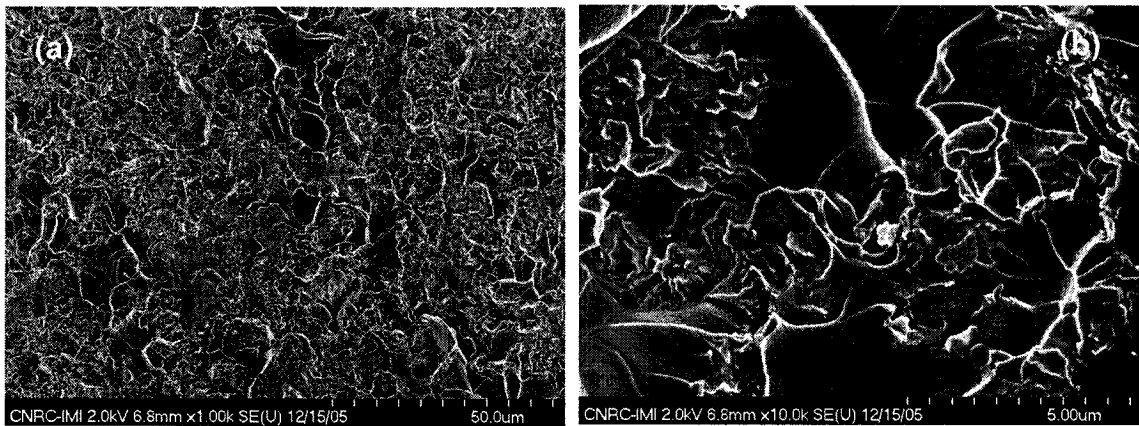


**Figure 6.12. Fracture surface for sample with room temperature stirring at high speed (2 wt% C30B); samples cured at 120°C for 2 h: (a) low magnification, (b) high magnification**

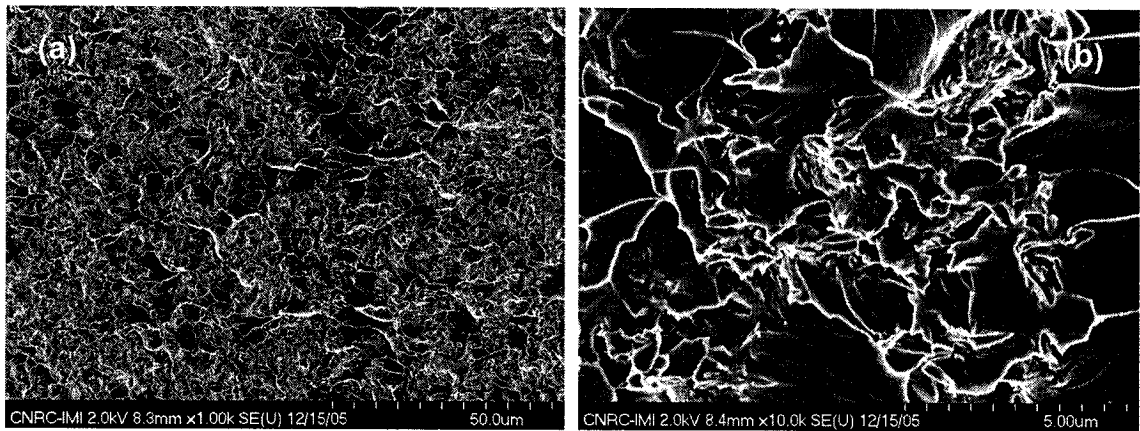


**Figure 6.13. Fracture surface for sample with high temperature stirring (120°C) at high speed (2 wt% C30B); samples cured at 120°C for 2 h: (a) low magnification, (b) high magnification**

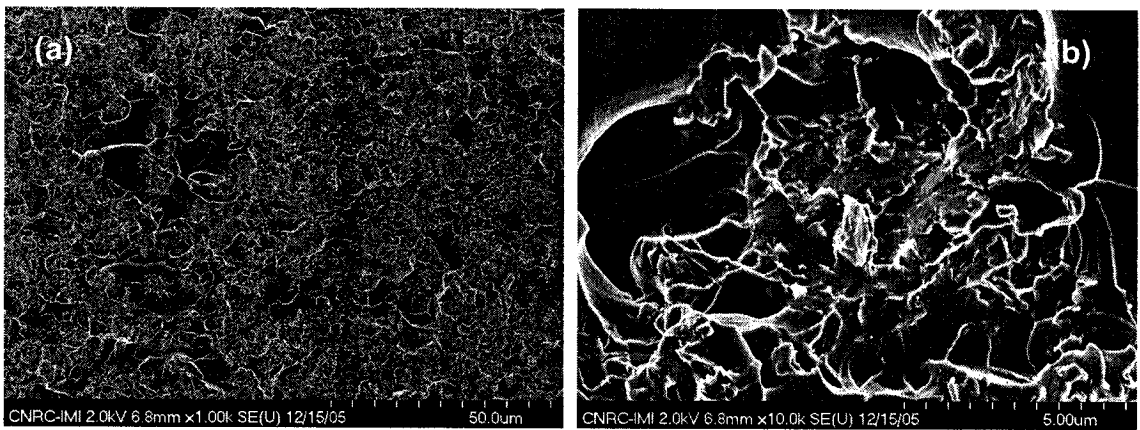


**Figure 6.14. Fracture surface for sample with high pressure (2 wt% C30B); samples cured at 120°C for 2 h: (a) low magnification, (b) high magnification**

### 6.3.2.2. The effect of stirring speed and clay loading on fracture toughness properties

The  $K_{IC}$  and  $G_{IC}$  for the EPON828-D230 system and its nanocomposites at different clay concentrations made by the Tm, TS and HP methods are shown in Figure 6.15.

Obviously, the presence of clay increases the  $K_{IC}$  and  $G_{IC}$  of the epoxy system (EPON828-D230). However,  $K_{IC}$  and  $G_{IC}$  do not increase linearly with the clay loading for this epoxy system. It may be because of the poorer dispersion of clay in this system at higher clay loading (4 and 6 wt%) and it results in lower fracture toughness compared to 2 wt%. The results agree with those of Zhao and Hoa [149], that for certain particle size, there would be an optimum volume fraction to obtain the maximum energy release. The results again show that even though  $K_{IC}$  and  $G_{IC}$  decrease with clay loading, the TS mixing method still gives higher fracture toughness than the HP and Tm mixing methods. Comparing the results for the two different stirring methods Tm and TS, the results confirm that stirring speed has a strong effect on  $K_{IC}$  and  $G_{IC}$ .

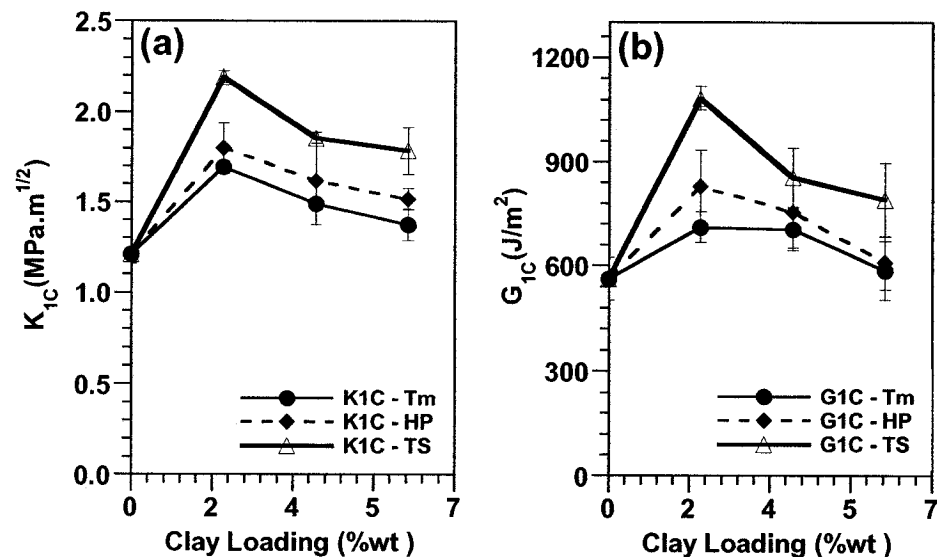


Figure 6.15. (a)  $K_{IC}$  and (b)  $G_{IC}$  for EPON828-D230 resin and its nanocomposites at different clay concentrations made by Tm, TS and HP methods



### 6.3.3. Dynamic mechanical properties

#### 6.3.3.1. The effect of stirring temperature and speed on DMA properties

The effects of nanoclay reinforcement on the mechanical properties of the EPON828-D230 system were also investigated by dynamic mechanical analysis (DMA). In the DMA technique an oscillatory force is applied to a sample and the response to that force is analyzed. Two different moduli are determined as a function of temperature, an elastic or storage modulus ( $E'$ ), which is related to the ability of the material to return or store energy, and an imaginary or loss modulus ( $E''$ ), which relates to the ability of the polymer to disperse energy. The temperature dependence of the ratio  $E''/E'$ , also called  $\tan \delta$  ( $\tan \delta$ ), is related to the mechanical properties of the (nano) composites. The curves in Figure 6.16 show the dependence of the storage modulus and the loss modulus on temperature, as determined by the three-point bending (flexural) DMA method. The data in Table 6.3 provides the storage modulus values of the pristine epoxy and the nanocomposite samples at 30 and 60°C (i.e., in the glassy region below  $T_g = \tan \delta_{max}$ ) and at 120° C (i.e., in the rubbery region above  $T_g = \tan \delta_{max}$ ). The percentage of improvement in the storage modulus of nanocomposites compared to pristine epoxy and  $T_g$  values of the samples as determined from  $\tan \delta_{max}$  are also provided in Table 6.3.

The storage modulus in both the glassy and rubbery regions is higher for the nanocomposite samples compared to the neat epoxy system. However, the level of increase in modulus in the rubbery region is higher than in the glassy region. Clearly, the reinforcing effect of nanoclay is strongly dependent on the nature of the neat polymer and the nanoclay has a more positive effect on mechanical properties in the rubbery region

than in the glassy one. With the same 2 wt% of clay in epoxy, the stirring at high speed and high temperature (TS) shows a better increase in modulus for nanocomposite than the other methods. The better the dispersion of clay in epoxy, the higher is the storage modulus of the nanocomposite (Figure 6.16a and Table 6.3).

The glass transition temperatures ( $T_g$ ) of epoxy and its nanocomposites are listed in Table 6.3. It was observed that the presence of nanoclay C30B does not significantly affect the  $T_g$  of the epoxy systems even at different levels of dispersion. C30B, a montmorillonite treated with methyl tallow bis-(2-hydroxyethyl) quaternary ammonium, might be expected to undergo some interaction (for example hydrogen bonding) with the epoxy resin at the temperatures used in the study. Such interaction should increase the  $T_g$  of the system significantly, but this is not the case, probably because the hydroxyethyl groups are “hidden” under the long hydrocarbon chains of the tallow of intercalant, thus inhibiting a direct interaction between these groups and the epoxy resin (See the structure of intercalant of C30B in Table 3.3).

It can be seen clearly that the storage modulus of ENC prepared with the Tm stirring method is higher than the storage modulus of ENC prepared with the Rm stirring method, and the storage modulus of ENC prepared with the TS stirring method is higher than the storage modulus of ENC prepared with the RS stirring method. This again confirms the positive effect of stirring temperature on the mechanical performance of ENC.

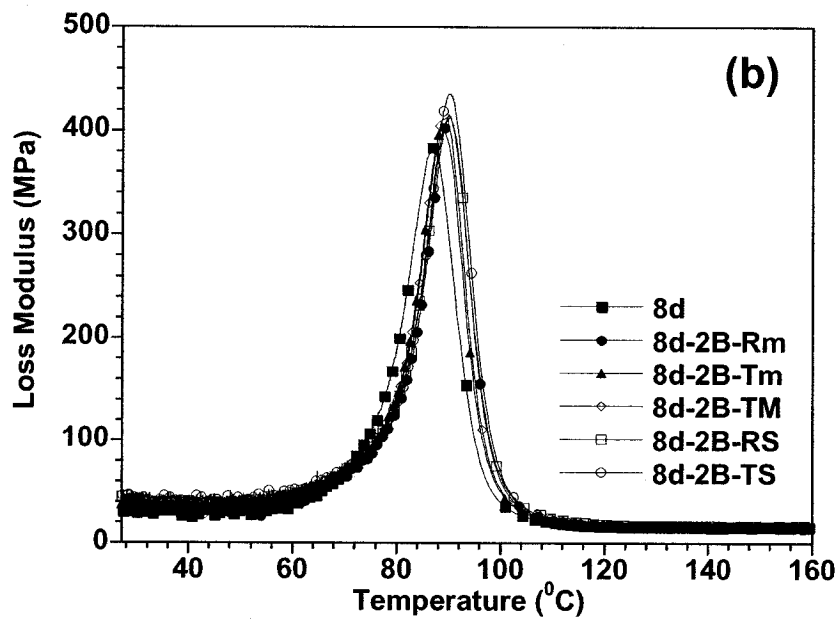
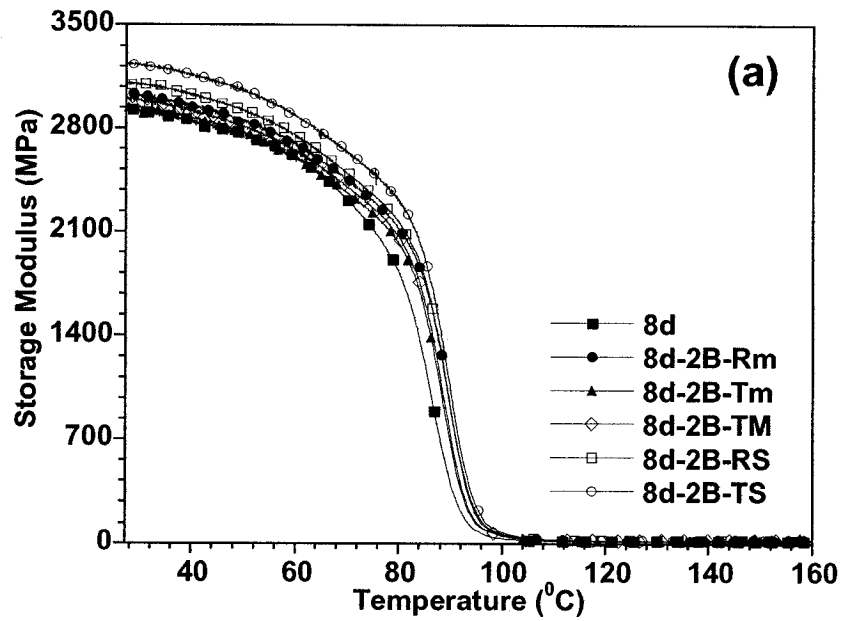


**Figure 6.16. Dynamic mechanical analysis measurements: (a) storage modulus vs temperature, (b) loss modulus vs temperature for the EPON828-D230 system and its nanocomposites for different stirring methods**

Stirring speed also shows its effect on storage modulus of ENC. At the same stirring temperature of room temperature, the storage modulus of ENC prepared with the RS stirring method is higher than the storage modulus of ENC prepared with the Rm stirring method. This is similar for stirring at 120°C; the storage modulus of ENC prepared with the high speed stirring method (TS) is higher than the storage modulus of ENC prepared with the low speed stirring method (TM) and without stirring (Tm). Both stirring temperature and speed show a positive effect on the storage modulus of ENC. However, it seems that stirring speed is the dominant one.

#### **6.3.3.2. The effect of stirring speed and clay loading on DMA properties**

The dependence of the storage modulus and loss modulus on temperature according to the clay concentration prepared with high speed at high temperature (TS) and at high temperature without mechanical stirring (Tm) are shown in Figure 6.17. The modulus increases with clay loading. The modulus shows a similar trend for both stirring with and without high speed at high temperature (Figure 6.17a). However, at the same clay loading, the storage modulus of epoxy nanocomposite prepared by high speed and high temperature (TS) is higher than the one without mechanical stirring at high temperature (Tm).

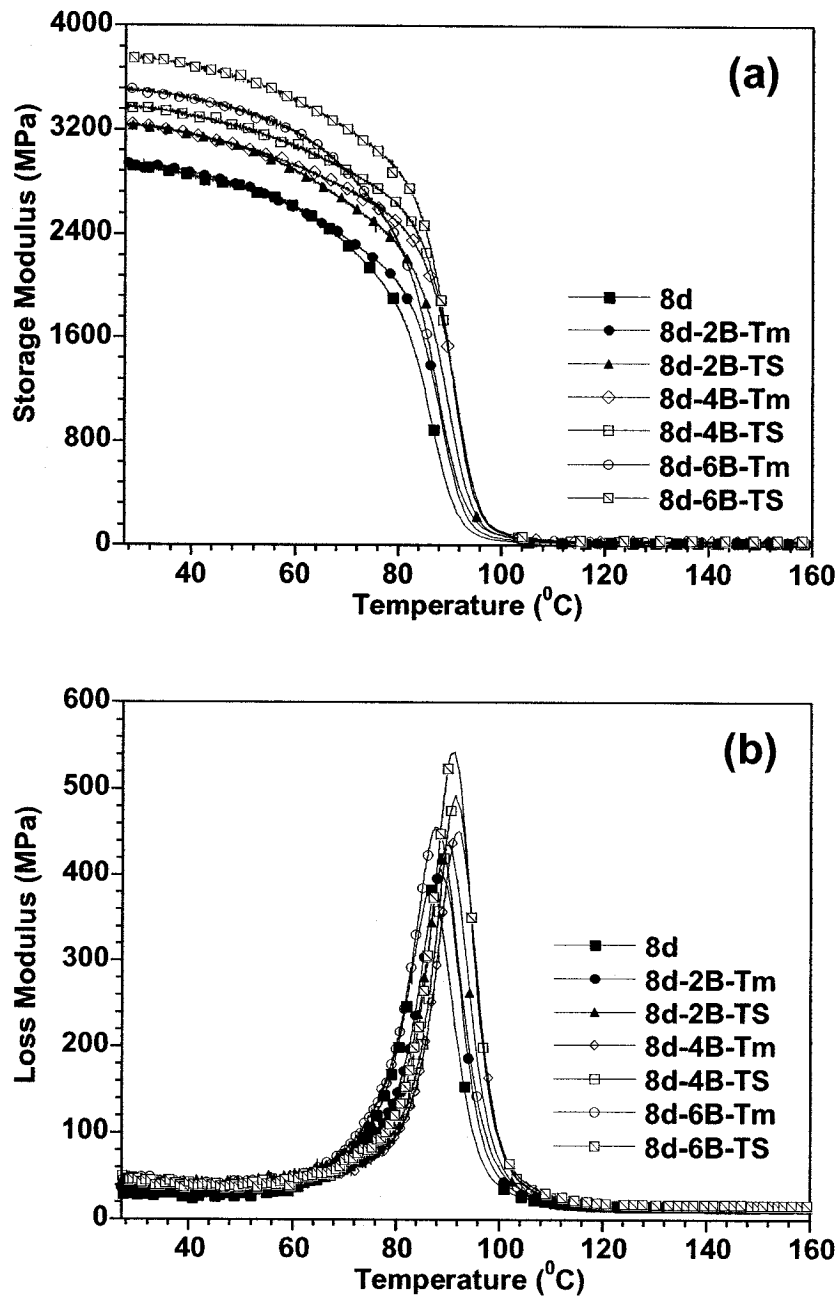


**Figure 6.17. Dynamic mechanical analysis measurements: (a) storage modulus vs temperature, (b) loss modulus vs temperature for the EPON828-D230 system and its nanocomposites at different clay concentrations for methods Tm and TS**

**Table 6.3. Dynamic Mechanical Analysis for pristine EPON828-D230 epoxy and its nanocomposites**

Materials	Storage Modulus $E'$ ( $\pm 2\%$ )						$T_g = \tan \delta_{max}$ ( $^{\circ}\text{C}$ )
	30 $^{\circ}\text{C}$ (GPa)	X(%)	60 $^{\circ}\text{C}$ (GPa)	X(%)	120 $^{\circ}\text{C}$ (MPa)	X(%)	
Epoxy 8d	2.9	-	2.6	-	15.1	-	96.8
8d-2B-Rm	3.0	3.5	2.7	3.9	16.6	9.9	97.9
8d-2B-Tm	3.0	3.5	2.7	3.9	17.5	15.9	96.5
8d-2B-TM	3.0	3.5	2.7	3.9	18.0	19.2	96.5
8d-2B-RS	3.1	6.9	2.7	3.9	18.6	21.2	98.1
8d-2B-TS	3.2	10.3	2.9	11.5	20.9	38.4	97.6
8d-4B-Tm	3.2	10.3	2.9	11.5	22.2	47.0	98.5
8d-4B-TS	3.4	17.2	3.1	19.2	25.2	66.9	97.5
8d-6B-Tm	3.5	20.7	3.2	23.1	26.7	76.8	96.5
8d-6B-TS	3.8	31.0	3.4	30.8	31.1	106.0	97.0

$X = 100 (E'_{nanocomposite} - E'_{epoxy}) / E'_{epoxy}$

### 6.3.4. Thermal properties

#### 6.3.4.1. The effect of stirring time, speed and clay loading on thermal stability properties

Thermogravimetric analysis data of C30B, EPON828-D230 and their nanocomposites with heating rate of 20 $^{\circ}\text{C}\cdot\text{min}^{-1}$  are shown in Figure 6.18. Figure 6.18a shows typical TGA plots of C30B, EPON828-D230 and their nanocomposites. Typical DTG thermograms (the first derivative curves of TGA) are shown in Figure 6.18b. It can be seen that there is 29.16% of weight loss in C30B up to 1000 $^{\circ}\text{C}$ . This means there is 70.84 wt% of remaining materials in C30B at 1000 $^{\circ}\text{C}$ . These values represent the inorganic silicates in C30B.

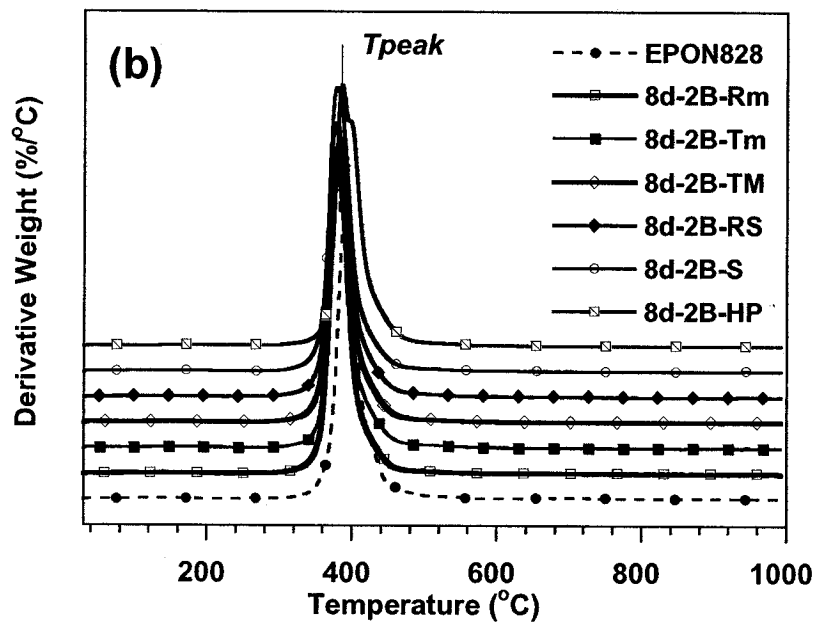
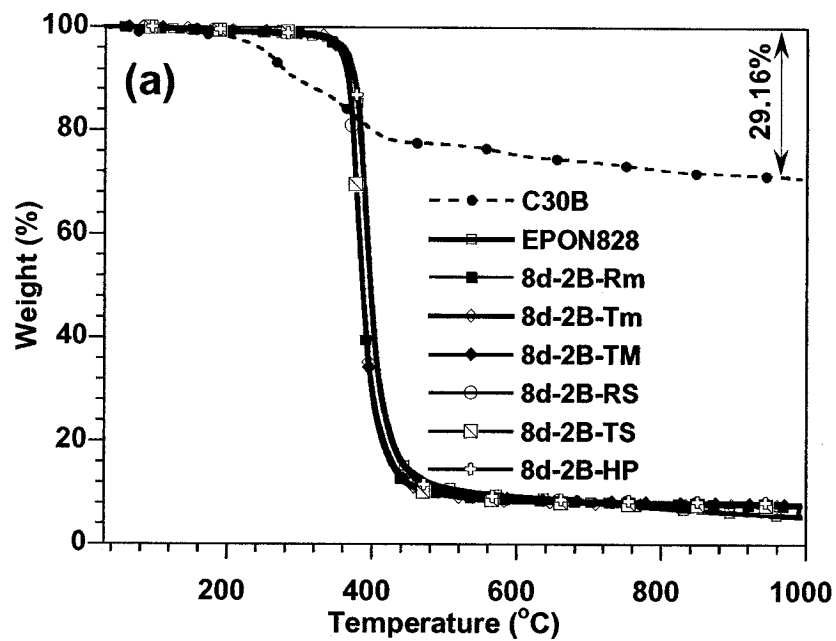


**Figure 6.18. TGA results for EPON828 resin and its nanocomposites made by different stirring methods**

The result indicates that the presence of clay C30B does not significantly influence the TGA results of this epoxy system. The  $T_{peak}$  values of decomposition (Figure 6.18b) are almost the same for the epoxy system and its nanocomposites (Note here that these

curves were shifted up in order to separate them). As discussed in Section 6.3.3, probably the hydroxyethyl groups of intercalant of C30B are “hidden” under the long hydrocarbon chains of the tallow of intercalant, thus inhibiting a direct interaction between these groups and the epoxy resin and resulting in an unchanged network. Therefore, the TGA characteristic of EPON828-D230 does not change with the presence of C30B.

TGA characteristics of EPON828-D230 and its nanocomposites made by Tm and TS stirring methods at different clay loadings at 200°C for 12 hours are shown in Figure 6.19. Again, the presence of clay C30B does not significantly influence the TGA results of this epoxy system if the error of 0.5 % is considered.

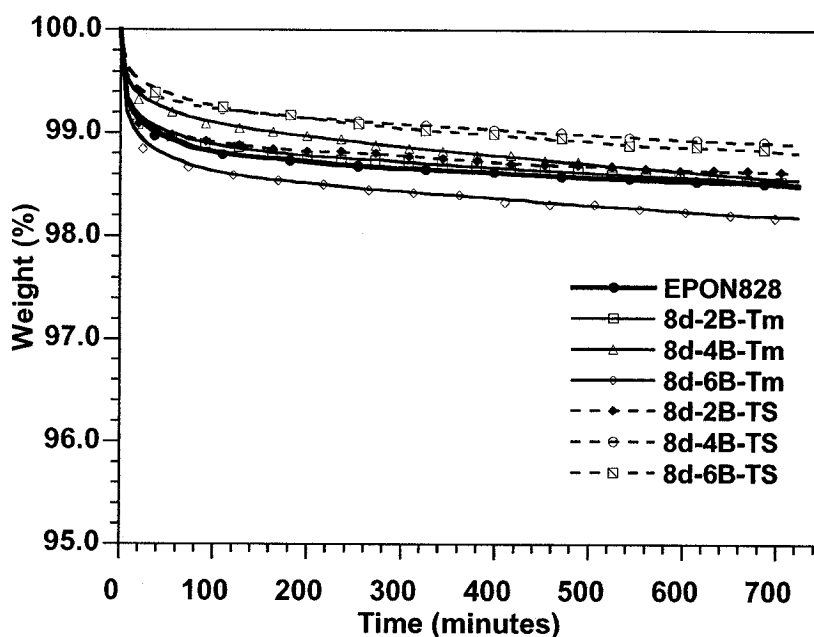


**Figure 6.19. TGA results for EPON828 resin and its nanocomposites made by Tm and TS stirring methods at different clay loadings**



#### 6.3.4.2. The effect of stirring time, speed and clay loading on LOI properties

The LOI test is a standard test to evaluate the flammability of materials. A high LOI value means that the flame is difficult to spread vertically from the top to the bottom. The LOI results for the epoxy system and its ENC based on EPON828 and 2 wt% C30B which were made by different mixing methods and cured with D230 are shown in Figure 6.20. It can be seen that the addition of 2 wt% of clay with Rm stirring improves LOI by 1.0 (from 24.0 to 25.0). With the same amount of clay with the Tm, TM, RS and HP methods, the LOI improves LOI by 1.5 (from 24.0 to 25.5) and 2.0 (from 24.0 to 26.0) with TS method. This shows that the addition of nanoclay improves the flame retardancy of the epoxy system. The better dispersion somewhat improves the LOI of nanocomposites. This may be explained by the fact that the diffusion of oxygen into the sample and transportation of the burning gas product out of the sample decrease with the presence of clay. After burning, nanocomposites show more char remains. It was also reported that one of nanocomposites flame retardant mechanisms is a consequence of high performance carbonaceous-silicate char built up on the surface during burning, which insulates the underlying materials and slows down the mass loss decomposition [150]. In addition, H<sub>2</sub>O can be formed during the burning due to the dehydration of HO-clay and results in a decrease in the temperature of the sample. Thus it slows down the burning process.

Stirring temperature does not show a strong effect on LOI results of nanocomposites in this case. There is a slight increase in the LOI of ENC prepared with the Tm stirring method compared to the LOI of ENC prepared with the Rm stirring method (from 25.0

for Rm method to 25.5 for Tm). Similarly for stirring at high speed, there is a slight increase in the LOI of ENC prepared with the TS stirring method as compared to the LOI of ENC prepared with the RS stirring method (from 25.5 for RS method to 26.0 for TS).

Stirring speed also shows its effect on the storage modulus of ENC. At the same stirring temperature of room temperature, the LOI of ENC prepared with the RS stirring method is higher than the LOI of ENC prepared with the Rm stirring method (from 25.0 for Rm method to 25.5 for RS). This is similar for stirring at 120°C; the LOI of ENC prepared with high speed stirring method (TS) is higher than LOI of ENC prepared with low speed stirring method (TM) and without stirring (Tm), respectively (from 25.5 for Tm and TM methods to 26.0 for TS).

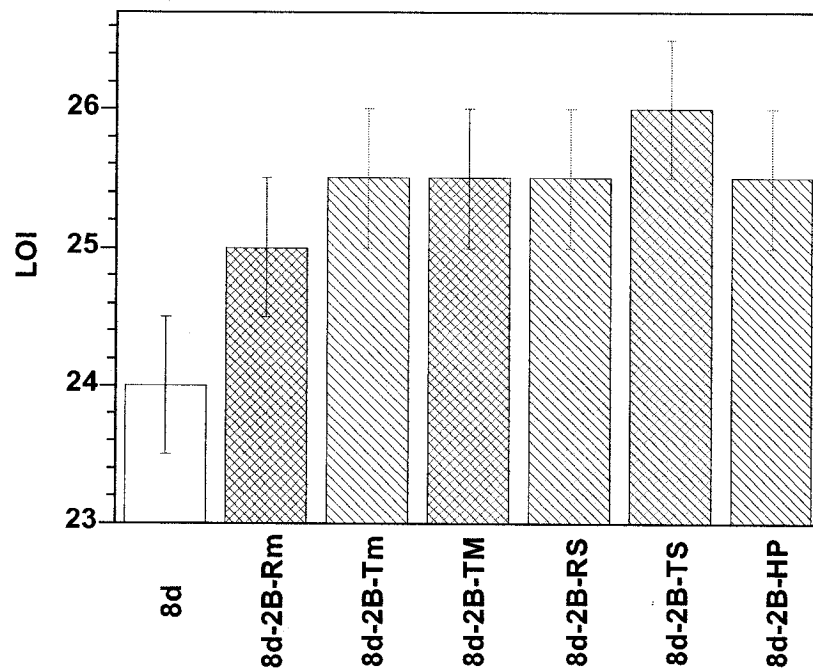


**Figure 6.20. LOI for EPON828-D230 system and its nanocomposites made by different stirring methods**

The LOI results for the epoxy system and its ENC based on EPON828 and different clay loadings made by Tm and TS methods and cured with D230 are shown in Figure 6.21. The result shows that the variation of clay loading does not show an effect on the LOI. However, it confirms the better improvement in LOI for nanocomposite prepared by TS stirring than by Tm stirring method. From the results obtained so far, it seems that the influence of both stirring temperature and speed on the thermal properties of ENC in this case are not significant.

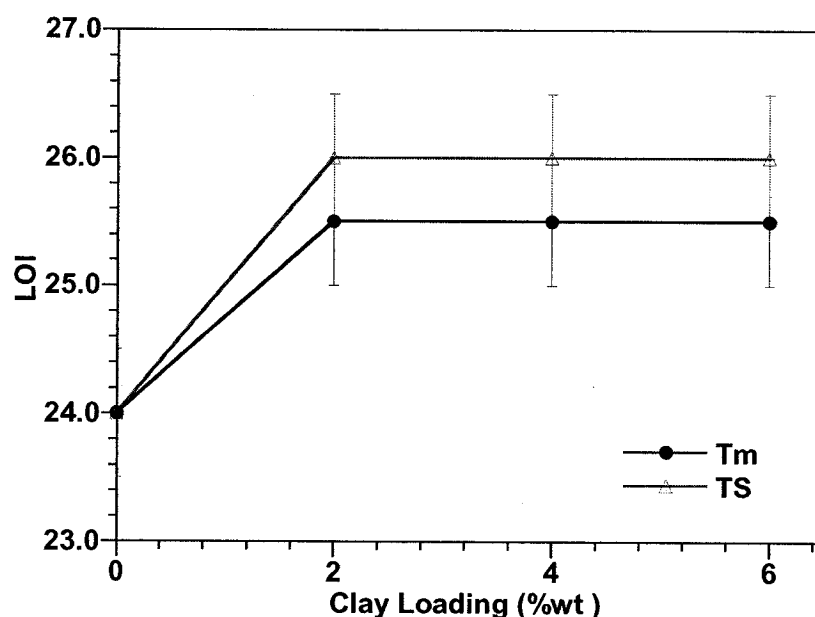


**Figure 6.21. LOI of 8d system and its nanocomposites at different clay loading made by Tm and TS methods**

### 6.3.5. Barrier properties

#### 6.3.5.1. The effect of stirring time and speed on water absorption

Water sorption as a function of time is illustrated in Figure 6.22 for the series of EPON828-D230 system and its nanocomposites made by different stirring methods.

Equilibrium water sorption values for all systems are shown in Table 6.4. It can be seen that the EPON828-D230 system reaches equilibrium at a low moisture content of about 1.9%. Similar results on the water absorption for DGEBA epoxy systems were reported [17, 151]. The equilibrium values show that the neat epoxy systems generally absorb more water than the layered silicate nanocomposite materials.

The mechanism of moisture diffusion in polymers has been extensively studied [152-154]. Moisture diffusion in epoxy resin can be represented by Fick's second law with a constant diffusivity,  $D$ , which describes the non-steady-state diffusion of a substance in the Cartesian coordinate system,  $x$ ,  $y$  and  $z$ :

$$\frac{\partial c}{\partial t} = D \left( \frac{\partial^2 c}{\partial x^2} + \frac{\partial^2 c}{\partial y^2} + \frac{\partial^2 c}{\partial z^2} \right) \quad (6.1)$$

where  $c$  is the concentration of the diffusing substance (water), and  $t$  is time. For one-dimensional diffusion through an infinite plate of thickness,  $h$ , Equation 6.2 can be reduced to:

$$\frac{\partial C}{\partial t} = D \frac{\partial^2 C}{\partial x^2} \quad (6.2)$$

The analytical solution of Equation 6.2 for the concentration profiles of a diffusing substance in an isotropic plane sheet of finite thickness can be described as a function of time  $t$  and distance  $x$ :

$$\frac{c_{(x,t)}}{c_{\infty}} = 1 - \frac{4}{\pi} \sum_{m=0}^{\infty} \frac{1}{(2m+1)} \times \exp\left[-\frac{D(2m+1)^2 \pi^2 t}{h^2}\right] \times \sin\left[\frac{(2m+1)\pi x}{h}\right] \quad (6.3)$$

where  $c_{\infty}$  is the saturation concentration of the absorbed substance. Upon solving Equation 6.2 with the following boundary conditions:  $c = 0$  when  $t = 0$ ,  $0 \leq x \leq h$ ;  $c = c_{\infty}$  when  $t > 0$ ,  $x = 0$ ,  $x = h$ ; and  $\partial c/\partial x = 0$  when  $x = 0$ ,  $t > 0$ , the relative moisture uptake is expressed as [17]:

$$\frac{M_t}{M_{\infty}} = 1 - \sum_{n=0}^{\infty} \frac{8}{(2n+1)^2 \pi^2} \times \exp\left[-\frac{D(2n+1)^2 \pi^2 t}{h^2}\right] \quad (6.4)$$

where  $M_t$  is the mass gain at reduced time and  $M_{\infty}$  is the maximum mass gain at the equilibrium state. In the initial stages of diffusion, Equation 6.4 can be approximated by:

$$\frac{M_t}{M_{\infty}} = 4 \left( \frac{Dt}{\pi h^2} \right)^{1/2} \quad (6.5)$$

Therefore, the diffusivity  $D$  can be calculated from the initial slope of the moisture gain,  $M_t/M_{\infty}$  versus time ( $t^{1/2}/h$ ):

$$D = \frac{\pi}{16} \left( \frac{M_t / M_{\infty}}{\sqrt{t} / h} \right)^2 \quad (6.6)$$

Data from the first few measurements of our experimental series have been fitted to this equation and the diffusion coefficient was determined. The prediction curves based on Equation 6.5 are also superimposed in the Figure 6.22. Results for the diffusion coefficient,  $D$ , are shown in Table 6.4.

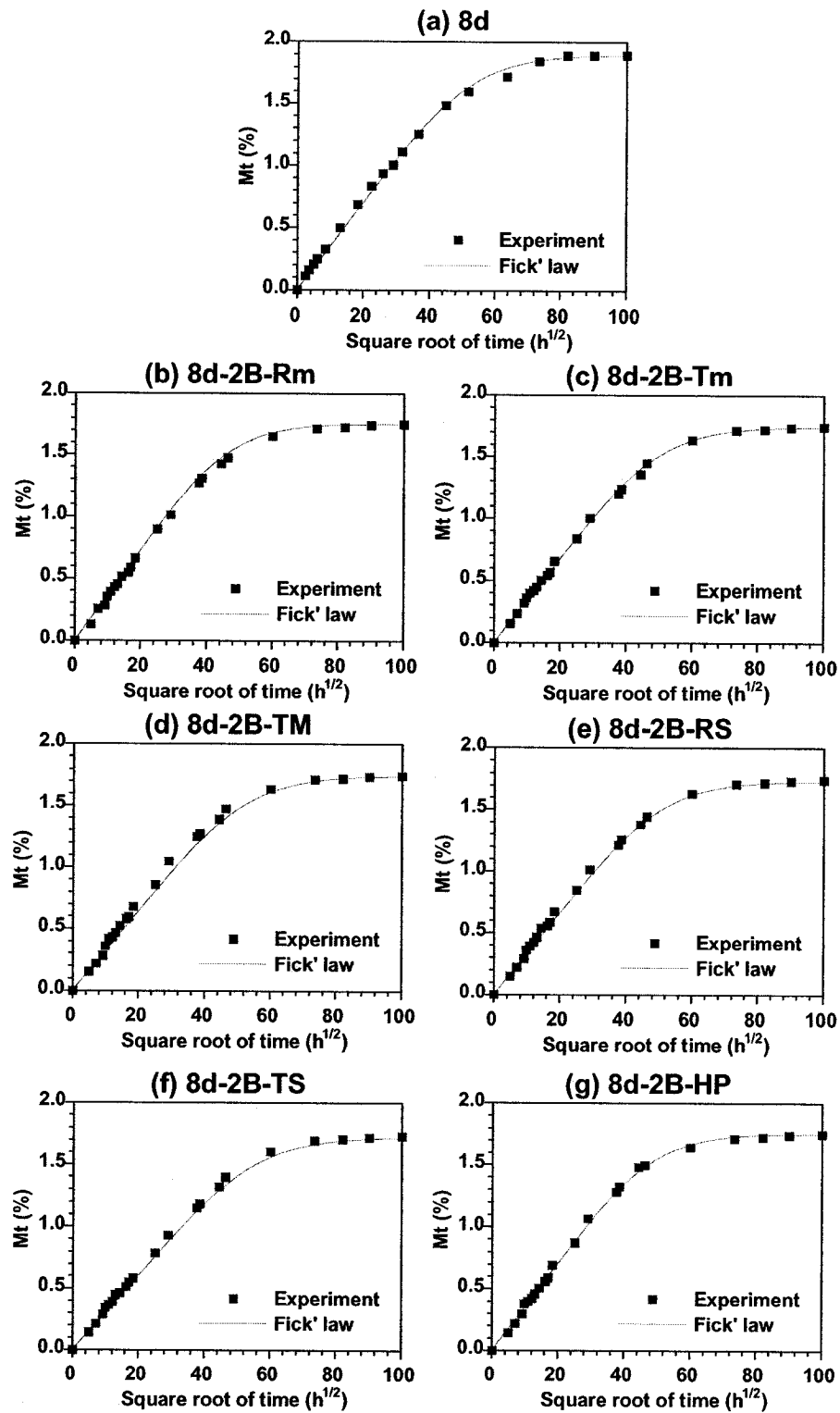


**Figure 6.22. Water absorption profiles for EPON828-D230 system and its nanocomposites made by different stirring methods**

**Table 6.4. Water uptake parameters for EPON828-D230 system and its nanocomposites made by different stirring methods**

Material	$M_{\infty}$ (%)	$D$ (mm <sup>2</sup> /s)
8d	1.90	$1.71 \times 10^{-7}$
8d-2B-Rm	1.75	$1.63 \times 10^{-7}$
8d-2B-Tm	1.74	$1.58 \times 10^{-7}$
8d-2B-TM	1.74	$1.44 \times 10^{-7}$
8d-2B-RS	1.73	$1.43 \times 10^{-7}$
8d-2B-TS	1.72	$1.21 \times 10^{-7}$
8d-2B-HP	1.75	$1.48 \times 10^{-7}$

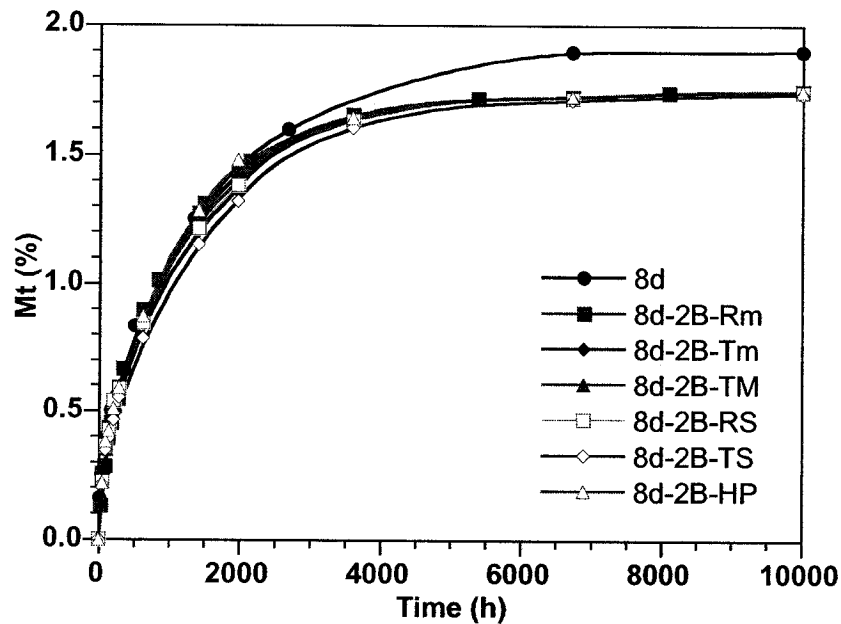


**Figure 6.23. Summary of water absorption for EPON828-D230 system and its nanocomposites made by different stirring methods**

The diffusion behavior of water into the epoxy system and its nanocomposites has been shown to be in good agreement with Fick's second law of diffusion [107, 155, 156]. The results show the decrease in diffusion coefficient with the presence of clay. The results also show that the level of dispersion has somewhat of an effect on the diffusion behavior

of water in nanocomposites. However, the level of dispersion does not show a strong effect on the  $M_{\infty}$ . It can also be seen that the addition of 2 wt% C30B decreases the water absorption of the epoxy system based on EPON828-D230 (Table 6.4 and Figure 6.23).

From the literature, nanoclay can be dispersed in epoxy to form conventional composite, intercalated nanocomposites, ordered and disordered exfoliated nanocomposites. Since nanoclay has a large ratio of length to thickness, gases and liquids should take a longer and more tortuous route to diffuse in or out of epoxy due to exfoliated nanoclay; this is called the barrier effect (as shown in Figure 6.24).

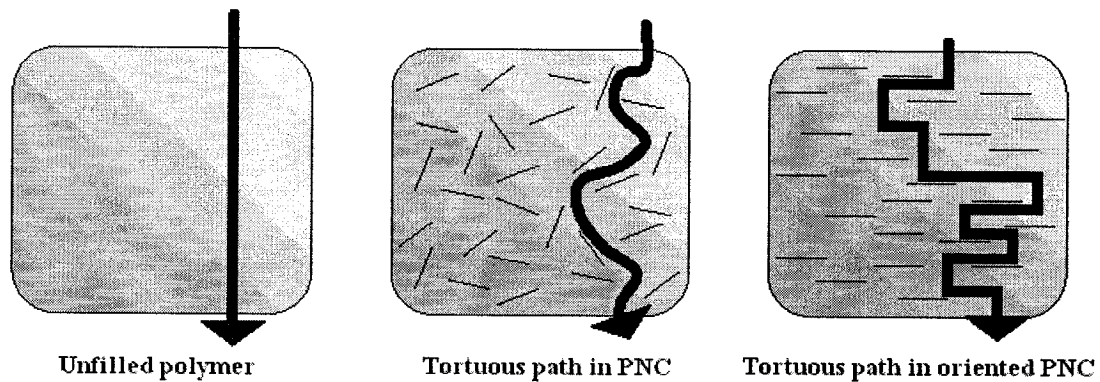


**Figure 6.24. Nanoclay improves barrier properties [157]**

#### **6.3.5.2. The effect of stirring time and speed on solvent resistance**

The solvent resistance results for the epoxy system and its ENCs based on EPON828 and 2 wt% C30B made by different stirring methods and cured with D230 are shown in Figures 6.25, 6.26 and Table 6.5. Apparently, the presence of 2 wt% of C30B increases the solvent resistance. The results also show that better dispersion and intercalation/exfoliation result in better solvent resistance. For instance, the solvent



resistance is in the order of TS > RS > TM > Tm > Rm > Epoxy, except for the specimen which was prepared by the HP method.

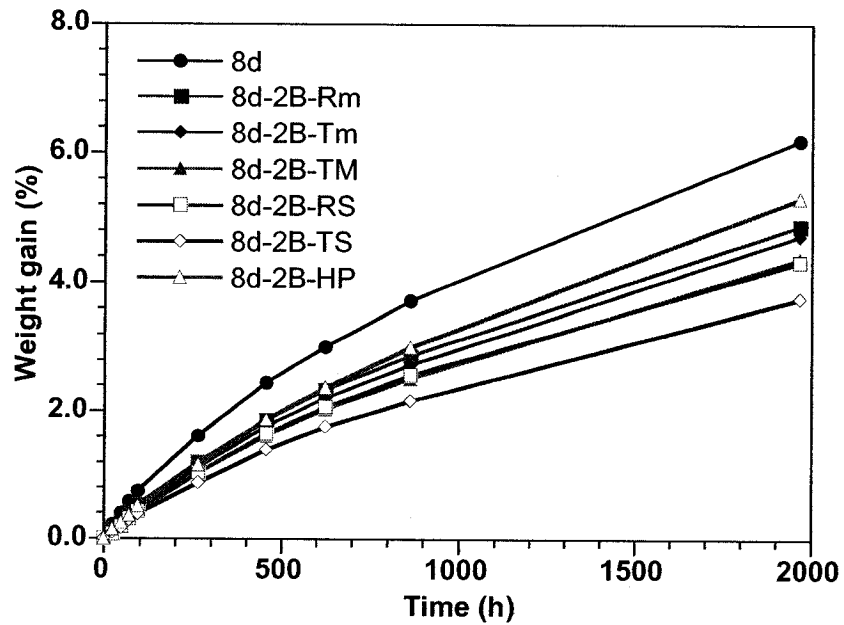


**Figure 6.25. Ethanol absorption for the EPON828-D230 system and its nanocomposites made by different stirring methods**

It is also very interesting that the presence of clay improves the toluene resistance much more than the ethanol resistance of epoxy. This may be explained by the fact that the toluene molecule is larger than the ethanol one. Thus it is more difficult for toluene to penetrate through the network of the ENCs than for ethanol.

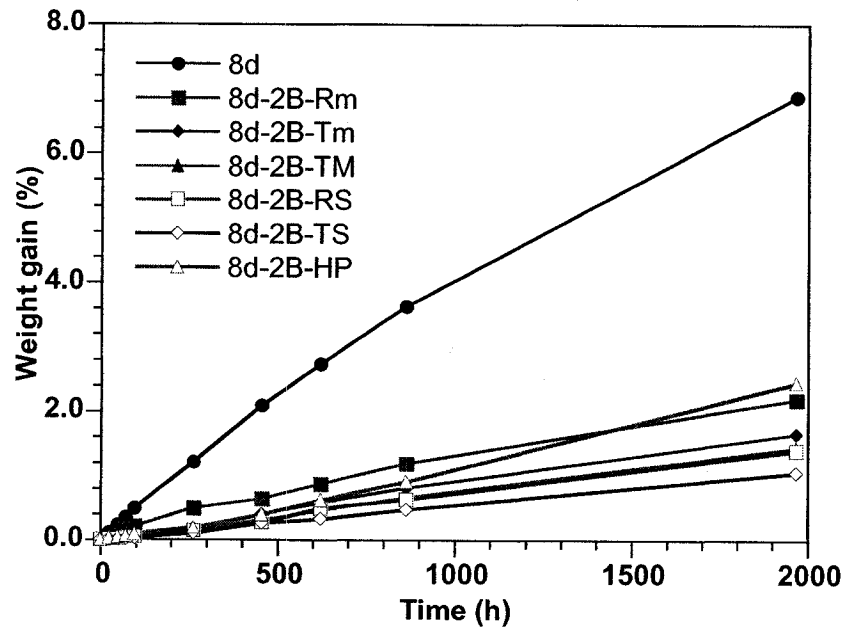


**Figure 6.26. Toluene absorption of the EPON828-D230 system and its nanocomposites made by different stirring methods**

**Table 6.5. Solvent resistance for the EPON828-D230 system and its nanocomposites made by different stirring methods after 1970 hrs**

Material	Absorption Percentage after 1970 hrs (%)	
	Ethanol	Toluene
8d	6.19	6.88
8d-2B-Rm	4.87	2.19
8d-2B-Tm	4.72	1.65
8d-2B-TM	4.36	1.44
8d-2B-RS	4.31	1.40
8d-2B-TS	3.76	1.06
8d-2B-HP	5.31	2.45

## 6.4. Effect of the chemistry of clays

Sample specifications for experiment set 6.4 are given in Table 6.6. These samples here are the same as the samples that were studied in section 5.4.

**Table 6.6. Sample specifications for experiment set 6.4**

Designation	Epon 828	Epicure 3046	Nanoclay	Mixing Method
8EP	100	35	0	-
<b>Cloisite 30B</b>				
8EP-2pB-Rm	100	35	2	Rm
8EP-2pB-Tm	100	35	2	Tm
8EP-4pB-Tm	100	35	4	Tm
8EP-2B-Tm	100	35	2.69	Tm
8EP-4B-Tm	100	35	5.5	Tm
8EP-6B-Tm	100	35	8.43	Tm
8EP-2B-TS	100	35	2.69	TS
8EP-4B-TS	100	35	5.5	TS
8EP-6B-TS	100	35	8.43	TS
<b>Nanomer I30E</b>				
8EP-2pE-Rm	100	35	2	Rm
8EP-2pE-Tm	100	35	2	Tm
8EP-4pE-Tm	100	35	4	Tm

### 6.4.1. Tensile and flexural properties

Tensile and flexural properties of 8EP and its nanocomposites were evaluated and are shown in Figures 6.27 and 6.28. Both clays result in an increase in modulus. A similar effect was discussed above in section 6.3 for both modulus and strength. The modulus of the nanocomposites can be improved by adding nanoclay. However, the strength does not follow the same trends as the modulus.

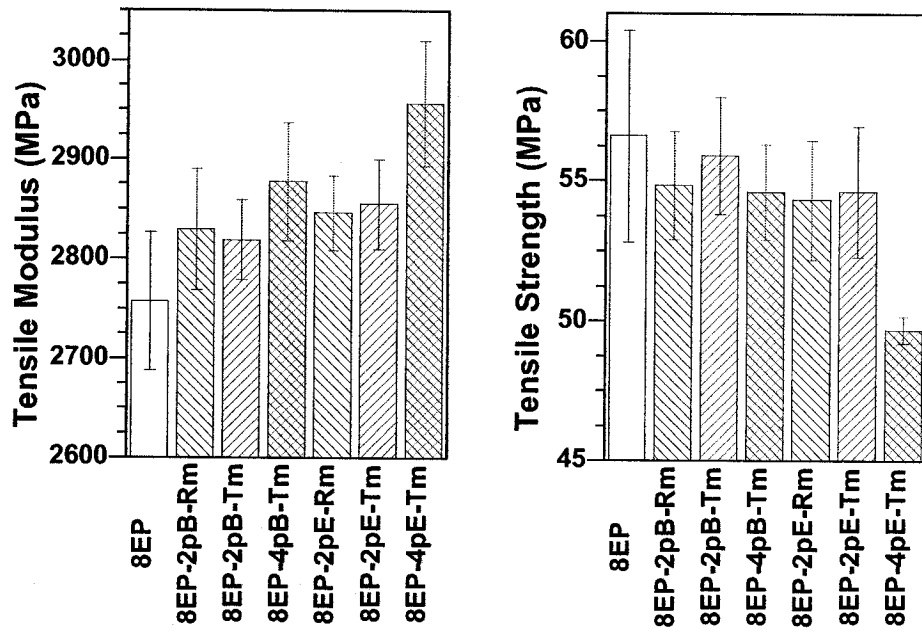


Figure 6.27. Tensile properties for 8EP and its nanocomposites: (a) tensile modulus and (b) tensile strength

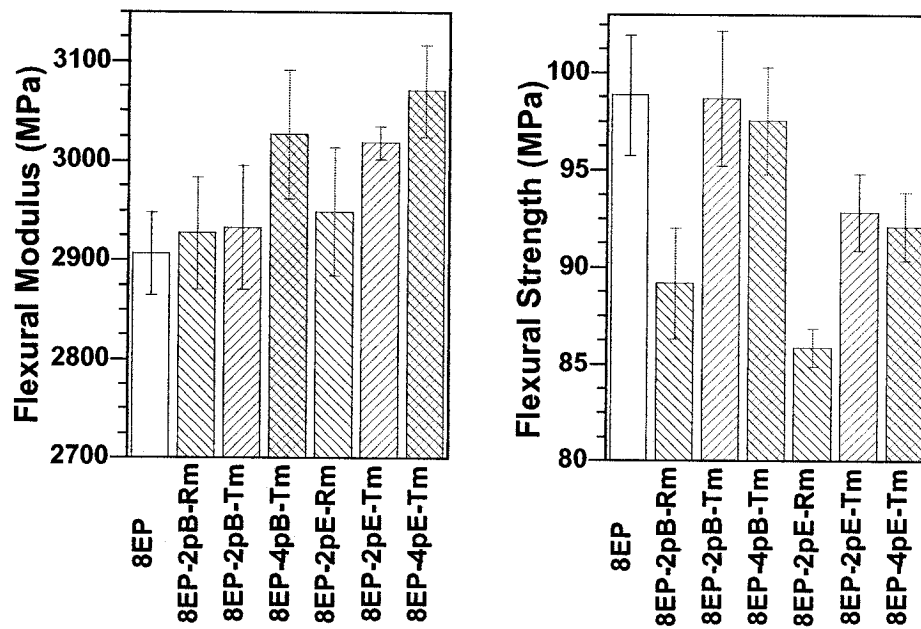


Figure 6.28. Flexural properties for 8EP and its nanocomposites: (a) flexural modulus and (b) flexural strength

As confirmed by X-ray diffraction and TEM and SEM photographs, stirring at higher temperature gives a better dispersion of nanoclay in epoxy and a lower concentration of voids in the aggregates than stirring at room temperature, as discussed earlier. This explains why, at the same 2 phr level of nanoclay, the 8EP-2pB-Tm sample in which the epoxy and clay were stirred at high temperature (Tm) gives higher strength (especially in flexion) than 8EP-2pB-Rm in which the epoxy and clay were stirred at room temperature (Rm).

Generally speaking, other conditions being equal, I30E gives a higher modulus than C30B but the inverse holds true for the strength. The I30E nanocomposites are more brittle than the C30B nanocomposites. This may be caused by the occurrence of homopolymerization inside the galleries of I30E, creating denser crosslinks around the clay particles. On the other hand, this homopolymerization can also create a nonuniform structure, since fewer epoxy groups form crosslinks with amine curing agent, possibly resulting in some free amine groups in the final structure. This may explain why the strength (and possibly to some extent the  $T_g$ ) are reduced for I30E nanocomposites as compared with C30B nanocomposites. In addition, after stirring clay with epoxy, the viscosity of the I30E series increases significantly. As a result, as discussed earlier, it is much more difficult to remove micro-voids inside the aggregates in these samples (although vacuum has been used in order to reduce the impact of such effects).

#### **6.4.2. Flammability - LOI**

The LOI results for epoxy and ENCs based on EPON828 and C30B, I30E which were made by Rm and Tm then cured with EPICURE3046 are shown in Figure 6.29. The LOI

improves by 1.5, 2.5 and 4.0 (from 25.5 to 27.0, 28.0 and 29.5) for nanocomposites with 2phr C30B made by the Rm, Tm methods and 4 phr of C30B made by the Tm method, respectively. The same effect on the LOI is observed with the presence of I30E; the LOI improves by 1.0, 2.0 and 4.5 (from 25.5 to 26.5, 27.5 and 30.0) for nanocomposites with 2phr I30E made by the Rm, Tm methods and 4 phr of I30E made by the Tm method, respectively. During burning, oil-like flaming materials dripped down for the neat epoxy system, but no drip can be seen for epoxy nanocomposite specimens. Since dripping flaming materials may help to spread fire and harm the surroundings, the reduction of flaming drips is also important for resisting fire. After burning, nanocomposites also show more char remains than the epoxy system.

The LOI results for EPON828- EPICURE 3046 and its nanocomposites (at different clay loadings) made by the Tm and TS methods are shown in Figure 6.30. The LOI improves by 3.0, 4.0 and 4.0 (from 25.5 to 28.5, 29.5 and 29.5) for nanocomposites made by the Tm method with 2, 4 and 6 wt% C30B, respectively, while it improves by 5.0, 5.5 and 5.0 (from 25.5 to 30.5, 31.0 and 30.5) for nanocomposites made by the TS method with 2, 4 and 6 wt% C30B, respectively. The result confirms better improvement in LOI for the TS stirring method than for the Tm method. The variation of clay loading does not show linear improvement in the LOI of epoxy nanocomposites. This may be because of the poorer dispersion of clay in epoxy systems at high clay loading.

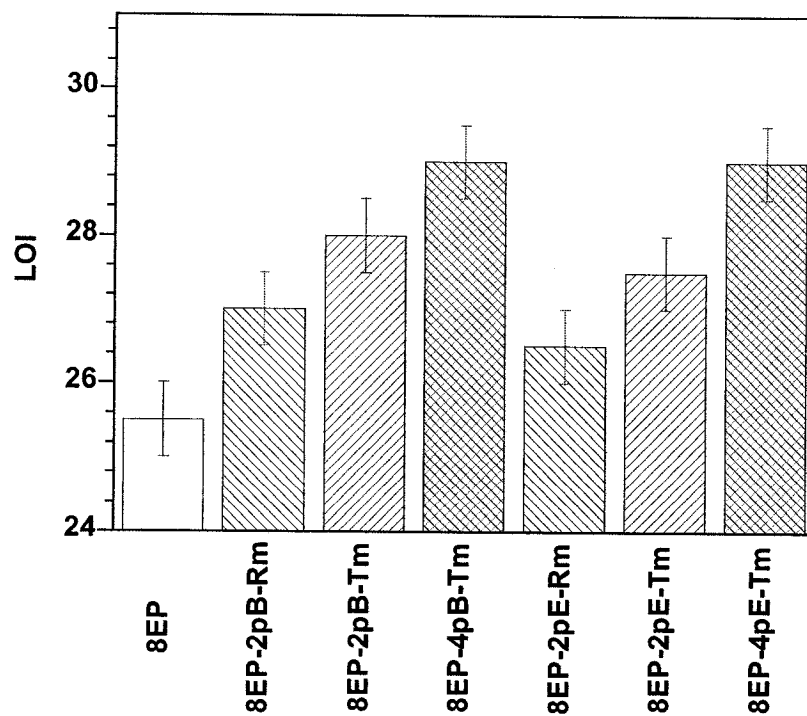


Figure 6.29. LOI for 8EP system and its nanocomposites with two different types of clay made by different stirring methods

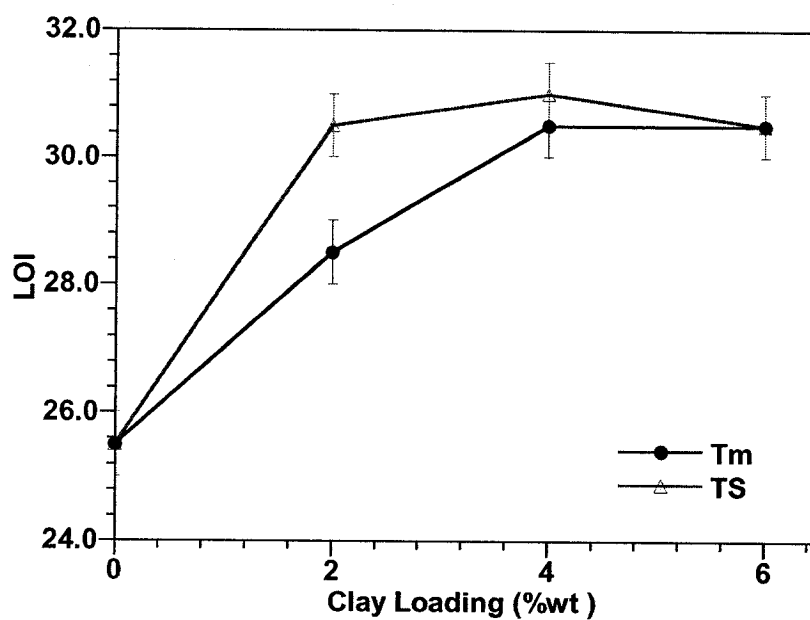


Figure 6.30. LOI of 8EP system and its nanocomposites at different clay loading made by Tm and TS methods

## 6.5. Effect of the chemistry of hardeners

Sample specifications for experiment set 6.5 are given in Table 6.7.

**Table 6.7. Sample specifications for experiment set 6.5**

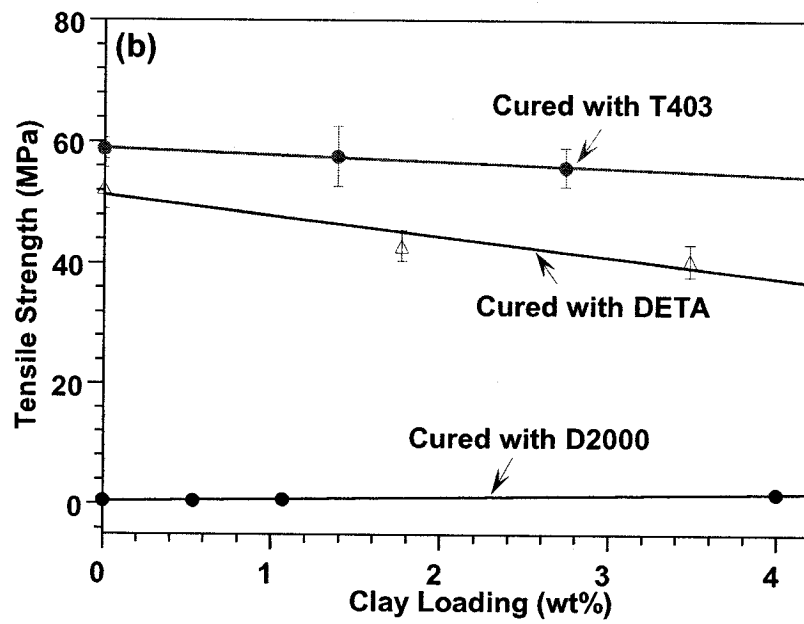
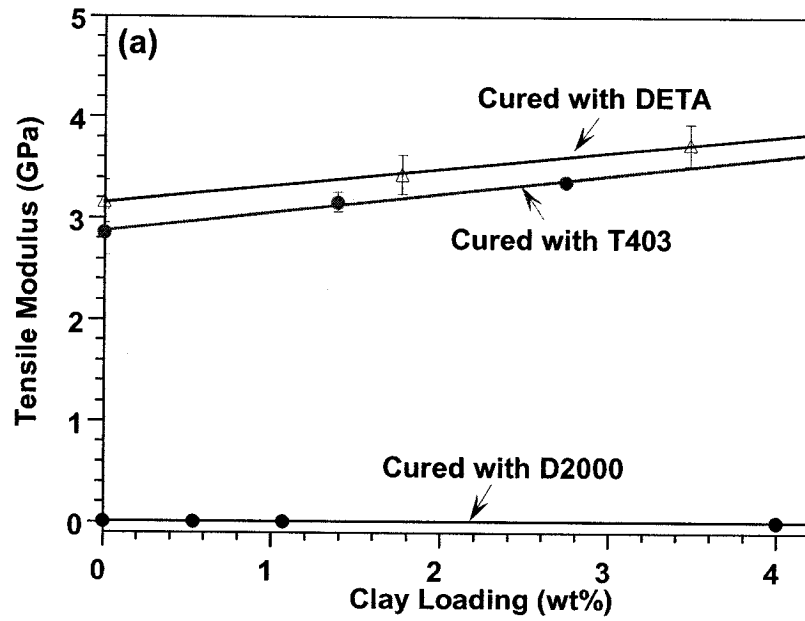
Designation	EPON 828	Hardener	Cloisite 30B	Stirring method
<b>DETA (DE)</b>				
8DE	100	10.9	0	-
8DE-xB-Tm	100	10.9	2, 4, 4.6	Tm
<b>Jeffamine T403 (T)</b>				
8T	100	42	0	-
8T-xB-Tm	100	42	2, 4, 5.9	Tm
<b>Jeffamine D2000 (D)</b>				
8D	100	270	0	-
8D-xB-Tm	100	270	2, 4, 15.4, 23.6	Tm
8D-6B-TS	100	270	23.6	TS
<b>Jeffamine D230 (d)</b>				
8d	100	32	0	-
8d-6B-TS	100	32	8.4	TS
<b>Boron trifluoride BF<sub>3</sub> (BF)</b>				
8BF	100	3	0	-
8BF-6B-TS	100	3	6.6	TS

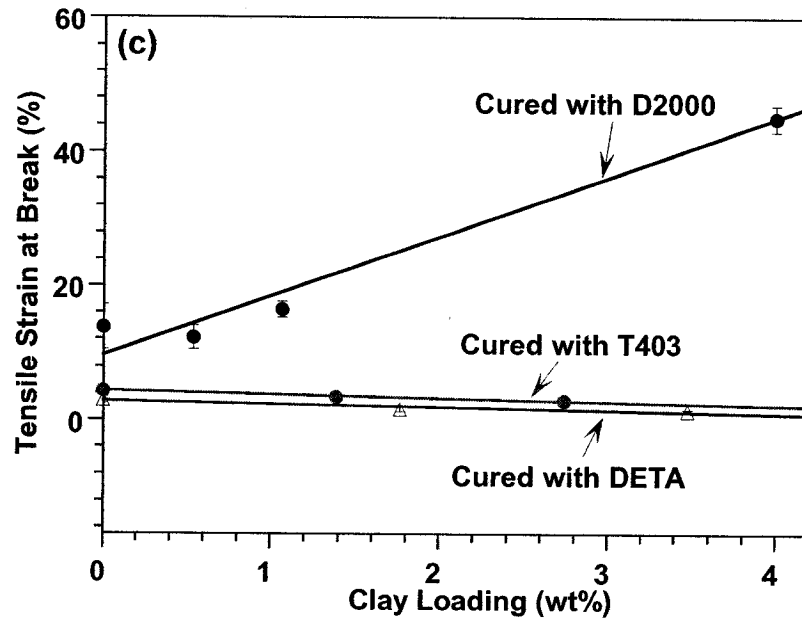
### 6.5.1. Tensile properties

Figure 6.31 provides the tensile properties of epoxy and its nanocomposites cured with the three types of curing agent (DETA, T403 and D2000). The presence of nanoclay results in an increase in modulus for all cases [11, 22]. In addition, the higher is the concentration of organoclay, the higher is the modulus. All cases show a linear increase in modulus with the clay loading. However, the level of improvement in modulus is very much dependent on the type of curing agent. Compared to the EPON828-DETA system and the EPON828-T403 system, the EPON828-D2000 (Figure 6.31a) exhibited a much



higher improvement in modulus with the presence of nanoclay. With only 1.07 wt% of clay, the modulus improves up to 31%. The modulus increases more than 120% (2 times higher compared to neat epoxy) at 6 wt% of the clay loading. This means that the presence of clay has a strong effect on the modulus of soft epoxy. For a rigid system, the presence of nanoclay has less influence on the modulus than for soft epoxy. The presence of 3.5 wt% nanoclay C30B improves the modulus by 18.4%. On the other hand, for the nanocomposite cured with T403; the presence of 2.74 wt% nanoclay C30B improves the modulus by 18.0 %. The presence of clay has different effects on the strength and strain at break depending on the behavior of the neat epoxy (Figures 6.31b and 6.31c). For the rigid EPON828-DETA system, the presence of clay reduces the strength and strain at break of nanocomposite compared to neat epoxy. For the nanocomposites EPON828-T403, the presence of clay has less negative effect (as discussed above) on the strength and the strain at break compared to EPON828-DETA system. On the other hand, the presence of clay increases the strength and the strain at break for the system cured with D2000, which is representative of soft and weak materials. With only 1.07 wt% of clay, strength improves up to 43% and strain at break up to 19%. When the clay loading increases to 6 wt%, the strength and strain at break increase up to 430% and 410% compared to the epoxy system, respectively.





**Figure 6.31. Tensile properties for epoxy and its nanocomposites cured with D2000, T403, and DETA: (a) tensile modulus, (b) tensile strength, and (c) strain at break**

From the above curves, the slopes of tensile curves versus clay loading are summarized in Table 6.8. It is clear that the effect of clay on the mechanical behavior of the epoxy nanocomposites which were cured with different curing agents is quite distinct. The slope of modulus is positive for all cases. However, it is very much dependent on the epoxy system for strength and strain.

**Table 6.8. Slope of tensile properties curves versus clay loading**

Nanocomposites	Slope of curves		
	D2000	T403	DETA
Tensile modulus	+0.0008	+0.18	+0.17
Tensile strength	+0.35	-0.79	-3.40
Tensile strain at break	+8.96	-0.51	-0.53

### 6.5.2. Flammability - LOI

The LOI results for epoxy and ENC cured with D2000, T403 and DETA are shown in Figure 6.32. The results indicate that the LOI are different for epoxy systems which were prepared by the Tm method and cured with D2000, T403 and DETA. The results also show that the addition of C30B somewhat improves the LOI of ENCs compared to neat epoxy systems. This is very similar like those cured with D230 (Figure 6.21). However, the level of improvement in LOI for these three hardeners (D2000, T403 and DETA) and D230 is small compared to EPICURE 3046 (Figure 6.30). With D2000, the LOI improves by 1.0 and 1.5 (from 20.5 to 21.5 and 22.0) for nanocomposites containing 1.07% and 4.0% C30B. With T403, the LOI improves by 0.5 and 1.1 (from 24.5 to 25.0 and 25.6) for nanocomposites which contain 1.4% and 4% C30B, respectively. With DETA, the LOI improves by 1.5 and 1.7 (from 27.0 to 28.5 and 28.7) for nanocomposites which contain 1.8% and 4.0% C30B, respectively. Again, nanocomposites also show more char remaining after burning than the epoxy system cured with the same hardener. Chemistry of hardener shows an influence on the LOI of epoxy systems and epoxy nanocomposites. Among these hardeners used, the presence of nanoclay only has a strong effect on the LOI of epoxy system based on EPICURE 3046. Recalling the structure of these hardeners (from Chapter 3), one can see that DETA, D230, and D2000 are diamines (primary amines) while T403 is a triamine but it also belongs to the primary amine group. On the other hand, EPICURE 3046 is an aliphatic amidoamine containing triethylene tetramine and tall oil fatty acid polyamide. Tall oil fatty acid is produced by the fractional distillation of tall oil. It is predominately straight chain, 18 carbon mono- and di-unsaturated fatty acids, mainly oleic and linoleic acid). EPICURE 3046 contains both

primary amine and polyamide. This difference in chemistry of hardener may influence the LOI of nanocomposites compared to neat epoxy. Generally speaking, there are three items necessary to support the combustion of polymer: oxygen, heat source and decomposition products of polymer. They must all be present in the same place at the same time to support the combustion of polymer. If any of them is missing, the fire will be extinguished. During the combustion process, both diffusion of decomposition products out of epoxy and diffusion of oxygen into epoxy can be inhibited. Therefore, the flame combustion can be retarded.

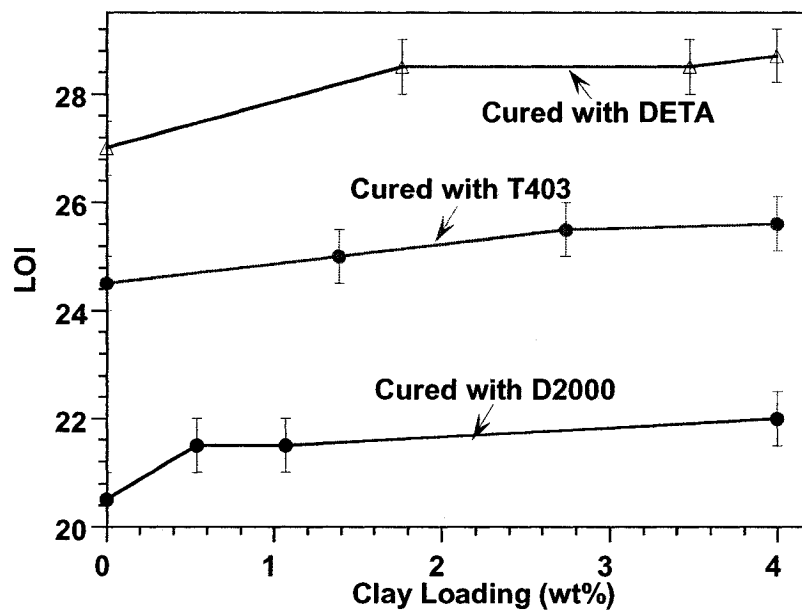


**Figure 6.32. LOI of epoxy systems and their nanocomposites cured different hardeners**

### 6.5.3. Fracture toughness

From the results obtained so far, the TS method has a strong positive effect on the critical stress intensity factor and the critical strain energy release rate for EPON828-D230 resin (section 6.3.2). It is interesting to know the effect of this stirring method on fracture toughness for other epoxy systems. The  $K_{IC}$  and  $G_{IC}$  for EPON828-D2000 and EPON828-BF<sub>3</sub> systems and their nanocomposites at 6 wt% C30B made by the TS method are shown in Figures 6.33 and 6.34. For the EPON828-D2000 system, it shows 377% (4.77 times) and 838% (9.38 times) increases respectively, in  $K_{IC}$  and  $G_{IC}$  at 6 wt% C30B compared to neat epoxy system, but 117% (2.17 times) and 363% (4.63 times) increase for EPON828-BF<sub>3</sub>. However only 47.9 % (1.48 times) and 40.7% (1.41 times) increase in  $K_{IC}$  and  $G_{IC}$  at 6 wt% C30B were observed for EPON828-D230 (as indicated in Figure 6.15 and redrawn in Figure 6.35), respectively compared to neat epoxy system. The results show the huge improvement in fracture toughness for nanocomposites based on two epoxy systems EPON828-D2000 and EPON828-BF<sub>3</sub> in the presence of 6 wt% C30B. But there is not much improvement in  $K_{IC}$  and  $G_{IC}$  for EPON828-D230. The level of increase in  $K_{IC}$  and  $G_{IC}$  may depend on the behaviour of the systems (One can see that the  $K_{IC} \text{ (EPON828-D230)} > K_{IC} \text{ (EPON828-BF}_3\text{)} > K_{IC} \text{ (EPON828-D2000)}$ ). It also depends on the level of dispersion and intercalation/exfoliation of organoclay in nanocomposites (as discussed above). The XRD results for the EPON828-D2000, EPON828-D230, EPON828-BF<sub>3</sub> systems and their nanocomposites based on 6 wt% C30B shown in Figure 6.36 confirm that the level of intercalation/exfoliation of the nanocomposites based on the three epoxy systems follows the order 8D-6B-TS > 8BF-6B-TS > 8d-6B-TS.

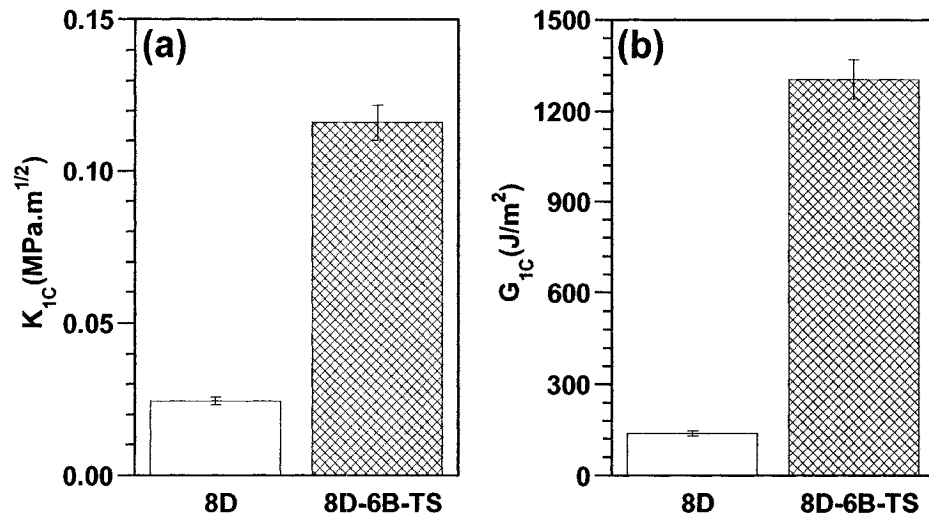


Figure 6.33. (a)  $K_{1C}$  and (b)  $G_{1C}$  for EPON828-D2000 resin and its nanocomposites made by the TS method

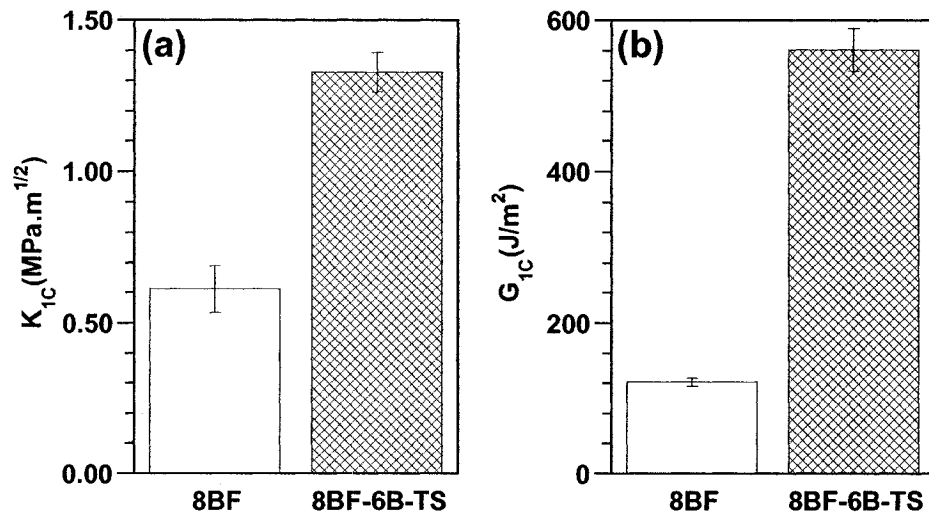


Figure 6.34. (a)  $K_{1C}$  and (b)  $G_{1C}$  for EPON828-BF<sub>3</sub> resin and its nanocomposites made by the TS method

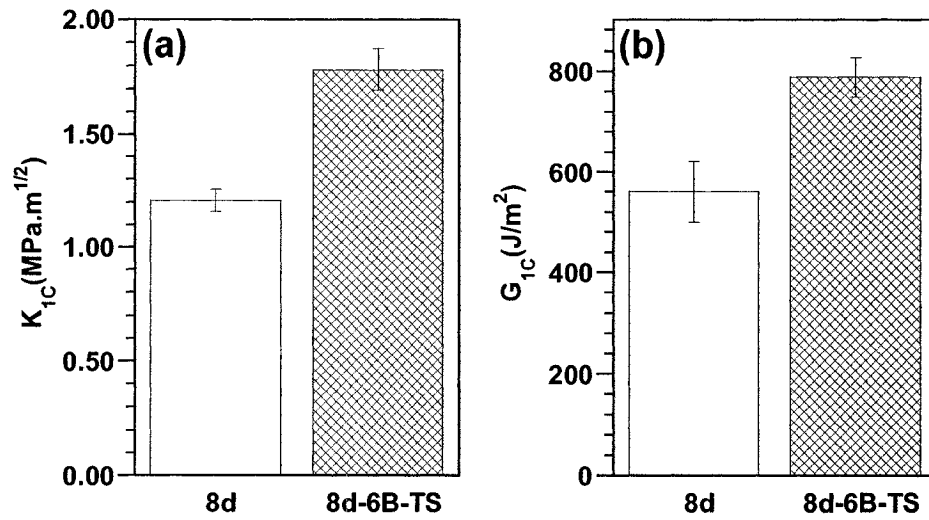


Figure 6.35. (a)  $K_{1C}$  and (b)  $G_{1C}$  for EPON828-D230 resin its nanocomposites made by TS method (results from Figure 6.15)

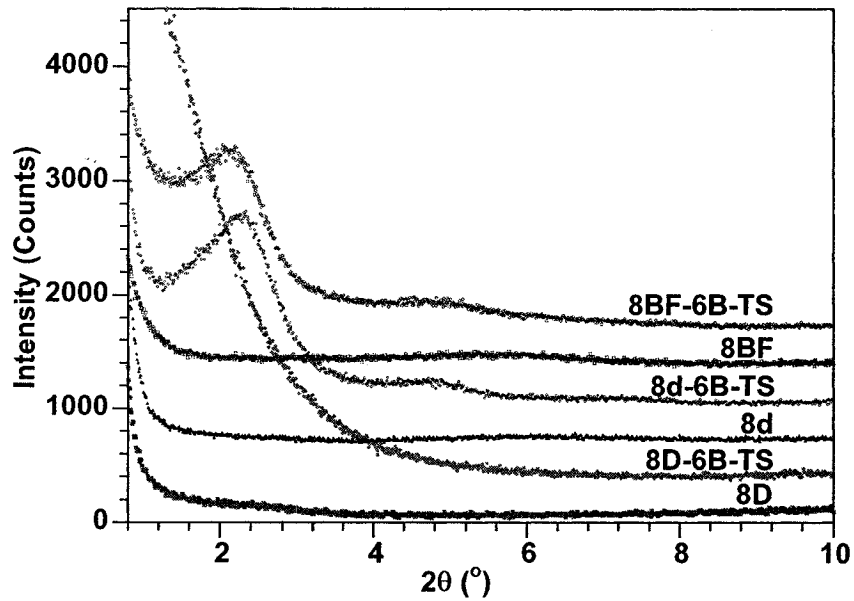


Figure 6.36. XRD results for EPON828-D2000, EPON828-D230, EPON828-BF<sub>3</sub> systems and their nanocomposites with 6wt% C30B made by TS method



## 6.6. Summary

As for conventional composites, the mechanical properties of epoxy clay nanocomposites are strongly influenced by the quality of clay dispersion, the interface interaction between organoclay and matrix, and the clay loading. As shown in Chapter 4 there are several different levels of dispersion of organoclays in the matrix, ranging from exfoliated or delaminated clay layers to non-intercalated stacks or intercalated stack, multiple-stack aggregates and macro-aggregates. The quality of clay dispersion and clay size distribution are strongly dependent on the stirring technique and conditions, the curing conditions and the chemistries of hardener and organoclays. The intercalation and exfoliation do not automatically provide the best mechanical performance because the mechanical performance is not only controlled by the nano-structure but also by the macro- and micro-structure that exist in the system. The presence of aggregates even at the micro-size can have a great negative impact on the mechanical performance (especially the strength, strain and ductility) because they are the weakest points in the system, which will initiate and promote failure under stress.

The findings in this study are quite superior to other data reported in the literature for glassy ENC's, where only a loss in tensile strength was reported [11, 12, 18, 27, 41, 45, 91]. The increase in tensile strength seems to reach a plateau at 4wt% clay loading. The modulus is quite linearly proportional to clay loading in the studied loading range, which likely indicates that this relationship obeys the rule of mixture. Further studies on the rule of mixture and other mechanical theory will be addressed in the following chapter. A significant loss in strain as the result of increase in high modulus for the ENC's was also

seen. A similar trend was also observed for compressive properties.

Processing parameters have an important influence on the dispersion of clay in the matrix and thus on mechanical properties of epoxy nanocomposites. A new processing method developed and employed to make well-dispersed epoxy layered silicate nanocomposites is described. Well dispersed nanocomposites have been achieved with high speed and high-temperature stirring. This technique is simple; no solvent is needed to achieve a good dispersion and intercalation/exfoliation of clay into an epoxy system. Stirring with high speed breaks down clay aggregates into smaller ones and results in better intercalation/exfoliation of clay in epoxy especially for curing at high temperature. The presence of C30B does not influence the  $T_g$  of epoxy, but it affects the mechanical properties of epoxy materials. The presence of clay results in an increase in modulus for all cases of stirring. The better is the dispersion of clay in epoxy, the higher is the storage modulus of nanocomposite. It is interesting that high speed (RS and TS) can help to break down the aggregates to a sub-micro dispersion and bring back the strength equal to or even higher than the neat epoxy (EPON828-D230). The reinforcing effect of nanoclay is strongly dependent on the nature of the neat polymer, and the nanoclay has a more positive effect on the mechanical properties in the rubbery region (as indicated in DMA results) than in the glassy one.

Better dispersion with the homogenizer provides improvement in the fracture toughness of epoxy systems. The level of increase in  $K_{IC}$  and  $G_{IC}$  depends on the behaviour of the systems. It also depends on the level of dispersion and intercalation/exfoliation of organoclay in nanocomposites (as discussed above). There is a huge improvement in

fracture toughness of EPON828-D2000 and EPON828-BF<sub>3</sub> epoxy systems with the presence of clay. For the EPON828-D2000 system, it shows 377% (4.77 times) and 838% (9.38 times) increases respectively, in  $K_{IC}$  and  $G_{IC}$  at 6 wt% C30B compared to the neat epoxy system.  $K_{IC}$  and  $G_{IC}$  increase 117% (2.17 times) and 363% (4.63 times), respectively for EPON828-BF<sub>3</sub>.

Chemistry of clay and hardeners has an effect on the properties of epoxy nanocomposites. At the same clay loading, I30E gives a higher modulus than C30B but the inverse holds true for the strength. Different hardeners result in different behavior of epoxy systems and hence the presence of clay shows different effects on mechanical properties. Flammability of epoxy nanocomposites decreases with the presence of clay, especially in the epoxy system cured with EPICURE 3046.

The addition of clay in the epoxy matrix also results in an improvement in water and solvent resistance. The diffusion behavior of water into the epoxy system and its nanocomposites has been shown to be in good agreement with Fick's second law of diffusion. The results show a decrease in diffusion coefficient with the presence of clay. The results also show that the level of dispersion has somewhat of an effect on the diffusion behavior of water nanocomposites. The dispersion level of clay in epoxy has a great effect on the solvent resistance, especially with toluene. The results show that better dispersion and intercalation/exfoliation result in better solvent resistance. It is also very interesting that the presence of clay improves the toluene resistance much more than the ethanol resistance of epoxy. The level of ethanol and toluene absorption of epoxy was reduced 1.6 times and 6.5 times (after 1970 hours) respectively with the presence of 2

wt% C30B (nanocomposite was prepared by the TS stirring method).

The dispersion and curing process of nanoclays in epoxy have been studied in Chapters 4 and 5. The following stage is the performance properties of epoxy nanocomposites. One knows that the properties of composite materials are strongly influenced by the properties of the components, by the geometry of the filler phase (the size, the shape and the size distribution, thus the aspect ratio), by the morphology of the system, by the nature of the interface between the phases and by the volume fraction of reinforcements etc. For nanocomposites reinforced with nanoclay, their properties also depend on the level of dispersion and intercalation/exfoliation of nanoclay in the matrix. Nanoclay fillers can be present in the form of sheets of one nanometer thick and hundreds to thousands nanometers wide or in the form of stacks or even large aggregates, depending on the quality of dispersion of clays in the matrix. Therefore, they can make a great contribution to the properties of the materials.

# Chapter 7

## **Reinforcing effect of organoclay in epoxy resins with characteristics varying over a broad range from rubbery to glassy**

### **7.1. Challenges and objectives**

Chapter 6 investigated the performance of ENCs with different levels of dispersion and different chemistries of clays and hardeners. The effect of adding nanoclay on the mechanical properties of epoxy has been discussed; however, it has not been clear what mechanism governs the reinforcing effect of organoclay in thermoset epoxy systems with characteristics varying over a broad range from rubbery to glassy. Moreover, there has been no study on this topic.

The objective of this chapter is to understand how the clay disperses in epoxy matrices with large differences in behavior at room temperature, as well as how the clay affects the  $T_g$  and mechanical properties of these epoxy matrices.

## 7.2. Methodology and experiment

In order to understand the reinforcing effect of organoclay in thermoset epoxy resins, whose characteristics can vary over a broad range from rubbery to glassy, different epoxy systems from rubbery to glassy are chosen to have very similar chemistry in order to minimize its impact on the comparison of properties. In addition, all the fabrication steps of the nanocomposites, such as dispersing clay in the epoxy resin, mixing this mixture with hardener, curing, etc., were also kept the same. As in all experiments throughout this study, only one type of epoxy resin (EPON828), two types of hardener come from the same chemical family (Jeffamine D2000 and Jeffamine D230) as well as their mixtures were used. With this design of materials, the structure of rubbery and glassy epoxy system after being cured is presented schematically in Figure 7.1.

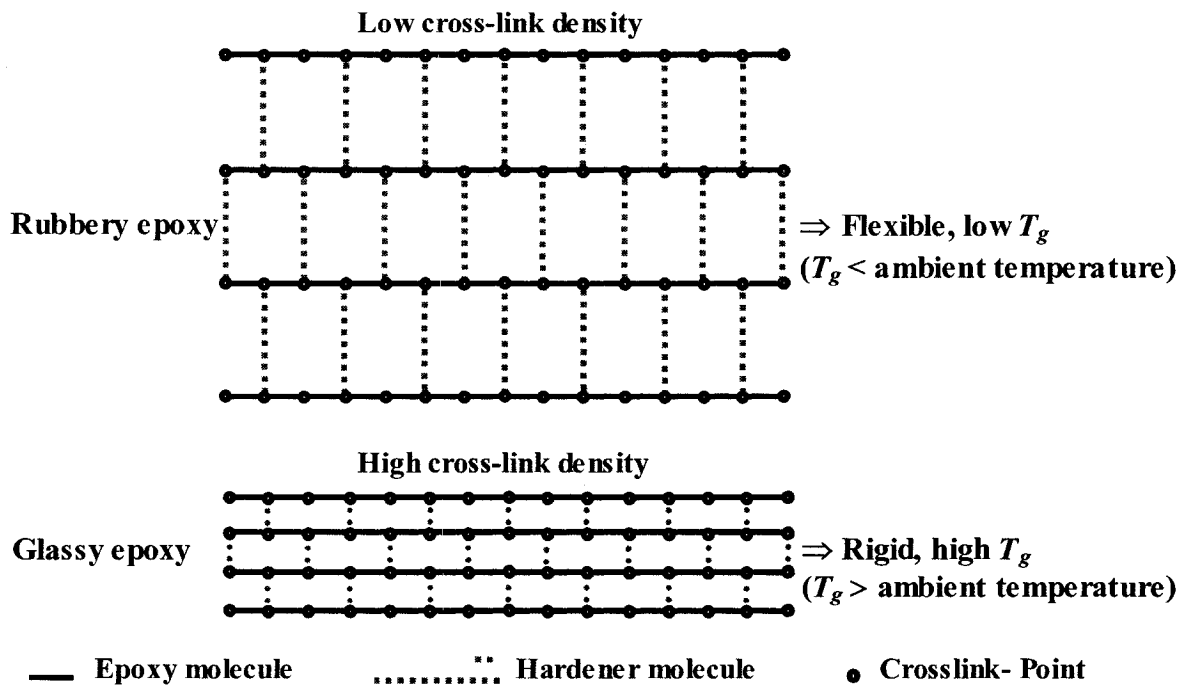


Figure 7.1. An example for the structure of rubbery and glassy epoxy systems

The intercalation/exfoliation of the nanoclay in the polymer matrix was studied by WAXRD on the surface of the samples with a Bruker Discover 8 powder X-ray diffractometer with  $\text{CuK}\alpha$  radiation. The experiments were conducted on the exposed surface of specimens prepared by casting. A Hitachi-S4700 FEGSEM was used to observe the dispersion of clay in the epoxy matrix at the micro-level, as well as the fracture surface of the cured epoxies and epoxy nanocomposites. For clay dispersion at the nano-level, ultra-thin (50 to 80 nm) sections of nanocomposite samples were prepared with a cryo-ultramicrotome and supported on a copper 200 mesh grid for observation with a Hitachi H9000 TEM. To determine the  $T_g$  and to confirm the absence of any residual curing, the cured samples (at 120°C for 2 hours, with subsequent post cure at 140°C for 2 hours) were heated in a Perkin-Elmer Pyris 1 DSC instrument using helium atmosphere from -100°C to 150°C at 20°C·min<sup>-1</sup> and then cooled to -100°C at 20°C·min<sup>-1</sup> to minimize the enthalpy relaxation in the second heating scan. Finally, the sample was reheated to 150°C at 20°C·min<sup>-1</sup>. TGA data were obtained on a TA-Q50 instrument using nitrogen atmosphere. The samples were heated from 30°C to 1000°C (dynamic scan) at heating rate of 20°C·min<sup>-1</sup>. The flexural and tensile properties of the epoxy system with and without clay were determined at room temperature and 50% relative humidity according to ASTM D790-2000 and ASTM D638-2002 on an Instron Material Testing Machine with crosshead speeds of 1.3mm/min and 5mm/min, respectively. The impact testing of epoxy and epoxy nanocomposites was done at room temperature and 50% relative humidity according to ASTM D256-2002 on impact tester-Tmi testing machines Inc. The hardness of epoxy and epoxy nanocomposites was determined at room temperature and relative humidity of 50% according to ASTM D2240-00 using a Shore

Conveloader Instrument. The density of materials was obtained on a Mettler AE 163 balance and kit at room temperature.

The fabrication steps of the nanocomposites were designed as follows. A masterbatch of epoxy and 23.6 phr clay was prepared using Tm stirring method at 120°C for 1 hour then stored at room temperature. For curing, the required amounts of masterbatch, epoxy resin, and hardener(s) to obtain 6 wt% organoclay in the final products were mixed at room temperature for 5 min then subjected to vacuum for another 30 min. Samples were finally cured at 120°C for 2 hours, with subsequent post cure at 140°C for another 2 hours. Sample preparation for this study is shown in Figure 7.2. Sample specifications are shown in Table 7.1.

**Table 7.1. Sample specifications for Chapter 7**

<b>Sample name</b>	<b>D230 : D2000 weight ratio</b>	<b>EPON828</b>	<b>D230</b>	<b>D2000</b>	<b>Nanoclay</b>
8d0D100	0:100	100	0	270	0
8d25D75	25:75	100	23.6	70.8	0
8d35D65	35:65	100	26.2	48.7	0
8d60D40	60:40	100	29.7	19.8	0
8d100D0	100:0	100	32	0	0
<b>C30B</b>					
8d0D100-6B	0:100	100	0	270	23.6
8d25D75-6B	25:75	100	23.6	70.8	12.4
8d35D65-6B	35:65	100	26.2	48.7	11.2
8d60D40-6B	60:40	100	29.7	19.8	9.5
8d100D0-6B	100:0	100	32	0	8.4
<b>I30E</b>					
8d0D100-6E	0:100	100	0	270	23.6
8d25D75-6E	25:75	100	23.6	70.8	12.4
8d35D65-6E	35:65	100	26.2	48.7	11.2
8d60D40-6E	60:40	100	29.7	19.8	9.5
8d100D0-6E	100:0	100	32	0	8.4



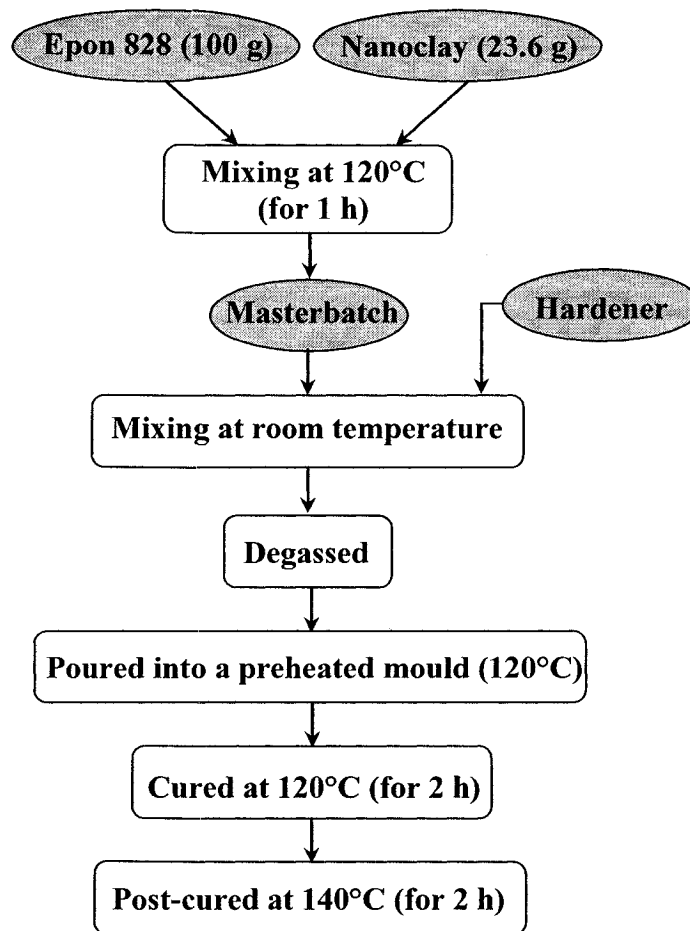


Figure 7.2. Flowchart of sample preparation

## 7.3. Results and discussion

### 7.3.1. Dispersion

WAXRD analysis of the epoxy nanocomposites based on C30B and I30E are illustrated in Figures 7.3 and 7.4. In Figure 7.3, the clay layer separation (degree of intercalation) in the nanocomposites based on C30B is more than twice as large as in the original C30B, showing that the clay has been further intercalated by the epoxy matrix. It is also noticed

that D2000 leads to a much greater clay gallery distance compared to D230 and the clays can be considered to be exfoliated in this system as  $d_{001}$  is greater than 7 nm. The molecular weight of D230 is smaller than that of D2000, so D230 would be expected to diffuse into the clay galleries more easily during curing, and hence to increase further the clay gallery distance. However, the curing rate of the D2000 system is much slower compared to the D230 system (as indicated by DSC study, see section 4.4.3). As a consequence, it is reasonable to believe that D2000 and possibly EPON828 would have more time to diffuse into the clay galleries to exfoliate the clays. The results show there is a correlation between the reactivity of epoxy system and the intercalation/exfoliation of clay in the corresponding nanocomposites. Thus, the lower is the curing reactivity of the epoxy system, the greater is the clay intercalation in the nanocomposites. This observation is in good agreement with the literature [18]. Moreover, it is also believed that the length of the D2000 molecules contributes significantly to the intercalation/exfoliation of clay C30B in epoxy matrix. With a longer length compared to D230, D2000 can push the clay platelets apart and expand the clay galleries more than D230. It is worth stressing here that in thermoset systems, the intercalation and exfoliation process can continue during curing and is controlled not only by the rate of diffusion of organic molecules (in this case, the curing agent and the epoxy molecules) into the clay gallery but also by the curing rate of the epoxy system and by the size of epoxy and hardener molecules.

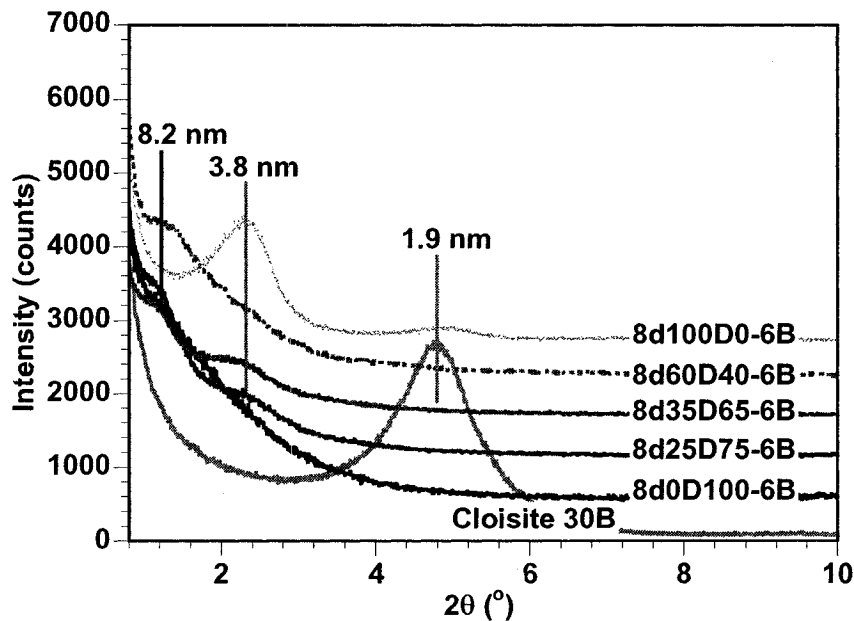


**Figure 7.3. X-ray diffraction curves of epoxy-nanocomposites based on 6 wt% C30B and cured with different ratios of D230/D2000**

Figure 7.4 shows X-ray diffraction of I30E nanocomposites. The peaks almost disappear on all XRD curves. It looks like that the intercalation of I30E in these epoxy systems is superior to C30B (except for the one which was cured with D2000). This may be due to the difference in chemistry of their intercalants. I30E was treated with octadecyl amine, the primary amine base while C30B was treated with quaternary amine (methyl tallow bis-2-hydroxyethyl). One may speculate that the active amine of octadecyl amine in I30E provides a better interaction with the hardener via hydrogen bond. A high molecular weight D2000 is probably less compatible with saturated  $C_{18}$  of the octadecyl amine intercalant than low molecular weight D230. This may explain for the small peak on the XRD curve of 8d0D100-6E.

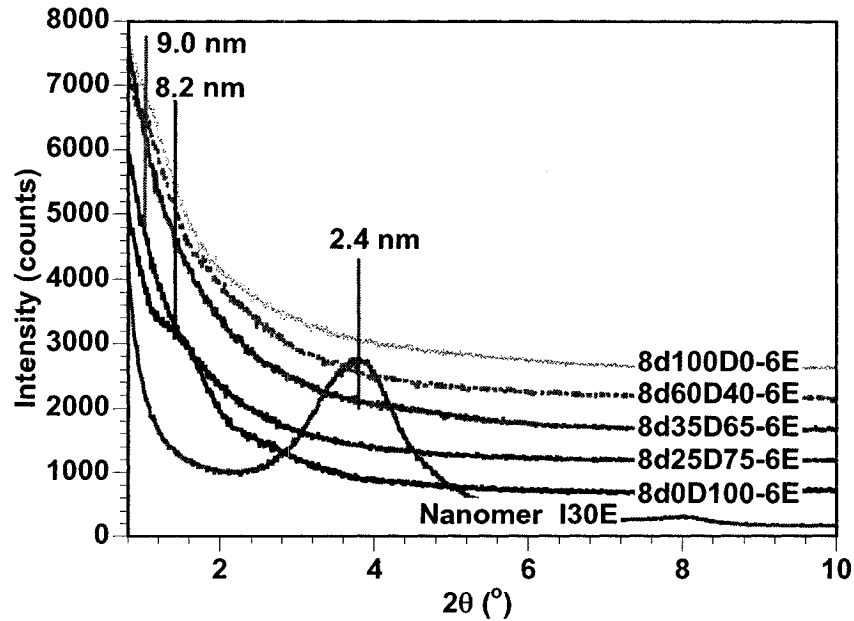


**Figure 7.4. X-ray diffraction curves of epoxy-nanocomposites based on 6wt% I30E and cured with different ratios of D230/D2000**

The microstructures of nanocomposite samples observed by FEGSEM are shown in Figures 7.5 and 7.6. The bright spots on the backscattered images correspond to clay aggregates. Apparently, a portion of the clay remains at the micro-scale level with different size populations depending on the types of hardener and clay. For nanocomposites based on C30B, there is a greater density of small particles with size below 2  $\mu\text{m}$  and a lower density of large particles in the nanocomposite cured with D2000 (Figure 7.5a) than in the nanocomposite cured with D230 (Figure 7.5e). This means that the nanoclay C30B has been dispersed better in the nanocomposite cured with D2000 than in the one cured with D230. Furthermore, samples cured with mixtures of these two hardeners showed intermediate results. This indicates that the longer hardener molecule and the lower curing rate of the D2000 epoxy system have a positive effect not

only on the intercalation (as identified by XRD) but also on the dispersion of the clay at the micro level in the epoxy.

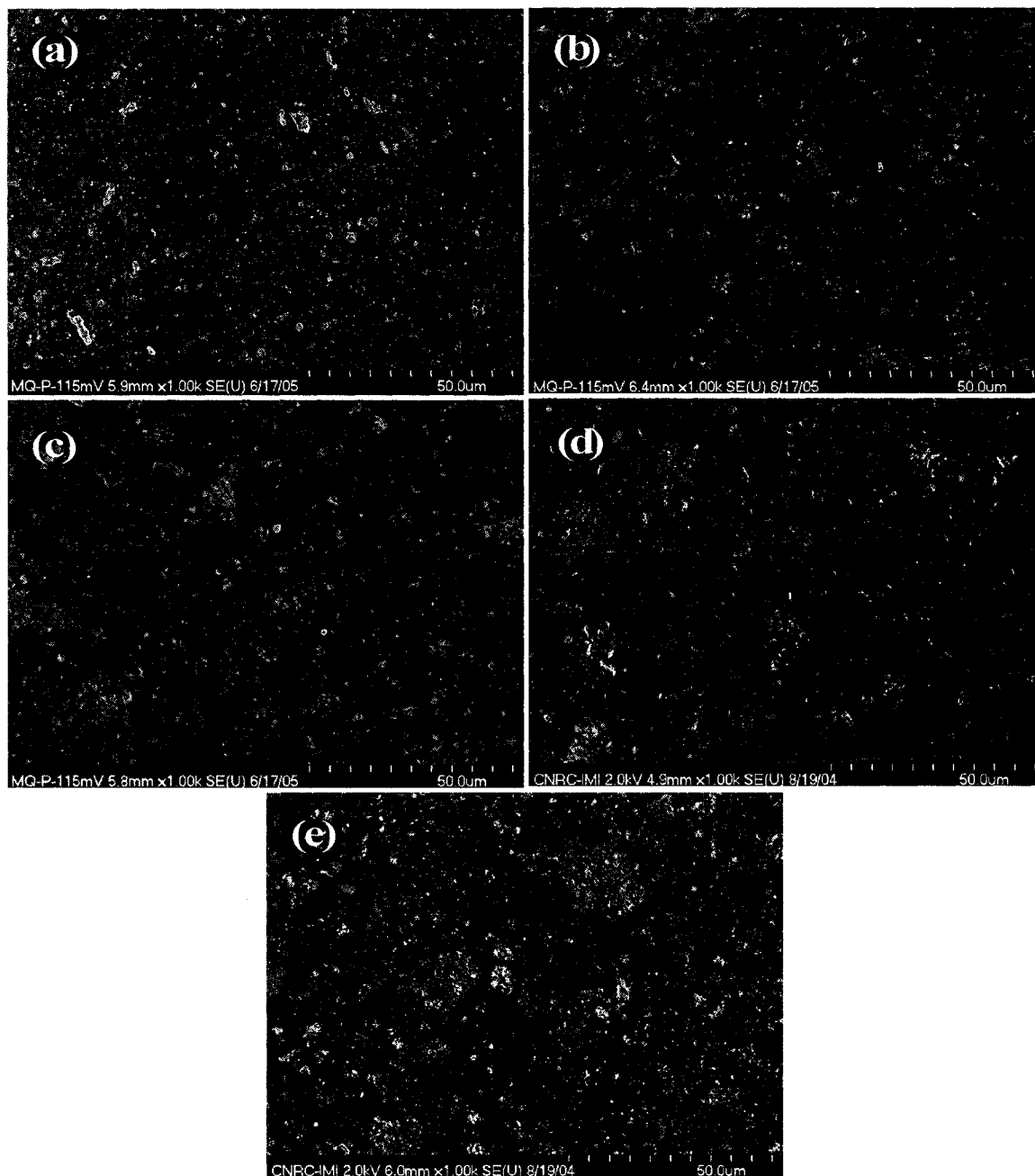


**Figure 7.5. FEGSEM micrographs of 6 wt% C30B nanocomposites cured with (a) d0D100 (D2000), (b) d25D75, (c) d35D65, (d) d60D40 and (e) d100D0 (D230)**

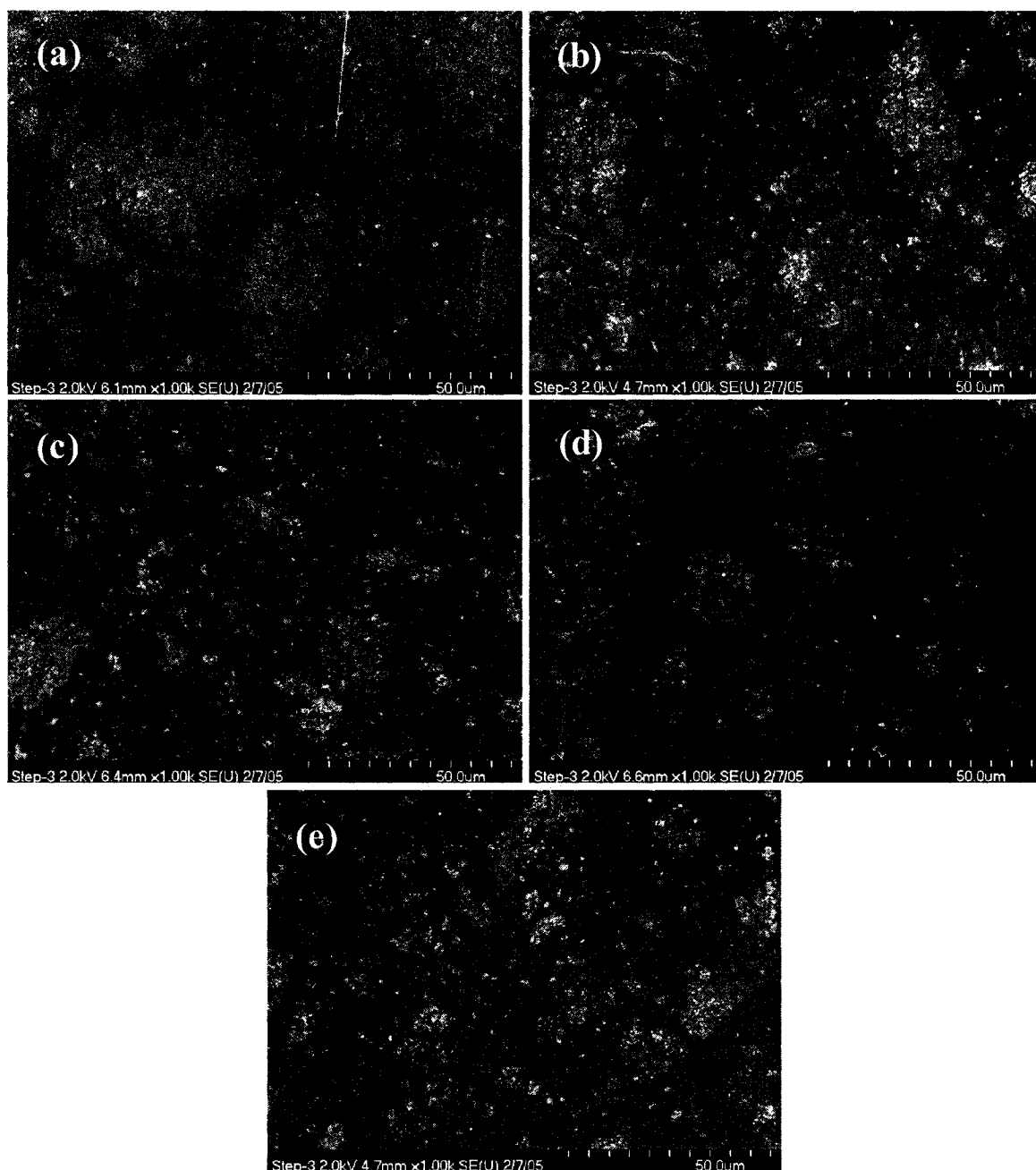


**Figure 7.6. FEGSEM micrographs of 6 wt% I30E nanocomposites cured with (a) d0D100 (D2000), (b) d25D75, (c) d35D65, (d) d60D40 and (e) d100D0 (D230)**

A different phenomenon appears for the case of I30E, as can be seen in Figure 7.6a. There is a greater density of big particles and a lower density of small particles than in

Figure 7.6e. This means that the nanoclay I30E has been dispersed more poorly in the nanocomposite cured with D2000 than the one cured with D230. Again, samples cured with the mixtures of these two hardeners also showed intermediate results. This result supports the discussion for the XRD results earlier. FEGSEM micrographs also indicated that the micro dispersion of C30B is better than I30E in systems cured with the same hardener.

TEM micrographs for the two nanocomposites based on C30B at different magnifications are shown in Figure 7.7. It is clear that the clay particles were not completely exfoliated into individual platelets. However, epoxy matrix has entered into the clay galleries, as a significant increase in the clay gallery distance can be seen for the two nanocomposites. Figure 7.7 confirms that the clay has been better intercalated and better dispersed in nanocomposite cured with D2000 than in nanocomposite cured with D230 (as identified by XRD and FEGSEM). From the TEM images, the average *d*-spacing (taken at different location) is estimated to be around 7 nm and 3 nm for the D2000 and the D230 systems, respectively, which is in fairly good agreement with the XRD results. Again it is confirmed that D2000 leads to greater clay intercalation compared to D230. However, it is surprising that, although the gallery distance in the D2000 is fairly large (to an extent often considered as full exfoliation), the platelets still remain ordered into stacks. This may be related to the fact that the intercalation took place in the absence of shear forces; hardener and epoxy molecules diffused into the galleries very gradually with time. So far, the results from XRD, SEM and TEM combined indicate that in this particular case a longer chain length of curing agent and a lower curing rate of the epoxy system has a positive effect on the dispersion and

intercalation/exfoliation of clay in the epoxy system. This indicates that the use of mechanical force to facilitate the exfoliation is really important. However, during curing the use of mechanical force is not possible.

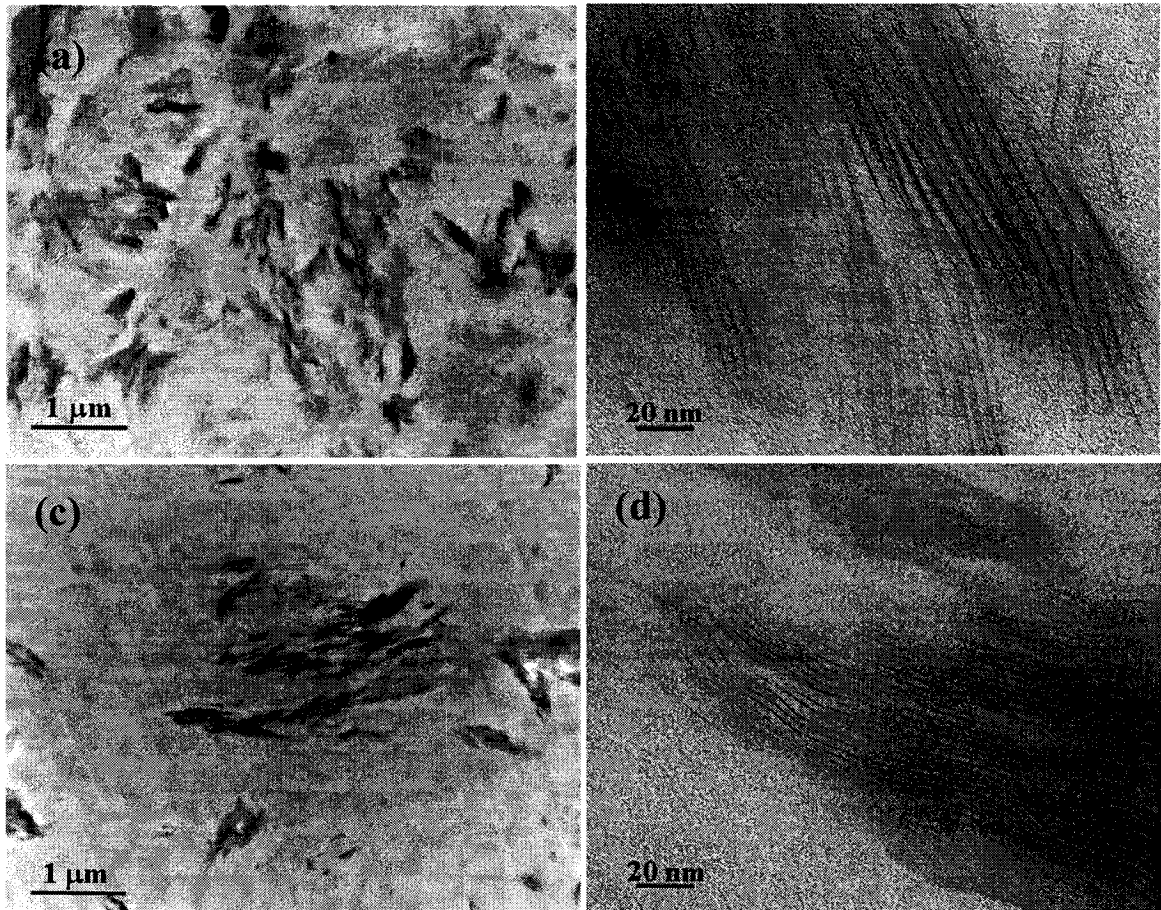


**Figure 7.7. TEM micrographs of 6 wt% C30B nanocomposites cured with (a, b) D2000 and (c, d) D230**

### **7.3.2. Thermal, physical and mechanical properties**

The  $T_g$  of epoxy and epoxy nanocomposites was determined by DSC and the results are shown in Figure 7.8. The  $T_g$  values of samples (with and without clay) cured with D2000



are much lower than those of samples cured with D230. After curing at 120°C the epoxy matrix prepared with D2000 is a soft rubbery material with  $T_g = -46.3^\circ\text{C}$ , whereas the one prepared with D230 is hard and glassy with a high  $T_g = 86.8^\circ\text{C}$ . As a result of the difference in molecular weights of curing agent, the distance between crosslinks in EPON828-D2000 is expected to be greater than in EPON828-D230. This explains the difference in the  $T_g$  of the two systems. The samples cured with the mixtures of two hardeners showed a  $T_g$  in between the  $T_g$  of the D2000 and D230 systems which is reasonable. The higher is the ratio of D230/D2000, the higher is  $T_g$ . Based on the  $T_g$  of the systems, 8d0D100 (EPON828-D2000) and 8d25D75 systems can be classified as rubbery systems; while 8d60D40 and 8d100D0 (EPON828-D230) systems can be classified as glassy systems. However 8d35D65 system can be classified as the intermediate one.

It was also observed that the presence of nanoclay does not significantly affect the  $T_g$  of the epoxy systems, if the error of 2°C is considered. If the clay has interaction with the epoxy matrix, one may expect an increase in the  $T_g$  of ENC systems, but this is not the case. Probably the long hydrocarbon chains of the tallow inhibit a direct interaction between the epoxy matrix and the clay surface. It was also observed that there was only one transition step in the DSC curves for the two systems (Figure 7.9), and the transition step was quite narrow and identical, indicating that there is only one phase in the system. This may allow us to exclude the possibility that the curing is different inside and outside the clay galleries [18].

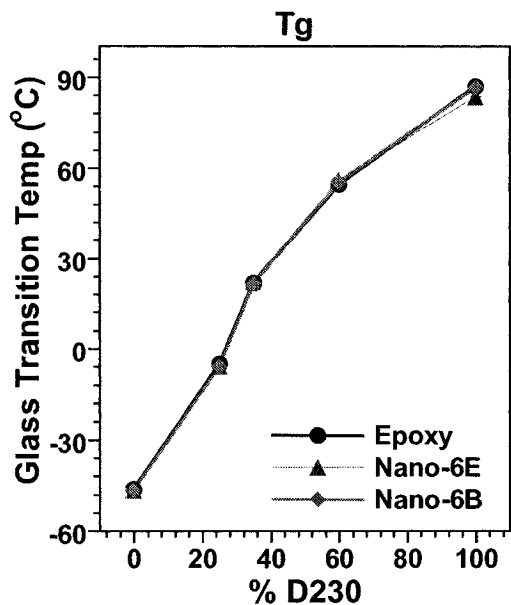


Figure 7.8.  $T_g$  of epoxy systems and their 6 wt% C30B and 6 wt% I30E nanocomposites versus the amount of D230

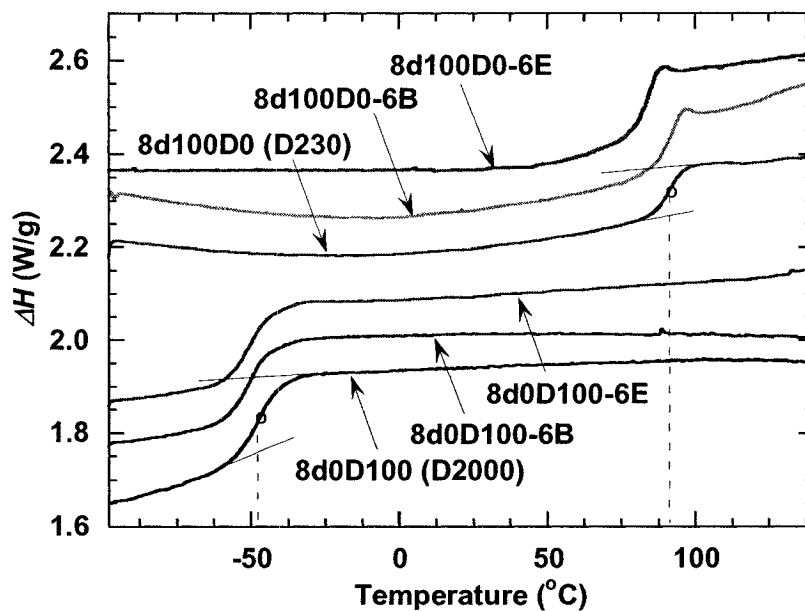


Figure 7.9.  $T_g$  for epoxy systems and their nanocomposites cured with D2000 and D230

TGA characteristics of C30B, I30E, EPON828-D2000, EPON828-D230 and their nanocomposites are shown in Figure 7.10 and Table 7.2. Figure 7.10a shows the typical TGA weight loss plots of C30B, I30E, EPON828-D2000, EPON828-D230 and their nanocomposites. It can be seen that there is 29.16% and 29.67% of weight loss in C30B and I30E, respectively, up to 1000°C. This means there is 70.84 and 70.33 wt% of remaining materials in C30B and I30E at 1000°C respectively. These values represent the inorganic silicates in C30B and I30E. It also can be seen in Figure 7.10a and Table 7.2 that the EPON828-D230 system is more thermally stable than the EPON828-D2000 system as its  $T_{onset}$  temperature is higher and the temperature corresponding to any given weight loss is higher. This can be attributed to the shorter polyoxypropylene links, resulting in a lower overall polyoxypropylene content. Such groups would be expected to decompose at a lower temperature than the more stable bisphenol A units of the epoxy resin. In addition, the short chain hardener provides a denser crosslink network and inhibits the volatilization of the structure which was broken down during degradation. The presence of clay C30B and I30E have only minor influence on the TGA results of these two epoxy systems if the error 5°C is considered. Typical DTG thermograms (the first derivative curves of TGA) of rubbery and glassy epoxy systems and their nanocomposites are shown in Figure 7.10b. They reveal that the thermal degradation of these systems consisted of only one step. Their maximum degradation rate temperatures  $T_{peak}$  from Figure 7.10b is shown in Table 7.2. The presence of clay increases  $T_{peak}$  for D2000 systems but not for the D230 systems. It is still unclear the cause but probably due to the change of structure during burning. D2000 systems have less dense structure,

during the burning, the clay may have a greater flexibility to align on the sample surface which preventing the transportation of the burning gas outside the samples.

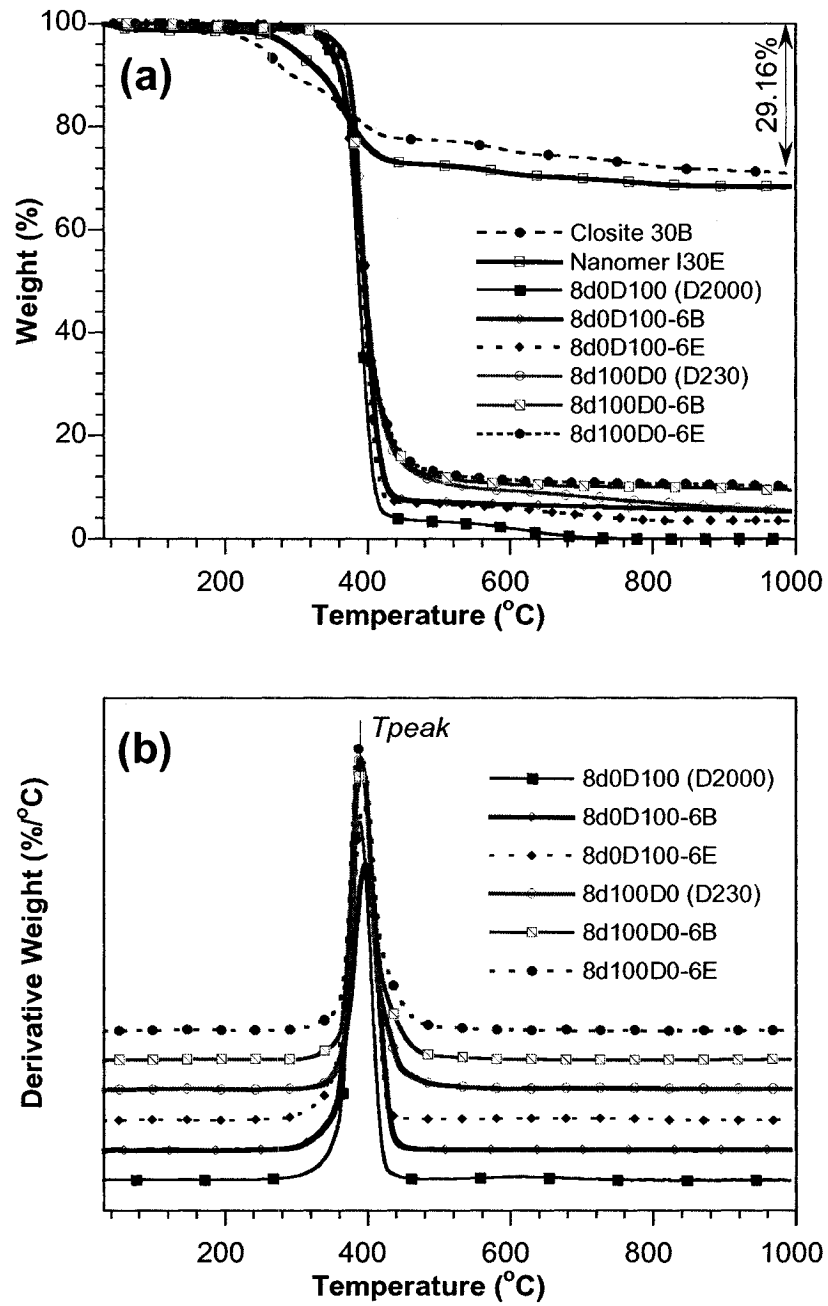
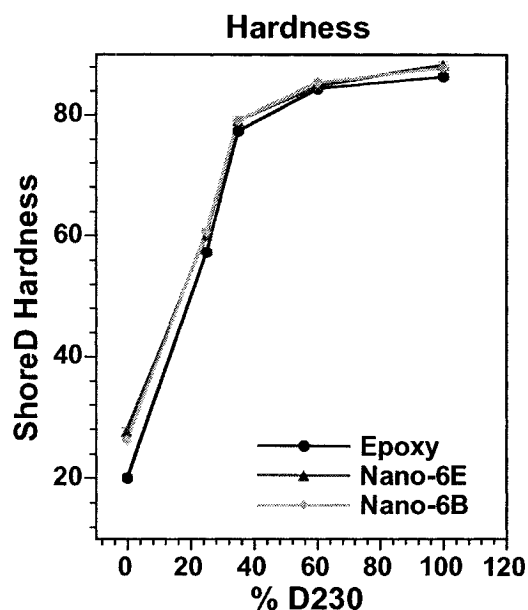


Figure 7.10. TGA results of C30B, I30E and their nanocomposites cured with D2000 and D230

**Table 7.2. Summary of TGA results for D2000, D230 epoxy systems and their nanocomposites**

Materials	8d0D100 (D2000)	8d0D100-6B	8d0D100-6E	8d100D0 (D230)	8d100D0-6B	8d100D0-6E
Temperature (°C)						
$T_{onset}$	367.7	369.3	369.6	375.1	370.9	370.8
$T_{peak}$	388.9	396.8	394.3	389.4	389.2	389.4

The surface hardness of the samples with and without clay was determined at room temperature and the results are shown in Figure 7.11. As expected, adding nanoclay increases the surface hardness for all the epoxy systems ranging from rubbery to glassy. However, the level of increase in the hardness for the rubbery system (D2000) is greater than for the glassy system (D230). The higher is the ratio of D2000/D230, the higher is the level of increase in hardness. Clay has a much greater surface hardness because of its ceramic nature. Therefore, at the same clay concentration, the contribution of clay to the hardness is greater for the rubbery epoxy matrix than for the glassy epoxy. Furthermore, the better dispersion and better intercalation/exfoliation of the clay in the D2000 sample may also be a contributing factor.



**Figure 7.11. Surface hardness of epoxy systems and their 6 wt% C30B, 6 wt% I30E nanocomposites versus percentage of D230**

Typical stress-versus-strain curves for the epoxy and epoxy-clay are shown in Figure 7.12. The response of the materials to applied stress is described as ductile to brittle depending on the curing agent used. The comparison of the typical stress-versus-strain curves for the epoxy systems and their nanocomposites at the same scale is shown in Figure 7.13. One can see that the D2000 systems are very weak compared to D230 systems. For the D2000 systems, stress-strain curves of ENC and matrix are quite distinct, the great improvement over all mechanical performance in term of strength, stiffness, toughness and ductility of ENC compared to the matrix. However, for D230 systems, the ENC do not show differ from the matrix except a great loss in the ductility. The systems cured with the mixture of these two hardeners show the intermediate results. More detail of discussions on the mechanical performance as follows.

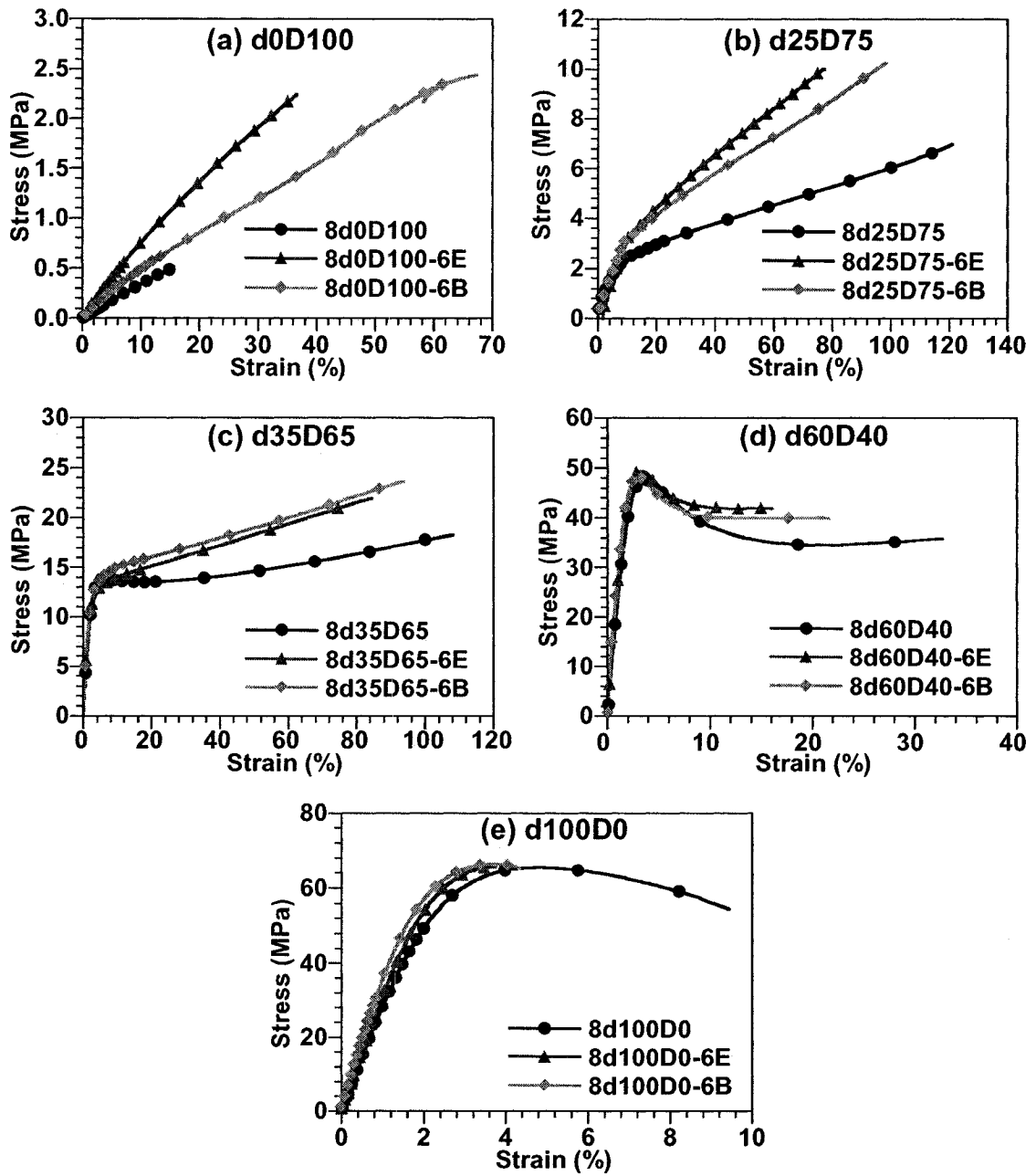


**Figure 7.12. Typical stress-strain curves for epoxy and its 6 wt% C30B, 6 wt% I30E nanocomposites cured with (a) d0D100 (D2000), (b) d25D75, (c) d35D65, (d) d60D40, and (e) d100D0 (D230)**

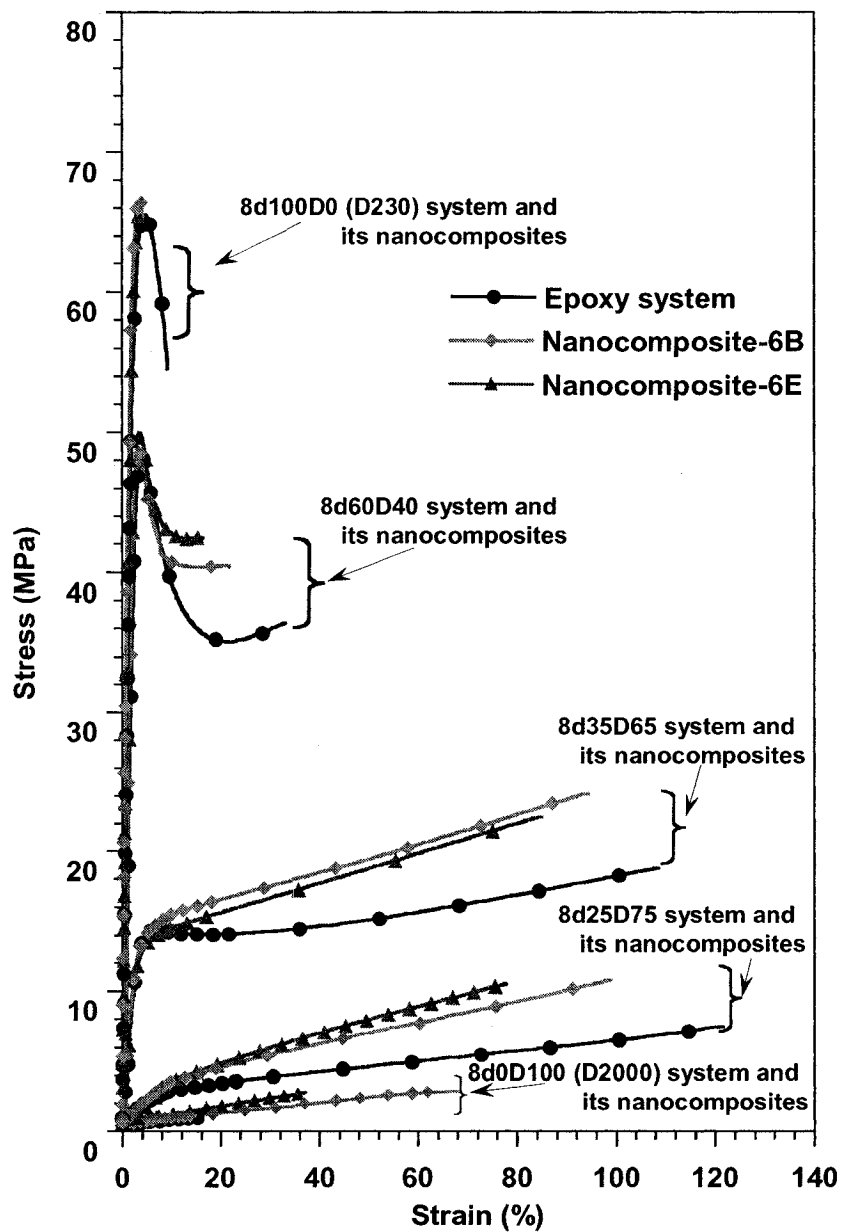


**Figure 7.13. Comparison of typical stress-strain curves for epoxy systems and their 6 wt% C30B, 6 wt% I30E nanocomposites in the same scale**

Figures 7.14 to 7.17 show the details the tensile properties of the epoxy matrices and their nanocomposites. Figure 7.14 shows that with increase of the ratio of D230/D2000, the modulus of the epoxy materials increases. As a result of the difference in molecular



weights, the distance between crosslinks in EPON828-D230 is shorter than in EPON828-D2000. Because of this, systems cured with hardeners which contain a higher proportion of D230 are more brittle and have higher modulus than systems cured with a lower proportion of D230.

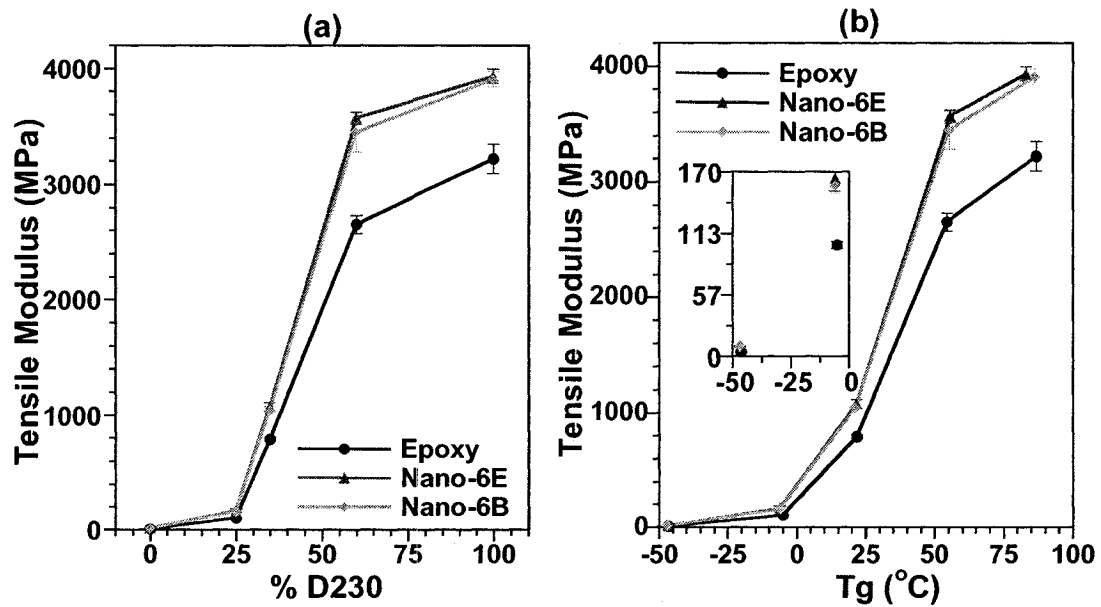


Figure 7.14. Tensile modulus of epoxy systems and their nanocomposites versus (a) percentage of D230, and (b)  $T_g$

The presence of organoclays results in a significant increase in modulus, whether the epoxy matrix is rubbery or glassy regardless the clay type. Again, a similar effect was also reported by other researchers [10, 11, 19, 28] and also in Chapter 6. Since the modulus of clay is superior to that of the matrix, this improvement can be simply explained by the rule of mixture. The presence of 6 wt% of nanoclay increases the tensile modulus more than twice in the presence of both C30B and I30E relative to the pristine elastomeric polymer (Figure 7.15a). For the glassy system with the same clay content, the tensile modulus increases by only 21% for the nanocomposite based on C30B and 22%

for the nanocomposite based on I30E, relative to the neat glassy epoxy (Figure 7.15e). The modulus of the 8d25D75, 8d35D65 and 8d60D40 systems increases by about 32, 35 and 55 %, respectively, with addition of 6 wt% of nanoclay (C30B, I30E).

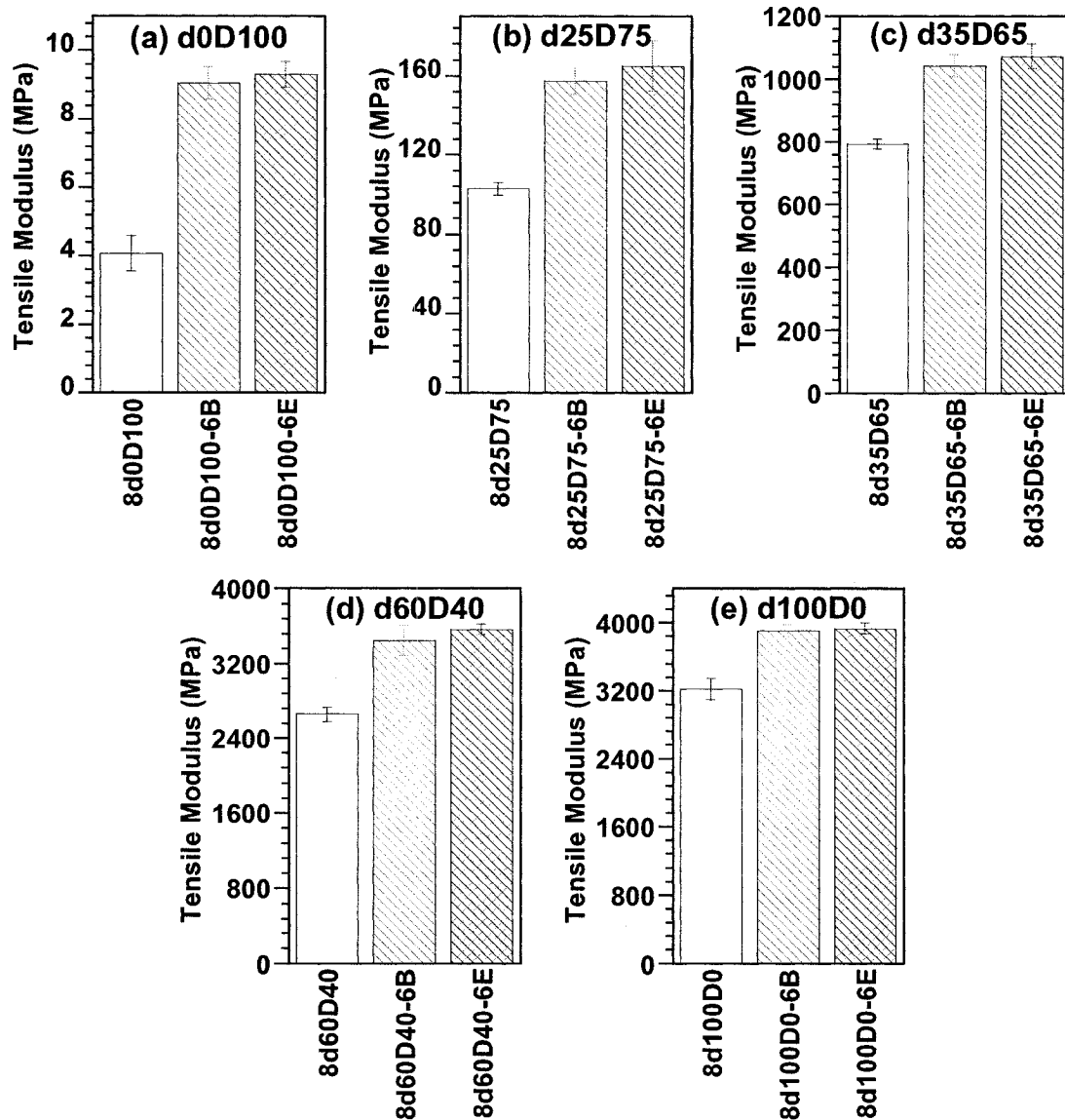
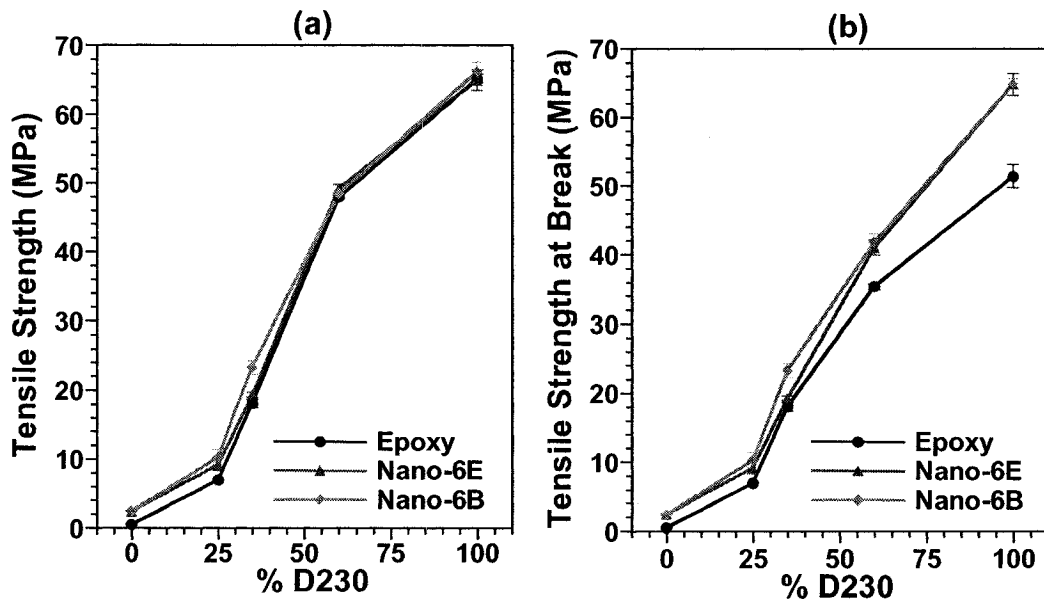


Figure 7.15. Tensile modulus of epoxy systems and their nanocomposites cured with different hardeners (a) d0D100 (D2000), (b) d25D75, (c) d35D65, (d) d60D40, and (e) d100D0 (D230)

Tensile strength (the maximum point on the stress-strain curve), tensile strength at break (the last or break point on the stress-strain curve), tensile strain at break and energy to break are shown in Figures 7.16 and 7.17. The results illustrate a substantial increase in strength, ductility and toughness for the nanocomposite system cured with D2000, which is representative of soft and weak materials. The presence of 6 wt% of I30E nanoclay increases the strengths more than 5 times, the strain at break 2 times, and the energy to break (the area under the stress-strain curve) more than 12 times relative to the pristine elastomeric polymer. Moreover, the presence of 6 wt% of C30B nanoclay substantially increases the strength more than 5 times, the strain at break 5 times, and the energy to break more than 23 times relative to the pristine elastomeric polymer. A similar effect was also obtained by other researchers [11, 28, 46, 158, 159, 160]. On the other hand, for the glassy system with the same clay content the strength remains almost unchanged, The strength at break improves about 20% while the strain at break and energy to break decrease significantly. This means that for high  $T_g$  epoxy thermoset, the presence of organoclay does not lead to an improvement of the tensile strength but rather makes the materials more brittle [45, 95]. For the mixture systems, the strain decreases with the presence of nanoclay. The strength either increases or remains the same as that of the neat epoxy system depending on curing agents. The strength at break improves from 20 to 50% depending on system. The change in energy to break also depends on curing agents and clay.

The effect of clay on the toughness of epoxy systems depends on curing agents. It is clear that the toughness of the EPON828-D2000 nanocomposites is significantly improved compared to the neat epoxy, whereas the reverse is true for the glassy EPON828-D230.

The type of clay also contributes to the toughness of epoxy. With the same curing agent, nanocomposites based on C30B show a higher strain and higher toughness than nanocomposites based on I30E. This may be explained by either the difference in level of micro dispersion of the nanoclay in the epoxy system or interaction between the epoxy system and the clay (Figures 7.5, 7.6 and 7.17) which indicated that the micro dispersion of C30B is better than I30E systems cured with the same hardener).



**Figure 7.16. Tensile strength and tensile strength at break of epoxy systems and their nanocomposites versus percentage of D230 (a) tensile strength (the maximum point on the stress-strain curve), and (b) tensile strength at break (the last or break point on the stress-strain curve)**

Clearly, the reinforcing effect of nanoclay is strongly dependent on the nature of the neat polymer and the nanoclay has a more positive effect on the mechanical properties of the rubbery material than on those of the glassy one. Firstly, a better reinforcing effect of

nanoclay in the rubbery system can be expected based on the rule of mixture. Since its strength and modulus are many times smaller than those of the glassy one, the positive impact of the organoclay becomes relatively more important. Secondly, the improvement can be explained by the fact that, owing to the ability of nanoparticles to dissipate energy because of their mobility under applied stress [161, 162], the nanoclay can provide temporary physical crosslinks between polymer chains, providing localized regions of enhanced strength. There is also the possibility that the looser structure of the nanoclay in the rubbery structure can allow a better realignment of clay layers according to the stress direction, thus resulting in a greater reinforcing effect [11]. In addition, the better dispersion and intercalation/exfoliation in the rubbery system can also be of importance.

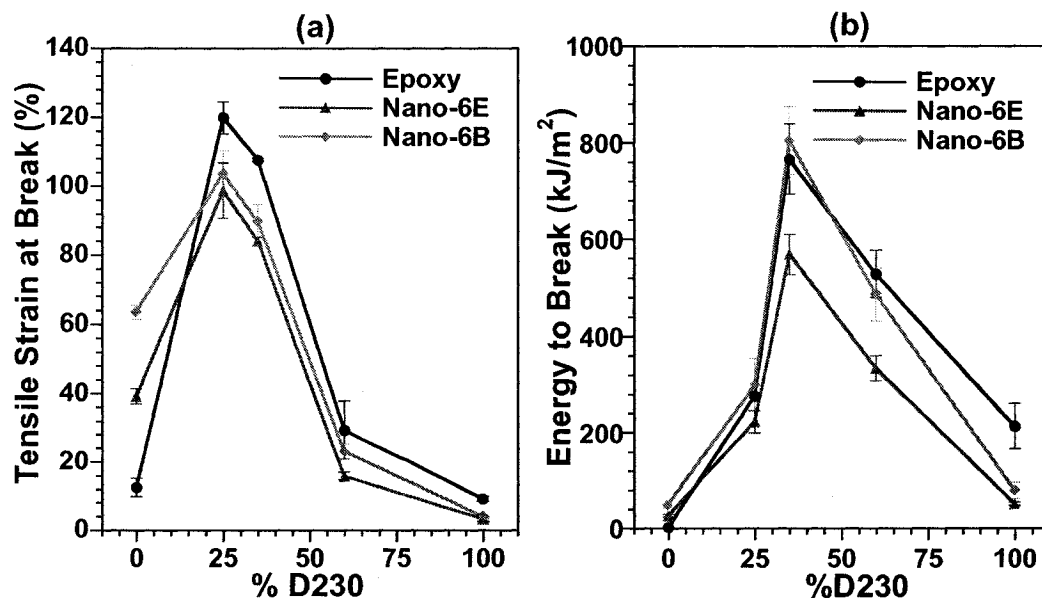


**Figure 7.17. Tensile strain at break and energy to break (the area under the stress-strain curve) of epoxy systems and their nanocomposites versus percentage of D230**

**(a) tensile strain at break, and (b) energy to break**

Flexural properties of epoxy systems and their nanocomposites based on C30B and I30E are shown in Figures 7.18 and 7.19. The behavior in flexural is quite similar in tension.

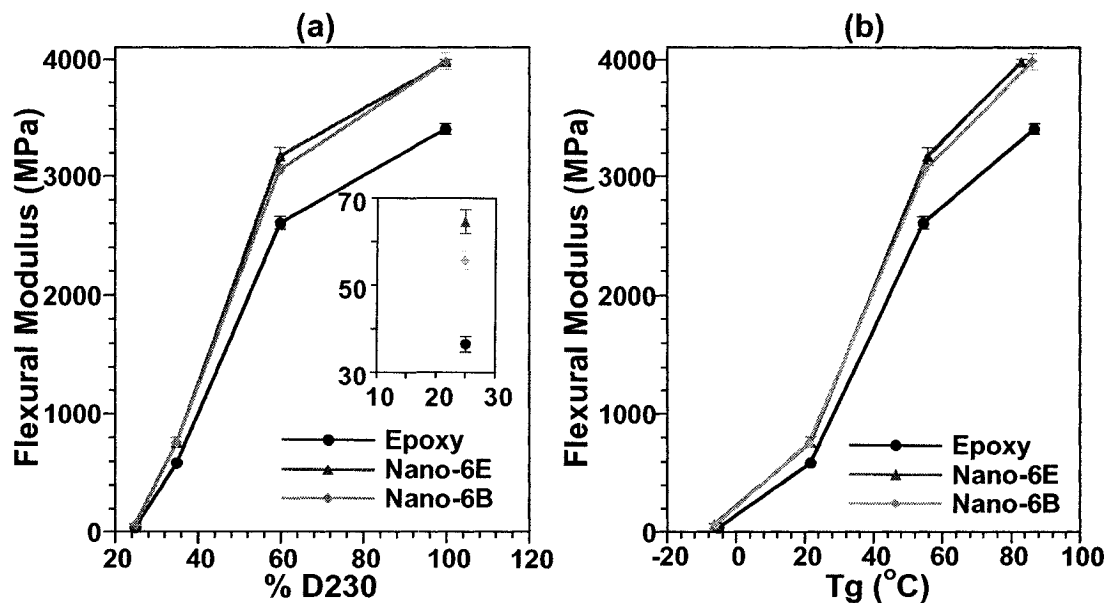


Figure 7.18. Flexural modulus of epoxy systems and their nanocomposites cured with different hardeners (a) modulus versus %D230, and (b) modulus versus  $T_g$

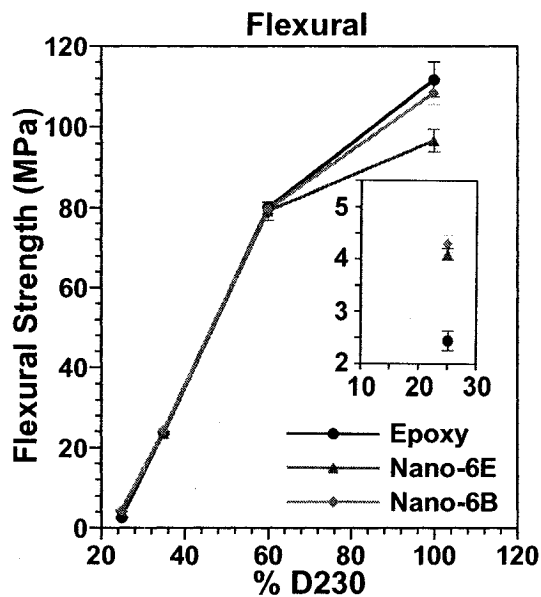
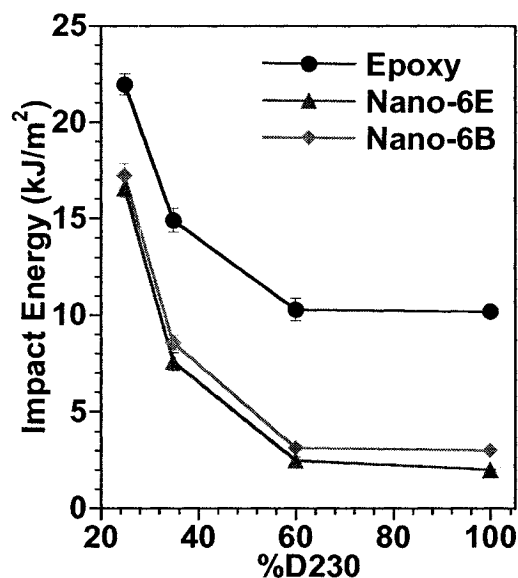


Figure 7.19. Flexural strength of epoxy systems and their nanocomposites versus  $T_g$

The impact properties of the epoxy systems and their nanocomposites based on the two types of nanoclay are shown in Figure 7.20. Generally speaking, the impact energy decreases with the increase in ratio of D230/D2000. This is because the system cured with D230 represents a glassy epoxy and the system cured with D2000 represents a rubbery system. This explains why the impact energy of the system decreases with increasing D230/D2000 ratio. Regardless the type of clay used in the ENCs, the presence of clay reduces the impact energy which is good agreement with most publications [41, 69, 97]. This result is also seen in Figure 6.15 for the fracture toughness of 6 wt% C30B (Tm method) except the decrease in impact energy here is more than fracture toughness in Figure 6.15. This may due to the difference in the rate of loading.



**Figure 7.20. Impact energy of epoxy systems and their nanocomposites versus percentage of D230**

Figure 7.21 summarizes the change in mechanical properties of the nanocomposites compared to the neat resin. It confirms that nanoclay has a more significant effect on the

properties of soft rubbery materials (typical of material in the rubbery region above  $T_g$ ), namely the system cured by D2000 for both nanoclays.

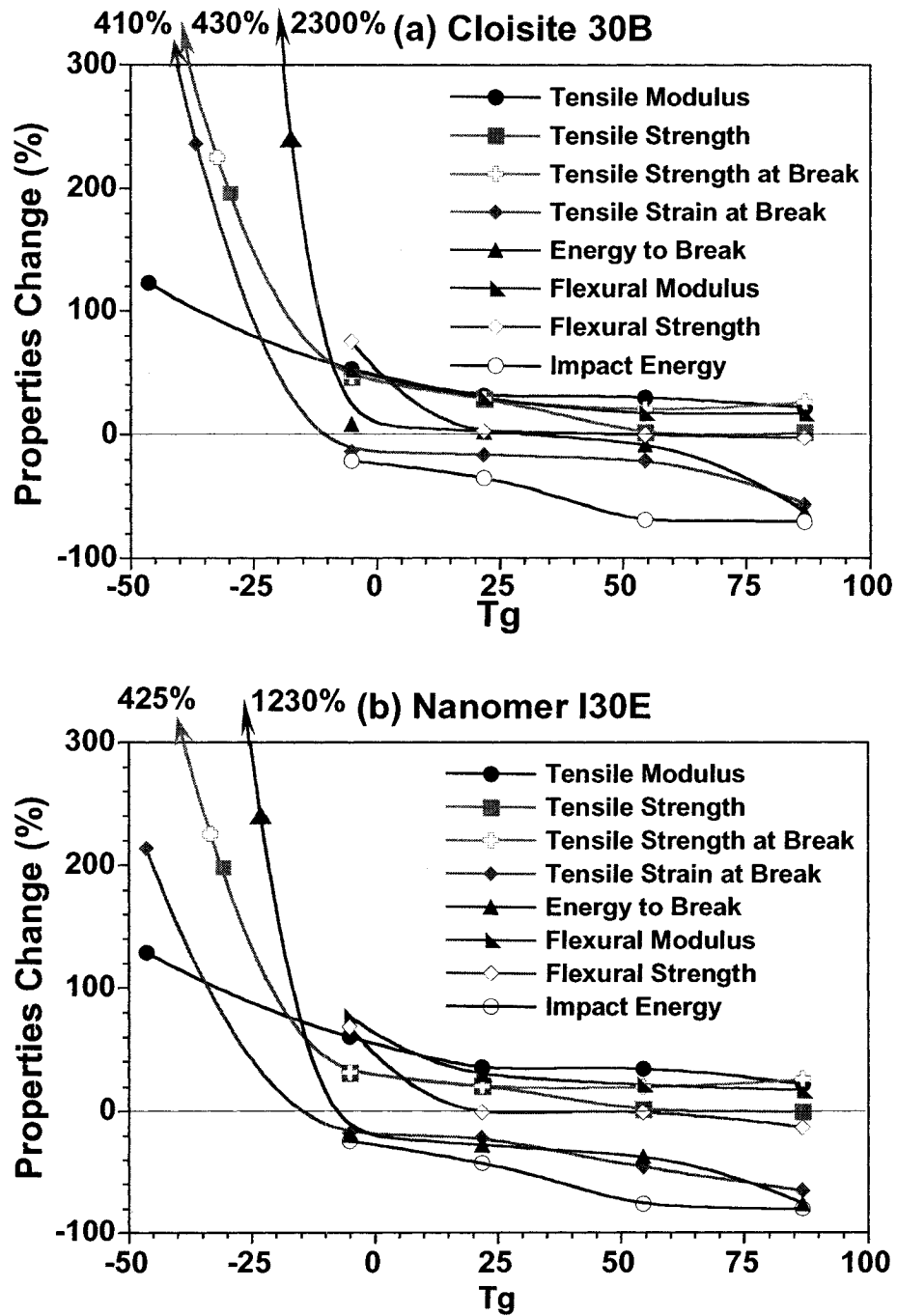


Figure 7.21. Summary of the reinforcing effect of nanoclay on mechanical properties of epoxy (a) Cloisite 30B, and (b) Nanomer I30E



For  $T_g > 0$ , the effect of clay is not large and is about the same for all epoxy systems. However for  $T_g < 0$ , some properties are affected more than the others and the effect can be quite large for a few properties. This shows that  $T_g$  can be used as an indication of the effect of clay addition on epoxy properties, regardless of the type of epoxy system.

To further understand the reinforcing mechanism of C30B and I30E on epoxy resins, whose characteristics vary over a broad range from rubbery to glassy, the fracture surfaces of tensile-tested specimens were observed by FEGSEM (Figures 7.22, 7.23 and 7.24).

It can be seen that neat epoxy resin exhibits a relatively smooth fracture surface. The difference in the fracture of rubbery and glassy states of the neat epoxy can be seen clearly in Figures 7.22a and 7.22e. There is yielding behavior on the fracture surface of the rubbery-state epoxy, which is a typical fractography feature of soft fracture behavior (Figure 7.22a). Compared with rubbery epoxy, the fracture surface of glassy epoxy is rougher and there are more cracks in different planes but almost parallel to the crack-propagation direction, indicated by a white arrow (Figure 7.22e). This is a typical fractography feature of brittle fracture behavior, thus accounting for the low fracture toughness of the unfilled epoxy.

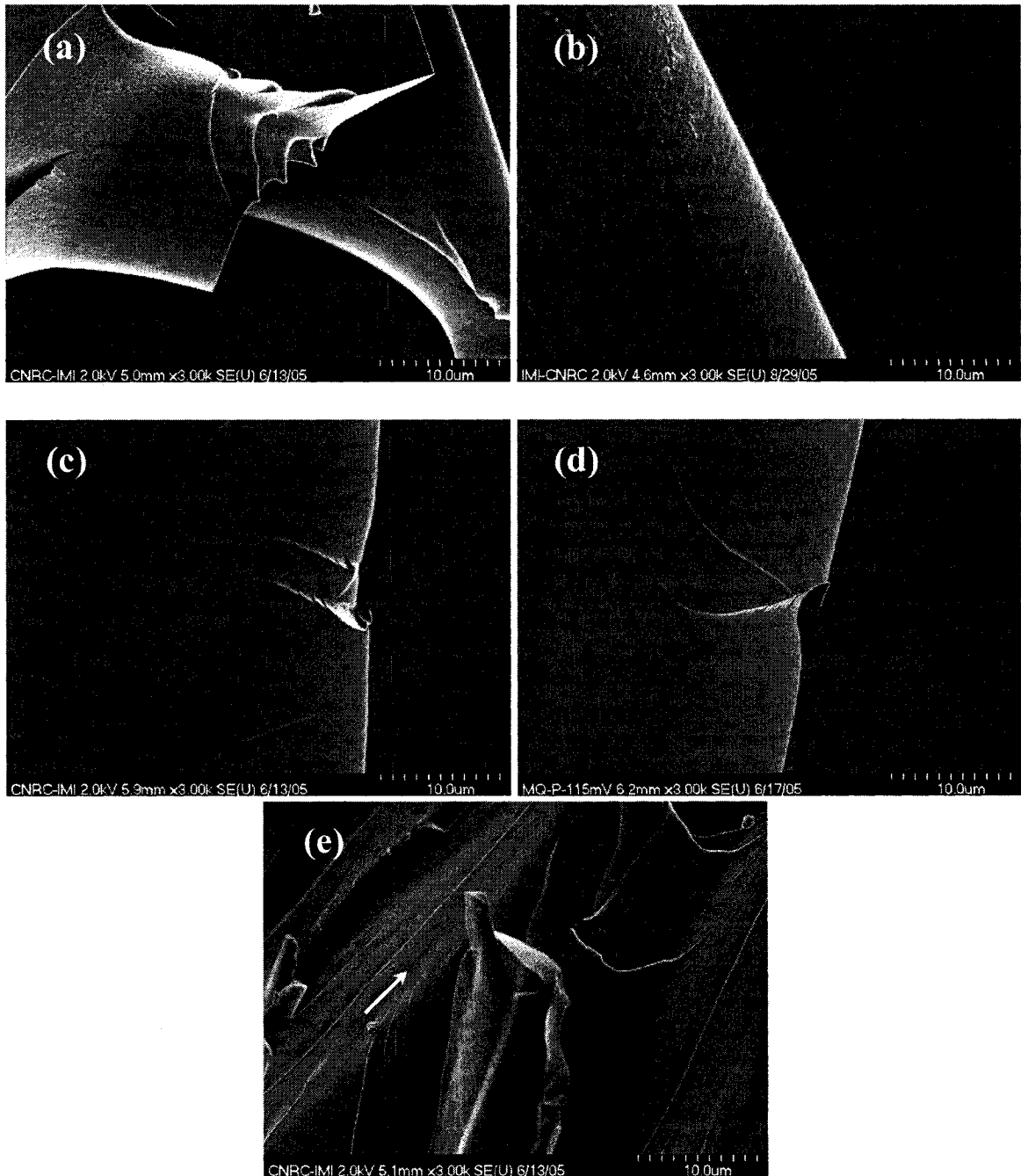


**Figure 7.22. Fracture surfaces for epoxy cured with different D230-D2000 mixtures, (a) with d0D100, (b) d25D75, (c) d35D65, (e) d60D40, and (e) d100D0**

The failure surface of the nanocomposites containing 6 wt% C30B and 6 wt% I30E which were cured with different mixtures of D230-D2000 is shown in Figures 7.23 and

7.24. Generally, a much rougher fracture surface is seen upon adding nanoclay into the epoxy matrix for all states of epoxy. In addition, although the roughness of the fracture surface is quite similar in both nanocomposites, the extent of increase in roughness is more evident for the case of soft material (Figures 7.22a, 7.23a, and 7.24a) compared to rigid material (Figures 7.22e, 7.23e, and 7.24e). The increased surface roughness implies that the path of the crack tip is distorted because of the clay platelets, making crack propagation more difficult. More precisely, the clay is able to interact with the growing crack front. Therefore, the presence of clay particles or aggregates would cause perturbations along the crack front, thus altering the path of the propagating crack from the straight unperturbed growth seen in the neat resin (as evidenced by an incline relative to the initial crack propagation direction that is indicated by a white arrow). Consequently, the cracks are deflected by the clay particles into the rougher regions surrounding them. Clearly, the crack deflection observed is responsible for the increase of strength and toughness observed on incorporating clay into the epoxy matrix. On the other hand, clay particles are also very likely to act as stress concentration sites, thus usually resulting in (1) clay-matrix debonding and (2) cleavage of clay tactoids, consequently producing some micro- or nanovoids and finally reducing the performance. With C30B nanocomposites, Figure 7.23 shows that many clay aggregates are observed on the fracture surface of the glassy systems (several distinct agglomerations are indicated by circles). The Figure also demonstrates a poorer micro-dispersion of the glassy system. Therefore, it can be believed that the negative effect of the cleavage of clay tactoids aspect plays a more important role in the fracture toughness of the glassy system, which is not the case for the rubbery system.

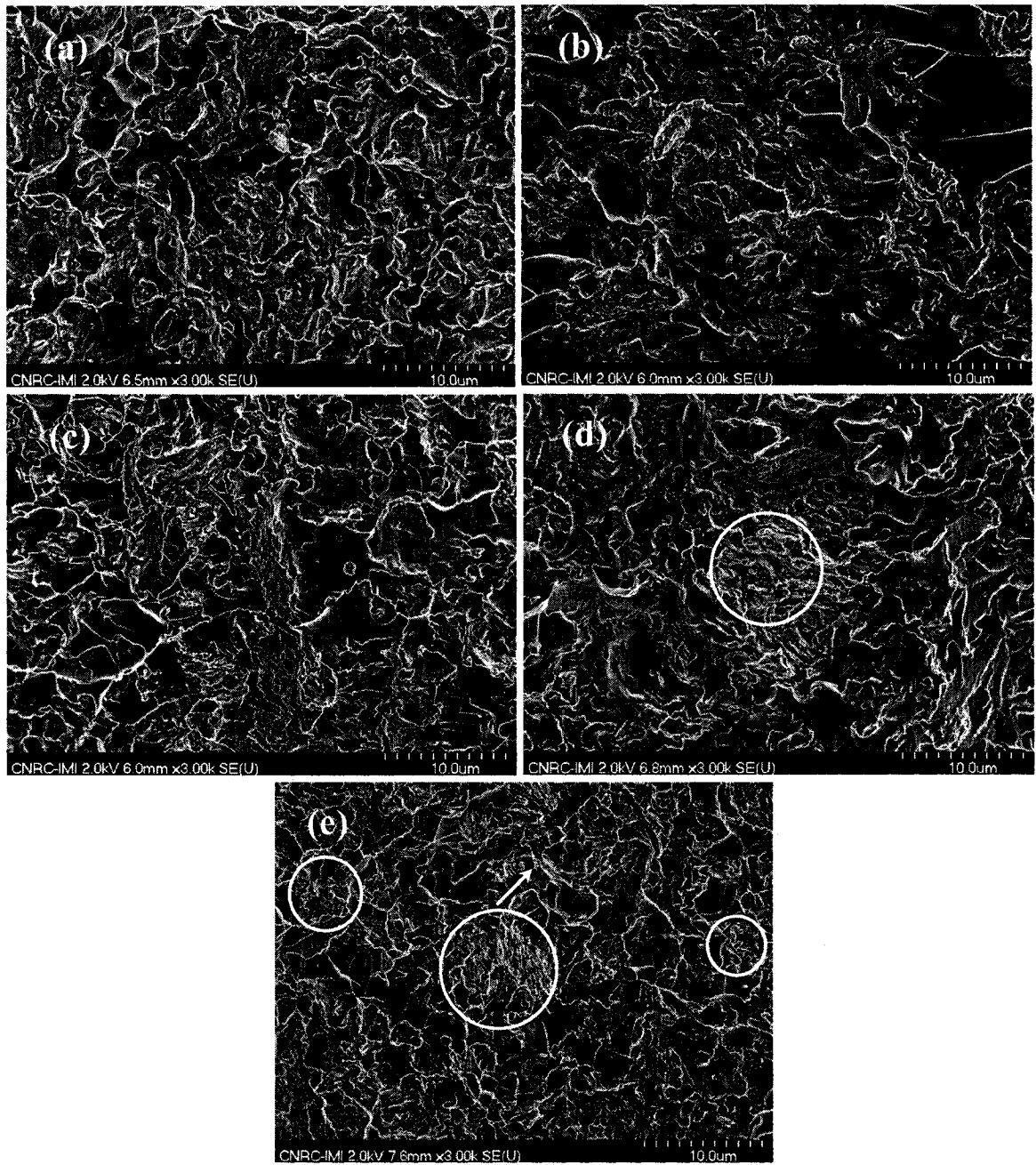


**Figure 7.23. Fracture surfaces for 6 wt% C30B epoxy nanocomposites cured with different D230-D2000 mixtures, (a) d0D100, (b) d25D75, (c) d35D65, (e) d60D40, and (e) d100D0**

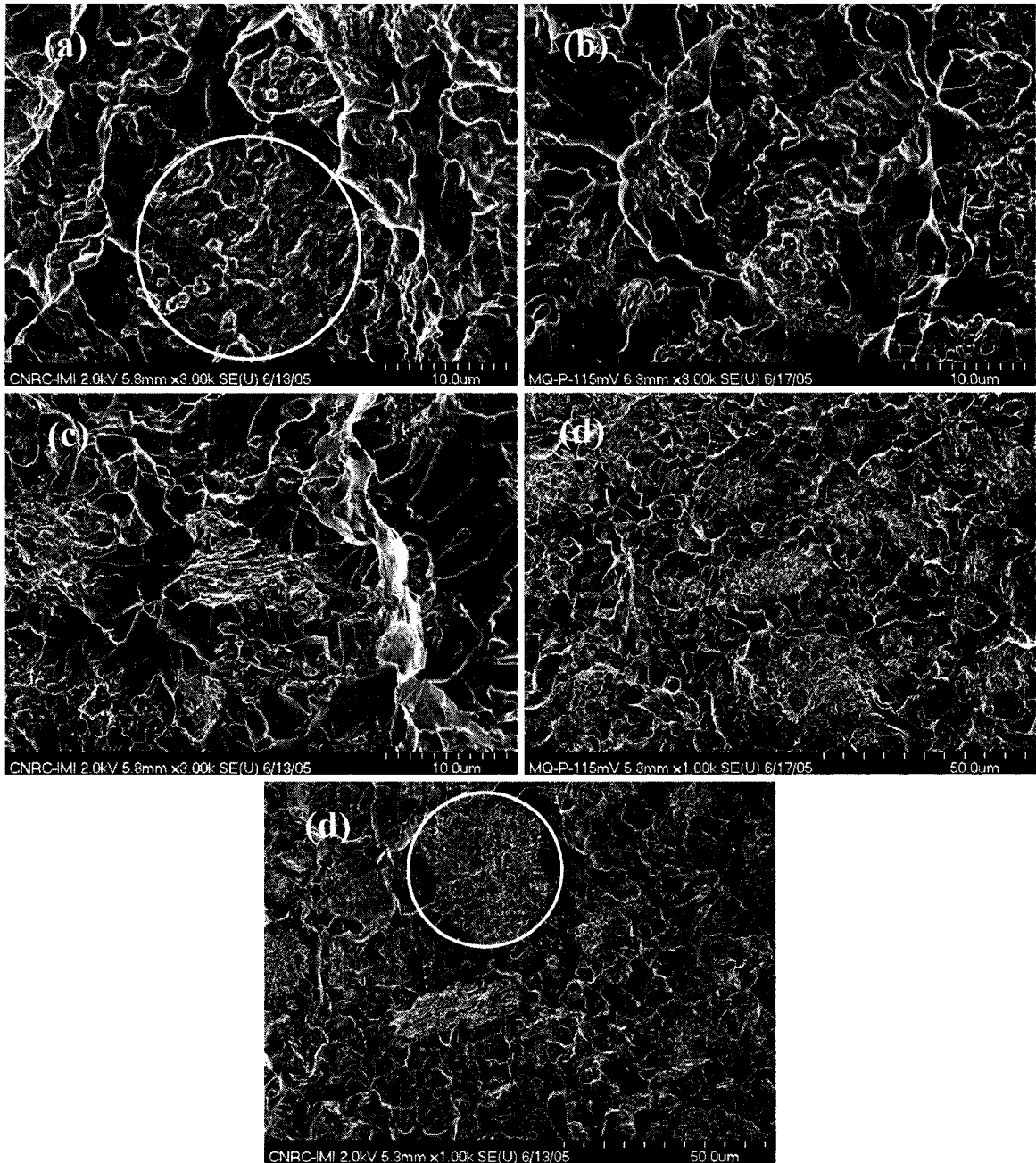


**Figure 7.24. Fracture surfaces for 6 wt% I30E epoxy nanocomposites cured with different D230-D2000 mixtures, (a) d0D100, (b) d25D75, (c) d35D65, (e) d60D40, and (e) d100D0**

However, with I30E nanocomposites, the clay aggregates are observed on the fracture surface of the all systems (Figure 7.24). Moreover, for the rubbery system, owing to the much greater elongation upon stress above the  $T_g$ , the improved performance of rubbery nanocomposite may largely be due to shear deformation [11], where nanoclay under strain may align as discussed earlier, thus further contributing to the improved performance. FEGSEM micrographs for fracture surfaces also indicated that the micro dispersion of C30B is better than I30E in epoxy systems which were cured with the same hardener.

From the results we can see that the quality of dispersion and intercalation/exfoliation, and the mechanical behavior of the glassy and rubbery epoxy nanocomposites are distinct. Because of this, it is interesting to further understand the reinforcing effect of nanoclay on mechanical properties of the two epoxy systems. Modulus is one target issue which is described in the following section.

## **7.4. Modulus prediction**

### **7.4.1. Halpin-Tsai and Mori-Tanaka models**

Prediction of the mechanical properties of discontinuous fiber/flake composite materials has been a subject of extensive study. The composite of interest is considered to consist of two homogeneous phases of matrix and high-aspect-ratio particles. The particle and matrix domains are shown in Figure 7.25.

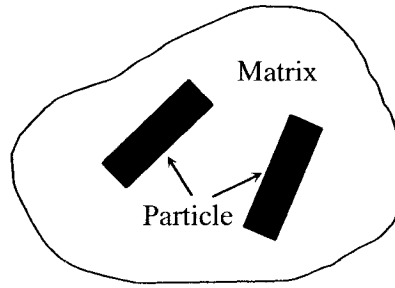


**Figure 7.25. Illustration of the ‘particle’ and ‘matrix’ domains in conventional composite**

Halpin and Tsai developed a well known composite theory for predicting the stiffness of unidirectional composites as a function of aspect ratio [163-165]. This theory can be adapted for a variety of reinforcement geometries, including discontinuous filler reinforcement such as clay particle. The Halpin-Tsai equation for prediction of the longitudinal stiffness of composites filled with unidirectional disk-like particles is given by

$$\frac{E}{E_m} = \frac{1 + 2A_p \eta_p f_p}{1 - \eta_p f_p} \quad (7.1)$$

where,  $E$  and  $E_m$  represent the Young’s modulus of composite and matrix, respectively,  $A_p$  is the aspect ratio of the particles ( $A_p$  is defined as length divided by thickness of the particles  $L/t$ ),  $f_p$  is the volume fraction of particles in the composite, and  $\eta_p$  is given by

$$\eta_p = \frac{(E_p / E_m) - 1}{(E_p / E_m) + 2A_p} \quad (7.2)$$

where,  $E_p$  represents the Young’s modulus of the particles.

The Mori-Tanaka average stress theory has also received considerable attention in the literature [166]. It was derived on the principles of Eshelby's inclusion model for predicting an elastic stress field in and around an ellipsoidal particle in an infinite matrix [167]. To account for finite filler concentrations, Mori and Tanaka [166], however, considered a non-dilute composite consisting of many identical spheroidal particles that cause the matrix to experience an average stress different from that of the applied stress; to satisfy equilibrium conditions the volume average stress over the entire composite was forced to be equal to the applied stress. Tandon and Weng [168] used this assumption and Eshelby's solution to derive complete analytical solutions for the elastic moduli of an isotropic matrix filled with aligned spheroidal inclusions. The result for closed-form solution based on the Mori-Tanaka model is

$$\frac{E}{E_m} = \frac{1}{1 - f_p \zeta} \quad (7.3)$$

$$\zeta = [-2\nu_m A_3 + (1 - \nu_m)A_4 + (1 + \nu_m)A_5 A] / (-2A) \quad (7.4)$$

where  $f_p$  is particle volume fraction,  $\zeta$  is a positive coefficient depending on the matrix Poisson ratio,  $\nu_m$ , and constants  $A$  and  $A_i$ ;  $A$  and  $A_i$  can be calculated from the matrix/particle properties and components of the Eshelby tensor [167], which depend on the particle aspect ratio ( $L/t$ ) and dimensionless elastic constants of the matrix [168].

For aligned disk-shaped particles, Figures 7.26 and 7.27 depict the dependence of  $E/E_m$  on volume fraction  $f_p$ , aspect ratio  $A_p = L/t$ , and ratio of  $E_p/E_m$ , as predicted by Equations 7.1 and 7.3.



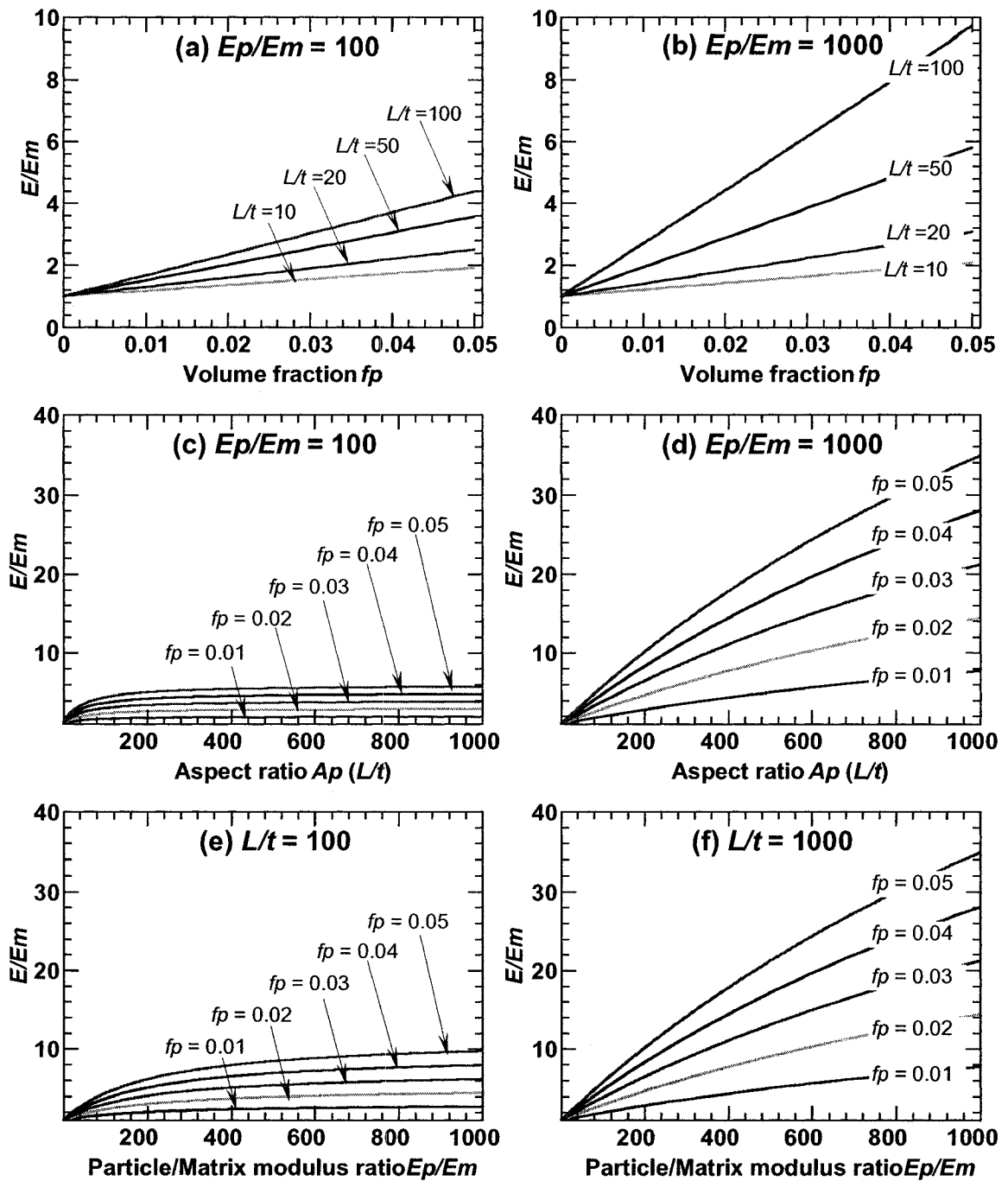


Figure 7.26. Results of the Halpin-Tsai model (H-T): dependence of  $E/E_m$  on (a), (b)  $f_p$ ; (c), (d)  $L/t$  and (e), and (f)  $E_p/E_m$

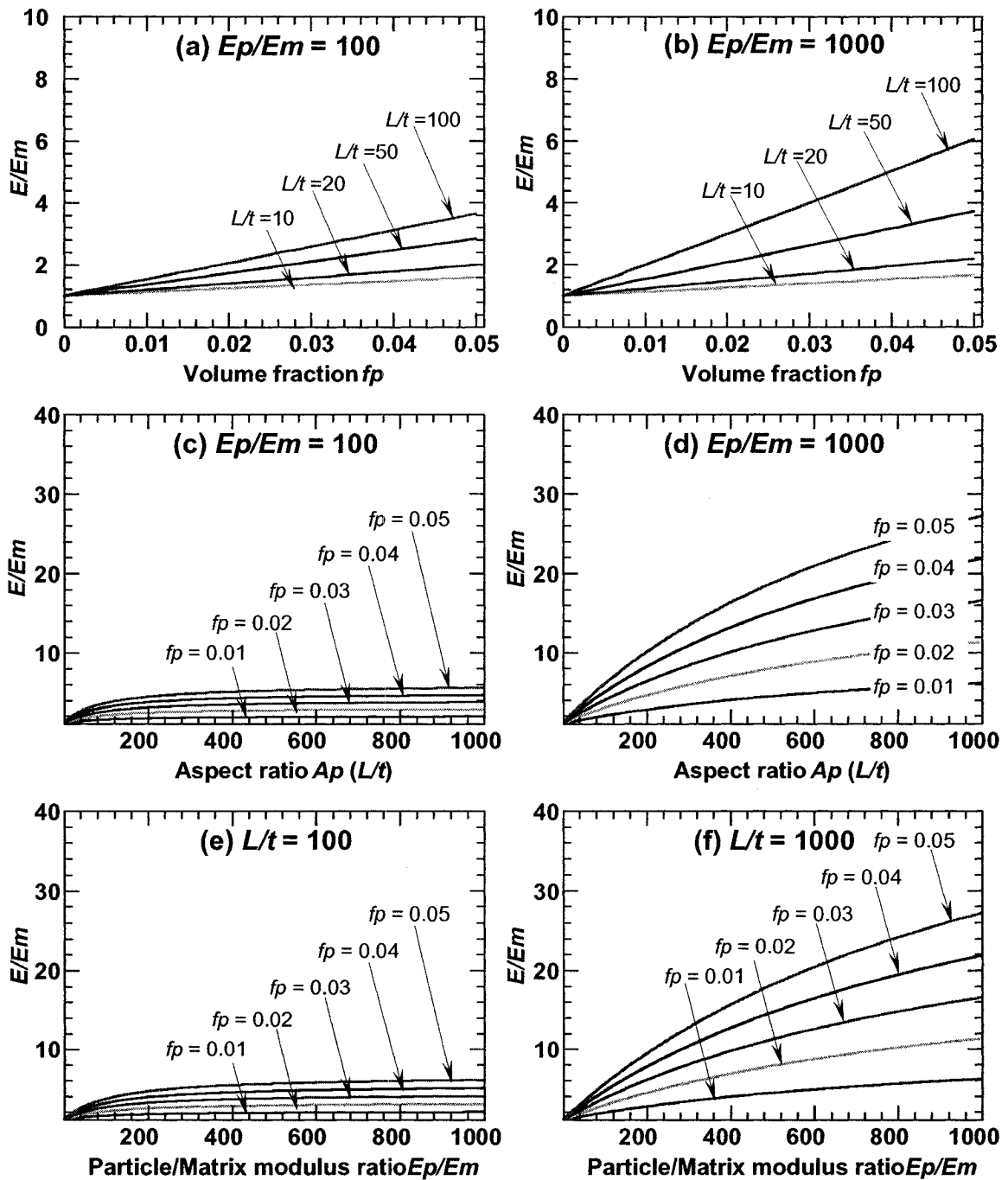


Figure 7.27. Results of the Mori-Tanaka model (M-T): dependence of  $E/E_m$  on (a),

(b)  $f_p$ ; (c), (d)  $L/t$  and (e), and (f)  $E_p/E_m$

Figures 7.26a, 7.26b, 7.27a, and 7.27b indicate that  $E/E_m$  increases almost linearly with the volume fraction of particles  $f_p$  for a fixed  $L/t$  and  $E_p/E_m$ . Figures 7.26 and 7.27 also show a greater reinforcing effect of particle on the  $E/E_m$  with large aspect ratio  $L/t$  or high  $E_p/E_m$ . However, the dependencies of  $E/E_m$  on aspect ratio of particles  $L/t$  (Figures 7.26c, 7.26d, 7.27c, and 7.27d) and particle/matrix modulus  $E_p/E_m$  (Figures 7.26e, 7.26f, 7.27e, and 7.27f) are nonlinear for a fixed  $f_p$ . In general, both models show the same expected trends, but the Halpin-Tsai model is consistently stiffer than the Mori-Tanaka model.

#### 7.4.2. Representation of intercalated/exfoliated nanoclay

From TEM micrographs, a clearly defined particle does not exist in most polymer-clay nanocomposites. It is obvious that often one has incompletely exfoliated stacks of clay platelets, containing some intercalant and matrix between the clay platelets in each stack. These stacks can contain several clay platelets and the platelets within a stack can be at various distances from each other. The ‘effective particles’ which are incompletely exfoliated stacks of individual platelets have been proposed by Brune and Bicerano [165]. The ‘effective particle’ is identified by a well-defined spatial volume, occupied by both the silicate layers and the inter-layer galleries, as shown in Figure 7.28 [169].

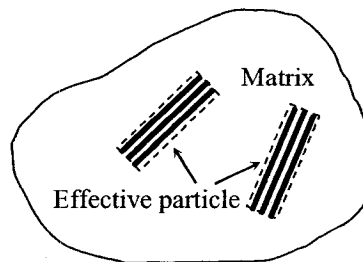


**Figure 7.28. Illustration of the ‘effective particle’ and ‘matrix’ domains in nanocomposite**

For simplicity, the internal structure of an intercalated clay particle (effective particle) is idealized as a multi-layer stack containing  $N$  single silicate sheets (platelets) with uniform inter-layer spacing  $d_{001}$  as shown in Figure 7.29. Separating adjacent sheets is a so-called gallery layer comprising both intercalants or surfactants and polymer matrix chains that have penetrated the inter-silicate layers during various stages of synthesis and processing. The particle thickness  $t$  can be related to the internal structural parameters  $N$  and  $d_{001}$  through

$$t = (N-1) d_{001} + d_s \quad (7.5)$$

Where  $d_s$  is the silicate sheet thickness ( $d_s = 0.96$  nm [41]). Therefore,  $N$  can be calculated as follows:

$$N = \frac{t - d_s}{d_{001}} + 1 \quad (7.6)$$

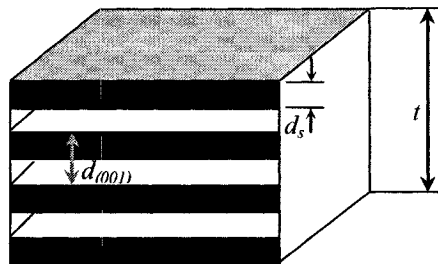


**Figure 7.29. Multi-layer structure of intercalated nanoclay (effective particle)**

The volume fraction of platelets in the effective particle is

$$\chi = \frac{V_s}{V_p} = \frac{Nd_s}{(N-1)d_{001} + d_s} \quad (7.7)$$

Where  $V_s$  and  $V_p$  are the volumes assigned to the silicate sheets (platelets) in a stack and to the ‘effective particles’, respectively.

Figure 7.30 shows the relationship between silicate volume fraction  $\chi$  and  $d_{001}$  at different  $N$ . It indicates a decrease in silicate volume fraction  $\chi$  with increased  $d_{001}$  (with  $N > 1$ ). The case  $N = 1$  stands out from the others.

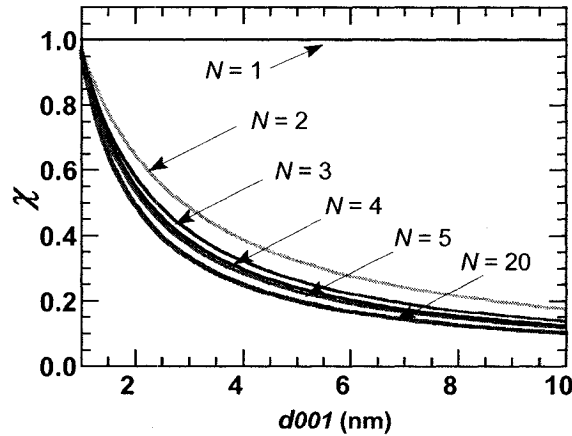


**Figure 7.30. Relation between volume fraction of clay platelets ( $\chi$ ) and  $d_{001}$  at different  $N$**

According to the simple rule of mixture relation (ROM) [165], the modulus of ‘effective particles’ can be predicted as follows

$$E_p = \chi E_s + (1 - \chi) E_m \quad (7.8)$$

Since the clay content is provided in terms of weight fraction  $W_s$  (ash weight), it is necessary to establish a quantitative connection between  $W_s$  and the volume fraction of the ‘effective particles’  $f_p$ . First, consider a two-phase composite consisting of matrix and particles (or effective particles in the case of a nanocomposite); the ‘effective particles’ volume fraction  $f_p$  and ‘effective particles’ weight fraction  $W_p$  are related according to

$$f_p = \frac{W_p / \rho_p}{W_p / \rho_p + (1 - W_p) / \rho_m} \quad (7.9)$$

where  $\rho_p$  and  $\rho_m$  are the mass densities of ‘effective particles’ and matrix, respectively.

For an intercalated nanocomposite,  $W_s$  differs from the ‘effective particles’ weight fraction  $W_p$ , since the ‘effective particles’ consists of both silicate sheets and the inter-layer galleries. The two quantities are related through

$$\frac{W_p}{W_s} = \frac{\rho_p V_p}{\rho_s V_s} = \left( \frac{\rho_p}{\rho_s} \right) / \left( \frac{V_s}{V_p} \right) = \left( \frac{\rho_p}{\rho_s} \right) \frac{1}{\chi} \quad (7.10)$$

where  $\rho_s$  is the mass density of the silicate sheet (platelet), and the ratio  $W_p/W_s$  is defined as  $\alpha$ .

Taking  $W_p = \alpha W_s$  into Equation 7.9, we can write  $f_p$  as a function of  $W_s$

$$f_p = \frac{W_s / \rho_p}{W_s / \rho_p + (1 / \alpha - W_s) / \rho_m} \quad (7.11)$$

When  $W_s$  is small, as it often is for the nanocomposite, Equation 7.11 can be linearized as

$$f_p \approx \left( \frac{\alpha \rho_m}{\rho_p} \right) W_s = \left( \frac{\rho_m}{\rho_p} \frac{\rho_p}{\rho_s} \frac{1}{\chi} \right) W_s = \left( \frac{\rho_m}{\rho_s} \frac{1}{\chi} \right) W_s \quad (7.12)$$

Figure 7.31 shows the relationship between  $f_p/W_s$  and  $d_{001}$  at different  $N$ . This figure indicates that the increase in  $d_{001}$  leads to increase of  $f_p/W_s$  ratio (with  $N > 1$ ).

With effective representation of the nanoclay, Figures 7.32 and 7.33 depict the dependence of  $E/E_m$  on  $W_s$ ,  $N$  and  $E_s/E_m$ , as predicted by Equations 7.1 and 7.3 for aligned ‘effective particles’ instead of particles as in conventional composite. Figures 7.32a, 7.32b, 7.33a, and 7.33b indicate that  $E$  (for both of the two models) increases almost linearly with increasing  $W_s$  for a fixed  $N$  and  $E_s/E_m$ . There is a greater reinforcing effect of particle on the  $E/E_m$  with smaller values of  $N$ . With the same  $N$ , the higher is the ratio of  $E_s/E_m$ , the higher is the influence of clay on  $E/E_m$  (comparing Figures 7.32a and 7.32b, Figure 7.33a and 7.33b). Figures 7.32c and 7.33c show the effect of  $d_{001}$  on  $E/E_m$  at  $N$  of 5. These figures indicate that the higher is  $d_{001}$  (better intercalation/exfoliation), the stronger is the reinforcing effect of particles on the  $E/E_m$ . That means better intercalation/exfoliation provides a better reinforcing effect.

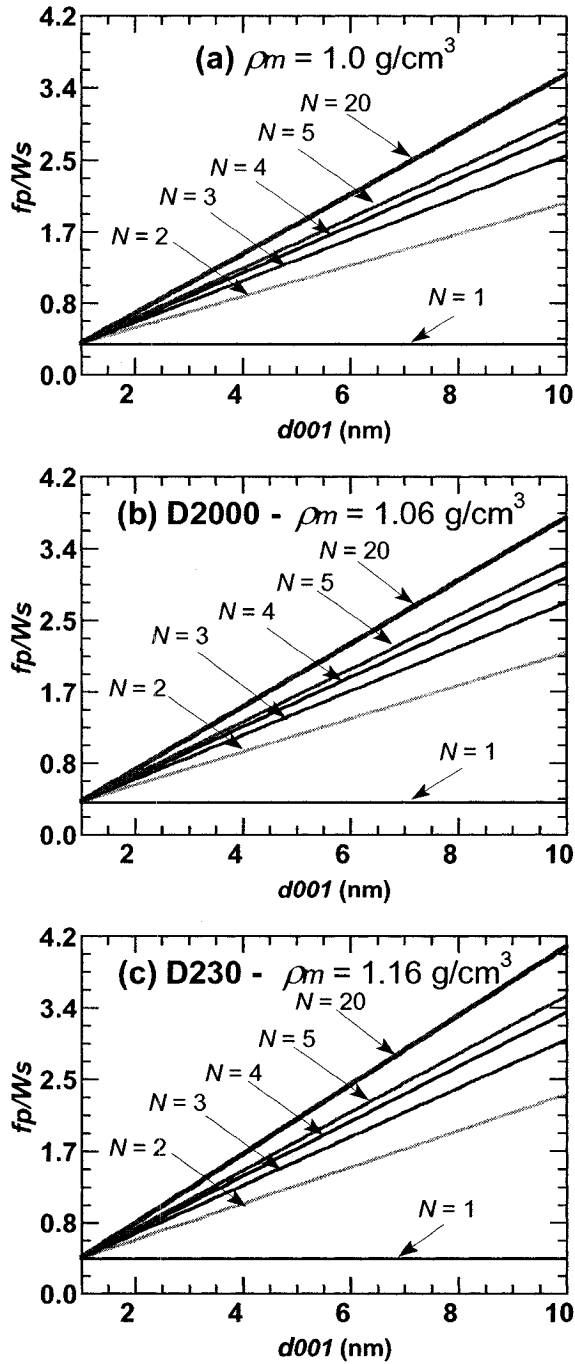


Figure 7.31. Relation between  $f_p/W_s$  and  $d_{001}$  at different  $N$  with  $\rho_m$  of (a)  $1.0 \text{ g/cm}^3$ , (b)  $1.06 \text{ g/cm}^3$  (D2000), and (c)  $1.16 \text{ g/cm}^3$  (D230)



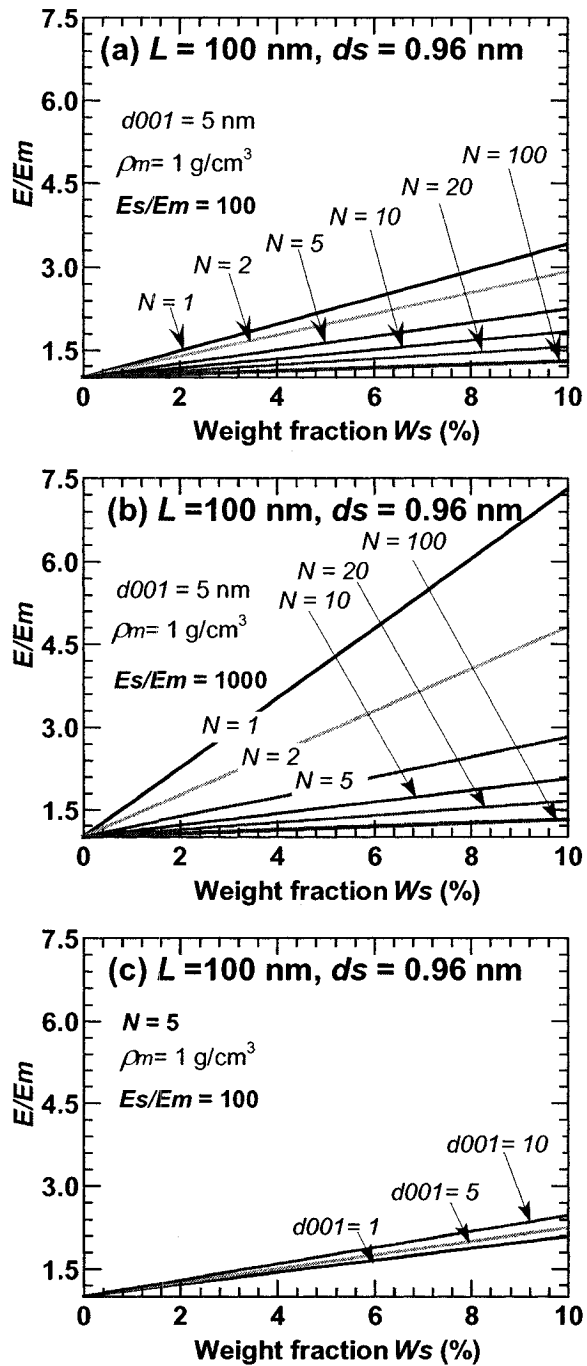


Figure 7.32. Effect of clay structural parameters ( $N$ ,  $d_{001}$ ), weight fraction of clay and ratio of  $E_s/E_m$  on the macroscopic modulus, predicted by the Halpin-Tsai model

(a)  $d_{001} = 5 \text{ nm}$ ,  $\rho_m = 1 \text{ g/cm}^3$ ,  $E_s/E_m = 100$ , (b)  $d_{001} = 5 \text{ nm}$ ,  $\rho_m = 1 \text{ g/cm}^3$ ,  $E_s/E_m = 1000$ ,

and (c)  $N = 5 \text{ nm}$ ,  $\rho_m = 1 \text{ g/cm}^3$ ,  $E_s/E_m = 100$

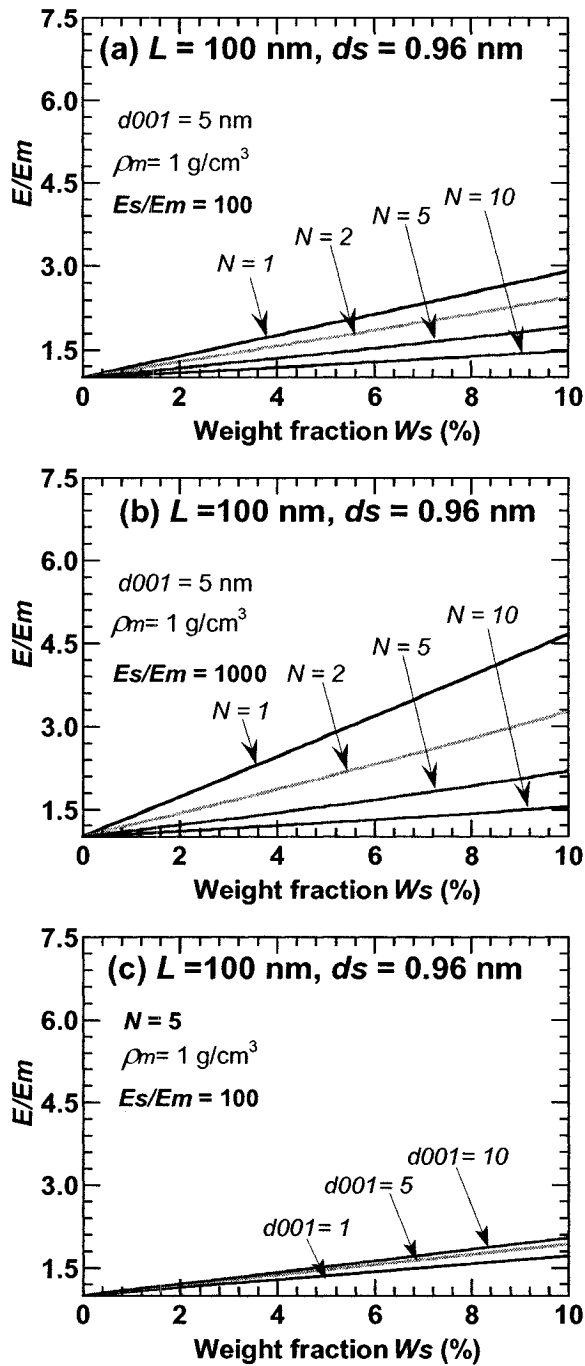


Figure 7.33. Effect of clay structural parameters ( $N$ ,  $d_{001}$ ), weight fraction of clay and ratio of  $E_s/E_m$  on the macroscopic modulus, predicted by the Mori-Tanaka model (a)  $d_{001} = 5 \text{ nm}$ ,  $\rho_m = 1 \text{ g/cm}^3$ ,  $E_s/E_m = 100$ , (b)  $d_{001} = 5 \text{ nm}$ ,  $\rho_m = 1 \text{ g/cm}^3$ ,  $E_s/E_m = 1000$ , and (c)  $N = 5 \text{ nm}$ ,  $\rho_m = 1 \text{ g/cm}^3$ ,  $E_s/E_m = 100$

The result from TGA testing shows there is 70.84% of inorganic material remaining for C30B at 1000°C (Figure 7.10). This value represents the percentage of silicate in C30B. From there, the weight fraction of silicate in these two nanocomposites (6% of organo nanoclay)  $W_s$  is 4.25%. The length of the platelet  $L$  is about 100 nm (evaluated from TEM). The data for calculation are shown in Table 7.3.

**Table 7.3. Component property data used for calculating composite modulus**

System	$\rho_s$ (g/cm <sup>3</sup> ) [170-173]	$\rho_m$ (g/cm <sup>3</sup> )	$E_m$ (MPa)	$E_s$ (GPa) [168-170]	$W_s$ (%)	$d_s$ (nm)	$L$ (nm)
D2000	2.83	1.06	4.06	178	4.25	0.96	100
D230		1.16	3218				
<i>Experiment:</i> D230 6wt% clay $N \sim 10-15$ : poor dispersion; 2 wt% clay $N \sim 4$ : good dispersion D2000 6wt% clay $N \sim 1-2$ ( $N$ is the number of clay layers/stack)							

Figure 7.34 shows the results obtained from the rule of mixture ( $E = E_s V_s + (1 - V_s) E_m$ ), Halpin-Tsai, Mori-Tanaka equations, and experiment, for both completely exfoliated and incompletely exfoliated systems. If the clay is fully exfoliated in nanocomposites, all of the clay sheets separate from each other. The shape parameter in this case is  $A_p = L/t = L/d_s = 104.17$ . From there, with polymer-clay nanocomposites, the value of  $A_p$  can not be infinity for the clay platelets. This explains why the values of modulus that were calculated from the simple rule of mixture (Figures 7.34a, and 7.34b) do not correspond to the results obtained from experiment. Apparently, the increase of  $N$  leads to lower reinforcement efficiencies, especially for the incompletely exfoliated system. It also can be seen clearly that clay has a better reinforcing effect in the rubbery system than the glassy one (Figures 7.34c, 7.34d, 7.34e, and 7.34f).

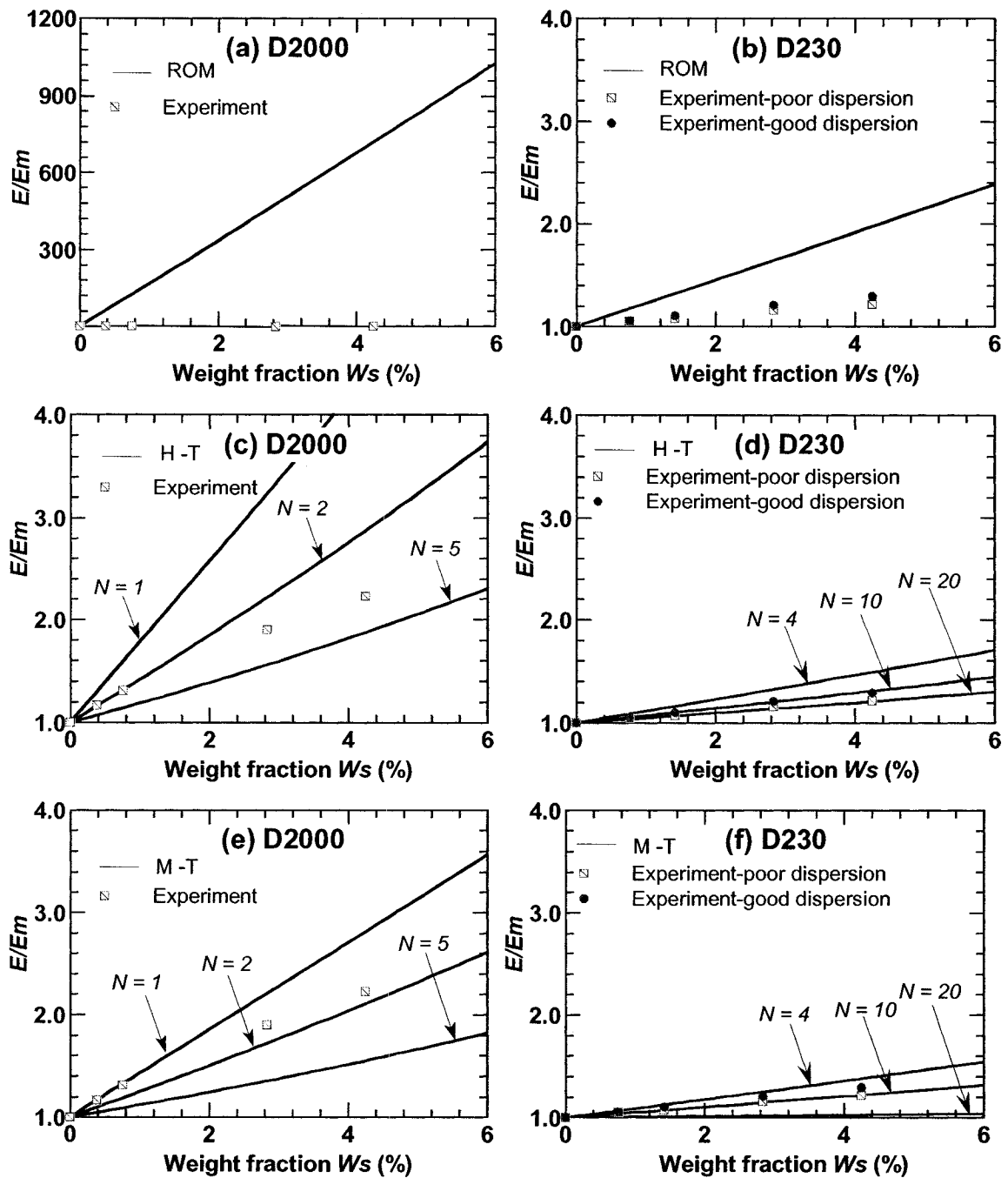


**Figure 7.34. Effect of weight fraction  $W_s$  and  $N$  on the macroscopic modulus of D2000 and D230 nanocomposite systems, predicted by (a, b) the rule of mixture-ROM, (c, d) the Halpin-Tsai model, and (e, f) the Mori-Tanaka model**

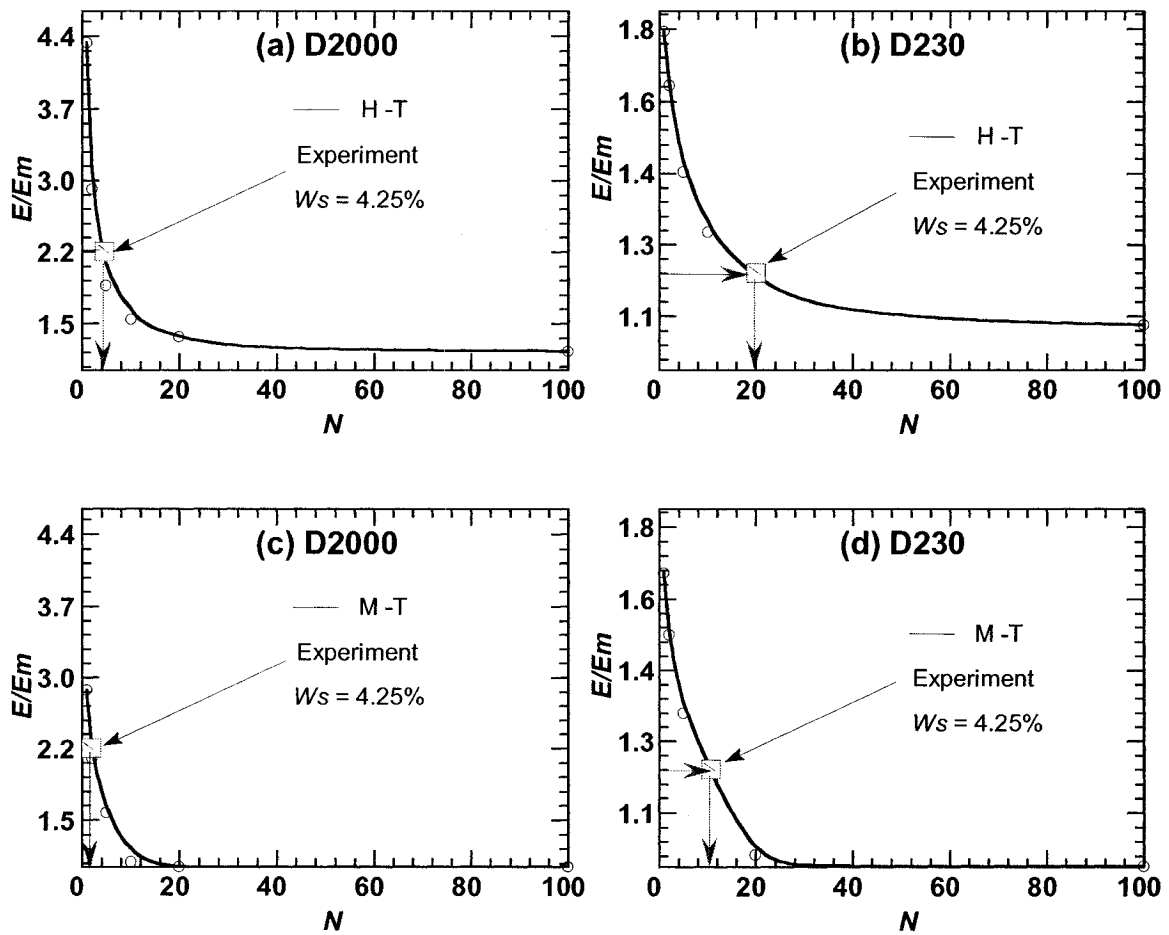


**Figure 7.35. Effect of  $N$  on the macroscopic modulus of D230 and D2000 nanocomposite systems, predicted by (a, b) the Halpin-Tsai and (c, d) the Mori-Tanaka models compared to experiment results**

At the same value of  $N$  the reinforcement of C30B in EPON828-D2000 is higher than in the EPON828-D230 system. The largest drop in reinforcement is experienced when going from one platelet to two platelets per stack for the rubbery system. The effect of the value of  $N$  on the modulus of nanocomposite at  $W_s = 4.25\%$  is plotted and shown in Figure 7.35. The Halpin-Tsai model gave a value of  $E$  close to experiment at  $N$  about 3 to 4 and 20 for nanocomposite based on D2000 and D230, respectively. However, The

Mori-Tanaka model gave a value of  $E$  close to experiment at  $N$  about 1 to 2 and 10 for nanocomposite based on D2000 and D230, respectively. The results are in good agreement with the experimental result that clay has been better dispersed into smaller stacks in the D2000 system (rubbery system) than in the D230 one (glassy system) for both models. Again the results confirm that the Halpin-Tsai model is stiffer than the Mori-Tanaka model. According to the XRD and TEM results (Figure 7.3 and Table 7.3), C30B is almost exfoliated by EPON828-D2000. This means the value of  $N$  is almost 1 for this case. From this result, one can see that the Mori-Tanaka model gives the best results for large aspect ratio fillers. A similar result was also reported by other researchers [166, 168, 169].

The Halpin-Tsai and Mori-Tanaka models describe the reinforcing effect of nanoclay for rubbery and glassy systems. They confirm the clay has a greater reinforcing effect on rubbery epoxy system than on a glassy system.

## 7.5. Summary

Epoxy resins can display totally different behavior at room temperature, depending upon whether their glass transition temperature occurs above or below room temperature. The reinforcing effect of nanoclay in epoxy systems whose characteristics can vary over a broad range from rubbery to glassy rubbery was evaluated. Although the presence of C30B and I30E does not influence the  $T_g$  of epoxy systems except the system which was based on I30E and cured with D230, it significantly affects the mechanical properties of materials. Tensile strength, modulus, and toughness improve significantly in the rubbery system with the presence of nanoclay. However, in the glassy system the presence of clay

increases only the modulus and does not lead to an improvement of the tensile strength while it reduces the toughness and ductility. The fracture surface was also found to be influenced by the presence of nanoclay. In this particular study, the organoclay C30B is better dispersed and better intercalated/exfoliated in the rubbery epoxy system than in the glassy one, mainly because of its lower curing rate and the size of the hardener molecule. However, a different phenomenon appears for the case of nanoclay I30E, which is less well dispersed in the rubbery system than in the glassy one. Micro dispersion of C30B is better than I30E in an epoxy system cured with the same hardener.

A better reinforcing effect of organoclay in the rubbery system can involve different contributions: 1) better micro-dispersion, 2) better intercalation/exfoliation, 3) a greater relative contribution of the clay mechanical properties because of the lower matrix properties compared to the glassy one, and 4) alignment ability of clay in response to the applied stress.

The Halpin-Tsai and Mori-Tanaka models confirm the clay has a greater reinforcing effect on a rubbery epoxy system than on a glassy system, and Mori-Tanaka model shows better agreement with the result from experiments.

From the experimental results described in Chapters 4 and 7, we can represent the effect of reactivity of clays and hardeners on the intercalation/exfoliation of clay in epoxy nanocomposites as in Figure 7.36.

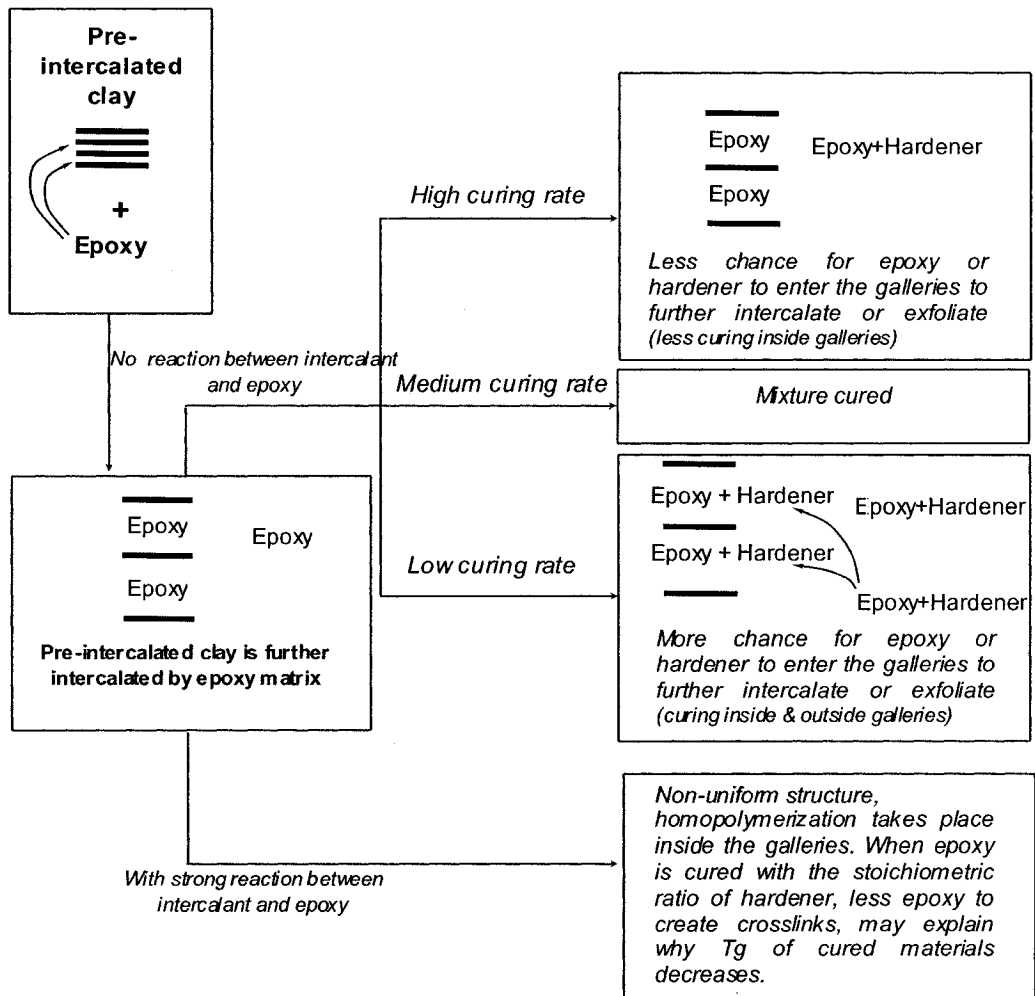


**Figure 7.36. Intercalation/exfoliation of clay during the stirring and curing of epoxy nanocomposites**



# Chapter 8

## Summary, conclusions, contributions and recommendations for future work

### 8.1. Summary

The formation and the properties of montmorillonite clay based ENC<sub>s</sub> have been investigated in this thesis. A new solvent-free stirring method using a homogenizer was implicated to fabricate the ENC<sub>s</sub>. The effects of clays, curing agents and processing parameters on the fabrication, curing process and performance of ENC<sub>s</sub> were studied.

#### **In Chapter 4:**

- Dispersion of organoclays in ENC<sub>s</sub> is a very complex process. The results have confirmed that there are several different levels of dispersion of organoclays in ENC<sub>s</sub> depending on the processing conditions. They include: 1) exfoliated or delaminated clay layers; 2) non-intercalated stacks (multiple layers not intercalated) or intercalated stacks (multiple layers intercalated); and 3) multiple-stack aggregates (multiple stacks forming aggregates on the micro-scale).
- The quality of dispersion can be controlled during the stirring (pre-mixing) of the clay with epoxy as well as during the curing. Mechanical force and thermodynamic rules

govern the dispersion process. Since it is difficult to apply conventional mechanical forces and because of the limited gellation time of the resin in the curing step, it is favorable to emphasize the effort in the mixing step, in which the resin has extended shelf life and it is possible to use different types of force to facilitate the dispersion process.

– Intercalation is controlled by the diffusion of epoxy resin (both epoxy and hardener) into the clay galleries, which is governed by thermodynamic rules. The chosen organoclays (C30B and I30E) have an acceptable compatibility with the epoxy, therefore it can diffuse quite easily into the clay galleries even at room temperature. However, high temperature and sufficient time are required to facilitate the diffusion and to obtain a uniform intercalation. On the other hand, breaking the macro-aggregates down into multiple-stack aggregates can be effectively achieved by using mechanical shear forces. However, exfoliation cannot be achieved by using the shear force alone that was generated from the devices used in this study. Exfoliation is more likely controlled by diffusion of the resin into the galleries. It is also evident that although the shear force cannot delaminate the clay stacks into individual platelets, it breaks down the large aggregates into smaller stacks, thus facilitating the diffusion of polymer molecules into the clay galleries. As a consequence, the organoclays have a finer dispersion as well as a more uniform distribution and a more uniform intercalation in the pre-mixing of clay and epoxy. The dispersion, intercalation and exfoliation are favorable when the stirring intensity and temperature increase.

– Intercalation and exfoliation continue to take place during the curing step by the diffusion of the monomers and oligomers into the clay galleries. However, the diffusion of monomers and oligomers into the clay galleries in this step may be inhibited by the

curing reaction that limits or restricts the molecule mobility. It is important to control the curing process either by controlling the curing temperature or the chemistry of hardener in order to favor the intercalation and exfoliation process. A good temperature range for favoring the intercalation and exfoliation is dependent on the chemical reactivity and mobility of hardener, and the compatibility between hardener and organoclays.

– The effects of different stirring parameters (temperature, speed, and duration), chemistry of clay, and hardeners (chemical reactivity) on the formation of ENC<sub>s</sub> were studied. Temperature, speed and duration of stirring have a positive effect on dispersion and intercalation/exfoliation of clay in epoxy at the stirring step. However, stirring speed is more powerful compared to temperature and duration in terms of breaking down the clay aggregates. Agglomerates of organoclay were broken down to very small tactoids with high speed stirring, which results in well dispersed and well intercalated/exfoliated ENC<sub>s</sub>. With mechanical stirring at high temperatures, organoclay C30B exists in ENC<sub>s</sub> in the form of aggregates, whose size is on a micro-scale (maximum about 15 μm and minimum about 3 μm). However, these aggregates were broken down into the smaller ones with only high speed (maximum about 5.8 μm and minimum about 0.56 μm) and uniformly distributed in epoxy nanocomposites. Moreover with high speed and high temperature stirring, these aggregates could be broken down to tactoids consisting less than 4 silicate layers, and much more uniformly distributed in ENC.

– The chemical reactivity of the studied organoclay does not seem to have a strong effect on intercalation/exfoliation at the stirring step (with R<sub>m</sub> and T<sub>m</sub> methods). However, it affected the quality of clay dispersion and clay intercalation at the curing

step. The more reactive organoclay I30E has better intercalation in the ENC's compared to C30B. On the other hand, C30B shows a better micro dispersion in nanocomposites than I30E.

– Chemical reactivity of hardener is a main factor that controls the dispersion and intercalation/exfoliation of clay in epoxy matrix. It is worth stressing here that in thermoset systems, the intercalation and exfoliation process can continue during the curing, and is controlled not only by the rate of diffusion of organic molecules (in this case, the curing agent and the epoxy molecules) into the clay gallery but also by the curing rate of the epoxy system and by the size of epoxy and hardener molecules. For reactive clay (I30E), one has better intercalation/exfoliation with fast and medium curing rate epoxy systems but not for long molecular and low curing rate hardeners. On the other hand, the longer is the molecule and the lower is the curing rate of the hardener, the better is the intercalation/exfoliation of C30B.

– A model for flow in a concentric cylinder high shear stirrer was developed and applied to predict the processing conditions necessary for achieving delamination of the clay layers. The model provides a useful tool for determining the required processing parameters to separate the clay layers in thermosetting polymers. It can also be used to design a new stirrer to give the desired shearing force.

#### **In Chapter 5:**

– Effects of different types of organoclay and curing agent on the curing kinetics of epoxy nanocomposites were examined. There is a certain effect of the organoclay type and clay dispersion on the curing kinetics as studied by dynamic scan, but it is quite

minor. The I30E was expected to have a great impact on the results due to its chemical reactivity with the epoxy. However, the reaction with epoxy and amine takes place quite fast even at room temperature and because in this study the temperature was raised slowly in the DSC device, the epoxy and hardener had enough time to react before the sample reached the critical temperatures. Therefore, the reactions of I30E with epoxy were almost negligible. The presence of clay does not seem to have a tremendous effect on the growing of microgels in the epoxy systems during the curing, with the possible exception of fast cure epoxy systems such as DETA.

– The  $E_a$  of the Nanomer I30E mixture is lower than that of the Cloisite 30B mixture. The influence of clay also depends on the rate of cure and behavior of curing agent. The change of activation energy  $E_a$  vs  $\alpha$  cure for epoxy and epoxy nanocomposites depends on hardeners. The presence of organoclay also results in a slight increase in the curing rate of epoxy nanocomposite compared to epoxy system.

– It is very important to stress here that depending on the intercalant chemistry of the organoclay, the organoclay either can generate or promote certain chemical reactions with the matrix. The C30B, which is based on quaternary ammonium intercalant does not undergo chemical reaction with the epoxy matrix. The I30E was treated with an excess amount of primary amine intercalant. Both the primary amine bound to the clay surface and the free amine can react with the epoxy matrix in different ways. The primary amine bound to the clay surface can catalyze the polymerization of the epoxy ring and the hydroxyl group of the DGEBA, while the free primary amine can react with the epoxy group (in the absence of hardener). The first case leads to a dangerous practice since the

polymerization liberates a high amount of heat that can generate fire and possible explosion if a large quantity used. However, the reaction only takes place at high temperatures (above 150°C). The second reaction is also not favorable because it causes a significant increase in viscosity which is always a challenge in the fabrication of epoxy-based products. However, the reaction is more noticeable at temperatures above 120°C. It is very important to remark here that in the preparation of ENCs with I30E, full attention must be paid to these reactions in order to avoid accident, especially when high temperature is involved. The recommended temperature for the preparation of ENCs with I30E is 120°C and below. If curing temperature above 120°C is required, it is recommended to raise the temperature slowly or begin the reaction at low temperature for a certain period of time in order to allow the epoxy to react with hardener first. This means that the concentration of epoxy has to be sufficiently reduced before the system reaches that temperature in order to minimize the heat release by the above-mentioned reaction.

#### **In Chapter 6:**

– The intercalation and exfoliation do not automatically provide the best mechanical performance because the mechanical performance is controlled not only by the nano-structure but also by the macro- and micro-structure, because the macro- and micro-aggregates exist in the system. The presence of aggregates even at the micro-size can have a great negative impact on the mechanical performance (especially the strength, strain and ductility) because they are the weakest points in the system, and will initiate and promote failure under stress. To obtain good performance, it is important to reduce the size of the aggregates in the systems as much as possible.

- Processing parameters have an important influence on the dispersion of clay in the matrix and thus on the mechanical properties of ENCs. The better is the dispersion of clay in epoxy, the higher is the storage modulus of nanocomposite. It is interesting that shear can help to break down the aggregates to a sub-micro dispersion and bring back the strength equal to or even higher than the neat brittle epoxy.
- The findings in this study are quite superior to other data reported in the literature for glassy ENCs, where only a loss in tensile strength was reported [11, 12, 18, 27, 41, 45, 91]. The increase in tensile strength seems to reach a plateau at 4wt% clay loading. The modulus is quite linearly proportional to clay loading in the studied loading range. A significant loss in tensile strain as the result of increase in high modulus for the ENCs was also observed. A similar trend was also obtained for compressive properties.
- Better dispersion with the homogenizer provides improvement in fracture toughness of epoxy systems. The level of increase in  $K_{IC}$  and  $G_{IC}$  for ENCs depends on the behaviour of the epoxy systems.  $K_{IC}$  and  $G_{IC}$  increase significantly for soft and very brittle epoxy systems with the presence of clay. It also depends on the level of dispersion and intercalation/exfoliation of organoclay in nanocomposites (as discussed above). There is a huge improvement in fracture toughness of EPON828-D2000 and EPON828-BF<sub>3</sub> epoxy systems with the presence of clay (377% (4.77 times) and 838% (9.38 times) increases respectively, in  $K_{IC}$  and  $G_{IC}$  at 6 wt% C30B compared to neat EPON828-D2000 system, 117% (2.17 times) and 363% (4.63 times) increase for EPON828-BF<sub>3</sub>).
- The addition of clay in the epoxy matrix results in a decrease in water absorption. The diffusion behavior of water into the epoxy system and its nanocomposites has been

shown to be in good agreement with Fick's second law of diffusion. The presence of clay results in a decrease of diffusion coefficient in epoxy. The level of dispersion has somewhat of an effect on the diffusion behavior of water in nanocomposites.

- The addition of clay in the epoxy matrix also results in an improvement in solvent resistance. The level of dispersion of clay in epoxy has a great effect on the solvent resistance especially with toluene. The level of ethanol and toluene absorption of epoxy is reduced 1.6 times and 6.5 times (after 1970 hours) respectively with the presence of only 2 wt% C30B (nanocomposite was prepared by high speed and high temperature stirring method).

- The chemical reactivity of clays and hardeners has an effect on the properties of ENC. Nanocomposites containing the more reactive nanoclay I30E show slightly higher modulus than the nanocomposites containing less reactive C30B, but the inverse holds true for the strength. Different hardeners result in a difference in behavior of epoxy systems and hence the presence of clay shows different effects on mechanical properties.

- Flammability of ENCs decreases with the presence of clay, especially for the epoxy system which was cured with EPICURE 3046. The LOI of EPON828-EPICURE 3046 containing 4 wt% C30B (prepared by TS stirring method) increases 22% compared to that of neat EPON828-EPICURE 3046.

**In Chapter 7:**

- The reinforcing effect of nanoclay in epoxy systems whose characteristics can vary over a broad range from rubbery to glassy was evaluated (Different epoxy systems from



rubbery to glassy were chosen to have very similar chemistry in order to minimize its impact on the comparison of properties.). Although the presence of C30B and I30E does not influence the  $T_g$  of epoxy systems except for the system which was based on I30E and cured with D230, it significantly affects the mechanical properties of materials. Tensile strength, modulus, and toughness improve significantly in the rubbery system with the presence of nanoclay. However, in the glassy system the presence of clay does not lead to an improvement of the tensile strength and reduces the strain at break. The fracture surface was also found to be influenced by the presence of nanoclay. In this particular study, the organoclay C30B is better dispersed and better intercalated/exfoliated in the rubbery epoxy system than in the glassy one, mainly because of its lower curing rate and the size of the hardener molecule. However, nanoclay I30E has been more poorly dispersed in the rubbery system than in the glassy system. Micro dispersion of C30B is better than I30E in the system which was cured with the same hardener.

A better reinforcing effect of organoclay in the rubbery system can involve different contributions: 1) better micro-dispersion, 2) better intercalation/exfoliation, 3) a greater relative contribution of the clay mechanical properties because of the lower matrix properties compared to the glassy one, and 4) alignment ability of clay in response to the applied stress. The Halpin-Tsai and Mori-Tanaka models confirm that the clay has a greater reinforcing effect on a rubbery epoxy system than on a glassy system, and the Mori-Tanaka model shows better agreement with the result from experiments.

## 8.2. Conclusions

Development of ENCs with fine dispersion and exfoliated morphologies is a challenge, since high shear is always required but epoxy has low viscosity. Direct stirring of organoclay and epoxy with mechanical stirring and sonication is widely used to disperse nanoclay in epoxy. However it is not enough for good dispersion of clay in epoxy. The solvent assistance method can help to improve the dispersion of clay in epoxy. However, a lot of solvent was used and significant time was required for removing the solvent. In this thesis, a solvent-free stirring method was used to fabricate the epoxy nanocomposites. The effects of clays, curing agents and processing parameters on the fabrication, curing process and performance of epoxy nanocomposites were studied by various characterizations. The following conclusions can be made:

### **Dispersion of nanoclay in epoxy at the stirring and curing steps:**

- The processing parameters (temperature  $T$ , stirring speed  $\nu$ , and stirring duration  $t$ ), chemistry of clay and hardeners (chemical reactivity) involved in the formation of epoxy nanocomposites have a positive effect on dispersion and intercalation/exfoliation of clay in epoxy at the stirring step.
- Stirring speed is more powerful compared to temperature and duration in terms of breaking down the clay aggregates. There may be a critical speed to achieve uniformly distributed dispersion of clay aggregates in epoxy (suggestion 10000 rpm).

– Temperature helps to improve the diffusion of epoxy and hardener molecules into the clay galleries and expand them, especially at the curing step (curing at 120°C shows a strong effect on the delamination of clay).

– Duration of stirring does not have a strong effect on the *d*-spacing of clay at the stirring step. However, it helps to reduce the size of clay aggregates (stirring has to be at least 10 minutes) and has an indirect effect on delamination at the curing step. The chemical reactivity of the clay seems does not seem to have a strong effect on intercalation/exfoliation at the stirring step (with Rm and Tm methods). However, it affected the quality of clay dispersion and clay intercalation at the curing step. The more reactive clay I30E showed better intercalation/exfoliation in nanocomposites compared to C30B. On the other hand, C30B shows better micro dispersion in nanocomposites than I30E.

– The chemical reactivity of the hardener is also a main factor that controls the dispersion and intercalation/exfoliation of clay in an epoxy matrix. One obtains better intercalation/exfoliation with fast and medium curing rate epoxy systems than for long molecular and low curing rate hardeners with the reactive clay I30E. On the other hand, the longer is the molecule and the lower is the curing rate of hardeners, the better is the intercalation/exfoliation of the less reactive clay C30B.

#### **Curing process of epoxy nanocomposites:**

– The presence of the clay does not have a strong influence on the curing of epoxy nanocomposites (The presence of organoclay results in a slight increase in the curing rate

of epoxy nanocomposite compared to epoxy system. There is a minor steric effect of the clay on the cure of the nanocomposite).

#### **Performance of epoxy nanocomposites:**

- Better dispersion with a homogenizer provides an improvement in fracture toughness of epoxy systems. The level of increase in  $K_{IC}$  and  $G_{IC}$  for epoxy nanocomposites depends on the behaviour of the epoxy systems.  $K_{IC}$  and  $G_{IC}$  increase quite substantially for soft and very brittle epoxy systems with the presence of clay. The level of dispersion has an effect on the diffusion behavior of water in nanocomposites. The level of dispersion of clay in epoxy has a great effect on the solvent resistance, especially with toluene.
- The chemical reactivity of clays and hardeners has an effect on the properties of epoxy nanocomposites. Nanocomposites containing the more reactive nanoclay I30E show a higher modulus than the nanocomposites containing the less reactive nanoclay C30B, but the inverse holds true for the strength.
- Different hardeners can generate epoxy and epoxy nanocomposites with different properties. Usually, longer molecule hardeners result in softer materials than the shorter ones. Tensile strength, modulus, and toughness improve significantly in the rubbery system with the presence of nanoclay. Flammability of epoxy nanocomposite decreases with the presence of clay, especially in the epoxy system cured with EPICURE 3046.

### **8.3. Contributions**

In this study, many factors that affect the formulation, curing process and properties of epoxy nanocomposites have been investigated, including different clay types, different curing agents and processing parameters. The study did not only focus on a single parameter but also a combination of these parameters. These effects have tremendous impact on the manufacture of epoxy nanocomposites, which have not been fully explored so far. This thesis was designed to contribute to the understanding of these effects in more complex features as follows.

– Better understanding of the effects of different process parameters (temperature  $T$ , stirring speed  $\nu$ , and stirring duration  $t$ ), chemistry of clay, hardeners (chemical reactivity) on formation of epoxy nanocomposites in a more systematic manner. The clay aggregates are broken down into the smaller ones with increasing stirring temperature, speed and duration. Moreover the speed shows greater effect than other parameters. In terms of delamination, stirring temperature plays a more important role than the other parameters. The more reactive clay I30E shows a better intercalation/exfoliation in epoxy nanocomposites than C30B. However, C30B shows better micro dispersion in epoxy nanocomposites than I30E. The longer hardener molecule and the lower curing rate of the epoxy system have a positive effect not only on the intercalation but also on the dispersion of the C30B clay at the micro level in the epoxy. However, the inverse holds true for I30E clay.

– The equation  $F_{DT} = D + \tau = D + \eta \frac{d\nu}{dh}$  was proposed for the first time to explain the effect of stirring temperature, speed and duration on the intercalation and exfoliation of clay at the stirring step for thermoset polymer.

- A model for flow in a concentric cylinder high shear stirrer was developed and applied to predict the processing conditions necessary for achieving delamination of the clay layers. The model provides a useful tool for determining the required processing parameters to separate the clay layers in thermosetting polymers. It can also be used to design a new stirrer to give the desired shearing force.
  
- A new method to generate the high shear to disperse organoclays into organic media, a high speed stirring method, is proposed. Agglomerates of organoclay are broken down into very small tactoids of clay and form high surface area in the epoxy matrix with high speed stirring. Well dispersed and well intercalated/exfoliated epoxy nanocomposites are achieved. Aggregates were broken down to tactoids consisting of fewer than 4 silicate layers, and uniformly distributed in glassy epoxy nanocomposites. The advantages of this method are that it is simple, fast and easy to carry out. This method also eliminates the use of solvent for dispersing clay in epoxy. Due to free solvent, it can save a lot of time and cost as well as be environmentally friendly.
  
- The kinetics of the curing process of epoxy nanocomposites, containing different types of clay and hardener was systematically studied. The presence of clay facilitates the curing reaction (the presence of organoclay also results in a slight increase in the curing rate of epoxy nanocomposite compared to epoxy system). There is a minor steric effect of the clay on the cure of the nanocomposite. Generally speaking, the presence of the clay does not have a strong influence on the curing of epoxy nanocomposites.
  
- The risk involved in the preparation of ENCs with reactive organoclays (such as Nanomer I30E) has been discovered. It is important to study the reactivity of the

organoclay before using it, especially at high temperature.

– The effect on formation of epoxy nanocomposites of different types of curing agents, which involve different molecular weights, chain size and curing rate were for the first time systematically studied. The intercalation and exfoliation process is controlled not only by the rate of diffusion of organic molecules (in this case, the curing agent and the epoxy molecules) into the clay gallery but also by the curing rate of the epoxy system and by the size of epoxy and hardener molecules.

– Results have been generated for different systems. The dispersed nanoclay particles have an important effect on the mechanical properties of nanocomposites. Tensile properties, compression properties, and especially fracture toughness greatly improve with the high speed stirring method. The findings in this study are quite superior to other data reported in the literature for glassy ENCs, where only a loss in tensile strength was reported [11, 12, 18, 27, 41, 45, 91]. High speed stirring also provides a great improvement in the solvent resistance of epoxy nanocomposite compared to other stirring methods and of course to the neat epoxy. The better is the dispersion of clay, the lower is the water absorption and the higher is the solvent resistance. A great improvement on the LOI for epoxy nanocomposites (based on EPICURE 3046 curing agent) prepared by this stirring method was observed that has not been reported. The correlation between the dispersion of clay and the critical stress intensity factor ( $K_{IC}$ ) and the critical strain energy release rate ( $G_{IC}$ ) was studied. The size of clay aggregates has a great effect on  $K_{IC}$  and  $G_{IC}$ . The smaller is the particle size, the higher are  $K_{IC}$  and  $G_{IC}$ . The correlation between the dispersion of clay in epoxy nanocomposites and water or solvent absorption was developed. The reinforcing effect of nanoclay in epoxy systems whose

characteristics can vary over a broad range from rubbery to glassy rubbery was for the first time systematically evaluated. It confirms that nanoclay has a more significant effect on the properties of soft rubbery materials (typical of material in the rubbery region above  $T_g$ ). For  $T_g > 0$ , the effect of clay is not large and is about the same for all epoxy systems. However for  $T_g < 0$ , some properties are affected more than the others and the effect can be quite large for a few properties. This research shows for the first time that  $T_g$  can be used as an indication of the effect of clay addition on epoxy properties, regardless of the type of epoxy system.

– The improvement in modulus of epoxy nanocomposites based on rubbery and glassy epoxy systems has been evaluated for the first time by means of the Halpin-Tsai and Mori-Tanaka models. The Halpin-Tsai and Mori-Tanaka models confirm that the clay has a greater reinforcing effect on a rubbery epoxy system than on a glassy system. The results have provided a very good fundamental understand of the reinforcing effect of nanoclay on epoxy properties. The Mori-Tanaka model shows a better agreement with the experimental results.

## **8.4. List of publications**

1. Ngo T.-D., Ton-That M.-T., Hoa S. V. and Cole K. C. “Reinforcing effect of organoclay in epoxy resins with characteristics varying over a broad range from rubbery to glassy”, to be submitted.
2. Ngo T.-D., Ton-That M.-T., Hoa S. V. “Dispersion methods and performance of epoxy nanocomposites”, to be submitted.



3. Ngo T.-D., Hoa S. V., Ton-That M.-T., and Wood-Adams P. M., “Shear mixing and dispersion of thermoset polymer nanocomposites: modeling the delamination process”, to be submitted.
4. Ngo T.-D., Ton-That M.-T., Hoa S. V. and Cole K. C. “Reinforcing effect of organoclay in rubbery and glassy epoxy resins– part 2: modulus prediction”, to be submitted to *J. Appl. Polym. Sci.*
5. Ngo T.-D., Ton-That M.-T., Hoa S. V. and Cole K. C. “Reinforcing effect of organoclay in rubbery and glassy epoxy resins – part 1: dispersion and properties”, submitted to *J. Appl. Polym. Sci.*
6. Ngo T.-D., Ton-That M.-T., Hoa S. V. and Cole K. C. “Curing kinetics and mechanical properties of epoxy nanocomposites based on different organoclays”, in press, *Polymer Engineering and Science*, Vol. 47, No. 5.
7. Hoa S. V., Ouellette P., Ngo T.-D. “Monitoring the history of shrinkage and modulus development of thermosetting resins”, submitted to *Journal of Composites Science and Technology*.
8. Ton-That M.-T., Ngo T.-D., Cole K. C., Ding P., Fang G., and Hoa S. V. (2004) “Epoxy nanocomposites: analysis and kinetics of cure”, *Polymer Engineering and Science*, Vol. 44, No.6, 1132-1141.
9. Ngo T.-D., Ton-That M.-T., Hoa S. V., Cole K. C. (2007) “The influence of type of curing agents on dispersion and performance of epoxy nanocomposites”, to be submitted to *the four international symposium on Polymer Nanocomposites and Technology*,

Boucherville, Canada.

10. Ngo T.-D., Ton-That M.-T., Hoa S. V. “Understanding the effect of adding nanoclays into epoxy: the effect of mixing temperature and speed on dispersion”, *AES – ATEMA-2007 - International conference on advances and trends in engineering materials and their applications*, Montreal, Canada.

11. Ngo T.-D., Ton-That M.-T., Hoa S. V., Wood-Adams P. (2007) “Effect Shearing Time and Temperature on the Dispersion of Clay in Thermoset Nanocomposites”, *CANCOM 2007*, Winnipeg, Canada.

12. Ngo T.-D., Ton-That M.-T., Hoa S. V. (2007) “Effect of shearing on dispersion, intercalation/exfoliation of clay in epoxy”, *The 16<sup>th</sup> international conference on Composite Materials*, Kyoto, Japan.

13. Ngo T.-D., Ton-That M.-T., Hoa S. V., Cole K. C. (August 24-26, 2006) “Rubbery and glassy epoxy-clay nanocomposites”, *The sixth joint Canada-Japan workshop on Composites*, Toronto, Canada.

14. Ngo T.-D., Ton-That M.-T., Hoa S. V., Cole K. C. (September, 2005) “The influence of type of organo-nanoclay and preparation methods on curing kinetics and mechanical properties of epoxy nanocomposites”, *Third international symposium on Polymer Nanocomposites and Technology*, Boucherville, Canada.

15. Ngo T.-D., Ton-That M.-T., Cole K. C., Hoa S. V. (August, 2005) “Epoxy nanocomposites: the effect of organo-nanoclay on curing kinetics and mechanical properties”, *CANCOM 2005*, Vancouver, Canada.

16. Ngo T.-D., Ton-That M.-T., Cole K. C., Hoa S. V. (Oct-2005) “The effect of organo-nanoclay and preparation methods on curing kinetics and mechanical properties of epoxy nanocomposite”, *The 9<sup>th</sup> conference on Science and Technology*, Ho Chi Minh, Vietnam.

17. Ton-That M.-T., Ngo T.-D., Cole K. C., Ding P., Fang G., Hoa S. V. (Oct-2003) “Curing kinetics of epoxy nanocomposites”, *Second international symposium on Polymer Nanocomposites and Technology*, Montreal, Canada.

## **8.5. Recommendations for future work**

In this thesis, many effects have been studied to obtain high performance epoxy nanocomposites. The following works are felt necessary to be done in the future:

- It is very difficult to control the temperature of the resin during stirring by the present homogenizer since the high stirring power of the device generates a large amount of heat in the system. As a result, the high shear force decreases as the viscosity of the system drops with the increase of temperature. A more dynamic flow should be considered in order to bring the heat out of the system.
- High temperature favors intercalation and exfoliation but it reduces the system viscosity, so it is difficult to obtain a good shear force. The stirring step should be split into two sub-steps, in which the first one will work with the homogenizer at low temperatures and the latter one will work with a conventional mechanical stirrer at high temperatures.
- The commercial organoclays can only be intercalated in the epoxy resin in the stirring

step, indicating that these are not fully compatible with the epoxy resin. The chemistry of the organoclays should be studied in order to obtain full exfoliation in this step. A chemical bond between the epoxy and the clay is favorable.

- To quantify accurately the level of exfoliation, XRD is not reliable while TEM is very time-consuming and expensive. AFM techniques should be adapted for this kind of analysis.
- When the level of exfoliation can be quantified accurately it should be interesting to use different models to predict other mechanical properties like strength, toughness, etc.
- The study should be expanded to other epoxy systems, including different epoxy resins and different hardeners and even multiphase epoxy systems.
- The study should also be expanded to hybrid clay nanocomposite-composite systems, in which a conventional reinforcement like fibers will be used together with nanoclays. The role of nanoclays will be to reinforce the properties of the composite which are contributed by the matrix, for example the interlaminar shear, the transverse properties in unidirectional composites, barrier, etc.
- Long-term mechanical performance of the nanocomposites should be studied, such as fatigue, creep, durability, etc.
- In order to obtain a better understanding of the LOI results, further work on the mechanism of fire resistance of the clays should be carried out.
- The procedure needs to be scaled up.

# References

- [1] Mark J. E., "Ceramic reinforced polymers and polymer-modified ceramics", *Polym. Eng. Sci.*, **36**, 2905-2920 (1996).
- [2] Reynaud E., Gauthier C. and Perez J., "Nanophases in polymers", *Rev. Metall./Cah. Inf. Tech.*, **96**, 169-176 (1999).
- [3] Werne T. Von and Patten T. E., "Preparation of structurally well defined polymer-nanoparticle hybrids with controlled/ living radical polymerization", *J. Am. Chem. Soc.*, **121**, 7409-7410 (1999).
- [4] Kornmann X., "Synthesis and characterisation of thermoset-clay nanocomposites", *PhD thesis, Lulå University of Technology*, Sweden (1999).
- [5] Herron N. and Thorn D. L., "Nanoparticles. Uses and relationships to molecular clusters", *Adv. Mater.*, **10**, 1173-1184 (1998).
- [6] Calvert P., "Potential applications of nanotubes, in: T. W. Ebbesen (Ed.), Carbon Nanotubes", *CRC Press, Boca Raton, FL*, 277-292 (1997).
- [7] Favier V., Canova G.R., Shrivastava S. C. and Cavaille J.Y., "Mechanical percolation in cellulose whiskers nanocomposites", *Polym. Eng. Sci.*, **37**, 1732-1739 (1997).
- [8] Chazeau L., Cavaille J. Y., Canova G., Dendievel R. and Bouterin B., "Viscoelastic properties of plasticized PVC reinforced with cellulose whiskers", *J. Appl. Polym. Sci.*, **71**, 1797-1808 (1999).
- [9] Messersmith P. B. and Giannelis E. P., "Synthesis and characterisation of layered silicate-epoxy nanocomposites", *Chem. Mater.*, **6**, 1719-1725 (1994).

- [10] Kornmann X., Linberg H. and Berglund L. A., "Synthesis of epoxy-clay nanocomposites- Influence of the nature of the curing agent on structure", *Polymer*, **42**, 4493-4499 (2001).
- [11] Lan T. and Pinnavaia T. J., "Clay-reinforced epoxy nanocomposites", *Chem. Mater.*, **6**, 2216-2219 (1994).
- [12] Massam J. and Pinnavaia T. J., "Clay nanolayer reinforcement of glassy epoxy polymer", *Mater. Res. Soc. Symp. Proc. Spring Meeting*, San Francisco, CA (US), Vol. **520**, 223-232 (1998).
- [13] Brown J. M., Curliss D. and Vaia R. A., "Thermoset-layered silicate nanocomposites. Quaternary ammonium montmorillonite with primary diamine cured epoxies", *Chem. Mater.*, **12**, 3376-3384 (2000).
- [14] Kornmann X., Thomann R., Mülhaupt R., Finter J. and Berglund L. A., "High performance epoxy-layered silicate nanocomposites", *Polym. Eng. Sci.*, Vol. **42**, No. 9, 1815-1826 (2002).
- [15] Gilman J. W., Kashiwagi T., Nyden M., Brown J. E. T., Jackson C. L., Lomakin S., Giannelis E. P. and Manias E., "Flammability studies of polymer layered silicate nanocomposites: polyolefin, epoxy and vinyl ester resins", Chapter 14 in Al-Malaika S., Golovoy A. and Wilkie C. A. (eds)- "Chemistry and technology of Polymer Additives", *Blackwell Science*, Oxford, UK (1999).
- [16] Wang M. S. and Pinnavaia T. J., "Clay-Polymer Nanocomposites formed from acidic derivatives of montmorillonite and an epoxy resin", *Chem. Mater.*, Vol. **6**, No. 4, 468-474 (1994).

- [17] Becker O., Varley R. J. and Simon G. P., "Thermal stability and water uptake of high performance epoxy layered silicate nanocomposites", *Eur. Polym. J.*, **Vol. 40**, No. 1, 187-195 (2004).
- [18] Kornmann X., Lindberg H. and Berglund L. A., "Synthesis of epoxy-clay nanocomposites: influence of the nature of the clay on structure", *Polymer*, **Vol. 42**, No. 4, 1303-1310 (2001).
- [19] Yasmin A., Abot J. L. and Daniel I. M., "Processing of clay/epoxy nanocomposites by shear mixing", *Scripta Materialia*, **Vol. 49**, No. 1, 81-86 (2003).
- [20] Chen C. and Tolle T. B., "Fully exfoliated layered silicate epoxy nanocomposites", *J. Polym. Sci. Part B: Polym. Phys.*, **Vol. 42**, No. 21, 3981-3986 (2004).
- [21] Liu W. P., Hoa S. V. and Pugh M., "Morphology and performance of epoxy nanocomposites modified with organoclay and rubber", *Polym. Eng. Sci.*, **Vol. 44**, No. 6, 1178-1186 (2004).
- [22] Liu W. P., Hoa S. V. and Pugh M., "Organoclay-modified high performance epoxy nanocomposites", *Compos. Sci. Technol.*, **Vol. 65**, 307-316 (2004).
- [23] Liu W. P., Hoa S. V. and Pugh M., "Fracture toughness and water uptake of high-performance epoxy/nanoclay nanocomposites", *Compos. Sci. Technol.*, **Vol. 65**, 2364-2373 (2005).
- [24] Theng B. K. G., "Formation and properties of clay-polymer complexes", *Elsevier, Amsterdam* (1979).

- [25] Blumstein A., "Etude des polymerizations en couche adsorbée I", *Bull Chim. Soc.*, 899-905 (1961).
- [26] Okada A., Kawasumi M., Usuki A., Kojima Y., Kurauchi T. and Kamigaito O., "Nylon 6-clay hybrid", *Mater. Res. Soc. Proc.*, **171**, 45-50 (1990).
- [27] Nanocor Inc. Web site: [www.nanocor.com](http://www.nanocor.com)
- [28] Wang Z., Lan T. and Pinnavaia T. J., "Hybrid organic-inorganic nanocomposites formed from an epoxy polymer and a layered silicic acid (Magadiite)", *Chem. Mater.*, **8**, 2200-2204 (1996).
- [29] Munzy C. D., Butler B. D., Hanley H. J. M., Tsvetkov F. and Pfeiffer D. G., "Clay platelet dispersion in a polymer matrix", *Materials Letters*, **28**, 379-384 (1996).
- [30] Lan T. and Pinnavaia T. J., "Nanolayer ordering in an epoxy-exfoliated clay hybrid composite", *Mat. Res. Soc. Symp. Proc.*, **435**, 79-84 (1996).
- [31] Deer W. A. and Howie R. A., "Rock-forming minerals", *Wiley*, New York, **3**, p 240 (1962).
- [32] Damour A. A. and Salvetat D., "Analyses sur un hydrosilicate d'alumine trouvé à montmorillon", *Ann. Chim. Phys. Ser.*, **21**, 376-383 (1847).
- [33] Theng B. K. G., "The chemistry of clay-organic reactions", *Wiley*, New York (1974).
- [34] Giannelis E. P., Krishnamoorti R. and Manias E., "Polymer-silicate nanocomposites: model systems for confined polymers and polymer brushes", *Adv. Polym. Sci.*, **138**, 107-147 (1999).
- [35] <http://www.ill.fr/dif/3Dcrystals/layers.html>



- [36] Sinha Ray S. and Okamoto M., "Polymer/layered silicate nanocomposites: a review from preparation to processing", *Prog. Polym. Sci.*, **28**, 1539–641 (2003).
- [37] Sinha Ray S. and Bousmina M., "Biodegradable polymers and their layered silicate nanocomposites: in greening the 21st century materials world", *Progress in Materials Science*, **50**, 962-1079 (2005).
- [38] Lagaly G., "Introduction: from clay mineral-polymer interactions to clay mineral-polymer nanocomposites", *Applied Clay Science*, **15**, 1-9 (1999).
- [39] Worrall W. E., "Clay and ceramic raw materials 2nd edition", *Elsevier applied science publishers*, New York (1986).
- [40] Worall W. E., "Clays: their nature, origin and general properties", *MacLaren & sons*, London (1968).
- [41] Utracki L. A., "Clay-containing polymeric nanocomposites", *Rapra Technology* (2004).
- [42] Usuki A., Kawasumi M., Kojima Y., Okada A., Kurauchi T. and Kamigaito O., "Swelling behaviour of montmorillonite cation-exchanged for  $\omega$ -amino acids by  $\epsilon$ -caprolactam", *J. Mater. Res.*, **8**, 1174-1178 (1993).
- [43] Jordan J. W., "Organophilic bentonites", *J. Phys. Colloid Chem.*, **53**, 294-306 (1949).
- [44] Weiss A., "Organic derivatives of mica-type layer silicates", *Angew. Chem. internat. Edit.*, **2**, 134-143 (1963).
- [45] Lan T., Kaviratna P. D. and Pinnavaia T. J., "Mechanism of clay tactoid exfoliation in epoxy-clay nanocomposites", *Chem. Mater.*, **Vol. 7**, No. 11, 2144-2150 (1995).

- [46] Wang Z. and Pinnavaia T. J., "Hybrid organic-inorganic nanocomposites: exfoliation of magadiite nanolayers in an elastomeric epoxy polymer", *Chem. Mater.*, **10**, 1820-1826 (1998).
- [47] Plueddemann E. P., "Silane coupling agents, 2nd Ed.", New York (1991).
- [48] Ogawa M. and Kuroda K., "Preparation of inorganic-organic nanocomposites through intercalation of organoammonium ions into layered silicates", *Bull. Chem. Soc., Jpn.*, **70**, 2593-2618 (1997).
- [49] Southern Clay Product. Website: <http://www.nanoclay.com>
- [50] Pinnavaia T. J. and Beall G. W., "Polymer-clay nanocomposites", *John Wiley & Sons*, New York (2000).
- [51] Alexandre M. and Dubois P., "Polymer-layered silicate nanocomposites: preparation, properties and uses of a new class of materials", *Mater. Sci. & Eng.*, **28**, 1-63 (2000).
- [52] Giannelis E. P., "Polymer layered silicate nanocomposites", *Adv. Mater.*, **8**, 29-35 (1996).
- [53] Chin I. J. , Thrun-Albrecht T., Kim H.C., Russell T.P. and Wang J., "On exfoliation of montmorillonite in epoxy", *Polymer*, **42**, 5947-5952 (2001).
- [54] Kornmann X., Berglund L. A., Sterte J. and Giannelis E. P., "Nanocomposites based on montmorillonite and unsaturated polyester", *Polym. Eng. Sci*, **38**, 1351-1358 (1998).
- [55] Wang Z. and Pinnavaia T. J., "Nanolayer reinforcement of elastomeric polyurethane", *Chem. Mater.*, **10**, 3769-3771 (1998).

- [56] Zilg C., Thomann R., Mülhaupt R. and Finter J., "Polyurethane nanocomposites containing laminated anisotropic nanoparticles derived from organophilic layered silicates", *Adv. Mater.*, **11**, 49-51 (1999).
- [57] Chen C. and Curliss D., "Resin matrix composites: organoclay-aerospace epoxy Nanocomposites Part II", *Sample Journal*, Vol. **37**, No. 5, 11-18 (2001).
- [58] Wang H., "The study of clay/epoxy nanocomposites: their synthesis, microstructure and properties", *Master thesis, Concordia University, Montreal* (2004).
- [59] Messersmith P. B. and Giannelis E. P., "Synthesis and barrier properties of poly( $\epsilon$ -caprolactone)-layered silicate nanocomposites", *J. Appl. Polym. Sci. Part A*, **33**, 1047-1057 (1995).
- [60] Ke Y., Long C. and Qi Z., "Crystallization, properties, and crystal and nanoscale morphology of PET clay nanocomposites", *J. Appl. Polymer. Sci.*, **71**, 1139-1146 (1999).
- [61] Ma J. S., Qi Z. N. and Hu Y. L., "Synthesis and characterization of polypropylene/clay nanocomposites", *J. Appl. Polym. Sci.*, **82**(14), 3611-3617, (2001).
- [62] Jeon H. G., Jung H.-T. and Hudson S. D., "Morphology of polymer/silicate nanocomposites", *Polymer Bulletin*, **41**, 107-113 (1998).
- [63] Yano K., Usuki A., Okada A., Kurauchi T. and Kamigaito O., "Synthesis and properties of polyimide clay hybrid", *J. Polym. Sci. Part A*, **31**, 2493-2498 (1993).

- [64] Kawasumi M., Hasegawa N., Usuki A. and Akane O., "Nematic liquid crystal/clay mineral composites", *Mater. Eng. Sci.*, **6**, 135-143 (1998).
- [65] Vaia R. A., Sauer B. B., Tse O. K. and Giannelis E. P., "Relaxations of confined chains in polymer nanocomposites: glass transition properties of poly(ethylene oxide) intercalated in montmorillonite", *J. Polym. Sci.: Part B*, **35**, 59-67 (1997).
- [66] Lee D. C. and Jang L. W., "Preparation and characterisation of PMMA-clay hybrid composite by emulsion polymerisation", *J. Appl. Polym. Sci.*, **61**, 1117-1122 (1996).
- [67] Vaia R. A., Ishii H. and Giannelis E. P., "Synthesis and properties of two-dimensional nanostructures by direct intercalation of polymer melts in layered silicates", *Chem. Mater.*, **5**, 1694-1696 (1993).
- [68] Kojima Y., Usuki A., Kawasumi M., Okada A., Kurauchi T., Kamigaito O. and Kaji K., "Fine structure of nylon 6-clay hybrid", *J. Polym. Sci., Part B*, **32**, 625-630 (1994).
- [69] Liu L., Qi Z. and Zhu X., "Studies on nylon 6/clay nanocomposites by melt-intercalation process", *J. Appl. Polym. Sci.*, **71**, 1133-1138 (1999).
- [70] Vaia R. A., Jandt K. D., Kramer E. J. and Giannelis E. P., "Microstructural evolution of melt intercalated polymer-organically modified layered silicates nanocomposites", *Chem. Mater.*, **8**, 2628-2635 (1996).
- [71] Kawasumi M., Hasegawa N., Kato M., Usuki A. and Okada A., "Preparation and mechanical properties of polypropylene-clay hybrids", *Macromolecules*, **30**, 6333-6338 (1997).
- [72] Petrie E. M., "Epoxy Adhesive Formulations", *McGraw-Hill* (2006).

- [73] Lee H. and Neville K., "Handbook of epoxy resin", *McGraw-Hill* (1967).
- [74] Clayton A. May., "Epoxy resins- chemistry and technology", *Marcel Dekker*, New York (1988).
- [75] Varma I. K. and Gupta V. B., "Thermosetting resin- properties", *Comprehensive Composite Materials, Vol. 2 - Polymer Matrix Composites*, 1-56 (2000)
- [76] Dow Chemical. Website: <http://www.dow.com>
- [77] Resolution group of Companies. Website: <http://www.resins-versatics.com/resins>
- [78] Huntsman LLC. Website: <http://www.huntsman.com>
- [79] Sigma-Aldrich. Website: <http://www.sigmaaldrich.com>
- [80] Cole K. C., "A new Approach to modeling the cure kinetics of epoxy amine thermosetting resins. 1. Mathematical development", *Macromolecules*, **24**, 3093-3097 (1991).
- [81] Lan T., Kaviratna P. D. and Pinnavaia T. J., "Epoxy self-polymerization in smectite clays", *J. Phys. Chem. Solids.*, Vol. **57**, No. 6-8, 1005-1010 (1996).
- [82] Pinnavaia T. J., Lan T., Wang Z., Shi H. and Kaviratna P. D., "Clay-reinforced epoxy nanocomposites: synthesis, properties, and mechanism of formation", *ACS Symp Ser*, Vol. **622**, 250-261 (1996).
- [83] Ke Y., Lü J., Yi X., Zhao J., and Qi Z., "The effect of promoter and curing process on exfoliation behavior of epoxy/clay nanocomposites", *J. Appl. Polym. Sci.*, Vol. **78**, 808-815 (2000).
- [84] Lü J., Ke Y., Zhao J., Qi Z., and Yi X.-S., "Study on intercalation and exfoliation behavior of organoclays in epoxy resin", *J. Polym. Sci. B: Polym Phys.*, **39**, 115-120 (2001).

- [85] Becker O., Simon G. P., Varley R. J., and Halley P. J., "Layered silicate nanocomposites based on various high-functionality epoxy resins: The influence of an organoclay on resin cure", *Polym. Eng. Sci.*, **43**, No.4, 850-862 (2003).
- [86] Barton J. M., "The application of differential scanning calorimetry (DSC) to the study of epoxy resin curing reactions", *Adv. Polym. Sci.*, **72**, 111-154 (1985).
- [87] Butzloff P., D'Souza N. A., Golden T. D. and Garrett D., "Epoxy-montmorillonite nanocomposite: Effect of composition on reaction kinetics", *Polym. Eng. Sci.*, **Vol. 41**, No.10, 1794-1802 (2001).
- [88] Chen D. Z., He P. S. and Pan L. J., "Cure kinetics of epoxy-based nanocomposites analyzed by Avrami theory of phase change", *Polymer Testing*, **Vol. 22**, 689-697 (2003).
- [89] Chen D. Z., He P. S., "Monitoring the curing process of epoxy resin nanocomposites based on organo-montmorillonite – a new application of resin curemeter", *Compos. Sci. Technol.*, **Vol. 64**, 2501-2507 (2004).
- [90] Xu W. B., Zhou Z. F., He P. S. and Pan W.-P., "Cure behavior of epoxy resin/MMT/DETA nanocomposite", *Journal of Thermal Analysis and Calorimetry*, **Vol. 78**, 113-124 (2004).
- [91] Zilg C., Thomann R., Finter J. and Mülhaupt R., "The influence of silicate modification and compatibilizers on mechanical properties and morphology of anhydride-cured epoxy nanocomposites", *Macromol. Mater. Eng.*, **280/281**, 41-46 (2000).
- [92] Kornmann X., Thomann R., Mülhaupt R., Finter J. and Berglund L. A., "Synthesis of amine-cured, epoxy-layered silicate nanocomposites: the influence

- of the silicate surface modification on the properties”, *J. Appl. Polym. Sci.*, **86**, 2643-2652 (2002).
- [93] Qui B., Zhang Q. X., Bannister M., Mai Y.-W., “Investigation of the mechanical properties of DGEBA-based epoxy resin with nanoclay additives”, *Composite Structures*, **75**, 514-519 (2006).
- [94] Zerda A. S. and Lesser A. J., “Intercalated clay nanocomposites: morphology, mechanics, and fracture behavior”, *J. Polym. Sci. B: Polym Phys.*, **39**, 1137-1146 (2001).
- [95] Zilg C., Mülhaupt R. and Finter J., “Morphology and toughness/stiffness balance of nanocomposites based upon anhydride-cured epoxy resins and layered silicates”, *Macromol. Chem. Phys.*, **200**, No. 3, 661-670 (1999).
- [96] Wang L., Zhang K. L., Feing W., Wang F. and Li Z. B., “Preparation and characterization of modified montmorillonite reinforced and toughed epoxy resins nanocomposites”, *International Symposium on polymer nanocomposites, science and technology*, Montreal (2001).
- [97] Ratna D., Manoj N. R., Varley R., Raman R. K. S. and Simon G. P., “Clay-reinforced epoxy nanocomposites”, *Polym. Int.*, **52**, 1403-1407 (2003).
- [98] Gam K. T. , Lu J. J., Sue H. J. And Miyamoto M., “Mechanical property and toughening of epoxy nanocomposites”, *Annual Technical conference society of Plastics Engineers, 60th*, **Vol. 2**, 1524-1529 (2002).
- [99] Ratna D., Becker O., Krishnamurthy R., Simon G. P. and Varley R., “Nanocomposites based on a combination of epoxy resin, hyperbranched epoxy and a layered silicate”, *Polymer*, **44**, 7449-7457 (2003).

- [100] Liu T., Tjiu W. C, Tong Y., He C., Goh S. S. and Chung T. S., "Morphology and fracture behavior of intercalated epoxy/clay nanocomposites", *J. Appl. Polym. Sci.*, **Vol. 94**, 1236-1244 (2004).
- [101] Kelly P., Akelah A. Qutubuddin S. and Moet A., "Reduction of residual stress in montmorillonite/epoxy compounds", *J. Mater. Sci.*, **29**, 2274-2280 (1994).
- [102] Feng W., Ait-Kadi A., and Riedl B., "Polymerization compounding: epoxy-montmorillonite nanocomposites", *Polym. Eng. Sci.*, **Vol. 42**, No. 9, 1827-1835 (2002).
- [103] Becker O., Varley R. J. and Simon G. P., "Morphology, thermal relaxations and mechanical properties of layered silicate nanocomposites based upon high-functionality epoxy resins", *Polymer*, **43**, 4365-4373 (2002).
- [104] Chen K. H. and Yang S. M., "Synthesis of epoxy-montmorillonite nanocomposite", *J. Appl. Polym. Sci.*, **86**, 414-421 (2002).
- [105] Chen C., Khobaib M. and Curliss D., "Epoxy layered-silicate nanocomposites", *Progress in organic coating*, **47**, 376-383 (2003).
- [106] Mai Y.-W., Yu Z.-Z., "Polymer nanocomposite", *Woodhead Publishing in Materials*, FL (2006).
- [107] Liu W., "Epoxy-clay nanocomposites for structure applications", *PhD Thesis, Concordia University*, Montreal (2005).
- [108] Hoa S. V., Liu W. P., Pugh M. and Ton-That M.-T., "Process for the development of epoxy nanocomposites and products", *U. S. Patent, US 60/5315 18, Dec 2003*, in process.



- [109] Milton M. D., "X-ray diffraction and the identification and analysis of clay minerals", *Oxford, Oxford University press*, New York (1997).
- [110] Diagram courtesy of Iowa State university SEM homepage. Website: <http://www.purdue.e/sem.htm>
- [111] Williams D. B. and Carter C. B., "Transmission electron microscopy", *Plenum Press*, New York (1996).
- [112] ASTM-D2863-97. An American society for testing and materials standard, ASTM, West Conshohocken, PA, United States.
- [113] Sichina W. J., "Thermal analysis for the characterization of polymer impact resistance". *Thermal analysis-application note*, PerkinElmer instruments (2001).
- [114] Netzsch thermal analysis. Website: <http://www.netzch-thermal-analysis.com> .
- [115] MatWeb-Material properties data. Web site: <http://www.matweb.com>.
- [116] ASTM-D638-02a. An American society for testing and materials standard, ASTM, West Conshohocken, PA, United States.
- [117] ASTM-D790-03. An American society for testing and materials standard, ASTM, West Conshohocken, PA, United States.
- [118] ASTM-D695-02a. An American society for testing and materials standard, ASTM, West Conshohocken, PA, United States.
- [119] ASTM-D256-02. An American society for testing and materials standard, ASTM, West Conshohocken, PA, United States.
- [120] ASTM-D5045-99. An American society for testing and materials standard, ASTM, West Conshohocken, PA, United States.

- [121] ASTM-D2240-00. An American society for testing and materials standard, ASTM, West Conshohocken, PA, United States.
- [122] Ishida H., Campbell S., Blackwell J., “General approach to nanocomposite preparation”, *Chem. Mater.*, **12**, 1260-1267 (2000).
- [123] Xu W.-B., Bao S.-P., He and P.-S., “Intercalation and exfoliation behavior of epoxy resin/curing agent/montmorillonite nanocomposite”, *J Appl Polym Sci* , **84**, 842-849 (2002).
- [124] Stokes R. J. and Evans D. F., “Fundamentals of interfacial engineering”, *Wiley – VCH* (1997).
- [125] Hiemenz P. C., Rajagopalan R., “Principle of colloid and surface chemistry”, *Marcel Dekker* (1997).
- [126] Grimshaw R. W., “The chemistry and physics of clays”, *John Wiley & Sons*, New York (1971).
- [127] Morrison F. A., “Understanding rheology”, New York-Oxford (2001).
- [128] Bird R. B., Stewart W. E. and Lightfoot E. N., “Transport phenomena”, *John Wiley & Son*, New York (1960).
- [129] <http://www.syvum.com/eng/fluid/>
- [130] Larson R. G., “The Structure and rheology of complex fluids”, Oxford University Press, New York (1999).
- [131] Jeffery G. B., “The motion of ellipsoidal particles immersed in a viscous fluid”, *Proc. R. Soc. Lond. A*, **102**, 161-179 (1922).

- [132] Kim K., Utracki L. A. and Kamal M. R., "Numerical simulation of polymer nanocomposites using self-consistent mean-field model", *Journal of Chemical Physics*, **Vol. 121**, No. 21, 10766-10777 (2004).
- [133] Vial J. and Carré A., "Calculation of Hamaker constant and surface energy of polymers by a simple group contribution method", *Int. J. Adhesion Adhesive*, **11**, 140-143 (1991).
- [134] Médout-Marère V., "A simple experimental way of measuring the Hamaker constant  $A_{11}$  of divided solids by immersion calorimetry in polar liquids", *J. Colloid Interface Sci.*, **228**, 434-437 (2000).
- [135] Boey F. Y. C. and Qiang W., "Experimental modeling of the cure kinetics of an epoxy-hexa-anhydro-4-methylphthalicanhydride (MHHPA) system", *Polymer*, **41**, 2081-2094 (2000).
- [136] Lee J.-Y., Shim M.-J. and Kim S.-W., "Effect of modified rubber compound on the cure kinetics of DGEBA/MDA system by Kissinger and isoconversional methods", *Thermochim. Acta*, **371**, 45-51 (2001).
- [137] Zvetkov V. L., "Comparative DSC kinetics of the reaction of DGEBA with aromatic diamines.: I. Non-isothermal kinetic study of the reaction of DGEBA with *m*-phenylene diamine", *Polymer*, **42**, 6687-6697 (2001).
- [138] Pollard M. and Kardos J. L., "Analysis of epoxy resin curing kinetics using the Avrami theory of phase change", *Polym. Eng. Sci.*, **27**, 829-836 (1987).
- [139] Muzumdar S. V. and Lee L. J., "Chemorheological analysis of unsaturated polyester-styrene copolymerization", *Polym. Eng. Sci.*, **36**, 943-952 (1996).

- [140] Lu M. G., Shim M. J. and Kim S. W., "Curing behavior of an unsaturated polyester system analyzed by Avrami equation", *Thermochim. Acta*, **323**, 37-42 (1998).
- [141] Kim S.-W., Lu M.-G. and Shim M.-J., "The isothermal cure kinetic of epoxy/amine system analyzed by phase change theory", *Polym. J.*, **30**, 90-94 (1998).
- [142] Roşu D., Caşcaval C. N., Mustaţă F. and Ciobanu C., "Cure kinetics of epoxy resins studied by non-isothermal DSC data", *Thermochim. Acta*, **383**, 119-127 (2002).
- [143] He Y., "DSC and DEA studies of underfill curing kinetics ", *Thermochim. Acta*, **367**, 101-106 (2001).
- [144] Kamal M. R., "Thermoset characterization for moldability analysis", *Polym. Eng. Sci.*, **14**, 231-239 (1974).
- [145] Wunderlich B., "Macromolecular physics: crystal nucleation, growth, annealing", **Vol. 2**, Chapters 5 and 6, pp. 139ff, *Academic Press*, New York (1976).
- [146] Ozawa T., "Kinetics of non-isothermal crystallization", *Polymer*, **12**, 150-158 (1971).
- [147] Chuah K. P., Gan S. N. and Chee K. K., "Determination of Avrami exponent by differential scanning calorimetry for non-isothermal crystallization of polymers", *Polymer*, **40**, 253-259 (1998).
- [148] Ton-That M.-T., Ngo T.-D., Ding P., Fang G., Cole K. C. and Hoa S. V., "Epoxy nanocomposites: analysis and kinetics of cure", *Polym. Eng. Sci.*, **44**, 1132-1141 (2004).

- [149] Zhao Q. and Hoa S. V., "Toughening mechanism of epoxy resins with micro/nano particles", *J. Composite materials*, **Vol. 41**, No. 2, 201-219 (2007).
- [150] Horrocks A. R. and Price D., "Fire retardant materials", *CRC Press*, Cambridge England (2001)
- [151] Kim J.-K., Hu C., Woo R. S.C. and Sham M.-L., "Moisture barrier characteristics of organoclay-epoxy nanocomposites". *Compos. Sci. and Technol.*, **65**, 805-813 (2005).
- [152] Drozdov A. D., Christiansen J. D., Gupta R. K., Shah A. P., "Model for anomalous moisture diffusion through a polymer-clay nanocomposite", *J. Polym. Sci. Part B: Polym. Phys.*, **41**, 476-492 (2003).
- [153] Crank J., "The mathematics of diffusion", *Clarendon Press*, Oxford, UK (1956).
- [154] Shen C. H. and Springer G. S., "Moisture absorption and desorption of composite materials", *J. Compos. Mater.*, **10**, 2-10 (1976).
- [155] Grave C., McEwan I. and Pethrick R. A., "Influence of stoichiometric ratio on water absorption in epoxy resins", *J. Appl. Polym. Sci.*, **69**, 2369-2376 (1998).
- [156] Nogueira P., Ramirez C., Torres A., Abad M., Cano J., Lopez J., et al., "Effect of water sorption on the structure and mechanical properties of an epoxy resin system", *J. Appl. Polym. Sci.*, **80**, 71-80 (2001).
- [157] Manias E., Touny A., Wu L., Strawhecker K., Lu B. and Chung T. C., "Polypropylene/montmorillonite nanocomposites. Review of the synthetic routes and materials properties", *Chem. Mater.*, **13**, 3516-3523 (2001).

- [158] Wang Y., Zhang L., Tang C., and Yu D., "Preparation and characterization of rubber-clay nanocomposites", *J. Appl. Polym. Sci.*, **Vol. 78 (11)**, 1879-1883 (2000).
- [159] Bala P., Samantaray B. K., Srivastava S. K., and Nando G. B., "Organomodified montmorillonite as filler in natural and synthetic rubber", *J. Appl. Polym. Sci.*, **Vol. 92 (6)**, 3583-3592 (2004).
- [160] Wu Y.-P., Jia Q.-X., Yu D.-S., and Zhang L.-Q., "Structure and properties of nitrile rubber (NBR)-clay nanocomposites by Co-coagulating NBR latex and clay aqueous suspension", *J. Appl. Polym. Sci.*, **89 (14)**, 3855-3858 (2003).
- [161] Gersappe D., "Molecular mechanisms of failure in polymer nanocomposites", *Phys. Rev. Lett.*, **89**, 058301-1 – 50831-4 (2002).
- [162] Shah D., Maiti P., Gunn E., Schmidt D. F., Jiang D. D., Batt C. A. and Giannelis E. P., "Dramatic enhancements in toughness of polyvinylidene fluoride nanocomposites via nanoclay-directed crystal structure and morphology", *Adv. Mater.*, **16**, 1173-1177 (2004).
- [163] Halpin J. C. and Kardos J. L., "The Halpin-Tsai equations: a review", *Polym. Eng. Sci.*, **16**, 344-352 (1976).
- [164] Hull D. "An introduction to composite materials", *Cambridge University Press* (1981).
- [165] Brune D. A. and Bicerano J. U., "Micromechanics of nanocomposites: comparison of tensile and compressive elastic moduli, and prediction of effects of incomplete exfoliation and imperfect alignment on modulus", *Polymer*, **43**, 369-387 (2002).

- [166] Mori T. and Tanaka K., “Average stress in matrix and average elastic energy of materials with misfitting inclusions”, *Acta Metall*, **21**, 571-574 (1973).
- [167] Eshelby J. D., “The determination of elastic field of an ellipsoidal inclusion, and related problems”, *Proc. Roy. Soc. Long*, **A241**, 376-396 (1957).
- [168] Tandon G. P. and Weng G. J., “The effect of aspect ratio of inclusions on the elastic properties of unidirectionally aligned composites”, *Polym. Compos.*, **5(4)**, 327-333 (1984).
- [169] Sheng N., Boyce M. C., Parks D. M., Rutledge G. C., Abes J. I. and Cohen R. E., “Multiscale micromechanical modeling of polymer/clay nanocomposites and effective clay particle”, *J. Polymer*, **45**, 487-506 (2004).
- [170] Es M. van, Xiqiao F., Turnhout J. van and Giessen E. van der., “Specialty polymer additives: principles and applications. In: Al-Malaika S. and Golovoy A. W., editors. CA Malden-Chapter 21”, *MA: Blackwell Science* (2001).
- [171] Fornes T. D. and Paul D. R., “Modeling properties of nylon 6/clay nanocomposites using composite theories”, *Polymer*, **44**, 4993-5013 (2003).
- [172] Olphen H. Van, “An introduction to clay colloid chemistry: for clay technologists, geologists, and soil scientists, 2nd ed.”, New York: Wiley (1977).
- [173] Clark S. P., “Handbook of physical constants”, *New York: Geological Society of America, rev. ed.*, 50-89 (1966).